HOKKAIDO UNIVERSITY

Title	Early evolutionary history of soft-bodied cephalopods
Author(s)	池上, 森
Degree Grantor	北海道大学
Degree Name	博士(理学)
Dissertation Number	甲第16254号
Issue Date	2025-03-25
DOI	https://doi.org/10.14943/doctoral.k16254
Doc URL	https://hdl.handle.net/2115/97673
Type	doctoral thesis
File Information	Shin_Ikegami.pdf

Hokkaido University Collection of Scholarly and Academic Papers : HUSCAP

博士学位論文

Early evolutionary history of soft-bodied cephalopods

(軟体性頭足類の初期進化史)

池上 森

北海道大学大学院理学院

自然史科学専攻

2025 年 3 月

Contents

Abstract ····· 2

General Introduction ····· 3

Chapter 1. Squids (Oegopsida and Myopsida) ····· 8
Chapter 2. Octopoda ····· 101
Chapter 3. Vampyromorpha ····· 125
Chapter 4. New groups ····· 143

General Discussion ····· 159

Acknowledgements ····· 163

Abstract

Cephalopods have evolved through cycles of extinction and diversification over 500 Myr, dating back to the Cambrian period. By the loss of large and heavy shells, modern cephalopods have developed flexible bodies like lens eyes, chromatophores for rapid colour change, and a complex central nervous system, making them the only intelligent invertebrates with sophisticated cognition and behaviour. However, the loss of the shell brought extreme rarity of fossil record for soft-bodied cephalopods, leading to significant gaps in understanding their evolutionary history. Current research only implies the Cretaceous period as a critical evolutionary phase for them. Among known fossils of soft-bodied cephalopods, only beaks provide effective fossil evidence. However, the traditional methods for discovering, extracting, and observing fossils cannot treat this tiny, thin, and complex organ. This study shifted all of these processes into cyberspace and enabled to visualize all fossils embedded in rocks and separate them completely as a digital 3D model. By this method, I discovered numerous beak fossils, hidden as millimetre-sized microfossils, from the Late Cretaceous. These findings provide new insights into cephalopod diversity, origins, biomass, ecology, and early evolutionary history, overcoming previous limitations in the fossil record.

By thorough morphological investigations on fossil beaks, this study updated the classification methods of coleoid beaks. A total of 4 orders, 8 families, thirty genera, and fifty species were newly described among Late Cretaceous soft-bodied cephalopods. Continuous fossil records of these taxa for the Cretaceous period filled the significant gap in fossil records and revealed the origins of squid and Cirrata, and rise and fall of the unknown groups. The study also demonstrates that soft-bodied cephalopods dominated the Late Cretaceous Pacific, surpassing ammonites and teleost fishes, their ecological competitors, in biomass. The ecological examinations revealed a separation in niches, with squids being predatory, Cirrata being durophagous, and Vampyromorpha and unknown groups likely plankton feeders. A major shift from shelled to soft-bodied cephalopods at the Early/Late Cretaceous boundary was suggested, challenging the previous hypotheses of Cenozoic diversification and phylogeny. Diversity, biomass, and ecology of early soft-bodied cephalopods highlights their significant role in shaping modern marine ecosystems of adroit and intelligent animals.

General Introduction

Since they originated in the Cambrian period[1], cephalopods have repeatedly undergone cycles of extinction and diversification for over 500 Myr, all while retaining their pivotal role as large marine organisms. An immense quantity of cephalopod fossils has been discovered worldwide, showing substantial diversity[2,3]. These features have facilitated the continuous tracking of fossil records, leading to the development of numerous palaeontological theories and concepts, associated with fluctuations in diversity, variations in evolutionary rates, and mass extinction events[4–7].

In the course of their evolution, cephalopods have experienced a transformation in which they initially internalised their external shell and ultimately discarded it[1]. The living cephalopods belong to the subclass Coleoidea, with the exception of the few extant nautiloids[8–12]. This subclass is categorised into Decabrachia, encompassing squids and cuttlefish, and Octobrachia, encompassing octopuses and vampire squids[8–12]. The majority of these organisms are soft-bodied, devoid of the rigid calcium carbonate shells[13–15]. The evolutionary trajectory towards the shell loss has independently occurred in several lineages[14,15]. In Decabrachia, a progressive reduction of the shell was followed by decalcification, whereas in Octobrachia, decalcification preceded the reduction of the gladius, the vestigial shell[14,15]. These morphological adaptations have conferred upon cephalopods the ability to develop highly flexible and agile bodies[1,14,16]. Triggered by this innovation, they achieved lens eyes, flexible arms, chromatophores that rapidly alter body colouration, and a complex central nervous system[17]. With these characteristics, cephalopods have become the only intelligent invertebrate that show extraordinarily sophisticated cognition and behaviour, including effective feeding, defence, and communication strategies[1,17–19].

However, this evolutionary progression has resulted in significant gaps within the fossil record since cephalopod fossils predominantly consist of shells or gladii[1,20,21]. Consequently, the evolutionary history of soft-bodied cephalopods remains largely unsolved. Some attempts have been made to reconstruct their evolutionary history through molecular phylogenetics, but the absence of fossil records precludes the establishment of a precise timeline[16,22,23]. Previous studies of the evolutionary history of cephalopods indicated that shelled groups nearly became extinct by the end of the Cretaceous period[11], and that the shells and gladii of ancestral groups underwent significant changes during the Cretaceous[24,25]. Therefore, the Late Cretaceous is considered a critical period in their evolutionary history.

So far, only four types of soft-bodied cephalopod fossils are known: gladii, imprints of the soft body, statoliths, and beaks[20,21,26–33]. Gladius fossils are the most abundantly found among them. These fossils are, however, mostly limited to older Mesozoic forms such as Vampyromorpha and are concentrated in the Jurassic Lagerstätten, providing no continuous temporal data[3,20]. In the Late Cretaceous deposits, only four known Lagerstätten are known to yield fossils of soft-bodied cephalopods[3]. Imprints of the soft body are preserved under even more restricted conditions than gladii[21]. Most of these imprints show only outlines of the body without most taxonomic features, making identification at the order level impossible[34]. Consequently, their classification is often based on the associated gladius. Statoliths are very small calcareous particles located within the equilibrium organs[26], which have been reported as microfossils in previous studies[27]. For reasons not yet understood, statoliths are rarely found in Cretaceous sediments, as evidenced by the ratio of statoliths to fish otoliths in the same localities[27,35]. Mesozoic statoliths also cannot be reliably identified at the

order level since all of them are potentially attributed to belemnites[35]. Beaks, which this study focuses on, is an organ unique to cephalopods, with each individual possessing an upper and lower jaw[36]. Beaks are resistant to physical and chemical degradation, and their morphology accurately reflects taxonomic differences[37,38]. The lower jaws of the coleoids can be identified from the order to the species level, with detailed methods established for extant ones[39,40]. Due to their durability, beaks remain intact within the stomachs of predators such as whales and within sediments, making it possible to study predator diets, fauna, and biomass by identifying these beaks[37,38]. Research on beak identification methods has progressed by focusing on this utility, based on comprehensive morphological data from extant species. Additionally, beaks preserve a variety of information beyond taxonomic classification. Detailed morphological features are strongly influenced by phylogenetic constraints and are effective for classification[41], while the overall shape reflects dietary habits[36,42,43]. The size of the beak allows for the back-calculation of the size of the soft body[37–39,44], and the degree of pigmentation indicates growth stages[45,46]. These features make beaks the only effective material to provide a reliable fossil record of soft-bodied cephalopods from the Cretaceous.

However, small, thin, and complex fossil beaks are unable to be discovered, extracted, and observed through traditional methods. The most commonly used method, physically breaking the rock, often results in destroying the beak fossils, which are more fragile than the surrounding matrix. Chemical extraction using acids to dissolve the matrix poses difficulties in handling the fossils without damage, making thorough observation nearly impossible[47]. X-ray computed tomography (CT) is unable to visualize beaks sufficiently for taxonomic identification due to the low difference of density between the fossils and the matrix[48]. Consequently, over 200 years of fossil cephalopod research have yielded only 37 reported beak fossils[28–33,49]. All these specimens are larger than 50 mm, comparable in size to the beaks of the Giant Squid (*Architeuthis dux*)[39]. Given that the body size of hatchling cephalopods is typically less than 10 mm[11], this suggests a significant collection bias. These specimens often lack detailed morphological data, making identification and classification criteria ambiguous. The limitations shown above are hindering accurate understanding of diversity and biomass.

For documenting fossil beaks, this study developed a novel approach by conducting all processes, from fossil excavation to storage, within cyberspace. This method has enabled the discovery of numerous beak fossils of soft-bodied cephalopods from continuous time periods in the Late Cretaceous. The discovered fossils were then compared with previously reported specimens and with beaks of extant cephalopods, using updated methodologies for classification. Based on these results, this study elucidates diversity, estimates origins, biomass, and ecology, and reconstructs the early evolutionary history of these cephalopods in high resolution.

References for General Introduction

1. Kröger, B., Vinther, J. & Fuchs, D. Cephalopod origin and evolution: a congruent picture emerging from fossils, development and molecules: extant cephalopods are younger than previously realised and were under major selection to become agile, shell-less predators. *BioEssays* **33**, 602–613 (2011).
2. Yacobucci, M. M. Macroevolution and Paleobiogeography of Jurassic-Cretaceous Ammonoids. in *Ammonoid Paleobiology: From macroevolution to paleogeography* (eds. Klug, C., Korn, D., De Baets, K., Kruta, I. & Mapes, R. H.) vol. 44 189–228 (Springer Netherlands, Dordrecht, 2015).
3. Fuchs, D. Part M, Chapter 23G: Systematic descriptions: Octobrachia. *Treatise Online* **138**, 1–52 (2020).
4. House, M. R. Correlation of mid-Palaeozoic ammonoid evolutionary events with global sedimentary perturbations. *Nature* **313**, 17–22 (1985).
5. Brayard, A. *et al.* Good Genes and Good Luck: Ammonoid Diversity and the End-Permian Mass Extinction. *Science* **325**, 1118–1121 (2009).
6. Monnet, C., Brayard, A. & Bucher, H. Ammonoids and Quantitative Biochronology—A Unitary Association Perspective. in *Ammonoid Paleobiology: From macroevolution to paleogeography* (eds. Klug, C., Korn, D., De Baets, K., Kruta, I. & Mapes, R. H.) vol. 44 277–298 (Springer Netherlands, Dordrecht, 2015).
7. Monnet, C., Klug, C. & De Baets, K. Evolutionary Patterns of Ammonoids: Phenotypic Trends, Convergence, and Parallel Evolution. in *Ammonoid Paleobiology: From macroevolution to paleogeography* (eds. Klug, C., Korn, D., De Baets, K., Kruta, I. & Mapes, R. H.) vol. 44 95–142 (Springer Netherlands, Dordrecht, 2015).
8. Jereb, P. & Roper, C. F. E. *Cephalopods of the World. An Annotated and Illustrated Catalogue of Cephalopod Species Known to Date. Volume 1. Chambered Nautiluses and Sepioids (Nautilidae, Sepiidae, Sepiolidae, Sepiadariidae, Idiosepiidae and Spirulidae)*. (Food and Agriculture Organization of the United Nations, Rome, 2005).
9. Jereb, P. & Roper, C. F. E. *Cephalopods of the World. An Annotated and Illustrated Catalogue of Cephalopod Species Known to Date. Volume 2. Myopsid and Oegopsid Squids*. (Food and Agriculture Organization of the United Nations, Rome, 2010).
10. Jereb, P., Roper, C. F. E., Norman, M. D. & Finn, J. K. *Cephalopods of the World. An Annotated and Illustrated Catalogue of Cephalopod Species Known to Date: Volume 3. Octopods and Vampire Squids*. (Food and Agriculture Organization of the United Nations, Rome, 2016).
11. Boyle, P. & Rodhouse, P. *Cephalopods: Ecology and Fisheries*. (Blackwell Science, Oxford, 2005).
12. Nesis, K. N. Distribution of recent Cephalopoda and implications for Plio-Pleistocene events. *Berl. Paläobiol. Abh.* **3**, 199–224 (2003).
13. Young, R. E., Vecchione, M. & Donovan, D. T. The evolution of coleoid cephalopods and their present biodiversity and ecology. *African Journal of Marine Science* **20**, 393–420 (1998).
14. Fuchs, D. & Iba, Y. The gladiuses in coleoid cephalopods: homology, parallelism, or convergence? *Swiss J. Palaeontol.* **134**, 187–197 (2015).
15. Fuchs, D. Homology problems in cephalopod morphology: deceptive (dis)similarities between different types of ‘caecum’. *Swiss J. Palaeontol.* **138**, 49–63 (2019).
16. Tanner, A. R. *et al.* Molecular clocks indicate turnover and diversification of modern coleoid

cephalopods during the Mesozoic Marine Revolution. *Proc. R. Soc. B.* **284**, 20162818 (2017).
17. Amodio, P. *et al.* Grow smart and die young: why did cephalopods evolve intelligence? *Trends Ecol. Evol.* **34**, 45–56 (2019).
18. Nixon, M. & Young, J. Z. *The Brains and Lives of Cephalopods*. (Oxford University Press, Oxford, 2003).
19. Hanlon, R. T. & Messenger, J. B. *Cephalopod Behaviour*. (Cambridge University Press, Cambridge, 2018).
20. Fuchs, D. Part M, Chapter 9B: The Gladius and Gladius Vestige in Fossil Coleoidea. *Treatise Online* **83**, 1–23 (2016).
21. Donovan, D. & Fuchs, D. Fossilized Soft Tissues in Coleoidea. *Treatise Online* **73**, (2016).
22. Uribe, J. E. & Zardoya, R. Revisiting the phylogeny of Cephalopoda using complete mitochondrial genomes. *J. Molluscan Stud.* **83**, 133–144 (2017).
23. López-Córdova, D. A. *et al.* Mesozoic origin of coleoid cephalopods and their abrupt shifts of diversification patterns. *Mol. Phylogenet. Evol.* **166**, 107331 (2022).
24. Fuchs, D. *et al. Longibelus* gen. nov., A new Cretaceous coleoid genus linking Belemnoidea and early Decabrachia. *Palaeontology* **56**, 1081–1106 (2013).
25. Fuchs, D. *et al.* The Muensterelloidea: phylogeny and character evolution of Mesozoic stem octopods. *Papers in Palaeontology* **6**, 31–92 (2020).
26. Arkhipkin, A. I. Statoliths as 'black boxes'(life recorders) in squid. *Marine and freshwater research* **56**, 573–583 (2005).
27. Neige, P., Lapierre, H. & Merle, D. New eocene coleoid (Cephalopoda) diversity from statolith remains: Taxonomic assignation, fossil record analysis, and new data for calibrating molecular phylogenies. *PLoS ONE* **11**, 1–24 (2016).
28. Tanabe, K., Hikida, Y. & Iba, Y. Two coleoid jaws from the Upper Cretaceous of Hokkaido, Japan. *J. Paleontol.* **80**, 138–145 (2006).
29. Tanabe, K., Trask, P., Ross, R. & Hikida, Y. Late Cretaceous Octobrachiate Coleoid Lower Jaws from the North Pacific Regions. *Journal of Paleontology* **82**, 398–408 (2008).
30. Tanabe, K. & Hikida, Y. Jaws of a New Species of *Nanaimoteuthis* (Coleoidea: Vampyromorphida) from the Tuironian of Hokkaido, Japan. *Paleontological Research* **14**, 145–150 (2010).
31. Tanabe, K., Misaki, A. & Ubukata, T. Late Cretaceous record of large soft-bodied coleoids based on lower jaw remains from Hokkaido, Japan. *Acta Palaeontol. Pol.* **60**, 27–38 (2015).
32. Tanabe, K., Misaki, A., Hikida, Y. & Nishimura, T. New records of coleoid cephalopod jaws from the Upper Cretaceous of Hokkaido, Japan, and their paleobiogeographic and evolutionary implications. *Cretaceous Research* **70**, 128–141 (2017).
33. Tanabe, K. & Misaki, A. Upper Cretaceous record of non-belemnitid coleoid jaws from Hokkaido, Japan, and its evolutionary implications. *Cret. Res.* **151**, 105624 (2023).
34. Mironenko, A. A. *et al.* First discovery of the soft-body imprint of an Oligocene fossil squid indicates its piscivorous diet. *Lethaia* **54**, 793–805 (2021).
35. Pindakiewicz, M. K., Hryniewicz, K., Janiszewska, K. & Kaim, A. First cretaceous cephalopod statoliths fill the gap between Jurassic and Cenozoic forms. *Comptes Rendus Palevol* **21**, 801–813 (2022).
36. Tanabe, K. & Fukuda, Y. Morphology and function of cephalopod buccal mass. in *Functional Morphology of the Invertebrate Skeleton* (ed. Savazzi, E.) 245–262 (John Wiley & Sons, New

York, 1999).
37. Xavier, J. C. *et al.* The significance of cephalopod beaks as a research tool: An update. *Frontiers in Physiology* **13**, 1038064 (2022).
38. Clarke, M. R. Significance of cephalopod beaks. *Nature* **193**, 560–561 (1962).
39. Clarke, M. R. *A Handbook for the Identification of Cephalopod Beaks*. (Clarendon Press, Oxford, 1986).
40. Young, R. E., Clarke, M. R., Vecchione, M. & Mangold, K. M. Beak terminology. *Tree of Life* http://tolweb.org/notes/?note_id=1980 (2000).
41. Clarke, M. R. & Maddock, L. Beaks of living coleoid Cephalopoda. in *Paleontology and neontology of cephalopods* (eds. Clarke, M. R. & Trueman, E. R.) 123–131 (Academic Press, Cambridge, 1988).
42. Roscian, M. *et al.* Every hooked beak is maintained by a prey: Ecological signal in cephalopod beak shape. *Functional Ecology* **36**, 2015–2028 (2022).
43. Souquet, L. *et al.* The growth of the buccal mass in Sepia officinalis: functional changes throughout ontogeny. *Mar Biol* **170**, 82 (2023).
44. Clarke, M. R. The identification of cephalopod 'beaks' and the relationship between beak size and total body weight. *Bull. Br. Mus. nat. Hist. (Zool.)* **8**, 419–480 (1962).
45. Hernańdez-García, V., Piatkowski, U. & Clarke, M. R. Development of the darkening of *Todarodes sagittatus* beaks and its relation to growth and reproduction. *South African Journal of Marine Science* **20**, 363–373 (1998).
46. Hernández-García, V. Growth and pigmentation process of the beaks of *Todaropsis Eblanae* (Cephalopoda: Ommastrephidae). *Berl. Paläobiol. Abh.* **3**, 131–140 (2003).
47. Harzhauser, M. Filling a gap - beaks and hooks of Cenozoic coleoids (Cephalopoda). *Annalen des Naturhistorischen Museums in Wien* **101 A**, 123–135 (1999).
48. Kruta, I., Landman, N., Rouget, I., Cecca, F. & Tafforeau, P. The role of ammonites in the mesozoic marine food web revealed by jaw preservation. *Science* **331**, 70–72 (2011).
49. Kanie, Y. New vampyromorph (Coleoidea: Cephalopoda) jaw apparatuses from the Late Cretaceous of Japan. *Bulletin of Gumma Museum of Natural History* **2**, 23–34 (1998).

Chapter 1. Squids (Oegopsida and Myopsida)

Summary

The evolution of soft-bodied squids, which provide a significant part of the biomass in modern oceans globally, is poorly understood due to their patchy fossil record. We provide a comprehensive evolutionary history of squids through “digital fossil-mining” techniques, revealing a new Lagerstätte. The more than 250 fossil beaks of 40 species show that squids originated and rapidly radiated by 100 million years ago. Our new data suggest that the radical shift from heavily shelled, slowly moving cephalopods to soft-bodied forms did not result from the end-Cretaceous mass extinction (66 Ma). Early squids had already formed large populations and their biomass exceeded that of ammonites and fishes. They pioneered the modern-type marine ecosystem as intelligent, fast swimmers.

1.1. Introduction

Squids (the order Oegopsida and Myopsida) are the most diverse and globally distributed group of cephalopods in modern oceans[1,2]. They are exceptional invertebrates with lens eyes, flexible arms, and a large brain[3–5], giving them a sophisticated cognition and mobility comparable to that of vertebrates[4–7]. They are adept predators, competing with fishes, while being essential prey for whales and sharks[7–9]. These characteristics make squids a principal component of the marine ecosystem.

The origin of squids is marked by the loss of the large, mineralized shell that was initially a key trait of cephalopods, probably occurring independently in Oegopsida and Myopsida[10,11]. These shell demineralization events are the greatest innovation in the 500 Myr history of cephalopods[10]. Squids benefitted from this evolution as faster swimming, coupled with complex cognitive abilities[10]. Modern squids are well studied[2], but little is known about their origin and evolution since soft-bodied organisms are rarely fossilized[10]. Only few squid fossils have been reported, almost all of which are from the middle Eocene (~45 Ma) onward[12]. Most of these fossils are statoliths, which are small calcareous particles functioning as a balance system[12]. In other approaches, molecular phylogenetics have attempted to estimate speciation ages from extant squids, but the lack of fossils prevented a precise understanding of their early evolution (~50 Myr of confidence intervals)[5,13,14]. Previous studies thus speculated that squids only radiated after the Cretaceous–Paleogene (K–Pg) mass extinction (~66 Ma), in which shelled cephalopods such as ammonites perished[14].

Mesozoic fossils of squids are absent even in Fossil-Lagerstätten due to the poor preservational potential of their soft-tissue bodies[15]. While fossil statoliths of non-squid cephalopods have Jurassic records, those of squids are not conserved in Mesozoic sediment for unknown reasons[12]. To overcome the limitations of the record of fossil squids, we focused on their beaks. All cephalopods have an upper and lower beak, a unique hard tissue composed of chitin-protein complexes[16]. The morphology of cephalopod lower beaks is constrained by phylogenetic relationships rather than feeding habits[17]. The lower beak morphology of squids varies on the species level[18,19]. Squid beaks also offer precise insights into body length based on their size and growth stage through pigmentation patterns[19,20]. These characteristics apply to fossil beaks, particularly in which their three-dimensional morphology is retained. Carbonate concretions are likely the best source for 3D preserved beaks. Fossil beaks are, however, difficult to discover and extract from hard rocks because of their fragility and morphological complexity. Therefore, only one fossil squid beak has been described (see systematic paleontology). Conventional fossil extraction techniques, including physical preparation and chemical dissolution, have not solved this problem (Fig. 1). X-ray computed tomography also cannot provide the solution even with synchrotron, which was the state of the art to date (Fig. 2).

This study developed “digital fossil-mining”, a new approach that replaces conventional techniques, allowing mass and flawless extraction of fossils (Fig. 1). Our method converts whole rocks into full-color digital volume data and allows us to discover all hidden fossils as 3D models. This breakthrough was enabled by a fully automated grinding tomography system with the highest resolution ever obtained and high-performance image processing using RGB data. Digitally, we collected fossil squid beaks from carbonate concretions of Cretaceous shelf deposits in Japan (interval of 110–70 Ma: Table 1).

1.2. Material

The 35 carbonate concretions studied here were collected from middle Albian to Early Maastrichtian

of the Yezo Group, exposed on Hokkaido Island, northern Japan. They were formed in an outer shelf sea, low-energy environment without wave influence[21]. Their geological age assignment is based on previous chronostratigraphic studies[22–32]. All fieldwork was carried out under the permission of the Hokkaido Regional Forest Office. The detailed localities, geological ages, and horizons are documented in Table 1.

Institutional abbreviations

KMNH: Kitakyushu Museum of Natural History and Human History, Kitakyushu, Japan.
NMA: Nakagawa Museum of Natural History, Nakagawa, Japan.
NMNS: National Museum of Nature and Science, Tokyo, Japan.

1.3. Methods

1.3.1. Digital fossil-mining

This study used a new grinding tomography system (Paleobiology Lab, Hokkaido University: Fig. 1) that scans rocks in their original colors with high resolution. (~3 times higher than previous systems)[33]. In a first step, whole rocks were automatically converted into sequential cross-sectional images, along with numerous fossils hidden inside the rocks. The rock samples were embedded into a plaster jacket and ground at equal intervals of 10, 25, or 50 μm (Table 1). High-precision diamond wheel were

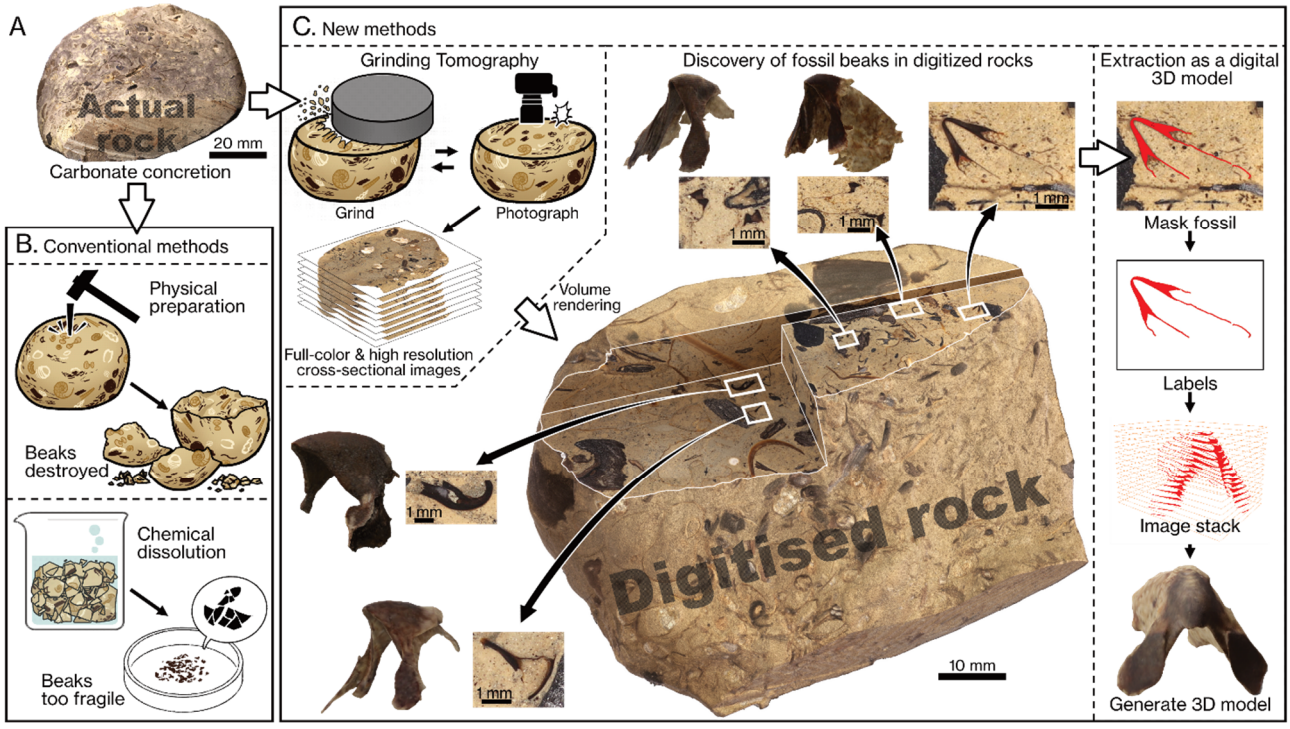


Fig. 1. Digital fossil-mining of squid beaks.

(**A**) A studied carbonate concretion (sample No. 6). (**B**) Conventional fossil extraction techniques, physical preparation and chemical dissolution. Thin, tiny, and complex fossil beaks cannot be discovered or extracted. (**C**) Digital fossil-mining applied in this study. Top left, concretions are converted into full-color digital volume data by automated grinding tomography. Middle, beak fossils are discovered in the digitized concretions that can be freely sliced and magnified. Top right, discovered fossils are completely separated from host rocks as label data and extracted as a 3D model.

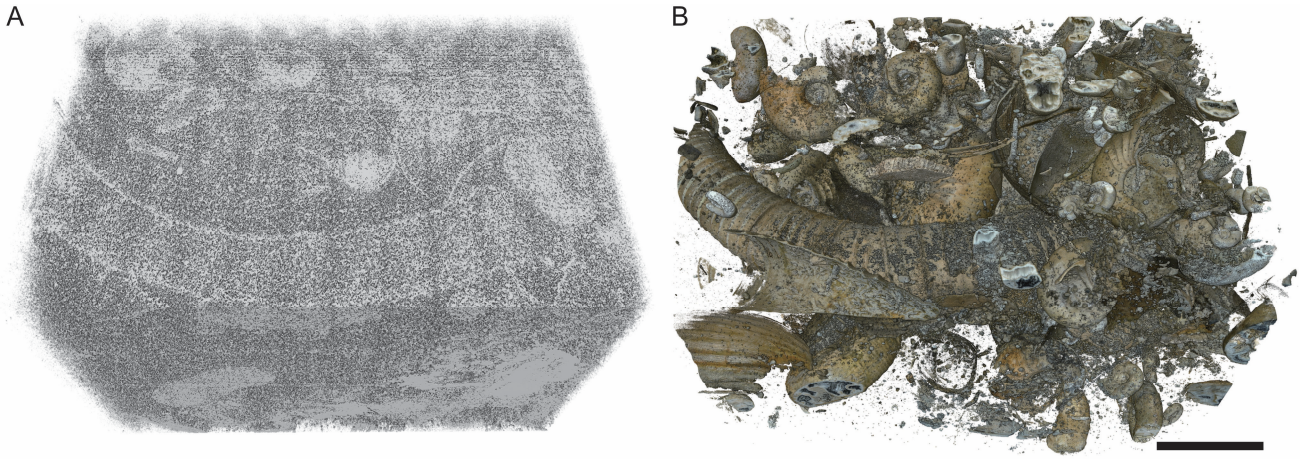


Fig. 2. Comparison between X-ray CT and grinding tomography.
(**A**) Synchrotron X-ray computed tomography. (**B**) Grinding tomography. In both panels, the exhibited rock is a studied carbonate concretion (sample No. 14). The cross-sectional data used in (A) was obtained by X-ray phase-contrast tomography with a pixel size 48 μm/pixel at energy of 113 keV, at BL20B2 of SPring-8, Japan. The data used in (B) were obtained through the grinding tomography system.

used for surface grinding (diamond size ~15 μm: Asahi Diamond Industrial Co., Ltd; ~20 μm: Noritake Co., Ltd). Each surface was then photographed in color with high-resolution digital cameras (8,688 x 5,792 pixels/image in EOS 5Ds, Canon; 19,008 x 12,672 pixels/image in α7R IV, SONY). These grinding–photographing processes were computerized, controlled numerically, and repeated automatically.

In the second step, the fossils of cephalopod beaks and vertebrae of bony fishes were discovered and counted from each image dataset and its animation. The areas of the beak fossils were subsequently masked by RGB values in the IV-Seg 1.3.2.0 (IVLab Co., Ltd.) and imported to Amira 6.2.0 (Thermo Fisher Scientific, Inc.) for 3D reconstruction. The 3D models underwent minimal smoothing to avoid modifying the diagnostic characters. The original colors of the fossil beaks were extracted from unprocessed tomographic images and superposed on the models. All measurements and taxonomical interpretations are based on these 3D models. Blender 3.2.1 (Blender Foundation) was used to display the 3D models in the figures.

1.3.2. Taxonomy

The identification of the upper and lower beaks of cephalopods and their subsequent taxonomic classification is based on previous studies[16,19]. The growth stages, including adults, subadults, and juveniles (Table 3), are distinguished based on criteria successfully applied for extant squid beaks by using pigmentation patterns[20]. Species-level classification and establishment of new taxa were conducted based on 120 lower beaks of adults and subadults in the specimens discovered here (Table 3). In addition, all fossil beak specimens reported as squids from the Late Cretaceous in previous studies[34–36] were re-examined.

Table 1. Carbonate concretions and their tomographic datasets.

Sample No. of carbonate concretion	Dimensions (cm^3)	Geological age	Horizon	Locality	Longitude and latitude
1	590	middle to late Albian, Late Cretaceous	Hikagenosawa Formation, Yezo Group	Ponbetsu creek, Ponbetsuhonsawachou, Mikasa, Hokkaido, Japan	43° 17' 37.92" N 141° 59' 54.73" E
2	290	middle to late Albian, Late Cretaceous	Hikagenosawa Formation, Yezo Group	Ponbetsu creek, Ponbetsuhonsawachou, Mikasa, Hokkaido, Japan	43° 18' 01.57" N 142° 00' 02.25" E
3	640	middle to late Albian, Late Cretaceous	Hikagenosawa Formation, Yezo Group	Ponbetsu creek, Ponbetsuhonsawachou, Mikasa, Hokkaido, Japan	43° 19' 54.64" N 142° 01' 34.94" E
4	600	middle to late Albian, Late Cretaceous	Hikagenosawa Formation, Yezo Group	Ponbetsu creek, Ponbetsuhonsawachou, Mikasa, Hokkaido, Japan	43° 19' 20.06" N 142° 00' 18.16" E
5	350	middle to late Albian, Late Cretaceous	Hikagenosawa Formation, Yezo Group	Ponbetsu creek, Ponbetsuhonsawachou, Mikasa, Hokkaido, Japan	43° 18' 50.28" N 142° 00' 44.01" E
6	100	earliest Cenomanian, Late Cretaceous	Unit My3, Yezo Group	Suribachi creek, a tributy of Souunnai creek, Soeushinai, Horokanai, Hokkaido, Japan	44° 13' 29" N 142° 04' 07" E
7	140	Early Cenomanian, Late Cretaceous	Unit My4, Yezo Group	Sanjussen creek, Soeushinai, Horokanai, Hokkaido, Japan	44° 14' 30" N 142° 04' 57" E
8	270	Late Cenomanian, Late Cretaceous	Saku Formation, Yezo Group	Obirashibe creek, Kawakami, Obira, Hokkaido, Japan	44° 05' 58" N 142° 00' 50" E
9	570	Early Turonian, Late Cretaceous	Takinosawa Formation, Yezo Group	Kamimaki creek, Oyubari, Yubari, Hokkaido, Japan	43° 07' 49.25" N 142° 07' 59.90" E
10	200	Middle Turonian, Late Cretaceous	Saku Formation, Yezo Group	Sato-no-sawa creek, a tributy of Kamikinenbetsu creek, Obira, Hokkaido, Japan	44° 02' 07" N 141° 35' 33" E
11	180	Late Turonian, Late Cretaceous	Mikasa Formation, Yezo Group	Kimunashibetsu creek, Okuashibetsu, Ashibetsu, Hokkaido, Japan	43° 17' 52" N 142° 05' 16" E
12	100	Late Turonian, Late Cretaceous	Saku Formation, Yezo Group	A tributy of Kamikinenbetsu creek, Kawakami, Obira, Hokkaido, Japan	44° 03' 47" N 141° 58' 55" E
13	580	Late Turonian, Late Cretaceous	Saku Formation, Yezo Group	Kamikinenbetsu creek, Kawakami, Obira, Hokkaido, Japan	44° 03' 30" N 141° 59' 28" E
14	100	Late Turonian, Late Cretaceous	Saku Formation, Yezo Group	Furuichi creek, Toyosato, Nakagawa, Hokkaido, Japan	44° 45' 41" N 142° 01' 40" E
15	100	Late Turonian, Late Cretaceous	Saku Formation, Yezo Group	Saku-gakko-no-sawa creek, Yasukawa, Nakagawa, Hokkaido, Japan	44° 44' 15.39" N 142° 00' 42.51" E
16	460	Late Turonian, Late Cretaceous	Saku Formation, Yezo Group	A tributy of Kamikinenbetsu creek, Kawakami, Obira, Hokkaido, Japan	44° 03' 43.28" N 141° 58' 50.69" E
17	150	Early Coniacian, Late Cretaceous	Haborogawa Formation, Yezo Group	Yutaka-sawa, a tributy of Sakasa creek, Kamihaboro, Haboro, Hokkaido, Japan	44° 17' 20" N 141° 00' 23" E
18	310	Late Coniacian, Late Cretaceous	Haborogawa Formation, Yezo Group	A tributy of Nakahutamata creek, Kamihaboro, Haboro, Hokkaido, Japan	44° 17' 43" N 142° 00' 10" E
19	180	Late Coniacian, Late Cretaceous	Haborogawa Formation, Yezo Group	Nakahutamata creek, Kamihaboro, Haboro, Hokkaido, Japan	44° 17' 55" N 142° 00' 04" E
20	170	Late Coniacian, Late Cretaceous	Haborogawa Formation, Yezo Group	A tributy of Obirashibe creek, Kawakami, Obira, Hokkaido, Japan	44° 05' 42" N 141° 58' 42" E
21	380	Santonian, Late Cretaceous	Haborogawa Formation, Yezo Group	Horotate creek, Kiritachi, Tomamae, Hokkaido, Japan	44° 10' 41" N 141° 58' 34" E
22	550	Santonian, Late Cretaceous	Haborogawa Formation, Yezo Group	Detofutamata creek, Kamihaboro, Haboro, Hokkaido, Japan	44° 19' 26" N 141° 57' 25" E
23	140	Santonian, Late Cretaceous	Haborogawa Formation, Yezo Group	Nakahutamata creek, Kamihaboro, Haboro, Hokkaido, Japan	44° 18' 05" N 141° 57' 42" E
24	140	Santonian, Late Cretaceous	Haborogawa Formation, Yezo Group	Kuma-no-sawa, a tributy of Kotanbetsu creek, Kiritachi, Tomamae, Hokkaido, Japan	44° 11' 24" N 141° 58' 14" E
25	200	Santonian, Late Cretaceous	Haborogawa Formation, Yezo Group	Machiyoi creek, a tibuty of Nakahutamata creek, Kamihaboro, Haboro, Hokkaido, Japan	44° 18' 04" N 141° 58' 56" E
26	210	Santonian, Late Cretaceous	Unit Ug, Haborogawa Formation, Yezo Group	Nakafutamata creek, Kamihaboro, Haboro, Hokkaido, Japan	44° 18' 06" N 141° 58' 04" E
27	150	Early Campanian, Late Cretaceous	Nagareya Formation, Yezo Group	Katakage creek, a tributy of Migi-no-sawa creek, Kamihaboro, Haboro, Hokkaido, Japan	44° 16' 50" N 141° 53' 16" E
28	200	Early Campanian, Late Cretaceous	Nigorigawa Formation, Yezo Group	Omoshirushibetsu creek, Higashino, Enbetsu, Hokkaido, Japan	44° 38' 00" N 141° 59' 16" E
29	100	Early Campanian, Late Cretaceous	Osoushinai Formation, Yezo Group	Abeshinai creek, Kyowa, Nakagawa, Hokkaido, Japan	44° 40' 29.7" N 142° 01' 22.3" E
30	310	Early Campanian, Late Cretaceous	Nagareya Formation, Yezo Group	Katakage creek, a tributy of Migi-no-sawa creek, Kamihaboro, Haboro, Hokkaido, Japan	44° 16' 50" N 141° 53' 16" E
31	280	Late Campanian, Late Cretaceous	Chinomigawa Formation, Yezo Group	Pankeushappu creek, Hidaka, Hidaka, Hokkaido, Japan	42° 54' 35.91" N 142° 25' 08.21" E
32	290	Late Campanian, Late Cretaceous	Chinomigawa Formation, Yezo Group	Pankeushappu creek, Hidaka, Hidaka, Hokkaido, Japan	42° 54' 48.66" N 142° 24' 44.65" E
33	360	Early Maastrichtian, Late Cretaceous	Heitaro-zawa Formation, Yezo Group	Utsunai creek, Utsunai, Hamatombetsu, Hokkaido, Japan	45° 01' 24.61" N 142° 12' 44.20" E
34	500	Early Maastrichtian, Late Cretaceous	Etanpakku Formation, Yezo Group	Onishibetsu creek, Koishi, Sarufutsu, Hokkaido, Japan	45° 18' 09.30" N 141° 59' 24.08" E
35	390	Early Maastrichtian, Late Cretaceous	Heitaro-zawa Formation, Yezo Group	Utsunai creek, Utsunai, Hamatombetsu, Hokkaido, Japan	45° 01' 27.42" N 142° 12' 03.34" E

Table 1. (continued)

Sample No. of carbonate concretion	Collection No. of cross-sectional images (NMNS: National Museum of Nature and Science, Tokyo)	Total number of images	Pixel size (μm/pixel)	Number of pixels	Image width (mm)	Image height (mm)	Spatial resolution (μm)	Animation of cross sectional images
1	NMNS_DS00178_wl_01_0001.tif–1400.tif	1400	5.893	19008×12672	112	74.67	50	NMNS_DS00178_wl_01_0001–1400_animation.mp4
2	NMNS_DS00180_wl_01_0001.tif–1060.tif	1060	4.762	19008×12672	90.51	60.34	50	NMNS_DS00180_wl_01_0001–1060_animation.mp4
3	NMNS_DS00224_wl_01_0001.tif–1485.tif	1485	6.131	19008×12672	116.5	77.69	50	NMNS_DS00224_wl_01_0001–1485_animation.mp4
4	NMNS_DS00249_wl_01_0001.tif–1540.tif	1540	5.693	19008×12672	108.2	72.14	50	NMNS_DS00249_wl_01_0001–1540_animation.mp4
5	NMNS_DS00250_wl_01_0001.tif–1140.tif	1140	5.117	19008×12672	97.26	64.84	50	NMNS_DS00250_wl_01_0001–1140_animation.mp4
6	NMNS_DS00068_20181123_c1_wl_01_0001.jpg–0954.jpg	954	10.715	8688×5792	93.09	62.06	50	NMNS_DS00068_20181123_c1_wl_01_0001–0954_animation.mp4
7	NMNS_DS00084_20190202_c1_wl_01_0001.jpg–0779.jpg	779	10.316	8688×5792	89.62	59.75	50	NMNS_DS00084_20190202_c1_wl_01_0001–0779_animation.mp4
8	NMNS_DS00082_20190127_c1_wl_01_0001.jpg–0933.jpg	933	11.864	8688×5792	103.1	68.72	50	NMNS_DS00082_20190127_c1_wl_01_0001–0933_animation.mp4
9	NMNS_DS00140_wl_02_0001.tif–1463.tif	1463	5.325	19008×12672	101.2	67.49	50	NMNS_DS00140_wl_02_0001–1463_animation.mp4
10	NMNS_DS00009_20170727_c1_wl_01_0001.jpg–1257.jpg	1257	13.567	8688×5792	117.9	78.58	10 and 50	NMNS_DS00009_20170727_c1_wl_01_0001–1257_animation.mp4
11	NMNS_DS00040_20180409_c1_wl_01_0001.jpg–0800.jpg	800	10.768	8688×5792	93.55	62.37	50	NMNS_DS00040_20180409_c1_wl_01_0001–0800_animation.mp4
12	NMNS_DS00041_20180414_c1_wl_01_0001.jpg–0780.jpg	780	12.287	8688×5792	106.8	71.17	50	NMNS_DS00041_20180414_c1_wl_01_0001–0780_animation.mp4
13	NMNS_DS00046_20180709_c1_wl_01_0001.jpg–0997.jpg	997	11.459	8688×5792	99.56	66.37	50	NMNS_DS00046_20180709_c1_wl_01_0001–0997_animation.mp4
14	NMNS_DS00135_wl_01_0001.tif–4059.tif	4059	3.381	19008×12672	64.25	42.83	10	NMNS_DS00135_wl_01_0001–4059_animation.mp4
15	NMNS_DS00141_wl_02_0001.tif–1615.tif	1615	3.369	19008×12672	64.04	42.69	25	NMNS_DS00141_wl_02_0001–1615_animation.mp4
16	NMNS_DS00173_wl_01_0001.tif–1400.tif	1400	5.339	19008×12672 and 9504×6336	101.5	67.66	50	NMNS_DS00173_wl_01_0001–1400_animation.mp4
17	NMNS_DS00034_20180207_c1_wl_01_0001.jpg–0800.jpg	800	12.157	8688×5792	105.6	70.41	50	NMNS_DS00034_20180207_c1_wl_01_0001–0800_animation.mp4
18	NMNS_DS00081_20190124_c1_wl_01_0001.jpg–1000.jpg	1000	11.865	8688×5792	103.1	68.73	50	NMNS_DS00081_20190124_c1_wl_01_0001–1000_animation.mp4
19	NMNS_DS00083_20190130_c1_wl_01_0001.jpg–0900.jpg	900	11.861	8688×5792	103.1	68.70	50	NMNS_DS00083_20190130_c1_wl_01_0001–0900_animation.mp4
20	NMNS_DS00089_20190223_c1_wl_01_0001.jpg–0836.jpg	836	8.871	8688×5792	77.07	51.38	50	NMNS_DS00089_20190223_c1_wl_01_0001–0836_animation.mp4
21	NMNS_DS00004_20170519_c1_wl_01_0001.jpg–1054.jpg	1054	17.852	8688×5792	155.1	103.40	50	NMNS_DS00004_20170519_c1_wl_01_0001–1054_animation.mp4
22	NMNS_DS00011_20170806_c1_wl_01_0001.jpg–1000.jpg	1000	16.751	8688×5792	145.5	97.02	50	NMNS_DS00011_20170806_c1_wl_01_0001–1000_animation.mp4
23	NMNS_DS00039_20180406_c1_wl_01_0001.jpg–0500.jpg	500	13.321	8688×5792	115.7	77.15	50	NMNS_DS00039_20180406_c1_wl_01_0001–0500_animation.mp4
24	NMNS_DS00042_20180419_c1_wl_02_0001.jpg–0601.jpg	601	10.503	8688×5792	91.25	60.83	50	NMNS_DS00042_20180419_c1_wl_02_0001–0601_animation.mp4
25	NMNS_DS00090_20190228_c1_wl_01_0001.jpg–0732.jpg	732	10.120	8688×5792	87.92	58.61	50	NMNS_DS00090_20190228_c1_wl_01_0001–0732_animation.mp4
26	NMNS_DS00104_wl_01_0001.jpg–0800.jpg	800	9.768	8688×5792	84.86	56.57	50	NMNS_DS00104_wl_01_0001–0800_animation.mp4
27	NMNS_DS00073_20181212_c1_wl_01_0001.jpg–0893.jpg	893	8.715	8688×5792	75.72	50.48	50	NMNS_DS00073_20181212_c1_wl_01_0001–0893_animation.mp4
28	NMNS_DS00097_wl_01_0001.jpg–0920.jpg	920	8.711	8688×5792	75.68	50.45	50	NMNS_DS00097_wl_01_0001–0920_animation.mp4
29	NMNS_DS00134_wl_01_0001.tif–1690.tif	1690	3.317	19008×12672	63.05	42.03	25	NMNS_DS00134_wl_01_0001–1690_animation.mp4
30	NMNS_DS00175_wl_01_0001.tif–1176.tif	1176	4.716	19008×12672	89.63	59.75	50	NMNS_DS00175_wl_01_0001–1176_animation.mp4
31	NMNS_DS00171_wl_01_0001.tif–1421.tif	1421	5.805	19008×12672	110.3	73.56	50	NMNS_DS00171_wl_01_0001–1421_animation.mp4
32	NMNS_DS00182_wl_01_0001.tif–1060.tif	1060	4.756	19008×12672	90.4	60.27	50	NMNS_DS00182_wl_01_0001–1060_animation.mp4
33	NMNS_DS00128_wl_01_0001.jpg–1200.jpg	1200	10.221	9504×6336	97.14	64.76	50	NMNS_DS00128_wl_01_0001–1200_animation.mp4
34	NMNS_DS00172_wl_01_0001.tif–1310.tif	1310	5.285	19008×12672	100.5	66.97	50	NMNS_DS00172_wl_01_0001–1310_animation.mp4
35	NMNS_DS00174_wl_01_0001.tif–1159.tif	1159	5.322	19008×12672	101.2	67.45	50	NMNS_DS00174_wl_01_0001–1159_animation.mp4

Published terminology and methods[19,37] were used here with respect to the measurements and higher classifications of the coleoid beaks (Fig. 3). The crest length, hood length, lower rostral length, wing length, and wing angle were measured in accordance with these studies[19,37]. Additionally, the following values were obtained in this study (Fig. 3): the extended jaw edge length, the jaw edge length in a lateral view, the angle between a jaw edge and the adjacent shoulder blade, and the rostral width. A total of 30 morphological features were used for the classification of this study. These include all 20 criteria hitherto used for the identification of modern squid beaks[19] and 10 morphological features that frequently appear in fossils. All diagnostic characters show sufficiently small intraspecific variations and ontogenetic changes in the adult and subadult stages.

The International Code of Zoological Nomenclature accepts the complete destruction of type

specimens and photograph-based establishment of a new species in the following cases: "*capture or preservation of specimens is not feasible for technical reasons or for conservation concerns, or when specimens must be destroyed to reliably diagnose a new species*"[38]. The diagnostic characters of the thin, tiny, and complex specimens cannot be observed and analyzed without the destructive method applied here (Fig. 1). The study results thus fall under the above cited rules. The code further recommends taxonomical studies without physical type specimens to provide "*extensive documentation of potentially diagnostic characters as completely as possible*"[38]. To satisfy this recommendation, this study stored all related files (a total of over 30 TB data size) in the National Museum of Nature and Science, Tokyo, with collection numbers (Tables 1 and 3). These files comprise all the original cross-sectional images of carbonate concretions (.arw, .dng, .tif, .jpg), their animation (.mov), the reconstructed 3D model of the fossil squid beaks (.stl), the label data corresponding to each model (.tif), and the cross-sectional images cropped for generating the label data (.jpg). In addition, the cross-sectional animations (DOI: 10.25452/figshare.plus.25735515), the 3D models, the label data, and the cropped cross-sectional images are archived in the Figshare+ digital repository. All four data sets are open to the public.

This document does not include nomenclatural acts. New taxonomic names shown here will be published in other papers at appropriate journals.

Terminology and Measurements for Systematic Paleontology

The following descriptive terms[19,37] were used for describing fossil squid beaks in this study.

Anglepoint: a ventrally pointed tip of the jaw edge extensions.

Bridge: the strip of beak material that connects the hood to the lateral wall on each side of the beak (Fig. 3D).

Anglepoint: a ventrally pointed tip of the jaw edge extensions (Fig. 3G).

Bridge: the strip of beak material that connects the hood to the lateral wall on each side of the beak (Fig. 3D).

Crest: the narrow region in which the top of the two lateral walls merge (Fig. 3C).

Hood: the outer region of the beak attached by the rostral edge (or bridges) to the lateral wall, which lies outside or lateral to the lateral walls (Fig. 3C).

Hood notch: an indentation of the posterior edge of the pigmented hood in the dorsal midline (Fig. 3E).

Hyaline matrix: a subset of unpigmented material that is usually found in the shoulder of coleoid lower beaks (Fig. 3G).

Jaw angle: the angle formed at the intersection of the jaw edge and the adjacent shoulder blade (Fig. 3D).

Jaw edge: the cutting edge of the beak formed from the anterior ends of a lateral wall and the hood or from those of a lateral wall and the adjacent bridge (Fig. 3C).

Jaw edge extension: the embedded extension of the jaw edge that is the junction of lateral walls and their adjacent shoulder blade (Fig. 3D).

Lateral wall: the sheet on each side which runs back from the jaw edge, medial to the hood (Fig. 3C).

Lateral wall fold: a fold in the lateral wall that may become a solid or partially solid ridge (Fig. 3E).

Rostrum: the anterior portion of the hood consisting of the heavy, biting region of the beak that

includes the jaw edges (Fig. 3C).

Rostral dent: a medially concave region on the lateral sides of the rostrum around jaw edges (Fig. 3F).

Rostral tip: the anterior end of the rostrum where the jaw edges converge (Fig. 3C).

Shoulder: the join of wings with the anterior end of the nearest lateral wall, approximately bounded by the bridge posteriorly and including some of the wing laterally (Fig. 3D).

Shoulder blade: the pigmented medial part of the shoulder (Fig. 3D).

Tooth: the upper edge of shoulder blades extending dorsally beyond the wings (Fig. 3F).

Wing: the part of the hood that extends anteroventrally (Fig. 3C).

Wing fold: a fold of wings in the region of the neighboring jaw angle (Fig. 3D).

Following measurements of lengths and angles[19,37] were used in this study. All measured values are documented in Table 3.

Crest length (CL): the distance from the rostral tip to the posterior end of the crest (Fig. 3H).

Extended jaw edge length (EJEL): the distance between the rostral tip and the anteroventral end of the lateral walls (Fig. 3I).

Hood length (HL): the distance from the rostral tip to the posterior end of the hood (Fig. 3H).

Jaw edge length in a lateral view (JELL): the length of the part in jaw edges that are observable in lateral view (Fig. 3H).

Lower rostral length (LRL): the distance from the apex of the jaw angles to the rostral tip (Fig. 3I).

Rostral width (RW): the length between both jaw angles (Fig. 3I).

Wing length (WL): the distance from the tip of the wings to the point where the jaw edge intercepts the jaw angle or wing fold in lateral view (Fig. 3H).

Angle between a jaw edge and the adjacent shoulder blade (AJS): the degree of the angle of the corner formed at jaw angles (Fig. 3K).

Wing angle (WA): the degree of the angle formed by the intersection of the jaw edge and the wing in lateral view (Fig. 3J).

The size of the rostrum was described as follows.

Small: JELL/EJEL < 0.4

Moderate: $0.4 \leq$ JELL/EJEL < 0.6

Large: JELL/EJEL ≥ 0.6

The width of the rostrum was described as follows.

Broad: LRL/RW < 0.8

Moderate: $0.8 \leq$ LRL/RW < 1.2

Narrow: $1.2 \leq$ LRL/RW < 1.5

Very narrow: LRL/RW ≥ 1.5

Diagnostic Characters

The following 30 characters were used to establish a taxonomy for the fossil squid beaks. The characters unique to fossil squid beaks are marked with an asterisk. The others are used for the identification of modern squid beaks[19].

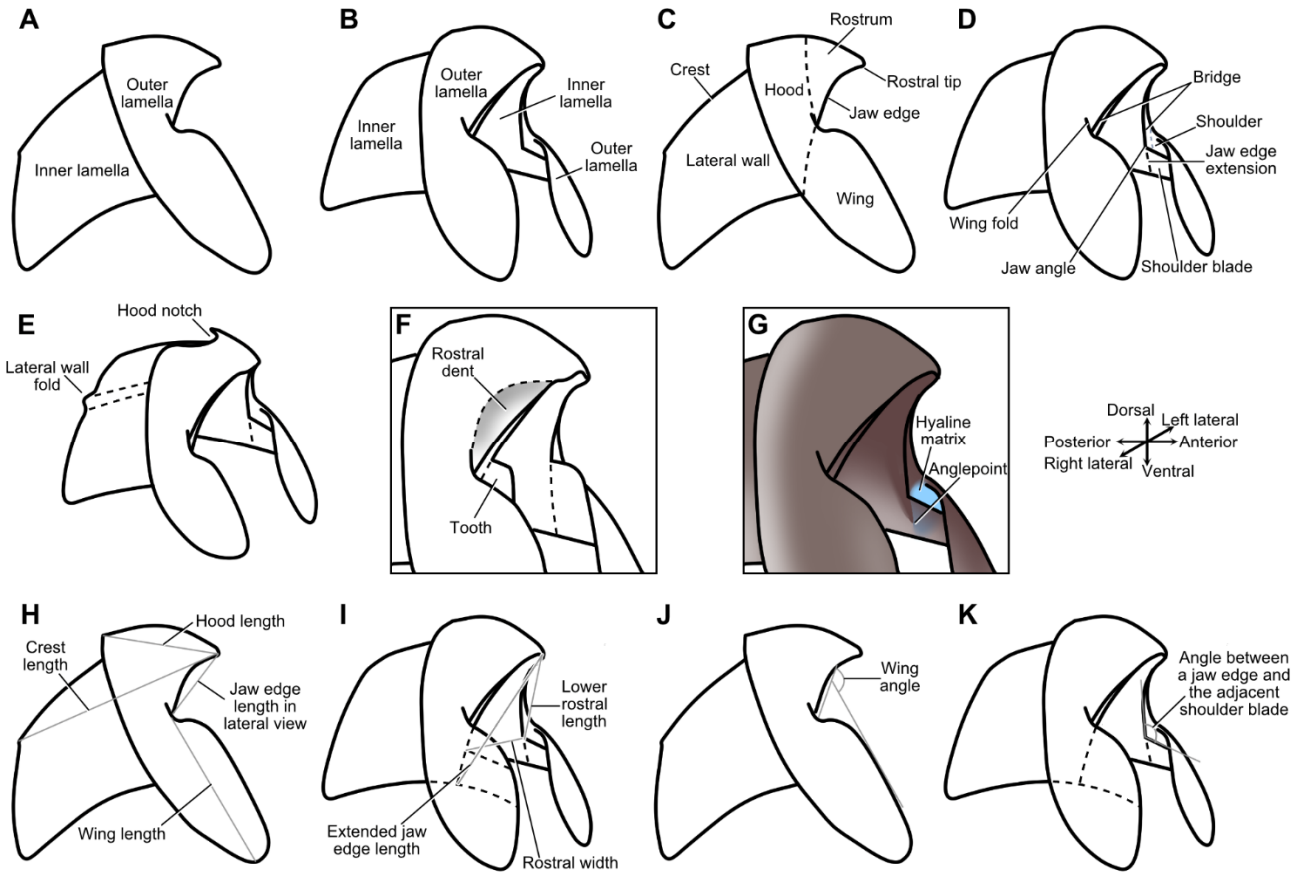


Fig. 3. Descriptive terms of the coleoid lower beak.
(**A** and **B**) Inner and outer lamellae. (**C** to **F**) Terms for morphology. (**G**) Terms related to pigmentation patterns. (**H** and **I**) Measurements of lengths. (**J** and **K**) Measurements of angles. (E) shows specific characters for the lateral walls and hood, and (F) shows those for the rostrum and shoulder. (A, C, H, and J) Left lateral view; (B, D to G, I, and K) oblique view.

The size of the rostrum is measured by JELL/EJEL (see Terminology and Measurements).

The width of the rostrum is measured by LRL/RW (see Terminology and Measurements).

Rostral dents are described based on whether the dents are present or absent, their width, and their depth.

The rostral hook is described based on the degree of its anterior protrusion.

The anterior protrusion of the rostrum is measured by the angle between the jaw edges and the crest in lateral view.

The presence of bridges is categorized as present or absent.

*The width of bridges** is categorized as constant, ventrally broadened, or ventrally tapered.

*The connection between bridges and the adjacent wing** is categorized as entirely connected or separated at their ventral part.

The development of shoulder blades is categorized as weak (only a narrow plate is present around the ventral part of jaw edges), thin, or thick.

*The connection between shoulder blades and the adjacent wing** is categorized as connected at the anterior edge of the wings or the thickened ridge on the medial side of the wings.

The presence of a step (sudden drop) is categorized as absent, present between the jaw edge extensions and the adjacent shoulder blade, or on the outer lamella neighbouring to the

jaw edge extensions.

*The connection between the dorsal edge of the shoulder blades and the adjacent wing** is categorized as not connected, directly connected, or connected by a flat plane.

The presence of teeth is categorized as present or absent.

*Bifurcation of jaw edges** is categorized as entirely single-edged or bifurcated at the ventral part.

The curvature of jaw edges is categorized as strongly curved, gently curved, or nearly straight.

*The curvature of jaw edge extensions** is categorized as posteriorly curved or nearly straight.

The roundness of jaw angles is categorized as angular or subrounded.

The shape of jaw angles is categorized as recessed or not recessed.

Visibility of jaw angles in lateral view is categorized as visible or hidden by a wing fold.

The angle between a jaw edge and the adjacent shoulder blade is categorized as acute, obtuse, or nearly perpendicular.

The presence of the hood notch is categorized as present or absent.

Constriction of wings is categorized as constricted around the adjacent jaw edges or not constricted.

*The angular ridge on wings** is described based on whether the ridge is present or absent and the angle between the ridge and the adjacent jaw edge.

The wing angle is categorized as obtuse or very obtuse.

The presence of wing folds is categorized as present or absent.

*The angle between the wing fold and jaw edge** is categorized as acute, obtuse, or nearly perpendicular.

*Thickness of wings** is categorized as thickened around the adjacent jaw edges or entirely thin.

The anterior margin of wings is categorized as ventrally curved, nearly straight, or having a pointed tip.

*The fold on the anterior part of wings** is categorized as present or absent.

Lateral wall folds are categorized as absent, ridged, or sulcate.

1.3.3. Body size estimation

This study used a correlation function between lower rostral length and mantle length of 42 extant species (40 oegopsids and two myopsids)[19] to estimate the size of the Late Cretaceous squids (Tables 4 and 5). The lower rostral length has been measured for 114 oegopsid and 41 myopsid fossil beak specimens. The average and quartile values of estimations were calculated for each geological stage (Table 6). Negative values were obtained from functions of six extant species: *Architeuthis dux*, *Thysanoteuthis rhombus*, *Gonatus* spp., *Ancistrocheirus lesueuri*, *Taningia danae*, and *Megalocranchia* spp. Since these species have exceptionally large body and beak sizes[19], estimations based on their correlation function were omitted from calculations of the average and quartile values.

The same as for squids, this study used a correlation function between the length of and the body length of 45 extant marine species[39] to reconstruct the body size of fossil bony fishes (Table 7). The length of vertebrae has been measured in 119 disarticulated fossil vertebrae out of a total of 161 specimens. The average and quartile values of estimated body length were obtained for each geological stage (Table 8).

1.3.4. Morphological disparity analyses of Cretaceous squid species

We evaluated the disparity of the lower beak morphology of all squid species discovered here based

on principal coordinates analysis. All 30 diagnostic characters used in taxonomy were tabulated as a character matrix, including continuous, ordinal, and nominal scales. This matrix was converted into a distance matrix based on Gower's similarity coefficient and then used to analyze the principal coordinates. These calculations were conducted using R 4.4.2 (the R Foundation). The plots of the morphospaces are shown in fig. S12. All data and R code for this analysis are available at Figshare+ (DOI: 10.25452/figshare.plus.28377848).

1.4. Results

A total of 263 squid lower beaks, documenting micrometer-scale structures and pigmentation patterns, were discovered in this study (Fig. 4). I obtained 1,000 cephalopod beaks, consisting of 671 coleoids (a cephalopod group without an external shell), 326 ammonites, and three nautiloids. The coleoid beaks include 322 upper and 349 lower beaks, indicating the absence of a fossilization bias among them. To avoid duplicate counts of paired beaks, subsequent examinations were only conducted for the lower beaks. These lower beaks descended from 263 squids, 48 Vampyromorpha, 12 octopuses, and 26 taxonomically indeterminate non-squid coleoids. Cuttlefishes, spirulids, and belemnites were not encountered (Table 2).The lengths of fossil squid beaks discovered here range from 1.23 to 19.32 mm (Table 3). The average is 3.87 mm, more than fifteen times smaller than the only known fossil squid beak[35]. The minimum thickness of these fossil beaks was always less than 10 μm.

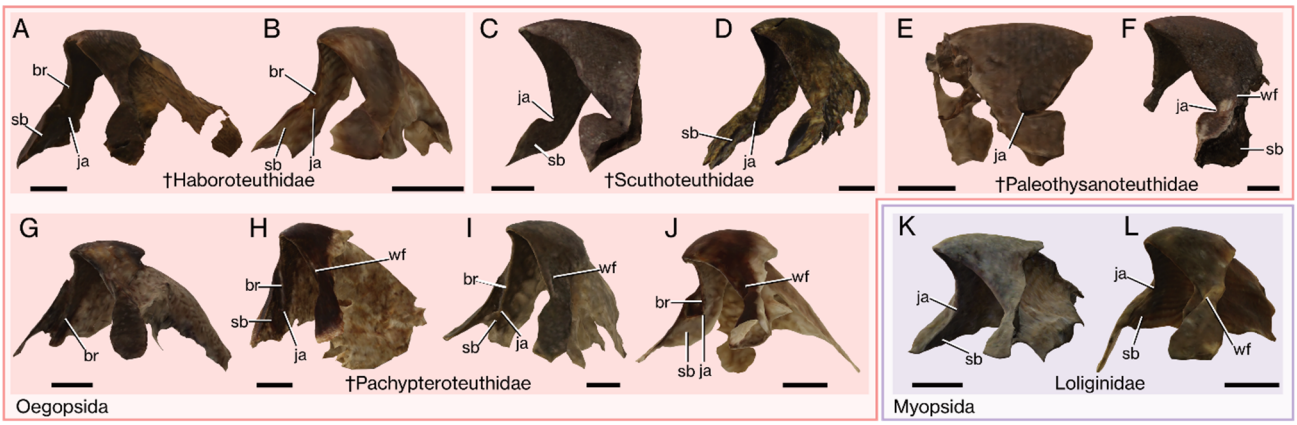


Fig. 4. Fossil lower beaks of squids from the Late Cretaceous (~100–70 Ma).
(**A**) *Pachygephyra callisto.* (**B**) *Hoplitopteryx solida.* (**C**) *Scuthoteuthis kawataro.* (**D**) *Grossiscapula angusta.* (**E**) *Paleothysanoteuthis complicatus.* (**F**) *Aetorhynchus incisus.* (**G**) *Pachypteroteuthis adiacens*. (**H**) *Gerontoteuthis acutissimus*. (**I**) *Thalassasboides watatsumi*. (**J**) *Sepultipons castor*. (**K**) *Psiloteuthis naucrates*. (**L**) *Streptopteryx bidentata*. All taxonomic orders and families discussed in this study are shown here. Important diagnostic characters are indicated for each model: br, bridge; ja, jaw angle; sb, shoulder blade; wf, wing fold. Scale bars: all 1 mm. See Table 3 for their accession numbers.

Table 2. Faunal counts.

Sample No. of carbonate concretion	Geological stage	Number of lower beaks												Number of upper beaks			Total of lower & upper beaks	Number of teleost vertebrae
		Coleoids										Ammonites	Nautiloids	Coleoids	Ammonites	Nautiloids		
		Squids			Cuttlefishes	Sepiolida	Spirulida	Vampyromorpha	Octopuse	Indeterminate	Total							
		Identifiable	Indeterminate	Total														
1	Albian	0	0	0	0	0	0	0	0	0	0	0	0	1	0	0	1	3
2		0	0	0	0	0	0	0	0	0	0	5	0	2	0	0	7	0
3		0	0	0	0	0	0	0	0	0	0	1	0	0	1	0	2	1
4		0	0	0	0	0	0	0	0	1	1	0	0	1	1	0	3	1
5		0	0	0	0	0	0	0	0	1	1	3	0	1	0	0	5	0
total		**0**	**0**	**0**	**0**	**0**	**0**	**0**	**0**	**2**	**2**	**9**	**0**	**5**	**2**	**0**	**18**	**5**
6	Cenomanian	11	4	15	0	0	0	1	1	4	21	14	0	28	5	0	68	0
7		8	5	13	0	0	0	0	0	1	14	2	1	9	0	0	26	0
8		9	9	18	0	0	0	3	0	1	22	7	0	20	6	0	55	9
total		**28**	**18**	**46**	**0**	**0**	**0**	**4**	**1**	**6**	**57**	**23**	**1**	**57**	**11**	**0**	**149**	**9**
9	Turonian	1	4	5	0	0	0	0	0	0	5	4	0	7	1	0	17	0
10		6	2	8	0	0	0	1	0	1	10	4	0	4	0	0	18	15
11		8	4	12	0	0	0	0	0	0	12	28	0	1	5	0	46	7
12		1	6	7	0	0	0	5	0	2	14	10	0	8	2	0	34	0
13		2	1	3	0	0	0	2	0	0	5	4	0	9	2	0	20	1
14		1	0	1	0	0	0	0	0	0	1	5	0	3	6	0	15	0
15		0	2	2	0	0	0	0	0	0	2	23	0	2	6	0	33	3
16		23	23	46	0	0	0	8	1	7	62	48	0	77	20	0	207	3
total		**42**	**42**	**84**	**0**	**0**	**0**	**16**	**1**	**10**	**111**	**126**	**0**	**111**	**42**	**0**	**390**	**29**
17	Coniacian	4	13	17	0	0	0	0	0	0	17	2	0	10	2	0	31	5
18		1	2	3	0	0	0	1	0	0	4	7	1	3	1	0	16	0
19		10	9	19	0	0	0	7	0	0	26	7	0	25	0	0	58	22
20		2	4	6	0	0	0	1	0	4	11	11	0	14	3	0	39	5
total		**17**	**28**	**45**	**0**	**0**	**0**	**9**	**0**	**4**	**58**	**27**	**1**	**52**	**6**	**0**	**144**	**32**
21	Santonian	0	3	3	0	0	0	1	0	1	5	4	0	6	0	0	15	1
22		2	6	8	0	0	0	2	0	0	10	0	0	8	0	0	18	5
23		0	0	0	0	0	0	0	0	0	0	0	0	0	1	0	1	2
24		0	1	1	0	0	0	1	1	0	3	0	0	1	0	0	4	4
25		2	1	3	0	0	0	2	0	0	5	2	0	3	0	0	10	1
26		2	4	6	0	0	0	0	0	2	8	7	0	11	10	0	36	1
total		**6**	**15**	**21**	**0**	**0**	**0**	**6**	**1**	**3**	**31**	**13**	**0**	**29**	**11**	**0**	**84**	**14**
27	Campanian	0	1	1	0	0	0	0	0	0	1	1	1	2	0	0	5	13
28		1	8	9	0	0	0	0	0	0	9	10	0	12	0	0	31	8
29		0	0	0	0	0	0	0	0	0	0	0	0	0	0	0	0	1
30		3	7	10	0	0	0	0	0	0	10	6	0	3	1	0	20	11
31		5	8	13	0	0	0	12	8	1	34	7	0	24	1	0	66	2
32		4	4	8	0	0	0	0	1	0	9	12	0	7	6	0	34	6
total		**13**	**28**	**41**	**0**	**0**	**0**	**12**	**9**	**1**	**63**	**36**	**1**	**48**	**8**	**0**	**156**	**41**
33	Maastrichtia	4	3	7	0	0	0	0	0	0	7	1	0	5	0	0	13	25
34		1	0	1	0	0	0	0	0	0	1	3	0	4	0	0	8	4
35		9	9	18	0	0	0	1	0	0	19	6	0	11	2	0	38	2
total		**14**	**12**	**26**	**0**	**0**	**0**	**1**	**0**	**0**	**27**	**10**	**0**	**20**	**2**	**0**	**59**	**31**
Albian-Maastrichtian total		**120**	**143**	**263**	**0**	**0**	**0**	**48**	**12**	**26**	**349**	**244**	**3**	**322**	**82**	**0**	**1000**	**161**

1.4.1. Systematic Palaeontology

Subclass **Coleoidea** Bather, 1888

Superorder **Decapodiformes** Leach, 1817

Order **Oegopsida** d'Orbigny, 1845

Remarks. The lower beak of the extant oegopsids can be distinguished from that of the other decapodiform orders by a clear separation of a lateral wall and a shoulder blade[17]. This separation is marked by a step, a distinct anglepoint, or a bridge[17]. Here I used these characters for identifying oegopsids in the fossil material. The Oegopsida is the only decapodiform order which shows lateral wall folds[17].

Family **Haboroteuthidae** fam. nov.

Type genus. *Haboroteuthis* Tanabe, Misaki and Ubukata, 2015

Diagnosis. The size of the rostrum ranges from small to very large, and the width of that from narrow to moderately wide. The rostral tip is not hooked or only slightly hooked and has no dents. The bridges are present in the ventral part, forming a bifurcated jaw edge. The bridges are tapered or not developed under jaw angles, and almost parallel to the transverse axis in horizontal sections. The shoulder blades are distinct. The shoulders are infilled with hyaline matrices or thickened to form a massive complex. No folds or grooves are discernible on the hood and lateral walls.

Comparison. The Haboroteuthidae is here assigned to the Oegopsida based on a distinct division between a lateral wall and the adjacent shoulder blade (Fig. 5D), and lateral wall folds in the holotype of *Haboroteuthis poseidon*[35]. The principal characters of the Haboroteuthidae are the bridges that form a bifurcated jaw edge (Fig. 5E) and extend around the ventral end of a lateral wall (Fig. 5F). This type of bridges is absent in other families of extant and fossil oegopsid squids.

Genus ***Haboroteuthis*** Tanabe, Misaki and Ubukata, 2015

Type species. *Haboroteuthis poseidon* Tanabe, Misaki and Ubukata, 2015

Emended diagnosis. The crest length of *Haboroteuthis* is extremely large (more than 50 mm in adults) among coleoids. The rostrum is large and narrow. It has a faint hook and no dents. The bridges are present in the ventral part to form a bifurcated jaw edge, tapered below jaw angles, and almost parallel to the transverse axis in horizontal sections. The shoulders are covered by a thin and distinct pigmented plate connected to a bridge on its lateral side and by a thin shoulder blade on its medial side. The jaw angles are covered by hyaline matrices that fill the inside of the shoulders in younger growth stages. The ventral parts of the shoulders and the adjacent wing merge directly. The anterior edge of the wings gently curves downward. No folds or grooves are discernible on the hood. The lateral walls are somewhat longer than high and have a fold running parallel to the crest on their dorsal part.

Comparison. This genus can be distinguished from *Pachygephyra* gen. nov. and *Placomoteuthis* gen. nov. by the lack of distinct shoulder planes (Figs. 5D and Q, and 6I). It differs from *Hoplitopteryx* gen. nov. by the absence of an angular ridge on the wings (Fig. 5A and T) and from *Bathmidoteuthis* gen. nov. by the absence of a step between shoulder blades and the adjacent lateral wall (Figs. 5G and 6D).

Occurrence. Late Cenomanian to Early Campanian; Yezo Group in Hokkaido, Japan.

Haboroteuthis poseidon Tanabe, Misaki and Ubukata, 2015

Fig. 5A–M

2023 *Longibelus matsumotoi*; Tanabe and Misaki, p. 5, Fig. 4.1A–D, 4.2A–D.

2023 Haboroteuthis poseidon; Fuchs, p. 29, Fig.13.1a-b.

Holotype. KMNH IvP 902002.

Material. KMNH IvP 902002, KMNH IvP 902008, KMNH IvP 902009, NMNS_DS00082_79XGc4h.stl, NMNS_DS00009_3F7VSzd.stl, and NMNS_DS00173_Ps2dDmF.stl (https://doi.org/10.25452/figshare.plus.25736631).

Emended diagnosis. Same as for the genus.

Description. The large, narrow rostrum shows a weak hook on its tip and does not exhibit dents (Fig. 5A, B, E, F, K, and L). The bridges appear slightly above the jaw angles to form a ventrally bifurcated jaw edge (Fig. 5D, E, G, and L). The bridges run parallel to the transverse axis in horizontal sections. Below the jaw angles, the bridges taper off and are surrounded by a shoulder blade and the pigmented lateral margin of a shoulder. The internal part of the shoulders is filled with a hyaline matrix, it is presumably gradually pigmented from the anteroventral part during growth (Fig. 5M). In the smallest specimen, a hyaline matrix covers the root of the wings, which may obscure a jaw angle (Fig. 5F–I). The dorsal parts of the shoulders and the adjacent wing directly merge and gently curve downward (Fig. 5A and F). The wing angle is obtuse. The hood is fairly short and has a deep notch (Fig. 5C). The lateral walls show an elongated parallelogram shape and have a relatively broad fold that runs parallel to the crest on their dorsal part.

Remarks. The identification of the specimens newly discovered in this study (NMNS_DS00082_79XGc4h.stl, NMNS_DS00009_3F7VSzd.stl, and NMNS_DS00173_Ps2dDmF.stl) are based on rostrum and wings characteristics, which are identical to the holotype. Their much smaller size and pigmentation in the lateral walls suggest that these specimens represent earlier ontogenetic growth stages than the holotype. The typical features of the bridges, jaw edges, and shoulders are clearly recognizable in these specimens. Ontogenetic changes are seen in the degree of pigmentation in the inner shoulders and lateral walls, but do not alter the general morphology. Based on these features, the lower beaks described as *Longibelus matsumotoi*[36] (KMNH IvP 902008 and KMNH IvP 902009) are here synonymized with this species. The original description distinguished two species based on the size of the entire beaks and the length of the inner lamella[36]. These differences are, however, due to the growth changes and incomplete preparation.

Occurrence. Late Cenomanian to Early Campanian; Yezo Group in Hokkaido, Japan.

Genus ***Pachygephyra*** gen. nov.

Etymology. Ancient Greek ‘pachys’ (thick) and ‘gephyra’ (bridge).

Type species. *Pachygephyra callisto* sp. nov.

Diagnosis. The rostrum is moderately large, moderately wide, and somewhat hooked. The bridges are very broad, broadening ventrally, almost parallel to the transverse axis in horizontal sections. A thick complex of a wing and a shoulder covers their ventral part. A broad plane exists in the shoulders, separated by a wing fold and the angular dorsal margin of a shoulder blade. The ventral surface of wing-shoulder complexes has no grooves. The jaw angles are angular. The angle between the jaw edges and the adjacent shoulder blade is slightly obtuse. Wings are fairly narrow around jaw angle. No fold or groove is discernible on the hood.

Comparison. This genus can be distinguished from *Placomoteuthis* gen. nov. by the rostral hook, exceedingly broad bridges, and thicker wings (Figs. 5R and 6J). It markedly differs from the other genera of the Haboroteuthidae fam. nov. by exceedingly broad bridges and the presence of distinct shoulder planes (Figs. 5D, Q, and V, and 6D).

Occurrence. Santonian; Yezo Group in Hokkaido, Japan.

Pachygephyra callisto sp. nov.
Fig. 5N–R
Etymology. Callisto in Greek mythology, who was transformed into a bear, referring to the outline of beaks that resembles a bear.
Material. NMNS_DS00011_JVM6xKK.stl (https://doi.org/10.25452/figshare.plus.25736631).
Diagnosis. Same as for the genus.
Description. The rostrum shows a moderate size, moderate width, and a somewhat hooked tip (Fig. 5N, O, and R), rostral dents are absent. The bridges are very broad and almost parallel to the transverse axis in horizontal sections (Fig. 5R), they form an entirely double jaw edge. Wings and shoulders are intensively thickened and merged to cover ventral parts of the bridges (Fig. 5N and O). The ventral surface of the wing-shoulder complexes has no groove between a shoulder blade and a wing. The inner jaw edges form a sharp jaw angle, and the outer ones are connected with a low, angular wing fold (Fig. 5Q). Wing folds and the dorsal margin of the adjacent shoulder blade are merged at their anterior part, forming a plane between them (Fig. 5P and Q). The angle between a jaw edge and the adjacent shoulder blade is slightly obtuse. Wings are medially inflected at a line along the adjacent jaw edge extension and constricted around a jaw angle (Fig. 5N and O). The hood is short. The lateral walls show a slightly elongated trapezoidal shape.
Occurrence. Santonian; Yezo Group in Hokkaido, Japan.

Genus ***Hoplitopteryx*** gen. nov.
Etymology. Ancient Greek ‘hoplites’ (armed) and ‘pteryx’ (wing).
Type species. *Hoplitopteryx solida* sp. nov.
Diagnosis. The rostrum is moderately large and wide. It has no hook or dents. Narrow bridges that form a bifurcated jaw edge are observable in the only short area above jaw angles of the external surface and almost parallel to the transverse axis in horizontal sections. A light-colored belt along the jaw edge extensions exists till the ventral end of lateral walls. Wings are thick, slightly constricted around jaw angles, and fused with a shoulder, forming a massive complex. No groove is present on the narrow ventral surface of the wing-shoulder complexes. The lateral surface of the wings has an angular ridge which runs parallel to the adjacent jaw edge extension. The jaw angles are angular. The angle between the jaw edges and the adjacent shoulder blade is almost perpendicular. No folds or grooves are discernible on the hood.
Comparison. This genus can be easily distinguished from other genera of the Haboroteuthidae fam. nov. by the presence of a remarkably angular ridge on the wings (Figs. 5N and T, and 6A and F). It differs from *Haboroteuthis* by the shoulder blades entirely fused with a wing (Fig. 5A and V) and from *Bathmidoteuthis* gen. nov. by the smaller rostrum and the absence of a step between the shoulder blades and the adjacent lateral wall (Figs. 5V and 6D). The absence of the shoulder planes in this genus is the main difference to *Pachygephyra* gen. nov. and *Placomoteuthis* gen. nov. (Figs. 5Q and V, and 6I).
Occurrence. Middle Turonian; Yezo Group in Hokkaido, Japan.

Hoplitopteryx solida sp. nov.
Fig. 5S–W
Etymology. Latin ‘solidus’ (complete).

Material. NMNS_DS00009_dvxb42e.stl (https://doi.org/10.25452/figshare.plus.25736631).
Diagnosis. Same as for the genus.
Description. The rostrum shows moderate size and width (Fig. 5S, T, and W). No hooks or dents are discernible around it. The jaw edges curve gently. Narrow bridges rise dorsally from a jaw angle, and their inner and outer edges fuse at a point slightly above the jaw angles (Fig. 5V and W). The wings are thickened and merged to the adjacent shoulder without forming a groove (Fig. 5V). The ventral surface of the wing-shoulder complexes is placed near the ventral end of the shoulder blades. A light-colored strip exists along the jaw edge extensions, showing slight constriction. Wings slightly curve downward and form an angular ridge and a valley behind that (Fig. 5S–U). They are parallel to and slightly anterior to the adjacent jaw edge extension. The wing angle is slightly obtuse. The jaw angles are angular, and the angle between a jaw edge and the adjacent shoulder blade is almost perpendicular (Fig. 5V). The hood is somewhat short and has a broad notch of which the most posteriorly extending parts are located at almost the same height as the jaw angles (Fig. 5U). The shape of the inner lamella is uncertain, but the crest shows a moderate length.
Occurrence. Middle Turonian; Yezo Group in Hokkaido, Japan.

Genus ***Bathmidoteuthis*** gen. nov.
Etymology. Ancient Greek ‘bathmis’ (step) and ‘teuthis’ (squid).

Type species. *Bathmidoteuthis altus* sp. nov.
Diagnosis. The rostrum is large, narrow, slightly hooked, and has no dents. Narrow bridges that form a bifurcated jaw edge are observable in the only short area above jaw angles of the external surface and almost parallel to the transverse axis in horizontal sections. A low step exists between the lateral walls and the adjacent shoulder blade. A low step is also present on the dorsal part of the wings just below the jaw angles. The shoulder blades are mostly fused with the adjacent wing. The anterior edge of the wings gently curves downward. The jaw angles are angular. The angle between the jaw edges and the adjacent shoulder blade is obtuse. No folds or grooves are discernible on the hood.
Comparison. This genus can be clearly distinguished from other genera of the Haboroteuthidae fam. nov. by the presence of a step between the shoulder blades and the adjacent lateral wall (Figs. 5D, Q, and V, and 6D and I) and the small ratio of HL to JELL (~0.75 in this genus while over 1.00 in the other genera; Figs. 5A, N, and S, 6A and F, and Table 3).
Occurrence. Early Cenomanian to Late Campanian; Yezo Group in Hokkaido, Japan.

Bathmidoteuthis altus sp. nov.
Fig. 6A–E
Etymology. Latin ‘altus’ (tall).
Material. NMNS_DS00084_a3ll9sj.stl and NMNS_DS00171_Lq1Jgoh.stl (https://doi.org/10.25452/figshare.plus.25736631).
Diagnosis. Same as for the genus.
Description. The large, narrow rostrum shows gently curved jaw edges and a faint hook (Fig. 6A, B, and E). The rostral dents are not discernible. Narrow bridges rise from a jaw angle, and their inner and

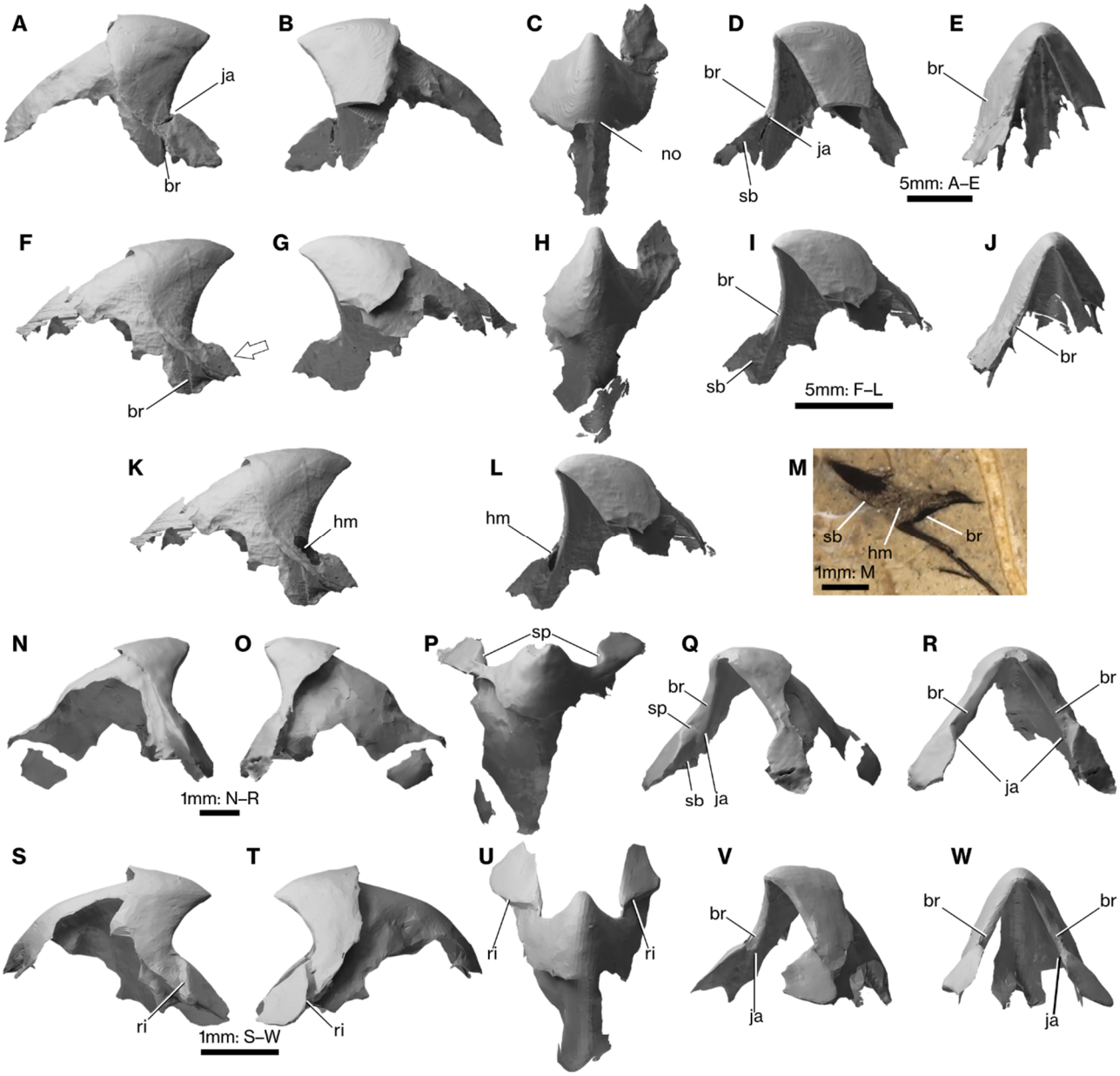


Fig. 5. Lower beaks of *Haboroteuthis*, *Pachygephyra*, and *Hoplitopteryx*.
(**A** to **E**) *Haboroteuthis poseidon* Tanabe, Misaki, and Ubukata, 2015, NMNS_DS00009_3F7VSzd.stl. (**F** to **M**) *Haboroteuthis poseidon* Tanabe, Misaki, and Ubukata, 2015, NMNS_DS00082_79XGc4h.stl (F to L) and A part of C_NMNS_DS00082_20190127_c1_wl_01_0491_79XGc4h.jpg (M). (**N** to **R**) *Pachygephyra callisto* sp. nov., NMNS_DS00011_JVM6xKK.stl. (**S** to **W**) *Hoplitopteryx solida* sp. nov., NMNS_DS00009_dvxb42e.stl. (A, F, K, N, and S) left lateral view; (B, G, O, and T) right lateral view; (C, H, P, and U) dorsal view; (D, I, L, Q, and V) oblique view; (E, J, R, and W) frontal view; (M) a transverse section around a wing (white arrow in (F)). In (K) and (L), hyaline matrices are shown as the region with a dark grey color. The specimens are available from Figshare+: 3D models and the cropped cross–sectional images (https://doi.org/10.25452/figshare.plus.25736631). Abbreviations: ja, jaw angle; br, bridge; hm, hyaline material; no, hood notch; ri, ridge; sb, shoulder blade; sp, shoulder plane.

outer edges fuse at a point slightly above the jaw angles (Fig. 6D and E). The wings are thickened and merged to the adjacent shoulder without forming a groove (Fig. 6C and D). A low step exists between the lateral walls and the adjacent shoulder blade (Fig. 6D). A step may also be present on the dorsal part of the wings, along the neighbouring jaw edge extension (Fig. 6A). The anterior edge of the wings gently curves downward (Fig. 6A). Jaw angles are angular, and the angle between a jaw edge and the adjacent shoulder blade is obtuse (Fig. 6A and D). The wing angle is fairly obtuse.
Occurrence. Early Cenomanian to Late Campanian; Yezo Group in Hokkaido, Japan.

Genus ***Placomoteuthis*** gen. nov.
Etymology. Ancient Greek 'plax (plane), 'omos' (shoulder), and 'teuthis' (squid),
Type species. *Placomoteuthis hercules* sp. nov.
Diagnosis. The rostrum is moderate in size and width. It has no hook or dents. The bridges bifurcate ventrally, forming the inner and outer jaw edges, taper abruptly under the jaw angles, and are almost parallel to the transverse axis in horizontal sections. A broad plane exists in the shoulders, separated by an angular wing fold and the dorsal margin of the nearest shoulder blade. The jaw angles are angular. The angle between the jaw edges and the adjacent shoulder blade is slightly obtuse. Wings are thin and fairly narrow around the jaw angles. No folds or grooves are discernible on the hood and the lateral walls.
Comparison. This genus can be distinguished from *Pachygephyra* gen. nov. by significantly narrower bridges and thinner wings (Figs. 5R and 6J). It markedly differs from the other genera of the Haboroteuthidae fam. nov. by the presence of distinct shoulder planes (Figs. 5D and V, and 6D and I) and the large ratio of HL to JELL (~1.60 in this genus while less than 1.20 in the other genera; Figs. 5A, N, and S, 6A and F, and Table 3).
Occurrence. Early Maastrichtian; Yezo Group in Hokkaido, Japan.

Placomoteuthis hercules sp. nov.
Fig. 6F–J
Etymology. After Hercules in Greek mythology, who has extraordinary toughness and ingenuity.
Material. NMNS_DS00174_bjM7Cpk.stl (https://doi.org/10.25452/figshare.plus.25736631).
Diagnosis. Same as for the genus.
Description. The rostrum shows moderate size and width. The rostral hook is absent (Fig. 6F, G, and J). The jaw edges are almost straight. A broad bridge is observable in the ventral half of jaw edges and abruptly tapers below the jaw angles (Fig. 6I and J). The bridges are almost parallel to the transverse axis in horizontal sections. The inner jaw edges form a sharp jaw angle with the dorsal margin of the adjacent shoulder blade, and the outer ones are connected with a low, angular wing fold (Fig. 6I). Wing folds and the dorsal margin of the adjacent shoulder blade are merged at their anterior part, forming a plane between them. The angle between a jaw edge and the adjacent shoulder blade is slightly obtuse. Well-developed shoulder blades are thin and smoothly connected with a lateral wall (Fig. 6I). The wings are relatively thin and have no folds or grooves (Fig. 6F and G). The hood is long and has no notches (Fig. 6H). The lateral walls show a moderately elongated parallelogram shape with a slightly curved crest (Fig. 6F and G).
Occurrence. Early Maastrichtian; Yezo Group in Hokkaido, Japan.

Family **Pachypteroteuthidae** fam. nov.

Type genus. *Pachypteroteuthis* gen. nov.
Diagnosis. The size of the rostrum ranges from small to large, and the width of that from very narrow to moderately wide. The rostrum is typically hooked and has dents around the jaw edges, surrounded by a fold extending from the hook. These folds are typically connected to a wing fold. The bridges extend to almost the ventral end of a lateral wall, forming an anglepoint. The jaw edges are single-edged. The wings are typically thick and almost straight in lateral view. Around the adjacent jaw edge, the wings are constricted and bent medially. The anterior edge of the wings is superposed on a jaw edge in the frontal view. The shoulder blades are faint or relatively small. Wing folds are high and not parallel to the dorsal edge of the shoulder blades.
Comparison. The Pachypteroteuthidae were assigned to the order Oegopsida due to the clear separation between the lateral walls and the neighboring shoulder blade, marked by a bridge (Fig. 6N). Some taxa of the Haboroteuthidae fam. nov. also have bridges clearly separated from the shoulder blades and the wings, but this family shows much higher wing folds (Figs. 5D and 6N). The Pachypteroteuthidae can be distinguished from the other families of fossil oegopsids by the apparently exposed bridges and the wing folds forming a groove medial to them. Developed wing folds not parallel to the dorsal edge of the shoulder blades are a crucial feature of this family. More than half of the extant oegopsid families (e.g., the Ommastrephidae and the Histioteuthidae) also exhibit the same feature[19]. The Pachypteroteuthidae differ from these extant families by the developed bridges that reach the ventral end of the lateral walls (Fig. 6N).

Genus ***Pachypteroteuthis*** gen. nov.
Etymology. Ancient Greek ‘pachys’ (thick), ‘pteryx’ (wing), and ‘teuthis’ (squid),
Type species. *Pachypteroteuthis adiacens* sp. nov.
Diagnosis. The adult beaks of some species become fairly large among Cretaceous squids, with a rostral length over 5 mm. The size of the rostrum ranges from small to moderate. The rostrum is moderately wide and hooked. It has dents surrounded by a low fold extending from the hook. The bridges are equal in width or ventrally tapered. The bridges are smoothly connected with a groove medial to the adjacent wing fold. The wing folds are high, extending at an acute angle with the adjacent jaw edge. The wings are thick, constricted around the adjacent jaw edge, and almost straight in lateral view. The anterior edge of the wings is superposed on a jaw edge in the frontal view. An angular ridge on the wings exists along the nearest jaw edge extension. The wings bend medially at this ridge.
Comparison. This genus differs from other genera in the Pachypteroteuthidae fam. nov. by the presence of an angular ridge on the wings (Fgs. 5K, 6, A, F, and U, 7, A, F, and Q, and 8, A and P). This genus resembles *Hoplitopteryx* gen. nov. in having the ridge, but the former can be distinguished by the wider bridges (Figs. 5W and 6O) and the less distinct shoulder blades (Figs. 5V and 6N).
Occurrence. earliest Cenomanian to Early Campanian; Yezo Group in Hokkaido, Japan.

Pachypteroteuthis adiacens sp. nov.
Fig. 6K–O
Etymology. Latin ‘adiacens’ (adjacent), referring to ridges positioned parallelly to a jaw edge.
Material. NMNS_DS00068_o0JKOmo.stl and NMNS_DS00068_EnU0Efh.stl (https://doi.org/10.25452/figshare.plus.25736631).
Diagnosis. The rostrum is small, moderately wide, and hooked. It has dents surrounded by a low fold extending from the hook to a wing fold. The bridges are entirely exposed, equal in width, and smoothly

connected with the groove medial to the neighbouring wing fold. The wing folds are high, extending at an acute angle with the adjacent jaw edge. The shoulder blades are not discernible. The wings are thick, constricted around the adjacent jaw edge, and almost straight in lateral view. The anterior edge of the wings is superposed on a jaw edge in the frontal view. An angular ridge on the wings exists along the nearest jaw edge extension. The wings bend medially at this ridge.

Description. The rostrum is small, moderately wide, and weakly hooked (Fig. 6K, L, and O). The shoulder blades are weak (Fig. 6N). The bridges are entirely exposed, equal in width, and nearly parallel to the transverse axis in horizontal sections of the ventral part (Fig. 6N). High wing folds extend at an acute angle with a jaw edge and are continuous with a low fold, extending from the rostral hook. These folds form a dent around the jaw edges (Fig. 6K and L). The basal part of the wings is constricted and has a laterally pointed small tip (Fig. 6K, L, and N). An angular ridge rises from this tip and extends posteroventrally along the adjacent jaw edge (Fig. 6K–M). The anterior edge of the wings is almost straight in lateral view (Fig. 6K and L) and superposed on a jaw edge in frontal view (Fig. 6O). The degree of the wing angle is obtuse. The hood shows a moderate length (Fig. 6M). The inner lamella is approximately twice as long as high (Fig. 6K and L).

Comparison. This species differs from *P. mortarii* sp. nov. by a smaller rostrum and the degree of angle between the wing ridges and the adjacent jaw edge (Fig. 6K and Q). This species can be distinguished from *P. magnus* sp. nov. by the less developed shoulder blades (Fig. 6N and X) and the wings that are not curved in lateral view (Fig. 6K and V). Unlike *P. sulcatus* sp. nov., the dorsal end of the wing ridges is not remarkably pointed in this species (Fig. 6K and AA).

Occurrence. earliest Cenomanian; Yezo Group in Hokkaido, Japan.

Pachypteroteuthis mortarii sp. nov.

Fig. 6P–T

Material. NMNS_DS00068_G7fBskP.stl (https://doi.org/10.25452/figshare.plus.25736631).

Etymology. Latin ‘mortarium’ (mortar), referring to the Suribachi Creek (the creek of a mortar), the locality where this species occurred.

Diagnosis. The rostrum is moderately large and wide. It has a hook and dents surrounded by a low fold extending from the hook to a wing fold. The bridges are entirely exposed, equal in width, and smoothly connected with the groove medial to the neighbouring wing fold. The wing folds are high, extending at an acute angle with the adjacent jaw edge. The shoulder blades are not discernible. The wings are thick, constricted around the adjacent jaw edge, and almost straight in lateral view. The anterior edge of the wings is superposed on a jaw edge in the frontal view. An angular ridge on the wings extends posteroventrally across the jaw edge in lateral view. The wings bend medially at this ridge.

Description. The rostrum shows a moderate size, moderate width, and a weak hook (Fig. 6P, Q, and T). The shoulder blades are not discernible (Fig. 6S). The bridges are entirely exposed, equal in width, and nearly parallel to the transverse axis in horizontal sections of the ventral part (Fig. 6S). High wing folds extend at an acute angle with a jaw edge and are continuous with a low fold, extending from the rostral hook. These folds form a dent around the jaw edges (Fig. 6P and Q). The basal part of the wings is constricted and has a laterally pointed small tip (Fig. 6P, Q, and S). An angular ridge rises from this tip and extends posteroventrally across the adjacent jaw edge in lateral view (Fig. 6P–R). The anterior edge of the wings is almost straight in lateral view (Fig. 6P and Q) and superposed on a jaw edge in frontal view (Fig. 6T). The degree of the wing angle is obtuse. The hood shows a moderate length (Fig.

6R).
Comparison. This species differs from *P. adiacens* sp. nov. by a larger rostrum and the degree of the angle between the wing ridges and the adjacent jaw edge (Fig. 6K and Q). This species can be distinguished from *P. magnus* sp. nov. by the less developed shoulder blades (Fig. 6S and X) and the wings that are not curved in lateral view (Fig. 6Q and V). Unlike *P. sulcatus* sp. nov., the dorsal end of the wing ridges is not remarkably pointed in this species (Fig. 6Q and AA).
Occurrence. earliest Cenomanian; Yezo Group in Hokkaido, Japan.

Pachypteroteuthis magnus sp. nov.
Fig. 6U–Y
Etymology. Latin 'magnus' (large).
Material. NMNS_DS00034_nv7HRSc.stl (https://doi.org/10.25452/figshare.plus.25736631).
Diagnosis. The adult beaks of this species become fairly large among the Cretaceous squids, with the rostral length over 5 mm. The rostrum is moderate-sized and hooked. It has dents surrounded by a low fold extending from the hook to a wing fold. The ventral part of the bridge is gradually covered by a shoulder from the lateral side and smoothly connected with the groove medial to the neighbouring wing fold. The wing folds are high, extending at an acute angle with the adjacent jaw edge. The bridges are detached from the adjacent wing below the jaw angles without forming a ridge on the lateral walls. The shoulder blades are distinct, but their dorsal margin is ambiguous. The anterior edge of the shoulder blades directly merged with that of the wing. The wings are thick, constricted around the adjacent jaw edge, and gently curved ventrally around their basal part. An angular ridge exists on the wings and is smoothly connected to the anterior edge of the wings with the same curvature. The ventral part of the ridges is parallel to the nearest jaw edge extension. The wings bend medially at this ridge.
Description. The rostrum shows moderate size, a hook, and probably moderate width (Fig. 6U, V, and W). The bridges are almost parallel to the transverse axis in horizontal sections and detached from the adjacent wing below the jaw angles without forming a ridge on the lateral walls. The ventral part of bridges is gradually covered up from the lateral side by a shoulder and completely covered around the midpoint of the shoulder (Fig. 6X). Distinct shoulder blades are smoothly connected to a lateral wall but do not exhibit a clear dorsal margin (Fig. 6X). High wing folds extend at an acute angle with the neighbouring jaw edge (Fig. 6V). The wing folds form a narrow dent around jaw edges. The wings are thick. The anterior edge of the wings curves anteroventrally with gentle curvature around their basal part. It is smoothly connected to an angular ridge on the wings, keeping the same curvature (Fig. 6V). The ventral part of the ridges extends along the adjacent jaw edge extension. The degree of the wing angle is obtuse (Fig. 6V).
Comparison. This species clearly differs from the other species of *Pachypteroteuthis* gen. nov. by developed shoulder blades (Fig. 6N, S, X, and AC) and the arced ridge on wings that is continuous with the anterior edge of a wing (Fig. 6L, Q, V, and AA). The adult beaks exceed 5 mm in LRL, which is significantly large among the Late Cretaceous squids (Table 3).
Occurrence. Early Coniacian; Yezo Group in Hokkaido, Japan.

Pachypteroteuthis sulcatus sp. nov.
Fig. 6Z–AD
Etymology. Latin 'sulcatus' (sulcate), referring to the characteristic grooves on the inner lamella.
Material. NMNS_DS00175_2UQENMZ.stl (https://doi.org/10.25452/figshare.plus.25736631).

Diagnosis. The adult beaks of this species become fairly large among the Cretaceous squids (the crest length surpasses 10 mm). The bridges are entirely exposed, broadened ventrally, and smoothly connected with the groove medial to the neighbouring wing fold. The wing folds are high, extending at a very acute angle with the adjacent jaw edge. The shoulder blades are not discernible. The wings are thick, constricted around the adjacent jaw edge, almost straight in lateral view, and have a pointed tip with strong dorsal protrusion. The anterior edge of the wings is superposed on a jaw edge in the frontal view. An angular ridge exists on the wings, nearly parallel to the jaw edge in lateral view. The wings bend medially at this ridge. Lateral wall groove parallel to crest, forming an angular ridge on the dorsal boundary.

Description. The extended line of the inner lamella suggests that the size and width of the rostrum are moderate (Fig. 6AA and AD). The jaw edges curve gently. The shoulder blades are not discernible (Fig. 6AC). The bridges are entirely exposed and ventrally tapered (Fig. 6AC). The ventral part of the bridges is detached from the adjacent wing and forms a ridge on a lateral wall. Thickened wings form a high wing fold and a strongly pointed tip on their dorsal margin (Fig. 6AA). The wing folds extend at a very acute angle with the nearest jaw edge. An angular ridge rises from this tip and extends parallel to and anterior to the adjacent jaw edge (Fig. 6AA and AB). The anterior edge of the wings is almost straight in lateral view (Fig. 6AA) and superposed on a jaw edge in frontal view (Fig. 6AD). The degree of the wing angle is obtuse. The lateral walls have a groove running by the crest (Fig. 6Z). The dorsal margin of this groove is angulated.

Comparison. This species markedly differs from the other species of *Pachypteroteuthis* gen. nov. by a remarkably pointed tip on the anterior edge of a wing (Fig. 6L, Q, V, and AA). The size of beaks exceeds 5 mm in WL at the subadult stage, which is quite large among for a Late Cretaceous squid (Table 3).

Occurrence. Early Campanian; Yezo Group in Hokkaido, Japan.

Genus ***Catantopteryx*** gen. nov.

Etymology. Ancient Greek ‘katantes’ (sloping down), referring to the obtuse wing angle, and ‘pteryx’ (wing).

Type species. *Catantopteryx altilis* sp. nov.

Diagnosis. The rostrum is small, moderately wide, and hooked. It has dents surrounded by a low fold extending from the hook to a wing fold. The bridges are entirely exposed, equal in width, and smoothly connected with the groove medial to the neighbouring wing fold. The wing folds are high, extending at a very acute angle with the nearest jaw edge. The shoulder blades are not discernible. The wings are thick, almost straight in lateral view, and have no ridge on the outer surface. Around the adjacent jaw edge, the wings are constricted and bend medially. The anterior edge of the wings is superposed on a jaw edge in frontal view. The wing angle is very obtuse.

Comparison. The small rostrum and the wings with exceedingly obtuse wing angles only coexist in this genus and *Orthoteuthis* gen. nov. of the Pachypteroteuthidae fam. nov. (Figs. 7A and 8A). The latter genus can be distinguished from the former by the acuter angle between the crest and the jaw edges (Figs. 7A and 8A).

Occurrence. Late Cenomanian to Late Turonian; Yezo Group in Hokkaido, Japan.

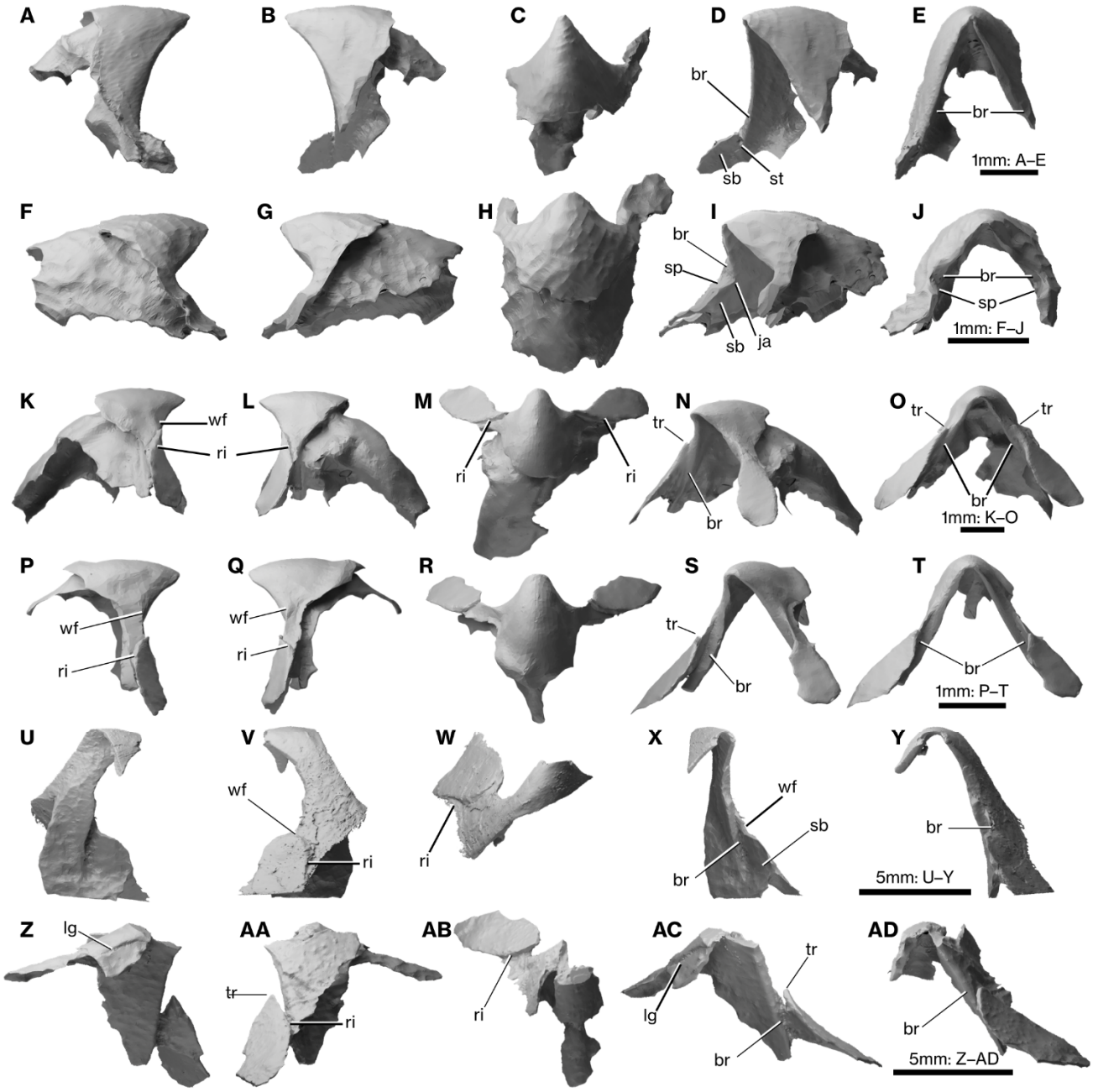


Fig. 6. Lower beaks of *Bathmidoteuthis*, *Placomoteuthis*, and *Pachypteroteuthis*. (**A** to **E**) *Bathmidoteuthis altus* sp. nov., NMNS_DS00084_a3ll9sj.stl. (**F** to **J**) *Placomoteuthis hercules* sp. nov., NMNS_DS00174_bjM7Cpk.stl. (**K** to **O**) *Pachypteroteuthis adiacens* sp. nov., NMNS_DS00068_EnU0Efh.stl. (**P** to **T**) *Pachypteroteuthis mortarii* sp. nov., NMNS_DS00068_G7fBskP.stl. (**U** to **Y**) *Pachypteroteuthis magnus* sp. nov., NMNS_DS00034_nv7HRSc.stl. (**Z** to **AD**) *Pachypteroteuthis sulcatus* sp. nov., NMNS_DS00175_2UQENMZ.stl. (A, F, K, P, U, and Z) left lateral view; (B, G, L, Q, V, and AA) right lateral view; (C, H, M, R, W, and AB) dorsal view; (D, I, N, S, X, and AC) oblique view; (E, J, O, T, Y, and AD) frontal view. The 3D models are available from Figshare+ (https://doi.org/10.25452/figshare.plus.25736631). Abbreviations: br, bridge; ja, jaw angle; lg, lateral wall groove; ri, ridge; sb, shoulder blade; sp, shoulder plane; st, step; tr, a tip on the anterodorsal end of a ridge; wf, wing fold.

Catantopteryx altilis sp. nov.
Fig. 7A–E
Etymology. Latin ‘altilis’ (fattened), referring to thickened wings and bridges.
Material. NMNS_DS00082_tntK5pM.stl and NMNS_DS00173_JGcVf5Q.stl (https://doi.org/10.25452/figshare.plus.25736631).
Diagnosis. Same as for the genus.
Description. The rostrum is small, moderately wide, and hooked (Fig. 7A, B, and E). The shoulder blades are not discernible (Fig. 7D). The bridges are entirely exposed, equal in width, and posterolaterally inclined (Fig. 7D). High wing folds extend at an acute angle with the nearest jaw edge and are continuous with a low fold, extending from the rostral hook. These folds form a dent around the jaw edges (Fig. 7A and B). Thickened wings are constricted and bend medially around the adjacent jaw edge (Fig. 7A–C). The anterior edge of the wings is almost straight in lateral view (Fig. 7A and B) and superposed on a jaw edge in frontal view (Fig. 7E). The degree of the wing angle is very obtuse (Fig. 7A and B).
Occurrence. Late Cenomanian to Late Turonian; Yezo Group in Hokkaido, Japan.

Genus ***Thalassasboides*** gen. nov.
Etymology. Ancient Greek ‘thalassa’ (sea), ‘asvos’ (badger), and suffix ‘-eides’ (-like).
Type species. *Thalassasboides watatsumi* sp. nov.
Diagnosis. The rostrum is moderate-sized and strongly hooked. It has dents surrounded by fold extending from the hook. The width of the rostrum ranges from very narrow to moderate. The bridges are entirely exposed, ventrally tapered, and smoothly connected with the groove medial to the neighbouring wing fold. The wing folds are high, extending at an acute angle with the adjacent jaw edge. The shoulder blades are thin and weakly developed. The shoulder blades are connected to a bridge and the thickened ridge on the medial side of the adjacent wing. The wings are thick, almost straight in lateral view, and have no ridge on the outer surface. Around the adjacent jaw edge, the wings are constricted and bend medially. The anterior edge of the wings is superposed on a jaw edge in frontal view. The wing angle is obtuse.
Comparison. This genus has no ridges on the wings, unlike *Pachypteroteuthis* gen. nov. (Figs. 6K and 7F). It differs from *Catantopteryx* gen. nov., *Pseudovampyroteuthis* gen. nov., *Orthoteuthis* gen. nov., and *Gerontoteuthis* gen. nov. by a larger rostrum (Figs. 7A, F, and U, and 8A and F). This genus can be distinguished from the morphologically related *Astathogephyra* gen. nov. by bridges that are entirely connected to a wing (Figs. 7I and 8N) and from *Sepultipons* gen. nov. by weakly developed shoulder blades (Figs. 7I and 9D). It differs from *Aspasmoteuthis* gen. nov. by ventrally tapered bridges (Fig. 7I and 9S) and from *Juroteuthis* gen. nov. by the acuter angle between the crest and jaw edges (Fig. 7F and 9Y).
Occurrence. earliest Cenomanian to Late Campanian; Yezo Group in Hokkaido, Japan.

Thalassasboides watatsumi sp. nov.
Fig. 7F–J
Etymology. After Watatsumi, a water deity in Japanese mythology.
Material. NMNS_DS00084_U3Z2mdm.stl, NMNS_DS00084_RAKM2iJ.stl, NMNS_DS00082_1H8UvDW.stl, NMNS_DS00082_ev6tAaJ.stl, NMNS_DS00082_egK7tIO.stl, NMNS_DS00009_MnRA9nb.stl, NMNS_DS00135_JM4f46S.stl, NMNS_DS00173_4dpfh14.stl,

NMNS_DS00173_A2DztKh.stl, NMNS_DS00173_TFD6EIX.stl, NMNS_DS00173_d50dzkI.stl, NMNS_DS00034_kJU1vwB.stl, NMNS_DS00083_SN4asC0.stl, NMNS_DS00011_UU1c7pj.stl, and NMNS_DS00182_F56YeDG.stl (https://doi.org/10.25452/figshare.plus.25736631).

Diagnosis. The rostrum is moderately large, moderately wide, and strongly hooked. It has dents surrounded by a low fold extending from the hook. The bridges are entirely exposed, ventrally tapered, and smoothly connected with the groove medial to the neighbouring wing fold. The wing folds are high, extending at an acute angle with the adjacent jaw edge. The shoulder blades are thin and weakly developed. The shoulder blades are connected to a bridge and the thickened ridge on the medial side of the adjacent wing. The wings are thick, almost straight in lateral view, and have no ridge on the outer surface. Around the adjacent jaw edge, the wings are constricted and bend medially. The anterior edge of the wings is superposed on a jaw edge in the frontal view. The wing angle is obtuse.

Description. The rostrum is of moderate size and width (Fig. 7F, G, and J). The jaw edges are almost straight at their ventral part and form a relatively strong hook on the rostral tip (Fig. 7F and G). Thin shoulder blades are discernible only around the ventral end of the bridges. The shoulder blades are connected to a bridge and the thickened ridge on the medial side of the adjacent wing (Fig. 7I). The bridges are entirely exposed, ventrally tapered, and posterolaterally inclined (Fig. 7I). High wing folds extend at an angle of ~30° with the adjacent jaw edge and are continuous with a fold, extending from the rostral hook. These folds form a somewhat deep dent around the jaw edges (Fig. 7F and G). Thickened wings are constricted and bend medially around the adjacent jaw edge (Fig. 7F and G). The anterior edge of the wings is almost straight in lateral view (Fig. 7F and G) and superposed on a jaw edge in frontal view (Fig. 7J). The degree of the wing angle is obtuse. The hood is relatively long (Fig. 7M). The lateral walls show a somewhat elongated trapezoidal shape (Fig. 7F and G).

Comparison. This species differs from *T. pulchellus* sp. nov. and *T. acutus* sp. nov. by a wider rostrum (this species: $1.08 \leq \mathrm{LRL/RW} \leq 1.16$, *T. pulchellus* sp. nov.: $1.29 \leq \mathrm{LRL/RW} \leq 1.47$, *T. acutus* sp. nov.: $\mathrm{LRL/RW} > 2.00$; Fig. 7J, O, and T, and Table 3). The rostral width is a significantly valuable character that reflects species-level differences in extant squid beaks[19].

Occurrence. Early Cenomanian to Late Campanian; Yezo Group in Hokkaido, Japan.

Thalassasboides pulchellus sp. nov.

Fig. 7K–O

Etymology. Latin ‘pulchellus’ (beautiful).

Material. NMNS_DS00068_pBrzD5i.stl, NMNS_DS00173_CLt5m2t.stl, NMNS_DS00173_8IkQbCV.stl, NMNS_DS00173_27C5zir.stl, NMNS_DS00081_V85MVoY.stl, and NMNS_DS00104_GDb7t8w.stl (https://doi.org/10.25452/figshare.plus.25736631).

Diagnosis. The rostrum is moderately large, narrow, and strongly hooked. It has dents surrounded by a low fold extending from the hook. The bridges are entirely exposed, ventrally tapered, and smoothly connected with the groove medial to the neighbouring wing fold. The wing folds are high, extending at an acute angle with the adjacent jaw edge. The shoulder blades are thin and weakly developed. The shoulder blades are connected to a bridge and the thickened ridge on the medial side of the adjacent wing. The wings are thick, almost straight in lateral view, and have no ridge on the outer surface. Around the adjacent jaw edge, the wings are constricted and bend medially. The anterior edge of the wings is superposed on a jaw edge in frontal view. The wing angle is obtuse.

Description. The rostrum is of moderate size and narrow (Fig. 7K, L, and O). The jaw edges are almost straight at their ventral part and form a relatively strong hook on the rostral tip (Fig. 7K and L). Thin

shoulder blades are discernible only around the ventral end of the bridges. The shoulder blades are connected to a bridge and the thickened ridge on the medial side of the adjacent wing (Fig. 7N). The bridges are entirely exposed, ventrally tapered, and posterolaterally inclined (Fig. 7N). High wing folds extend at an angle of ~30° with the adjacent jaw edge and are continuous with a low fold, extending from the rostral hook. These folds form a somewhat deep dent around the jaw edges (Fig. 7K and L). Thickened wings are constricted and bend medially around the adjacent jaw edge (Fig. 7K and L). The anterior edge of the wings is almost straight in lateral view (Fig. 7K and L) and superposed on a jaw edge in the frontal view (Fig. 7O). The degree of the wing angle is obtuse. The hood is relatively long (Fig. 7M). The lateral walls show a somewhat elongated trapezoidal shape (Fig. 7K and L).
Comparison. The rostrum of this species is narrower than that of *T. watatsumi* sp. nov. and wider than that of *T. acutus* sp. nov. (this species: $1.29 \leq \text{LRL/RW} \leq 1.47$, *T. watatsumi* sp. nov.: $1.08 \leq \text{LRL/RW} \leq 1.16$, *T. acutus* sp. nov.: $\text{LRL/RW} > 2.00$; Fig. 7J, O, and T, and Table 3).
Occurrence. earliest Cenomanian and Santonian; Yezo Group in Hokkaido, Japan.

Thalassasboides acutus sp. nov.
Fig. 7P–T
Etymology. Latin 'acutus' (acute).
Material. NMNS_DS00173_w8T3Zp0.stl (https://doi.org/10.25452/figshare.plus.25736631).
Diagnosis. The rostrum is moderately large, very narrow, and strongly hooked. It has dents surrounded by a low fold extending from the hook. The bridges are entirely exposed, ventrally tapered, and smoothly connected with the groove medial to the neighbouring wing fold. The wing folds are high, extending at an acute angle with the adjacent jaw edge. The shoulder blades are thin and weakly developed. The shoulder blades are connected to a bridge and the thickened ridge on the medial side of the adjacent wing. The wings are thick, almost straight in lateral view, and have no ridge on the outer surface. Around the adjacent jaw edge, the wings are constricted and bend medially. The anterior edge of the wings is superposed on a jaw edge in frontal view. The wing angle is obtuse.
Description. The rostrum is of moderate size and very narrow (Fig. 7P, Q, and T). The jaw edges are almost straight at their ventral part and form a relatively strong hook on the rostral tip (Fig. 7P and Q). Thin shoulder blades are discernible only around the ventral end of the bridges. The shoulder blades are connected to a bridge and the thickened ridge on the medial side of the adjacent wing (Fig. 7S). The bridges are entirely exposed, ventrally tapered, and posterolaterally inclined (Fig. 7S). High wing folds extend at an angle of ~30° with the adjacent jaw edge and are continuous with a low fold, extending from the rostral hook. These folds form a somewhat deep dent around jaw edges (Fig. 7P and Q). Thickened wings are constricted and bend medially around the adjacent jaw edge (Fig. 7P and Q). The anterior edge of the wings is almost straight in lateral view (Fig. 7P and Q) and superposed on a jaw edge in the frontal view (Fig. 7T). The degree of the wing angle is obtuse. The hood is relatively long (Fig. 7R).
Comparison. This species has a narrower rostrum than the other two species of *Thalassasboides* gen. nov. (this species: $\text{LRL/RW} > 2.00$, *T. watatsumi* sp. nov.: $1.08 \leq \text{LRL/RW} \leq 1.16$, *T. pulchellus* sp. nov.: $1.29 \leq \text{LRL/RW} \leq 1.47$; Fig. 7J, O, and T, and Table 3).
Occurrence. Late Turonian; Yezo Group in Hokkaido, Japan.

Genus ***Pseudovampyroteuthis*** gen. nov.
Etymology. Ancient Greek 'pseudes' (false) and *Vampyroteuthis*, the vampire squid.

Type species. *Pseudovampyroteuthis hecate* sp. nov.
Diagnosis. The rostrum is small, moderately wide, and not hooked. It has narrow, faint dents surrounded by a low fold. The bridges are entirely exposed, equal in width, and smoothly connected with the groove medial to the neighbouring wing fold. The wing folds are high, extending at an acute angle with the adjacent jaw edge. The shoulder blades are faintly developed. The wings are thick, almost straight in lateral view, and have no ridge on the outer surface. Around the adjacent jaw edge, the wings are constricted and bend medially. The anterior edge of the wings is superposed on a jaw edge in the frontal view. The wing angle is obtuse.
Comparison. The rostral hook of this genus is not discernible (Fig. 7U and V), unlike the other genera of the Pachypteroteuthidae fam. nov. This genus differs from *Pachypteroteuthis* gen. nov. by having no ridges on the wings (Figs. 6K and 7U). It can be discriminated from *Catantopteryx* gen. nov. by the acuter wing angle (Fig. 7A and U) and from *Gerontoteuthis* gen. nov. by the significantly wider rostrum (Figs. 7Y and 8J). This genus can be distinguished from *Thalassasboides* gen. nov., *Astathogephyra* gen. nov., *Sepultipons* gen. nov., and *Aspasmoteuthis* gen. nov. by the smaller rostrum (Figs. 7F and U, 8K, and 9A and P). The angle between the crest and jaw edges of this genus are blunter than those in *Orthoteuthis* gen. nov. (Figs. 7U and 8A) and acuter than in *Juroteuthis* gen. nov. (Figs. 7U and 9U).
Occurrence. earliest Cenomanian; Yezo Group in Hokkaido, Japan.

Pseudovampyroteuthis hecate sp. nov.
Fig. 7U–Y
Etymology. After Hecate, a deity of the underworld in Greek mythology.
Material. NMNS_DS00068_gNqH3RQ.stl (https://doi.org/10.25452/figshare.plus.25736631).
Diagnosis. Same as for the genus.
Description. The rostrum is small, moderately wide, not hooked, and has narrow, faint dents surrounded by a low fold (Fig. 7U, V, and Y). The remnants of the shoulder blades can be observed around the ventral end of the bridges (Fig. 7X). The bridges are entirely exposed, equal in width, and almost parallel to the transverse axis in horizontal sections of the ventral part (Fig. 7X). High wing folds slightly extend posterior to the jaw edges (Fig. 7U and V). The wing folds form an angle of ~30° with the adjacent jaw edge. Thickened wings are constricted and bend medially around the adjacent jaw edge (Fig. 7U and V). The anterior edge of the wings is almost straight in lateral view (Fig. 7U and V) and superposed on a jaw edge in the frontal view (Fig. 7Y). The degree of the wing angle is obtuse. The hood is relatively long (Fig. 7W).
Occurrence. earliest Cenomanian; Yezo Group in Hokkaido, Japan.

Genus ***Orthoteuthis*** gen. nov.
Etymology. Ancient Greek ‘orthos’ (upright), referring to the upturned rostrum, and ‘teuthis’ (squid).
Type species. *Orthoteuthis subaru* sp. nov.
Diagnosis. The rostrum is small, moderately wide, and slightly hooked. It has dents surrounded by a low fold extending from the hook. The bridges are entirely exposed and observable in the ventral two-thirds of the jaw edge, including the potential jaw edge extension. The bridges are broadest at their midpoint. The angle between the crest and the jaw edges is fairly acute. Ridges are absent on the wings.
Comparison. This genus differs from *Pachypteroteuthis* gen. nov., *Catantopteryx* gen. nov., *Pseudovampyroteuthis* gen. nov., *Juroteuthis* gen. nov. by the acuter angle between the crest and the

jaw edges (~50° in lateral view of this genus; Figs. 6Q, 7A and U, 8A, and 9U). Compared with *Gerontoteuthis* gen. nov., it shows a significantly wider rostrum (Fig. 8E and J). It can be distinguished from the other genera of the Pachypteroteuthidae fam. nov. by the smaller rostrum (Figs. 7F, 8B, and 9A and P).
Occurrence. Late Coniacian; Yezo Group in Hokkaido, Japan.

Orthoteuthis subaru sp. nov.
Fig. 8A–E
Etymology. After the Subaru Telescope, referring to the upturned rostrum.
Material. NMNS_DS00083_UA2WR3Z.stl (https://doi.org/10.25452/figshare.plus.25736631).
Diagnosis. Same as for the genus.
Description. The rostrum shows a small size, moderate width, and a faint hook (Fig. 8A, B, and E). The faint folds extending from the rostral hook form a dent around the jaw edges. The jaw edges form a fairly acute angle (~50° in lateral view) with the crest (Fig. 8A and B). The shoulder blades are not discernible (Fig. 8D). The bridges are entirely exposed, they are observable in the ventral two-thirds of the jaw edges (including the potential jaw edge extension). The bridges have the broadest point on their midpoint and taper off ventrally from that point (Fig. 8D). The horizontal sections of the bridges are nearly parallel to the transverse axis. The wings exhibit no ridges around their basal part (Fig. 8B).
Occurrence. Late Coniacian; Yezo Group in Hokkaido, Japan.

Genus ***Gerontoteuthis*** gen. nov.
Etymology. Ancient Greek ‘geron’ (old man), referring to the curved crest, and ‘teuthis’ (squid).
Type species. *Gerontoteuthis acutissimus* sp. nov.
Diagnosis. The rostrum is small, very narrow, and hooked. It has dents surrounded by a low fold, extending from the hook to a wing fold. The ventral part of the bridges is gradually covered by the shoulder from the lateral side and smoothly connected with the groove medial to the neighbouring wing fold. The wing folds are high, extending at an acute angle with the adjacent jaw edge. The shoulder blades are distinct, but their dorsal margin is ambiguous. The anterior edge of the shoulder blades directly merges with that of the adjacent wing. The wings are thick, almost straight in lateral view, and have no ridge on the outer surface. Around the adjacent jaw edge, the wings are constricted and bend medially. The anterior edge of the wings is superposed on a jaw edge in the frontal view. The wing angle is obtuse.
Comparison. A small rostrum is also seen in *Pachypteroteuthis* gen. nov., *Catantopteryx* gen. nov., *Pseudovampyroteuthis* gen. nov., and *Orthoteuthis* gen. nov. (Figs. 6K, 7A and U, and 8A and F). The very narrow rostrum is in common with a species of *Thalassasboides* gen. nov. (Figs. 7T and 8J), and developed shoulder blades with the ambiguous dorsal margin occur in a species of *Pachypteroteuthis* gen. nov. (Figs. 6X and 8I). *Gerontoteuthis* can be clearly distinguished from all other genera of the Pachypteroteuthidae fam. nov. by the small and very narrow rostrum.
Occurrence. earliest Cenomanian; Yezo Group in Hokkaido, Japan.

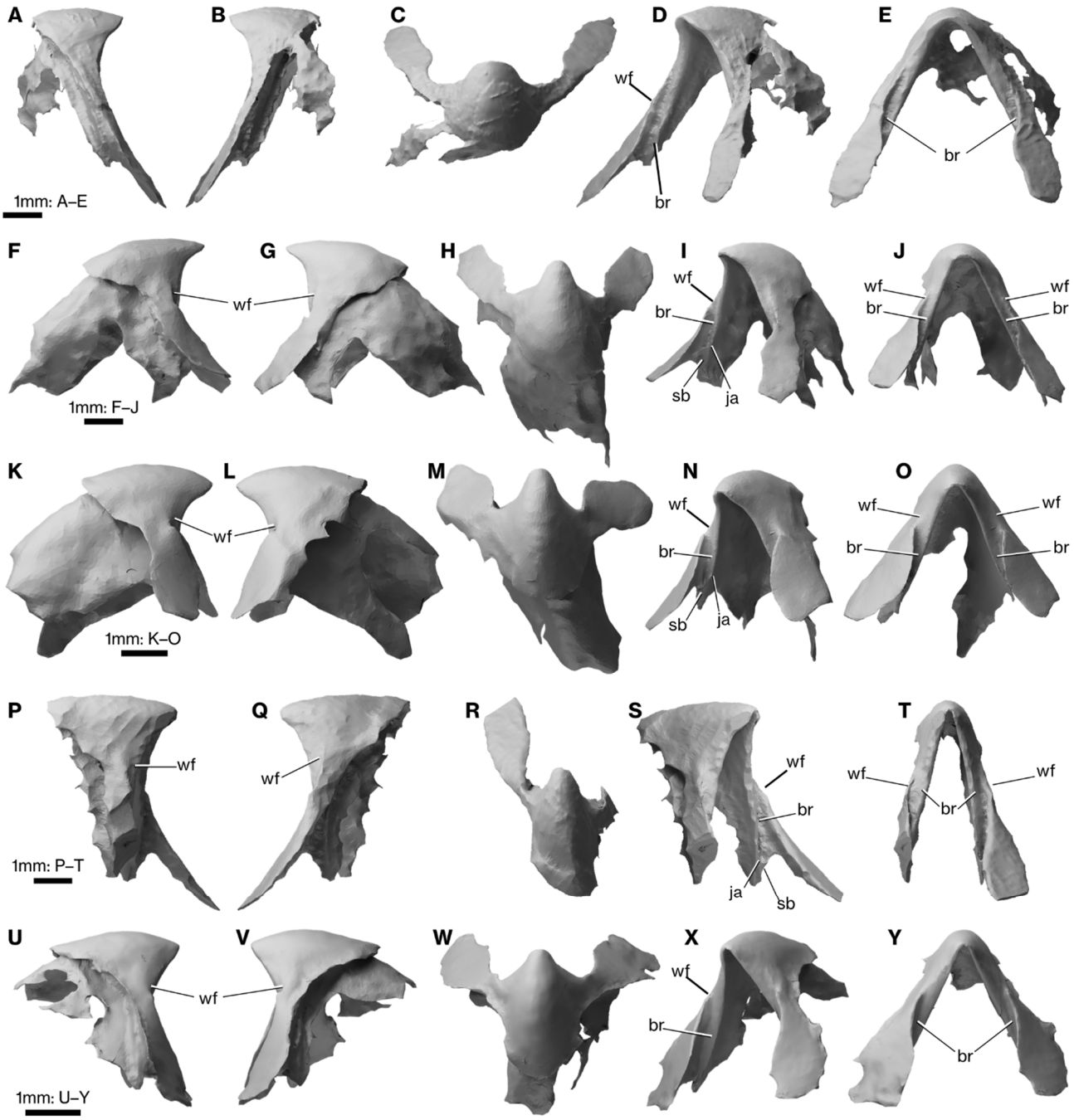


Fig. 7. Lower beaks of *Catantopteryx*, *Thalassasboides*, and *Pseudovampyroteuthis*. (**A** to **E**) *Catantopteryx altilis* sp. nov., NMNS_DS00082_tntK5pM.stl. (**F** to **J**) *Thalassasboides watatsumi* sp. nov., NMNS_DS00082_ev6tAaJ.stl. (**K** to **O**) *Thalassasboides pulchellus* sp. nov., NMNS_DS00068_pBrzD5i.stl. (**P** to **T**) *Thalassasboides acutus* sp. nov., NMNS_DS00173_w8T3Zp0.stl. (**U** to **Y**) *Pseudovampyroteuthis hecate* sp. nov., NMNS_DS00068_gNqH3RQ.stl. (A, F, K, P, and U) left lateral view; (B, G, L, Q, and V) right lateral view; (C, H, M, R, and W) dorsal view; (D, I, N, S, and X) oblique view; (E, J, O, T, and Y) frontal view. The 3D models are available from Figshare+ (https://doi.org/10.25452/figshare.plus.25736631). Abbreviations: br, bridge; ja, jaw angle; sb, shoulder blade; wf, wing fold.

Gerontoteuthis acutissimus sp. nov.
Fig. 8F–J
Etymology. superlative degree of the Latin ‘acutus’ (acute).
Material. NMNS_DS00068_6MhIFUS.stl (https://doi.org/10.25452/figshare.plus.25736631).
Diagnosis. Same as for the genus.
Description. The rostrum is small, very narrow, and hooked (Fig. 8F, G, and J). The bridges exhibit a slight posterolateral inclination. The ventral part of bridges is gradually covered up from the lateral side by a shoulder and completely blanketed around the midpoint of a shoulder (Fig. 8I). Distinct shoulder blades are smoothly connected to a lateral wall and do not exhibit a clear dorsal margin (Fig. 8I). Thickened wings are constricted and bend medially around the adjacent jaw edge (Fig. 8F and G). High wing folds extend at an acute angle with the adjacent jaw edge and are continuous with a low fold, extending from the rostral hook. These folds form a dent around the jaw edges (Fig. 8F and G). The degree of the wing angle is obtuse. The hood is moderately long (Fig. 8H). The lateral walls are slightly longer than high, have a strongly curved crest, and show a parallelogram shape (Fig. 8F and G).
Comparison. The ventral part of the bridges, gradually being covered by a shoulder from the lateral side is also seen in *Pachypteroteuthis magnus* sp. nov. However, *G. acutissimus* differs by the absence of angular wing ridges, the very narrow rostrum, and a different form of the wings (Figs. 6V and 8G). The very narrow rostrum and the wing form are common traits with *Thalassasboides acutus* sp. nov., but this genus can be distinguished by the developed shoulder blades and the small rostrum (Figs. 7Q and S, and 8G and I).
Occurrence. earliest Cenomanian; Yezo Group in Hokkaido, Japan.

Genus ***Astathogephyra*** gen. nov.
Etymology. Ancient Greek ‘astathis’ (unstable) and ‘gephyra’ (bridge).
Type species. *Astathogephyra metis* sp. nov.
Diagnosis. The size of the rostrum ranges from large to moderate, and the width from narrow to moderate. The rostrum is hooked and has dents surrounded by a low fold extending from the hook to a wing fold. The bridges are entirely exposed, ventrally tapered, and smoothly connected with the groove medial to the neighbouring wing fold. The wing folds extend at an acute angle with the adjacent jaw edge. The shoulder blades are thin. The wings are thick, almost straight in lateral view, and have no ridge on the outer surface. Around the adjacent jaw edge, the wings are constricted and bend medially. The wings are disengaged from the adjacent bridge at their basal part. The ventral part of the wings and the adjacent shoulder blade are connected. The wing angle is obtuse.
Comparison. In other genera of the Pachypteroteuthidae fam. nov., the medial side of the wings (often thickened to form a ridge) is entirely connected to a bridge or a shoulder blade (Figs. 6N, 7D, I, and X, 8I, and 9D and S). This genus can be clearly differentiated from these genera by the middle part of the ridge, which is free from the other pigmented parts (Fig. 8N).
Occurrence. Late Cenomanian to the Late Coniacian strata of Yezo Group.

Astathogephyra metis sp. nov.
Fig. 8K–O
Etymology. After Metis, whose name means ‘wisdom’ in Greek mythology.

Material. NMNS_DS00009_TkD5dWU.stl, NMNS_DS00009_MU8cSC4.stl, and NMNS_DS00083_VCCZZr4.stl (https://doi.org/10.25452/figshare.plus.25736631).

Diagnosis. The rostrum is moderately large, moderately wide, and hooked. It has dents surrounded by a low fold, extending from the hook to a wing fold. The bridges are entirely exposed, ventrally tapered, and smoothly connected with the groove medial to the neighbouring wing fold. High wing folds extend at an acute angle with the adjacent jaw edge. The shoulder blades are thin. The wings are thick, almost straight in lateral view, and have no ridge on the outer surface. Around the adjacent jaw edge, the wings are constricted and bend medially. The wings are disengaged from the adjacent bridge at their basal part. The ventral part of the ridge on the medial side of the wings and the adjacent shoulder blade are connected. The wing angle is obtuse.

Description. The rostrum is of moderate size, moderate width, and a relatively prominent hook (Fig. 8K, L, and O). Thin shoulder blades are discernible only around the ventral end of the bridges (Fig. 8N). The bridges are entirely exposed, ventrally tapered, and posterolaterally inclined (Fig. 8N). High wing folds extend at an angle of ~30° with the adjacent jaw edge and are continuous with a low fold, extending from the rostral hook. These folds form a somewhat deep dent around the jaw edges (Fig. 8K and L). Thickened wings are constricted and bend medially around the adjacent jaw edge (Fig. 8K–M). The anterior edge of the wings is almost straight in lateral view (Fig. 8K) and superposed on a jaw edge in the frontal view (Fig. 8O). The wings have a ridge on their medial side. This ridge is connected to a bridge at its dorsal part and to a shoulder blade at its ventral part (Fig. 8N). The middle part of the ridge is free from the other pigmented parts (Fig. 8N). The degree of the wing angle is obtuse. The hood is relatively long (Fig. 8M). The lateral walls show a somewhat elongated trapezoidal shape (Fig. 8K and L).

Comparison. This species differs from *A. himatium* sp. nov. by the smaller and wider rostrum (Fig. 8L, O, Q, and T), the absence of a dorsally pointed tip on the wings (Fig. 8L and Q), and the narrow rostral dents (Fig. 8L and Q). The size and width of the rostrum are important characters in the species-level identification of extant squid beaks[19].

Occurrence. Middle Turonian to Late Coniacian; Yezo Group in Hokkaido, Japan.

Astathogephyra himatium sp. nov.

Fig. 8P–T

Etymology. A thin clothing of the ancient Greek ‘himation’, referring to the extremely thin lamellae.

Material. NMNS_DS00082_ZxRP3bR.stl (https://doi.org/10.25452/figshare.plus.25736631).

Diagnosis. The rostrum is large, narrow, and hooked. It has dents surrounded by a low fold extending from the hook to the wing fold. The bridges are entirely exposed, ventrally tapered, and smoothly connected with the groove medial to the neighbouring wing fold. The wing folds are relatively low and extend at an acute angle with the adjacent jaw edge. The shoulder blades are thin. The wings are thick, almost straight in lateral view, and have no ridge on the outer surface. Around the adjacent jaw edge, the wings are constricted and bend medially. The wings are disengaged from the adjacent bridge at their basal part. The shoulder blades extend toward the anterior edge of the adjacent wing. The wing angle is obtuse.

Description. The rostrum is large, narrow, and weakly hooked (Fig. 8P, Q, and T). The shoulder blades are thin but distinct (Fig. 8S). The bridges are entirely exposed, ventrally tapered, and posterolaterally inclined (Fig. 8S). Relatively low wing folds extend at an angle of ~30° with the adjacent jaw edge and are continuous with a low fold. They stretch out from the rostral hook. These folds form a large

dent around jaw edges (Fig. 8P and Q). Thin wings bend medially around the adjacent jaw edge (Fig. 8Q and R). The anterior edge of the wings is almost straight in lateral view (Fig. 8Q), superposed on a jaw edge in the frontal view (Fig. 8T), and forms a dorsally pointed tip at a point slightly anterior to a jaw edge (Fig. 8Q). The medial side of the wings is connected to a bridge at the dorsal part and probably to a shoulder blade at the ventral part (Fig. 8S). Its middle part is free from other pigmented parts (Fig. 8S). The degree of the wing angle is obtuse. The hood is relatively long (Fig. 8S). The lateral walls show a somewhat elongated trapezoidal shape (Fig. 8P and Q).
Comparison. This species differs from *A. metis* sp. nov. by the larger and narrower rostrum (Fig. 8L, O, Q, and T), the presence of a dorsally pointed tip on the wings (Fig. 8L and Q), and the very wide rostral dents (Fig. 8L and Q).
Occurrence. Late Cenomanian; Yezo Group in Hokkaido, Japan.

Genus ***Sepultipons*** gen. nov.
Etymology. Latin 'sepultus' (buried) and 'pons' (bridge).
Type species. *Sepultipons castor* sp. nov.
Diagnosis. The rostrum is large or moderate-sized, moderately wide, and strongly hooked. It has dents surrounded by a fold extending from the hook to a wing fold. The bridges taper ventrally and are smoothly connected with the groove medial to the neighbouring wing fold. The wing folds are high and extend at an acute angle with the adjacent jaw edge. The ventral part of the bridges is covered with a massive shoulder. The shoulder blades are distinct and connected to the adjacent wing at their anterior margin. The dorsal edge of the shoulder blades is straight, forming a slightly obtuse angle with a jaw edge. The wings are thick, almost straight in the lateral views, and have no ridge on the outer surface. Around the adjacent jaw edge, the wings are constricted and bend medially. The anterior edge of the wings is superposed on a jaw edge in the frontal view. The wing angle is obtuse.
Comparison. *Gerontoteuthis* gen. nov. and *Pachypteroteuthis magnus* sp. nov. are similar to*Sepultipons* in having the robust shoulders covering the ventral part of a bridge. *Sepultipons* differs from *Gerontoteuthis* and *Pachypteroteuthis* by its shoulder blades with a clear dorsal margin (Figs. 6X, 8I, and 9D) and from the other genera of the Pachypteroteuthidae fam. nov. by the significantly thickened shoulder blades (Figs. 6N, 7D, F, and X, 8D and N, and 9D, S, and X).
Occurrence. Middle Turonian to Early Maastrichtian; Yezo Group in Hokkaido, Japan.

Sepultipons castor sp. nov.
Fig. 9A–E
Etymology. After Castor and Pollux, known as twins in Greek mythology, referring to the highly similar form to *S. pollux* sp. nov. described below.
Material. NMNS_DS00009_vxf2tIr.stl, NMNS_DS00041_b4BWTEx.stl, NMNS_DS00173_bIJ7zso.stl, NMNS_DS00173_f2mBoiP.stl, NMNS_DS00173_BbCw7oa.stl, NMNS_DS00173_UXkxZH5.stl, NMNS_DS00173_001WWW9.stl, NMNS_DS00173_54IvJ9D.stl, NMNS_DS00174_kRFX5Fg.stl, NMNS_DS00174_L1VyDDh.stl, NMNS_DS00174_7H4Gb53.stl, and NMNS_DS00174_jWDHdZ1.stl (https://doi.org/10.25452/figshare.plus.25736631).

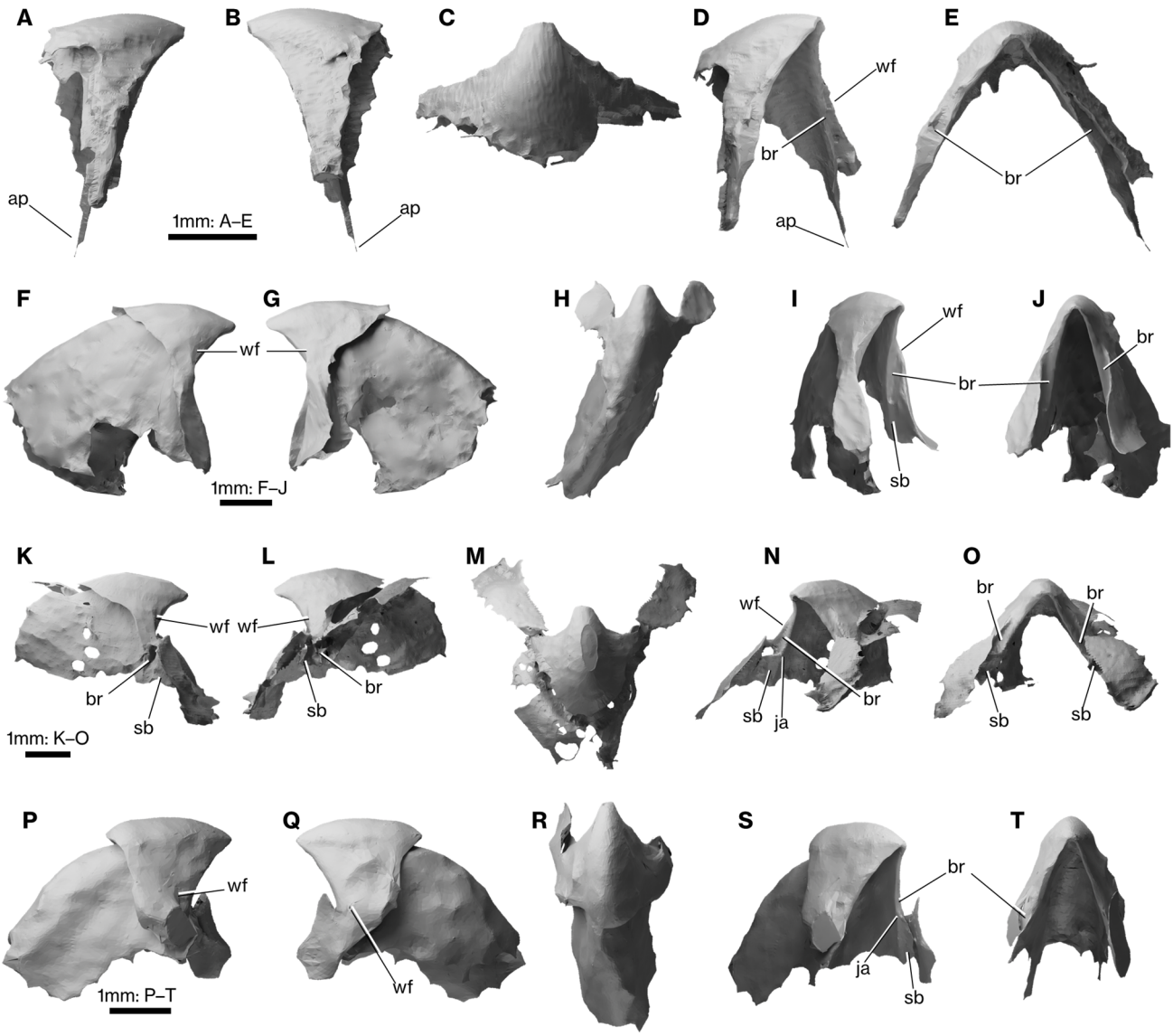


Fig. 8. Lower beaks of *Orthoteuthis*, *Gerontoteuthis*, and *Astathogephyra*.
(**A** to **E**) *Orthoteuthis subaru* sp. nov., NMNS_DS00083_UA2WR3Z.stl. (**F** to **J**) *Gerontoteuthis acutissimus* sp. nov., NMNS_DS00068_6MhIFUS.stl. (**K** to **O**) *Astathogephyra metis* sp. nov., NMNS_DS00009_MU8cSC4.stl. (**P** to **T**) *Astathogephyra himatium* sp. nov., NMNS_DS00082_ZxRP3bR.stl. (A, F, K, and P) left lateral view; (B, G, L, and Q) right lateral view; (C, H, M, and R) dorsal view; (D, I, N, and S) oblique view; (E, J, O, and T) frontal view. The 3D models are available from Figshare+ (https://doi.org/10.25452/figshare.plus.25736631). Abbreviations: ap, anglepoint; br, bridge; ja, jaw angle; sb, shoulder blade; wf, wing fold.

Diagnosis. The rostrum is large or moderate-sized, moderately wide, and strongly hooked. It has dents surrounded by a fold extending from the hook to a wing fold. The bridges taper ventrally and are smoothly connected with the groove medial to the neighbouring wing fold. The wing folds are high and extend at an acute angle with the adjacent jaw edge. The ventral part of the bridges is covered with a massive shoulder. The shoulder blades are distinct and connected to the adjacent wing at their anterior margin. The dorsal edge of the shoulder blades is straight, forming a slightly obtuse angle with a jaw edge. No step exists between the shoulder blades and the adjacent lateral wall. The wings are thick,

almost straight in the lateral views, and have no ridge or dorsally pointed tip on the outer surface. Around the adjacent jaw edge, the wings are constricted and bend medially. The anterior edge of the wings is superposed on a jaw edge in the frontal view. The wing angle is obtuse.

Description. The rostrum is large to moderate-sized, moderately wide, and strongly hooked (Fig. 9A, B, and E). The bridges are ventrally tapered and posterolaterally inclined (Fig. 9D). High wing folds extend at an angle of ~40° with the adjacent jaw edge and are continuous with a low fold, extending from the rostral hook. These folds form a deep dent around the jaw edges (Fig. 9A and B). The shoulders are fully pigmented and cover the ventral part of the bridges (Fig. 9D). The shoulder blades have a straight dorsal edge that forms a slightly obtuse angle with a jaw edge (Fig. 9D). The anterior edge of shoulder blades is connected to that of a wing. The posterior edge of the shoulder blades is smoothly attached to a lateral wall (Fig. 9D). The wing folds and the adjacent shoulder blade are not parallel and form a concave area (Fig. 9D). The wings are thickened, constricted, and bend medially around the adjacent jaw edge (Fig. 9A–C). The anterior edge of the wings is almost straight in the lateral views (Fig. 9A and B) and superposed on a jaw edge in the frontal view (Fig. 9E). The degree of the wing angle is obtuse. The hood is relatively long (Fig. 9C). The lateral walls show a somewhat elongated trapezoidal shape (Fig. 9A and B).

Comparison. This genus can be easily distinguished from *S. pollux* sp. nov. by the absence of a dorsally pointed tip on the wings (Fig. 9B, D, I, and J). It differs from *S. gradus* sp. nov. by the wing folds forming a blunter angle with a jaw edge (Fig. 9A and K) and the absence of a step between the lateral walls and the adjacent shoulder blade (Fig. 9D and N).

Occurrence. Middle Turonian to Early Maastrichtian; Yezo Group in Hokkaido, Japan.

Sepultipons pollux sp. nov.

Fig. 9F–J

Etymology. After Castor and Pollux, known as twins in Greek mythology, referring to the highly similar form to *S. castor* sp. nov.

Material. NMNS_DS00040_e0mxqWi.stl, NMNS_DS00173_JvLSs02.stl, and NMNS_DS00083_qxUALq6.stl (https://doi.org/10.25452/figshare.plus.25736631).

Diagnosis. The rostrum is large or moderate-sized, moderately wide, and strongly hooked. It has dents surrounded by a fold extending from the hook to a wing fold. The bridges taper ventrally and are smoothly connected with the groove medial to the neighbouring wing fold. The wing folds are high and extend at an acute angle with the adjacent jaw edge. The ventral part of the bridges is covered with a massive shoulder. The shoulder blades are distinct and connected to the adjacent wing at their anterior margin. The dorsal edge of the shoulder blades is straight, forming a slightly obtuse angle with a jaw edge. No step exists between the shoulder blades and the adjacent lateral wall. The wings are thick, almost straight in the lateral views, and have no ridge on the outer surface. A dorsally pointed tip exists on the basal part of the wings. Around the adjacent jaw edge, the wings are constricted and bend medially. The anterior edge of the wings is superposed on a jaw edge in the frontal view. The wing angle is obtuse.

Description. The rostrum is large to moderate-sized, moderately wide, and strongly hooked (Fig. 9F, G, and J). The bridges are ventrally tapered and posterolaterally inclined (Fig. 9I). High wing folds extend at an angle of ~40° with the adjacent jaw edge and are continuous with a low fold, extending from the rostral hook. These folds form a deep dent around the jaw edges (Fig. 9G). The shoulders are fully pigmented and cover the ventral part of a bridge (Fig. 9I). The shoulder blades have a straight

dorsal edge that forms a slightly obtuse angle with a jaw edge (Fig. 9I). The anterior edge of the shoulder blades is connected to a thickened wing. The posterior edge of the shoulder blades is smoothly attached to a lateral wall (Fig. 9I). The wing folds and the adjacent shoulder blade are not parallel and form a concave area (Fig. 9I). The wings are constricted and bend medially around the adjacent jaw edge (Fig. 9G and H). A dorsally pointed small tip exists on the basal part of the wings. The anterior edge of the wings is almost straight in the lateral view (Fig. 9G) and superposed on a jaw edge in the frontal view (Fig. 9J). The degree of the wing angle is obtuse. The hood is relatively long (Fig. 9H). The lateral walls show a somewhat elongated trapezoidal shape (Fig. 9G).

Comparison. This species shows remarkable similarity to *S. castor* sp. nov., but the former has an acute tip on the basal part of the wings (Fig. 9B, D, I, and J). It markedly differs from *S. gradus* sp. nov. by the wing folds forming a blunter angle with a jaw edge (Fig. 9G and K) and no step between the lateral walls and the adjacent shoulder blade (Fig. 9I and N).

Occurrence. Late Turonian and Late Coniacian; Yezo Group in Hokkaido, Japan.

Sepultipons gradus sp. nov.

Fig. 9K–O

Etymology. Latin 'gradus' (step).

Material. NMNS_DS00173_h0qQoNN.stl, NMNS_DS00083_3h8PCFD.stl, NMNS_DS00128_oRE3wgv.stl, and NMNS_DS00174_Nu50pFy.stl (https://doi.org/10.25452/figshare.plus.25736631).

Diagnosis. The rostrum is large to moderate-sized, moderately wide, and strongly hooked. It has very narrow dents surrounded by a fold extending from the hook to the wing fold. The bridges taper ventrally and are smoothly connected with the groove medial to the neighbouring wing fold. The wing folds are high and extend at an acute angle with the adjacent jaw edge. The ventral part of the bridges is covered with a massive shoulder. The shoulder blades are distinct and connected to the adjacent wing at their anterior margin. The dorsal edge of the shoulder blades is straight, forming a slightly obtuse angle with a jaw edge. A low step exists between the shoulder blades and the adjacent lateral wall. The wings are thick, almost straight in the lateral views, and have no ridge or dorsally pointed tip on the outer surface. Around the adjacent jaw edge, the wings are constricted and bend medially. The anterior edge of the wings is superposed on a jaw edge in the frontal view. The wing angle is obtuse.

Description. The rostrum is large to moderate-sized, moderately wide, and strongly hooked (Fig. 9K, L, and O). The bridges are ventrally tapered and posterolaterally inclined (Fig. 9N). High wing folds extend at a very acute angle with the adjacent jaw edge and are continuous with a low fold, extending from the rostral hook. These folds form a very narrow dent around the jaw edges (Fig. 9K and L). The shoulders are fully pigmented and cover the ventral part of a bridge (Fig. 9N). The shoulder blades have a straight dorsal edge that forms a nearly perpendicular or somewhat acute angle with a jaw edge (Fig. 9N). The anterior edge of shoulder blades is connected to a thickened wing. The posterior edge of shoulder blades is attached to a lateral wall, forming a low step between them (Fig. 9N). The wing folds and the adjacent shoulder blade are not parallel and form a concave area between them (Fig. 9N). The wings are constricted and bend medially around the adjacent jaw edge (Fig. 9K, L, and M). The anterior edge of the wings is almost straight in the lateral views (Fig. 9K and L) and superposed on a jaw edge in the frontal view (Fig. 9O). The degree of the wing angle is obtuse (Fig. 9K and L). The hood of moderate length has no notch (Fig. 9M). The lateral walls show an elongated trapezoidal shape

and a slightly curved crest (Fig. 9K and L).
Comparison. This species can be easily distinguished from *S. pollux* sp. nov. and *S. castor* sp. nov. by the wing folds forming an acuter angle with the jaw edge (Fig. 9A, G, and K) and a low step between the lateral walls and the adjacent shoulder blade (Fig. 9D, I, and N).
Occurrence. Late Turonian to Early Maastrichtian; Yezo Group in Hokkaido, Japan.

Genus ***Aspasmoteuthis*** gen. nov.
Etymology. Ancient Greek 'aspasmos' (embrace), referring to the relatively strong medial curve of wings, and 'teuthis' (squid).
Type species. *Aspasmoteuthis peltatus* sp. nov.
Diagnosis. The rostrum is moderately large, moderately wide, and strongly hooked. It has large dents surrounded by a low fold extending from the hook to a wing fold. The bridges are entirely exposed, equal in width, and smoothly connected with the groove medial to the neighbouring wing fold. The wing folds are high, extending at an acute angle with the adjacent jaw edge. The shoulder blades are not discernible. The wings are thick, almost straight in the lateral views, and have no ridge on the outer surface. Around the adjacent jaw edge, the wings are constricted and bend medially. The anterior edge of the wings is superposed on a jaw edge in the frontal view. The wing angle is obtuse.
Comparison. *Pachypteroteuthis* gen. nov., *Catantopteryx* gen. nov., *Pseudovampyroteuthis* gen. nov., and *Orthoteuthis* gen. nov. also have bridges of equal width, but these genera do not show the large rostral dents formed by a developed wing fold as in *Aspasmoteuthis* (Figs. 6K, 7A and U, 8B, and 9P). *Aspasmoteuthis* differs from *Thalassasboides* gen. nov. and *Sepultipons* gen. nov. by the bridges being of equal width and the absence of the developed shoulder blades (Figs. 7I, and 9D and S). The major differences to *Astathogephyra* gen. nov. are the bridges that show a much weaker combination with a wing (Figs. 8N and 9S).
Occurrence. Early Coniacian; Yezo Group in Hokkaido, Japan.

Aspasmoteuthis peltatus sp. nov.
Fig. 9P–T
Etymology. Latin 'peltatus' (shield-bearing), referring to the shield-like form of wings.
Material. NMNS_DS00034_OJDNCD8.stl (https://doi.org/10.25452/figshare.plus.25736631).
Diagnosis. Same as for the genus.
Description. The rostrum shows moderate size and width (Fig. 9P, Q, and T). It has a strong hook and large dents surrounded by a fold extending from the hook to a shoulder (Fig. 9P and Q). The shoulder blades are not discernible (Fig. 9S). The bridges are entirely exposed, equal in width, and show strong posterolateral inclination (Fig. 9S). High wing folds extend at an angle of ~45° with the adjacent jaw edge (Fig. 9P and Q). The wings are thickened, constricted, and bend medially around the adjacent jaw edge (Fig. 9P, Q, and R). The anterior edge of the wings is almost straight in the lateral views (Fig. 9P and Q) and superposed on a jaw edge in the frontal view (Fig. 9T). The degree of the wing angle is obtuse. The hood is moderately long (Fig. 9R).
Occurrence. Early Coniacian; Yezo Group in Hokkaido, Japan.

Genus ***Juroteuthis*** gen. nov.
Etymology. After Jurojin, a god of fortune in Japanese mythology with elongated head, referring to the hood that looks posteriorly elongated.

Type species. *Juroteuthis arrectus* sp. nov.
Diagnosis. The rostrum is moderately wide and strongly hooked. It has very deep dents surrounded by a fold extending from the hook to the outer edge of the bridges. The bridges are entirely exposed and ventrally tapered. The shoulder blades are thin and very weakly developed. The jaw edges extend nearly perpendicular to the crest.
Comparison. This genus differs from all other genera of the Pachypteroteuthidae fam. nov. by its extraordinarily deep rostral dents (Figs. 6O, 7E, J, and Y, 8E, J, and O, and 9E, T, and Y) and the jaw edges extending perpendicularly to the crest (Figs. 6K, 7A, F, and U, 8A, F, and K, and 9A, P, and V).
Occurrence. Late Turonian to Early Coniacian; Yezo Group in Hokkaido, Japan.

Juroteuthis arrectus sp. nov.
Fig. 9U–Y
Etymology. Latin 'arrectus' (perpendicular), referring to jaw edges extending vertically.
Material. NMNS_DS00173_X7NQkzW.stl, NMNS_DS00173_IHj1roq.stl, and NMNS_DS00034_MDF4xvB.stl (https://doi.org/10.25452/figshare.plus.25736631).
Diagnosis. Same as for the genus.
Description. The rostrum shows moderate width, a strong hook, and very deep dents surrounded by a subangular margin (Fig. 9U, V, and Y). Its size is probably moderate, inferred from the possible wing folds. Very weak shoulder blades may exist on the ventral one-third of the jaw edges (including jaw edge extension). The bridges are entirely exposed, ventrally tapered, and show strong posterolateral inclination (Fig. 9X). The ventral part of the jaw edges is almost straight and perpendicular to the crest and the dorsal margin of the dents (Fig. 9U and V). The hood of moderate length has no notch (Fig. 9W).
Occurrence. Late Turonian to Early Coniacian; Yezo Group in Hokkaido, Japan.

Family **Scuthoteuthidae** fam. nov.
Type genus. *Scuthoteuthis* gen. nov.
Diagnosis. The size of the rostrum ranges from moderate to large, and its width from very narrow to moderate. The jaw edges are single-edged. The bridges are significantly reduced. The jaw angles are angular. The shoulder blades are directly connected to a wing at their anterior margin. The wings are less well-developed than the shoulder blades.
Comparison. All taxa of the Scuthoteuthidae have developed shoulder blades that form an angular jaw angle (Fig. 9D). The dorsal to anterior margins of the shoulder blades is typically connected to that of the adjacent wing (Fig. 10L). The bridges do not reach the ventral end of the lateral walls. Below the jaw angles, the bridges are often covered up with a complex of a shoulder and a wing (Fig. 10B). A groove or fold on the outer lamella might be present along them. The Scuthoteuthidae can be attributed the order Oegopsida due to the clear separation between the lateral walls and the adjacent shoulder blade marked by a bridge (Fig. 10B). The shoulder blades with similar forms are also seen in some taxa of the Haboroteuthidae fam. nov., but the Scuthoteuthidae can be distinguished from those taxa by the single-edged rostrum (Figs. 5E and 10E). The Scuthoteuthidae differ from the Pachypteroteuthidae fam. nov. by the shoulder blades that are more developed than the wings (Figs. 6N and 10D). Difference from the Paleothysanoteuthidae fam. nov. is the ventral part of the jaw edges, which is not posteriorly curved (Figs. 10B and 11K). The Scuthoteuthidae show a similar form of the shoulders and wings with

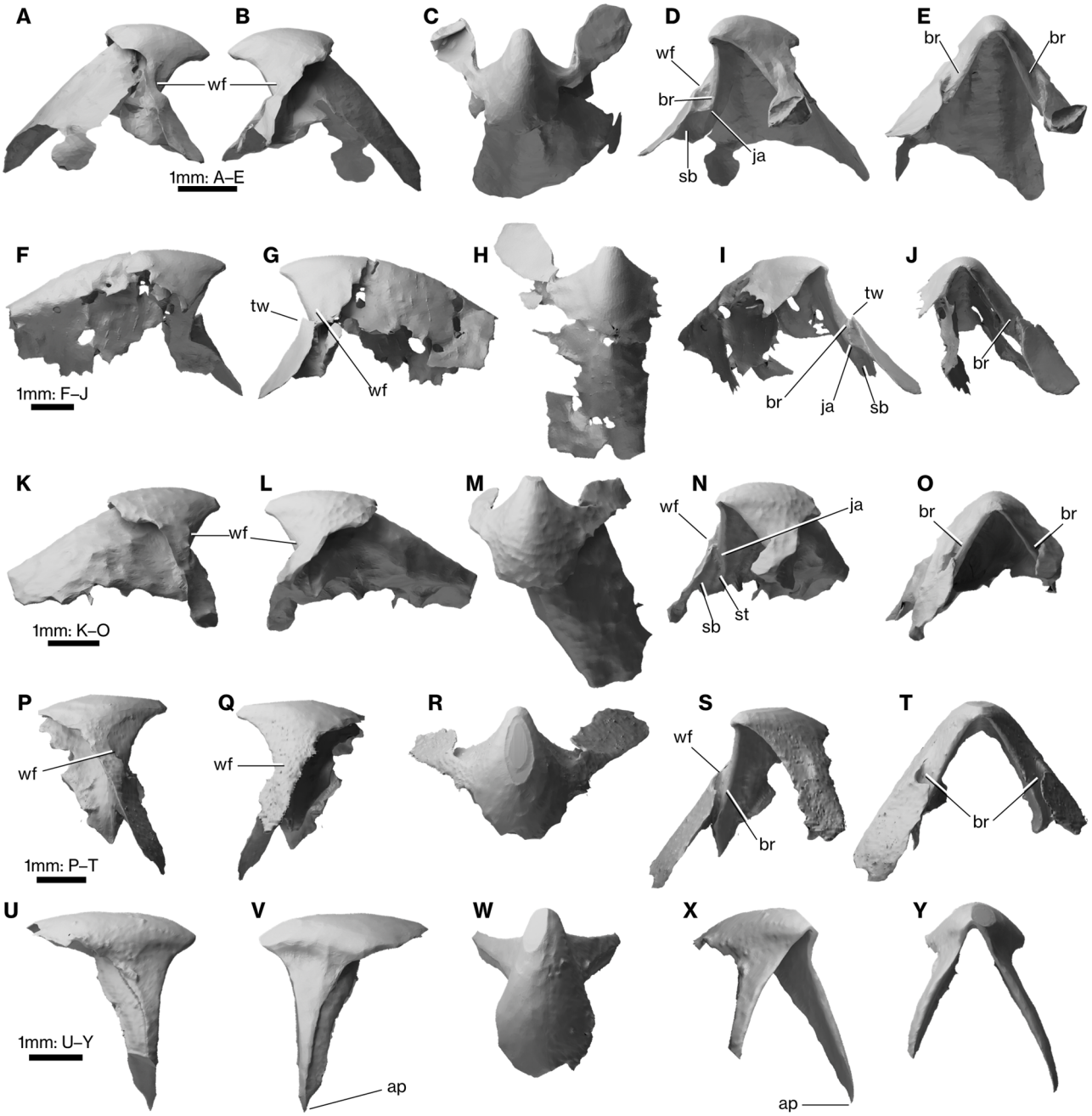


Fig. 9. Lower beaks of *Sepultipons*, *Aspasmoteuthis*, and *Juroteuthis*.
(**A** to **E**) *Sepultipons castor* sp. nov., NMNS_DS00009_vxf2tIr.stl. (**F** to **J**) *Sepultipons pollux* sp. nov., NMNS_DS00040_e0mxqWi.stl. (**K** to **O**) *Sepultipons gradus* sp. nov., NMNS_DS00174_Nu50pFy.stl. (**P** to **T**) *Aspasmoteuthis peltatus* sp. nov., NMNS_DS00034_OJDNCD8.stl. (**U** to **Y**) *Juroteuthis arrectus* sp. nov., NMNS_DS00034_MDF4xvB.stl. (A, F, K, P, and U) left lateral view; (B, G, L, Q, and V) right lateral view; (C, H, M, R, and W) dorsal view; (D, I, N, S, and X) oblique view; (E, J, O, T, and Y) frontal view. The 3D models are available from Figshare+ (https://doi.org/10.25452/figshare.plus.25736631). Abbreviations: ap, anglepoint; br, bridge; ja, jaw angle; sb, shoulder blade; st, step between a shoulder blade and a lateral wall; tw, a dorsally pointed tip on a wing; wf, wing fold.

extant oegopsids families, the Lepidoteuthidae and the Octopoteuthidae[19]. The Scuthoteuthidae differ by the bridges that remarkably extend below the jaw angles (Fig. 10B).

Genus ***Scuthoteuthis*** gen. nov.
Etymology. Ancient Greek 'skuthes' (scythe) and 'teuthis' (squid).
Type species. *Scuthoteuthis kawataro* sp. nov.
Diagnosis. The size of the rostrum ranges from moderate to large, and its width from very narrow to moderate. The rostrum is strongly projected toward the front. The jaw edges are single-edged. The bridges are significantly reduced. The jaw angles are angular. The shoulder blades are directly connected to a wing at their anterior and dorsal margins. The wings are less developed than the shoulder blades.
Comparison. This genus can be distinguished from *Grossiscapula* gen. nov. by the absence of the shoulder planes (Fig. 10D and X) and from *Amblyscuthes* gen. nov. by the strong anterior projection of the rostrum (Figs. 10A and 11A).
Occurrence. Early Cenomanian to Late Campanian; Yezo Group in Hokkaido, Japan.

Scuthoteuthis kawataro sp. nov.
Fig. 10A–E
Etymology. After Kawataro, a reptiloid in Japanese folklore whose beak shows a similar form to the rostrum of this species.
Material. NMNS_DS00084_XCCa3MD.stl (https://doi.org/10.25452/figshare.plus.25736631).
Diagnosis. The rostrum is large, narrow, and strongly projected toward the front. The rostral hook and dents are absent. The jaw edges are single-edged. The bridges are short and covered by a thick complex of a wing and a shoulder. A groove on the outer lamella exists along the bridges. The angle between the jaw edges and the adjacent shoulder blade is fairly acute. The shoulder blades are directly connected to a wing at their anterior and dorsal margins. The wings are less developed than the shoulder blades and strongly curve downward.
Description. The rostrum is large, narrow, and strongly projected toward the front. It has no hooks or dents (Fig. 10A, B, and E). The jaw edges are sharp, single-edged, and gently curved. The angle between a jaw edge and the adjacent shoulder blade is fairly acute (Fig. 10A, B, and D). The dorsal parts of the shoulder blades and the adjacent wing merge directly and form a somewhat thickened complex, which tapers laterally (Fig. 10A, B, and D). The bridges are entirely covered up with this complex and form a groove on the outer lamella (Fig. 10A, B, and D). The dorsal edge of the wings extends anteriorly in its basal part and then strongly curves downward (Fig. 10A and B). A posterodorsally curved fold might be present around the jaw angles. The hood is relatively long, not notched, and almost entirely merged with the inner lamella (Fig. 10C).
Comparison. The angle between a jaw edge and the adjacent shoulder blade of this species is significantly acuter than in other species of *Scuthoteuthis* gen. nov. (AJS is 56.0° in *S. kawataro*, > 80.0° in all other species; Fig. 10B, G, L, and Q, and Table 3). The rostrum of *S. kawataro* is wider than in *S. falcatus* sp. nov. and narrower than in *S. tenuis* sp. nov. (*S. kawataro*: LRL/RW = 1.28, *S. falcatus*: LRL/RW ≥ 1.42, *S. tenuis*: LRL/RW = 0.90; Fig. 10E, J, O, and T, and Table 3). The rostral width is a significantly valuable character that reflects species-level differences in extant squid beaks[19].
Occurrence. Early Cenomanian; Yezo Group in Hokkaido, Japan.

Scuthoteuthis fragilis sp. nov.
Fig. 10F–J
Etymology. Latin 'fragilis' (fragile), referring to the severely deformed state of the holotype.
Material. NMNS_DS00182_VHJhp0K.stl (https://doi.org/10.25452/figshare.plus.25736631).
Diagnosis. The rostrum is large, strongly hooked, and strongly projected toward the front. It has large dents bordered by a fold extending from the rostral hook. The jaw edges are single-edged. The shoulders are thin and smoothly connected to the neighbouring lateral wall. The dorsal part of the shoulders directly merges with that of the adjacent wing. The shoulder blades are thin. Traces of bridges exist around the jaw angles as a small step on the outer lamella. The wings are thin and less well-developed than the shoulder blades.
Description. The rostrum is large, strongly hooked, and strongly projected toward the front (Fig. 10F, G, and J). Its width is presumably somewhat narrow. The jaw edges are sharp, single-edged, and almost straight. The dorsal part of the shoulders directly merges with that of the adjacent wing and forms a probably perpendicular angle with a jaw edge (Fig. 10J). The wings and shoulders are thin, but the wings are less developed. Below the jaw angles, a short bridge is observable as a low step on the outer lamella extending along the neighbouring jaw edge extension (Fig. 10G). A fold extends from the jaw angles, forming an angle of ~30° with the adjacent jaw edge (Fig. 10G). The rostrum has large and deep dents surrounded by this fold and an extension of the rostral hook (Fig. 10F and G). The hood notch is absent (Fig. 10H). The lateral walls are longer than high (Fig. 10F and G).
Comparison. This species can be distinguished from the other species of *Scuthoteuthis* gen. nov. by the well-developed rostral dents and the very short bridges (Fig. 10B, G, L, and Q). The size of the adult beaks exceeds 5 mm in LRL, which is currently the second largest species among the Late Cretaceous squids, next to *Haboroteuthis poseidon*[35] (Table 3).
Occurrence. Late Campanian; Yezo Group in Hokkaido, Japan.

Scuthoteuthis falcatus sp. nov.
Fig. 10K–O
Etymology. Latin 'falcatus' (sickle-shaped), referring to the rostrum morphology.
Material. NMNS_DS00046_Tf7vfru.stl, NMNS_DS00089_cdL9i2R.stl, NMNS_DS00090_uJIwH0a.stl (https://doi.org/10.25452/figshare.plus.25736631).
Diagnosis. The rostrum is large, very narrow, and strongly projected toward the front. The rostral hook and dents are absent. The jaw edges are single-edged. The bridges are narrow, extending around the midpoint of the shoulder blade, and covered by a thin complex of a wing and a shoulder. A low step on the outer lamella exists along the bridges. The angle between the jaw edges and the adjacent shoulder blade is almost perpendicular. The shoulder blades are directly connected to a wing at their anterior and dorsal margins. The wings are less developed than the shoulder blades and strongly curve downward.
Description. The rostrum is large, very narrow, and strongly projected toward the front. It has no hook or dents (Fig. 10K, L, and O). The jaw edges are sharp, single-edged, and gently curved. The shoulder blades are thin but distinct (Fig. 10N). The angle between a jaw edge and the adjacent shoulder blade is almost perpendicular (Fig. 10N). The dorsal half of the shoulder blades merges with the adjacent wing to form a thin complex, which tapers laterally (Fig. 10L and N). Narrow bridges are entirely covered with this complex and form a low step on the outer lamella (Fig. 10K and L). The dorsal edges of the wings extend anteriorly in its basal part and then strongly curve downward (Fig. 10K and L).

The hood is relatively long and mostly merged with the inner lamella (Fig. 10M).
Comparison. This species differs from other species of *Scuthoteuthis* gen. nov. by the very narrow rostrum (LRL/RW is more than 1.42 in this species while it is less than 1.28 in the other ones; Fig. 10E, J, O, and T, and Table 3).
Occurrence. Late Turonian to Santonian; Yezo Group in Hokkaido, Japan.

Scuthoteuthis tenuis sp. nov.
Fig. 10P–T
Etymology. Latin 'tenuis' (thin).
Material. NMNS_DS00083_wMN7Xl9.stl (https://doi.org/10.25452/figshare.plus.25736631).
Diagnosis. The rostrum is moderately large, moderately narrow, slightly hooked, and strongly projected toward the front. The rostral dents are absent. The jaw edges are single-edged. The bridges are narrow, extending around the midpoint of the shoulder blade, and covered by a thin complex of a wing and a shoulder. A low step on the outer lamella exists along the bridges. The angle between the jaw edges and the adjacent shoulder blade is obtuse. The shoulder blades are directly connected to a wing at their anterior and dorsal margins. The wings are less well-developed than the shoulder blades and gently curve downward.
Description. The rostrum is moderately large, moderately wide, and strongly projected toward the front. It has a faint hook and no dents (Fig. 10P, Q, and T). The jaw edges are sharp, single-edged, and gently curved. The shoulder blades are thin but distinct (Fig. 10S). The angle between a jaw edge and the adjacent shoulder blade is obtuse. The dorsal half of the shoulder blades merges with the adjacent wing to form a thin complex, which tapers laterally (Fig. 10P, Q, and S). Narrow bridges are entirely covered up with this complex and form a low step on the outer lamella (Fig. 10P, Q, and S). The dorsal edges of the wings gently curve downward (Fig. 10P and Q). The hood has a fairly deep notch (Fig. 10R).
Comparison. This species can be distinguished from the other species of *Scuthoteuthis* gen. nov. by the deep hood notch (Fig. 10C, H, M, and R) and the rostrum of moderate size and width (LRL/RW is less than 0.90 in this species while it is more than 1.28 in the other ones; Fig. 10E, J, O, and T, and Table 3).
Occurrence. Late Coniacian; Yezo Group in Hokkaido, Japan.

Genus ***Grossiscapula*** gen. nov.
Etymology. Latin 'grossus' (thick) and 'scapula' (shoulder blade).
Type species. *Grossiscapula angusta* sp. nov.
Diagnosis. The rostrum is large, narrow, and strongly projected toward the front. It has a distinct hook and no dents. The jaw edges are single-edged and form an angle of ~45° with a wing fold around the jaw angles. The bridges abruptly taper below the jaw angles. The shoulder blades are directly connected to a wing at their anterior margin. The dorsal part of the shoulder blades is thick. A broad plane exists in the shoulders, separated by an angular wing fold and the dorsal margin of a shoulder blade. The jaw angles are angular. The angle between the jaw edges and the adjacent shoulder blade is almost perpendicular. The wings are thin and constricted around the jaw angles.
Comparison. This genus differs from *Scuthoteuthis* gen. nov. and *Amblyscuthes* gen. nov. by the well-developed shoulder planes (Figs. 10D and X, and 11D). The shoulder planes, surrounded by angular boundaries, are also seen in the genera *Pachygephyra* gen. nov. and *Placomoteuthis* gen. nov. Both

genera differ from *Grossiscapula* gen. nov. by the broader and smaller rostrum, the double jaw edges, and the absence of the wing folds (Figs. 5R, 6J, and 10Y).
Occurrence. Early Maastrichtian; Yezo Group in Hokkaido, Japan.

Grossiscapula angusta sp. nov.
Fig. 10U–Y
Etymology. Latin 'angustus' (narrow).
Material. NMNS_DS00172_cWN9lDD.stl (https://doi.org/10.25452/figshare.plus.25736631).
Diagnosis. Same as for the genus.
Description. The rostrum is large, narrow, and strongly projected toward the front. It has a distinct hook and no dents (Fig. 10U, V, and Y). The jaw edges are single-edged and gently curved. The bridges abruptly taper off below the jaw angles (Fig. 10U and V). Low, angular wing folds extend at ~45° with the adjacent jaw edge around a jaw angle and curve posterodorsally (Fig. 10U and V). The wing folds and the dorsal margin of the adjacent shoulder blade border thick shoulder planes (Fig. 10X). The angle between a jaw edge and the adjacent shoulder blade is almost perpendicular. The wing angle is somewhat obtuse. The shoulder blades are smoothly connected with a lateral wall and thickened around their anterior margin (Fig. 10X). The wings are thin, constricted around a jaw angle, and not ornamented with ridges (Fig. 10U and V). The hood is of moderate length and has no notch (Fig. 10W). The lateral walls are as long as high (Fig. 10U and V).
Occurrence. Early Maastrichtian; Yezo Group in Hokkaido, Japan.

Genus ***Amblyscuthes*** gen. nov.
Etymology. Ancient Greek 'amblys' (blunt) and 'skuthes' (scythe), referring to the less projected rostrum.
Type species. *Amblyscuthes apterus* sp. nov.

Diagnosis. The rostrum is large, hooked, and moderately projected toward the front. The width of the rostrum ranges from narrow to very narrow. The jaw edges are single-edged. The shoulders are thin, distinct, and smoothly connected to a lateral wall. The dorsal part of the shoulder blades is directly connected to the neighbouring wing. The angle between the jaw edges and the adjacent shoulder blade is almost perpendicular or slightly obtuse. The wings are less developed than the shoulder blades. The bridges are narrow, extending around the midpoint of the adjacent shoulder blade, and covered by a thin wing-shoulder complex. A low step exists on the outer lamella along the bridges.
Comparison. *Amblyscuthes* gen. nov. differs from *Scuthoteuthis* gen. nov. by the less projected rostrum (Figs. 10A and 11A) and from *Grossiscapula* gen. nov. by the absence of the developed shoulder planes (Figs. 10X and 11D).
Occurrence. Early Cenomanian to Early Campanian; Yezo Group in Hokkaido, Japan.

Amblyscuthes apterus sp. nov.
Fig. 11A–E
Etymology. Ancient Greek prefix 'a-' (-less) and 'pteryx' (wing).
Material. NMNS_DS00082_9VBER8O.stl and NMNS_DS00175_1oEjNpv.stl (https://doi.org/10.25452/figshare.plus.25736631).

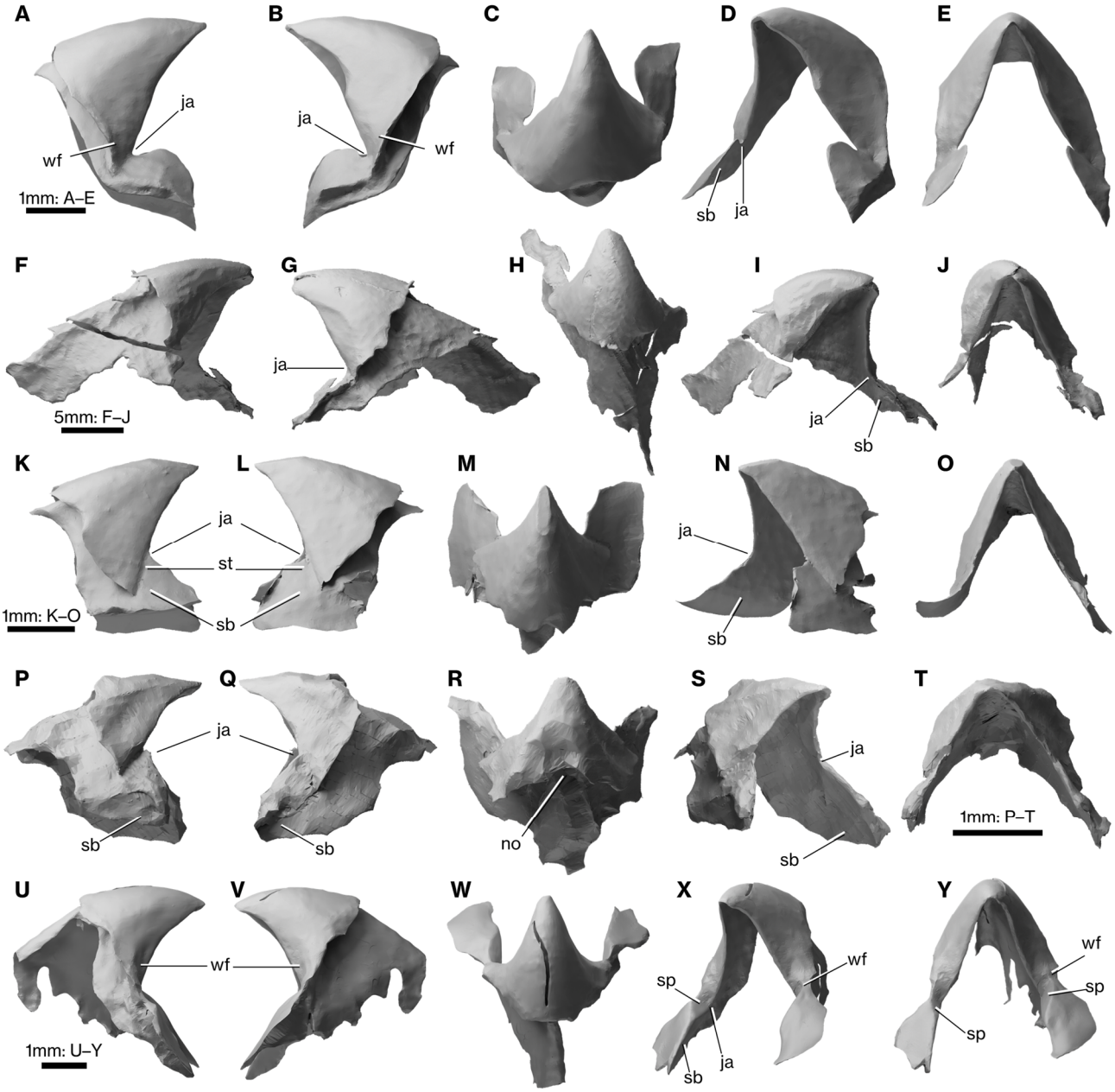


Fig. 10. Lower beaks of *Scuthoteuthis* and *Grossiscapula*.
(**A** to **E**) *Scuthoteuthis kawataro* sp. nov., NMNS_DS00084_XCCa3MD.stl. (**F** to **J**) *Scuthoteuthis fragilis* sp. nov., NMNS_DS00182_VHJhp0K.stl. (**K** to **O**) *Scuthoteuthis falcatus* sp. nov., NMNS_DS00090_uJIwH0a.stl. (**P** to **T**) *Scuthoteuthis tenuis* sp. nov., NMNS_DS00083_wMN7Xl9.stl. (**U** to **Y**) *Grossiscapula angusta* sp. nov., NMNS_DS00172_cWN9lDD.stl. (A, F, K, P, and U) left lateral view; (B, G, L, Q, and V) right lateral view; (C, H, M, R, and W) dorsal view; (D, I, N, S, and X) oblique view; (E, J, O, T, and Y) frontal view. The 3D models are available from Figshare+ (https://doi.org/10.25452/figshare.plus.25736631). Abbreviations: ja, jaw angle; no, hood notch; sb, shoulder blade; sp, shoulder plane; st, step around a jaw edge extension; wf, wing fold.

Diagnosis. The rostrum is large, narrow, hooked, and moderately projected toward the front. The jaw edges are single-edged. The shoulders are thin, distinct, and smoothly connected to a lateral wall. The dorsal part of the shoulder blades is directly connected to the neighbouring wing. The angle between the jaw edges and the adjacent shoulder blade is almost perpendicular or slightly obtuse. The wings are less developed than the shoulder blades. The bridges are narrow, extending around the midpoint of the adjacent shoulder blade, and covered by a thin wing-shoulder complex. A low step exists on the outer lamella along the bridges.

Description. The rostrum is large, narrow, hooked, moderately projected toward the front, and has no dents (Fig. 11A, B, and E). The jaw edges are sharp, single-edged, and gently curved. The shoulder blades are thin but distinct (Fig. 11D). The angle between a jaw edge and the adjacent shoulder blade is obtuse. The dorsal half of the shoulder blades merges with the adjacent wing, forming a thin complex, which tapers laterally (Fig. 11A and B). Narrow bridges are entirely covered with this complex (Fig. 11D) and form a low step on the outer lamella (Fig. 11A, B, and C). The dorsal edges of the wings extend anteriorly in its basal part and then strongly curve downward (Fig. 11A and B).

Comparison. This species differs from *A. pyrgoides* sp. nov. by the wider rostrum (LRL/RW is 1.29 in this species while it is more than 1.63 in *A. pyrgoides* sp. nov.; Fig. 11E and J, and Table 3). The rostral width strongly reflects species-level differences in extant squids[19].

Occurrence. Late Cenomanian to Early Campanian; Yezo Group in Hokkaido, Japan.

Amblyscuthes pyrgoides sp. nov.

Fig. 11F–J

Etymology. Ancient Greek ‘pyrgos’ (tower) and suffix ‘-eides’ (-like).

Material. NMNS_DS00084_0iYtIfF.stl, NMNS_DS00046_ikc7ZzK.stl, NMNS_DS00083_hbPNRL6.stl, NMNS_DS00097_bizU8mn.stl, and NMNS_DS00175_nhUN0gO.stl (https://doi.org/10.25452/figshare.plus.25736631).

Diagnosis. The rostrum is large, very narrow, hooked, and moderately projected toward the front. The jaw edges are single-edged. The shoulders are thin, distinct, and smoothly connected to the lateral wall. The dorsal part of the shoulder blades is directly connected to the neighbouring wing. The angle between the jaw edges and the adjacent shoulder blade is slightly obtuse. The wings are less well-developed than the shoulder blades. The bridges are narrow, extending around the midpoint of the adjacent shoulder blade, and covered by a thin wing-shoulder complex. A low step exists on the outer lamella along the bridges.

Description. The rostrum is large, very narrow, hooked, moderately projected toward the front, and has no dents (Fig. 11F, G, and J). The jaw edges are sharp, single-edged, and gently curved. The shoulder blades are thin but distinct (Fig. 11I). The angle between a jaw edge and the adjacent shoulder blade is obtuse. The dorsal half of the shoulder blades merges with the adjacent wing, forming a thin complex, which tapers laterally (Fig. 11F and G). Narrow bridges are entirely covered with this complex (Fig. 11I) and form a low step on the outer lamella (Fig. 11F, G, and H). The dorsal edges of the wings extend anteriorly in its basal part and then strongly curve downward (Fig. 11F and G).

Comparison. This species differs from *A. apterus* sp. nov. by the narrower rostrum (LRL/RW is 1.63 to 2.36 in this species while it is 1.29 in *A. apterus* sp. nov.; Fig. 11E and J, and Table 3).

Occurrence. Early Cenomanian to Early Campanian; Yezo Group in Hokkaido, Japan.

Family **Paleothysanoteuthidae** fam. nov.

Type genus. *Paleothysanoteuthis* gen. nov.
Diagnosis. The size of the rostrum ranges from moderate to large, and its width from moderate to narrow. The rostrum is strongly projected toward the front. The bridges are significantly reduced. The jaw edges are single-edged and posteriorly curved. The ventral part of the jaw edges may be in contact with the dorsal edge of a shoulder blade. The jaw angles are recessed. The distinct shoulder blades are directly connected to the adjacent wing at the anterior and dorsal margins. The wings are thin, dorsally convex, and form a low wing fold.
Comparison. This family can be distinguished from the other extinct oegopsid families by the jaw edges that curve posteriorly around a jaw angle (Fig. 11K). In extant oegopsid families, these jaw edges are only present in the Thysanoteuthidae. In the Paleothysanoteuthidae fam. nov. the jaw edges curve, however, strongly above the jaw angles, forming a deeply recessed jaw angle.

Genus ***Paleothysanoteuthis*** gen. nov.
Etymology. Ancient Greek 'palaios' (ancient) and *Thysanoteuthis*, the diamond squid.
Type species. *Paleothysanoteuthis complicatus* sp. nov.
Diagnosis. The rostrum is moderate-sized or large, moderately wide, and strongly projected toward the front. The rostral hook and dents are absent. The bridges are significantly reduced. The jaw edges are single-edged and posteriorly curved. The ventral part of the jaw edges is adjacent or occasionally in contact with the dorsal edge of a shoulder blade. The jaw angles are recessed. The distinct shoulder blades are directly connected to the adjacent wing at the anterior and dorsal margins, forming a thin, large complex. The wings are thin, dorsally convex, and more developed than the shoulder blades. A dorsally pointed subangular tip exists on the dorsal margin of the wings. The inflecting point of the jaw edges is slightly posterior to this tip. The low wing folds extend from the jaw angles perpendicular to the dorsal margin of the nearest shoulder blade. The wing folds bend abruptly toward the dorsal tip of the nearest wing at the jaw angles.
Comparison. This genus clearly differs from *Aetorhynchus* gen. nov. by the smaller rostrum without a hook or dents, the sharp jaw angles, and the almost straight wing folds (Fig. 11K, Q, and V). The beak morphology of *Paleothysanoteuthis* gen. nov. is similar to that of the extant genera *Thysanoteuthis* and *Architeuthis*, with respect to the rostrum and the wings[19]. *Paleothysanoteuthis* gen. nov. differs, however, by the jaw edges that curve more strongly above jaw angles, forming a deeply recessed jaw angle (Fig. 11K, P, and Q).
Occurrence. Santonian; Yezo Group in Hokkaido, Japan.

Paleothysanoteuthis complicatus sp. nov.
Fig. 11K–T
Etymology. Latin 'complicatus' (folded up), referring to the recessed jaw angles.
Material. NMNS_DS00090_uO7uJwu.stl and NMNS_DS00104_ZNFObG0.stl (https://doi.org/10.25452/figshare.plus.25736631).
Diagnosis. Same as for the genus.
Description. The rostrum is moderately wide and strongly projected toward the front. It has no hooks or dents (Fig. 11K, L, P, Q, and O). The size of the rostrum might be moderate to somewhat large, inferred from shoulder form. The jaw edges are sharp, single-edged, almost straight in the dorsal part, and posteriorly curved in the ventral part (Fig. 11K, P, and Q). The ventral part of the jaw edges extends parallelly to, or even is in contact with the dorsal edge of the adjacent shoulder blade. The jaw angles

are deeply recessed (Fig. 11K, P, and Q). The bridges are not discernible, but weak anglepoints are present (Fig. 11N and S). The dorsal part of the shoulders merges directly with that of the neighbouring wing, forming a thin and large complex (Fig. 11M and R). The shoulder blades are weakly developed (Fig. 11N and S). The wings are relatively broad and form a subangular tip on their dorsal edge (Fig. 11K, P, and Q). This tip is somewhat anterior to the inflexion point of the jaw edges. From the jaw angles, a low wing fold runs perpendicularly to the dorsal margin of the nearest shoulder blade (Fig. 11K, P, and Q). It curves abruptly toward the dorsal tip of the nearest wing at a jaw angle.
Occurrence. Santonian; Yezo Group in Hokkaido, Japan.

Genus ***Aetorhynchus*** gen. nov.
Etymology. Ancient Greek 'aetos' (eagle) and 'rhynkhos' (beak).
Type species. *Aetorhynchus incisus* sp. nov.
Diagnosis. The rostrum is large, narrow, strongly hooked, and strongly projected toward the front. It has large dents bordered by a fold extending from the rostral hook to a wing fold. The bridges are significantly reduced, extend around the midpoint of the shoulder blades, and detach from the adjacent wing below the jaw angles. The jaw edges are single-edged and posteriorly curved. The jaw angles are recessed and rounded. The thick, distinct shoulder blades are directly connected to the adjacent wing at the anterior and dorsal margins, forming a thin, large complex. The wings are thin, dorsally convex, and less well-developed than the shoulder blades. The wings gently curve downward at a point slightly anterior to the inflecting point of the jaw edges. The broad wing folds extend posterodorsally from the anterior part of the wings. The wing folds curve slightly around the jaw angles and run nearly perpendicular to the ventral part of the adjacent jaw edges.
Comparison. This genus markedly differs from *Paleothysanoteuthis* gen. nov. by the larger rostrum, the strong rostral hook, the large rostral dents, the rounded jaw angles, and the wing folds that curve gently around the jaw angle (Fig. 11K, Q, and V).
Occurrence. earliest Cenomanian; Yezo Group in Hokkaido, Japan.

Aetorhynchus incisus sp. nov.
Fig. 11U–Y
Etymology. Latin 'incisus' (carved), referring to recessed jaw angles.
Material. NMNS_DS00068_z6nASvr.stl (https://doi.org/10.25452/figshare.plus.25736631).
Diagnosis. Same as for the genus.
Description. The rostrum is large, narrow, strongly hooked, and strongly projected toward the front (Fig. 11U, V, and Y). Large rostral dents are bordered by a fold extending from the hook to a wing fold (Fig. 11V). The jaw edges are sharp, single-edged, and posteriorly curved in the ventral part. The jaw angles are deeply recessed and rounded (Fig. 11V). The bridges abruptly taper off below the jaw angles (Fig. 11V). The shoulder blades merge directly with the adjacent wing at their dorsal part, forming a thin, large complex (Fig. 11V and X). The shoulder blades are thick. The wings are weakly developed. The anterior edge of wings gently curves downward, and its inflecting point is somewhat anterior to that of the jaw edges (Fig. 11V). Slightly curved wing folds rise from the anterior part of wings and run almost perpendicular to the recessed part of the nearest jaw edge (Fig. 11V). The hood is moderately long (Fig. 11W).
Occurrence. earliest Cenomanian; Yezo Group in Hokkaido, Japan.

Order **Myopsida** d'Orbigny, 1841

Remarks. The lower beak of myopsids can be distinguished from the order Oegopsida by the ambiguous boundary between the shoulder blades and the adjacent lateral wall[17]. It can be discriminated from the extant order Sepiida by the presence of the jaw angles, from the Sepiolida by the absence of rostral dents, and from the Spirulida by the remarkably less curved jaw edges[17]. The fossil myopsids in this study are identified based on these characters.

Family **Loliginidae** Lesueur, 1821

Remarks. The Loliginidae comprises all genera and species in the extant myopsids except for *Australiteuthis aldrichi*[40]. They show the following characters for the lower beak[19]. The rostrum is moderately wide and slightly hooked; the rostral dents, bridges, and anglepoints are not discernible; the jaw edges are sharp, single-edged, and gently curved; the dorsal parts of the shoulders and wings merge directly, form a subrounded jaw angle, and gently curve downward; the angle between a jaw edge and the adjacent shoulder blade is obtuse or nearly perpendicular; the boundary between the shoulder blades and the adjacent lateral wall is ambiguous; the wings are thin, form no or a low wing fold, and have no angular ridges. The newly erected genera *Psiloteuthis* gen. nov., *Streptopteryx* gen. nov., and *Camptoteuthis* gen. nov. are referable to the Loliginidae since they show the same characters in the jaw edges, jaw angles, shoulders, and ornamentations on the outer lamella (Figs. 12A and 13A and K). The lower beak of this family differs from beaks of the family Australiteuthidae, another known family of the Myopsida, by the absence of the serration in the jaw edges and shoulders[40] (Fig. 12A).

Genus ***Psiloteuthis*** gen. nov.

Etymology. Ancient Greek 'psilos' (smooth) and 'teuthis' (squid).

Type species. *Psiloteuthis naucrates* sp. nov.

Diagnosis. The rostrum is slightly hooked. The width of the rostrum ranges from moderate to narrow. The rostral dents, wing folds, bridges, and anglepoints are absent. The jaw angles are subrounded. Theangle between the jaw edges and the adjacent shoulder blade is obtuse. The boundary between the shoulder blades and the adjacent lateral wall is ambiguous. The region around the jaw edge extensions is thick. The wings are thin. The anterior part of the shoulder blades and wings are directly merged and gently curved downward.

Comparison. This genus can be distinguished from *Streptopteryx* gen. nov. and *Camptoteuthis* gen. nov. by the absence of the wing folds (Figs. 12E and 13E and O). It resembles the extant genera of the family Loliginidae, but differs by the presence of thickened parts around jaw edge extensions (Fig. 12K).

Occurrence. earliest Cenomanian to Early Maastrichtian; Yezo Group in Hokkaido, Japan.

Psiloteuthis naucrates sp. nov.

Fig. 12A–E

Etymology. Ancient Greek 'naukrates' (supremacy in the sea).

Material. NMNS_DS00068_uZlnAz0.stl, NMNS_DS00068_tj22YEq.stl, NMNS_DS00068_mb5AJPm.stl, NMNS_DS00084_N272hY0.stl, NMNS_DS00082_fh6e497.stl, NMNS_DS00040_Tt7lr4y.stl, NMNS_DS00040_CN8PI3W.stl, NMNS_DS00040_xQd37Tu.stl, NMNS_DS00040_FgRWr9e.stl, NMNS_DS00173_tRj5kxm.stl, NMNS_DS00083_SKAsE98.stl,

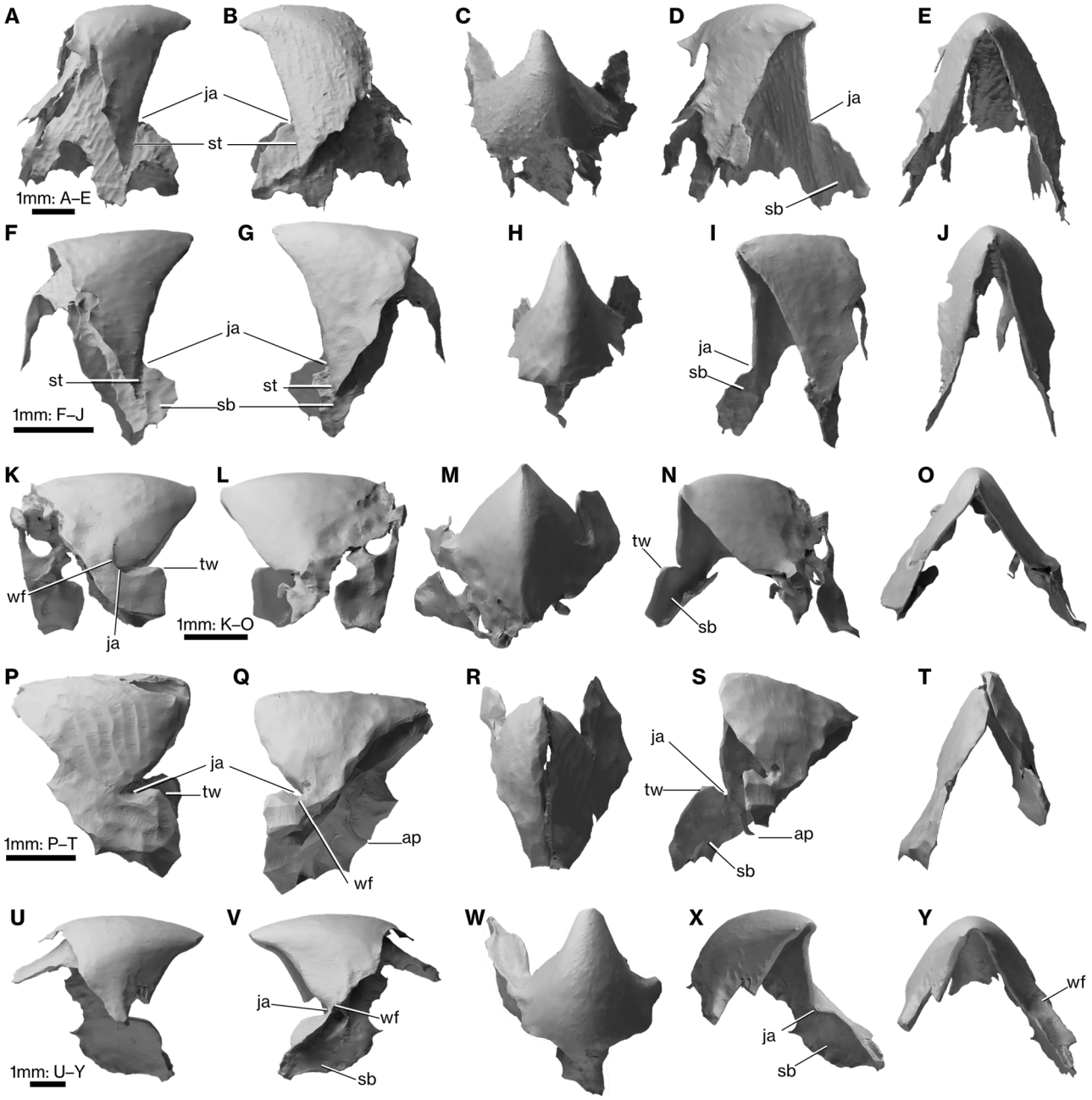


Fig. 11. Lower beaks of *Amblyscuthes*, *Paleothysanoteuthis*, and *Aetorhynchus*. (**A** to **E**) *Amblyscuthes apterus* sp. nov., NMNS_DS00175_1oEjNpv.stl. (**F** to **J**) *Amblyscuthes pyrgoides* sp. nov., NMNS_DS00046_ikc7ZzK.stl. (**K** to **O**) *Paleothysanoteuthis complicatus* sp. nov., NMNS_DS00104_ZNFObG0.stl. (**P** to **T**) *Paleothysanoteuthis complicatus* sp. nov., NMNS_DS00090_uO7uJwu.stl. (**U** to **Y**) *Aetorhynchus incisus* sp. nov., NMNS_DS00068_z6nASvr.stl. (A, F, K, P, and U) left lateral view; (B, G, L, Q, and V) right lateral view; (C, H, M, R, and W) dorsal view; (D, I, N, S, and X) oblique view; (E, J, O, T, and Y) frontal view. The 3D models are available from Figshare+ (https://doi.org/10.25452/figshare.plus.25736631). Abbreviations: ap, anglepoint; ja, jaw angle; sb, shoulder blade; st, step around a jaw edge extension; tw, a dorsally pointed tip on a wing; wf, wing fold.

NMNS_DS00083_XZzD8hv.stl, NMNS_DS00182_oF5mYlz.stl, NMNS_DS00182_UPRVv9A.stl, NMNS_DS00128_NN6zaGU.stl, and NMNS_DS00128_zGiAOX1.stl (https://doi.org/10.25452/figshare.plus.25736631).

Diagnosis. The rostrum is moderately wide and slightly hooked. The rostral dents, wing folds, bridges, and anglepoints are absent. The jaw angles are subrounded. The angle between the jaw edges and the adjacent shoulder blade is obtuse. The boundary between the shoulder blades and the adjacent lateral wall is ambiguous. The region around the jaw edge extensions is thick. No dents or grooves exist on the shoulders. The wings are thin. The anterior part of the shoulder blades and wings are directly merged and gently curved downward.

Description. The rostrum is small to large and moderately wide. It has a faint hook and no dents (Fig. 12A, B, and E). The bridges and anglepoints are not discernible (Fig. 12D). The jaw edges are sharp, single-edged, and gently curved. The dorsal parts of the shoulders and the adjacent wing merge directly, they form a subrounded jaw angle, and gently curve downward (Fig. 12A and B). The angle between the jaw edge and the adjacent shoulder blade is obtuse. The shoulder blades and lateral walls are thickened around the jaw edge extensions, and their boundary is ambiguous (Fig. 12A, B, and D). The wings are thin and have no ridges (Fig. 12A and B). Grooves, dents, or folds are absent from the shoulder parts (Fig. 12D). The hood is moderately long, and the hood notch is not discernible (Fig. 12C). The lateral walls show a somewhat elongated trapezoidal shape (Fig. 12A and B).

Comparison. This species differs from *P. atalante* sp. nov. by the wider rostrum (LRL/RW is 0.88 to 1.02 in this species while it is 1.27 to 1.41 in *P. atalante* sp. nov.; Fig. 12E and J, and Table 3). The rostral width strongly reflects species-level differences in extant squid beaks[19]. It can be clearly distinguished from *P. sculptus* sp. nov. and *P. transitus* sp. nov. by the shoulder parts without grooves or dents (Fig. 12D, N, and S).

Occurrence. earliest Cenomanian to Early Maastrichtian; Yezo Group in Hokkaido, Japan.

Psiloteuthis atalante sp. nov.

Fig. 12F–J

Etymology. After Atalantē, a huntress in Greek mythology, who is known as a fast runner.

Material. NMNS_DS00089_N7pALkd.stl, NMNS_DS00171_R5TOKQL.stl, and NMNS_DS00171_9qzKEcc.stl (https://doi.org/10.25452/figshare.plus.25736631).

Diagnosis. The rostrum is large, narrow, and slightly hooked. The rostral dents, wing folds, bridges, and anglepoints are absent. The jaw angles are subrounded. The angle between the jaw edges and the adjacent shoulder blade is obtuse. The boundary between the shoulder blades and the adjacent lateral wall is ambiguous. The region around the jaw edge extensions is thick. No dents or grooves exist on the shoulders. The wings are thin. The anterior part of the shoulder blades and wings are directly merged and gently curved downward.

Description. The rostrum is large, narrow, slightly hooked, and has no dents (Fig. 12F, G, and J). The bridges and anglepoints are not discernible (Fig. 12I). The jaw edges are sharp, single-edged, and gently curved. The dorsal parts of the shoulders and the adjacent wing merge directly, form a subrounded jaw angle, and gently curve downward (Fig. 12F and G). They occasionally form a large complex. The angle between a jaw edge and the adjacent shoulder blade is obtuse. The shoulder blades and lateral walls are thickened around the jaw edge extensions, and their boundary is ambiguous (Fig. 12F, G, and I). The wings are thin and have no ridges (Fig. 12F and G). Grooves, dents, or folds are absent from the shoulder parts (Fig. 12I). The hood is moderately long, and the hood notch is not

discernible (Fig. 12H).
Comparison. This species differs from *P. naucrates* sp. nov. by the narrower rostrum (LRL/RW is 1.27 to 1.41 in this species while it is 0.88 to 1.02 in *P. naucrates* sp. nov.; Fig. 12E and J, and Table 3). It can be easily distinguished from *P. sculptus* sp. nov. and *P. transitus* sp. nov. by the shoulder parts missing grooves or dents (Fig. 12I, N, and S).
Occurrence. Late Coniacian to Late Campanian; Yezo Group in Hokkaido, Japan.

Psiloteuthis sculptus sp. nov.
Fig. 12K–O
Etymology. Latin 'sculptus' (sculpted), referring to the characteristic dent on wings.
Material. NMNS_DS00171_0gcEN28.stl (https://doi.org/10.25452/figshare.plus.25736631).
Diagnosis. The rostrum is moderately large, moderately wide, slightly hooked, and strongly projected toward the front. Rostral dents, wing folds, bridges, and anglepoints are absent. The jaw angles are subrounded. The angle between the jaw edges and the adjacent shoulder blade is obtuse. The boundary between the shoulder blades and the adjacent lateral wall is ambiguous. The region around the jaw edge extensions is thick. The wings are thin. The anterior part of the shoulder blades and wings are directly merged and almost straight in the lateral views. A short and deep dent exists on the midpoint of the shoulder-wing complexes.
Description. The rostrum shows a moderate size, moderate width, and strong anterior projection (Fig. 12K, L, and O). It might have a small hook, but dents are not discernible. Bridges and anglepoints are not discernible (Fig. 12N). The jaw edges are sharp, single-edged, and slightly curved. The almost straight dorsal parts of the shoulders and the adjacent wing merge directly, form a subrounded jaw angle, and have a short and deep dent on their intermediate point (Fig. 12N and O). The angle between a jaw edge and the adjacent shoulder blade is obtuse. The shoulder blades and lateral walls are thickened around the jaw edge extensions, and their boundary is ambiguous (Fig. 12K, L, and N). The wing folds are absent. The wings are thin and have no ridges (Fig. 12K and L). The hood is moderately long, and the hood notch is not discernible (Fig. 12M). The lateral walls are as long as high and show a trapezoidal shape (Fig. 12K and L).
Comparison. This species clearly differs from all other species of *Psiloteuthis* gen. nov. by the presence of the dent on the shoulders (Fig. 12D, I, N, and S).
Occurrence. Late Campanian; Yezo Group in Hokkaido, Japan.

Psiloteuthis transitus sp. nov.
Fig. 12P–T
Etymology. Latin 'transitus' (transition), referring to the intermediate form between *Psiloteuthis* gen. nov. and *Streptopteryx* gen. nov..
Material. NMNS_DS00171_opgN0Hg.stl (https://doi.org/10.25452/figshare.plus.25736631).
Diagnosis. The rostrum is moderately large, narrow, and slightly hooked. The rostral dents, wing folds, bridges, and anglepoints are absent. The jaw angles are subrounded. The angle between the jaw edges and the adjacent shoulder blade is obtuse. The boundary between the shoulder blades and the adjacent lateral wall is ambiguous. The region around the jaw edge extensions is thick. The wings are thin. The anterior part of the shoulder blades and wings are directly merged and gently curved downward. A shallow groove exists between the anterior edge of the shoulder blades and the adjacent wing.
Description. The rostrum is moderately large, moderately wide, and slightly hooked (Fig. 12P, Q, and

T). The rostral dents, bridges, and anglepoints are not discernible (Fig. 12S). The jaw edges are sharp, single-edged, and slightly curved. The dorsal parts of the shoulders and the adjacent wing merge directly, form a subrounded jaw angle, and gently curve downward (Fig. 12P and Q). The angle between the jaw edge and the adjacent shoulder blade is obtuse. The shoulder blades and lateral walls are thickened around jaw edge extensions, and their boundary is ambiguous (Fig. 12P, Q, and S). The wings are thin and have no ridges (Fig. 12P and Q). A shallow groove exists between the anterior edge of the shoulder blades and the adjacent wing (Fig. 12S). The hood is moderately long, and the hood notch is not discernible (Fig. 12S and T). The lateral walls are somewhat longer than high and show a trapezoidal shape (Fig. 12P and Q).

Comparison. This species can be clearly distinguished from all other species of *Psiloteuthis* gen. nov. by the presence of the groove between the anterior edges of the shoulder blades and the adjacent wing (Fig. 12D, I, N, and S).

Occurrence. Late Campanian; Yezo Group in Hokkaido, Japan.

Genus ***Streptopteryx*** gen. nov.

Etymology. Ancient Greek ‘streptos’ (twisted) and ‘pteryx’ (wing).

Type species. *Streptopteryx glabra* sp. nov.

Diagnosis. The rostrum is moderately wide, slightly hooked, and relatively projected toward the front. The rostral dents, bridges, and anglepoints are absent. The jaw angles are subrounded. The angle between the jaw edges and the adjacent shoulder blade is obtuse or nearly perpendicular. The boundary between the shoulder blades and the adjacent lateral wall is ambiguous. The region around the jaw edge extensions is thick. No dents or grooves exist on the shoulders. The wings are thin. A low wing folds run lateral to the dorsal margin of the shoulder blades without distinctive inflexion around the jaw angles. The anterior part of the shoulder blades and wings are directly merged and gently curved downward.

Comparison. This genus differs from *Psiloteuthis* gen. nov. by the presence of the distinct wing folds (Figs. 12E and 13E). It differs from *Camptoteuthis* gen. nov. by the blunter angle between the crestand jaw edges in the lateral views (this genus ~45°, *Camptoteuthis* gen. nov.: ~30°; Fig. 13A and K).

Occurrence. earliest Cenomanian to Early Maastrichtian; Yezo Group in Hokkaido, Japan.

Streptopteryx glabra sp. nov.

Fig. 13A–E

Etymology. Latin ‘glabrus’ (smooth).

Material. NMNS_DS00068_okmTU54.stl, NMNS_DS00084_Erg3dY7.stl, NMNS_DS00084_pAh4xpP.stl, NMNS_DS00040_OuBYd2G.stl, NMNS_DS00040_fBilvb5.stl, NMNS_DS00173_ACI2D9e.stl, and NMNS_DS00174_6Ga0IDF.stl (https://doi.org/10.25452/figshare.plus.25736631).

Diagnosis. The rostrum is moderately wide, slightly hooked, and relatively projected toward the front. The rostral dents, bridges, and anglepoints are absent. The jaw angles are subrounded. The angle between the jaw edges and the adjacent shoulder blade is obtuse. The boundary between the shoulder blades and the adjacent lateral wall is ambiguous. The region around the jaw edge extensions is thick. The shoulder teeth are absent. The wings are thin. A low wing folds run lateral to the dorsal margin of the shoulder blades without distinct inflexion around the jaw angles. The anterior part of the shoulder blades and wings are directly merged and gently curved downward.

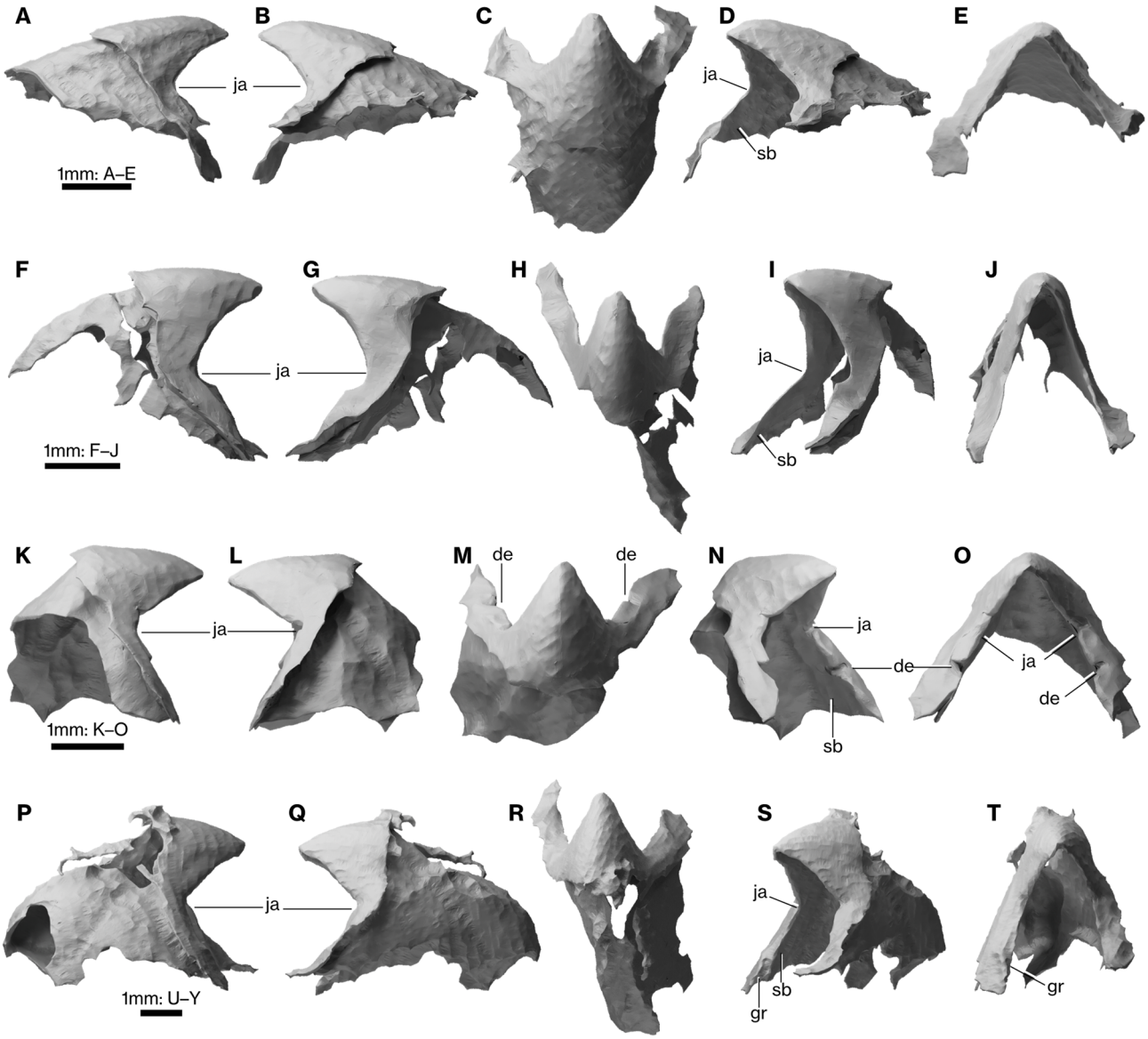


Fig. 12. Lower beaks of *Psiloteuthis*.
(**A** to **E**) *Psiloteuthis naucrates* sp. nov., NMNS_DS00182_UPRVv9A.stl. (**F** to **J**) *Psiloteuthis atalante* sp. nov., NMNS_DS00171_9qzKEcc.stl. (**K** to **O**) *Psiloteuthis sculptus* sp. nov., NMNS_DS00171_0gcEN28.stl. (**P** to **T**) *Psiloteuthis transitus* sp. nov., NMNS_DS00171_opgN0Hg.stl. (A, F, K, and P) left lateral view; (B, G, L, and Q) right lateral view; (C, H, M, and R) dorsal view; (D, I, N, and S) oblique view; (E, J, O, and T) frontal view. The 3D models are available from Figshare+ (https://doi.org/10.25452/figshare.plus.25736631). Abbreviations: de, dent; ja, jaw angle; gr, groove; sb, shoulder blade.

Description. The rostrum is large to moderate-sized, moderately wide, and slightly hooked (Fig. 13A, B, and E). The rostral dents, bridges, and anglepoints are not discernible (Fig. 13D). The jaw edges are sharp, single-edged, and gently curved. The dorsal parts of the shoulders and the adjacent wing merge directly, form a subrounded jaw angle, and gently curve downward (Fig. 13A and B). The angle between a jaw edge and the adjacent shoulder blade is obtuse. The shoulder blades and lateral walls are thickened around jaw edge extensions, and their boundary is ambiguous (Fig. 13A, B, and D). The shoulder teeth are absent (Fig. 13D and E). A low wing fold exists next to the dorsal edge of the

shoulder blades and runs across a jaw edge at an angle of ~50° (Fig. 13A, B, and D). The wings are thin and have no ridges (Fig. 13A and B). The hood is moderately long, and the hood notch is not discernible (Fig. 13C). The lateral walls show a somewhat elongated trapezoidal shape (Fig. 13A and B).

Comparison. This species markedly differs from *S. bidentata* sp. nov. by the absence of the shoulder teeth (Fig. 13D, E, I, and J) and a slightly more obtuse angle between the wing folds and the adjacent jaw edge (this species: ~50°, *S. bidentata* sp. nov.: ~30°; Fig. 13A, B, F, and G).

Occurrence. earliest Cenomanian to Early Maastrichtian; Yezo Group in Hokkaido, Japan.

Streptopteryx bidentata sp. nov.

Fig. 13F–J

Etymology. Latin prefix 'bi-' (two) and 'dentatus' (having tooth).

Material. NMNS_DS00040_CdEhX1r.stl, NMNS_DS00083_HFkq7tj.stl, NMNS_DS00128_k1LIu1T.stl, NMNS_DS00174_RmFzKT4.stl, and NMNS_DS00174_TWaF8yT.stl (https://doi.org/10.25452/figshare.plus.25736631).

Diagnosis. The rostrum is moderately wide, slightly hooked, and relatively projected toward the front. Rostral dents, bridges, and anglepoints are absent. The jaw angles are subrounded. The angle between the jaw edges and the adjacent shoulder blade is obtuse or nearly perpendicular. The boundary between the shoulder blades and the adjacent lateral wall is ambiguous. The region around the jaw edge extensions is thick. The shoulder teeth are thin. The wings are thin. A low wing folds run lateral to the dorsal margin of the shoulder blades without distinct inflexion around the jaw angles. The anterior part of the shoulder blades and wings are directly merged and gently curved downward.

Description. The rostrum is large to moderate-sized, moderately wide, slightly hooked, and has no dents (Fig. 13F, G, and J). The bridges and anglepoints are not discernible (Fig. 13I). The jaw edges are sharp, single-edged, and gently curved. The dorsal parts of the shoulders and the adjacent wing merge directly, form a subrounded jaw angle, and gently curve downward (Fig. 13F and G). The angle between the jaw edge and the adjacent shoulder blade is slightly obtuse or nearly perpendicular. The shoulder blades and lateral walls are thickened around the jaw edge extensions, and their boundary is ambiguous (Fig. 13F, G, and I). The shoulder teeth are thin (Fig. 13I and J). A low wing fold exists near the dorsal edge of the shoulder blades and runs across a jaw edge at an angle of ~30° (Fig. 13F and G). The wings are thin and have no ridges (Fig. 13F and G). The hood is moderately long, and the hood notch is not discernible (Fig. 13H). The lateral walls show a somewhat elongated trapezoidal shape (Fig. 13F and G).

Comparison. This species markedly differs from *S. glabra* sp. nov. by the presence of shoulder teeth (Fig. 13D, E, I, and J) and an acuter angle between jaw edges and wing folds (this species: ~30°, *S. glabra* sp. nov.: ~50°; Fig. 13A, B, F, and G).

Occurrence. Late Turonian to Early Maastrichtian; Yezo Group in Hokkaido, Japan.

Genus ***Camptoteuthis*** gen. nov.

Etymology. Ancient Greek 'kamptos' (bent), referring to jaw edges showing strong curvature, and 'teuthis' (squid).

Type species. *Camptoteuthis acrorhynchus* sp. nov.

Diagnosis. The rostrum is large, moderately wide, slightly hooked, and exceedingly projected toward the front. The rostral dents, bridges, and anglepoints are absent. The jaw angles are subrounded. The

angle between the jaw edges and the adjacent shoulder blade is nearly perpendicular. The boundary between the shoulder blades and the adjacent lateral wall is ambiguous. The region around the jaw edge extensions is thick. The wings are thin. A low wing folds run lateral to the dorsal margin of the shoulder blades.

Comparison. This genus can be distinguished from *Psiloteuthis* gen. nov. by the presence of the distinct wing folds (Figs. 12E and 13O). It differs from *Streptopteryx* gen. nov. by the acuter angle between the crest and jaw edges in the lateral views (this genus: ~30°, *Streptopteryx* gen. nov.: ~45°; Fig. 13A and K).

Occurrence. Late Cenomanian to Late Turonian; Yezo Group in Hokkaido, Japan.

Camptoteuthis acrorhynchus sp. nov.

Fig. 13K–O

Etymology. Ancient Greek 'akros' (sharp) and 'rhynkhos' (beak).

Material. NMNS_DS00140_3qYJhEx.stl and NMNS_DS00173_OWxR12l.stl (https://doi.org/10.25452/figshare.plus.25736631).

Diagnosis. The rostrum is large, moderately wide, slightly hooked, and exceedingly projected toward the front. The rostral dents, bridges, and anglepoints are absent. The jaw angles are subrounded. The angle between the jaw edges and the adjacent shoulder blade is nearly perpendicular. The boundary between the shoulder blades and the adjacent lateral wall is ambiguous. The region around the jaw edge extensions is thick. The wings are thin. Relatively high wing folds run lateral to the dorsal margin of the shoulder blades. The degree of the angle between the wing folds and the adjacent jaw edge is ~60°. A small step exists on the wing folds around the jaw angles.

Description. The rostrum is large, moderately wide, slightly hooked, and exceedingly projected toward the front (Fig. 13K, L, and O). The rostral dents, bridges, and anglepoints are not discernible (Fig. 13N). The jaw edges are sharp, single-edged, and gently curved. The dorsal parts of the shoulders and the adjacent wing merge directly, form a subrounded jaw angle, and gently curve downward (Fig. 13K). The angle between the jaw edge and the adjacent shoulder blade is nearly perpendicular. The shoulder blades and lateral walls are thickened around jaw edge extensions, and their boundary is ambiguous (Fig. 13K). The shoulder teeth are absent (Fig. 13N). A distinct wing fold exists by the dorsal edge of the shoulder blades and runs across a jaw edge at an angle of ~60° (Fig. 13K, N, and O). Around the jaw angle, a small step exists on the wing folds (Fig. 13N and O). The wings are thin and have no ridges (Fig. 13K). The wing folds are relatively high to hide the jaw angles in the lateral views (Fig. 13K, N, and O). The hood is moderately long (Fig. 13M).

Comparison. This species differs from *C. cunabuli* sp. nov. by the higher wing folds that hide the jaw angles in lateral view and the presence of a step on the wing folds (Fig. 13K, N, P, and Q).

Occurrence. Early to Late Turonian; Yezo Group in Hokkaido, Japan.

Camptoteuthis cunabuli sp. nov.

Fig. 13P–T

Etymology. Latin 'cunabulum' (cradle).

Material. NMNS_DS00082_p4vjY3G.stl (https://doi.org/10.25452/figshare.plus.25736631).

Diagnosis. The rostrum is large, moderately wide, slightly hooked, and exceedingly projected toward the front. The rostral dents, bridges, and anglepoints are absent. The jaw angles are subrounded. The angle between the jaw edges and the adjacent shoulder blade is nearly perpendicular. The boundary

between the shoulder blades and the adjacent lateral wall is ambiguous. The region around the jaw edge extensions is thick. The wings are thin. A low wing folds run lateral to the dorsal margin of the shoulder blades. The wing folds run across the adjacent jaw edge without forming step. The degree of the angle between the wing folds and the adjacent jaw edge is ~60°.

Description. The rostrum is large, moderately wide, slightly hooked, and exceedingly projected toward the front (Fig. 13P, Q, and T). The rostral dents, bridges, and anglepoints are not discernible (Fig. 13S). The jaw edges are sharp, single-edged, and gently curved. The dorsal parts of the shoulders and the adjacent wing merge directly, they form a subrounded jaw angle, and gently curve downward (Fig. 13P and Q). The angle between a jaw edge and the adjacent shoulder blade is nearly perpendicular. The shoulder blades and lateral walls are thickened around jaw edges, and their boundary is ambiguous (Fig. 13P and Q). A low wing fold exists near the dorsal edge of the shoulder blades and runs across the jaw edge at an angle of ~60° without forming a step around it (Fig. 13P, Q, and T). The wings are thin and have no ridges (Fig. 13P and Q). The hood is moderately long, and the hood notch is not discernible.

Comparison. This species differs from *C. acrorhynchus* sp. nov. by the lower wing folds that do not hide the jaw angles in the lateral view and the absence of a step on the wing folds (Fig. 13K, N, P, and Q).

Occurrence. Late Cenomanian; Yezo Group in Hokkaido, Japan.

Order and Family uncertain

Remarks. A potential taxonomic relevance of the morphology of the upper beak has been studied intensively in the past[41,42]. According to these studies, this feature cannot be used taxonomically at the order or family level. *Yezoteuthis* was attributed to the order Oegopsida[34,36] based on a morphometric analysis of coleoid upper beaks[43]. The criteria for this identification are, however, insufficient because only three species of the Oegopsida were examined. This low number does not reflect the morphological variations present in the Oegopsida. Significant taxonomic variations are reported in the morphology of oegopsid upper beaks[42] which are not reflected by these criteria. The observation of the holotype further revealed that the diagnostic characters of shoulders, wings, and lateral walls are not preserved.

Another fossil upper beak (gen. et sp. indet.) has also been attributed to the Oegopsida based on the morphological similarity of the rostrum[36]. This specimen had been excluded from the morphologically related order Vampyromorpha based on the larger ratio between the rostral length and hood length[36]. This published ratio is unfortunately not accurate since the posterior part of the hood is not preserved. A study of extant cephalopod beaks pointed out that the Vampyromorpha can only be distinguished from the Oegopsida by bridges that extend more posteriorly[44]. Whether these upper beaks have such characteristics cannot be confirmed due to the lack of the posterior hood. The taxonomic classification of these two fossil upper beaks on the order and family level therefore remains open.

Genus ***Yezoteuthis*** Tanabe, Hikida and Iba, 2006

Type genus. *Yezoteuthis giganteus* Tanabe, Hikida and Iba, 2006

Emended diagnosis. The size of adult beaks is extremely large (more than 50 mm in the crest length). The rostrum is thick and sharply pointed. The hood is gently arched. The shoulder blades are connected to the hood without making a step. The crest line is gently arched. The hood and lateral walls are

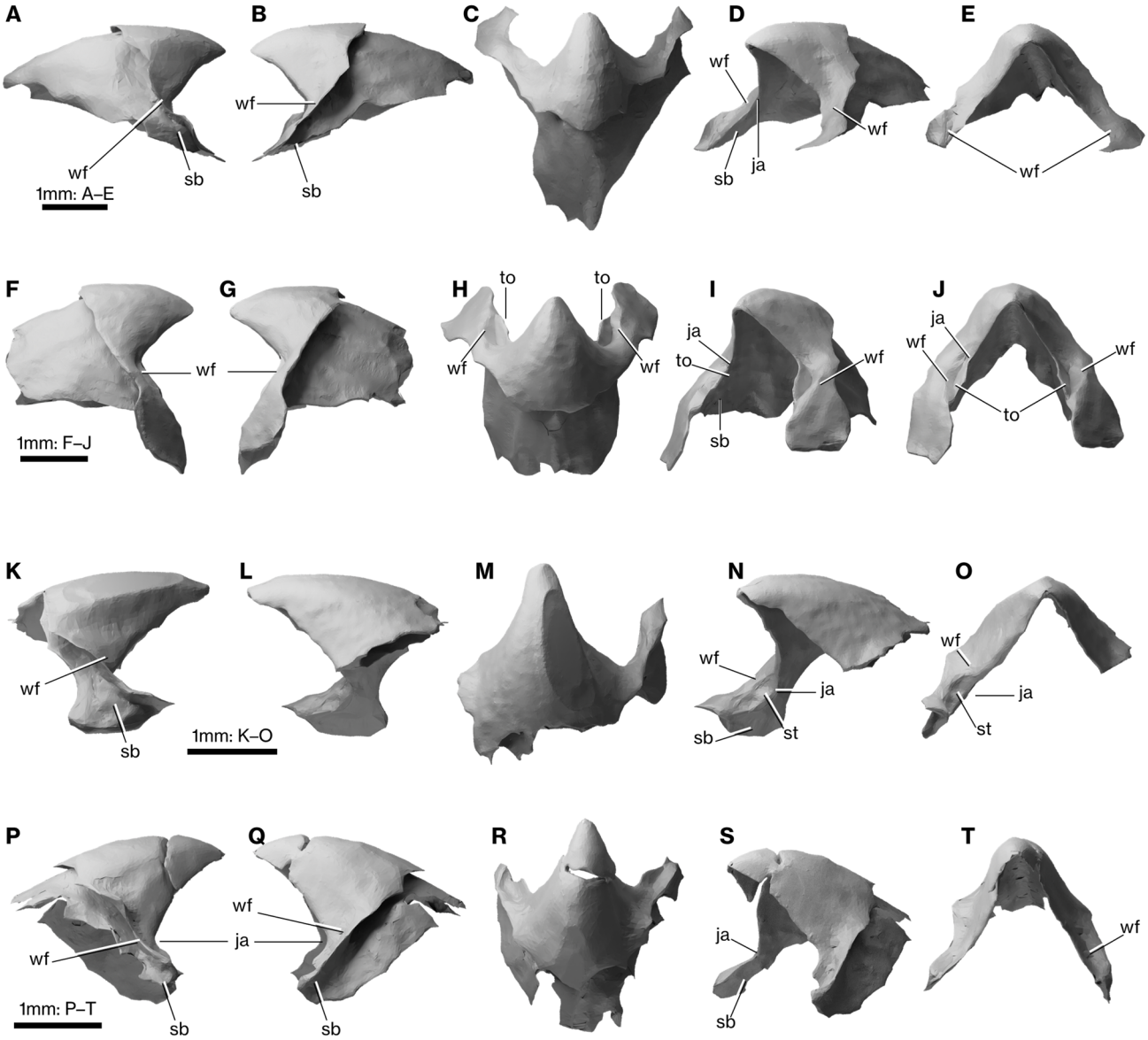


Fig. 13. Lower beaks of *Streptopteryx* and *Camptoteuthis*.
(**A** to **E**) *Streptopteryx glabra* sp. nov., NMNS_DS00040_fBilvb5.stl. (**F** to **J**) *Streptopteryx bidentata* sp. nov., NMNS_DS00128_k1LIu1T.stl. (**K** to **O**) *Camptoteuthis acrorhynchus* sp. nov., NMNS_DS00140_3qYJhEx.stl. (**P** to **T**) *Camptoteuthis cunabuli* sp. nov., NMNS_DS00082_p4vjY3G.stl. (A, F, K, and P) left lateral view; (B, G, L, and Q) right lateral view; (C, H, M, and R) dorsal view; (D, I, N, and S) oblique view; (E, J, O, and T) frontal view. The 3D models are available from Figshare+ (https://doi.org/10.25452/figshare.plus.25736631). Abbreviations: ja, jaw angle; sb, shoulder blade; st, step around a jaw angle; to, shoulder tooth; wf, wing fold.

ornamented with fine radial striations.

Remarks. The shape of the jaw angles, shoulders, and the posterior part of the lateral walls are regarded as the diagnostic characters in the original description[34]. These characters are, however, not reliable due to damage during deposition, diagenesis and preparation.

Occurrence. Early Campanian; Yezo Group in Hokkaido, Japan.

Table 3. Summary of squid lower beaks.

No.	Classification				Geological age	Growth stage	Measurements										
	Order	Family	Genus	Species			CL (mm)	HL (mm)	WL (mm)	AJS (degree)	WA (degree)	LRL (mm)	RW (mm)	LRL/RW	JEL (mm)	JELL (mm)	JELL/JEL
1	Oegopsida	Haboroteuthidae	*Haboroteuthis*	*poseidon*	Late Cenomanian	subadult	11.83	5.83	-	-	125.7	5.97	-	1.27	8.19	5.03	0.61
2	Oegopsida	Haboroteuthidae	*Haboroteuthis*	*poseidon*	Middle Turonian	subadult	17.82	7.68	5.98	64.2	114.3	7.56	5.30	1.43	11.40	7.56	0.66
3	Oegopsida	Haboroteuthidae	*Haboroteuthis*	*poseidon*	Late Turonian	uncertain	-	-	4.93	-	-	-	-	-	-	-	-
4	Oegopsida	Haboroteuthidae	*Pachygephyra*	*callisto*	Santonian	adult	5.17	1.87	1.99	105.0	136.9	2.43	2.67	0.91	3.35	1.65	0.49
5	Oegopsida	Haboroteuthidae	*Hoplitopteryx*	*solida*	Middle Turonian	adult	2.88	1.13	1.08	85.3	109.0	1.12	1.10	1.02	1.87	1.06	0.57
6	Oegopsida	Haboroteuthidae	*Bathmidoteuthis*	*altus*	Early Cenomanian	subadult	-	1.95	-	120.7	142.1	2.67	2.04	-	3.22	2.67	0.83
7	Oegopsida	Haboroteuthidae	*Bathmidoteuthis*	*altus*	Late Campanian	subadult	2.31	1.34	1.20	-	135.6	1.78	1.58	1.13	2.28	1.78	0.78
8	Oegopsida	Haboroteuthidae	*Placomoteuthis*	*hercules*	Early Maastrichtian	adult	2.24	1.30	1.03	97.8	114.0	1.11	1.20	0.93	1.62	0.80	0.50
9	Oegopsida	Pachyteroteuthidae	*Pachypteroteuthis*	*adiacens*	earliest Cenomanian	subadult	-	2.58	-	-	127.7	2.12	-	0.81	2.75	0.96	0.35
10	Oegopsida	Pachyteroteuthidae	*Pachypteroteuthis*	*adiacens*	earliest Cenomanian	adult	4.56	2.06	2.34	-	137.9	2.43	2.58	0.93	2.92	1.02	0.35
11	Oegopsida	Pachyteroteuthidae	*Pachypteroteuthis*	*mortarii*	earliest Cenomanian	subadult	-	2.06	1.64	-	143.6	1.31	1.15	1.14	2.65	1.20	0.45
12	Oegopsida	Pachyteroteuthidae	*Pachypteroteuthis*	*magnus*	Early Coniacian	subadult	-	-	-	-	144.0	5.18	-	-	7.71	3.60	0.47
13	Oegopsida	Pachyteroteuthidae	*Pachypteroteuthis*	*sulcatus*	Early Campanian	subadult	-	-	5.29	-	144.1	-	-	-	-	-	-
14	Oegopsida	Pachyteroteuthidae	*Catantopteryx*	*altilis*	Late Cenomanian	subadult	-	-	4.14	-	151.5	-	-	-	4.26	1.66	0.39
15	Oegopsida	Pachyteroteuthidae	*Catantopteryx*	*altilis*	Late Turonian	subadult	-	3.40	4.37	-	154.9	4.20	3.77	1.11	4.92	2.52	0.51
16	Oegopsida	Pachyteroteuthidae	*Thalassasboides*	*watatsumi*	Early Cenomanian	subadult	-	2.36	1.33	-	131.2	-	-	-	2.52	1.09	0.43
17	Oegopsida	Pachyteroteuthidae	*Thalassasboides*	*watatsumi*	Early Cenomanian	subadult	-	1.95	1.68	105.1	137.5	2.01	1.83	1.10	2.69	1.20	0.45
18	Oegopsida	Pachyteroteuthidae	*Thalassasboides*	*watatsumi*	Late Cenomanian	adult	2.58	1.46	1.22	-	125.9	-	-	-	1.52	0.83	0.54
19	Oegopsida	Pachyteroteuthidae	*Thalassasboides*	*watatsumi*	Late Cenomanian	subadult	4.20	2.92	2.31	136.2	136.2	2.74	2.44	1.12	4.09	1.93	0.47
20	Oegopsida	Pachyteroteuthidae	*Thalassasboides*	*watatsumi*	Late Cenomanian	subadult	-	2.79	-	-	-	-	-	-	3.38	2.00	0.59
21	Oegopsida	Pachyteroteuthidae	*Thalassasboides*	*watatsumi*	Middle Turonian	subadult	6.25	2.60	3.12	-	127.9	4.03	3.59	1.12	4.03	2.24	0.56
22	Oegopsida	Pachyteroteuthidae	*Thalassasboides*	*watatsumi*	Late Turonian	subadult	3.02	1.48	1.38	-	127.3	1.77	1.57	1.13	1.97	1.15	0.58
23	Oegopsida	Pachyteroteuthidae	*Thalassasboides*	*watatsumi*	Late Turonian	subadult	4.67	3.12	3.14	-	147.5	3.58	3.30	1.08	4.34	2.01	0.46
24	Oegopsida	Pachyteroteuthidae	*Thalassasboides*	*watatsumi*	Late Turonian	subadult	-	2.85	3.68	98.5	144.2	2.79	2.40	1.16	4.17	1.65	0.40
25	Oegopsida	Pachyteroteuthidae	*Thalassasboides*	*watatsumi*	Late Turonian	subadult	3.53	1.88	1.24	-	138.7	1.83	1.59	1.15	2.20	1.10	0.50
26	Oegopsida	Pachyteroteuthidae	*Thalassasboides*	*watatsumi*	Late Turonian	subadult	-	2.79	2.96	130.4	144.8	2.95	-	-	4.38	1.76	0.40
27	Oegopsida	Pachyteroteuthidae	*Thalassasboides*	*watatsumi*	Early Coniacian	adult	5.18	2.61	1.58	-	131.0	1.69	-	-	2.95	1.50	0.51
28	Oegopsida	Pachyteroteuthidae	*Thalassasboides*	*watatsumi*	Late Coniacian	subadult	-	2.10	1.93	-	-	-	-	-	2.68	1.33	0.50
29	Oegopsida	Pachyteroteuthidae	*Thalassasboides*	*watatsumi*	Santonian	adult	3.96	1.78	1.61	-	133.4	-	-	-	2.54	1.14	0.45
30	Oegopsida	Pachyteroteuthidae	*Thalassasboides*	*watatsumi*	Late Campanian	subadult	2.90	1.49	1.64	-	132.6	-	-	-	1.91	0.95	0.50
31	Oegopsida	Pachyteroteuthidae	*Thalassasboides*	*pulchellus*	earliest Cenomanian	adult	3.87	2.25	2.12	123.6	137.5	1.86	1.44	1.29	2.40	1.11	0.46
32	Oegopsida	Pachyteroteuthidae	*Thalassasboides*	*pulchellus*	Late Turonian	subadult	5.75	3.07	3.12	72.0	137.3	3.05	2.37	1.29	3.90	2.01	0.52
33	Oegopsida	Pachyteroteuthidae	*Thalassasboides*	*pulchellus*	Late Turonian	adult	4.90	2.66	2.84	-	149.3	2.58	1.76	1.47	3.65	1.51	0.41
34	Oegopsida	Pachyteroteuthidae	*Thalassasboides*	*pulchellus*	Late Turonian	adult	6.05	3.92	4.64	131.1	133.8	3.92	3.05	1.29	4.67	2.19	0.47
35	Oegopsida	Pachyteroteuthidae	*Thalassasboides*	*pulchellus*	Late Coniacian	subadult	-	2.27	2.23	-	145.6	2.72	1.93	1.41	3.42	1.50	0.44
36	Oegopsida	Pachyteroteuthidae	*Thalassasboides*	*pulchellus*	Santonian	adult	-	4.11	-	-	133.7	-	-	1.35	-	-	-
37	Oegopsida	Pachyteroteuthidae	*Thalassasboides*	*acutus*	Late Turonian	subadult	-	3.02	3.26	-	140.6	3.50	1.69	2.07	4.22	2.13	0.50
38	Oegopsida	Pachyteroteuthidae	*Thalassasboides*	uncertain	Early Coniacian	juvenile	6.87	3.88	3.56	-	-	3.63	-	-	4.25	-	-
39	Oegopsida	Pachyteroteuthidae	*Thalassasboides*	uncertain	Late Coniacian	juvenile	4.87	2.43	1.92	-	-	-	-	-	3.17	1.68	0.53
40	Oegopsida	Pachyteroteuthidae	*Thalassasboides*	uncertain	Late Campanian	juvenile	-	-	1.99	-	-	-	-	-	-	-	-
41	Oegopsida	Pachyteroteuthidae	*Pseudovampyroteuthis*	*hecate*	earliest Cenomanian	subadult	-	2.26	2.19	-	137.9	2.34	2.12	1.10	2.84	1.08	0.38
42	Oegopsida	Pachyteroteuthidae	*Orthoteuthis*	*subaru*	Late Coniacian	subadult	-	1.78	-	-	-	0.88	0.97	0.91	3.50	0.88	0.25
43	Oegopsida	Pachyteroteuthidae	*Gerontoteuthis*	*acutissimus*	earliest Cenomanian	adult	4.85	2.53	2.09	90.4	134.9	2.21	1.14	1.94	2.94	1.09	0.37
44	Oegopsida	Pachyteroteuthidae	*Astathogephyra*	*metis*	Middle Turonian	adult	5.71	3.15	3.05	-	129.9	2.43	2.17	1.12	3.52	1.54	0.44
45	Oegopsida	Pachyteroteuthidae	*Astathogephyra*	*metis*	Middle Turonian	adult	-	2.55	2.64	-	134.8	1.87	1.97	0.95	2.73	1.44	0.53
46	Oegopsida	Pachyteroteuthidae	*Astathogephyra*	*metis*	Late Coniacian	subadult	3.19	1.56	-	-	143.7	1.78	1.59	1.12	2.27	1.04	0.46
47	Oegopsida	Pachyteroteuthidae	*Astathogephyra*	*himatium*	Late Cenomanian	adult	4.00	2.02	1.27	129.6	129.7	1.38	1.08	1.28	2.24	1.37	0.61
48	Oegopsida	Pachyteroteuthidae	*Sepultipons*	*castor*	Middle Turonian	adult	3.65	1.87	1.60	81.5	119.0	1.62	1.57	1.03	2.37	1.24	0.52
49	Oegopsida	Pachyteroteuthidae	*Sepultipons*	*castor*	Late Turonian	adult	3.36	1.76	1.41	96.8	121.9	1.56	1.75	0.89	2.01	1.07	0.53
50	Oegopsida	Pachyteroteuthidae	*Sepultipons*	*castor*	Late Turonian	subadult	-	2.02	1.23	-	124.5	1.62	1.76	0.92	2.11	1.22	0.58
51	Oegopsida	Pachyteroteuthidae	*Sepultipons*	*castor*	Late Turonian	subadult	-	2.07	1.18	107.2	140.1	1.67	1.61	1.04	2.15	1.31	0.61
52	Oegopsida	Pachyteroteuthidae	*Sepultipons*	*castor*	Late Turonian	subadult	-	2.11	1.16	125.1	120.6	1.71	1.71	1.00	2.33	1.38	0.59
53	Oegopsida	Pachyteroteuthidae	*Sepultipons*	*castor*	Late Turonian	adult	-	1.90	1.00	111.0	130.6	1.58	1.47	1.07	2.18	1.31	0.60
54	Oegopsida	Pachyteroteuthidae	*Sepultipons*	*castor*	Late Turonian	subadult	-	1.91	1.20	-	142.7	2.00	2.11	0.95	2.36	1.34	0.57
55	Oegopsida	Pachyteroteuthidae	*Sepultipons*	*castor*	Late Turonian	subadult	-	1.64	1.51	114.3	138.4	1.73	1.55	1.12	2.50	1.37	0.55
56	Oegopsida	Pachyteroteuthidae	*Sepultipons*	*castor*	Early Maastrichtian	adult	3.59	1.87	1.49	95.5	127.5	1.64	1.68	0.98	2.14	1.17	0.55
57	Oegopsida	Pachyteroteuthidae	*Sepultipons*	*castor*	Early Maastrichtian	subadult	-	1.75	1.12	-	124.3	-	-	-	1.92	0.97	0.50
58	Oegopsida	Pachyteroteuthidae	*Sepultipons*	*castor*	Early Maastrichtian	adult	4.00	1.93	1.90	107.6	131.2	1.38	1.43	0.97	2.18	0.96	0.44
59	Oegopsida	Pachyteroteuthidae	*Sepultipons*	*castor*	Early Maastrichtian	adult	-	1.96	1.44	112.6	126.8	1.43	1.51	0.95	2.30	1.10	0.48
60	Oegopsida	Pachyteroteuthidae	*Sepultipons*	*pollux*	Late Turonian	adult	4.45	1.82	1.92	102.0	129.6	1.96	2.08	0.94	2.80	1.37	0.49
61	Oegopsida	Pachyteroteuthidae	*Sepultipons*	*pollux*	Late Turonian	subadult	-	1.56	0.97	-	126.2	1.41	1.30	1.08	1.74	0.92	0.53
62	Oegopsida	Pachyteroteuthidae	*Sepultipons*	*pollux*	Late Coniacian	adult	3.47	1.80	1.88	125.8	-	1.41	1.36	1.04	2.10	1.26	0.60
63	Oegopsida	Pachyteroteuthidae	*Sepultipons*	*gradus*	Late Turonian	adult	-	2.02	-	75.4	145.7	1.74	2.02	0.86	2.20	1.20	0.55
64	Oegopsida	Pachyteroteuthidae	*Sepultipons*	*gradus*	Late Coniacian	subadult	-	2.28	-	93.8	-	2.11	-	-	2.50	1.68	0.67
65	Oegopsida	Pachyteroteuthidae	*Sepultipons*	*gradus*	Early Maastrichtian	adult	6.25	3.40	3.52	64.2	126.8	2.83	2.49	1.14	3.63	1.49	0.41
66	Oegopsida	Pachyteroteuthidae	*Sepultipons*	*gradus*	Early Maastrichtian	adult	4.66	2.14	1.76	-	128.4	1.66	1.73	0.96	2.57	1.29	0.50

Table 3. (continued)

No.	Dataset and Collection No. (NMNS: National Museum of Nature and Science, Tokyo)				Figure
	3D model	Label data of 3D models	Cross-sectional images of 3D models	Original cross-sectional images of carbonate concretions (animations of cross-sectional images are available from	
1	NMNS_DS00082_79XGc4h.stl	L_NMNS_DS00082_20190127_c1_wl_01_0360_79XGc4h.tif–0535_79XGc4h.tif	C_NMNS_DS00082_20190127_c1_wl_01_0360_79XGc4h.jpg–0535_79XGc4h.jpg	NMNS_DS00082_20190127_c1_wl_01_0360.jpg–0535.jpg	Fig. 4F–M
2	NMNS_DS00009_3F7VSzd.stl	L_NMNS_DS00009_20170720_c1_wl_01_0532_3F7VSzd.tif–0774_3F7VSzd.tif	C_NMNS_DS00009_20170720_c1_wl_01_0532_3F7VSzd.jpg–0774_3F7VSzd.jpg	NMNS_DS00009_20170720_c1_wl_01_0532.jpg–0774.jpg	Fig. 4A–E
3	NMNS_DS00173_Ps2dDmF.stl	L_NMNS_DS00173_wl_01_0843_Ps2dDmF.tif–0945_Ps2dDmF.tif	C_NMNS_DS00173_wl_01_0843_Ps2dDmF.jpg–0945_Ps2dDmF.jpg	NMNS_DS00173_wl_01_0843.tif–0945.tif	-
4	NMNS_DS00011_JVM6xKK.stl	L_NMNS_DS00011_20170806_c1_wl_01_0475_JVM6xKK.tif–0573_JVM6xKK.tif	C_NMNS_DS00011_20170806_c1_wl_01_0475_JVM6xKK.jpg–0573_JVM6xKK.jpg	NMNS_DS00011_20170806_c1_wl_01_0475.jpg–0573.jpg	Figs 3A & 4N–R
5	NMNS_DS00009_dvxb42e.stl	L_NMNS_DS00009_20170720_c1_wl_01_0468_dvxb42e.tif–0514_dvxb42e.tif	C_NMNS_DS00009_20170720_c1_wl_01_0468_dvxb42e.jpg–0514_dvxb42e.jpg	NMNS_DS00009_20170720_c1_wl_01_0468.jpg–0514.jpg	Figs 3B & 4S–W
6	NMNS_DS00084_a3ll9sj.stl	L_NMNS_DS00084_20190202_c1_wl_01_0277_a3ll9sj.tif–0332_a3ll9sj.tif	C_NMNS_DS00084_20190202_c1_wl_01_0277_a3ll9sj.jpg–0332_a3ll9sj.jpg	NMNS_DS00084_20190202_c1_wl_01_0277.jpg–0332.jpg	Fig. 5A–E
7	NMNS_DS00171_Lq1Jgoh.stl	L_NMNS_DS00171_wl_01_0296_Lq1Jgoh.tif–0340_Lq1Jgoh.tif	C_NMNS_DS00171_wl_01_0296_Lq1Jgoh.jpg–0340_Lq1Jgoh.jpg	NMNS_DS00171_wl_01_0296.tif–0340.tif	-
8	NMNS_DS00174_bjM7Cpk.stl	L_NMNS_DS00174_wl_01_0313_bjM7Cpk.tif–0356_bjM7Cpk.tif	C_NMNS_DS00174_wl_01_0313_bjM7Cpk.jpg–0356_bjM7Cpk.jpg	NMNS_DS00174_wl_01_0313.jpg–0356.jpg	Fig. 5F–J
9	NMNS_DS00068_o0JKOmo.stl	L_NMNS_DS00068_20181123_c1_wl_01_0317_o0JKOmo.tif–0378_o0JKOmo.tif	C_NMNS_DS00068_20181123_c1_wl_01_0317_o0JKOmo.jpg–0378_o0JKOmo.jpg	NMNS_DS00068_20181123_c1_wl_01_0317.jpg–0378.jpg	-
10	NMNS_DS00068_EnU0Efh.stl	L_NMNS_DS00068_20181123_c1_wl_01_0369_EnU0Efh.tif–0449_EnU0Efh.tif	C_NMNS_DS00068_20181123_c1_wl_01_0369_EnU0Efh.jpg–0449_EnU0Efh.jpg	NMNS_DS00068_20181123_c1_wl_01_0369.jpg–0449.jpg	Figs 3G & 5K–O
11	NMNS_DS00068_G7fBskP.stl	L_NMNS_DS00068_20181123_c1_wl_01_0638_G7fBskP.tif–0708_G7fBskP.tif	C_NMNS_DS00068_20181123_c1_wl_01_0638_G7fBskP.jpg–0708_G7fBskP.jpg	NMNS_DS00068_20181123_c1_wl_01_0638.jpg–0708.jpg	Fig. 5P–T
12	NMNS_DS00034_nv7HRSc.stl	L_NMNS_DS00034_20180207_c1_wl_01_0407_nv7HRSc.tif–0533_nv7HRSc.tif	C_NMNS_DS00034_20180207_c1_wl_01_0407_nv7HRSc.jpg–0533_nv7HRSc.jpg	NMNS_DS00034_20180207_c1_wl_01_0407.jpg–0533.jpg	Fig. 5U–Y
13	NMNS_DS00175_2UQENMZ.stl	L_NMNS_DS00175_wl_01_0953_2UQENMZ.tif–1083_2UQENMZ.tif	C_NMNS_DS00175_wl_01_0953_2UQENMZ.jpg–1083_2UQENMZ.jpg	NMNS_DS00175_wl_01_0953.tif–1083.tif	Fig. 5Z–AD
14	NMNS_DS00082_tntK5pM.stl	L_NMNS_DS00082_20190127_c1_wl_01_0513_tntK5pM.tif–0577_tntK5pM.tif	C_NMNS_DS00082_20190127_c1_wl_01_0513_tntK5pM.jpg–0577_tntK5pM.jpg	NMNS_DS00082_20190127_c1_wl_01_0513.jpg–0577.jpg	Fig. 6A–E
15	NMNS_DS00173_JGcVf5Q.stl	L_NMNS_DS00173_wl_01_1168_JGcVf5Q.tif–1265_JGcVf5Q.tif	C_NMNS_DS00173_wl_01_1168_JGcVf5Q.jpg–1265_JGcVf5Q.jpg	NMNS_DS00173_wl_01_1168.tif–1265.tif	-
16	NMNS_DS00084_U3Z2mdm.stl	L_NMNS_DS00084_20190202_c1_wl_01_0037_U3Z2mdm.tif–0090_U3Z2mdm.tif	C_NMNS_DS00084_20190202_c1_wl_01_0037_U3Z2mdm.jpg–0090_U3Z2mdm.jpg	NMNS_DS00084_20190202_c1_wl_01_0037.jpg–0090.jpg	-
17	NMNS_DS00084_RAKM2iJ.stl	L_NMNS_DS00084_20190202_c1_wl_01_0253_RAKM2iJ.tif–0302_RAKM2iJ.tif	C_NMNS_DS00084_20190202_c1_wl_01_0253_RAKM2iJ.jpg–0302_RAKM2iJ.jpg	NMNS_DS00084_20190202_c1_wl_01_0253.jpg–0302.jpg	-
18	NMNS_DS00082_1H8UvDW.stl	L_NMNS_DS00082_20190127_c1_wl_01_0125_1H8UvDW.tif–0156_1H8UvDW.tif	C_NMNS_DS00082_20190127_c1_wl_01_0125_1H8UvDW.jpg–0156_1H8UvDW.jpg	NMNS_DS00082_20190127_c1_wl_01_0125.jpg–0156.jpg	-
19	NMNS_DS00082_ev6tAaJ.stl	L_NMNS_DS00082_20190127_c1_wl_01_0149_ev6tAaJ.tif–0242_ev6tAaJ.tif	C_NMNS_DS00082_20190127_c1_wl_01_0149_ev6tAaJ.jpg–0242_ev6tAaJ.jpg	NMNS_DS00082_20190127_c1_wl_01_0149.jpg–0242.jpg	Figs 3I & Fig. 6F–J
20	NMNS_DS00082_egK7tIO.stl	L_NMNS_DS00082_20190127_c1_wl_01_0422_egK7tIO.tif–0477_egK7tIO.tif	C_NMNS_DS00082_20190127_c1_wl_01_0422_egK7tIO.jpg–0477_egK7tIO.jpg	NMNS_DS00082_20190127_c1_wl_01_0422.jpg–0477.jpg	-
21	NMNS_DS00009_MnRA9nb.stl	L_NMNS_DS00009_20170720_c1_wl_01_0684_MnRA9nb.tif–0767_MnRA9nb.tif	C_NMNS_DS00009_20170720_c1_wl_01_0684_MnRA9nb.jpg–0767_MnRA9nb.jpg	NMNS_DS00009_20170720_c1_wl_01_0684.jpg–0767.jpg	-
22	NMNS_DS00135_JM4f46S.stl	L_NMNS_DS00135_wl_01_0441_JM4f46S.tif–0661_JM4f46S.tif	C_NMNS_DS00135_wl_01_0441_JM4f46S.jpg–0661_JM4f46S.jpg	NMNS_DS00135_wl_01_0441.tif–0661.tif	-
23	NMNS_DS00173_4dpfh14.stl	L_NMNS_DS00173_wl_01_0508_4dpfh14.tif–0597_4dpfh14.tif	C_NMNS_DS00173_wl_01_0508_4dpfh14.jpg–0597_4dpfh14.jpg	NMNS_DS00173_wl_01_0508.tif–0597.tif	-
24	NMNS_DS00173_A2DztKh.stl	L_NMNS_DS00173_wl_01_0658_A2DztKh.tif–0777_A2DztKh.tif	C_NMNS_DS00173_wl_01_0658_A2DztKh.jpg–0777_A2DztKh.jpg	NMNS_DS00173_wl_01_0658.tif–0777.tif	-
25	NMNS_DS00173_TFD6EIX.stl	L_NMNS_DS00173_wl_01_0903_TFD6EIX.tif–0946_TFD6EIX.tif	C_NMNS_DS00173_wl_01_0903_TFD6EIX.jpg–0946_TFD6EIX.jpg	NMNS_DS00173_wl_01_0903.tif–0946.tif	-
26	NMNS_DS00173_d50dzkI.stl	L_NMNS_DS00173_wl_01_0962_d50dzkI.tif–1019_d50dzkI.tif	C_NMNS_DS00173_wl_01_0962_d50dzkI.jpg–1019_d50dzkI.jpg	NMNS_DS00173_wl_01_0962.tif–1019.tif	-
27	NMNS_DS00034_kJU1vwB.stl	L_NMNS_DS00034_20180207_c1_wl_01_0238_kJU1vwB.tif–0310_kJU1vwB.tif	C_NMNS_DS00034_20180207_c1_wl_01_0238_kJU1vwB.jpg–0310_kJU1vwB.jpg	NMNS_DS00034_20180207_c1_wl_01_0238.jpg–0310.jpg	-
28	NMNS_DS00083_SN4asC0.stl	L_NMNS_DS00083_20190130_c1_wl_01_0384_SN4asC0.tif–0420_SN4asC0.tif	C_NMNS_DS00083_20190130_c1_wl_01_0384_SN4asC0.jpg–0420_SN4asC0.jpg	NMNS_DS00083_20190130_c1_wl_01_0384.jpg–0420.jpg	-
29	NMNS_DS00011_UU1c7pj.stl	L_NMNS_DS00011_20170806_c1_wl_01_0668_UU1c7pj.tif–0733_UU1c7pj.tif	C_NMNS_DS00011_20170806_c1_wl_01_0668_UU1c7pj.jpg–0733_UU1c7pj.jpg	NMNS_DS00011_20170806_c1_wl_01_0668.jpg–0733.jpg	-
30	NMNS_DS00182_F56YeDG.stl	L_NMNS_DS00182_wl_01_0403_F56YeDG.tif–0455_F56YeDG.tif	C_NMNS_DS00182_wl_01_0403_F56YeDG.jpg–0455_F56YeDG.jpg	NMNS_DS00182_wl_01_0403.tif–0455.tif	-
31	NMNS_DS00068_pBrzD5i.stl	L_NMNS_DS00068_20181123_c1_wl_01_0788_pBrzD5i.tif–0851_pBrzD5i.tif	C_NMNS_DS00068_20181123_c1_wl_01_0788_pBrzD5i.jpg–0851_pBrzD5i.jpg	NMNS_DS00068_20181123_c1_wl_01_0788.jpg–0851.jpg	Fig. 6K–O
32	NMNS_DS00173_CLt5m2t.stl	L_NMNS_DS00173_wl_01_0221_CLt5m2t.tif–0297_CLt5m2t.tif	C_NMNS_DS00173_wl_01_0221_CLt5m2t.jpg–0297_CLt5m2t.jpg	NMNS_DS00173_wl_01_0221.tif–0297.tif	-
33	NMNS_DS00173_8IkQbCV.stl	L_NMNS_DS00173_wl_01_0417_8IkQbCV.tif–0499_8IkQbCV.tif	C_NMNS_DS00173_wl_01_0417_8IkQbCV.jpg–0499_8IkQbCV.jpg	NMNS_DS00173_wl_01_0417.tif–0499.tif	-
34	NMNS_DS00173_27C5zir.stl	L_NMNS_DS00173_wl_01_1131_27C5zir.tif–1230_27C5zir.tif	C_NMNS_DS00173_wl_01_1131_27C5zir.jpg–1230_27C5zir.jpg	NMNS_DS00173_wl_01_1131.tif–1230.tif	-
35	NMNS_DS00081_V85MVoY.stl	L_NMNS_DS00081_20190124_c1_wl_01_0776_V85MVoY.tif–0851_V85MVoY.tif	C_NMNS_DS00081_20190124_c1_wl_01_0776_V85MVoY.jpg–0851_V85MVoY.jpg	NMNS_DS00081_20190124_c1_wl_01_0776.jpg–0851.jpg	-
36	NMNS_DS00104_GDb7t8w.stl	L_NMNS_DS00104_wl_01_0391_GDb7t8w.tif–0524_GDb7t8w.tif	C_NMNS_DS00104_wl_01_0391_GDb7t8w.jpg–0524_GDb7t8w.jpg	NMNS_DS00104_wl_01_0391.jpg–0524.jpg	-
37	NMNS_DS00173_w8T3Zp0.stl	L_NMNS_DS00173_wl_01_0406_w8T3Zp0.tif–0460_w8T3Zp0.tif	C_NMNS_DS00173_wl_01_0406_w8T3Zp0.jpg–0460_w8T3Zp0.jpg	NMNS_DS00173_wl_01_0406.tif–0460.tif	Fig. 6P–T
38	NMNS_DS00034_GA9MzKt.stl	L_NMNS_DS00034_20180207_c1_wl_01_0033_GA9MzKt.tif–0101_GA9MzKt.tif	C_NMNS_DS00034_20180207_c1_wl_01_0033_GA9MzKt.jpg–0101_GA9MzKt.jpg	NMNS_DS00034_20180207_c1_wl_01_0033.jpg–0101.jpg	-
39	NMNS_DS00083_LNaCE2f.stl	L_NMNS_DS00083_20190130_c1_wl_01_0090_LNaCE2f.tif–0147_LNaCE2f.tif	C_NMNS_DS00083_20190130_c1_wl_01_0090_LNaCE2f.jpg–0147_LNaCE2f.jpg	NMNS_DS00083_20190130_c1_wl_01_0090.jpg–0147.jpg	-
40	NMNS_DS00171_H6o1Nxu.stl	L_NMNS_DS00171_wl_01_0883_H6o1Nxu.tif–0918_H6o1Nxu.tif	C_NMNS_DS00171_wl_01_0883_H6o1Nxu.jpg–0918_H6o1Nxu.jpg	NMNS_DS00171_wl_01_0883.tif–0918.tif	-
41	NMNS_DS00068_gNqH3RQ.stl	L_NMNS_DS00068_20181123_c1_wl_01_0768_gNqH3RQ.tif–0829_gNqH3RQ.tif	C_NMNS_DS00068_20181123_c1_wl_01_0768_gNqH3RQ.jpg–0829_gNqH3RQ.jpg	NMNS_DS00068_20181123_c1_wl_01_0768.jpg–0829.jpg	Fig. 6U–Y
42	NMNS_DS00083_UA2WR3Z.stl	L_NMNS_DS00083_20190130_c1_wl_01_0236_UA2WR3Z.tif–0271_UA2WR3Z.tif	C_NMNS_DS00083_20190130_c1_wl_01_0236_UA2WR3Z.jpg–0271_UA2WR3Z.jpg	NMNS_DS00083_20190130_c1_wl_01_0236.jpg–0271.jpg	Fig. 7A–E
43	NMNS_DS00068_6MhIFUS.stl	L_NMNS_DS00068_20181123_c1_wl_01_0764_6MhIFUS.tif–0850_6MhIFUS.tif	C_NMNS_DS00068_20181123_c1_wl_01_0764_6MhIFUS.jpg–0850_6MhIFUS.jpg	NMNS_DS00068_20181123_c1_wl_01_0764.jpg–0850.jpg	Fig. 3H & Fig. 7F–J
44	NMNS_DS00009_TkD5dWU.stl	L_NMNS_DS00009_20170720_c1_wl_01_0425_TkD5dWU.tif–0517_TkD5dWU.tif	C_NMNS_DS00009_20170720_c1_wl_01_0425_TkD5dWU.jpg–0517_TkD5dWU.jpg	NMNS_DS00009_20170720_c1_wl_01_0425.jpg–0517.jpg	-
45	NMNS_DS00009_MU8cSC4.stl	L_NMNS_DS00009_20170720_c1_wl_01_0958_MU8cSC4.tif–1021_MU8cSC4.tif	C_NMNS_DS00009_20170720_c1_wl_01_0958_MU8cSC4.jpg–1021_MU8cSC4.jpg	NMNS_DS00009_20170720_c1_wl_01_0958.jpg–1021.jpg	Fig. 7K–O
46	NMNS_DS00083_VCCZZr4.stl	L_NMNS_DS00083_20190130_c1_wl_01_0277_VCCZZr4.tif–0340_VCCZZr4.tif	C_NMNS_DS00083_20190130_c1_wl_01_0277_VCCZZr4.jpg–0340_VCCZZr4.jpg	NMNS_DS00083_20190130_c1_wl_01_0277.jpg–0340.jpg	-
47	NMNS_DS00082_ZxRP3bR.stl	L_NMNS_DS00082_20190127_c1_wl_01_0274_ZxRP3bR.tif–0318_ZxRP3bR.tif	C_NMNS_DS00082_20190127_c1_wl_01_0274_ZxRP3bR.jpg–0318_ZxRP3bR.jpg	NMNS_DS00082_20190127_c1_wl_01_0274.jpg–0318.jpg	Fig. 7P–T
48	NMNS_DS00009_vxf2tIr.stl	L_NMNS_DS00009_20170720_c1_wl_01_0761_vxf2tIr.tif–0836_vxf2tIr.tif	C_NMNS_DS00009_20170720_c1_wl_01_0761_vxf2tIr.jpg–0836_vxf2tIr.jpg	NMNS_DS00009_20170720_c1_wl_01_0761.jpg–0836.jpg	Fig. 3J & Fig. 8A–E
49	NMNS_DS00041_b4BWTEx.stl	L_NMNS_DS00041_20180414_c1_wl_01_0001_b4BWTEx.tif–0037_b4BWTEx.tif	C_NMNS_DS00041_20180414_c1_wl_01_0001_b4BWTEx.jpg–0037_b4BWTEx.jpg	NMNS_DS00041_20180414_c1_wl_01_0001.jpg–0037.jpg	-
50	NMNS_DS00173_bIJ7zso.stl	L_NMNS_DS00173_wl_01_0102_bIJ7zso.tif–0138_bIJ7zso.tif	C_NMNS_DS00173_wl_01_0102_bIJ7zso.jpg–0138_bIJ7zso.jpg	NMNS_DS00173_wl_01_0102.tif–0138.tif	-
51	NMNS_DS00173_f2mBoiP.stl	L_NMNS_DS00173_wl_01_0651_f2mBoiP.tif–0690_f2mBoiP.tif	C_NMNS_DS00173_wl_01_0651_f2mBoiP.jpg–0690_f2mBoiP.jpg	NMNS_DS00173_wl_01_0651.tif–0690.tif	-
52	NMNS_DS00173_BbCw7oa.stl	L_NMNS_DS00173_wl_01_0776_BbCw7oa.tif–0817_BbCw7oa.tif	C_NMNS_DS00173_wl_01_0776_BbCw7oa.jpg–0817_BbCw7oa.jpg	NMNS_DS00173_wl_01_0776.tif–0817.tif	-
53	NMNS_DS00173_UXkxZH5.stl	L_NMNS_DS00173_wl_01_0799_UXkxZH5.tif–0851_UXkxZH5.tif	C_NMNS_DS00173_wl_01_0799_UXkxZH5.jpg–0851_UXkxZH5.jpg	NMNS_DS00173_wl_01_0799.tif–0851.tif	-
54	NMNS_DS00173_001WWW9.stl	L_NMNS_DS00173_wl_01_0780_001WWW9.tif–0836_001WWW9.tif	C_NMNS_DS00173_wl_01_0780_001WWW9.jpg–0836_001WWW9.jpg	NMNS_DS00173_wl_01_0780.tif–0836.tif	-
55	NMNS_DS00173_54IvJ9D.stl	L_NMNS_DS00173_wl_01_1335_54IvJ9D.tif–1378_54IvJ9D.tif	C_NMNS_DS00173_wl_01_1335_54IvJ9D.jpg–1378_54IvJ9D.jpg	NMNS_DS00173_wl_01_1335.tif–1378.tif	-
56	NMNS_DS00174_kRFX5Fg.stl	L_NMNS_DS00174_wl_01_0263_kRFX5Fg.tif–0311_kRFX5Fg.tif	C_NMNS_DS00174_wl_01_0263_kRFX5Fg.jpg–0311_kRFX5Fg.jpg	NMNS_DS00174_wl_01_0263.tif–0311.tif	-
57	NMNS_DS00174_L1VyDDh.stl	L_NMNS_DS00174_wl_01_0596_L1VyDDh.tif–0628_L1VyDDh.tif	C_NMNS_DS00174_wl_01_0596_L1VyDDh.jpg–0628_L1VyDDh.jpg	NMNS_DS00174_wl_01_0596.tif–0628.tif	-
58	NMNS_DS00174_7H4Gb53.stl	L_NMNS_DS00174_wl_01_0843_7H4Gb53.tif–0900_7H4Gb53.tif	C_NMNS_DS00174_wl_01_0843_7H4Gb53.jpg–0900_7H4Gb53.jpg	NMNS_DS00174_wl_01_0843.tif–0900.tif	-
59	NMNS_DS00174_jWDHdZ1.stl	L_NMNS_DS00174_wl_01_0945_jWDHdZ1.tif–1006_jWDHdZ1.tif	C_NMNS_DS00174_wl_01_0945_jWDHdZ1.jpg–1006_jWDHdZ1.jpg	NMNS_DS00174_wl_01_0945.tif–1006.tif	-
60	NMNS_DS00040_e0mxqWi.stl	L_NMNS_DS00040_20180409_c1_wl_01_0357_e0mxqWi.tif–0441_e0mxqWi.tif	C_NMNS_DS00040_20180409_c1_wl_01_0357_e0mxqWi.jpg–0441_e0mxqWi.jpg	NMNS_DS00040_20180409_c1_wl_01_0357.jpg–0441.jpg	Fig. 8F–J
61	NMNS_DS00173_JvLSs02.stl	L_NMNS_DS00173_wl_01_0829_JvLSs02.tif–0863_JvLSs02.tif	C_NMNS_DS00173_wl_01_0829_JvLSs02.jpg–0863_JvLSs02.jpg	NMNS_DS00173_wl_01_0829.tif–0863.tif	-
62	NMNS_DS00083_qxUALq6.stl	L_NMNS_DS00083_20190130_c1_wl_01_0001_qxUALq6.tif–0058_qxUALq6.tif	C_NMNS_DS00083_20190130_c1_wl_01_0001_qxUALq6.jpg–0058_qxUALq6.jpg	NMNS_DS00083_20190130_c1_wl_01_0001.jpg–0058.jpg	-
63	NMNS_DS00173_h0qQoNN.stl	L_NMNS_DS00173_wl_01_1209_h0qQoNN.tif–1273_h0qQoNN.tif	C_NMNS_DS00173_wl_01_1209_h0qQoNN.jpg–1273_h0qQoNN.jpg	NMNS_DS00173_wl_01_1209.tif–1273.tif	-
64	NMNS_DS00083_3h8PCFD.stl	L_NMNS_DS00083_20190130_c1_wl_01_0342_3h8PCFD.tif–0372_3h8PCFD.tif	C_NMNS_DS00083_20190130_c1_wl_01_0342_3h8PCFD.jpg–0372_3h8PCFD.jpg	NMNS_DS00083_20190130_c1_wl_01_0342.jpg–0372.jpg	-
65	NMNS_DS00128_oRE3wgv.stl	L_NMNS_DS00128_wl_01_1097_oRE3wgv.tif–1186_oRE3wgv.tif	C_NMNS_DS00128_wl_01_1097_oRE3wgv.jpg–1186_oRE3wgv.jpg	NMNS_DS00128_wl_01_1097.jpg–1186.jpg	-
66	NMNS_DS00174_Nu50pFy.stl	L_NMNS_DS00174_wl_01_1016_Nu50pFy.tif–1100_Nu50pFy.tif	C_NMNS_DS00174_wl_01_1016_Nu50pFy.jpg–1100_Nu50pFy.jpg	NMNS_DS00174_wl_01_1016.tif–1100.tif	Fig. 8K–O

Table 3. (continued)

No.	Classification				Geological age	Growth stage	Measurements										
	Order	Family	Genus	Species			CL (mm)	HL (mm)	WL (mm)	AJS (degree)	WA (degree)	LRL (mm)	RW (mm)	LRL/RW	JEL (mm)	JELL (mm)	JELL/JEL
67	Oegopsida	Pachypteroteuthidae	*Aspasmoteuthis*	*peltatus*	Early Coniacian	subadult	-	2.72	2.48	-	145.1	2.67	2.56	-	3.38	1.80	0.53
68	Oegopsida	Pachypteroteuthidae	*Juroteuthis*	*arrectus*	Late Turonian	subadult	-	2.69	-	-	-	-	-	-	4.10	-	-
69	Oegopsida	Pachypteroteuthidae	*Juroteuthis*	*arrectus*	Late Turonian	subadult	-	2.78	-	-	-	-	-	-	3.59	-	-
70	Oegopsida	Pachypteroteuthidae	*Juroteuthis*	*arrectus*	Early Coniacian	subadult	-	3.03	-	-	-	-	-	1.03	3.54	-	-
71	Oegopsida	Pachypteroteuthidae	uncertain	uncertain	earliest Cenomanian	juvenile	-	-	-	-	-	-	-	-	2.33	1.26	0.54
72	Oegopsida	Pachypteroteuthidae	uncertain	uncertain	Early Cenomanian	juvenile	-	-	-	-	136.6	-	-	-	2.61	-	-
73	Oegopsida	Pachypteroteuthidae	uncertain	uncertain	Early Cenomanian	juvenile	-	1.91	-	-	-	-	-	-	2.13	-	-
74	Oegopsida	Pachypteroteuthidae	uncertain	uncertain	Late Cenomanian	juvenile	-	-	-	-	-	-	-	-	3.51	-	-
75	Oegopsida	Pachypteroteuthidae	uncertain	uncertain	Late Cenomanian	juvenile	-	2.92	-	-	139.2	-	-	-	3.10	1.44	0.46
76	Oegopsida	Pachypteroteuthidae	uncertain	uncertain	Late Cenomanian	juvenile	-	-	-	-	-	3.15	-	-	3.38	2.46	0.73
77	Oegopsida	Pachypteroteuthidae	uncertain	uncertain	Late Cenomanian	juvenile	-	1.13	-	-	-	1.12	0.98	1.14	1.27	0.72	0.57
78	Oegopsida	Pachypteroteuthidae	uncertain	uncertain	Early Turonian	adult	2.80	1.58	1.55	-	-	-	-	-	2.50	1.01	0.40
79	Oegopsida	Pachypteroteuthidae	uncertain	uncertain	Early Turonian	juvenile	4.93	3.08	-	-	-	-	-	-	-	1.97	-
80	Oegopsida	Pachypteroteuthidae	uncertain	uncertain	Middle Turonian	juvenile	4.26	2.34	-	-	-	2.03	2.00	1.02	2.85	-	-
81	Oegopsida	Pachypteroteuthidae	uncertain	uncertain	Middle Turonian	adult	2.86	1.78	1.26	-	126.1	2.06	2.33	-	2.06	1.50	0.73
82	Oegopsida	Pachypteroteuthidae	uncertain	uncertain	Late Turonian	juvenile	-	3.11	-	-	-	-	-	1.76	3.34	1.93	0.58
83	Oegopsida	Pachypteroteuthidae	uncertain	uncertain	Late Turonian	juvenile	-	1.76	1.34	99.1	132.0	1.87	1.87	1.00	2.10	1.22	0.58
84	Oegopsida	Pachypteroteuthidae	uncertain	uncertain	Late Turonian	juvenile	-	1.88	-	-	-	1.30	1.32	0.98	1.63	-	-
85	Oegopsida	Pachypteroteuthidae	uncertain	uncertain	Late Turonian	juvenile	-	1.61	-	-	-	-	-	-	1.69	-	-
86	Oegopsida	Pachypteroteuthidae	uncertain	uncertain	Late Turonian	juvenile	-	1.59	-	-	-	-	-	-	2.38	1.18	0.50
87	Oegopsida	Pachypteroteuthidae	uncertain	uncertain	Late Turonian	juvenile	-	1.38	-	-	-	-	-	-	1.80	-	-
88	Oegopsida	Pachypteroteuthidae	uncertain	uncertain	Late Turonian	adult	2.55	1.27	1.28	-	-	-	-	-	1.97	-	-
89	Oegopsida	Pachypteroteuthidae	uncertain	uncertain	Late Turonian	juvenile	-	1.26	-	-	-	-	-	-	1.83	-	-
90	Oegopsida	Pachypteroteuthidae	uncertain	uncertain	Late Turonian	juvenile	-	2.88	2.49	-	-	-	-	-	5.02	2.42	0.48
91	Oegopsida	Pachypteroteuthidae	uncertain	uncertain	Late Turonian	juvenile	-	2.78	3.51	-	-	-	-	-	3.93	-	-
92	Oegopsida	Pachypteroteuthidae	uncertain	uncertain	Late Turonian	juvenile	-	2.89	-	-	-	3.32	2.56	1.30	4.43	-	-
93	Oegopsida	Pachypteroteuthidae	uncertain	uncertain	Late Turonian	uncertain	-	-	-	-	-	-	-	-	-	-	-
94	Oegopsida	Pachypteroteuthidae	uncertain	uncertain	Early Coniacian	juvenile	3.97	1.86	1.26	-	-	1.79	1.24	1.44	2.14	1.41	0.66
95	Oegopsida	Pachypteroteuthidae	uncertain	uncertain	Early Coniacian	juvenile	-	1.22	1.82	-	125.7	1.32	0.87	1.52	1.68	1.05	0.63
96	Oegopsida	Pachypteroteuthidae	uncertain	uncertain	Early Coniacian	adult	4.35	1.93	-	-	-	-	-	1.03	1.39	-	-
97	Oegopsida	Pachypteroteuthidae	uncertain	uncertain	Early Coniacian	juvenile	2.05	0.89	-	-	146.7	1.12	0.87	1.29	1.55	0.76	0.49
98	Oegopsida	Pachypteroteuthidae	uncertain	uncertain	Early Coniacian	juvenile	-	-	-	-	-	-	-	1.17	3.76	1.90	0.51
99	Oegopsida	Pachypteroteuthidae	uncertain	uncertain	Early Coniacian	juvenile	-	2.89	-	143.8	-	-	-	1.60	4.03	2.14	0.53
100	Oegopsida	Pachypteroteuthidae	uncertain	uncertain	Late Coniacian	juvenile	-	-	-	-	-	-	-	-	-	-	-
101	Oegopsida	Pachypteroteuthidae	uncertain	uncertain	Late Coniacian	juvenile	-	1.52	-	-	-	-	-	-	2.03	1.09	0.54
102	Oegopsida	Pachypteroteuthidae	uncertain	uncertain	Santonian	juvenile	1.95	1.10	-	-	-	1.18	1.11	1.06	1.31	-	-
103	Oegopsida	Pachypteroteuthidae	uncertain	uncertain	Early Campanian	juvenile	-	2.80	1.95	-	137.3	-	-	-	-	-	-
104	Oegopsida	Pachypteroteuthidae	uncertain	uncertain	Early Campanian	juvenile	2.72	-	-	-	-	-	-	-	2.58	-	-
105	Oegopsida	Pachypteroteuthidae	uncertain	uncertain	Late Campanian	uncertain	-	-	2.46	-	-	-	-	-	-	2.06	-
106	Oegopsida	Pachypteroteuthidae	uncertain	uncertain	Late Campanian	juvenile	-	-	-	-	-	-	-	-	3.42	1.83	0.54
107	Oegopsida	Pachypteroteuthidae	uncertain	uncertain	Early Campanian	juvenile	3.41	2.60	1.84	-	123.8	-	-	-	2.80	1.31	0.47
108	Oegopsida	Pachypteroteuthidae	uncertain	uncertain	Early Campanian	juvenile	-	1.33	-	111.5	-	1.42	-	-	2.41	1.20	0.50
109	Oegopsida	Pachypteroteuthidae	uncertain	uncertain	Late Campanian	juvenile	-	-	1.94	-	-	-	-	-	3.02	1.53	0.51
110	Oegopsida	Pachypteroteuthidae	uncertain	uncertain	Early Maastrichtian	juvenile	-	1.98	-	-	-	-	-	-	2.12	-	-
111	Oegopsida	Pachypteroteuthidae	uncertain	uncertain	Early Maastrichtian	juvenile	-	1.87	-	-	-	1.65	-	-	2.22	-	-
112	Oegopsida	Pachypteroteuthidae	uncertain	uncertain	Early Maastrichtian	juvenile	3.77	2.54	-	-	-	1.84	2.01	0.92	2.48	0.94	0.38
113	Oegopsida	Pachypteroteuthidae	uncertain	uncertain	Early Maastrichtian	juvenile	2.80	-	-	-	-	1.65	1.44	1.15	2.11	0.92	0.44
114	Oegopsida	Pachypteroteuthidae	uncertain	uncertain	Early Maastrichtian	adult	2.95	1.45	1.07	-	-	-	-	-	1.57	0.80	0.51
115	Oegopsida	Pachypteroteuthidae	uncertain	uncertain	Early Maastrichtian	juvenile	-	-	-	-	-	-	-	-	1.71	1.12	0.65
116	Oegopsida	Pachypteroteuthidae	uncertain	uncertain	Early Maastrichtian	adult	3.07	1.80	1.52	-	-	1.70	1.59	1.07	2.03	0.97	0.48
117	Oegopsida	Pachypteroteuthidae	uncertain	uncertain	Early Maastrichtian	adult	3.19	1.96	2.37	-	124.8	1.65	1.70	0.97	2.18	0.72	0.33
118	Oegopsida	Scuthoteuthidae	*Scuthoteuthis*	*kawataro*	Early Cenomanian	subadult	-	2.73	-	56.0	144.1	2.81	2.20	1.28	3.57	2.81	0.79
119	Oegopsida	Scuthoteuthidae	*Scuthoteuthis*	*fragilis*	Late Campanian	adult	19.32	8.68	-	-	-	7.99	-	-	11.19	7.99	0.71
120	Oegopsida	Scuthoteuthidae	*Scuthoteuthis*	*falcatus*	Late Turonian	subadult	-	2.74	-	83.9	-	2.34	-	-	3.45	2.34	0.68
121	Oegopsida	Scuthoteuthidae	*Scuthoteuthis*	*falcatus*	Late Coniacian	subadult	-	2.55	-	95.3	-	2.07	1.16	1.78	3.55	2.07	0.58
122	Oegopsida	Scuthoteuthidae	*Scuthoteuthis*	*falcatus*	Santonian	subadult	-	2.91	-	100.6	-	2.21	1.56	1.42	4.07	-	-
123	Oegopsida	Scuthoteuthidae	*Scuthoteuthis*	*tenuis*	Late Coniacian	subadult	2.24	1.08	-	119.8	-	1.21	1.35	0.90	2.58	1.21	0.47
124	Oegopsida	Scuthoteuthidae	*Grossiscapula*	*angusta*	Early Maastrichtian	adult	4.40	2.80	2.25	92.3	127.1	3.00	2.22	1.35	3.60	2.31	0.64
125	Oegopsida	Scuthoteuthidae	*Amblyscuthes*	*apterus*	Late Cenomanian	subadult	-	1.47	-	78.1	130.9	1.56	1.21	1.29	2.55	1.56	0.61
126	Oegopsida	Scuthoteuthidae	*Amblyscuthes*	*apterus*	Early Campanian	subadult	-	3.02	-	105.1	-	3.31	2.45	-	5.74	3.31	0.58
127	Oegopsida	Scuthoteuthidae	*Amblyscuthes*	*pyrgoides*	Early Cenomanian	subadult	4.29	2.72	-	-	-	1.81	0.77	2.36	3.02	1.81	0.60
128	Oegopsida	Scuthoteuthidae	*Amblyscuthes*	*pyrgoides*	Late Turonian	subadult	-	1.85	-	104.1	-	1.88	1.02	1.84	2.91	1.88	0.65
129	Oegopsida	Scuthoteuthidae	*Amblyscuthes*	*pyrgoides*	Late Coniacian	subadult	-	2.17	-	-	-	-	-	-	2.72	-	-
130	Oegopsida	Scuthoteuthidae	*Amblyscuthes*	*pyrgoides*	Early Campanian	subadult	-	1.85	-	-	-	-	-	1.87	2.48	-	-
131	Oegopsida	Scuthoteuthidae	*Amblyscuthes*	*pyrgoides*	Early Campanian	subadult	-	1.48	-	100.7	125.7	1.35	0.83	1.63	2.40	-	-
132	Oegopsida	Scuthoteuthidae	uncertain	uncertain	Early Cenomanian	juvenile	-	2.62	-	65.0	-	3.37	-	-	3.81	3.37	0.88
133	Oegopsida	Scuthoteuthidae	uncertain	uncertain	Early Coniacian	juvenile	2.74	2.20	-	131.3	-	2.64	-	-	3.57	2.64	0.74

Table 3. (continued)

No.	Dataset and Collection No. (NMNS: National Museum of Nature and Science, Tokyo)				Figure
	3D model	Label data of 3D models	Cross-sectional images of 3D models	Original cross-sectional images of carbonate concretions (animations of cross-sectional images are available from	
67	NMNS_DS00034_OJDNCD8.stl	L_NMNS_DS00034_20180207_c1_wl_01_0379_OJDNCD8.tif–0456_OJDNCD8.tif	C_NMNS_DS00034_20180207_c1_wl_01_0379_OJDNCD8.jpg–0456_OJDNCD8.jpg	NMNS_DS00034_20180207_c1_wl_01_0379.jpg–0456.jpg	Fig. 8P–T
68	NMNS_DS00173_X7NQkzW.stl	L_NMNS_DS00173_wl_01_0910_X7NQkzW.tif–0963_X7NQkzW.tif	C_NMNS_DS00173_wl_01_0910_X7NQkzW.jpg–0963_X7NQkzW.jpg	NMNS_DS00173_wl_01_0910.tif–0963.tif	-
69	NMNS_DS00173_IHj1roq.stl	L_NMNS_DS00173_wl_01_1034_IHj1roq.tif–1104_IHj1roq.tif	C_NMNS_DS00173_wl_01_1034_IHj1roq.jpg–1104_IHj1roq.jpg	NMNS_DS00173_wl_01_1034.tif–1104.tif	-
70	NMNS_DS00034_MDF4xvB.stl	L_NMNS_DS00034_20180207_c1_wl_01_0492_MDF4xvB.tif–0546_MDF4xvB.tif	C_NMNS_DS00034_20180207_c1_wl_01_0492_MDF4xvB.jpg–0546_MDF4xvB.jpg	NMNS_DS00034_20180207_c1_wl_01_0492.jpg–0546.jpg	Fig. 8U–Y
71	NMNS_DS00068_o0hmWAZ.stl	L_NMNS_DS00068_20181123_c1_wl_01_0176_o0hmWAZ.tif–0232_o0hmWAZ.tif	C_NMNS_DS00068_20181123_c1_wl_01_0176_o0hmWAZ.jpg–0232_o0hmWAZ.jpg	NMNS_DS00068_20181123_c1_wl_01_0176.jpg–0232.jpg	-
72	NMNS_DS00084_Z7XZtlw.stl	L_NMNS_DS00084_20190202_c1_wl_01_0001_Z7XZtlw.tif–0037_Z7XZtlw.tif	C_NMNS_DS00084_20190202_c1_wl_01_0001_Z7XZtlw.jpg–0037_Z7XZtlw.jpg	NMNS_DS00084_20190202_c1_wl_01_0001.jpg–0037.jpg	-
73	NMNS_DS00084_vmtPsX9.stl	L_NMNS_DS00084_20190202_c1_wl_01_0140_vmtPsX9.tif–0174_vmtPsX9.tif	C_NMNS_DS00084_20190202_c1_wl_01_0140_vmtPsX9.jpg–0174_vmtPsX9.jpg	NMNS_DS00084_20190202_c1_wl_01_0140.jpg–0174.jpg	-
74	NMNS_DS00082_H8vz3ua.stl	L_NMNS_DS00082_20190127_c1_wl_01_0011_H8vz3ua.tif–0093_H8vz3ua.tif	C_NMNS_DS00082_20190127_c1_wl_01_0011_H8vz3ua.jpg–0093_H8vz3ua.jpg	NMNS_DS00082_20190127_c1_wl_01_0011.jpg–0093.jpg	-
75	NMNS_DS00082_2PRzcqr.stl	L_NMNS_DS00082_20190127_c1_wl_01_0127_2PRzcqr.tif–0179_2PRzcqr.tif	C_NMNS_DS00082_20190127_c1_wl_01_0127_2PRzcqr.jpg–0179_2PRzcqr.jpg	NMNS_DS00082_20190127_c1_wl_01_0127.jpg–0179.jpg	-
76	NMNS_DS00082_rGYynE6.stl	L_NMNS_DS00082_20190127_c1_wl_01_0336_rGYynE6.tif–0392_rGYynE6.tif	C_NMNS_DS00082_20190127_c1_wl_01_0336_rGYynE6.jpg–0392_rGYynE6.jpg	NMNS_DS00082_20190127_c1_wl_01_0336.jpg–0392.jpg	-
77	NMNS_DS00082_O57xtDF.stl	L_NMNS_DS00082_20190127_c1_wl_01_0482_O57xtDF.tif–0505_O57xtDF.tif	C_NMNS_DS00082_20190127_c1_wl_01_0482_O57xtDF.jpg–0505_O57xtDF.jpg	NMNS_DS00082_20190127_c1_wl_01_0482.jpg–0505.jpg	-
78	NMNS_DS00140_6dLPkjD.stl	L_NMNS_DS00140_wl_03_0202_6dLPkjD.tif–0265_6dLPkjD.tif	C_NMNS_DS00140_wl_03_0202_6dLPkjD.jpg–0265_6dLPkjD.jpg	NMNS_DS00140_wl_03_0202.tif–0265.tif	-
79	NMNS_DS00140_0vO7jym.stl	L_NMNS_DS00140_wl_03_0867_0vO7jym.tif–0936_0vO7jym.tif	C_NMNS_DS00140_wl_03_0867_0vO7jym.jpg–0936_0vO7jym.jpg	NMNS_DS00140_wl_03_0867.tif–0936.tif	-
80	NMNS_DS00009_U4Gf3fX.stl	L_NMNS_DS00009_20170720_c1_wl_01_0820_U4Gf3fX.tif–0886_U4Gf3fX.tif	C_NMNS_DS00009_20170720_c1_wl_01_0820_U4Gf3fX.jpg–0886_U4Gf3fX.jpg	NMNS_DS00009_20170720_c1_wl_01_0820.jpg–0886.jpg	-
81	NMNS_DS00009_6SkvYgx.stl	L_NMNS_DS00009_20170720_c1_wl_01_1137_6SkvYgx.tif–1178_6SkvYgx.tif	C_NMNS_DS00009_20170720_c1_wl_01_1137_6SkvYgx.jpg–1178_6SkvYgx.jpg	NMNS_DS00009_20170720_c1_wl_01_1137.jpg–1178.jpg	-
82	NMNS_DS00040_ezp57pJ.stl	L_NMNS_DS00040_20180409_c1_wl_01_0441_ezp57pJ.tif–0495_ezp57pJ.tif	C_NMNS_DS00040_20180409_c1_wl_01_0441_ezp57pJ.jpg–0495_ezp57pJ.jpg	NMNS_DS00040_20180409_c1_wl_01_0441.jpg–0495.jpg	-
83	NMNS_DS00046_zxab88O.stl	L_NMNS_DS00046_20180709_c1_wl_01_0760_zxab88O.tif–0799_zxab88O.tif	C_NMNS_DS00046_20180709_c1_wl_01_0760_zxab88O.jpg–0799_zxab88O.jpg	NMNS_DS00046_20180709_c1_wl_01_0760.jpg–0799.jpg	-
84	NMNS_DS00173_Ud7AGGR.stl	L_NMNS_DS00173_wl_01_0068_Ud7AGGR.tif–0102_Ud7AGGR.tif	C_NMNS_DS00173_wl_01_0068_Ud7AGGR.jpg–0102_Ud7AGGR.jpg	NMNS_DS00173_wl_01_0068.tif–0102.tif	-
85	NMNS_DS00173_i7RkpPt.stl	L_NMNS_DS00173_wl_01_0177_i7RkpPt.tif–0214_i7RkpPt.tif	C_NMNS_DS00173_wl_01_0177_i7RkpPt.jpg–0214_i7RkpPt.jpg	NMNS_DS00173_wl_01_0177.tif–0214.tif	-
86	NMNS_DS00173_MT5y8SL.stl	L_NMNS_DS00173_wl_01_0391_MT5y8SL.tif–0423_MT5y8SL.tif	C_NMNS_DS00173_wl_01_0391_MT5y8SL.jpg–0423_MT5y8SL.jpg	NMNS_DS00173_wl_01_0391.tif–0423.tif	-
87	NMNS_DS00173_vnX5JU7.stl	L_NMNS_DS00173_wl_01_0577_vnX5JU7.tif–0613_vnX5JU7.tif	C_NMNS_DS00173_wl_01_0577_vnX5JU7.jpg–0613_vnX5JU7.jpg	NMNS_DS00173_wl_01_0577.tif–0613.tif	-
88	NMNS_DS00173_k4Zi6cM.stl	L_NMNS_DS00173_wl_01_0679_k4Zi6cM.tif–0720_k4Zi6cM.tif	C_NMNS_DS00173_wl_01_0679_k4Zi6cM.jpg–0720_k4Zi6cM.jpg	NMNS_DS00173_wl_01_0679.tif–0720.tif	-
89	NMNS_DS00173_RS2ows3.stl	L_NMNS_DS00173_wl_01_0826_RS2ows3.tif–0851_RS2ows3.tif	C_NMNS_DS00173_wl_01_0826_RS2ows3.jpg–0851_RS2ows3.jpg	NMNS_DS00173_wl_01_0826.tif–0851.tif	-
90	NMNS_DS00173_BSp1Uzp.stl	L_NMNS_DS00173_wl_01_1079_BSp1Uzp.tif–1136_BSp1Uzp.tif	C_NMNS_DS00173_wl_01_1079_BSp1Uzp.jpg–1136_BSp1Uzp.jpg	NMNS_DS00173_wl_01_1079.tif–1136.tif	-
91	NMNS_DS00173_Nv9fbhp.stl	L_NMNS_DS00173_wl_01_1184_Nv9fbhp.tif–1276_Nv9fbhp.tif	C_NMNS_DS00173_wl_01_1184_Nv9fbhp.jpg–1276_Nv9fbhp.jpg	NMNS_DS00173_wl_01_1184.tif–1276.tif	-
92	NMNS_DS00173_eVvAn7U.stl	L_NMNS_DS00173_wl_01_1264_eVvAn7U.tif–1331_eVvAn7U.tif	C_NMNS_DS00173_wl_01_1264_eVvAn7U.jpg–1331_eVvAn7U.jpg	NMNS_DS00173_wl_01_1264.tif–1331.tif	-
93	NMNS_DS00173_GtZcR9a.stl	L_NMNS_DS00173_wl_01_1303_GtZcR9a.tif–1347_GtZcR9a.tif	C_NMNS_DS00173_wl_01_1303_GtZcR9a.jpg–1347_GtZcR9a.jpg	NMNS_DS00173_wl_01_1303.tif–1347.tif	-
94	NMNS_DS00034_Pt2Sm0S.stl	L_NMNS_DS00034_20180207_c1_wl_01_0053_Pt2Sm0S.tif–0091_Pt2Sm0S.tif	C_NMNS_DS00034_20180207_c1_wl_01_0053_Pt2Sm0S.jpg–0091_Pt2Sm0S.jpg	NMNS_DS00034_20180207_c1_wl_01_0053.jpg–0091.jpg	-
95	NMNS_DS00034_3Ec0EI7.stl	L_NMNS_DS00034_20180207_c1_wl_01_0316_3Ec0EI7.tif–0345_3Ec0EI7.tif	C_NMNS_DS00034_20180207_c1_wl_01_0316_3Ec0EI7.jpg–0345_3Ec0EI7.jpg	NMNS_DS00034_20180207_c1_wl_01_0316.jpg–0345.jpg	-
96	NMNS_DS00034_GFK1LYI.stl	L_NMNS_DS00034_20180207_c1_wl_01_0441_GFK1LYI.tif–0483_GFK1LYI.tif	C_NMNS_DS00034_20180207_c1_wl_01_0441_GFK1LYI.jpg–0483_GFK1LYI.jpg	NMNS_DS00034_20180207_c1_wl_01_0441.jpg–0483.jpg	-
97	NMNS_DS00034_ilTGm9n.stl	L_NMNS_DS00034_20180207_c1_wl_01_0443_ilTGm9n.tif–0468_ilTGm9n.tif	C_NMNS_DS00034_20180207_c1_wl_01_0443_ilTGm9n.jpg–0468_ilTGm9n.jpg	NMNS_DS00034_20180207_c1_wl_01_0443.jpg–0468.jpg	-
98	NMNS_DS00034_nf9Ejgu.stl	L_NMNS_DS00034_20180207_c1_wl_01_0461_nf9Ejgu.tif–0521_nf9Ejgu.tif	C_NMNS_DS00034_20180207_c1_wl_01_0461_nf9Ejgu.jpg–0521_nf9Ejgu.jpg	NMNS_DS00034_20180207_c1_wl_01_0461.jpg–0521.jpg	-
99	NMNS_DS00034_Z2XS2EX.stl	L_NMNS_DS00034_20180207_c1_wl_01_0510_Z2XS2EX.tif–0570_Z2XS2EX.tif	C_NMNS_DS00034_20180207_c1_wl_01_0510_Z2XS2EX.jpg–0570_Z2XS2EX.jpg	NMNS_DS00034_20180207_c1_wl_01_0510.jpg–0570.jpg	-
100	NMNS_DS00089_EbQv3XX.stl	L_NMNS_DS00089_20190223_c1_wl_01_0033_EbQv3XX.tif–0088_EbQv3XX.tif	C_NMNS_DS00089_20190223_c1_wl_01_0033_EbQv3XX.jpg–0088_EbQv3XX.jpg	NMNS_DS00089_20190223_c1_wl_01_0033.jpg–0088.jpg	-
101	NMNS_DS00089_favO32g.stl	L_NMNS_DS00089_20190223_c1_wl_01_0579_favO32g.tif–0609_favO32g.tif	C_NMNS_DS00089_20190223_c1_wl_01_0579_favO32g.jpg–0609_favO32g.jpg	NMNS_DS00089_20190223_c1_wl_01_0579.jpg–0609.jpg	-
102	NMNS_DS00011_qpwW1R1.stl	L_NMNS_DS00011_20170806_c1_wl_01_0282_qpwW1R1.tif–0309_qpwW1R1.tif	C_NMNS_DS00011_20170806_c1_wl_01_0282_qpwW1R1.jpg–0309_qpwW1R1.jpg	NMNS_DS00011_20170806_c1_wl_01_0282.jpg–0309.jpg	-
103	NMNS_DS00097_bdk7qIo.stl	L_NMNS_DS00097_wl_01_0001_bdk7qIo.tif–0044_bdk7qIo.tif	C_NMNS_DS00097_wl_01_0001_bdk7qIo.jpg–0044_bdk7qIo.jpg	NMNS_DS00097_wl_01_0001.jpg–0044.jpg	-
104	NMNS_DS00097_PmwMgn0.stl	L_NMNS_DS00097_wl_01_0310_PmwMgn0.tif–0360_PmwMgn0.tif	C_NMNS_DS00097_wl_01_0310_PmwMgn0.jpg–0360_PmwMgn0.jpg	NMNS_DS00097_wl_01_0310.jpg–0360.jpg	-
105	NMNS_DS00171_nNE3rJU.stl	L_NMNS_DS00171_wl_01_0595_nNE3rJU.tif–0653_nNE3rJU.tif	C_NMNS_DS00171_wl_01_0595_nNE3rJU.jpg–0653_nNE3rJU.jpg	NMNS_DS00171_wl_01_0595.tif–0653.tif	-
106	NMNS_DS00171_zi2h0sv.stl	L_NMNS_DS00171_wl_01_0725_zi2h0sv.tif–0780_zi2h0sv.tif	C_NMNS_DS00171_wl_01_0725_zi2h0sv.jpg–0780_zi2h0sv.jpg	NMNS_DS00171_wl_01_0725.tif–0780.tif	-
107	NMNS_DS00175_oPtCSM5.stl	L_NMNS_DS00175_wl_01_0108_oPtCSM5.tif–0179_oPtCSM5.tif	C_NMNS_DS00175_wl_01_0108_oPtCSM5.jpg–0179_oPtCSM5.jpg	NMNS_DS00175_wl_01_0108.tif–0179.tif	-
108	NMNS_DS00175_fonSGM6.stl	L_NMNS_DS00175_wl_01_0618_fonSGM6.tif–0664_fonSGM6.tif	C_NMNS_DS00175_wl_01_0618_fonSGM6.jpg–0664_fonSGM6.jpg	NMNS_DS00175_wl_01_0618.tif–0664.tif	-
109	NMNS_DS00182_SYDC0zH.stl	L_NMNS_DS00182_wl_01_0962_SYDC0zH.tif–1009_SYDC0zH.tif	C_NMNS_DS00182_wl_01_0962_SYDC0zH.jpg–1009_SYDC0zH.jpg	NMNS_DS00182_wl_01_0962.tif–1009.tif	-
110	NMNS_DS00128_R1IzaWx.stl	L_NMNS_DS00128_wl_01_1141_R1IzaWx.tif–1187_R1IzaWx.tif	C_NMNS_DS00128_wl_01_1141_R1IzaWx.jpg–1187_R1IzaWx.jpg	NMNS_DS00128_wl_01_1141.jpg–1187.jpg	-
111	NMNS_DS00174_53ff8oD.stl	L_NMNS_DS00174_wl_01_0123_53ff8oD.tif–0164_53ff8oD.tif	C_NMNS_DS00174_wl_01_0123_53ff8oD.jpg–0164_53ff8oD.jpg	NMNS_DS00174_wl_01_0123.tif–0164.tif	-
112	NMNS_DS00174_WNYvS2g.stl	L_NMNS_DS00174_wl_01_0229_WNYvS2g.tif–0276_WNYvS2g.tif	C_NMNS_DS00174_wl_01_0229_WNYvS2g.jpg–0276_WNYvS2g.jpg	NMNS_DS00174_wl_01_0229.tif–0276.tif	-
113	NMNS_DS00174_q1CFxaH.stl	L_NMNS_DS00174_wl_01_0255_q1CFxaH.tif–0304_q1CFxaH.tif	C_NMNS_DS00174_wl_01_0255_q1CFxaH.jpg–0304_q1CFxaH.jpg	NMNS_DS00174_wl_01_0255.tif–0304.tif	-
114	NMNS_DS00174_P1KHcht.stl	L_NMNS_DS00174_wl_01_0286_P1KHcht.tif–0319_P1KHcht.tif	C_NMNS_DS00174_wl_01_0286_P1KHcht.jpg–0319_P1KHcht.jpg	NMNS_DS00174_wl_01_0286.tif–0319.tif	-
115	NMNS_DS00174_tYi8udG.stl	L_NMNS_DS00174_wl_01_0305_tYi8udG.tif–0336_tYi8udG.tif	C_NMNS_DS00174_wl_01_0305_tYi8udG.jpg–0336_tYi8udG.jpg	NMNS_DS00174_wl_01_0305.tif–0336.tif	-
116	NMNS_DS00174_xil2BIU.stl	L_NMNS_DS00174_wl_01_0645_xil2BIU.tif–0694_xil2BIU.tif	C_NMNS_DS00174_wl_01_0645_xil2BIU.jpg–0694_xil2BIU.jpg	NMNS_DS00174_wl_01_0645.tif–0694.tif	-
117	NMNS_DS00174_je66P5f.stl	L_NMNS_DS00174_wl_01_1089_je66P5f.tif–1147_je66P5f.tif	C_NMNS_DS00174_wl_01_1089_je66P5f.jpg–1147_je66P5f.jpg	NMNS_DS00174_wl_01_1089.tif–1147.tif	-
118	NMNS_DS00084_XCCa3MD.stl	L_NMNS_DS00084_20190202_c1_wl_01_0395_XCCa3MD.tif–0454_XCCa3MD.tif	C_NMNS_DS00084_20190202_c1_wl_01_0395_XCCa3MD.jpg–0454_XCCa3MD.jpg	NMNS_DS00084_20190202_c1_wl_01_0395.jpg–0454.jpg	Figs 3C & 9A–E
119	NMNS_DS00182_VHJhp0K.stl	L_NMNS_DS00182_wl_01_0729_VHJhp0K.tif–0910_VHJhp0K.tif	C_NMNS_DS00182_wl_01_0729_VHJhp0K.jpg–0910_VHJhp0K.jpg	NMNS_DS00182_wl_01_0729.tif–0910.tif	Fig. 9F–J
120	NMNS_DS00046_Tf7vfru.stl	L_NMNS_DS00046_20180709_c1_wl_01_0510_Tf7vfru.tif–0572_Tf7vfru.tif	C_NMNS_DS00046_20180709_c1_wl_01_0510_Tf7vfru.jpg–0572_Tf7vfru.jpg	NMNS_DS00046_20180709_c1_wl_01_0510.jpg–0572.jpg	-
121	NMNS_DS00089_cdL9i2R.stl	L_NMNS_DS00089_20190223_c1_wl_01_0315_cdL9i2R.tif–0377_cdL9i2R.tif	C_NMNS_DS00089_20190223_c1_wl_01_0315_cdL9i2R.jpg–0377_cdL9i2R.jpg	NMNS_DS00089_20190223_c1_wl_01_0315.jpg–0377.jpg	-
122	NMNS_DS00090_uJIwH0a.stl	L_NMNS_DS00090_20190228_c1_wl_01_0408_uJIwH0a.tif–0478_uJIwH0a.tif	C_NMNS_DS00090_20190228_c1_wl_01_0408_uJIwH0a.jpg–0478_uJIwH0a.jpg	NMNS_DS00090_20190228_c1_wl_01_0408.jpg–0478.jpg	Figs 9K–O
123	NMNS_DS00083_wMN7XI9.stl	L_NMNS_DS00083_20190130_c1_wl_01_0221_wMN7XI9.tif–0268_wMN7XI9.tif	C_NMNS_DS00083_20190130_c1_wl_01_0221_wMN7XI9.jpg–0268_wMN7XI9.jpg	NMNS_DS00083_20190130_c1_wl_01_0221.jpg–0268.jpg	Fig. 9P–T
124	NMNS_DS00172_cWN9IDD.stl	L_NMNS_DS00172_wl_01_0598_cWN9IDD.tif–0682_cWN9IDD.tif	C_NMNS_DS00172_wl_01_0598_cWN9IDD.jpg–0682_cWN9IDD.jpg	NMNS_DS00172_wl_01_0598.tif–0682.tif	Figs 3D & 9U–Y
125	NMNS_DS00082_9VBER8O.stl	L_NMNS_DS00082_20190127_c1_wl_01_0032_9VBER8O.tif–0070_9VBER8O.tif	C_NMNS_DS00082_20190127_c1_wl_01_0032_9VBER8O.jpg–0070_9VBER8O.jpg	NMNS_DS00082_20190127_c1_wl_01_0032.jpg–0070.jpg	-
126	NMNS_DS00175_1oEjNpv.stl	L_NMNS_DS00175_wl_01_0154_1oEjNpv.tif–0248_1oEjNpv.tif	C_NMNS_DS00175_wl_01_0154_1oEjNpv.jpg–0248_1oEjNpv.jpg	NMNS_DS00175_wl_01_0154.tif–0248.tif	Fig. 10A–E
127	NMNS_DS00084_0iYtfF.stl	L_NMNS_DS00084_20190202_c1_wl_01_0641_0iYtfF.tif–0685_0iYtfF.tif	C_NMNS_DS00084_20190202_c1_wl_01_0641_0iYtfF.jpg–0685_0iYtfF.jpg	NMNS_DS00084_20190202_c1_wl_01_0641.jpg–0685.jpg	-
128	NMNS_DS00046_ikc7ZzK.stl	L_NMNS_DS00046_20180709_c1_wl_01_0643_ikc7ZzK.tif–0679_ikc7ZzK.tif	C_NMNS_DS00046_20180709_c1_wl_01_0643_ikc7ZzK.jpg–0679_ikc7ZzK.jpg	NMNS_DS00046_20180709_c1_wl_01_0643.jpg–0679.jpg	Fig. 10F–J
129	NMNS_DS00083_hbPNRL6.stl	L_NMNS_DS00083_20190130_c1_wl_01_0242_hbPNRL6.tif–0281_hbPNRL6.tif	C_NMNS_DS00083_20190130_c1_wl_01_0242_hbPNRL6.jpg–0281_hbPNRL6.jpg	NMNS_DS00083_20190130_c1_wl_01_0242.jpg–0281.jpg	-
130	NMNS_DS00097_bizU8mn.stl	L_NMNS_DS00097_wl_01_0152_bizU8mn.tif–0187_bizU8mn.tif	C_NMNS_DS00097_wl_01_0152_bizU8mn.jpg–0187_bizU8mn.jpg	NMNS_DS00097_wl_01_0152.jpg–0187.jpg	-
131	NMNS_DS00175_nhUN0gO.stl	L_NMNS_DS00175_wl_01_0645_nhUN0gO.tif–0682_nhUN0gO.tif	C_NMNS_DS00175_wl_01_0645_nhUN0gO.jpg–0682_nhUN0gO.jpg	NMNS_DS00175_wl_01_0645.tif–0682.tif	-
132	NMNS_DS00084_skNkAF7.stl	L_NMNS_DS00084_20190202_c1_wl_01_0438_skNkAF7.tif–0491_skNkAF7.tif	C_NMNS_DS00084_20190202_c1_wl_01_0438_skNkAF7.jpg–0491_skNkAF7.jpg	NMNS_DS00084_20190202_c1_wl_01_0438.jpg–0491.jpg	-
133	NMNS_DS00034_yjFV2Xr.stl	L_NMNS_DS00034_20180207_c1_wl_01_0523_yjFV2Xr.tif–0571_yjFV2Xr.tif	C_NMNS_DS00034_20180207_c1_wl_01_0523_yjFV2Xr.jpg–0571_yjFV2Xr.jpg	NMNS_DS00034_20180207_c1_wl_01_0523.jpg–0571.jpg	-

Table 3. (continued)

No.	Classification				Geological age	Growth stage	Measurements										
	Order	Family	Genus	Species			CL (mm)	HL (mm)	WL (mm)	AJS (degree)	WA (degree)	LRL (mm)	RW (mm)	LRL/RW	JEL (mm)	JELL (mm)	JELL/JEL
134	Oegopsida	Paleothysanoteuthidae	*Paleothysanoteuthis*	*complicatus*	Santonian	subadult	-	-	-	40.0	121.5	1.69	-	-	2.42	1.69	0.70
135	Oegopsida	Paleothysanoteuthidae	*Paleothysanoteuthis*	*complicatus*	Santonian	subadult	-	2.53	-	69.9	139.9	1.64	1.60	1.03	-	1.64	-
136	Oegopsida	Paleothysanoteuthidae	*Aetorhynchus*	*incisus*	earliest Cenomanian	subadult	-	4.78	-	55.3	135.1	3.58	-	1.29	5.37	3.58	0.67
137	Oegopsida	uncertain	uncertain	uncertain	earliest Cenomanian	juvenile	-	1.35	-	-	-	-	-	-	1.69	-	-
138	Oegopsida	uncertain	uncertain	uncertain	Early Cenomanian	juvenile	-	1.59	-	-	-	-	-	-	2.61	-	-
139	Oegopsida	uncertain	uncertain	uncertain	Late Cenomanian	juvenile	-	1.46	-	88.0	135.9	1.35	-	-	1.80	-	-
140	Oegopsida	uncertain	uncertain	uncertain	Late Cenomanian	juvenile	-	1.70	-	-	-	-	-	-	2.35	-	-
141	Oegopsida	uncertain	uncertain	uncertain	Late Cenomanian	juvenile	-	1.17	-	-	-	-	-	-	1.55	-	-
142	Oegopsida	uncertain	uncertain	uncertain	Late Cenomanian	juvenile	-	1.60	-	-	-	1.42	-	-	2.18	1.42	0.65
143	Oegopsida	uncertain	uncertain	uncertain	Late Cenomanian	juvenile	-	1.95	-	-	-	1.80	1.62	1.11	2.68	-	-
144	Oegopsida	uncertain	uncertain	uncertain	Early Turonian	juvenile	-	4.07	-	-	-	6.85	-	-	7.74	-	-
145	Oegopsida	uncertain	uncertain	uncertain	Late Turonian	juvenile	2.26	1.21	-	90.6	132.9	1.18	1.11	1.06	1.80	1.18	0.66
146	Oegopsida	uncertain	uncertain	uncertain	Late Turonian	juvenile	-	1.90	-	-	-	-	-	1.55	2.12	-	-
147	Oegopsida	uncertain	uncertain	uncertain	Late Turonian	juvenile	5.34	3.07	-	-	-	-	-	0.97	3.28	-	-
148	Oegopsida	uncertain	uncertain	uncertain	Late Turonian	juvenile	1.37	1.05	-	-	-	-	-	0.79	0.80	-	-
149	Oegopsida	uncertain	uncertain	uncertain	Late Turonian	juvenile	-	2.65	-	-	-	-	-	1.31	2.81	-	-
150	Oegopsida	uncertain	uncertain	uncertain	Late Turonian	juvenile	2.59	1.58	1.16	-	-	-	-	1.04	1.59	1.21	0.76
151	Oegopsida	uncertain	uncertain	uncertain	Late Turonian	juvenile	2.47	1.69	-	-	-	1.54	1.51	1.02	2.06	-	-
152	Oegopsida	uncertain	uncertain	uncertain	Late Turonian	juvenile	-	1.12	-	-	-	-	-	1.22	1.40	-	-
153	Oegopsida	uncertain	uncertain	uncertain	Late Turonian	juvenile	-	2.21	-	133.3	-	1.88	1.42	1.32	2.78	-	-
154	Oegopsida	uncertain	uncertain	uncertain	Late Turonian	juvenile	4.33	3.17	-	101.2	-	2.57	-	-	4.00	-	-
155	Oegopsida	uncertain	uncertain	uncertain	Late Turonian	juvenile	-	1.49	-	92.3	-	1.45	-	-	2.44	1.45	0.59
156	Oegopsida	uncertain	uncertain	uncertain	Late Turonian	juvenile	-	1.11	-	-	-	-	-	-	1.62	-	-
157	Oegopsida	uncertain	uncertain	uncertain	Late Turonian	juvenile	2.57	1.79	-	-	-	1.44	-	-	1.83	-	-
158	Oegopsida	uncertain	uncertain	uncertain	Late Turonian	juvenile	-	1.12	-	-	-	-	-	-	1.62	-	-
159	Oegopsida	uncertain	uncertain	uncertain	Late Turonian	juvenile	-	2.31	-	-	-	-	-	-	-	-	-
160	Oegopsida	uncertain	uncertain	uncertain	Late Turonian	juvenile	-	1.16	-	-	-	-	-	-	1.32	-	-
161	Oegopsida	uncertain	uncertain	uncertain	Late Turonian	juvenile	-	1.83	-	-	-	1.76	1.64	1.07	2.28	-	-
162	Oegopsida	uncertain	uncertain	uncertain	Late Turonian	juvenile	-	2.41	-	-	-	2.46	-	-	3.23	-	-
163	Oegopsida	uncertain	uncertain	uncertain	Late Turonian	juvenile	-	1.85	-	-	-	1.46	1.11	1.32	1.96	-	-
164	Oegopsida	uncertain	uncertain	uncertain	Late Turonian	juvenile	-	2.03	-	-	-	1.49	1.22	1.22	2.91	-	-
165	Oegopsida	uncertain	uncertain	uncertain	Late Turonian	juvenile	-	1.55	-	-	-	-	-	-	1.67	-	-
166	Oegopsida	uncertain	uncertain	uncertain	Early Coniacian	juvenile	-	1.67	-	-	-	1.87	1.94	0.96	2.17	-	-
167	Oegopsida	uncertain	uncertain	uncertain	Early Coniacian	juvenile	3.64	2.06	-	-	-	-	-	1.21	2.11	-	-
168	Oegopsida	uncertain	uncertain	uncertain	Early Coniacian	juvenile	-	-	-	-	-	-	-	-	-	-	-
169	Oegopsida	uncertain	uncertain	uncertain	Early Coniacian	juvenile	-	1.91	-	-	-	-	-	1.00	2.13	-	-
170	Oegopsida	uncertain	uncertain	uncertain	Early Coniacian	juvenile	-	-	-	-	-	-	-	-	-	-	-
171	Oegopsida	uncertain	uncertain	uncertain	Late Coniacian	juvenile	-	-	-	-	-	-	-	-	3.24	-	-
172	Oegopsida	uncertain	uncertain	uncertain	Late Coniacian	juvenile	-	1.32	-	-	-	-	-	-	1.67	-	-
173	Oegopsida	uncertain	uncertain	uncertain	Late Coniacian	juvenile	-	-	-	-	-	-	-	-	1.94	-	-
174	Oegopsida	uncertain	uncertain	uncertain	Late Coniacian	juvenile	2.72	1.33	-	-	-	-	-	-	1.92	-	-
175	Oegopsida	uncertain	uncertain	uncertain	Late Coniacian	juvenile	-	1.06	-	-	-	-	-	-	-	-	-
176	Oegopsida	uncertain	uncertain	uncertain	Late Coniacian	juvenile	-	1.37	-	-	-	-	-	-	2.26	-	-
177	Oegopsida	uncertain	uncertain	uncertain	Late Coniacian	juvenile	-	1.58	-	-	-	-	-	-	2.16	-	-
178	Oegopsida	uncertain	uncertain	uncertain	Late Coniacian	juvenile	-	-	-	-	-	2.89	-	-	4.16	2.89	0.69
179	Oegopsida	uncertain	uncertain	uncertain	Late Coniacian	juvenile	-	-	-	-	-	-	-	-	2.21	-	-
180	Oegopsida	uncertain	uncertain	uncertain	Late Coniacian	juvenile	-	2.23	-	-	-	-	-	-	3.16	-	-
181	Oegopsida	uncertain	uncertain	uncertain	Late Coniacian	juvenile	-	5.68	-	-	-	-	-	-	7.13	4.67	0.65
182	Oegopsida	uncertain	uncertain	uncertain	Late Coniacian	juvenile	-	1.72	-	-	-	-	-	-	3.24	-	-
183	Oegopsida	uncertain	uncertain	uncertain	Santonian	juvenile	-	1.99	-	-	-	-	-	-	2.39	-	-
184	Oegopsida	uncertain	uncertain	uncertain	Santonian	juvenile	1.63	1.02	-	-	-	1.63	-	-	1.64	-	-
185	Oegopsida	uncertain	uncertain	uncertain	Santonian	juvenile	-	-	-	-	-	-	-	-	-	-	-
186	Oegopsida	uncertain	uncertain	uncertain	Santonian	juvenile	2.41	1.38	-	-	-	-	-	-	1.54	-	-
187	Oegopsida	uncertain	uncertain	uncertain	Santonian	juvenile	-	2.37	-	-	-	-	-	-	3.59	-	-
188	Oegopsida	uncertain	uncertain	uncertain	Santonian	juvenile	-	1.58	-	-	-	-	-	-	2.67	-	-
189	Oegopsida	uncertain	uncertain	uncertain	Santonian	juvenile	-	-	-	-	-	-	-	-	2.94	-	-
190	Oegopsida	uncertain	uncertain	uncertain	Santonian	juvenile	-	1.23	-	-	-	-	-	-	1.80	-	-
191	Oegopsida	uncertain	uncertain	uncertain	Santonian	juvenile	4.86	2.98	-	107.2	-	3.00	2.12	1.42	4.28	3.00	0.70
192	Oegopsida	uncertain	uncertain	uncertain	Santonian	juvenile	-	2.04	-	-	-	-	-	1.78	2.88	-	-
193	Oegopsida	uncertain	uncertain	uncertain	Santonian	juvenile	3.70	1.52	-	-	-	1.95	-	-	2.79	-	-
194	Oegopsida	uncertain	uncertain	uncertain	Santonian	juvenile	-	2.20	-	-	-	-	-	1.10	2.43	-	-
195	Oegopsida	uncertain	uncertain	uncertain	Santonian	juvenile	-	1.37	-	-	-	-	-	-	-	-	-
196	Oegopsida	uncertain	uncertain	uncertain	Santonian	uncertain	-	1.42	-	-	-	-	-	-	-	-	-

Table 3. (continued)

No.	Dataset and Collection No. (NMNS: National Museum of Nature and Science, Tokyo)				Figure
	3D model	Label data of 3D models	Cross-sectional images of 3D models	Original cross-sectional images of carbonate concretions (animations of cross-sectional images are available from	
134	NMNS_DS00090_uO7uJwu.stl	L_NMNS_DS00090_20190228_c1_wl_01_0482_uO7uJwu.tif–0523_uO7uJwu.tif	C_NMNS_DS00090_20190228_c1_wl_01_0482_uO7uJwu.jpg–0523_uO7uJwu.jpg	NMNS_DS00090_20190228_c1_wl_01_0482.jpg–0523.jpg	Fig. 10P–T
135	NMNS_DS00104_ZNFObG0.stl	L_NMNS_DS00104_wl_01_0131_ZNFObG0.tif–0189_ZNFObG0.tif	C_NMNS_DS00104_wl_01_0131_ZNFObG0.jpg–0189_ZNFObG0.jpg	NMNS_DS00104_wl_01_0131.jpg–0189.jpg	Figs 3E & 10K–O
136	NMNS_DS00068_z6nASvr.stl	L_NMNS_DS00068_20181123_c1_wl_01_0582_z6nASvr.tif–0673_z6nASvr.tif	C_NMNS_DS00068_20181123_c1_wl_01_0582_z6nASvr.jpg–0673_z6nASvr.jpg	NMNS_DS00068_20181123_c1_wl_01_0582.jpg–0673.jpg	Figs 3F & 10U–Y
137	NMNS_DS00068_jPw6ko4.stl	L_NMNS_DS00068_20181123_c1_wl_01_0856_jPw6ko4.tif–0887_jPw6ko4.tif	C_NMNS_DS00068_20181123_c1_wl_01_0856_jPw6ko4.jpg–0887_jPw6ko4.jpg	NMNS_DS00068_20181123_c1_wl_01_0856.jpg–0887.jpg	-
138	NMNS_DS00084_IG3g9n4.stl	L_NMNS_DS00084_20190202_c1_wl_01_0331_IG3g9n4.tif–0380_IG3g9n4.tif	C_NMNS_DS00084_20190202_c1_wl_01_0331_IG3g9n4.jpg–0380_IG3g9n4.jpg	NMNS_DS00084_20190202_c1_wl_01_0331.jpg–0380.jpg	-
139	NMNS_DS00082_KEtUN3n.stl	L_NMNS_DS00082_20190127_c1_wl_01_0034_KEtUN3n.tif–0050_KEtUN3n.tif	C_NMNS_DS00082_20190127_c1_wl_01_0034_KEtUN3n.jpg–0050_KEtUN3n.jpg	NMNS_DS00082_20190127_c1_wl_01_0034.jpg–0050.jpg	-
140	NMNS_DS00082_S4gN8WC.stl	L_NMNS_DS00082_20190127_c1_wl_01_0582_S4gN8WC.tif–0617_S4gN8WC.tif	C_NMNS_DS00082_20190127_c1_wl_01_0582_S4gN8WC.jpg–0617_S4gN8WC.jpg	NMNS_DS00082_20190127_c1_wl_01_0582.jpg–0617.jpg	-
141	NMNS_DS00082_QZjjRl8.stl	L_NMNS_DS00082_20190127_c1_wl_01_0578_QZjjRl8.tif–0602_QZjjRl8.tif	C_NMNS_DS00082_20190127_c1_wl_01_0578_QZjjRl8.jpg–0602_QZjjRl8.jpg	NMNS_DS00082_20190127_c1_wl_01_0578.jpg–0602.jpg	-
142	NMNS_DS00082_t4UOvaO.stl	L_NMNS_DS00082_20190127_c1_wl_01_0653_t4UOvaO.tif–0679_t4UOvaO.tif	C_NMNS_DS00082_20190127_c1_wl_01_0653_t4UOvaO.jpg–0679_t4UOvaO.jpg	NMNS_DS00082_20190127_c1_wl_01_0653.jpg–0679.jpg	-
143	NMNS_DS00082_pS6AQhr.stl	L_NMNS_DS00082_20190127_c1_wl_01_0698_pS6AQhr.tif–0754_pS6AQhr.tif	C_NMNS_DS00082_20190127_c1_wl_01_0698_pS6AQhr.jpg–0754_pS6AQhr.jpg	NMNS_DS00082_20190127_c1_wl_01_0698.jpg–0754.jpg	-
144	NMNS_DS00140_IWPZJL0.stl	L_NMNS_DS00140_wl_03_0334_IWPZJL0.tif–0530_IWPZJL0.tif	C_NMNS_DS00140_wl_03_0334_IWPZJL0.jpg–0530_IWPZJL0.jpg	NMNS_DS00140_wl_03_0334.tif–0530.tif	-
145	NMNS_DS00040_f5baG18.stl	L_NMNS_DS00040_20180409_c1_wl_01_0091_f5baG18.tif–0124_f5baG18.tif	C_NMNS_DS00040_20180409_c1_wl_01_0091_f5baG18.jpg–0124_f5baG18.jpg	NMNS_DS00040_20180409_c1_wl_01_0091.jpg–0124.jpg	-
146	NMNS_DS00040_5UEmEw7.stl	L_NMNS_DS00040_20180409_c1_wl_01_0501_5UEmEw7.tif–0533_5UEmEw7.tif	C_NMNS_DS00040_20180409_c1_wl_01_0501_5UEmEw7.jpg–0533_5UEmEw7.jpg	NMNS_DS00040_20180409_c1_wl_01_0501.jpg–0533.jpg	-
147	NMNS_DS00041_qf2yg91.stl	L_NMNS_DS00041_20180414_c1_wl_01_0407_qf2yg91.tif–0481_qf2yg91.tif	C_NMNS_DS00041_20180414_c1_wl_01_0407_qf2yg91.jpg–0481_qf2yg91.jpg	NMNS_DS00041_20180414_c1_wl_01_0407.jpg–0481.jpg	-
148	NMNS_DS00041_I7gRaRg.stl	L_NMNS_DS00041_20180414_c1_wl_01_0446_I7gRaRg.tif–0470_I7gRaRg.tif	C_NMNS_DS00041_20180414_c1_wl_01_0446_I7gRaRg.jpg–0470_I7gRaRg.jpg	NMNS_DS00041_20180414_c1_wl_01_0446.jpg–0470.jpg	-
149	NMNS_DS00041_hs6nJ9o.stl	L_NMNS_DS00041_20180414_c1_wl_01_0568_hs6nJ9o.tif–0646_hs6nJ9o.tif	C_NMNS_DS00041_20180414_c1_wl_01_0568_hs6nJ9o.jpg–0646_hs6nJ9o.jpg	NMNS_DS00041_20180414_c1_wl_01_0568.jpg–0646.jpg	-
150	NMNS_DS00041_UX7j93Q.stl	L_NMNS_DS00041_20180414_c1_wl_01_0643_UX7j93Q.tif–0689_UX7j93Q.tif	C_NMNS_DS00041_20180414_c1_wl_01_0643_UX7j93Q.jpg–0689_UX7j93Q.jpg	NMNS_DS00041_20180414_c1_wl_01_0643.jpg–0689.jpg	-
151	NMNS_DS00041_HZotSP0.stl	L_NMNS_DS00041_20180414_c1_wl_01_0699_HZotSP0.tif–0745_HZotSP0.tif	C_NMNS_DS00041_20180414_c1_wl_01_0699_HZotSP0.jpg–0745_HZotSP0.jpg	NMNS_DS00041_20180414_c1_wl_01_0699.jpg–0745.jpg	-
152	NMNS_DS00041_iP6QMdc.stl	L_NMNS_DS00041_20180414_c1_wl_01_0755_iP6QMdc.tif–0779_iP6QMdc.tif	C_NMNS_DS00041_20180414_c1_wl_01_0755_iP6QMdc.jpg–0779_iP6QMdc.jpg	NMNS_DS00041_20180414_c1_wl_01_0755.jpg–0779.jpg	-
153	NMNS_DS00141_G9KsSm2.stl	L_NMNS_DS00141_wl_02_0134_G9KsSm2.tif–0190_G9KsSm2.tif	C_NMNS_DS00141_wl_02_0134_G9KsSm2.jpg–0190_G9KsSm2.jpg	NMNS_DS00141_wl_02_0134.tif–0190.tif	-
154	NMNS_DS00141_WR23hLl.stl	L_NMNS_DS00141_wl_02_0208_WR23hLl.tif–0286_WR23hLl.tif	C_NMNS_DS00141_wl_02_0208_WR23hLl.jpg–0286_WR23hLl.jpg	NMNS_DS00141_wl_02_0208.tif–0286.tif	-
155	NMNS_DS00173_gs5MGgw.stl	L_NMNS_DS00173_wl_01_0134_gs5MGgw.tif–0171_gs5MGgw.tif	C_NMNS_DS00173_wl_01_0134_gs5MGgw.jpg–0171_gs5MGgw.jpg	NMNS_DS00173_wl_01_0134.tif–0171.tif	-
156	NMNS_DS00173_zOCQ5aH.stl	L_NMNS_DS00173_wl_01_0514_zOCQ5aH.tif–0533_zOCQ5aH.tif	C_NMNS_DS00173_wl_01_0514_zOCQ5aH.jpg–0533_zOCQ5aH.jpg	NMNS_DS00173_wl_01_0514.tif–0533.tif	-
157	NMNS_DS00173_t9bcfa5.stl	L_NMNS_DS00173_wl_01_0527_t9bcfa5.tif–0551_t9bcfa5.tif	C_NMNS_DS00173_wl_01_0527_t9bcfa5.jpg–0551_t9bcfa5.jpg	NMNS_DS00173_wl_01_0527.tif–0551.tif	-
158	NMNS_DS00173_ojJzal0.stl	L_NMNS_DS00173_wl_01_0670_ojJzal0.tif–0697_ojJzal0.tif	C_NMNS_DS00173_wl_01_0670_ojJzal0.jpg–0697_ojJzal0.jpg	NMNS_DS00173_wl_01_0670.tif–0697.tif	-
159	NMNS_DS00173_4wSYQi9.stl	L_NMNS_DS00173_wl_01_0721_4wSYQi9.tif–0775_4wSYQi9.tif	C_NMNS_DS00173_wl_01_0721_4wSYQi9.jpg–0775_4wSYQi9.jpg	NMNS_DS00173_wl_01_0721.tif–0775.tif	-
160	NMNS_DS00173_jE5iVdb.stl	L_NMNS_DS00173_wl_01_0715_jE5iVdb.tif–0735_jE5iVdb.tif	C_NMNS_DS00173_wl_01_0715_jE5iVdb.jpg–0735_jE5iVdb.jpg	NMNS_DS00173_wl_01_0715.tif–0735.tif	-
161	NMNS_DS00173_l1Etvnw.stl	L_NMNS_DS00173_wl_01_0920_l1Etvnw.tif–0968_l1Etvnw.tif	C_NMNS_DS00173_wl_01_0920_l1Etvnw.jpg–0968_l1Etvnw.jpg	NMNS_DS00173_wl_01_0920.tif–0968.tif	-
162	NMNS_DS00173_DhR5iVE.stl	L_NMNS_DS00173_wl_01_1028_DhR5iVE.tif–1097_DhR5iVE.tif	C_NMNS_DS00173_wl_01_1028_DhR5iVE.jpg–1097_DhR5iVE.jpg	NMNS_DS00173_wl_01_1028.tif–1097.tif	-
163	NMNS_DS00173_ZPmlNa6.stl	L_NMNS_DS00173_wl_01_1055_ZPmlNa6.tif–1090_ZPmlNa6.tif	C_NMNS_DS00173_wl_01_1055_ZPmlNa6.jpg–1090_ZPmlNa6.jpg	NMNS_DS00173_wl_01_1055.tif–1090.tif	-
164	NMNS_DS00173_IuDK6XN.stl	L_NMNS_DS00173_wl_01_1155_IuDK6XN.tif–1222_IuDK6XN.tif	C_NMNS_DS00173_wl_01_1155_IuDK6XN.jpg–1222_IuDK6XN.jpg	NMNS_DS00173_wl_01_1155.tif–1222.tif	-
165	NMNS_DS00173_62PofvF.stl	L_NMNS_DS00173_wl_01_1339_62PofvF.tif–1364_62PofvF.tif	C_NMNS_DS00173_wl_01_1339_62PofvF.jpg–1364_62PofvF.jpg	NMNS_DS00173_wl_01_1339.tif–1364.tif	-
166	NMNS_DS00034_y1A99ab.stl	L_NMNS_DS00034_20180207_c1_wl_01_0382_y1A99ab.tif–0415_y1A99ab.tif	C_NMNS_DS00034_20180207_c1_wl_01_0382_y1A99ab.jpg–0415_y1A99ab.jpg	NMNS_DS00034_20180207_c1_wl_01_0382.jpg–0415.jpg	-
167	NMNS_DS00034_1GB8eu3.stl	L_NMNS_DS00034_20180207_c1_wl_01_0403_1GB8eu3.tif–0441_1GB8eu3.tif	C_NMNS_DS00034_20180207_c1_wl_01_0403_1GB8eu3.jpg–0441_1GB8eu3.jpg	NMNS_DS00034_20180207_c1_wl_01_0403.jpg–0441.jpg	-
168	NMNS_DS00034_24pKfeh.stl	L_NMNS_DS00034_20180207_c1_wl_01_0475_24pKfeh.tif–0517_24pKfeh.tif	C_NMNS_DS00034_20180207_c1_wl_01_0475_24pKfeh.jpg–0517_24pKfeh.jpg	NMNS_DS00034_20180207_c1_wl_01_0475.jpg–0517.jpg	-
169	NMNS_DS00034_h0A3Z03.stl	L_NMNS_DS00034_20180207_c1_wl_01_0643_h0A3Z03.tif–0681_h0A3Z03.tif	C_NMNS_DS00034_20180207_c1_wl_01_0643_h0A3Z03.jpg–0681_h0A3Z03.jpg	NMNS_DS00034_20180207_c1_wl_01_0643.jpg–0681.jpg	-
170	NMNS_DS00034_3AO7Q0Z.stl	L_NMNS_DS00034_20180207_c1_wl_01_0665_3AO7Q0Z.tif–0714_3AO7Q0Z.tif	C_NMNS_DS00034_20180207_c1_wl_01_0665_3AO7Q0Z.jpg–0714_3AO7Q0Z.jpg	NMNS_DS00034_20180207_c1_wl_01_0665.jpg–0714.jpg	-
171	NMNS_DS00081_mtrue9M.stl	L_NMNS_DS00081_20190124_c1_wl_01_0031_mtrue9M.tif–0069_mtrue9M.tif	C_NMNS_DS00081_20190124_c1_wl_01_0031_mtrue9M.jpg–0069_mtrue9M.jpg	NMNS_DS00081_20190124_c1_wl_01_0031.jpg–0069.jpg	-
172	NMNS_DS00081_nsA03VV.stl	L_NMNS_DS00081_20190124_c1_wl_01_0698_nsA03VV.tif–0725_nsA03VV.tif	C_NMNS_DS00081_20190124_c1_wl_01_0698_nsA03VV.jpg–0725_nsA03VV.jpg	NMNS_DS00081_20190124_c1_wl_01_0698.jpg–0725.jpg	-
173	NMNS_DS00083_bcQb89y.stl	L_NMNS_DS00083_20190130_c1_wl_01_0133_bcQb89y.tif–0158_bcQb89y.tif	C_NMNS_DS00083_20190130_c1_wl_01_0133_bcQb89y.jpg–0158_bcQb89y.jpg	NMNS_DS00083_20190130_c1_wl_01_0133.jpg–0158.jpg	-
174	NMNS_DS00083_Cbzbvh5.stl	L_NMNS_DS00083_20190130_c1_wl_01_0292_Cbzbvh5.tif–0330_Cbzbvh5.tif	C_NMNS_DS00083_20190130_c1_wl_01_0292_Cbzbvh5.jpg–0330_Cbzbvh5.jpg	NMNS_DS00083_20190130_c1_wl_01_0292.jpg–0330.jpg	-
175	NMNS_DS00083_uHk9pZQ.stl	L_NMNS_DS00083_20190130_c1_wl_01_0408_uHk9pZQ.tif–0424_uHk9pZQ.tif	C_NMNS_DS00083_20190130_c1_wl_01_0408_uHk9pZQ.jpg–0424_uHk9pZQ.jpg	NMNS_DS00083_20190130_c1_wl_01_0408.jpg–0424.jpg	-
176	NMNS_DS00083_e3595mK.stl	L_NMNS_DS00083_20190130_c1_wl_01_0539_e3595mK.tif–0566_e3595mK.tif	C_NMNS_DS00083_20190130_c1_wl_01_0539_e3595mK.jpg–0566_e3595mK.jpg	NMNS_DS00083_20190130_c1_wl_01_0539.jpg–0566.jpg	-
177	NMNS_DS00083_DI1gKuG.stl	L_NMNS_DS00083_20190130_c1_wl_01_0538_DI1gKuG.tif–0567_DI1gKuG.tif	C_NMNS_DS00083_20190130_c1_wl_01_0538_DI1gKuG.jpg–0567_DI1gKuG.jpg	NMNS_DS00083_20190130_c1_wl_01_0538.jpg–0567.jpg	-
178	NMNS_DS00083_6QWWA3O.stl	L_NMNS_DS00083_20190130_c1_wl_01_0556_6QWWA3O.tif–0600_6QWWA3O.tif	C_NMNS_DS00083_20190130_c1_wl_01_0556_6QWWA3O.jpg–0600_6QWWA3O.jpg	NMNS_DS00083_20190130_c1_wl_01_0556.jpg–0600.jpg	-
179	NMNS_DS00083_x87tvtw.stl	L_NMNS_DS00083_20190130_c1_wl_01_0579_x87tvtw.tif–0600_x87tvtw.tif	C_NMNS_DS00083_20190130_c1_wl_01_0579_x87tvtw.jpg–0600_x87tvtw.jpg	NMNS_DS00083_20190130_c1_wl_01_0579.jpg–0600.jpg	-
180	NMNS_DS00083_eiHii2r.stl	L_NMNS_DS00083_20190130_c1_wl_01_0713_eiHii2r.tif–0759_eiHii2r.tif	C_NMNS_DS00083_20190130_c1_wl_01_0713_eiHii2r.jpg–0759_eiHii2r.jpg	NMNS_DS00083_20190130_c1_wl_01_0713.jpg–0759.jpg	-
181	NMNS_DS00089_KofdLo4.stl	L_NMNS_DS00089_20190223_c1_wl_01_0140_KofdLo4.tif–0274_KofdLo4.tif	C_NMNS_DS00089_20190223_c1_wl_01_0140_KofdLo4.jpg–0274_KofdLo4.jpg	NMNS_DS00089_20190223_c1_wl_01_0140.jpg–0274.jpg	-
182	NMNS_DS00089_TjB6DJr.stl	L_NMNS_DS00089_20190223_c1_wl_01_0337_TjB6DJr.tif–0390_TjB6DJr.tif	C_NMNS_DS00089_20190223_c1_wl_01_0337_TjB6DJr.jpg–0390_TjB6DJr.jpg	NMNS_DS00089_20190223_c1_wl_01_0337.jpg–0390.jpg	-
183	NMNS_DS00004_3BN7XMT.stl	L_NMNS_DS00004_20170519_c1_wl_01_0159_3BN7XMT.tif–0204_3BN7XMT.tif	C_NMNS_DS00004_20170519_c1_wl_01_0159_3BN7XMT.jpg–0204_3BN7XMT.jpg	NMNS_DS00004_20170519_c1_wl_01_0159.jpg–0204.jpg	-
184	NMNS_DS00004_yLSdup5.stl	L_NMNS_DS00004_20170519_c1_wl_01_0281_yLSdup5.tif–0311_yLSdup5.tif	C_NMNS_DS00004_20170519_c1_wl_01_0281_yLSdup5.jpg–0311_yLSdup5.jpg	NMNS_DS00004_20170519_c1_wl_01_0281.jpg–0311.jpg	-
185	NMNS_DS00004_eR8PLKv.stl	L_NMNS_DS00004_20170519_c1_wl_01_0780_eR8PLKv.tif–0805_eR8PLKv.tif	C_NMNS_DS00004_20170519_c1_wl_01_0780_eR8PLKv.jpg–0805_eR8PLKv.jpg	NMNS_DS00004_20170519_c1_wl_01_0780.jpg–0805.jpg	-
186	NMNS_DS00011_zfqX101.stl	L_NMNS_DS00011_20170806_c1_wl_01_0216_zfqX101.tif–0254_zfqX101.tif	C_NMNS_DS00011_20170806_c1_wl_01_0216_zfqX101.jpg–0254_zfqX101.jpg	NMNS_DS00011_20170806_c1_wl_01_0216.jpg–0254.jpg	-
187	NMNS_DS00011_rlyT1aF.stl	L_NMNS_DS00011_20170806_c1_wl_01_0487_rlyT1aF.tif–0548_rlyT1aF.tif	C_NMNS_DS00011_20170806_c1_wl_01_0487_rlyT1aF.jpg–0548_rlyT1aF.jpg	NMNS_DS00011_20170806_c1_wl_01_0487.jpg–0548.jpg	-
188	NMNS_DS00011_JVxT9Gj.stl	L_NMNS_DS00011_20170806_c1_wl_01_0717_JVxT9Gj.tif–0767_JVxT9Gj.tif	C_NMNS_DS00011_20170806_c1_wl_01_0717_JVxT9Gj.jpg–0767_JVxT9Gj.jpg	NMNS_DS00011_20170806_c1_wl_01_0717.jpg–0767.jpg	-
189	NMNS_DS00011_4IY3Bn9.stl	L_NMNS_DS00011_20170806_c1_wl_01_0882_4IY3Bn9.tif–0945_4IY3Bn9.tif	C_NMNS_DS00011_20170806_c1_wl_01_0882_4IY3Bn9.jpg–0945_4IY3Bn9.jpg	NMNS_DS00011_20170806_c1_wl_01_0882.jpg–0945.jpg	-
190	NMNS_DS00011_U2ovTAd.stl	L_NMNS_DS00011_20170806_c1_wl_01_0917_U2ovTAd.tif–0954_U2ovTAd.tif	C_NMNS_DS00011_20170806_c1_wl_01_0917_U2ovTAd.jpg–0954_U2ovTAd.jpg	NMNS_DS00011_20170806_c1_wl_01_0917.jpg–0954.jpg	-
191	NMNS_DS00042_zPgCX6g.stl	L_NMNS_DS00042_20180419_c1_wl_02_0521_zPgCX6g.tif–0601_zPgCX6g.tif	C_NMNS_DS00042_20180419_c1_wl_02_0521_zPgCX6g.jpg–0601_zPgCX6g.jpg	NMNS_DS00042_20180419_c1_wl_02_0521.jpg–0601.jpg	-
192	NMNS_DS00090_AMpLdq5.stl	L_NMNS_DS00090_20190228_c1_wl_01_0322_AMpLdq5.tif–0361_AMpLdq5.tif	C_NMNS_DS00090_20190228_c1_wl_01_0322_AMpLdq5.jpg–0361_AMpLdq5.jpg	NMNS_DS00090_20190228_c1_wl_01_0322.jpg–0361.jpg	-
193	NMNS_DS00104_xBccT1Q.stl	L_NMNS_DS00104_wl_01_0294_xBccT1Q.tif–0371_xBccT1Q.tif	C_NMNS_DS00104_wl_01_0294_xBccT1Q.jpg–0371_xBccT1Q.jpg	NMNS_DS00104_wl_01_0294.jpg–0371.jpg	-
194	NMNS_DS00104_gX4su0i.stl	L_NMNS_DS00104_wl_01_0337_gX4su0i.tif–0391_gX4su0i.tif	C_NMNS_DS00104_wl_01_0337_gX4su0i.jpg–0391_gX4su0i.jpg	NMNS_DS00104_wl_01_0337.jpg–0391.jpg	-
195	NMNS_DS00104_GJ9lpVN.stl	L_NMNS_DS00104_wl_01_0616_GJ9lpVN.tif–0644_GJ9lpVN.tif	C_NMNS_DS00104_wl_01_0616_GJ9lpVN.jpg–0644_GJ9lpVN.jpg	NMNS_DS00104_wl_01_0616.jpg–0644.jpg	-
196	NMNS_DS00104_zr7SWaY.stl	L_NMNS_DS00104_wl_01_0644_zr7SWaY.tif–0667_zr7SWaY.tif	C_NMNS_DS00104_wl_01_0644_zr7SWaY.jpg–0667_zr7SWaY.jpg	NMNS_DS00104_wl_01_0644.jpg–0667.jpg	-

Table 3. (continued)

No.	Classification				Geological age	Growth stage	Measurements										
	Order	Family	Genus	Species			CL (mm)	HL (mm)	WL (mm)	AJS (degree)	WA (degree)	LRL (mm)	RW (mm)	LRL/RW	JEL (mm)	JELL (mm)	JELL/JEL
197	Oegopsida	uncertain	uncertain	uncertain	Early Campanian	juvenile	-	1.70	-	-	-	1.22	1.19	1.03	1.95	1.22	0.63
198	Oegopsida	uncertain	uncertain	uncertain	Early Campanian	juvenile	-	-	-	-	-	-	-	-	-	-	-
199	Oegopsida	uncertain	uncertain	uncertain	Early Campanian	juvenile	-	1.58	-	-	-	-	-	-	2.48	-	-
200	Oegopsida	uncertain	uncertain	uncertain	Early Campanian	juvenile	-	1.41	-	-	-	-	-	-	2.38	-	-
201	Oegopsida	uncertain	uncertain	uncertain	Early Campanian	juvenile	-	1.99	-	-	-	-	-	1.18	2.77	-	-
202	Oegopsida	uncertain	uncertain	uncertain	Early Campanian	juvenile	-	-	-	-	-	-	-	-	2.15	-	-
203	Oegopsida	uncertain	uncertain	uncertain	Early Campanian	juvenile	-	-	-	-	-	-	-	-	2.43	-	-
204	Oegopsida	uncertain	uncertain	uncertain	Late Campanian	juvenile	4.43	2.46	-	123.3	144.4	1.90	-	-	3.40	1.90	0.56
205	Oegopsida	uncertain	uncertain	uncertain	Late Campanian	uncertain	7.37	3.25	-	-	-	-	-	-	-	-	-
206	Oegopsida	uncertain	uncertain	uncertain	Late Campanian	uncertain	-	-	-	-	-	-	-	-	-	-	-
207	Oegopsida	uncertain	uncertain	uncertain	Late Campanian	juvenile	-	2.34	-	-	-	-	-	-	-	-	-
208	Oegopsida	uncertain	uncertain	uncertain	Early Campanian	uncertain	-	-	-	-	-	-	-	-	-	-	-
209	Oegopsida	uncertain	uncertain	uncertain	Early Campanian	juvenile	-	1.13	-	120.1	-	0.87	0.73	1.20	1.35	-	-
210	Oegopsida	uncertain	uncertain	uncertain	Early Campanian	juvenile	2.01	0.93	-	-	-	0.94	0.81	1.16	1.27	-	-
211	Oegopsida	uncertain	uncertain	uncertain	Early Campanian	juvenile	-	1.23	-	-	-	-	-	-	1.30		-
212	Oegopsida	uncertain	uncertain	uncertain	Early Campanian	juvenile	-	1.97	-	-	-	1.40	-	-	2.17	-	-
213	Oegopsida	uncertain	uncertain	uncertain	Late Campanian	juvenile	3.82	2.56	-	117.7	-	2.35	-	-	3.89	-	-
214	Oegopsida	uncertain	uncertain	uncertain	Late Campanian	juvenile	-	-	-	-	-	-	-	-	3.63	-	-
215	Oegopsida	uncertain	uncertain	uncertain	Early Maastrichtian	juvenile	3.22	1.62	-	-	-	1.24	-	-	-	-	-
216	Oegopsida	uncertain	uncertain	uncertain	Early Maastrichtian	juvenile	-	1.13	-	-	-	-	-	-	2.36	-	-
217	Oegopsida	uncertain	uncertain	uncertain	Early Maastrichtian	juvenile	3.32	1.41	-	-	-	-	-	-	2.06	-	-
218	Oegopsida	uncertain	uncertain	uncertain	Early Maastrichtian	juvenile	2.01	1.05	-	-	-	-	-	-	-	-	-
219	Myopsida	Loliginidae	*Psiloteuthis*	*naucrates*	earliest Cenomanian	adult	3.28	2.15	-	136.0	136.0	1.48	1.58	0.94	2.32	1.48	0.64
220	Myopsida	Loliginidae	*Psiloteuthis*	*naucrates*	earliest Cenomanian	subadult	-	1.83	-	124.5	124.5	1.34	1.40	0.96	2.13	1.34	0.63
221	Myopsida	Loliginidae	*Psiloteuthis*	*naucrates*	earliest Cenomanian	subadult	3.51	2.12	-	128.5	128.5	1.42	1.42	1.00	2.16	1.42	0.66
222	Myopsida	Loliginidae	*Psiloteuthis*	*naucrates*	Early Cenomanian	adult	2.86	2.06	-	126.0	126.0	1.68	1.65	1.02	2.33	1.68	0.72
223	Myopsida	Loliginidae	*Psiloteuthis*	*naucrates*	Late Cenomanian	subadult	-	1.85	-	143.5	143.5	1.63	1.61	1.01	2.30	1.63	0.71
224	Myopsida	Loliginidae	*Psiloteuthis*	*naucrates*	Late Turonian	adult	2.79	1.85	-	130.0	130.0	1.22	1.23	0.99	2.19	1.22	0.56
225	Myopsida	Loliginidae	*Psiloteuthis*	*naucrates*	Late Turonian	adult	3.16	1.87	-	126.9	126.9	1.36	1.49	0.91	2.13	1.36	0.64
226	Myopsida	Loliginidae	*Psiloteuthis*	*naucrates*	Late Turonian	adult	3.46	1.93	-	122.0	122.0	1.37	1.55	0.88	2.34	1.37	0.59
227	Myopsida	Loliginidae	*Psiloteuthis*	*naucrates*	Late Turonian	adult	3.36	1.59	-	122.2	122.2	1.38	-	-	2.20	1.38	0.63
228	Myopsida	Loliginidae	*Psiloteuthis*	*naucrates*	Late Turonian	adult	3.11	1.73	-	99.9	112.1	1.36	1.46	0.93	1.89	1.36	0.72
229	Myopsida	Loliginidae	*Psiloteuthis*	*naucrates*	Late Coniacian	adult	2.46	1.57	-	122.0	122.0	1.52	1.64	0.93	2.48	1.52	0.61
230	Myopsida	Loliginidae	*Psiloteuthis*	*naucrates*	Late Coniacian	subadult	4.24	-	-	136.3	-	2.22	-	-	4.02	2.22	0.55
231	Myopsida	Loliginidae	*Psiloteuthis*	*naucrates*	Late Campanian	adult	2.65	1.75	-	127.1	-	1.47	1.56	0.94	1.82	1.20	0.66
232	Myopsida	Loliginidae	*Psiloteuthis*	*naucrates*	Late Campanian	adult	3.25	1.87	-	118.1	-	1.28	1.35	0.95	2.13	1.28	0.60
233	Myopsida	Loliginidae	*Psiloteuthis*	*naucrates*	Early Maastrichtian	adult	2.02	0.90	0.80	135.7	135.7	0.58	0.77	0.76	1.29	0.58	0.45
234	Myopsida	Loliginidae	*Psiloteuthis*	*naucrates*	Early Maastrichtian	adult	2.64	1.32	1.22	114.9	114.9	0.66	0.88	0.75	1.84	0.66	0.36
235	Myopsida	Loliginidae	*Psiloteuthis*	*atalante*	Late Coniacian	subadult	-	3.51	-	117.9	-	2.73	2.04	1.34	4.30	2.73	0.63
236	Myopsida	Loliginidae	*Psiloteuthis*	*atalante*	Late Campanian	adult	3.93	2.00	-	105.7	-	1.65	1.30	1.27	2.48	1.65	0.67
237	Myopsida	Loliginidae	*Psiloteuthis*	*atalante*	Late Campanian	subadult	3.52	1.66	-	109.6	-	1.55	1.10	1.41	2.26	1.55	0.69
238	Myopsida	Loliginidae	*Psiloteuthis*	*sculptus*	Late Campanian	adult	2.89	1.94	1.74	130.6	125.6	1.48	1.42	1.04	2.67	1.48	0.55
239	Myopsida	Loliginidae	*Psiloteuthis*	*transitus*	Late Campanian	adult	7.07	2.85	2.70	120.2	111.6	2.31	1.83	1.26	4.34	2.31	0.53
240	Myopsida	Loliginidae	*Psiloteuthis*	uncertain	earliest Cenomanian	juvenile	-	-	-	-	-	2.60	-	-	-	-	-
241	Myopsida	Loliginidae	*Psiloteuthis*	uncertain	earliest Cenomanian	juvenile	-	1.97	-	150.5	-	1.33	1.57	0.85	2.38	1.33	0.56
242	Myopsida	Loliginidae	*Psiloteuthis*	uncertain	Late Turonian	juvenile	-	1.44	-	-	-	-	-	-	2.08	-	-
243	Myopsida	Loliginidae	*Psiloteuthis*	uncertain	Late Campanian	adult	-	-	-	-	-	1.57	-	-	-	1.57	-
244	Myopsida	Loliginidae	*Streptopteryx*	*glabra*	earliest Cenomanian	adult	2.32	-	-	134.4	-	1.20	1.49	0.81	2.12	1.16	0.55
245	Myopsida	Loliginidae	*Streptopteryx*	*glabra*	Early Cenomanian	adult	-	1.06	-	129.3	-	1.05	1.04	1.01	1.82	1.05	0.58
246	Myopsida	Loliginidae	*Streptopteryx*	*glabra*	Early Cenomanian	adult	1.23	0.75	-	112.7	-	0.81	-	-	1.19	0.69	0.58
247	Myopsida	Loliginidae	*Streptopteryx*	*glabra*	Late Turonian	subadult	-	-	-	123.5	-	1.43	1.21	1.18	2.22	1.19	0.54
248	Myopsida	Loliginidae	*Streptopteryx*	*glabra*	Late Turonian	adult	3.32	1.80	-	136.6	-	1.42	1.52	0.93	2.62	1.42	0.54
249	Myopsida	Loliginidae	*Streptopteryx*	*glabra*	Late Turonian	adult	-	1.87	-	114.0	-	1.42	1.22	1.16	2.13	1.42	0.67
250	Myopsida	Loliginidae	*Streptopteryx*	*glabra*	Early Maastrichtian	adult	1.34	0.86	-	102.6	121.7	0.73	0.78	0.93	1.19	0.65	0.55
251	Myopsida	Loliginidae	*Streptopteryx*	*bidentata*	Late Turonian	subadult	-	1.39	-	84.5	-	1.30	-	-	1.89	1.30	0.69
252	Myopsida	Loliginidae	*Streptopteryx*	*bidentata*	Late Coniacian	adult	-	-	-	100.1	-	1.38	1.57	0.88	2.26	1.31	0.58
253	Myopsida	Loliginidae	*Streptopteryx*	*bidentata*	Early Maastrichtian	adult	2.63	1.78	2.10	109.8	107.4	1.36	1.41	0.96	2.18	1.36	0.62
254	Myopsida	Loliginidae	*Streptopteryx*	*bidentata*	Early Maastrichtian	adult	2.31	1.16	-	132.0	-	1.05	-	-	1.66	1.05	0.63
255	Myopsida	Loliginidae	*Streptopteryx*	*bidentata*	Early Maastrichtian	adult	1.78	1.00	-	113.6	-	0.88	0.85	1.04	1.41	0.82	0.58
256	Myopsida	Loliginidae	*Camptoteuthis*	*acrorhynchus*	Early Turonian	subadult	-	2.17	-	92.6	-	2.05	-	-	2.74	1.86	0.68
257	Myopsida	Loliginidae	*Camptoteuthis*	*acrorhynchus*	Late Turonian	subadult	3.15	1.97	-	-	-	2.07	-	-	2.45	2.07	0.84
258	Myopsida	Loliginidae	*Camptoteuthis*	*cunabuli*	Late Cenomanian	subadult	-	1.81	-	-	-	1.32	1.18	1.12	1.98	1.32	0.67
259	Myopsida	Loliginidae	uncertain	uncertain	Early Turonian	juvenile	-	1.81	-	-	-	-	-	-	-	-	-
260	Myopsida	Loliginidae	uncertain	uncertain	Late Turonian	adult	1.49	-	-	105.8	-	0.77	0.89	0.86	1.10	0.68	0.62
261	Myopsida	Loliginidae	uncertain	uncertain	Late Campanian	adult	-	-	-	-	-	1.46	-	-	-	-	-
262	Oegopsida or Myopsida	uncertain	uncertain	uncertain	Early Cenomanian	juvenile	-	1.74	-	-	-	-	-	-	-	-	-
263	Oegopsida or Myopsida	uncertain	uncertain	uncertain	Late Turonian	juvenile	2.41	1.66	-	-	-	1.25	-	-	1.25	-	-
						Average CL	3.87										

Table 3. (continued)

No.	Dataset and Collection No. (NMNS: National Museum of Nature and Science, Tokyo)				Figure
	3D model	Label data of 3D models	Cross-sectional images of 3D models	Original cross-sectional images of carbonate concretions (animations of cross-sectional images are available from	
197	NMNS_DS00073_UD0ygnM.stl	L_NMNS_DS00073_20181212_c1_wl_01_0376_UD0ygnM.tif–0420_UD0ygnM.tif	C_NMNS_DS00073_20181212_c1_wl_01_0376_UD0ygnM.jpg–0420_UD0ygnM.jpg	NMNS_DS00073_20181212_c1_wl_01_0376.jpg–0420.jpg	-
198	NMNS_DS00097_a2Birz2.stl	L_NMNS_DS00097_wl_01_0001_a2Birz2.tif–0013_a2Birz2.tif	C_NMNS_DS00097_wl_01_0001_a2Birz2.jpg–0013_a2Birz2.jpg	NMNS_DS00097_wl_01_0001.jpg–0013.jpg	-
199	NMNS_DS00097_tEhZh41.stl	L_NMNS_DS00097_wl_01_0409_tEhZh41.tif–0454_tEhZh41.tif	C_NMNS_DS00097_wl_01_0409_tEhZh41.jpg–0454_tEhZh41.jpg	NMNS_DS00097_wl_01_0409.jpg–0454.jpg	-
200	NMNS_DS00097_uvDU6Xd.stl	L_NMNS_DS00097_wl_01_0425_uvDU6Xd.tif–0456_uvDU6Xd.tif	C_NMNS_DS00097_wl_01_0425_uvDU6Xd.jpg–0456_uvDU6Xd.jpg	NMNS_DS00097_wl_01_0425.jpg–0456.jpg	-
201	NMNS_DS00097_IDZOyQ0.stl	L_NMNS_DS00097_wl_01_0501_IDZOyQ0.tif–0552_IDZOyQ0.tif	C_NMNS_DS00097_wl_01_0501_IDZOyQ0.jpg–0552_IDZOyQ0.jpg	NMNS_DS00097_wl_01_0501.jpg–0552.jpg	-
202	NMNS_DS00097_uvzfA6L.stl	L_NMNS_DS00097_wl_01_0603_uvzfA6L.tif–0621_uvzfA6L.tif	C_NMNS_DS00097_wl_01_0603_uvzfA6L.jpg–0621_uvzfA6L.jpg	NMNS_DS00097_wl_01_0603.jpg–0621.jpg	-
203	NMNS_DS00097_g5Xmmpa.stl	L_NMNS_DS00097_wl_01_0875_g5Xmmpa.tif–0920_g5Xmmpa.tif	C_NMNS_DS00097_wl_01_0875_g5Xmmpa.jpg–0920_g5Xmmpa.jpg	NMNS_DS00097_wl_01_0875.jpg–0920.jpg	-
204	NMNS_DS00171_Cgg2Zfk.stl	L_NMNS_DS00171_wl_01_0362_Cgg2Zfk.tif–0435_Cgg2Zfk.tif	C_NMNS_DS00171_wl_01_0362_Cgg2Zfk.jpg–0435_Cgg2Zfk.jpg	NMNS_DS00171_wl_01_0362.tif–0435.tif	-
205	NMNS_DS00171_uD0WryB.stl	L_NMNS_DS00171_wl_01_0608_uD0WryB.tif–0743_uD0WryB.tif	C_NMNS_DS00171_wl_01_0608_uD0WryB.jpg–0743_uD0WryB.jpg	NMNS_DS00171_wl_01_0608.tif–0743.tif	-
206	NMNS_DS00171_CC67Bow.stl	L_NMNS_DS00171_wl_01_0912_CC67Bow.tif–0969_CC67Bow.tif	C_NMNS_DS00171_wl_01_0912_CC67Bow.jpg–0969_CC67Bow.jpg	NMNS_DS00171_wl_01_0912.tif–0969.tif	-
207	NMNS_DS00171_43DOJaP.stl	L_NMNS_DS00171_wl_01_1029_43DOJaP.tif–1066_43DOJaP.tif	C_NMNS_DS00171_wl_01_1029_43DOJaP.jpg–1066_43DOJaP.jpg	NMNS_DS00171_wl_01_1029.tif–1066.tif	-
208	NMNS_DS00175_UlgqLn1.stl	L_NMNS_DS00175_wl_01_0108_UlgqLn1.tif–0283_UlgqLn1.tif	C_NMNS_DS00175_wl_01_0108_UlgqLn1.jpg–0283_UlgqLn1.jpg	NMNS_DS00175_wl_01_0108.tif–0283.tif	-
209	NMNS_DS00175_P1OdOSW.stl	L_NMNS_DS00175_wl_01_0465_P1OdOSW.tif–0486_P1OdOSW.tif	C_NMNS_DS00175_wl_01_0465_P1OdOSW.jpg–0486_P1OdOSW.jpg	NMNS_DS00175_wl_01_0465.tif–0486.tif	-
210	NMNS_DS00175_y4Zl5IT.stl	L_NMNS_DS00175_wl_01_0691_y4Zl5IT.tif–0721_y4Zl5IT.tif	C_NMNS_DS00175_wl_01_0691_y4Zl5IT.jpg–0721_y4Zl5IT.jpg	NMNS_DS00175_wl_01_0691.tif–0721.tif	-
211	NMNS_DS00175_7ESIH1Z.stl	L_NMNS_DS00175_wl_01_0814_7ESIH1Z.tif–0839_7ESIH1Z.tif	C_NMNS_DS00175_wl_01_0814_7ESIH1Z.jpg–0839_7ESIH1Z.jpg	NMNS_DS00175_wl_01_0814.tif–0839.tif	-
212	NMNS_DS00175_MO6fdKX.stl	L_NMNS_DS00175_wl_01_1127_MO6fdKX.tif–1174_MO6fdKX.tif	C_NMNS_DS00175_wl_01_1127_MO6fdKX.jpg–1174_MO6fdKX.jpg	NMNS_DS00175_wl_01_1127.tif–1174.tif	-
213	NMNS_DS00182_9vHtXfk.stl	L_NMNS_DS00182_wl_01_0695_9vHtXfk.tif–0770_9vHtXfk.tif	C_NMNS_DS00182_wl_01_0695_9vHtXfk.jpg–0770_9vHtXfk.jpg	NMNS_DS00182_wl_01_0695.tif–0770.tif	-
214	NMNS_DS00182_o6cWgkd.stl	L_NMNS_DS00182_wl_01_0778_o6cWgkd.tif–0853_o6cWgkd.tif	C_NMNS_DS00182_wl_01_0778_o6cWgkd.jpg–0853_o6cWgkd.jpg	NMNS_DS00182_wl_01_0778.tif–0853.tif	-
215	NMNS_DS00128_7Kb5OEo.stl	L_NMNS_DS00128_wl_01_0055_7Kb5OEo.tif–0084_7Kb5OEo.tif	C_NMNS_DS00128_wl_01_0055_7Kb5OEo.jpg–0084_7Kb5OEo.jpg	NMNS_DS00128_wl_01_0055.jpg–0084.jpg	-
216	NMNS_DS00128_XDB2mts.stl	L_NMNS_DS00128_wl_01_0700_XDB2mts.tif–0733_XDB2mts.tif	C_NMNS_DS00128_wl_01_0700_XDB2mts.jpg–0733_XDB2mts.jpg	NMNS_DS00128_wl_01_0700.jpg–0733.jpg	-
217	NMNS_DS00174_j7AcHlc.stl	L_NMNS_DS00174_wl_01_0933_j7AcHlc.tif–0973_j7AcHlc.tif	C_NMNS_DS00174_wl_01_0933_j7AcHlc.jpg–0973_j7AcHlc.jpg	NMNS_DS00174_wl_01_0933.tif–0973.tif	-
218	NMNS_DS00174_J39bDB6.stl	L_NMNS_DS00174_wl_01_1065_J39bDB6.tif–1093_J39bDB6.tif	C_NMNS_DS00174_wl_01_1065_J39bDB6.jpg–1093_J39bDB6.jpg	NMNS_DS00174_wl_01_1065.tif–1093.tif	-
219	NMNS_DS00068_uZlnAz0.stl	L_NMNS_DS00068_20181123_c1_wl_01_0040_uZlnAz0.tif–0092_uZlnAz0.tif	C_NMNS_DS00068_20181123_c1_wl_01_0040_uZlnAz0.jpg–0092_uZlnAz0.jpg	NMNS_DS00068_20181123_c1_wl_01_0040.jpg–0092.jpg	-
220	NMNS_DS00068_tj22YEq.stl	L_NMNS_DS00068_20181123_c1_wl_01_0385_tj22YEq.tif–0429_tj22YEq.tif	C_NMNS_DS00068_20181123_c1_wl_01_0385_tj22YEq.jpg–0429_tj22YEq.jpg	NMNS_DS00068_20181123_c1_wl_01_0385.jpg–0429.jpg	-
221	NMNS_DS00068_mb5AJPm.stl	L_NMNS_DS00068_20181123_c1_wl_01_0442_mb5AJPm.tif–0490_mb5AJPm.tif	C_NMNS_DS00068_20181123_c1_wl_01_0442_mb5AJPm.jpg–0490_mb5AJPm.jpg	NMNS_DS00068_20181123_c1_wl_01_0442.jpg–0490.jpg	-
222	NMNS_DS00084_N272hY0.stl	L_NMNS_DS00084_20190202_c1_wl_01_0274_N272hY0.tif–0316_N272hY0.tif	C_NMNS_DS00084_20190202_c1_wl_01_0274_N272hY0.jpg–0316_N272hY0.jpg	NMNS_DS00084_20190202_c1_wl_01_0274.jpg–0316.jpg	-
223	NMNS_DS00082_fh6e497.stl	L_NMNS_DS00082_20190127_c1_wl_01_0464_fh6e497.tif–0506_fh6e497.tif	C_NMNS_DS00082_20190127_c1_wl_01_0464_fh6e497.jpg–0506_fh6e497.jpg	NMNS_DS00082_20190127_c1_wl_01_0464.jpg–0506.jpg	-
224	NMNS_DS00040_Tt7lr4y.stl	L_NMNS_DS00040_20180409_c1_wl_01_0193_Tt7lr4y.tif–0243_Tt7lr4y.tif	C_NMNS_DS00040_20180409_c1_wl_01_0193_Tt7lr4y.jpg–0243_Tt7lr4y.jpg	NMNS_DS00040_20180409_c1_wl_01_0193.jpg–0243.jpg	-
225	NMNS_DS00040_CN8Pl3W.stl	L_NMNS_DS00040_20180409_c1_wl_01_0192_CN8Pl3W.tif–0234_CN8Pl3W.tif	C_NMNS_DS00040_20180409_c1_wl_01_0192_CN8Pl3W.jpg–0234_CN8Pl3W.jpg	NMNS_DS00040_20180409_c1_wl_01_0192.jpg–0234.jpg	-
226	NMNS_DS00040_xQd37Tu.stl	L_NMNS_DS00040_20180409_c1_wl_01_0262_xQd37Tu.tif–0315_xQd37Tu.tif	C_NMNS_DS00040_20180409_c1_wl_01_0262_xQd37Tu.jpg–0315_xQd37Tu.jpg	NMNS_DS00040_20180409_c1_wl_01_0262.jpg–0315.jpg	-
227	NMNS_DS00040_FgRWr9e.stl	L_NMNS_DS00040_20180409_c1_wl_01_0363_FgRWr9e.tif–0422_FgRWr9e.tif	C_NMNS_DS00040_20180409_c1_wl_01_0363_FgRWr9e.jpg–0422_FgRWr9e.jpg	NMNS_DS00040_20180409_c1_wl_01_0363.jpg–0422.jpg	-
228	NMNS_DS00173_tRj5kxm.stl	L_NMNS_DS00173_wl_01_0164_tRj5kxm.tif–0202_tRj5kxm.tif	C_NMNS_DS00173_wl_01_0164_tRj5kxm.jpg–0202_tRj5kxm.jpg	NMNS_DS00173_wl_01_0164.tif–0202.tif	-
229	NMNS_DS00083_SKAsE98.stl	L_NMNS_DS00083_20190130_c1_wl_01_0322_SKAsE98.tif–0363_SKAsE98.tif	C_NMNS_DS00083_20190130_c1_wl_01_0322_SKAsE98.jpg–0363_SKAsE98.jpg	NMNS_DS00083_20190130_c1_wl_01_0322.jpg–0363.jpg	-
230	NMNS_DS00083_XZzD8hv.stl	L_NMNS_DS00083_20190130_c1_wl_01_0618_XZzD8hv.tif–0695_XZzD8hv.tif	C_NMNS_DS00083_20190130_c1_wl_01_0618_XZzD8hv.jpg–0695_XZzD8hv.jpg	NMNS_DS00083_20190130_c1_wl_01_0618.jpg–0695.jpg	-
231	NMNS_DS00182_oF5mYlz.stl	L_NMNS_DS00182_wl_01_0033_oF5mYlz.tif–0082_oF5mYlz.tif	C_NMNS_DS00182_wl_01_0033_oF5mYlz.jpg–0082_oF5mYlz.jpg	NMNS_DS00182_wl_01_0033.tif–0082.tif	Fig. 3K
232	NMNS_DS00182_UPRVv9A.stl	L_NMNS_DS00182_wl_01_0517_UPRVv9A.tif–0574_UPRVv9A.tif	C_NMNS_DS00182_wl_01_0517_UPRVv9A.jpg–0574_UPRVv9A.jpg	NMNS_DS00182_wl_01_0517.tif–0574.tif	Fig. 11A–E
233	NMNS_DS00128_NN6zaGU.stl	L_NMNS_DS00128_wl_01_0102_NN6zaGU.tif–0133_NN6zaGU.tif	C_NMNS_DS00128_wl_01_0102_NN6zaGU.jpg–0133_NN6zaGU.jpg	NMNS_DS00128_wl_01_0102.jpg–0133.jpg	-
234	NMNS_DS00128_zGiAOX1.stl	L_NMNS_DS00128_wl_01_0310_zGiAOX1.tif–0371_zGiAOX1.tif	C_NMNS_DS00128_wl_01_0310_zGiAOX1.jpg–0371_zGiAOX1.jpg	NMNS_DS00128_wl_01_0310.jpg–0371.jpg	-
235	NMNS_DS00089_N7pALkd.stl	L_NMNS_DS00089_20190223_c1_wl_01_0034_N7pALkd.tif–0078_N7pALkd.tif	C_NMNS_DS00089_20190223_c1_wl_01_0034_N7pALkd.jpg–0078_N7pALkd.jpg	NMNS_DS00089_20190223_c1_wl_01_0034.jpg–0078.jpg	-
236	NMNS_DS00171_R5TOKQL.stl	L_NMNS_DS00171_wl_01_0607_R5TOKQL.tif–0654_R5TOKQL.tif	C_NMNS_DS00171_wl_01_0607_R5TOKQL.jpg–0654_R5TOKQL.jpg	NMNS_DS00171_wl_01_0607.tif–0654.tif	-
237	NMNS_DS00171_9qzKEcc.stl	L_NMNS_DS00171_wl_01_0716_9qzKEcc.tif–0752_9qzKEcc.tif	C_NMNS_DS00171_wl_01_0716_9qzKEcc.jpg–0752_9qzKEcc.jpg	NMNS_DS00171_wl_01_0716.tif–0752.tif	Fig. 11F–J
238	NMNS_DS00171_0gcEN28.stl	L_NMNS_DS00171_wl_01_0581_0gcEN28.tif–0626_0gcEN28.tif	C_NMNS_DS00171_wl_01_0581_0gcEN28.jpg–0626_0gcEN28.jpg	NMNS_DS00171_wl_01_0581.tif–0626.tif	Fig. 11K–O
239	NMNS_DS00171_opgN0Hg.stl	L_NMNS_DS00171_wl_01_1306_opgN0Hg.tif–1409_opgN0Hg.tif	C_NMNS_DS00171_wl_01_1306_opgN0Hg.jpg–1409_opgN0Hg.jpg	NMNS_DS00171_wl_01_1306.tif–1409.tif	Fig. 11P–T
240	NMNS_DS00068_r0HPqbb.stl	L_NMNS_DS00068_20181123_c1_wl_01_0097_r0HPqbb.tif–0178_r0HPqbb.tif	C_NMNS_DS00068_20181123_c1_wl_01_0097_r0HPqbb.jpg–0178_r0HPqbb.jpg	NMNS_DS00068_20181123_c1_wl_01_0097.jpg–0178.jpg	-
241	NMNS_DS00068_4NffBTu.stl	L_NMNS_DS00068_20181123_c1_wl_01_0434_4NffBTu.tif–0494_4NffBTu.tif	C_NMNS_DS00068_20181123_c1_wl_01_0434_4NffBTu.jpg–0494_4NffBTu.jpg	NMNS_DS00068_20181123_c1_wl_01_0434.jpg–0494.jpg	-
242	NMNS_DS00173_Yij4eBp.stl	L_NMNS_DS00173_wl_01_0289_Yij4eBp.tif–0326_Yij4eBp.tif	C_NMNS_DS00173_wl_01_0289_Yij4eBp.jpg–0326_Yij4eBp.jpg	NMNS_DS00173_wl_01_0289.tif–0326.tif	-
243	NMNS_DS00171_CA61a5q.stl	L_NMNS_DS00171_wl_01_0527_CA61a5q.tif–0581_CA61a5q.tif	C_NMNS_DS00171_wl_01_0527_CA61a5q.jpg–0581_CA61a5q.jpg	NMNS_DS00171_wl_01_0527.tif–0581.tif	-
244	NMNS_DS00068_okmTU54.stl	L_NMNS_DS00068_20181123_c1_wl_01_0459_okmTU54.tif–0508_okmTU54.tif	C_NMNS_DS00068_20181123_c1_wl_01_0459_okmTU54.jpg–0508_okmTU54.jpg	NMNS_DS00068_20181123_c1_wl_01_0459.jpg–0508.jpg	-
245	NMNS_DS00084_Erg3dY7.stl	L_NMNS_DS00084_20190202_c1_wl_01_0517_Erg3dY7.tif–0545_Erg3dY7.tif	C_NMNS_DS00084_20190202_c1_wl_01_0517_Erg3dY7.jpg–0545_Erg3dY7.jpg	NMNS_DS00084_20190202_c1_wl_01_0517.jpg–0545.jpg	-
246	NMNS_DS00084_pAh4xpP.stl	L_NMNS_DS00084_20190202_c1_wl_01_0757_pAh4xpP.tif–0779_pAh4xpP.tif	C_NMNS_DS00084_20190202_c1_wl_01_0757_pAh4xpP.jpg–0779_pAh4xpP.jpg	NMNS_DS00084_20190202_c1_wl_01_0757.jpg–0779.jpg	-
247	NMNS_DS00040_OuBYd2G.stl	L_NMNS_DS00040_20180409_c1_wl_01_0385_OuBYd2G.tif–0425_OuBYd2G.tif	C_NMNS_DS00040_20180409_c1_wl_01_0385_OuBYd2G.jpg–0425_OuBYd2G.jpg	NMNS_DS00040_20180409_c1_wl_01_0385.jpg–0425.jpg	-
248	NMNS_DS00040_fBilvb5.stl	L_NMNS_DS00040_20180409_c1_wl_01_0441_fBilvb5.tif–0494_fBilvb5.tif	C_NMNS_DS00040_20180409_c1_wl_01_0441_fBilvb5.jpg–0494_fBilvb5.jpg	NMNS_DS00040_20180409_c1_wl_01_0441.jpg–0494.jpg	Fig. 11A–E
249	NMNS_DS00173_ACI2D9e.stl	L_NMNS_DS00173_wl_01_0977_ACI2D9e.tif–1031_ACI2D9e.tif	C_NMNS_DS00173_wl_01_0977_ACI2D9e.jpg–1031_ACI2D9e.jpg	NMNS_DS00173_wl_01_0977.tif–1031.tif	-
250	NMNS_DS00174_6Ga0IDF.stl	L_NMNS_DS00174_wl_01_0651_6Ga0IDF.tif–0677_6Ga0IDF.tif	C_NMNS_DS00174_wl_01_0651_6Ga0IDF.jpg–0677_6Ga0IDF.jpg	NMNS_DS00174_wl_01_0651.tif–0677.tif	-
251	NMNS_DS00040_CdEhX1r.stl	L_NMNS_DS00040_20180409_c1_wl_01_0001_CdEhX1r.tif–0025_CdEhX1r.tif	C_NMNS_DS00040_20180409_c1_wl_01_0001_CdEhX1r.jpg–0025_CdEhX1r.jpg	NMNS_DS00040_20180409_c1_wl_01_0001.jpg–0025.jpg	-
252	NMNS_DS00083_HFkq7tj.stl	L_NMNS_DS00083_20190130_c1_wl_01_0331_HFkq7tj.tif–0370_HFkq7tj.tif	C_NMNS_DS00083_20190130_c1_wl_01_0331_HFkq7tj.jpg–0370_HFkq7tj.jpg	NMNS_DS00083_20190130_c1_wl_01_0331.jpg–0370.jpg	-
253	NMNS_DS00128_k1LIu1T.stl	L_NMNS_DS00128_wl_01_0193_k1LIu1T.tif–0261_k1LIu1T.tif	C_NMNS_DS00128_wl_01_0193_k1LIu1T.jpg–0261_k1LIu1T.jpg	NMNS_DS00128_wl_01_0193.jpg–0261.jpg	Figs 3L & 12F–J
254	NMNS_DS00174_RmFzKT4.stl	L_NMNS_DS00174_wl_01_0992_RmFzKT4.tif–1038_RmFzKT4.tif	C_NMNS_DS00174_wl_01_0992_RmFzKT4.jpg–1038_RmFzKT4.jpg	NMNS_DS00174_wl_01_0992.tif–1038.tif	-
255	NMNS_DS00174_TWaF8yT.stl	L_NMNS_DS00174_wl_01_1083_TWaF8yT.tif–1113_TWaF8yT.tif	C_NMNS_DS00174_wl_01_1083_TWaF8yT.jpg–1113_TWaF8yT.jpg	NMNS_DS00174_wl_01_1083.tif–1113.tif	-
256	NMNS_DS00140_3qYJhEx.stl	L_NMNS_DS00140_wl_03_0993_3qYJhEx.tif–1021_3qYJhEx.tif	C_NMNS_DS00140_wl_03_0993_3qYJhEx.jpg–1021_3qYJhEx.jpg	NMNS_DS00140_wl_03_0993.tif–1021.tif	Fig. 12K–O
257	NMNS_DS00173_OWxR12l.stl	L_NMNS_DS00173_wl_01_0173_OWxR12l.tif–0220_OWxR12l.tif	C_NMNS_DS00173_wl_01_0173_OWxR12l.jpg–0220_OWxR12l.jpg	NMNS_DS00173_wl_01_0173.tif–0220.tif	-
258	NMNS_DS00082_p4vjY3G.stl	L_NMNS_DS00082_20190127_c1_wl_01_0386_p4vjY3G.tif–0422_p4vjY3G.tif	C_NMNS_DS00082_20190127_c1_wl_01_0386_p4vjY3G.jpg–0422_p4vjY3G.jpg	NMNS_DS00082_20190127_c1_wl_01_0386.jpg–0422.jpg	Fig. 12P–T
259	NMNS_DS00140_s5yjXbC.stl	L_NMNS_DS00140_wl_03_0342_s5yjXbC.tif–0411_s5yjXbC.tif	C_NMNS_DS00140_wl_03_0342_s5yjXbC.jpg–0411_s5yjXbC.jpg	NMNS_DS00140_wl_03_0342.tif–0411.tif	-
260	NMNS_DS00173_7Ob4vJ8.stl	L_NMNS_DS00173_wl_01_1250_7Ob4vJ8.tif–1272_7Ob4vJ8.tif	C_NMNS_DS00173_wl_01_1250_7Ob4vJ8.jpg–1272_7Ob4vJ8.jpg	NMNS_DS00173_wl_01_1250.tif–1272.tif	-
261	NMNS_DS00182_Ua4EcEk.stl	L_NMNS_DS00182_wl_01_0491_Ua4EcEk.tif–0544_Ua4EcEk.tif	C_NMNS_DS00182_wl_01_0491_Ua4EcEk.jpg–0544_Ua4EcEk.jpg	NMNS_DS00182_wl_01_0491.tif–0544.tif	-
262	NMNS_DS00084_OWZo5r8.stl	L_NMNS_DS00084_20190202_c1_wl_01_0185_OWZo5r8.tif–0218_OWZo5r8.tif	C_NMNS_DS00084_20190202_c1_wl_01_0185_OWZo5r8.jpg–0218_OWZo5r8.jpg	NMNS_DS00084_20190202_c1_wl_01_0185.jpg–0218.jpg	-
263	NMNS_DS00040_Yq5i0Nj.stl	L_NMNS_DS00040_20180409_c1_wl_01_0516_Yq5i0Nj.tif–0547_Yq5i0Nj.tif	C_NMNS_DS00040_20180409_c1_wl_01_0516_Yq5i0Nj.jpg–0547_Yq5i0Nj.jpg	NMNS_DS00040_20180409_c1_wl_01_0516.jpg–0547.jpg	-

Yezoteuthis giganteus Tanabe, Hikida and Iba, 2006

2023 gen. and sp. indet.; Tanabe and Misaki, p. 9, Fig. 5A–D (KMNH IvP 902007).

2023 Yezoteuthis giganteus; Fuchs, p. 30, Fig.13.2a-b.

Holotype. NMA-335.

Material. NMA-335 and KMNH IvP 902007.

Emended diagnosis. Same as for the genus.

Description. The rostrum forms a long and sharply pointed tip. The crest is relatively close to the hood. The jaw angles are damaged, but the angle between the jaw edges and the adjacent shoulder blade seems to be nearly perpendicular. The hood is gently arched and at least three times longer than the rostral length. The shoulders are well-developed, connected to the hood without forming a step, and as broad as the rostral length in the preserved part. The anterior margin of shoulders might be slightly posterior to that of the lateral walls. The inner lamella is narrow, gently arched around the crest, and slightly curved inward in the ventral half. The lateral walls are at least five times longer and three times higher than the rostral length. The shape of lateral walls is uncertain since the ventral and posterior margins are not preserved. The lateral walls and the hood are ornamented with fine radial striations. Equal-spaced fine growth lines are also present around the shoulders.

Remarks. KMNH IvP 902007 has been described as gen. et sp. indet. The original description stated that it differs from *Y. giganteus* by the size of the entire beak and the size of the rostrum compared with the hood[36]. The posterior part of the hood is, however, apparently damaged. The specimen can thus not be used for identification on the species level. Since the characters of the preserved parts are identical to this species, this specimen is here classified into this species. It probably represents a younger growth stage than the holotype.

Occurrence. Early Campanian; Yezo Group in Hokkaido, Japan.

1.4.2. The key for identifying Cretaceous squid species

1. Jaw edges are bifurcated (Fig. 5E) ……2

   Jaw edges are single-edged (Fig. 10E) ……5

2. The dorsal edge of the shoulder blades is connected to the adjacent wing by a narrow …… ridge (Fig. 5D)……3

   The dorsal edge of the shoulder blades is connected to the adjacent wing by a flat plane…… (Fig. 5Q)……4

3. A step or ridge is absent in wings and shoulder blades (Fig. 5A and D) …… …… *Haboroteuthis poseidon*

   An angular ridge exists on wings (Fig. 5S) …… *Hoplitopteryx solida*

   A step exists between shoulder blades and the adjacent lateral walls (Fig. 6D) …… …… *Bathmidoteuthis altus*

4. Wings are very thick (Fig. 5Q)……*Pachygephyra Callisto*

   Wings are thin (Fig. 6I)……*Placomoteuthis hercules*

5. Jaw edges curves posteriorly in their ventral part (Fig. 11N) ……6

Jaw edges are entirely straight (Fig. 6N) ····· 7

6. The rostrum is not hooked (Fig. 11K) ····· *Paleothysanoteuthis complicates*

   The rostrum has a strong hook (Fig. 11V) ····· *Aetorhynchus incisus*

7. Shoulder blades are less developed than wings and form an angular jaw angle (Fig. 9D) ····· 8

   Shoulder blades are more developed than wings and form an angular jaw angle (Fig. 10A) ····· 21

   Shoulder blades are more developed than wings and form a subrounded jaw angle (Fig. 12D) 26

8. An angular ridge exists on wings (Fig. 6K) ····· 9

   No angular ridge exists on wings (Fig. 7F) ····· 11

9. Shoulder blades are distinct (Fig. 6X) ····· *Pachypteroteuthis magnus*

   Shoulder blades are very indistinct (Fig. 6N) ····· 10

10. The ridge on the wings is parallel to the adjacent jaw edge and does not form a dorsally pointed tip (Fig. 6L) ····· *Pachypteroteuthis adiacens*

    The ridge on the wings is parallel to the adjacent jaw edge and forms a tip with strong dorsal protrusion (Fig. 6AA) ····· *Pachypteroteuthis sulcatus*

    The ridge on the wings is not parallel to the adjacent jaw edge (Fig. 6Q) ····· *Pachypteroteuthis mortarii*

11. Shoulder blades are distinct (Fig. 9D) ····· 12

    Shoulder blades are tiny and indistinct (Fig. 7I) ····· 16

12. The ventral part of the bridges is free (Fig. 8K) ····· 13

    The ventral part of the bridges is covered by a massive shoulder (Fig. 9D) ····· 14

13. The rostrum shows moderate size and width (Fig. 8O) ····· *Astathogephyra metis*

    The rostrum is large and narrow (Fig. 8T) ····· *Astathogephyra himatium*

14. The dorsal edge of the shoulder blades is ambiguous (Fig. 8I) ····· *Gerontoteuthis acutissimus*

    The dorsal edge of the shoulder blades has a clear edge (Fig. 9D) ····· 15

15. A pointed tip or step is absent on wings and shoulder blades (Fig. 9D) ····· *Sepultipons castor*

    A pointed tip exists on the wings, and a step is absent in the shoulder blades (Fig. 9I) ····· *Sepultipons pollux*

    A pointed tip is absent in the wings, and a step exists between the shoulder blades and the adjacent lateral walls (Fig. 9N) ····· *Sepultipons gradus*

16. Shoulder blades are connected to the medial ridge of the adjacent wing (Fig. 7I) ····· 17

Shoulder blades are very indistinct (Fig. 7D)····· 18

17. 1.08 ≤ LRL/RW ≤ 1.16 (Fig. 7J) ····· *Thalassasboides watatsumi*

    1.29 ≤ LRL/RW ≤ 1.47 (Fig. 7O) ····· *Thalassasboides pulchellus*

    LRL/RW > 2.00 (Fig. 7T)····· *Thalassasboides acutus*

18. The rostral hook is distinct (Fig. 7A) ····· 19

    The rostral hook is faint or absent (Fig. 7U)····· 20

19. The rostrum shows moderate anterior protrusion and narrow dents (Fig. 7A)·····
    ····· *Catantopteryx altilis*

    The rostrum shows moderate anterior protrusion and wide dents (Fig. 9P) ·····
    ····· *Aspasmoteuthis peltatus*

    The rostrum shows very weak anterior protrusion and wide dents (Fig. 9U) ·····
    ····· *Juroteuthis arrectus*

20. The rostrum is moderately protruded forward (Fig. 7U)····· *Pseudovampyroteuthis Hecate*

    The rostrum is strongly protruded forward (Fig. 8A) ····· *Orthoteuthis Subaru*

21. The rostrum is moderately protruded forward (Fig. 11A) ····· 22

    The rostrum is strongly protruded forward (Fig. 10A) ····· 23

22. LRL/RW ≤ 1.29 (Fig. 11E) ····· *Amblyscuthes apterus*

    LRL/RW ≥ 1.63 (Fig. 11J)····· *Amblyscuthes pyrgoides*

23. The dorsal edge of the shoulder blades is connected to the adjacent wing by a flat plane (Fig. 10X)
    ····· *Grossiscapula angusta*

    The dorsal edge of the shoulder blades is connected to the adjacent wing at a narrow ····· ridge
    (Fig. 10D) ····· 24

24. The rostrum has distinct dents (Fig. 10G) ····· *Scuthoteuthis fragilis*

    The rostrum has no dents (Fig. 10A) ····· 23

25. LRL/RW = ~0.90 (Fig. 10T)····· *Scuthoteuthis tenuis*

    LRL/RW = ~1.28 (Fig. 10E)····· *Scuthoteuthis kawataro*

    LRL/RW > 1.42 (Fig. 10O)····· *Scuthoteuthis falcatus*

26. Wing folds are absent (Fig. 12D) ····· 27

    Wing folds are present (Fig. 13I)····· 29

27. No dent or groove exists on the merger part of the wings and the adjacent shoulder blade ·····
    (Fig. 12D) ····· 28

    A dent exists on the merger part of the wings and the adjacent shoulder blade (Fig. 12N) ·····
    ····· *Psiloteuthis sculptus*

    A groove exists between the wings and the adjacent shoulder blade (Fig. 12S)·····

…… *Psiloteuthis transitus*

28. LRL/RW ≤ 1.02 (Fig. 12E) …… *Psiloteuthis naucrates*

    LRL/RW ≥ 1.27 (Fig. 12J)…… *Psiloteuthis atalante*

29. The rostrum is moderately protruded forward (Fig. 13A) …… 30

    The rostrum is strongly protruded forward (Fig. 13K)…… 31

30. Shoulder teeth are absent (Fig. 13D) …… *Streptopteryx glabra*

    Shoulder teeth are present (Fig. 13I)…… *Streptopteryx bidentata*

31. Wing folds have no step (Fig. 13O) …… *Camptoteuthis cunabuli*

    Wing folds have a step around a jaw angle (Fig. 13T) …… *Camptoteuthis acrorhynchus*

1.4.3. Morphological disparity analyses of Cretaceous squid species

The principal coordinates analysis (PCoA) plot shows that all 40 species encountered in this study differ from each other by occupying disjunct, not overlapping positions in the disparity system (Fig. 14). The individual species are also well-clustered in their individual, higher-ranking taxonomic groups (genus, family, and order).

For five of the 40 species (*Pachypteroteuthis adiacens*, *P. mortarii*, *P. magnus*, *P. sulcatus*, and *Grossiscapula angusta*), the results of PCoA show minor differences to those of Systematic Paleontology. These are explained as follows:

1. *P. adiacens* and *P. mortarii* are positioned close to each other according to the PCoA (Fig. 14). They differ, however, clearly by the orientation of their wing ridges (Fig. 6L and Q).
2. The PCoA positions of *P. magnus* and *P. sulcatus* are distant from those of all other species of the genus *Pachypteroteuthis* (Fig. 14) Their rostral parts are not completely preserved, giving their PCoA positions a certain tolerance. Both species are included in *Pachypteroteuthis* because of their wing ridges, which are not present in any other genus of the family Pachypteroteuthidae (Fig. 6V and AA).
3. The PCoA plots *G. angusta* in an isolated position of the family Scuthoteuthidae, due to the presence of shoulder planes. The shoulder planes are a shared character with *Pachygephyra callisto* and *Placomoteuthis hercules* of the Haboroteuthidae. *G. angusta* can, however, be clearly classified into Scuthoteuthidae because of its single-edged rostrum (Fig. 10X).

1.5. Discussion and Conclusion

1.5.1. Discovery of numerous fossil squid beaks

The numerous fossil squids discovered here represent 40 species, 23 genera, and five families (Fig 13A). All species were assigned to the Oegopsida or Myopsida, these two orders include all extant squid taxa. The size of discovered beaks demonstrate that numerous squid beaks are hidden as millimeter-scaled microfossils and explain why they have been overlooked in previous studies. The digital approach transfers the fossiliferous carbonate concretions into a “Fossil-Lagerstätte of squids”.

1.5.2. Squids originated 100 million years ago

Our findings document that squids originated near the Early–Late Cretaceous (100 Ma) boundary

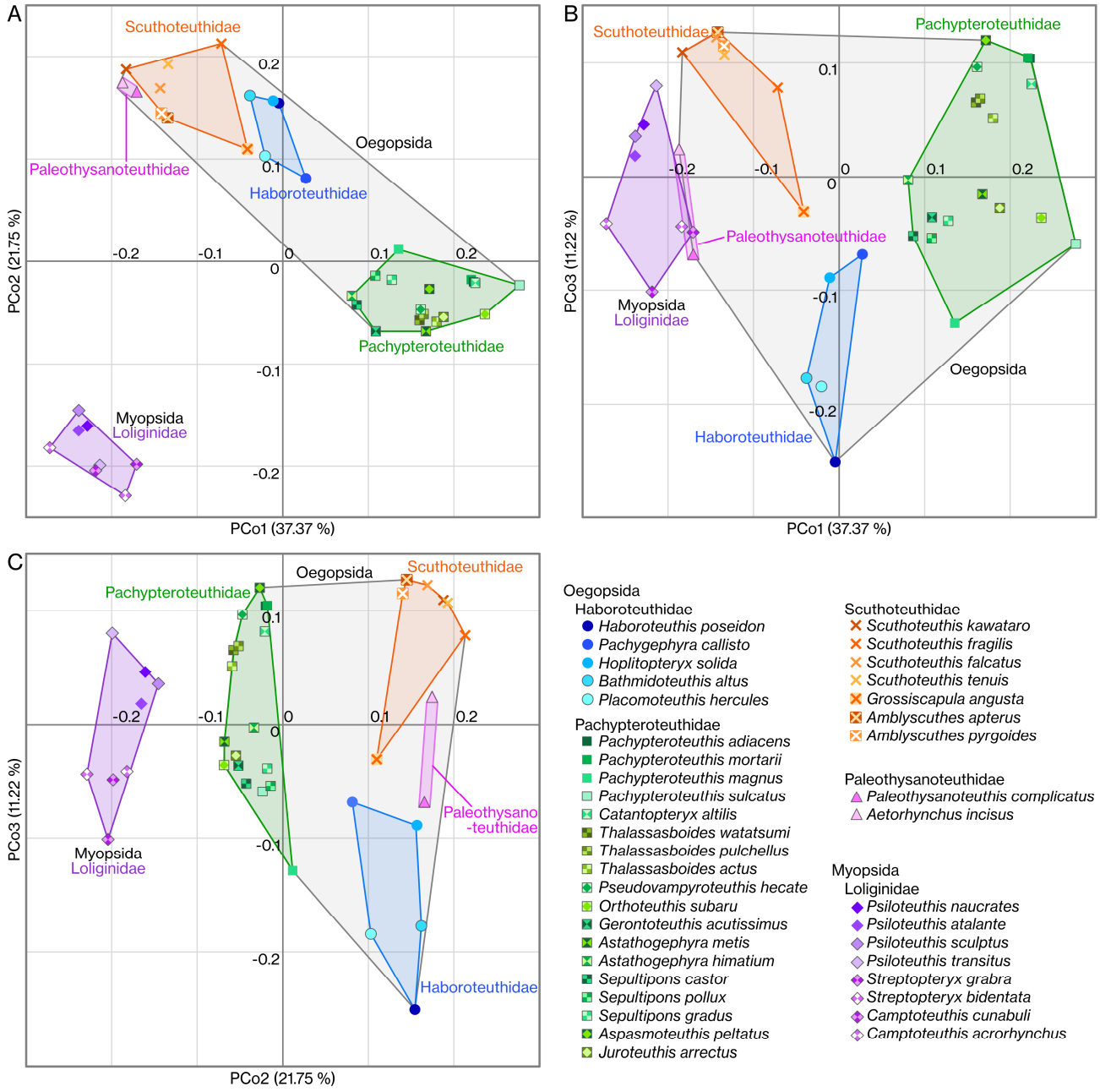


Fig.14. Morphospace of discovered squid species from the principal coordinate analysis. (**A** to **C**) Principal coordinates analysis plot showing principal coordinate 1 versus principal coordinate 2 (A), principal coordinate 1 versus principal coordinate 3 (B), and principal coordinate 2 versus principal coordinate 3 (C). The correspondence between markers in the plots and species names is exhibited on the bottom right.

followed by a rapid diversification (Fig. 15B). Throughout the Late Cretaceous, squid diversity maintained at a high level (Fig. 15B). The oldest squids reported here include both Oegopsida and Myopsida (Fig. 15A). The so far oldest record of the Oegopsida is from the middle Late Cretaceous (~85 Ma)[35], and that of Myopsida from the middle Eocene (~45 Ma)[13]. This study thus eextends the fossil record of both orders by ~15 Myr and ~50 Myr, respectively. The five oldest oegopsid species all possess characters rarely seen in stratigraphically younger specimens, such as a small rostrum and indistinct shoulder blades. Within six million years after the origination of these species, which all

belong to one family, all other fossil families appeared. These findings suggest a fast morphological evolution of the early Oegopsida. All myopsid species encountered here can be included in one extant family, showing the early origin of true modern forms. These results reveal that Oegopsida and Myopsida emerged earlier than all other living orders of ten-armed cephalopods like Sepiida[16,45].

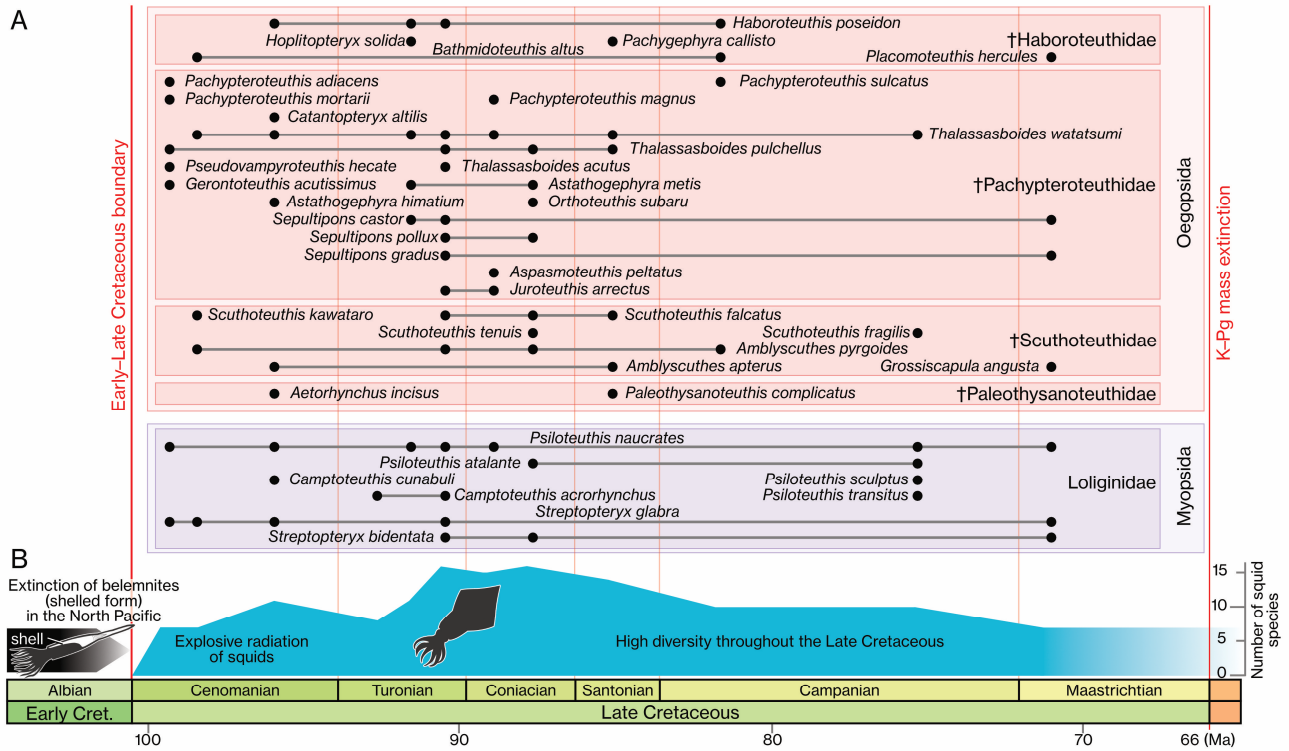


Fig. 15. Stratigraphic distribution and diversity pattern of early squids.
(**A**) Stratigraphic distribution of the fossil squid species based on the new findings. Occurrences of fossils are indicated as dots. The stratigraphic ranges are shown by horizontal lines. (**B**) Species diversity curve compiled from (A).

The rise of squids uncovered here is synchronous with a local extinction of belemnites, a Mesozoic internal shelled cephalopod occupying the same niche, across many oceanic regions (e.g., Tethys and North Pacific: Fig. 15)[46,47]. These opposing trends indicate that the turnover in cephalopods from heavily shelled to soft-bodied forms is not the consequence of the K–Pg mass extinction (66 Ma). Squids outcompeted shelled forms at least in the North Pacific, the largest ocean in the Cretaceous, and survived this extinction.

1.5.3. The Cretaceous squid ocean

Our data suggest that the abundance of Late Cretaceous squids exceeded that of co-occurring ammonites and bony fishes (Fig. 16 and Table S2). Since carbonate concretions formed in a few weeks and were not reworked[48], the faunal composition can be examined even based on fragile beaks that would have been decomposed quickly. The chemical composition of beaks excludes a fossilization bias and thus enables reliable population analyses of cephalopods with and without shells. Throughout the Late Cretaceous the number of squids discovered here is 1.1 to 2.6 times higher than that of ammonites. It is only in the Turonian that squids came second to ammonites, but they still formed a

major component of the cephalopod assemblage. I also obtained 161 disarticulated vertebrae of bony fishes (Table 2). These data indicate that squids are much more common than bony fishes (Fig. 16) since individuals of the latter group are known to have more than 16 vertebrae each[49]. Fish vertebrae are thicker and have a more robust structure than beaks so would be expected to fossilize at higher rates. Ammonites are known as extremely successful Mesozoic cephalopods, and bony fishes were most likely leading competitors of squids in the Cretaceous[7,50].

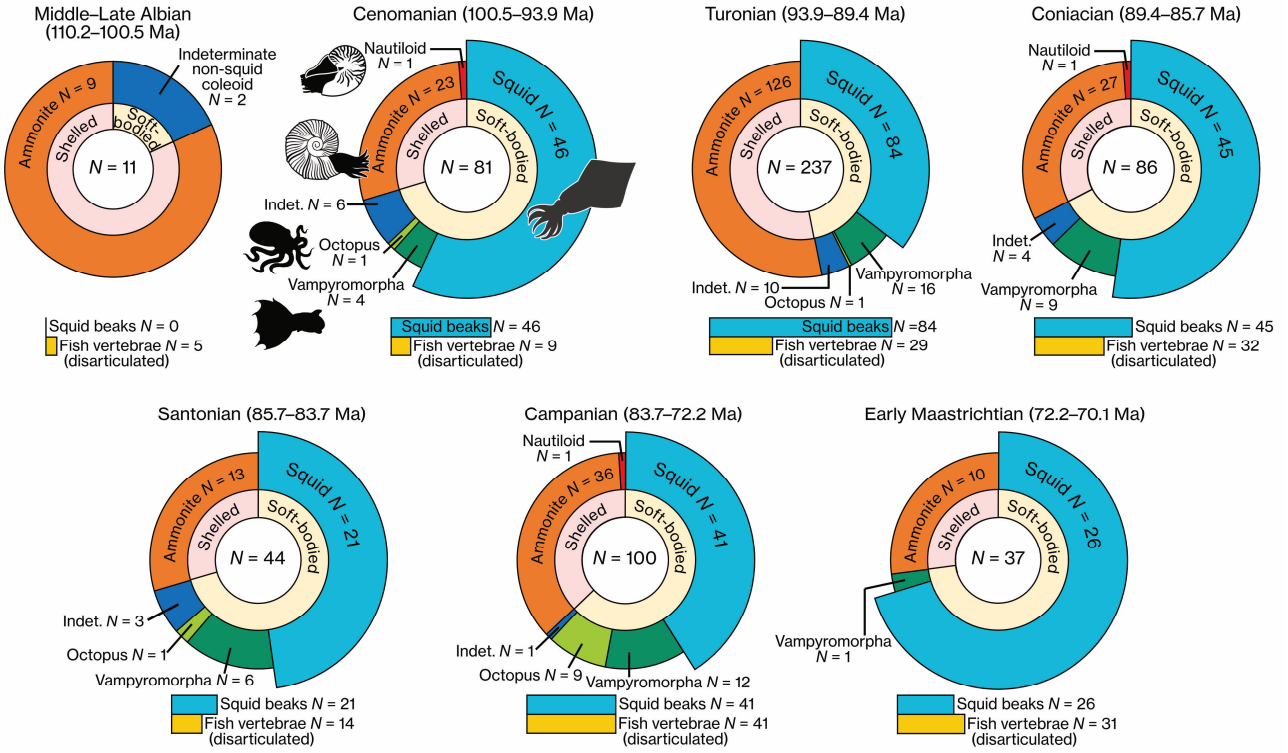


Fig. 16. Relative abundance of squids throughout the Albian–Maastrichtian.
Pie charts show the abundance of squids, Vampyromorpha, octopuses, indeterminate non-squid coleoids, ammonites, and nautiloids. In the center, N indicates the total number of lower beaks observed. The two horizontal bars show the numbers of squid beaks (blue) and bony fish vertebrae (yellow), respectively. These pie charts and bars include all discovered specimens (Table 2).

Further comparisons of the estimated body sizes, based on material from the same concretions, suggest that squids were larger than ammonites, having the size of bony fishes. Squids have long arms, a head, and a mantle; the beak is small with respect to the entire body[2]. Extant squids that reach 100 mm lengths have beaks that are only 2 mm long[19]. The beak sizes observed in the fossil material suggest an average mantle size of 70.33–90.99 mm for the Oegopsida and of 50.29–157.92 mm for the Myopsida (Tables 4–6). These sizes are similar to those of typical modern squids (e.g., California market squid)[51].

Large-sized ammonites are known from the studied sections, but they are quantitatively a minor component. Only 18 out of more than 1,000 ammonite shells encountered in the examined concretions were larger than 50 mm. This result implies that squids were larger than ammonites since the mantle of the latter lies inside their shell[16]. The average body length of co-occurring bony fishes, estimated from the size of vertebral bones, ranges from 122.06 to 238.93 mm (Tables 7 and 8). Considering that the estimates for the size of squids do not include the length of their head and the long arms, Cretaceous

squids are probably as large as bony fishes. The estimated body sizes, along with relative abundance, indicate that Late Cretaceous squids provided a larger biomass than any other co-existing nektonic organism.

The origin of squids would have imposed crucial effects on the evolution of the marine ecosystem. The present marine food web is characterized by intelligent fast-swimmers, in which bony fishes, marine mammals, and squids are dominant[52,53]. The radiation of bony fishes and marine mammals is well known to have occurred after the K–Pg mass extinction[54,55]. Our study reveals that squids prospered more than 30 Myr earlier than these groups, shaping the modern-type ecosystem as pioneers.

Table 4. Body size estimations of the Late Cretaceous oegopsid squids.

No.	Classification			3D model collection No. (NMNS: National Museum of Nature and Science, Tokyo)	Geological age	LRL (mm)	ML (mm) estimated from the relationship between LRL (mm) and ML (mm) of modern oegopsid squids (Clarke, 1986)[19]																	
	Family	Genus	Species				*Architeuthis dux* : 109.38 × LRL - 180.4	*Thysanoteuthis rhombus* : 110.53 × LRL - 112.6	*Dosidicus gigas* : 35.79 × LRL + 44.2	*Ommastrephes caroli* : 27.61 × LRL + 52.7	*Sthenoteuthis aulaniensis* : 39.25 × LRL + 6.98	*Hyaloteuthis hyadesi* : 24.31 × LRL + 20.65	*Todarodes sagittus* : 41.36 × LRL - 11.3	*Todarodes pacificus* : 37.44 × LRL + 18.53	*Notodarodes hawaiiensis* : 18.61 × LRL + 33.55	*Notodarodes gouldi* : 16.5 × LRL + 155	*Todaropsis eblanae* : 35.04 × LRL - 10.32	*Eucleoteuthis luminosa* : 37.61 × LRL + 11.12	*Ornithoteuthis volatilis* : 38.81 × LRL - 16.96	*Onychoteuthis banksi* : 61.0 × LRL - 28.9	*Pholidoteuthis boschmai* : 41.09 × LRL + 11.3	*Brachioteuthis* spp.: 20.18 × LRL + 16.31	*Gonatus* spp.: 42.87 × LRL - 43.4
1	Haboroteuthidae	*Haboroteuthis*	*poseidon*	NMNS_DS00082_79XGc4h.stl	Cenomanian	5.97	472.60	547.26	257.87	217.53	241.30	165.78	235.62	242.05	144.65	253.51	198.87	235.65	214.74	335.27	256.61	136.78	212.53
2	Haboroteuthidae	*Haboroteuthis*	*poseidon*	NMNS_DS00009_3F7VSzd.stl	Turonian	7.56	646.51	723.01	314.77	261.43	303.71	204.43	301.38	301.58	174.24	279.74	254.58	295.45	276.44	432.26	321.94	168.87	280.70
3	Haboroteuthidae	*Haboroteuthis*	*poseidon*	NMNS_DS00173_Px2dDmF.stl	Turonian	-	-	-	-	-	-	-	-	-	-	-	-	-	-	-	-	-	-
4	Haboroteuthidae	*Pachygephyra*	*callisto*	NMNS_DS00011_JVM6xKK.stl	Santonian	2.43	85.39	155.99	131.17	119.79	102.36	79.72	89.20	109.51	78.77	195.10	74.83	102.51	77.35	119.33	111.15	65.35	60.77
5	Haboroteuthidae	*Hoplitopteryx*	*solida*	NMNS_DS00009_dvxb42e.stl	Turonian	1.12	-57.89	11.19	84.28	83.62	50.94	47.88	35.02	60.46	54.39	173.48	28.92	53.24	26.51	39.42	57.32	38.91	4.61
6	Haboroteuthidae	*Bathmidoteuthis*	*altus*	NMNS_DS00084_a3lBsj.stl	Cenomanian	2.67	111.64	182.52	139.76	126.42	111.78	85.56	99.13	118.49	83.24	199.06	83.24	111.54	86.66	133.97	121.01	70.19	71.06
7	Haboroteuthidae	*Bathmidoteuthis*	*altus*	NMNS_DS00171_LqIJgoh.stl	Campanian	1.78	14.30	84.14	107.91	101.85	76.85	63.92	62.32	85.17	66.68	184.37	52.05	78.07	52.12	79.68	84.44	52.23	32.91
8	Haboroteuthidae	*Placomoteuthis*	*hercules*	NMNS_DS00174_bjM7Cpk.stl	Maastrichtian	1.11	-58.99	10.09	83.93	83.35	50.55	47.63	34.61	60.09	54.21	173.32	28.57	52.87	26.12	38.81	56.91	38.71	4.19
9	Pachypteroteuthidae	*Pachypteroteuthis*	*aduncens*	NMNS_DS00068_c0JKOmo.stl	Cenomanian	2.12	51.49	121.72	120.07	111.23	90.19	72.19	76.38	97.90	73.00	189.98	63.96	90.85	65.32	100.42	98.41	59.09	47.48
10	Pachypteroteuthidae	*Pachypteroteuthis*	*aduncens*	NMNS_DS00068_EnU0Efh.stl	Cenomanian	2.43	85.39	155.99	131.17	119.79	102.36	79.72	89.20	109.51	78.77	195.10	74.83	102.51	77.35	119.33	111.15	65.35	60.77
11	Pachypteroteuthidae	*Pachypteroteuthis*	*mortarii*	NMNS_DS00068_G7fBskP.stl	Cenomanian	1.31	-37.11	32.19	91.08	88.87	58.40	52.50	42.88	67.58	57.93	176.62	35.58	60.39	33.88	51.01	65.13	42.75	12.76
12	Pachypteroteuthidae	*Pachypteroteuthis*	*magnus*	NMNS_DS00034_nv7HRSc.stl	Coniacian	5.18	386.19	459.95	229.59	195.72	210.30	146.58	202.94	212.47	129.95	240.47	171.19	205.94	184.08	287.08	224.15	120.84	178.67
13	Pachypteroteuthidae	*Pachypteroteuthis*	*sulcatus*	NMNS_DS00175_2UQENMZ.stl	Campanian	-	-	-	-	-	-	-	-	-	-	-	-	-	-	-	-	-	-
14	Pachypteroteuthidae	*Catantopteryx*	*altilis*	NMNS_DS00082_mK5pM.stl	Cenomanian	-	-	-	-	-	-	-	-	-	-	-	-	-	-	-	-	-	-
15	Pachypteroteuthidae	*Catantopteryx*	*altilis*	NMNS_DS00173_JGcVf5Q.stl	Turonian	4.20	279.00	351.63	194.52	168.66	171.83	122.75	162.41	175.78	111.71	224.30	136.85	169.08	146.04	227.30	183.88	101.07	136.65
16	Pachypteroteuthidae	*Thalassasboides*	*wakatsumi*	NMNS_DS00084_U3Z2mdm.stl	Cenomanian	-	-	-	-	-	-	-	-	-	-	-	-	-	-	-	-	-	-
17	Pachypteroteuthidae	*Thalassasboides*	*wakatsumi*	NMNS_DS00084_RAKM2iJ.stl	Cenomanian	2.01	39.45	109.57	116.14	108.20	85.87	69.51	71.83	93.78	70.96	188.17	60.11	86.72	61.05	93.71	93.89	56.87	42.77
18	Pachypteroteuthidae	*Thalassasboides*	*wakatsumi*	NMNS_DS00082_1H8UvDW.stl	Cenomanian	-	-	-	-	-	-	-	-	-	-	-	-	-	-	-	-	-	-
19	Pachypteroteuthidae	*Thalassasboides*	*wakatsumi*	NMNS_DS00082_ev6tAaJ.stl	Cenomanian	2.74	119.30	190.25	142.26	128.35	114.53	87.26	102.03	121.12	84.54	200.21	85.69	114.17	89.38	138.24	123.89	71.60	74.06
20	Pachypteroteuthidae	*Thalassasboides*	*wakatsumi*	NMNS_DS00082_egK7tIO.stl	Cenomanian	-	-	-	-	-	-	-	-	-	-	-	-	-	-	-	-	-	-
21	Pachypteroteuthidae	*Thalassasboides*	*wakatsumi*	NMNS_DS00009_MnRA9nb.stl	Turonian	4.03	260.40	332.84	188.43	163.97	165.16	118.62	155.38	169.41	108.55	221.50	130.89	162.69	139.44	216.93	176.89	97.64	129.37
22	Pachypteroteuthidae	*Thalassasboides*	*wakatsumi*	NMNS_DS00135_JM4f46S.stl	Turonian	1.77	13.20	83.04	107.55	101.57	76.45	63.68	61.91	84.80	66.49	184.21	51.70	77.69	51.73	79.07	84.03	52.03	32.48
23	Pachypteroteuthidae	*Thalassasboides*	*wakatsumi*	NMNS_DS00173_4dpfhl4.stl	Turonian	3.58	211.18	283.10	172.33	151.54	147.50	107.68	136.77	152.57	100.17	214.07	115.12	145.76	121.98	189.48	158.40	88.55	110.07
24	Pachypteroteuthidae	*Thalassasboides*	*wakatsumi*	NMNS_DS00173_A2DztKh.stl	Turonian	2.79	124.77	195.78	144.05	129.73	116.49	88.47	104.09	122.99	85.47	201.04	87.44	116.05	91.32	141.29	125.94	72.61	76.21
25	Pachypteroteuthidae	*Thalassasboides*	*wakatsumi*	NMNS_DS00173_TFD6EDX.stl	Turonian	1.83	19.77	89.67	109.70	103.23	78.81	65.14	64.39	87.05	67.61	185.20	53.80	79.95	54.06	82.73	86.49	53.24	35.05
26	Pachypteroteuthidae	*Thalassasboides*	*wakatsumi*	NMNS_DS00173_d50dzkLs.stl	Turonian	2.95	142.27	213.46	149.78	134.15	122.77	92.36	110.71	128.98	88.45	203.68	93.05	122.07	97.53	151.05	132.52	75.84	83.07
27	Pachypteroteuthidae	*Thalassasboides*	*wakatsumi*	NMNS_DS00034_kJU1vwB.stl	Coniacian	1.69	4.45	74.20	104.69	99.36	73.31	61.73	58.60	81.80	65.00	182.89	48.90	74.68	48.63	74.19	80.74	50.41	29.05
28	Pachypteroteuthidae	*Thalassasboides*	*wakatsumi*	NMNS_DS00083_SN4asC0.stl	Coniacian	-	-	-	-	-	-	-	-	-	-	-	-	-	-	-	-	-	-
29	Pachypteroteuthidae	*Thalassasboides*	*wakatsumi*	NMNS_DS00011_UU1c7pj.stl	Santonian	-	-	-	-	-	-	-	-	-	-	-	-	-	-	-	-	-	-
30	Pachypteroteuthidae	*Thalassasboides*	*wakatsumi*	NMNS_DS00182_F56YeDG.stl	Campanian	-	-	-	-	-	-	-	-	-	-	-	-	-	-	-	-	-	-
31	Pachypteroteuthidae	*Thalassasboides*	*pukhellus*	NMNS_DS00068_pBrzD5i.stl	Cenomanian	1.86	23.05	92.99	110.77	104.05	79.99	65.87	65.63	88.17	68.16	185.69	54.85	81.07	55.23	84.56	87.73	53.84	36.34
32	Pachypteroteuthidae	*Thalassasboides*	*pukhellus*	NMNS_DS00173_CLt5m2t.stl	Turonian	3.05	153.21	224.52	153.36	136.91	126.69	94.80	114.85	132.72	90.31	205.33	96.55	125.83	101.41	157.15	136.62	77.86	87.35
33	Pachypteroteuthidae	*Thalassasboides*	*pukhellus*	NMNS_DS00173_8lkQbCV.stl	Turonian	2.58	101.80	172.57	136.54	123.93	108.25	83.37	95.41	115.13	81.56	197.57	80.08	108.15	83.17	128.48	117.31	68.37	67.20
34	Pachypteroteuthidae	*Thalassasboides*	*pukhellus*	NMNS_DS00173_27C5zir.stl	Turonian	3.92	248.37	320.68	184.50	160.93	160.84	115.95	150.83	165.29	106.50	219.68	127.04	158.55	135.18	210.22	172.37	95.42	124.65
35	Pachypteroteuthidae	*Thalassasboides*	*pukhellus*	NMNS_DS00081_V85MVoY.stl	Coniacian	2.72	117.11	188.04	141.55	127.80	113.74	86.77	101.20	120.37	84.17	199.88	84.99	113.42	88.60	137.02	123.06	71.20	73.21
36	Pachypteroteuthidae	*Thalassasboides*	*pukhellus*	NMNS_DS00104_GDb7t8w.stl	Santonian	-	-	-	-	-	-	-	-	-	-	-	-	-	-	-	-	-	-
37	Pachypteroteuthidae	*Thalassasboides*	*acutus*	NMNS_DS00173_w8T3Zp0.stl	Turonian	3.50	202.43	274.26	169.47	149.34	144.36	105.74	133.46	149.57	98.69	212.75	112.32	142.76	118.88	184.60	155.12	86.94	106.65
38	Pachypteroteuthidae	*Thalassasboides*	uncertain	NMNS_DS00034_GA9MzKt.stl	Coniacian	3.63	216.65	288.62	174.12	152.92	149.46	108.90	138.84	154.44	101.10	214.90	116.88	147.64	123.92	192.53	160.46	89.56	112.22
39	Pachypteroteuthidae	*Thalassasboides*	uncertain	NMNS_DS00083_LNaCE2f.stl	Coniacian	-	-	-	-	-	-	-	-	-	-	-	-	-	-	-	-	-	-
40	Pachypteroteuthidae	*Thalassasboides*	uncertain	NMNS_DS00171_H6o1Nxu.stl	Campanian	-	-	-	-	-	-	-	-	-	-	-	-	-	-	-	-	-	-
41	Pachypteroteuthidae	*Pseudovampyroteuthis*	*hecate*	NMNS_DS00068_gNqH3RQ.stl	Cenomanian	2.34	75.55	146.04	127.95	117.31	98.83	77.54	85.48	106.14	77.10	193.61	71.67	99.13	73.86	113.84	107.45	63.53	56.92
42	Pachypteroteuthidae	*Orthoteuthis*	*subaru*	NMNS_DS00083_UA2WR3Z.stl	Coniacian	0.88	-84.15	-15.33	75.70	77.00	41.52	42.04	25.10	51.48	49.93	169.52	20.52	44.22	17.19	24.78	47.46	34.07	-5.67
43	Pachypteroteuthidae	*Gerontoteuthis*	*acutissimus*	NMNS_DS00068_6MhlFUS.stl	Cenomanian	2.21	61.33	131.67	123.30	113.72	93.72	74.38	80.11	101.27	74.68	191.47	67.12	94.24	68.81	105.91	102.11	60.91	51.34
44	Pachypteroteuthidae	*Asthathogephyra*	*metis*	NMNS_DS00009_TkD5dWU.stl	Turonian	2.43	85.39	155.99	131.17	119.79	102.36	79.72	89.20	109.51	78.77	195.10	74.83	102.51	77.35	119.33	111.15	65.35	60.77
45	Pachypteroteuthidae	*Asthathogephyra*	*metis*	NMNS_DS00009_MU8cSC4.stl	Turonian	1.87	24.14	94.09	111.13	104.33	80.38	66.11	66.04	88.54	68.35	185.86	55.20	81.45	55.61	85.17	88.14	54.05	36.77
46	Pachypteroteuthidae	*Asthathogephyra*	*metis*	NMNS_DS00083_VCCZZr4.stl	Coniacian	1.78	14.30	84.14	107.91	101.85	76.85	63.92	62.32	85.17	66.68	184.37	52.05	78.07	52.12	79.68	84.44	52.23	32.91
47	Pachypteroteuthidae	*Asthathogephyra*	*himatium*	NMNS_DS00082_ZxRP3bR.stl	Cenomanian	1.38	-29.46	39.93	93.59	90.80	61.15	54.20	45.78	70.20	59.23	177.77	38.04	63.02	36.60	55.28	68.00	44.16	15.76
48	Pachypteroteuthidae	*Septitipons*	*castor*	NMNS_DS00009_vxf2tIr.stl	Turonian	1.62	-3.20	66.46	102.18	97.43	70.57	60.03	55.70	79.18	63.70	181.73	46.44	72.05	45.91	69.92	77.87	49.00	26.05
49	Pachypteroteuthidae	*Septitipons*	*castor*	NMNS_DS00041_b4BWTEx.stl	Turonian	1.56	-9.77	59.83	100.03	95.77	68.21	58.57	53.22	76.94	62.58	180.74	44.34	69.79	43.58	66.26	75.40	47.79	23.48
50	Pachypteroteuthidae	*Septitipons*	*castor*	NMNS_DS00173_bU7zsos.stl	Turonian	1.62	-3.20	66.46	102.18	97.43	70.57	60.03	55.70	79.18	63.70	181.73	46.44	72.05	45.91	69.92	77.87	49.00	26.05
51	Pachypteroteuthidae	*Septitipons*	*castor*	NMNS_DS00173_f2mBoiP.stl	Turonian	1.67	2.26	71.99	103.97	98.81	72.53	61.25	57.77	81.05	64.63	182.56	48.20	73.93	47.85	72.97	79.92	50.01	28.19
52	Pachypteroteuthidae	*Septitipons*	*castor*	NMNS_DS00173_BbCw7oa.stl	Turonian	1.71	6.64	76.41	105.40	99.91	74.10	62.22	59.43	82.55	65.37	183.22	49.60	75.43	49.41	75.41	81.56	50.82	29.91
53	Pachypteroteuthidae	*Septitipons*	*castor*	NMNS_DS00173_UXkxZH5.stl	Turonian	1.58	-7.58	62.04	100.75	96.32	69.00	59.06	54.05	77.69	62.95	181.07	45.04	70.54	44.36	67.48	76.22	48.19	24.33
54	Pachypteroteuthidae	*Septitipons*	*castor*	NMNS_DS00173_001WWW9.stl	Turonian	2.00	38.36	108.46	115.78	107.92	85.48	69.27	71.42	93.41	70.77	188.00	59.76	86.34	60.66	93.10	93.48	56.67	42.34
55	Pachypteroteuthidae	*Septitipons*	*castor*	NMNS_DS00173_54IvJ9D.stl	Turonian	1.73	8.83	78.62	106.12	100.47	74.88	62.71	60.25	83.30	65.75	183.55	50.30	76.19	50.18	76.63	82.39	51.22	30.77
56	Pachypteroteuthidae	*Septitipons*	*castor*	NMNS_DS00174_kRFX5Fg.stl	Maastrichtian	1.64	-1.02	68.67	102.90	97.98	71.35	60.52	56.53	79.93	64.07	182.06	47.15	72.80	46.69	71.14	78.69	49.41	26.91
57	Pachypteroteuthidae	*Septitipons*	*castor*	NMNS_DS00174_L1VyDDh.stl	Maastrichtian	-	-	-	-	-	-	-	-	-	-	-	-	-	-	-	-	-	-
58	Pachypteroteuthidae	*Septitipons*	*castor*	NMNS_DS00174_7H4Gb53.stl	Maastrichtian	1.38	-29.46	39.93	93.59	90.80	61.15	54.20	45.78	70.20	59.23	177.77	38.04	63.02	36.60	55.28	68.00	44.16	15.76
59	Pachypteroteuthidae	*Septitipons*	*castor*	NMNS_DS00174_jWDHdZl.stl	Maastrichtian	1.43	-23.99	45.46	95.38	92.18	63.11	55.41	47.84	72.07	60.16	178.60	39.79	64.90	38.54	58.33	70.06	45.17	17.90
60	Pachypteroteuthidae	*Septitipons*	*pollux*	NMNS_DS00040_e0mxqWi.stl	Turonian	1.96	33.98	104.04	114.35	106.82	83.91	68.30	69.77	91.91	70.03	187.34	58.36	84.84	59.11	90.66	91.84	55.86	40.63
61	Pachypteroteuthidae	*Septitipons*	*pollux*	NMNS_DS00173_lvLSx02.stl	Turonian	1.41	-26.17	43.25	94.66	91.63	62.32	54.93	47.02	71.32	59.79	178.27	39.09	64.15	37.76	57.11	69.24	44.76	17.05
62	Pachypteroteuthidae	*Septitipons*	*pollux*	NMNS_DS00083_qxUALq6.stl	Coniacian	1.41	-26.17	43.25	94.66	91.63	62.32	54.93	47.02	71.32	59.79	178.27	39.09	64.15	37.76	57.11	69.24	44.76	17.05
63	Pachypteroteuthidae	*Septitipons*	*gradus*	NMNS_DS00173_h0qQoNN.stl	Turonian	1.74	9.92	79.72	106.47	100.74	75.28	62.95	60.67	83.68	65.93	183.71	50.65	76.56	50.57	77.24	82.80	51.42	31.19
64	Pachypteroteuthidae	*Septitipons*	*gradus*	NMNS_DS00083_3h8PCFD.stl	Coniacian	2.11	50.39	120.62	119.72	110.96	89.80	71.94	75.97	97.53	72.82	189.82	63.61	90.48	64.93	99.81	98.00	58.89	47.06
65	Pachypteroteuthidae	*Septitipons*	*gradus*	NMNS_DS00128_oRE3wgv.stl	Maastrichtian	2.83	129.15	200.20	145.49	130.84	118.06	89.45	105.75	124.49	86.22	201.70	88.84	117.56	92.87	143.73	127.58	73.42	77.92
66	Pachypteroteuthidae	*Septitipons*	*gradus*	NMNS_DS00174_Nu5pFy.stl	Maastrichtian	1.66	1.17	70.88	103.61	98.53	72.14	61.00	57.36	80.68	64.44	182.39	47.85	73.55	47.46	72.36	79.51	49.81	27.76
67	Pachypteroteuthidae	*Aspasmoteuthis*	*peltatus*	NMNS_DS00034_OJDNCD8.stl	Coniacian	2.67	111.64	182.52	139.76	126.42	111.78	85.56	99.13	118.49	83.24	199.06	83.24	111.54	86.66	133.97	121.01	70.19	71.06
68	Pachypteroteuthidae	*Juroteuthis*	*arrectus*	NMNS_DS00173_X7NQkzW.stl	Turonian	-	-	-	-	-	-	-	-	-	-	-	-	-	-	-	-	-	-
69	Pachypteroteuthidae	*Juroteuthis*	*arrectus*	NMNS_DS00173_Hfj1roq.stl	Turonian	-	-	-	-	-	-	-	-	-	-	-	-	-	-	-	-	-	-
70	Pachypteroteuthidae	*Juroteuthis*	*arrectus*	NMNS_DS00034_MDF4xvB.stl	Coniacian	-	-	-	-	-	-	-	-	-	-	-	-	-	-	-	-	-	-

Table 4. (continued)

No.	ML (mm) estimated from the relationship between LRL (mm) and ML (mm) of modern oegopsid squids (Clarke, 1986)[19]																						
	Gonatus onyx : 19.02 × LRL + 12.82	*Gonatopsis borealis* : 32.0 × LRL + 24.1	*Berryteuthis magister* : 43.99 × LRL - 5.14	*Psychroteuthis* spp.: 33.16 × LRL + 6.2	*Abraliopsis affinis* : 19.28 × LRL + 9.8	*Abraliopsis felis* : 40.55 × LRL - 2.66	*Ancistrocheirus lesueuri* : 40.75 × LRL - 41.3	*Octopoteuthis* spp.: 17.33 × LRL - 0.4	*Taningia danae* : 75.22 × LRL - 556.9	*Histioteuthis miranda* : 25.82 × LRL - 7.0	*Histioteuthis dofleini* (ML<180mm): 20.61 × LRL - 5.9	*Histioteuthis dofleini* (ML>90mm): 14.55 × LRL + 7.69	*Histioteuthis bonnellii* : 8.99 × LRL + 17.1	*Histioteuthis heteropsis* : 20.57 × LRL + 2.04	*Bathyteuthis abyssicola* : 51.59 × LRL + 1.68	*Ctenopteryx* spp.: 32.42 × LRL + 11.69	*Cycloteuthis* spp.: 31 × LRL	*Mastigoteuthis* spp.: 29.08 × LRL - 1.8	*Chiroteuthis* spp.: 24.46 × LRL + 11.4	*Cranchia scabra* : 28.03 × LRL + 17.7	*Liocranchia* spp.: 78.71 × LRL + 5.9	*Leachia* spp.: 67.94 × LRL + 18.22	*Megalocranchia* spp.: 68.13 × LRL - 70.9	*Teuthowenia megalops* : 40.78 × LRL + 12.2
1	126.37	215.14	257.48	204.17	124.90	239.42	201.98	103.06	-107.84	147.15	117.14	94.55	70.77	124.84	309.67	205.24	185.07	171.81	157.43	185.04	475.80	423.82	335.84	255.66
2	156.61	266.02	327.42	256.89	155.56	303.90	266.77	130.61	11.76	188.20	149.91	117.69	85.06	157.55	391.70	256.79	234.36	218.04	196.32	229.61	600.95	531.85	444.16	320.50
3	-	-	-	-	-	-	-	-	-	-	-	-	-	-	-	-	-	-	-	-	-	-	-	-
4	59.04	101.86	101.76	86.78	56.65	95.88	57.72	41.71	-374.12	55.74	44.18	43.05	38.95	52.03	127.04	90.47	75.33	68.86	70.84	85.81	197.17	183.31	94.66	111.30
5	34.12	59.94	44.13	43.34	31.39	42.76	4.34	19.01	-472.65	21.92	17.18	23.99	27.17	25.08	59.46	48.00	34.72	30.77	38.80	49.09	94.06	94.31	5.41	57.87
6	63.60	109.54	112.31	94.74	61.28	105.61	67.50	45.87	-356.06	61.94	49.13	46.54	41.10	56.96	139.43	98.25	82.77	75.84	76.71	92.54	216.06	199.62	111.01	121.08
7	46.68	81.06	73.16	65.22	44.12	69.52	31.24	30.45	-423.01	38.96	30.79	33.59	33.10	38.65	93.51	69.40	55.18	49.96	54.94	67.59	146.00	139.15	50.37	84.79
8	33.93	59.62	43.69	43.01	31.20	42.35	3.93	18.84	-473.41	21.66	16.98	23.84	27.08	24.87	58.94	47.68	34.41	30.48	38.55	48.81	93.27	93.63	4.72	57.47
9	53.14	91.94	88.12	76.50	50.67	83.31	45.09	36.34	-397.43	47.74	37.79	38.54	36.16	45.65	111.05	80.42	65.72	59.85	63.26	77.12	172.77	162.25	73.54	98.65
10	59.04	101.86	101.76	86.78	56.65	95.88	57.72	41.71	-374.12	55.74	44.18	43.05	38.95	52.03	127.04	90.47	75.33	68.86	70.84	85.81	197.17	183.31	94.66	111.30
11	37.74	66.02	52.49	49.64	35.06	50.46	12.08	22.30	-458.36	26.82	21.10	26.75	28.88	28.99	69.26	54.16	40.61	36.29	43.44	54.42	109.01	107.22	18.35	65.62
12	111.34	189.86	222.73	177.97	109.67	207.39	169.79	89.37	-167.26	126.75	100.86	83.06	63.67	108.59	268.92	179.63	160.58	148.83	138.10	162.90	413.62	370.15	282.01	223.44
13	-	-	-	-	-	-	-	-	-	-	-	-	-	-	-	-	-	-	-	-	-	-	-	-
14	-	-	-	-	-	-	-	-	-	-	-	-	-	-	-	-	-	-	-	-	-	-	-	-
15	92.70	158.50	179.62	145.47	90.78	167.65	129.85	72.39	-240.98	101.44	80.66	68.80	54.86	88.43	218.36	147.85	130.20	120.34	114.13	135.43	336.48	303.57	215.25	183.48
16	-	-	-	-	-	-	-	-	-	-	-	-	-	-	-	-	-	-	-	-	-	-	-	-
17	51.05	88.42	83.28	72.85	48.55	78.85	40.61	34.43	-405.71	44.90	35.53	36.94	35.17	43.39	105.38	76.85	62.31	56.65	60.56	74.04	164.11	154.78	66.04	94.17
18	-	-	-	-	-	-	-	-	-	-	-	-	-	-	-	-	-	-	-	-	-	-	-	-
19	64.93	111.78	115.39	97.06	62.63	108.45	70.36	47.08	-350.80	63.75	50.57	47.56	41.73	58.40	143.04	100.52	84.94	77.88	78.42	94.50	221.57	204.38	115.78	123.94
20	-	-	-	-	-	-	-	-	-	-	-	-	-	-	-	-	-	-	-	-	-	-	-	-
21	89.47	153.06	172.14	139.83	87.50	160.76	122.92	69.44	-253.76	97.05	77.16	66.33	53.33	84.94	209.59	142.34	124.93	115.39	109.97	130.66	323.10	292.02	203.66	176.54
22	46.49	80.74	72.72	64.89	43.93	69.11	30.83	30.27	-423.76	38.70	30.58	33.44	33.01	38.45	92.99	69.07	54.87	49.67	54.69	67.31	145.22	138.47	49.69	84.38
23	80.91	138.66	152.34	124.91	78.82	142.51	104.59	61.64	-287.61	85.44	67.88	59.78	49.28	75.68	186.37	127.75	110.98	102.31	98.97	118.05	287.68	261.45	173.01	158.19
24	65.89	113.38	117.59	98.72	63.59	110.47	72.39	47.95	-347.04	65.04	51.60	48.28	42.18	59.43	145.62	102.14	86.49	79.33	79.64	95.90	225.50	207.77	119.18	125.98
25	47.63	82.66	75.36	66.88	45.08	71.55	33.27	31.31	-419.25	40.25	31.82	34.32	33.55	39.68	96.09	71.02	56.73	51.42	56.16	68.99	149.94	142.55	53.78	86.83
26	68.93	118.50	124.63	104.02	66.68	116.96	78.91	50.72	-335.00	69.17	54.90	50.61	43.62	62.72	153.87	107.33	91.45	83.99	83.56	100.39	238.09	218.64	130.08	132.50
27	44.96	78.18	69.20	62.24	42.38	65.87	27.57	28.89	-429.78	36.64	28.93	32.28	32.29	36.80	88.87	66.48	52.39	47.35	52.74	65.07	138.92	133.04	44.24	81.12
28	-	-	-	-	-	-	-	-	-	-	-	-	-	-	-	-	-	-	-	-	-	-	-	-
29	-	-	-	-	-	-	-	-	-	-	-	-	-	-	-	-	-	-	-	-	-	-	-	-
30	-	-	-	-	-	-	-	-	-	-	-	-	-	-	-	-	-	-	-	-	-	-	-	-
31	48.20	83.62	76.68	67.88	45.66	72.76	34.50	31.83	-416.99	41.03	32.43	34.75	33.82	40.30	97.64	71.99	57.66	52.29	56.90	69.84	152.30	144.59	55.82	88.05
32	70.83	121.70	129.03	107.34	68.60	121.02	82.99	52.46	-327.48	71.75	56.96	52.07	44.52	64.78	159.03	110.57	94.55	86.89	86.00	103.19	245.97	225.44	136.90	136.58
33	61.89	106.66	108.35	91.75	59.54	101.96	63.84	44.31	-362.83	59.62	47.27	45.23	40.29	55.11	134.78	95.33	79.98	73.23	74.51	90.02	208.97	193.51	104.88	117.41
34	87.38	149.54	167.30	136.19	85.38	156.30	118.44	67.53	-262.04	94.21	74.89	64.73	52.34	82.67	203.91	138.78	121.52	112.19	107.28	127.58	314.44	284.54	196.17	172.06
35	64.55	111.14	114.51	96.40	62.24	107.64	69.54	46.74	-352.30	63.23	50.16	47.27	41.55	57.99	142.00	99.87	84.32	77.30	77.93	93.94	219.99	203.02	114.41	123.12
36	-	-	-	-	-	-	-	-	-	-	-	-	-	-	-	-	-	-	-	-	-	-	-	-
37	79.39	136.10	148.83	122.26	77.28	139.27	101.33	60.26	-293.63	83.37	66.24	58.62	48.57	74.04	182.25	125.16	108.50	99.98	97.01	115.81	281.39	256.01	167.56	154.93
38	81.86	140.26	154.54	126.57	79.79	144.54	106.62	62.51	-283.85	86.73	68.91	60.51	49.73	76.71	188.95	129.37	112.53	103.76	100.19	119.45	291.62	264.84	176.41	160.23
39	-	-	-	-	-	-	-	-	-	-	-	-	-	-	-	-	-	-	-	-	-	-	-	-
40	-	-	-	-	-	-	-	-	-	-	-	-	-	-	-	-	-	-	-	-	-	-	-	-
41	57.33	98.98	97.80	83.79	54.92	92.23	54.06	40.15	-380.89	53.42	42.33	41.74	38.14	50.17	122.40	87.55	72.54	66.25	68.64	83.29	190.08	177.20	88.52	107.63
42	29.56	52.26	33.57	35.38	26.77	33.02	-5.44	14.85	-490.71	15.72	12.24	20.49	25.01	20.14	47.08	40.22	27.28	23.79	32.92	42.37	75.16	78.01	-10.95	48.09
43	54.85	94.82	92.08	79.48	52.41	86.96	48.76	37.90	-390.66	50.06	39.65	39.85	36.97	47.50	115.69	83.34	68.51	62.47	65.46	79.65	179.85	168.37	79.67	102.32
44	59.04	101.86	101.76	86.78	56.65	95.88	57.72	41.71	-374.12	55.74	44.18	43.05	38.95	52.03	127.04	90.47	75.33	68.86	70.84	85.81	197.17	183.31	94.66	111.30
45	48.39	83.94	77.12	68.21	45.85	73.17	34.90	32.01	-416.24	41.28	32.64	34.90	33.91	40.51	98.15	72.32	57.97	52.58	57.14	70.12	153.09	145.27	56.50	88.46
46	46.68	81.06	73.16	65.22	44.12	69.52	31.24	30.45	-423.01	38.96	30.79	33.59	33.10	38.65	93.51	69.40	55.18	49.96	54.94	67.59	146.00	139.15	50.37	84.79
47	39.07	68.26	55.57	51.96	36.41	53.30	14.94	23.52	-453.10	28.63	22.54	27.77	29.51	30.43	72.87	56.43	42.78	38.33	45.15	56.38	114.52	111.98	23.12	68.48
48	43.63	75.94	66.12	59.92	41.03	63.03	24.72	27.67	-435.04	34.83	27.49	31.26	31.66	35.36	85.26	64.21	50.22	45.31	51.03	63.11	133.41	128.28	39.47	78.26
49	42.49	74.02	63.48	57.93	39.88	60.60	22.27	26.63	-439.56	33.28	26.25	30.39	31.12	34.13	82.16	62.27	48.36	43.56	49.56	61.43	128.69	124.21	35.38	75.82
50	43.63	75.94	66.12	59.92	41.03	63.03	24.72	27.67	-435.04	34.83	27.49	31.26	31.66	35.36	85.26	64.21	50.22	45.31	51.03	63.11	133.41	128.28	39.47	78.26
51	44.58	77.54	68.32	61.58	42.00	65.06	26.75	28.54	-431.28	36.12	28.52	31.99	32.11	36.39	87.84	65.83	51.77	46.76	52.25	64.51	137.35	131.68	42.88	80.30
52	45.34	78.82	70.08	62.90	42.77	66.68	28.38	29.23	-428.27	37.15	29.34	32.57	32.47	37.21	89.90	67.13	53.01	47.93	53.23	65.63	140.49	134.40	45.60	81.93
53	42.87	74.66	64.36	58.59	40.26	61.41	23.09	26.98	-438.05	33.80	26.66	30.68	31.30	34.54	83.19	62.91	48.98	44.15	50.05	61.99	130.26	125.57	36.75	76.63
54	50.86	88.10	82.84	72.52	48.36	78.44	40.20	34.26	-406.46	44.64	35.32	36.79	35.08	43.18	104.86	76.53	62.00	56.36	60.32	73.76	163.32	154.10	65.36	93.76
55	45.72	79.46	70.96	63.57	43.15	67.49	29.20	29.58	-426.77	37.67	29.76	32.86	32.65	37.63	90.93	67.78	53.63	48.51	53.72	66.19	142.07	135.76	46.96	82.75
56	44.01	76.58	67.00	60.58	41.42	63.84	25.53	28.02	-433.54	35.34	27.90	31.55	31.84	35.77	86.29	64.86	50.84	45.89	51.51	63.67	134.98	129.64	40.83	79.08
57	-	-	-	-	-	-	-	-	-	-	-	-	-	-	-	-	-	-	-	-	-	-	-	-
58	39.07	68.26	55.57	51.96	36.41	53.30	14.94	23.52	-453.10	28.63	22.54	27.77	29.51	30.43	72.87	56.43	42.78	38.33	45.15	56.38	114.52	111.98	23.12	68.48
59	40.02	69.86	57.77	53.62	37.37	55.33	16.97	24.38	-449.34	29.92	23.57	28.50	29.96	31.46	75.45	58.05	44.33	39.78	46.38	57.78	118.46	115.37	26.53	70.52
60	50.10	86.82	81.08	71.19	47.59	76.82	38.57	33.57	-409.47	43.61	34.50	36.21	34.72	42.36	102.80	75.23	60.76	55.20	59.34	72.64	160.17	151.38	62.63	92.13
61	39.64	69.22	56.89	52.96	36.98	54.52	16.16	24.04	-450.84	29.41	23.16	28.21	29.78	31.04	74.42	57.40	43.71	39.20	45.89	57.22	116.88	114.02	25.16	69.70
62	39.64	69.22	56.89	52.96	36.98	54.52	16.16	24.04	-450.84	29.41	23.16	28.21	29.78	31.04	74.42	57.40	43.71	39.20	45.89	57.22	116.88	114.02	25.16	69.70
63	45.91	79.78	71.40	63.90	43.35	67.90	29.61	29.75	-426.02	37.93	29.96	33.01	32.74	37.83	91.45	68.10	53.94	48.80	53.96	66.47	142.86	136.44	47.65	83.16
64	52.95	91.62	87.68	76.17	50.48	82.90	44.68	36.17	-398.19	47.48	37.59	38.39	36.07	45.44	110.53	80.10	65.41	59.56	63.01	76.84	171.98	161.57	72.85	98.25
65	66.65	114.66	119.35	100.04	64.36	112.10	74.02	48.64	-344.03	66.07	52.43	48.87	42.54	60.25	147.68	103.44	87.73	80.50	80.62	97.02	228.65	210.49	121.91	127.61
66	44.39	77.22	67.88	61.25	41.80	64.65	26.35	28.37	-432.03	35.86	28.31	31.84	32.02	36.19	87.32	65.51	51.46	46.47	52.00	64.23	136.56	131.00	42.20	79.89
67	63.60	109.54	112.31	94.74	61.28	105.61	67.50	45.87	-356.06	61.94	49.13	46.54	41.10	56.96	139.43	98.25	82.77	75.84	76.71	92.54	216.06	199.62	111.01	121.08
68	-	-	-	-	-	-	-	-	-	-	-	-	-	-	-	-	-	-	-	-	-	-	-	-
69	-	-	-	-	-	-	-	-	-	-	-	-	-	-	-	-	-	-	-	-	-	-	-	-
70	-	-	-	-	-	-	-	-	-	-	-	-	-	-	-	-	-	-	-	-	-	-	-	-

Table 4. (continued)

No.	Classification			3D model collection No. (NMNS: National Museum of Nature and Science, Tokyo)	Geological age	LRL (mm)	ML (mm) estimated from the relationship between LRL (mm) and ML (mm) of modern oegopsid squids (Clarke, 1986)[19]															
	Family	Genus	Species				*Architeuthis dux*: 109.38 × LRL - 180.4	*Thysanoteuthis rhombus*: 110.53 × LRL - 112.6	*Dosidicus gigas*: 35.79 × LRL + 44.2	*Ommastrephes caroli*: 27.61 × LRL + 52.7	*Sthenoteuthis oualaniensis*: 39.25 × LRL + 6.98	*Hyaloteuthis hyadesi*: 24.31 × LRL + 20.65	*Todarodes sagittus*: 41.36 × LRL - 11.3	*Todarodes pacificus*: 37.44 × LRL + 18.53	*Notodarodes hawaiiensis*: 18.61 × LRL + 33.55	*Notodarodes gouldi*: 16.5 × LRL + 155	*Todaropsis eblanae*: 35.04 × LRL - 10.32	*Eucleoteuthis luminosa*: 37.61 × LRL + 11.12	*Ornithoteuthis volatilis*: 38.81 × LRL - 16.96	*Onychoteuthis banksi*: 61.0 × LRL - 28.9	*Pholidoteuthis boschmai*: 41.09 × LRL + 11.3	*Brachioteuthis* spp.: 20.18 × LRL + 16.31	*Gonatus* spp.: 42.87 × LRL - 43.4
71	Pachyteroteuthidae	uncertain	uncertain	NMNS_DS00068_o0hmWAZ.stl	Cenomanian	-	-	-	-	-	-	-	-	-	-	-	-	-	-	-	-	-
72	Pachyteroteuthidae	uncertain	uncertain	NMNS_DS00084_Z7XZtlw.stl	Cenomanian	-	-	-	-	-	-	-	-	-	-	-	-	-	-	-	-	-
73	Pachyteroteuthidae	uncertain	uncertain	NMNS_DS00084_vmtPsX9.stl	Cenomanian	-	-	-	-	-	-	-	-	-	-	-	-	-	-	-	-	-
74	Pachyteroteuthidae	uncertain	uncertain	NMNS_DS00082_H8vz3ua.stl	Cenomanian	-	-	-	-	-	-	-	-	-	-	-	-	-	-	-	-	-
75	Pachyteroteuthidae	uncertain	uncertain	NMNS_DS00082_2PRzxqr.stl	Cenomanian	-	-	-	-	-	-	-	-	-	-	-	-	-	-	-	-	-
76	Pachyteroteuthidae	uncertain	uncertain	NMNS_DS00082_rGYynE6.stl	Cenomanian	3.15	164.15	235.57	156.94	139.67	130.62	97.23	118.98	136.47	92.17	206.98	100.06	129.59	105.29	163.25	140.73	79.88	91.64
77	Pachyteroteuthidae	uncertain	uncertain	NMNS_DS00082_O57xtDF.stl	Cenomanian	1.12	-57.89	11.19	84.28	83.62	50.94	47.88	35.02	60.46	54.39	173.48	28.92	53.24	26.51	39.42	57.32	38.91	4.61
78	Pachyteroteuthidae	uncertain	uncertain	NMNS_DS00140_6dLPkjD.stl	Turonian	-	-	-	-	-	-	-	-	-	-	-	-	-	-	-	-	-	-
79	Pachyteroteuthidae	uncertain	uncertain	NMNS_DS00140_0vO7jym.stl	Turonian	-	-	-	-	-	-	-	-	-	-	-	-	-	-	-	-	-	-
80	Pachyteroteuthidae	uncertain	uncertain	NMNS_DS00009_U4Gf3tX.stl	Turonian	2.03	41.64	111.78	116.85	108.75	86.66	70.00	72.66	94.53	71.33	188.50	60.81	87.47	61.82	94.93	94.71	57.28	43.63
81	Pachyteroteuthidae	uncertain	uncertain	NMNS_DS00009_6SkvYgx.stl	Turonian	2.06	44.92	115.09	117.93	109.58	87.84	70.73	73.90	95.66	71.89	188.99	61.86	88.60	62.99	96.76	95.95	57.88	44.91
82	Pachyteroteuthidae	uncertain	uncertain	NMNS_DS00140_ezp57pJ.stl	Turonian	-	-	-	-	-	-	-	-	-	-	-	-	-	-	-	-	-	-
83	Pachyteroteuthidae	uncertain	uncertain	NMNS_DS00046_zxab88O.stl	Turonian	1.87	24.14	94.09	111.13	104.33	80.38	66.11	66.04	88.54	68.35	185.86	55.20	81.45	55.61	85.17	88.14	54.05	36.77
84	Pachyteroteuthidae	uncertain	uncertain	NMNS_DS00173_Ud7AGGR.stl	Turonian	1.30	-38.21	31.09	90.73	88.59	58.01	52.25	42.47	67.20	57.74	176.45	35.23	60.01	33.49	50.40	64.72	42.54	12.33
85	Pachyteroteuthidae	uncertain	uncertain	NMNS_DS00173_i7RkpPt.stl	Turonian	-	-	-	-	-	-	-	-	-	-	-	-	-	-	-	-	-	-
86	Pachyteroteuthidae	uncertain	uncertain	NMNS_DS00173_MT5y8SL.stl	Turonian	-	-	-	-	-	-	-	-	-	-	-	-	-	-	-	-	-	-
87	Pachyteroteuthidae	uncertain	uncertain	NMNS_DS00173_vnX5JU7.stl	Turonian	-	-	-	-	-	-	-	-	-	-	-	-	-	-	-	-	-	-
88	Pachyteroteuthidae	uncertain	uncertain	NMNS_DS00173_k4Zf6cM.stl	Turonian	-	-	-	-	-	-	-	-	-	-	-	-	-	-	-	-	-	-
89	Pachyteroteuthidae	uncertain	uncertain	NMNS_DS00173_RS2ows3.stl	Turonian	-	-	-	-	-	-	-	-	-	-	-	-	-	-	-	-	-	-
90	Pachyteroteuthidae	uncertain	uncertain	NMNS_DS00173_BSp1Uzp.stl	Turonian	-	-	-	-	-	-	-	-	-	-	-	-	-	-	-	-	-	-
91	Pachyteroteuthidae	uncertain	uncertain	NMNS_DS00173_Nv9fbhp.stl	Turonian	-	-	-	-	-	-	-	-	-	-	-	-	-	-	-	-	-	-
92	Pachyteroteuthidae	uncertain	uncertain	NMNS_DS00173_eVvAn7U.stl	Turonian	3.32	182.74	254.36	163.02	144.37	137.29	101.36	126.02	142.83	95.34	209.78	106.01	135.99	111.89	173.62	147.72	83.31	98.93
93	Pachyteroteuthidae	uncertain	uncertain	NMNS_DS00173_GtZcR9a.stl	Turonian	-	-	-	-	-	-	-	-	-	-	-	-	-	-	-	-	-	-
94	Pachyteroteuthidae	uncertain	uncertain	NMNS_DS00034_Pt2Sm0S.stl	Coniacian	1.79	15.39	85.25	108.26	102.12	77.24	64.16	62.73	85.55	66.86	184.54	52.40	78.44	52.51	80.29	84.85	52.43	33.34
95	Pachyteroteuthidae	uncertain	uncertain	NMNS_DS00034_3Ez0EI7.stl	Coniacian	1.32	-36.02	33.30	91.44	89.15	58.79	52.74	43.30	67.95	58.12	176.78	35.93	60.77	34.27	51.62	65.54	42.95	13.19
96	Pachyteroteuthidae	uncertain	uncertain	NMNS_DS00034_GFK1LYI.stl	Coniacian	-	-	-	-	-	-	-	-	-	-	-	-	-	-	-	-	-	-
97	Pachyteroteuthidae	uncertain	uncertain	NMNS_DS00034_iiTGm6n.stl	Coniacian	1.12	-57.89	11.19	84.28	83.62	50.94	47.88	35.02	60.46	54.39	173.48	28.92	53.24	26.51	39.42	57.32	38.91	4.61
98	Pachyteroteuthidae	uncertain	uncertain	NMNS_DS00034_nf9Ejgu.stl	Coniacian	-	-	-	-	-	-	-	-	-	-	-	-	-	-	-	-	-	-
99	Pachyteroteuthidae	uncertain	uncertain	NMNS_DS00034_Z2XS2EX.stl	Coniacian	-	-	-	-	-	-	-	-	-	-	-	-	-	-	-	-	-	-
100	Pachyteroteuthidae	uncertain	uncertain	NMNS_DS00089_EbQv3XX.stl	Coniacian	-	-	-	-	-	-	-	-	-	-	-	-	-	-	-	-	-	-
101	Pachyteroteuthidae	uncertain	uncertain	NMNS_DS00089_favO32g.stl	Coniacian	-	-	-	-	-	-	-	-	-	-	-	-	-	-	-	-	-	-
102	Pachyteroteuthidae	uncertain	uncertain	NMNS_DS00111_qpvWIR1.stl	Santonian	1.18	-51.33	17.83	86.43	85.28	53.30	49.34	37.50	62.71	55.51	174.47	31.03	55.50	28.84	43.08	59.79	40.12	7.19
103	Pachyteroteuthidae	uncertain	uncertain	NMNS_DS00097_bdk7qIo.stl	Campanian	-	-	-	-	-	-	-	-	-	-	-	-	-	-	-	-	-	-
104	Pachyteroteuthidae	uncertain	uncertain	NMNS_DS00097_PnwMgn0.stl	Campanian	-	-	-	-	-	-	-	-	-	-	-	-	-	-	-	-	-	-
105	Pachyteroteuthidae	uncertain	uncertain	NMNS_DS00171_nNE3rJU.stl	Campanian	-	-	-	-	-	-	-	-	-	-	-	-	-	-	-	-	-	-
106	Pachyteroteuthidae	uncertain	uncertain	NMNS_DS00171_zi2h0sv.stl	Campanian	-	-	-	-	-	-	-	-	-	-	-	-	-	-	-	-	-	-
107	Pachyteroteuthidae	uncertain	uncertain	NMNS_DS00175_oPtCSM5.stl	Campanian	-	-	-	-	-	-	-	-	-	-	-	-	-	-	-	-	-	-
108	Pachyteroteuthidae	uncertain	uncertain	NMNS_DS00175_fonSGM6.stl	Campanian	1.42	-25.08	44.35	95.02	91.91	62.72	55.17	47.43	71.69	59.98	178.43	39.44	64.53	38.15	57.72	69.65	44.97	17.48
109	Pachyteroteuthidae	uncertain	uncertain	NMNS_DS00182_SYDC0zH.stl	Campanian	-	-	-	-	-	-	-	-	-	-	-	-	-	-	-	-	-	-
110	Pachyteroteuthidae	uncertain	uncertain	NMNS_DS00128_R1IzaWx.stl	Maastrichtian	-	-	-	-	-	-	-	-	-	-	-	-	-	-	-	-	-	-
111	Pachyteroteuthidae	uncertain	uncertain	NMNS_DS00174_53ff8oD.stl	Maastrichtian	1.65	0.08	69.77	103.25	98.26	71.74	60.76	56.94	80.31	64.26	182.23	47.50	73.18	47.08	71.75	79.10	49.61	27.34
112	Pachyteroteuthidae	uncertain	uncertain	NMNS_DS00174_WNYvS2g.stl	Maastrichtian	1.84	20.86	90.78	110.05	103.50	79.20	65.38	64.80	87.42	67.79	185.36	54.15	80.32	54.45	83.34	86.91	53.44	35.48
113	Pachyteroteuthidae	uncertain	uncertain	NMNS_DS00174_q1CFxaH.stl	Maastrichtian	1.65	0.08	69.77	103.25	98.26	71.74	60.76	56.94	80.31	64.26	182.23	47.50	73.18	47.08	71.75	79.10	49.61	27.34
114	Pachyteroteuthidae	uncertain	uncertain	NMNS_DS00174_P1KHcIt.stl	Maastrichtian	-	-	-	-	-	-	-	-	-	-	-	-	-	-	-	-	-	-
115	Pachyteroteuthidae	uncertain	uncertain	NMNS_DS00174_tYi8udG.stl	Maastrichtian	-	-	-	-	-	-	-	-	-	-	-	-	-	-	-	-	-	-
116	Pachyteroteuthidae	uncertain	uncertain	NMNS_DS00174_xil2BIU.stl	Maastrichtian	1.70	5.55	75.30	105.04	99.64	73.71	61.98	59.01	82.18	65.19	183.05	49.25	75.06	49.02	74.80	81.15	50.62	29.48
117	Pachyteroteuthidae	uncertain	uncertain	NMNS_DS00174_je66P5f.stl	Maastrichtian	1.65	0.08	69.77	103.25	98.26	71.74	60.76	56.94	80.31	64.26	182.23	47.50	73.18	47.08	71.75	79.10	49.61	27.34
118	Scuthoteuthidae	*Scuhoteuthis*	*kawakaro*	NMNS_DS00084_XCCa3MD.stl	Cenomanian	2.81	63.98	111.29	73.21	48.30	-345.53	65.55	52.01	48.58	42.36	59.84	146.65	102.79	87.11	79.91	80.13	96.46	227.08
119	Scuthoteuthidae	*Scuhoteuthis*	*fragilis*	NMNS_DS00182_VHJhp0K.stl	Campanian	7.99	163.85	321.33	284.29	138.07	44.11	199.30	158.77	123.94	88.93	166.39	413.88	270.73	247.69	230.55	206.84	241.66	634.79
120	Scuthoteuthidae	*Scuhoteuthis*	*falcatus*	NMNS_DS00046_Tf7vfru.stl	Turonian	2.34	54.92	92.23	54.06	40.15	-380.89	53.42	42.33	41.74	38.14	50.17	122.40	87.55	72.54	66.25	68.64	83.29	190.08
121	Scuthoteuthidae	*Scuhoteuthis*	*falcatus*	NMNS_DS00089_cdL9i2R.stl	Coniacian	2.07	49.71	81.28	43.05	35.47	-401.19	46.45	36.76	37.81	35.71	44.62	108.47	78.80	64.17	58.40	62.03	75.72	168.83
122	Scuthoteuthidae	*Scuhoteuthis*	*falcatus*	NMNS_DS00090_uJwH0a.stl	Santonian	2.21	52.41	86.96	48.76	37.90	-390.66	50.06	39.65	39.85	36.97	47.50	115.69	83.34	68.51	62.47	65.46	79.65	179.85
123	Scuthoteuthidae	*Scuhoteuthis*	*tenuis*	NMNS_DS00083_wMN7XJ9.stl	Coniacian	-	-	-	-	-	-	-	-	-	-	-	-	-	-	-	-	-	-
124	Scuthoteuthidae	*Grossiscapula*	*angusta*	NMNS_DS00172_cWN9IDD.stl	Maastrichtian	3.00	67.64	118.99	80.95	51.59	-331.24	70.46	55.93	51.34	44.07	63.75	156.45	108.95	93.00	85.44	84.78	101.79	242.03
125	Scuthoteuthidae	*Amblyscuthes*	*apterus*	NMNS_DS00082_9VBER8O.stl	Cenomanian	1.56	39.88	60.60	22.27	26.63	-439.56	33.28	26.25	30.39	31.12	34.13	82.16	62.27	48.36	43.56	49.56	61.43	128.69
126	Scuthoteuthidae	*Amblyscuthes*	*apterus*	NMNS_DS00175_1oEjNpv.stl	Campanian	3.31	73.62	131.56	93.58	56.96	-307.92	78.46	62.32	55.85	46.86	70.13	172.44	119.00	102.61	94.45	92.36	110.48	266.43
127	Scuthoteuthidae	*Amblyscuthes*	*pyrgoides*	NMNS_DS00084_0iYtIFF.stl	Cenomanian	1.81	44.70	70.74	32.46	30.97	-420.75	39.73	31.40	34.03	33.37	39.27	95.06	70.37	56.11	50.83	55.67	68.43	148.37
128	Scuthoteuthidae	*Amblyscuthes*	*pyrgoides*	NMNS_DS00046_ikc7ZzK.stl	Turonian	1.88	46.05	73.57	35.31	32.18	-415.49	41.54	32.85	35.04	34.00	40.71	98.67	72.64	58.28	52.87	57.38	70.40	153.87
129	Scuthoteuthidae	*Amblyscuthes*	*pyrgoides*	NMNS_DS00083_hbPNRL6.stl	Coniacian	-	-	-	-	-	-	-	-	-	-	-	-	-	-	-	-	-	-
130	Scuthoteuthidae	*Amblyscuthes*	*pyrgoides*	NMNS_DS00097_bizU8mn.stl	Campanian	-	-	-	-	-	-	-	-	-	-	-	-	-	-	-	-	-	-
131	Scuthoteuthidae	*Amblyscuthes*	*pyrgoides*	NMNS_DS00175_nhUN0gO.stl	Campanian	1.35	35.83	52.08	13.71	23.00	-455.35	27.86	21.92	27.33	29.24	29.81	71.33	55.46	41.85	37.46	44.42	55.54	112.16
132	Scuthoteuthidae	uncertain	uncertain	NMNS_DS00084_skNkAF7.stl	Cenomanian	3.37	74.77	133.99	96.03	58.00	-303.41	80.01	63.56	56.72	47.40	71.36	175.54	120.95	104.47	96.20	93.83	112.16	271.15
133	Scuthoteuthidae	uncertain	uncertain	NMNS_DS00034_yjFV2Xr.stl	Coniacian	2.64	60.70	104.39	66.28	45.35	-358.32	61.16	48.51	46.10	40.83	56.34	137.88	97.28	81.84	74.97	75.97	91.70	213.69
134	Paleothysanoteuthidae	*Paleothysanoteuthis*	*complicatus*	NMNS_DS00090_uO7uWu.stl	Santonian	1.69	42.38	65.87	27.57	28.89	-429.78	36.64	28.93	32.28	32.29	36.80	88.87	66.48	52.39	47.35	52.74	65.07	138.92
135	Paleothysanoteuthidae	*Paleothysanoteuthis*	*complicatus*	NMNS_DS00104_ZNFObG0.stl	Santonian	1.64	41.42	63.84	25.53	28.02	-433.54	35.34	27.90	31.55	31.84	35.77	86.29	64.86	50.84	45.89	51.51	63.67	134.98
136	Paleothysanoteuthidae	*Aetorhynchus*	*incisus*	NMNS_DS00068_z6nASvr.stl	Cenomanian	3.58	78.82	142.51	104.59	61.64	-287.61	85.44	67.88	59.78	49.28	75.68	186.37	127.75	110.98	102.31	98.97	118.05	287.68
137	uncertain	uncertain	uncertain	NMNS_DS00068_jPw6ko4.stl	Cenomanian	-	-	-	-	-	-	-	-	-	-	-	-	-	-	-	-	-	-
138	uncertain	uncertain	uncertain	NMNS_DS00084_IG3g9n4.stl	Cenomanian	-	-	-	-	-	-	-	-	-	-	-	-	-	-	-	-	-	-
139	uncertain	uncertain	uncertain	NMNS_DS00082_KBUN3ns.stl	Cenomanian	1.35	-32.74	36.62	92.52	89.97	59.97	53.47	44.54	69.07	58.67	177.28	36.98	61.89	35.43	53.45	44.42	55.54	112.16
140	uncertain	uncertain	uncertain	NMNS_DS00082_S4gN88WC.stl	Cenomanian	-	-	-	-	-	-	-	-	-	-	-	-	-	-	-	-	-	-
141	uncertain	uncertain	uncertain	NMNS_DS00082_QZjjRI8.stl	Cenomanian	-	-	-	-	-	-	-	-	-	-	-	-	-	-	-	-	-	-
142	uncertain	uncertain	uncertain	NMNS_DS00082_tUOvaO.stl	Cenomanian	1.42	-25.08	44.35	95.02	91.91	62.72	55.17	47.43	71.69	59.98	178.43	39.44	64.53	38.15	57.72	46.13	57.50	117.67
143	uncertain	uncertain	uncertain	NMNS_DS00082_pS6AQhr.stl	Cenomanian	1.80	16.48	86.35	108.62	102.40	77.63	64.41	63.15	85.92	67.05	184.70	52.75	78.82	52.90	80.90	55.43	68.15	147.58
144	uncertain	uncertain	uncertain	NMNS_DS00140_IWPZJL0.stl	Turonian	6.85	568.85	644.53	289.36	241.83	275.84	187.17	272.02	274.99	161.03	268.03	229.70	268.75	248.89	388.95	178.95	209.71	545.06

Table 4. (continued)

No.	ML (mm) estimated from the relationship between LRL (mm) and ML (mm) of modern oegopsid squids (Clarke, 1986)[19]																								
	Gonatus onyx: 19.02 × LRL + 12.82	*Gonatopsis borealis*: 32.0 × LRL + 24.1	*Berryteuthis magister*: 43.99 × LRL - 5.14	*Pterigioteuthis* spp.: 33.16 × LRL + 6.2	*Abraliopsis affinis*: 19.28 × LRL + 9.8	*Abraliopsis felis*: 40.55 × LRL - 2.66	*Ancistrocheirus lesueuri*: 40.75 × LRL - 41.3	*Octopoteuthis* spp.: 17.33 × LRL - 0.4	*Taningia danae*: 75.22 × LRL - 556.9	*Histioteuthis miranda*: 25.82 × LRL - 7.0	*Histioteuthis dofleini* (ML<180mm): 20.61 × LRL - 5.9	*Histioteuthis dofleini* (ML>90mm): 14.55 × LRL + 7.69	*Histioteuthis bonnellii*: 8.99 × LRL + 17.1	*Histioteuthis heteropsis*: 20.57 × LRL + 2.04	*Bathyteuthis abyssicola*: 51.59 × LRL + 1.68	*Clenopteryx* spp.: 32.42 × LRL + 11.69	*Cycloteuthis* spp.: 31 × LRL	*Mastigoteuthis* spp.: 29.08 × LRL - 1.8	*Chiroteuthis* spp.: 24.46 × LRL + 11.4	*Cranchia scabra*: 28.03 × LRL + 17.7	*Liocranchia* spp.: 78.71 × LRL + 5.9	*Leachia* spp.: 67.94 × LRL + 18.22	*Megalocranchia* spp.: 68.13 × LRL - 70.9	*Teuthowenia megalops*: 40.78 × LRL + 12.2
71	-	-	-	-	-	-	-	-	-	-	-	-	-	-	-	-	-	-	-	-	-	-	-	-	-
72	-	-	-	-	-	-	-	-	-	-	-	-	-	-	-	-	-	-	-	-	-	-	-	-	-
73	-	-	-	-	-	-	-	-	-	-	-	-	-	-	-	-	-	-	-	-	-	-	-	-	-
74	-	-	-	-	-	-	-	-	-	-	-	-	-	-	-	-	-	-	-	-	-	-	-	-	-
75	-	-	-	-	-	-	-	-	-	-	-	-	-	-	-	-	-	-	-	-	-	-	-	-	-
76	72.73	124.90	133.43	110.65	70.53	125.07	87.06	54.19	-319.96	74.33	59.02	53.52	45.42	66.84	164.19	113.81	97.65	89.80	88.45	105.99	253.84	232.23	143.71	140.66
77	34.12	59.94	44.13	43.34	31.39	42.76	4.34	19.01	-472.65	21.92	17.18	23.99	27.17	25.08	59.46	48.00	34.72	30.77	38.80	49.09	94.06	94.31	5.41	57.87
78	-	-	-	-	-	-	-	-	-	-	-	-	-	-	-	-	-	-	-	-	-	-	-	-	-
79	-	-	-	-	-	-	-	-	-	-	-	-	-	-	-	-	-	-	-	-	-	-	-	-	-
80	51.43	89.06	84.16	73.51	48.94	79.66	41.42	34.78	-404.20	45.41	35.94	37.23	35.35	43.80	106.41	77.50	62.93	57.23	61.05	74.60	165.68	156.14	67.40	94.98
81	52.00	90.02	85.48	74.51	49.52	80.87	42.65	35.30	-401.95	46.19	36.56	37.66	35.62	44.41	107.96	78.48	63.86	58.10	61.79	75.44	168.04	158.18	69.45	96.21
82	-	-	-	-	-	-	-	-	-	-	-	-	-	-	-	-	-	-	-	-	-	-	-	-	-
83	48.39	83.94	77.12	68.21	45.85	73.17	34.90	32.01	-416.24	41.28	32.64	34.90	33.91	40.51	98.15	72.32	57.97	52.58	57.14	70.12	153.09	145.27	56.50	88.46
84	37.55	65.70	52.05	49.31	34.86	50.06	11.68	22.13	-459.11	26.57	20.89	26.61	28.79	28.78	68.75	53.84	40.30	36.00	43.20	54.14	108.22	106.54	17.67	65.21
85	-	-	-	-	-	-	-	-	-	-	-	-	-	-	-	-	-	-	-	-	-	-	-	-	-
86	-	-	-	-	-	-	-	-	-	-	-	-	-	-	-	-	-	-	-	-	-	-	-	-	-
87	-	-	-	-	-	-	-	-	-	-	-	-	-	-	-	-	-	-	-	-	-	-	-	-	-
88	-	-	-	-	-	-	-	-	-	-	-	-	-	-	-	-	-	-	-	-	-	-	-	-	-
89	-	-	-	-	-	-	-	-	-	-	-	-	-	-	-	-	-	-	-	-	-	-	-	-	-
90	-	-	-	-	-	-	-	-	-	-	-	-	-	-	-	-	-	-	-	-	-	-	-	-	-
91	-	-	-	-	-	-	-	-	-	-	-	-	-	-	-	-	-	-	-	-	-	-	-	-	-
92	75.97	130.34	140.91	116.29	73.81	131.97	93.99	57.14	-307.17	78.72	62.53	56.00	46.95	70.33	172.96	119.32	102.92	94.75	92.61	110.76	267.22	243.78	155.29	147.59
93	-	-	-	-	-	-	-	-	-	-	-	-	-	-	-	-	-	-	-	-	-	-	-	-	-
94	46.87	81.38	73.60	65.56	44.31	69.92	31.64	30.62	-422.26	39.22	30.99	33.73	33.19	38.86	94.03	69.72	55.49	50.25	55.18	67.87	146.79	139.83	51.05	85.20
95	37.93	66.34	52.93	49.97	35.25	50.87	12.49	22.48	-457.61	27.08	21.31	26.90	28.97	29.19	69.78	54.48	40.92	36.59	43.69	54.70	109.80	107.90	19.03	66.03
96	-	-	-	-	-	-	-	-	-	-	-	-	-	-	-	-	-	-	-	-	-	-	-	-	-
97	34.12	59.94	44.13	43.34	31.39	42.76	4.34	19.01	-472.65	21.92	17.18	23.99	27.17	25.08	59.46	48.00	34.72	30.77	38.80	49.09	94.06	94.31	5.41	57.87
98	-	-	-	-	-	-	-	-	-	-	-	-	-	-	-	-	-	-	-	-	-	-	-	-	-
99	-	-	-	-	-	-	-	-	-	-	-	-	-	-	-	-	-	-	-	-	-	-	-	-	-
100	-	-	-	-	-	-	-	-	-	-	-	-	-	-	-	-	-	-	-	-	-	-	-	-	-
101	-	-	-	-	-	-	-	-	-	-	-	-	-	-	-	-	-	-	-	-	-	-	-	-	-
102	35.26	61.86	46.77	45.33	32.55	45.19	6.79	20.05	-468.14	23.47	18.42	24.86	27.71	26.31	62.56	49.95	36.58	32.51	40.26	50.78	98.78	98.39	9.49	60.32
103	-	-	-	-	-	-	-	-	-	-	-	-	-	-	-	-	-	-	-	-	-	-	-	-	-
104	-	-	-	-	-	-	-	-	-	-	-	-	-	-	-	-	-	-	-	-	-	-	-	-	-
105	-	-	-	-	-	-	-	-	-	-	-	-	-	-	-	-	-	-	-	-	-	-	-	-	-
106	-	-	-	-	-	-	-	-	-	-	-	-	-	-	-	-	-	-	-	-	-	-	-	-	-
107	-	-	-	-	-	-	-	-	-	-	-	-	-	-	-	-	-	-	-	-	-	-	-	-	-
108	39.83	69.54	57.33	53.29	37.18	54.92	16.57	24.21	-450.09	29.66	23.37	28.35	29.87	31.25	74.94	57.73	44.02	39.49	46.13	57.50	117.67	114.69	25.84	70.11
109	-	-	-	-	-	-	-	-	-	-	-	-	-	-	-	-	-	-	-	-	-	-	-	-	-
110	-	-	-	-	-	-	-	-	-	-	-	-	-	-	-	-	-	-	-	-	-	-	-	-	-
111	44.20	76.90	67.44	60.91	41.61	64.25	25.94	28.19	-432.79	35.60	28.11	31.70	31.93	35.98	86.80	65.18	51.15	46.18	51.76	63.95	135.77	130.32	41.51	79.49
112	47.82	82.98	75.80	67.21	45.28	71.95	33.68	31.49	-418.50	40.51	32.02	34.46	33.64	39.89	96.61	71.34	57.04	51.71	56.41	69.28	150.73	143.23	54.46	87.24
113	44.20	76.90	67.44	60.91	41.61	64.25	25.94	28.19	-432.79	35.60	28.11	31.70	31.93	35.98	86.80	65.18	51.15	46.18	51.76	63.95	135.77	130.32	41.51	79.49
114	-	-	-	-	-	-	-	-	-	-	-	-	-	-	-	-	-	-	-	-	-	-	-	-	-
115	-	-	-	-	-	-	-	-	-	-	-	-	-	-	-	-	-	-	-	-	-	-	-	-	-
116	45.15	78.50	69.64	62.57	42.58	66.28	27.98	29.06	-429.03	36.89	29.14	32.43	32.38	37.01	89.38	66.80	52.70	47.64	52.98	65.35	139.71	133.72	44.92	81.53
117	44.20	76.90	67.44	60.91	41.61	64.25	25.94	28.19	-432.79	35.60	28.11	31.70	31.93	35.98	86.80	65.18	51.15	46.18	51.76	63.95	135.77	130.32	41.51	79.49
118	209.13	120.55	126.79	99.38	63.98	111.29	73.21	48.30	-345.53	65.55	52.01	48.58	42.36	59.84	146.65	102.79	87.11	79.91	80.13	96.46	227.08	209.13	120.55	126.79
119	561.06	473.46	338.03	271.15	163.85	321.33	284.29	138.07	44.11	199.30	158.77	123.94	88.93	166.39	413.88	270.73	247.69	230.55	206.84	241.66	634.79	561.06	473.46	338.03
120	177.20	88.52	107.63	83.79	54.92	92.23	54.06	40.15	-380.89	53.42	42.33	41.74	38.14	50.17	122.40	87.55	72.54	66.25	68.64	83.29	190.08	177.20	88.52	107.63
121	158.86	70.13	96.61	74.84	49.71	81.28	43.05	35.47	-401.19	46.45	36.76	37.81	35.71	44.62	108.47	78.80	64.17	58.40	62.03	75.72	168.83	158.86	70.13	96.61
122	168.37	79.67	102.32	79.48	52.41	86.96	48.76	37.90	-390.66	50.06	39.65	39.85	36.97	47.50	115.69	83.34	68.51	62.47	65.46	79.65	179.85	168.37	79.67	102.32
123	-	-	-	-	-	-	-	-	-	-	-	-	-	-	-	-	-	-	-	-	-	-	-	-	-
124	222.04	133.49	134.54	105.68	67.64	118.99	80.95	51.59	-331.24	70.46	55.93	51.34	44.07	63.75	156.45	108.95	93.00	85.44	84.78	101.79	242.03	222.04	133.49	134.54
125	124.21	35.38	75.82	57.93	39.88	60.60	22.27	26.63	-439.56	33.28	26.25	30.39	31.12	34.13	82.16	62.27	48.36	43.56	49.56	61.43	128.69	124.21	35.38	75.82
126	243.10	154.61	147.18	115.96	73.62	131.56	93.58	56.96	-307.92	78.46	62.32	55.85	46.86	70.13	172.44	119.00	102.61	94.45	92.36	110.48	266.43	243.10	154.61	147.18
127	141.19	52.42	86.01	66.22	44.70	70.74	32.46	30.97	-420.75	39.73	31.40	34.03	33.37	39.27	95.06	70.37	56.11	50.83	55.67	68.43	148.37	141.19	52.42	86.01
128	145.95	57.18	88.87	68.54	46.05	73.57	35.31	32.18	-415.49	41.54	32.85	35.04	34.00	40.71	98.67	72.64	58.28	52.87	57.38	70.40	153.87	145.95	57.18	88.87
129	-	-	-	-	-	-	-	-	-	-	-	-	-	-	-	-	-	-	-	-	-	-	-	-	-
130	-	-	-	-	-	-	-	-	-	-	-	-	-	-	-	-	-	-	-	-	-	-	-	-	-
131	109.94	21.08	67.25	50.97	35.83	52.08	13.71	23.00	-455.35	27.86	21.92	27.33	29.24	29.81	71.33	55.46	41.85	37.46	44.42	55.54	112.16	109.94	21.08	67.25
132	247.18	158.70	149.63	117.95	74.77	133.99	96.03	58.00	-303.41	80.01	63.56	56.72	47.40	71.36	175.54	120.95	104.47	96.20	93.83	112.16	271.15	247.18	158.70	149.63
133	197.58	108.96	119.86	93.74	60.70	104.39	66.28	45.35	-358.32	61.16	48.51	46.10	40.83	56.34	137.88	97.28	81.84	74.97	75.97	91.70	213.69	197.58	108.96	119.86
134	133.04	44.24	81.12	62.24	42.38	65.87	27.57	28.89	-429.78	36.64	28.93	32.28	32.29	36.80	88.87	66.48	52.39	47.35	52.74	65.07	138.92	133.04	44.24	81.12
135	129.64	40.83	79.08	60.58	41.42	63.84	25.53	28.02	-433.54	35.34	27.90	31.55	31.84	35.77	86.29	64.86	50.84	45.89	51.51	63.67	134.98	129.64	40.83	79.08
136	261.45	173.01	158.19	124.91	78.82	142.51	104.59	61.64	-287.61	85.44	67.88	59.78	49.28	75.68	186.37	127.75	110.98	102.31	98.97	118.05	287.68	261.45	173.01	158.19
137	-	-	-	-	-	-	-	-	-	-	-	-	-	-	-	-	-	-	-	-	-	-	-	-	-
138	-	-	-	-	-	-	-	-	-	-	-	-	-	-	-	-	-	-	-	-	-	-	-	-	-
139	109.94	21.08	67.25	50.97	35.83	52.08	13.71	23.00	-455.35	27.86	21.92	27.33	29.24	29.81	71.33	55.46	41.85	37.46	44.42	55.54	112.16	109.94	21.08	67.25
140	-	-	-	-	-	-	-	-	-	-	-	-	-	-	-	-	-	-	-	-	-	-	-	-	-
141	-	-	-	-	-	-	-	-	-	-	-	-	-	-	-	-	-	-	-	-	-	-	-	-	-
142	114.69	25.84	70.11	53.29	37.18	54.92	16.57	24.21	-450.09	29.66	23.37	28.35	29.87	31.25	74.94	57.73	44.02	39.49	46.13	57.50	117.67	114.69	25.84	70.11
143	140.51	51.73	85.60	65.89	44.50	70.33	32.05	30.79	-421.50	39.48	31.20	33.88	33.28	39.07	94.54	70.05	55.80	50.54	55.43	68.15	147.58	140.51	51.73	85.60
144	483.61	395.79	291.54	233.35	141.87	275.11	237.84	118.31	-41.64	169.87	135.28	107.36	78.68	142.94	355.07	233.77	212.35	197.40	178.95	209.71	545.06	483.61	395.79	291.54

Table 4. (continued)

No.	Classification			3D model collection No. (NMNS: National Museum of Nature and Science, Tokyo)	Geological age	LRL (mm)	ML (mm) estimated from the relationship between LRL (mm) and ML (mm) of modern oegopsid squids (Clarke, 1986)[19]															
	Family	Genus	Species				*Architeuthis dux*: 109.38 × LRL - 180.4	*Thysanoteuthis rhombus*: 110.53 × LRL - 112.6	*Dosidicus gigas*: 35.79 × LRL + 44.2	*Onmastrephes caroli*: 27.61 × LRL + 52.7	*Sthenoteuthis oualaniensis*: 39.25 × LRL + 6.98	*Hyaloteuthis hyadesi*: 24.31 × LRL + 20.65	*Todarodes sagittus*: 41.36 × LRL - 11.3	*Todarodes pacificus*: 37.44 × LRL + 18.53	*Notodarodes hawaiiensis*: 18.61 × LRL + 33.55	*Notodarodes gouldi*: 16.5 × LRL + 155	*Todaropsis eblanae*: 35.04 × LRL - 10.32	*Eucleoteuthis luminosa*: 37.61 × LRL + 11.12	*Ornithoteuthis volatilis*: 38.81 × LRL - 16.96	*Onychoteuthis banksi*: 61.0 × LRL - 28.9	*Pholidoteuthis boschmai*: 41.09 × LRL + 11.3	*Brachioteuthis* spp.: 20.18 × LRL + 16.31	*Gonatus* spp.: 42.87 × LRL - 43.4
145	uncertain	uncertain	uncertain	NMNS_DS00040_f5baG18.stl	Turonian	1.18	-51.33	17.83	86.43	85.28	53.30	49.34	37.50	62.71	55.51	174.47	31.03	55.50	28.84	43.08	40.26	50.78	98.78
146	uncertain	uncertain	uncertain	NMNS_DS00040_5UEmEw7.stl	Turonian	-	-	-	-	-	-	-	-	-	-	-	-	-	-	-	-	-	-
147	uncertain	uncertain	uncertain	NMNS_DS00041_qf2yg91.stl	Turonian	-	-	-	-	-	-	-	-	-	-	-	-	-	-	-	-	-	-
148	uncertain	uncertain	uncertain	NMNS_DS00041_f7gRaRg.stl	Turonian	-	-	-	-	-	-	-	-	-	-	-	-	-	-	-	-	-	-
149	uncertain	uncertain	uncertain	NMNS_DS00041_hs6nl9o.stl	Turonian	-	-	-	-	-	-	-	-	-	-	-	-	-	-	-	-	-	-
150	uncertain	uncertain	uncertain	NMNS_DS00041_UX7j93Q.stl	Turonian	-	-	-	-	-	-	-	-	-	-	-	-	-	-	-	-	-	-
151	uncertain	uncertain	uncertain	NMNS_DS00041_HZotSP0.stl	Turonian	1.54	-11.95	57.62	99.32	95.22	67.43	58.09	52.39	76.19	62.21	180.41	43.64	69.04	42.81	65.04	49.07	60.87	127.11
152	uncertain	uncertain	uncertain	NMNS_DS00041_iP6QMdc.stl	Turonian	-	-	-	-	-	-	-	-	-	-	-	-	-	-	-	-	-	-
153	uncertain	uncertain	uncertain	NMNS_DS00141_G9KsSm2.stl	Turonian	1.88	25.23	95.20	111.49	104.61	80.77	66.35	66.46	88.92	68.54	186.02	55.56	81.83	56.00	85.78	57.38	70.40	153.87
154	uncertain	uncertain	uncertain	NMNS_DS00141_WR23hLl.stl	Turonian	2.57	100.71	171.46	136.18	123.66	107.85	83.13	95.00	114.75	81.38	197.41	79.73	107.78	82.78	127.87	74.26	89.74	208.18
155	uncertain	uncertain	uncertain	NMNS_DS00173_gs5MGgw.stl	Turonian	1.45	-21.80	47.67	96.10	92.73	63.89	55.90	48.67	72.82	60.53	178.93	40.49	65.65	39.31	59.55	46.87	58.34	120.03
156	uncertain	uncertain	uncertain	NMNS_DS00173_zOCQ5aH.stl	Turonian	-	-	-	-	-	-	-	-	-	-	-	-	-	-	-	-	-	-
157	uncertain	uncertain	uncertain	NMNS_DS00173_t9bcfa5.stl	Turonian	1.44	-22.89	46.56	95.74	92.46	63.50	55.66	48.26	72.44	60.35	178.76	40.14	65.28	38.93	58.94	46.62	58.06	119.24
158	uncertain	uncertain	uncertain	NMNS_DS00173_ojJzal0.stl	Turonian	-	-	-	-	-	-	-	-	-	-	-	-	-	-	-	-	-	-
159	uncertain	uncertain	uncertain	NMNS_DS00173_4wSYQi9.stl	Turonian	-	-	-	-	-	-	-	-	-	-	-	-	-	-	-	-	-	-
160	uncertain	uncertain	uncertain	NMNS_DS00173_jE5iVdb.stl	Turonian	-	-	-	-	-	-	-	-	-	-	-	-	-	-	-	-	-	-
161	uncertain	uncertain	uncertain	NMNS_DS00173_l1Etvnw.stl	Turonian	1.76	12.11	81.93	107.19	101.29	76.06	63.44	61.49	84.42	66.30	184.04	51.35	77.31	51.35	78.46	54.45	67.03	144.43
162	uncertain	uncertain	uncertain	NMNS_DS00173_DhR5iVE.stl	Turonian	2.46	88.67	159.30	132.24	120.62	103.54	80.45	90.45	110.63	79.33	195.59	75.88	103.64	78.51	121.16	71.57	86.65	199.53
163	uncertain	uncertain	uncertain	NMNS_DS00173_ZPmlNa6.stl	Turonian	1.46	-20.71	48.77	96.45	93.01	64.29	56.14	49.09	73.19	60.72	179.09	40.84	66.03	39.70	60.16	47.11	58.62	120.82
164	uncertain	uncertain	uncertain	NMNS_DS00173_luDK6XN.stl	Turonian	1.49	-17.42	52.09	97.53	93.84	65.46	56.87	50.33	74.32	61.28	179.59	41.89	67.16	40.87	61.99	47.85	59.46	123.18
165	uncertain	uncertain	uncertain	NMNS_DS00173_62PofvF.stl	Turonian	-	-	-	-	-	-	-	-	-	-	-	-	-	-	-	-	-	-
166	uncertain	uncertain	uncertain	NMNS_DS00034_y1A99ab.stl	Coniacian	1.87	24.14	94.09	111.13	104.33	80.38	66.11	66.04	88.54	68.35	185.86	55.20	81.45	55.61	85.17	57.14	70.12	153.09
167	uncertain	uncertain	uncertain	NMNS_DS00034_1GB8eu3.stl	Coniacian	-	-	-	-	-	-	-	-	-	-	-	-	-	-	-	-	-	-
168	uncertain	uncertain	uncertain	NMNS_DS00034_24pKfeh.stl	Coniacian	-	-	-	-	-	-	-	-	-	-	-	-	-	-	-	-	-	-
169	uncertain	uncertain	uncertain	NMNS_DS00034_h0A3Z03.stl	Coniacian	-	-	-	-	-	-	-	-	-	-	-	-	-	-	-	-	-	-
170	uncertain	uncertain	uncertain	NMNS_DS00034_3AO7Q0Z.stl	Coniacian	-	-	-	-	-	-	-	-	-	-	-	-	-	-	-	-	-	-
171	uncertain	uncertain	uncertain	NMNS_DS00081_mtrue9M.stl	Coniacian	-	-	-	-	-	-	-	-	-	-	-	-	-	-	-	-	-	-
172	uncertain	uncertain	uncertain	NMNS_DS00081_nsA03VV.stl	Coniacian	-	-	-	-	-	-	-	-	-	-	-	-	-	-	-	-	-	-
173	uncertain	uncertain	uncertain	NMNS_DS00083_bcQb89y.stl	Coniacian	-	-	-	-	-	-	-	-	-	-	-	-	-	-	-	-	-	-
174	uncertain	uncertain	uncertain	NMNS_DS00083_Cbzbvh5.stl	Coniacian	-	-	-	-	-	-	-	-	-	-	-	-	-	-	-	-	-	-
175	uncertain	uncertain	uncertain	NMNS_DS00083_uHk9jZQ.stl	Coniacian	-	-	-	-	-	-	-	-	-	-	-	-	-	-	-	-	-	-
176	uncertain	uncertain	uncertain	NMNS_DS00083_e3595mK.stl	Coniacian	-	-	-	-	-	-	-	-	-	-	-	-	-	-	-	-	-	-
177	uncertain	uncertain	uncertain	NMNS_DS00083_DI1gKuG.stl	Coniacian	-	-	-	-	-	-	-	-	-	-	-	-	-	-	-	-	-	-
178	uncertain	uncertain	uncertain	NMNS_DS00083_6QWWA3O.stl	Coniacian	2.89	135.71	206.83	147.63	132.49	120.41	90.91	108.23	126.73	87.33	202.69	90.95	119.81	95.20	147.39	82.09	98.71	233.37
179	uncertain	uncertain	uncertain	NMNS_DS00083_x87tvtw.stl	Coniacian	-	-	-	-	-	-	-	-	-	-	-	-	-	-	-	-	-	-
180	uncertain	uncertain	uncertain	NMNS_DS00083_eiHii2r.stl	Coniacian	-	-	-	-	-	-	-	-	-	-	-	-	-	-	-	-	-	-
181	uncertain	uncertain	uncertain	NMNS_DS00089_KofdLo4.stl	Coniacian	-	-	-	-	-	-	-	-	-	-	-	-	-	-	-	-	-	-
182	uncertain	uncertain	uncertain	NMNS_DS00089_TjB6DJr.stl	Coniacian	-	-	-	-	-	-	-	-	-	-	-	-	-	-	-	-	-	-
183	uncertain	uncertain	uncertain	NMNS_DS00004_3BN7XMT.stl	Santonian	-	-	-	-	-	-	-	-	-	-	-	-	-	-	-	-	-	-
184	uncertain	uncertain	uncertain	NMNS_DS00004_yLSdup5.stl	Santonian	1.63	-2.11	67.56	102.54	97.70	70.96	60.28	56.12	79.56	63.88	181.90	46.80	72.42	46.30	70.53	51.27	63.39	134.20
185	uncertain	uncertain	uncertain	NMNS_DS00004_eR8PLKv.stl	Santonian	-	-	-	-	-	-	-	-	-	-	-	-	-	-	-	-	-	-
186	uncertain	uncertain	uncertain	NMNS_DS00011_zfqX101.stl	Santonian	-	-	-	-	-	-	-	-	-	-	-	-	-	-	-	-	-	-
187	uncertain	uncertain	uncertain	NMNS_DS00011_rlyT1aF.stl	Santonian	-	-	-	-	-	-	-	-	-	-	-	-	-	-	-	-	-	-
188	uncertain	uncertain	uncertain	NMNS_DS00011_JVxT9Gj.stl	Santonian	-	-	-	-	-	-	-	-	-	-	-	-	-	-	-	-	-	-
189	uncertain	uncertain	uncertain	NMNS_DS00011_4IY3Bt9.stl	Santonian	-	-	-	-	-	-	-	-	-	-	-	-	-	-	-	-	-	-
190	uncertain	uncertain	uncertain	NMNS_DS00011_U2ovTAd.stl	Santonian	-	-	-	-	-	-	-	-	-	-	-	-	-	-	-	-	-	-
191	uncertain	uncertain	uncertain	NMNS_DS00042_zPgCX6g.stl	Santonian	3.00	147.74	218.99	151.57	135.53	124.73	93.58	112.78	130.85	89.38	204.50	94.80	123.95	99.47	154.10	84.78	101.79	242.03
192	uncertain	uncertain	uncertain	NMNS_DS00090_AMpLdq5.stl	Santonian	-	-	-	-	-	-	-	-	-	-	-	-	-	-	-	-	-	-
193	uncertain	uncertain	uncertain	NMNS_DS00104_xBccT1Q.stl	Santonian	1.95	32.89	102.93	113.99	106.54	83.52	68.05	69.35	91.54	69.84	187.18	58.01	84.46	58.72	90.05	59.10	72.36	159.38
194	uncertain	uncertain	uncertain	NMNS_DS00104_gX4su0i.stl	Santonian	-	-	-	-	-	-	-	-	-	-	-	-	-	-	-	-	-	-
195	uncertain	uncertain	uncertain	NMNS_DS00104_GJ9IpVN.stl	Santonian	-	-	-	-	-	-	-	-	-	-	-	-	-	-	-	-	-	-
196	uncertain	uncertain	uncertain	NMNS_DS00104_zr7SWaY.stl	Santonian	-	-	-	-	-	-	-	-	-	-	-	-	-	-	-	-	-	-
197	uncertain	uncertain	uncertain	NMNS_DS00073_UD0ygmM.stl	Campanian	1.22	-46.96	22.25	87.86	86.38	54.87	50.31	39.16	64.21	56.25	175.13	32.43	57.00	30.39	45.52	41.24	51.90	101.93
198	uncertain	uncertain	uncertain	NMNS_DS00097_a2Birz2.stl	Campanian	-	-	-	-	-	-	-	-	-	-	-	-	-	-	-	-	-	-
199	uncertain	uncertain	uncertain	NMNS_DS00097_tEhZh41.stl	Campanian	-	-	-	-	-	-	-	-	-	-	-	-	-	-	-	-	-	-
200	uncertain	uncertain	uncertain	NMNS_DS00097_uvDU6Xd.stl	Campanian	-	-	-	-	-	-	-	-	-	-	-	-	-	-	-	-	-	-
201	uncertain	uncertain	uncertain	NMNS_DS00097_IDZOyQ0.stl	Campanian	-	-	-	-	-	-	-	-	-	-	-	-	-	-	-	-	-	-
202	uncertain	uncertain	uncertain	NMNS_DS00097_uvzfA6L.stl	Campanian	-	-	-	-	-	-	-	-	-	-	-	-	-	-	-	-	-	-
203	uncertain	uncertain	uncertain	NMNS_DS00097_g5Xmmpa.stl	Campanian	-	-	-	-	-	-	-	-	-	-	-	-	-	-	-	-	-	-
204	uncertain	uncertain	uncertain	NMNS_DS00171_Cgg2ZIk.stl	Campanian	1.90	27.42	97.41	112.20	105.16	81.56	66.84	67.28	89.67	68.91	186.35	56.26	82.58	56.78	87.00	57.87	70.96	155.45
205	uncertain	uncertain	uncertain	NMNS_DS00171_uD0WryB.stl	Campanian	-	-	-	-	-	-	-	-	-	-	-	-	-	-	-	-	-	-
206	uncertain	uncertain	uncertain	NMNS_DS00171_CC67Bow.stl	Campanian	-	-	-	-	-	-	-	-	-	-	-	-	-	-	-	-	-	-
207	uncertain	uncertain	uncertain	NMNS_DS00171_43DOJaP.stl	Campanian	-	-	-	-	-	-	-	-	-	-	-	-	-	-	-	-	-	-
208	uncertain	uncertain	uncertain	NMNS_DS00175_UIgqLn1.stl	Campanian	-	-	-	-	-	-	-	-	-	-	-	-	-	-	-	-	-	-
209	uncertain	uncertain	uncertain	NMNS_DS00175_P1OdOSW.stl	Campanian	0.87	-85.24	-16.44	75.34	76.72	41.13	41.80	24.68	51.10	49.74	169.36	20.16	43.84	16.80	24.17	32.68	42.09	74.38
210	uncertain	uncertain	uncertain	NMNS_DS00175_y4Zl5lT.stl	Campanian	0.94	-77.58	-8.70	77.84	78.65	43.88	43.50	27.58	53.72	51.04	170.51	22.62	46.47	19.52	28.44	34.39	44.05	79.89
211	uncertain	uncertain	uncertain	NMNS_DS00175_7ESIH1Z.stl	Campanian	-	-	-	-	-	-	-	-	-	-	-	-	-	-	-	-	-	-
212	uncertain	uncertain	uncertain	NMNS_DS00175_MO6fdKX.stl	Campanian	1.40	-27.27	42.14	94.31	91.35	61.93	54.68	46.60	70.95	59.60	178.10	38.74	63.77	37.37	56.50	45.64	56.94	116.09
213	uncertain	uncertain	uncertain	NMNS_DS00182_9vHtXfk.stl	Campanian	2.35	76.64	147.15	128.31	117.58	99.22	77.78	85.90	106.51	77.28	193.78	72.02	99.50	74.24	114.45	68.88	83.57	190.87
214	uncertain	uncertain	uncertain	NMNS_DS00182_o6cWgkd.stl	Campanian	-	-	-	-	-	-	-	-	-	-	-	-	-	-	-	-	-	-
215	uncertain	uncertain	uncertain	NMNS_DS00128_7Kb5OEo.stl	Maastrichtian	1.24	-44.77	24.46	88.58	86.94	55.65	50.79	39.99	64.96	56.63	175.46	33.13	57.76	31.16	46.74	41.73	52.46	103.50
216	uncertain	uncertain	uncertain	NMNS_DS00128_XDB2mts.stl	Maastrichtian	-	-	-	-	-	-	-	-	-	-	-	-	-	-	-	-	-	-
217	uncertain	uncertain	uncertain	NMNS_DS00174_j7AcHlc.stl	Maastrichtian	-	-	-	-	-	-	-	-	-	-	-	-	-	-	-	-	-	-
218	uncertain	uncertain	uncertain	NMNS_DS00174_J39bDB6.stl	Maastrichtian	-	-	-	-	-	-	-	-	-	-	-	-	-	-	-	-	-	-

Table 4. (continued)

No.	ML (mm) estimated from the relationship between LRL (mm) and ML (mm) of modern oegopsid squids (Clarke, 1986)[19]																							
	Gonatus onyx: 19.02 × LRL + 12.82	*Gonatopsis borealis*: 32.0 × LRL + 24.1	*Berryteuthis magister*: 43.99 × LRL - 5.14	*Pterigioteuthis* spp.: 33.16 × LRL + 6.2	*Abraliopsis affinis*: 19.28 × LRL + 9.8	*Abraliopsis felis*: 40.55 × LRL - 2.66	*Ancistrocheirus lesueuri*: 40.75 × LRL - 41.3	*Octopoteuthis* spp.: 17.33 × LRL - 0.4	*Taningia danae*: 75.22 × LRL - 556.9	*Histioteuthis miranda*: 25.82 × LRL - 7.0	*Histioteuthis dofleini* (ML<180mm): 20.61 × LRL - 5.9	*Histioteuthis dofleini* (ML>90mm): 14.55 × LRL + 7.69	*Histioteuthis bonnellii*: 8.99 × LRL + 17.1	*Histioteuthis heteropsis*: 20.57 × LRL + 2.04	*Bathyteuthis abyssicola*: 51.59 × LRL + 1.68	*Ctenopteryx* spp.: 32.42 × LRL + 11.69	*Cycloteuthis* spp.: 31 × LRL	*Mastigoteuthis* spp.: 29.08 × LRL - 1.8	*Chiroteuthis* spp.: 24.46 × LRL + 11.4	*Cranchia scabra*: 28.03 × LRL + 17.7	*Liocranchia* spp.: 78.71 × LRL + 5.9	*Leachia* spp.: 67.94 × LRL + 18.22	*Megalocranchia* spp.: 68.13 × LRL - 70.9	*Teuthowenia megalops*: 40.78 × LRL + 12.2
145	98.39	9.49	60.32	45.33	32.55	45.19	6.79	20.05	-468.14	23.47	18.42	24.86	27.71	26.31	62.56	49.95	36.58	32.51	40.26	50.78	98.78	98.39	9.49	60.32
146	-	-	-	-	-	-	-	-	-	-	-	-	-	-	-	-	-	-	-	-	-	-	-	-
147	-	-	-	-	-	-	-	-	-	-	-	-	-	-	-	-	-	-	-	-	-	-	-	-
148	-	-	-	-	-	-	-	-	-	-	-	-	-	-	-	-	-	-	-	-	-	-	-	-
149	-	-	-	-	-	-	-	-	-	-	-	-	-	-	-	-	-	-	-	-	-	-	-	-
150	-	-	-	-	-	-	-	-	-	-	-	-	-	-	-	-	-	-	-	-	-	-	-	-
151	122.85	34.02	75.00	57.27	39.49	59.79	21.46	26.29	-441.06	32.76	25.84	30.10	30.94	33.72	81.13	61.62	47.74	42.98	49.07	60.87	127.11	122.85	34.02	75.00
152	-	-	-	-	-	-	-	-	-	-	-	-	-	-	-	-	-	-	-	-	-	-	-	-
153	145.95	57.18	88.87	68.54	46.05	73.57	35.31	32.18	-415.49	41.54	32.85	35.04	34.00	40.71	98.67	72.64	58.28	52.87	57.38	70.40	153.87	145.95	57.18	88.87
154	192.83	104.19	117.00	91.42	59.35	101.55	63.43	44.14	-363.58	59.36	47.07	45.08	40.20	54.90	134.27	95.01	79.67	72.94	74.26	89.74	208.18	192.83	104.19	117.00
155	116.73	27.89	71.33	54.28	37.76	56.14	17.79	24.73	-447.83	30.44	23.98	28.79	30.14	31.87	76.49	58.70	44.95	40.37	46.87	58.34	120.03	116.73	27.89	71.33
156	-	-	-	-	-	-	-	-	-	-	-	-	-	-	-	-	-	-	-	-	-	-	-	-
157	116.05	27.21	70.92	53.95	37.56	55.73	17.38	24.56	-448.58	30.18	23.78	28.64	30.05	31.66	75.97	58.37	44.64	40.08	46.62	58.06	119.24	116.05	27.21	70.92
158	-	-	-	-	-	-	-	-	-	-	-	-	-	-	-	-	-	-	-	-	-	-	-	-
159	-	-	-	-	-	-	-	-	-	-	-	-	-	-	-	-	-	-	-	-	-	-	-	-
160	-	-	-	-	-	-	-	-	-	-	-	-	-	-	-	-	-	-	-	-	-	-	-	-
161	137.79	49.01	83.97	64.56	43.73	68.71	30.42	30.10	-424.51	38.44	30.37	33.30	32.92	38.24	92.48	68.75	54.56	49.38	54.45	67.03	144.43	137.79	49.01	83.97
162	185.35	96.70	112.52	87.77	57.23	97.09	58.95	42.23	-371.86	56.52	44.80	43.48	39.22	52.64	128.59	91.44	76.26	69.74	71.57	86.65	199.53	185.35	96.70	112.52
163	117.41	28.57	71.74	54.61	37.95	56.54	18.20	24.90	-447.08	30.70	24.19	28.93	30.23	32.07	77.00	59.02	45.26	40.66	47.11	58.62	120.82	117.41	28.57	71.74
164	119.45	30.61	72.96	55.61	38.53	57.76	19.42	25.42	-444.82	31.47	24.81	29.37	30.50	32.69	78.55	60.00	46.19	41.53	47.85	59.46	123.18	119.45	30.61	72.96
165	-	-	-	-	-	-	-	-	-	-	-	-	-	-	-	-	-	-	-	-	-	-	-	-
166	145.27	56.50	88.46	68.21	45.85	73.17	34.90	32.01	-416.24	41.28	32.64	34.90	33.91	40.51	98.15	72.32	57.97	52.58	57.14	70.12	153.09	145.27	56.50	88.46
167	-	-	-	-	-	-	-	-	-	-	-	-	-	-	-	-	-	-	-	-	-	-	-	-
168	-	-	-	-	-	-	-	-	-	-	-	-	-	-	-	-	-	-	-	-	-	-	-	-
169	-	-	-	-	-	-	-	-	-	-	-	-	-	-	-	-	-	-	-	-	-	-	-	-
170	-	-	-	-	-	-	-	-	-	-	-	-	-	-	-	-	-	-	-	-	-	-	-	-
171	-	-	-	-	-	-	-	-	-	-	-	-	-	-	-	-	-	-	-	-	-	-	-	-
172	-	-	-	-	-	-	-	-	-	-	-	-	-	-	-	-	-	-	-	-	-	-	-	-
173	-	-	-	-	-	-	-	-	-	-	-	-	-	-	-	-	-	-	-	-	-	-	-	-
174	-	-	-	-	-	-	-	-	-	-	-	-	-	-	-	-	-	-	-	-	-	-	-	-
175	-	-	-	-	-	-	-	-	-	-	-	-	-	-	-	-	-	-	-	-	-	-	-	-
176	-	-	-	-	-	-	-	-	-	-	-	-	-	-	-	-	-	-	-	-	-	-	-	-
177	-	-	-	-	-	-	-	-	-	-	-	-	-	-	-	-	-	-	-	-	-	-	-	-
178	214.57	126.00	130.05	102.03	65.52	114.53	76.47	49.68	-339.51	67.62	53.66	49.74	43.08	61.49	150.78	105.38	89.59	82.24	82.09	98.71	233.37	214.57	126.00	130.05
179	-	-	-	-	-	-	-	-	-	-	-	-	-	-	-	-	-	-	-	-	-	-	-	-
180	-	-	-	-	-	-	-	-	-	-	-	-	-	-	-	-	-	-	-	-	-	-	-	-
181	-	-	-	-	-	-	-	-	-	-	-	-	-	-	-	-	-	-	-	-	-	-	-	-
182	-	-	-	-	-	-	-	-	-	-	-	-	-	-	-	-	-	-	-	-	-	-	-	-
183	-	-	-	-	-	-	-	-	-	-	-	-	-	-	-	-	-	-	-	-	-	-	-	-
184	128.96	40.15	78.67	60.25	41.23	63.44	25.12	27.85	-434.29	35.09	27.69	31.41	31.75	35.57	85.77	64.53	50.53	45.60	51.27	63.39	134.20	128.96	40.15	78.67
185	-	-	-	-	-	-	-	-	-	-	-	-	-	-	-	-	-	-	-	-	-	-	-	-
186	-	-	-	-	-	-	-	-	-	-	-	-	-	-	-	-	-	-	-	-	-	-	-	-
187	-	-	-	-	-	-	-	-	-	-	-	-	-	-	-	-	-	-	-	-	-	-	-	-
188	-	-	-	-	-	-	-	-	-	-	-	-	-	-	-	-	-	-	-	-	-	-	-	-
189	-	-	-	-	-	-	-	-	-	-	-	-	-	-	-	-	-	-	-	-	-	-	-	-
190	-	-	-	-	-	-	-	-	-	-	-	-	-	-	-	-	-	-	-	-	-	-	-	-
191	222.04	133.49	134.54	105.68	67.64	118.99	80.95	51.59	-331.24	70.46	55.93	51.34	44.07	63.75	156.45	108.95	93.00	85.44	84.78	101.79	242.03	222.04	133.49	134.54
192	-	-	-	-	-	-	-	-	-	-	-	-	-	-	-	-	-	-	-	-	-	-	-	-
193	150.70	61.95	91.72	70.86	47.40	76.41	38.16	33.39	-410.22	43.35	34.29	36.06	34.63	42.15	102.28	74.91	60.45	54.91	59.10	72.36	159.38	150.70	61.95	91.72
194	-	-	-	-	-	-	-	-	-	-	-	-	-	-	-	-	-	-	-	-	-	-	-	-
195	-	-	-	-	-	-	-	-	-	-	-	-	-	-	-	-	-	-	-	-	-	-	-	-
196	-	-	-	-	-	-	-	-	-	-	-	-	-	-	-	-	-	-	-	-	-	-	-	-
197	101.11	12.22	61.95	46.66	33.32	46.81	8.42	20.74	-465.13	24.50	19.24	25.44	28.07	27.14	64.62	51.24	37.82	33.68	41.24	51.90	101.93	101.11	12.22	61.95
198	-	-	-	-	-	-	-	-	-	-	-	-	-	-	-	-	-	-	-	-	-	-	-	-
199	-	-	-	-	-	-	-	-	-	-	-	-	-	-	-	-	-	-	-	-	-	-	-	-
200	-	-	-	-	-	-	-	-	-	-	-	-	-	-	-	-	-	-	-	-	-	-	-	-
201	-	-	-	-	-	-	-	-	-	-	-	-	-	-	-	-	-	-	-	-	-	-	-	-
202	-	-	-	-	-	-	-	-	-	-	-	-	-	-	-	-	-	-	-	-	-	-	-	-
203	-	-	-	-	-	-	-	-	-	-	-	-	-	-	-	-	-	-	-	-	-	-	-	-
204	147.31	58.55	89.68	69.20	46.43	74.39	36.13	32.53	-413.98	42.06	33.26	35.34	34.18	41.12	99.70	73.29	58.90	53.45	57.87	70.96	155.45	147.31	58.55	89.68
205	-	-	-	-	-	-	-	-	-	-	-	-	-	-	-	-	-	-	-	-	-	-	-	-
206	-	-	-	-	-	-	-	-	-	-	-	-	-	-	-	-	-	-	-	-	-	-	-	-
207	-	-	-	-	-	-	-	-	-	-	-	-	-	-	-	-	-	-	-	-	-	-	-	-
208	-	-	-	-	-	-	-	-	-	-	-	-	-	-	-	-	-	-	-	-	-	-	-	-
209	77.33	-11.63	47.68	35.05	26.57	32.62	-5.85	14.68	-491.46	15.46	12.03	20.35	24.92	19.94	46.56	39.90	26.97	23.50	32.68	42.09	74.38	77.33	-11.63	47.68
210	82.08	-6.86	50.53	37.37	27.92	35.46	-3.00	15.89	-486.19	17.27	13.47	21.37	25.55	21.38	50.17	42.16	29.14	25.54	34.39	44.05	79.89	82.08	-6.86	50.53
211	-	-	-	-	-	-	-	-	-	-	-	-	-	-	-	-	-	-	-	-	-	-	-	-
212	113.34	24.48	69.29	52.62	36.79	54.11	15.75	23.86	-451.59	29.15	22.95	28.06	29.69	30.84	73.91	57.08	43.40	38.91	45.64	56.94	116.09	113.34	24.48	69.29
213	177.88	89.21	108.03	84.13	55.11	92.63	54.46	40.33	-380.13	53.68	42.53	41.88	38.23	50.38	122.92	87.88	72.85	66.54	68.88	83.57	190.87	177.88	89.21	108.03
214	-	-	-	-	-	-	-	-	-	-	-	-	-	-	-	-	-	-	-	-	-	-	-	-
215	102.47	13.58	62.77	47.32	33.71	47.62	9.23	21.09	-463.63	25.02	19.66	25.73	28.25	27.55	65.65	51.89	38.44	34.26	41.73	52.46	103.50	102.47	13.58	62.77
216	-	-	-	-	-	-	-	-	-	-	-	-	-	-	-	-	-	-	-	-	-	-	-	-
217	-	-	-	-	-	-	-	-	-	-	-	-	-	-	-	-	-	-	-	-	-	-	-	-
218	-	-	-	-	-	-	-	-	-	-	-	-	-	-	-	-	-	-	-	-	-	-	-	-

Table 5. Body size estimations of the Late Cretaceous myopsid squids.

No.	Classification			3D model collection No. (NMNS: National Museum of Nature and Science, Tokyo)	Geological age	Growth stage	LRL (mm)	ML (mm) estimated from the relationship between LRL (mm) and ML (mm) of modern myopsid squids (Clarke, 1986)19	
	Family	Genus	Species					*Loligo* spp.: 84.274 × LRL - 44.22	*Alloteuthis* spp.: 113.97 × LRL - 30.99
1	Loliginidae	*Psiloteuthis*	*naucrates*	NMNS_DS00068_uZlnAz0.stl	Cenomanian	adult	1.48	82.51	137.69
2	Loliginidae	*Psiloteuthis*	*naucrates*	NMNS_DS00068_tj22YEq.stl	Cenomanian	subadult	1.34	70.71	121.73
3	Loliginidae	*Psiloteuthis*	*naucrates*	NMNS_DS00068_mb5AJPm.stl	Cenomanian	subadult	1.42	77.45	130.85
4	Loliginidae	*Psiloteuthis*	*naucrates*	NMNS_DS00084_N272hY0.stl	Cenomanian	adult	1.68	99.36	160.48
5	Loliginidae	*Psiloteuthis*	*naucrates*	NMNS_DS00082_fh6e497.stl	Cenomanian	subadult	1.63	95.15	154.78
6	Loliginidae	*Psiloteuthis*	*naucrates*	NMNS_DS00040_Tt7lr4y.stl	Turonian	adult	1.22	60.59	108.05
7	Loliginidae	*Psiloteuthis*	*naucrates*	NMNS_DS00040_CN8PI3W.stl	Turonian	adult	1.36	72.39	124.01
8	Loliginidae	*Psiloteuthis*	*naucrates*	NMNS_DS00040_xQd37Tu.stl	Turonian	adult	1.37	73.24	125.15
9	Loliginidae	*Psiloteuthis*	*naucrates*	NMNS_DS00040_FgRWr9e.stl	Turonian	adult	1.38	74.08	126.29
10	Loliginidae	*Psiloteuthis*	*naucrates*	NMNS_DS00173_tRj5kxm.stl	Turonian	adult	1.36	72.39	124.01
11	Loliginidae	*Psiloteuthis*	*naucrates*	NMNS_DS00083_SKAsE98.stl	Coniacian	adult	1.52	85.88	142.24
12	Loliginidae	*Psiloteuthis*	*naucrates*	NMNS_DS00083_XZzD8hv.stl	Coniacian	subadult	2.22	144.87	222.02
13	Loliginidae	*Psiloteuthis*	*naucrates*	NMNS_DS00182_oF5mYlz.stl	Campanian	adult	1.47	81.66	136.55
14	Loliginidae	*Psiloteuthis*	*naucrates*	NMNS_DS00182_UPRVv9A.stl	Campanian	adult	1.28	65.65	114.89
15	Loliginidae	*Psiloteuthis*	*naucrates*	NMNS_DS00128_NN6zaGU.stl	Maastrichtian	adult	0.58	6.66	35.11
16	Loliginidae	*Psiloteuthis*	*naucrates*	NMNS_DS00128_zGiAOX1.stl	Maastrichtian	adult	0.66	13.40	44.23
17	Loliginidae	*Psiloteuthis*	*atalante*	NMNS_DS00089_N7pALkd.stl	Coniacian	subadult	2.73	187.85	280.15
18	Loliginidae	*Psiloteuthis*	*atalante*	NMNS_DS00171_R5TOKQL.stl	Campanian	adult	1.65	96.83	157.06
19	Loliginidae	*Psiloteuthis*	*atalante*	NMNS_DS00171_9qzKEcc.stl	Campanian	subadult	1.55	88.40	145.66
20	Loliginidae	*Psiloteuthis*	*sculptus*	NMNS_DS00171_0gcEN28.stl	Campanian	adult	1.48	82.51	137.69
21	Loliginidae	*Psiloteuthis*	*transitus*	NMNS_DS00171_opgN0Hg.stl	Campanian	adult	2.31	152.45	232.28
22	Loliginidae	*Psiloteuthis*	uncertain	NMNS_DS00068_r0HPqbb.stl	Cenomanian	juvenile	2.60	176.89	265.33
23	Loliginidae	*Psiloteuthis*	uncertain	NMNS_DS00068_4NffBTu.stl	Cenomanian	juvenile	1.33	69.86	120.59
24	Loliginidae	*Psiloteuthis*	uncertain	NMNS_DS00173_Yij4eBp.stl	Turonian	juvenile	-	-	-
25	Loliginidae	*Psiloteuthis*	uncertain	NMNS_DS00171_CA61a5q.stl	Campanian	adult	1.57	90.09	147.94
26	Loliginidae	*Streptopteryx*	*glabra*	NMNS_DS00068_okmTU54.stl	Cenomanian	adult	1.20	58.91	105.77
27	Loliginidae	*Streptopteryx*	*glabra*	NMNS_DS00084_Erg3dY7.stl	Cenomanian	adult	1.05	46.27	88.68
28	Loliginidae	*Streptopteryx*	*glabra*	NMNS_DS00084_pAh4xpP.stl	Cenomanian	adult	0.81	26.04	61.33
29	Loliginidae	*Streptopteryx*	*glabra*	NMNS_DS00040_OuBYd2G.stl	Turonian	subadult	1.43	78.29	131.99
30	Loliginidae	*Streptopteryx*	*glabra*	NMNS_DS00040_fBilvb5.stl	Turonian	adult	1.42	77.45	130.85
31	Loliginidae	*Streptopteryx*	*glabra*	NMNS_DS00173_ACI2D9e.stl	Turonian	adult	1.42	77.45	130.85
32	Loliginidae	*Streptopteryx*	*glabra*	NMNS_DS00174_6Ga0IDF.stl	Maastrichtian	adult	0.73	19.30	52.21
33	Loliginidae	*Streptopteryx*	*bidentata*	NMNS_DS00040_CdEhX1r.stl	Turonian	subadult	1.30	67.34	117.17
34	Loliginidae	*Streptopteryx*	*bidentata*	NMNS_DS00083_HFkq7tj.stl	Coniacian	adult	1.38	74.08	126.29
35	Loliginidae	*Streptopteryx*	*bidentata*	NMNS_DS00128_k1LIu1T.stl	Maastrichtian	adult	1.36	72.39	124.01
36	Loliginidae	*Streptopteryx*	*bidentata*	NMNS_DS00174_RmFzKT4.stl	Maastrichtian	adult	1.05	46.27	88.68
37	Loliginidae	*Streptopteryx*	*bidentata*	NMNS_DS00174_TWaF8yT.stl	Maastrichtian	adult	0.88	31.94	69.30
38	Loliginidae	*Camptoteuthis*	*acrorhynchus*	NMNS_DS00140_3qYJhEx.stl	Turonian	subadult	2.05	130.54	202.65
39	Loliginidae	*Camptoteuthis*	*acrorhynchus*	NMNS_DS00173_OWxR12l.stl	Turonian	subadult	2.07	132.23	204.93
40	Loliginidae	*Camptoteuthis*	*cunabuli*	NMNS_DS00082_p4vjY3G.stl	Cenomanian	subadult	1.32	69.02	119.45
41	Loliginidae	uncertain	uncertain	NMNS_DS00140_s5yjXbC.stl	Turonian	juvenile	-	-	-
42	Loliginidae	uncertain	uncertain	NMNS_DS00173_7Ob4vJ8.stl	Turonian	adult	0.77	22.67	56.77
43	Loliginidae	uncertain	uncertain	NMNS_DS00182_Ua4EcEk.stl	Campanian	adult	1.46	80.82	135.41

Table 6. Estimated body size of squids in the Late Cretaceous.

Geological age	Order	Number of measurable lower beaks	Estimated mantle length (mm) (for details see Table 4 and 5)			
			Average	Median	Lower Quartile	Upper Quartile
Cenomanian	Oegopsida	21	89.51	75.82	53.12	111.19
	Myopsida	11	106.31	97.25	70.08	128.57
Turonian	Oegopsida	44	90.99	73.54	52.02	109.77
	Myopsida	12	105.06	112.61	73.02	130.62
Coniacian	Oegopsida	16	86.27	74.25	49.73	108.67
	Myopsida	4	157.92	143.56	116.19	196.39
Santonian	Oegopsida	8	77.39	69.03	49.30	94.81
	Myopsida	0	-	-	-	-
Campanian	Oegopsida	11	86.09	59.97	40.33	95.15
	Myopsida	8	121.62	125.15	86.93	146.23
Maastrichtian	Oegopsida	13	70.33	62.57	44.77	83.64
	Myopsida	6	50.29	45.25	28.78	70.08

Table 7. Measurements and body size estimations of the Late Cretaceous teleost fishes.

Sample No.	Geological age	Collection No. of cross-sectional image (NMNS: National Museum of Nature and Science, Tokyo)	Number of measurable teleost vertebrae	VL (mm)	TL (mm) estimated from the relationship between VL (mm) and TL (mm) of modern teleost fishes (Watt et al., 1997)[39]									
					Clupea harengus : exp(1.0204 × ln(VL) + 4.4552)	*Sprattus sprattus* : exp(0.9616 × ln(VL) + 4.2524)	*Salmo salar* & *S. trutta* : exp(0.8239 × ln(VL) + 4.7643)	*Argentina sphyraena* & *A. silus* : VL / 0.01	*Merluccius merluccius* : exp(0.9916 × ln(VL) + 4.4327)	*Molva molva* : exp(1.0306 × ln(VL) + 4.3205)	*Gaidropsarus vulgaris* : exp(1.0931 × ln(VL) + 4.0469)	*Rhinonemus cimbrius* : exp(1.3121 × ln(VL) + 3.8754)	*Ciliata mustela* : 78.51 × VL - 55.70	*Brosme brosme* : exp(0.9925 × ln(VL) + 4.3195)
1	Albian	NMNS_DS00178_wl_01_0001.tif–1400.tif	3	2.58	226.40	174.83	256.00	258.00	215.41	199.79	161.25	167.17	146.86	192.52
				2.09	182.62	142.77	215.22	209.00	174.81	160.81	128.08	126.80	108.39	156.20
				2.50	219.24	169.61	249.44	250.00	208.78	193.41	155.79	160.40	140.58	186.59
3	Albian	NMNS_DS00224_wl_01_0001.tif–1485.tif	1	2.37	207.62	161.12	238.71	237.00	198.01	183.06	146.95	149.55	130.37	176.96
4	Albian	NMNS_DS00249_wl_01_0001.tif–1540.tif	1	1.54	133.73	106.44	167.34	154.00	129.13	117.39	91.73	84.94	65.21	115.36
8	Cenomanian	NMNS_DS00082_20190127_c1_wl_01_0001.jpg–0933.jpg	6	1.88	163.92	128.95	197.24	188.00	157.38	144.18	114.08	110.35	91.90	140.62
				2.16	188.86	147.37	221.14	216.00	180.61	166.36	132.78	132.40	113.88	161.39
				2.32	203.15	157.85	234.55	232.00	193.87	179.08	143.57	145.42	126.44	173.25
				1.57	136.38	108.44	170.02	157.00	131.63	119.75	93.69	87.12	67.56	117.59
				2.93	257.79	197.58	284.29	293.00	244.37	227.78	185.30	197.53	174.33	218.42
				2.36	206.72	160.47	237.88	236.00	197.19	182.26	146.28	148.72	129.58	176.22
10	Turonian	NMNS_DS00009_20170720_c1_wl_01_0001.jpg–1257.jpg	13	0.99	85.20	69.60	116.28	99.00	83.32	74.45	56.59	47.57	22.02	74.41
				1.44	124.87	99.79	158.34	144.00	120.82	109.54	85.24	77.78	57.35	107.92
				1.10	94.86	77.02	126.83	110.00	92.50	82.99	63.50	54.62	30.66	82.61
				1.43	123.99	99.12	157.43	143.00	119.99	108.76	84.59	77.07	56.57	107.18
				1.28	110.73	89.10	143.69	128.00	107.50	97.02	74.94	66.64	44.79	96.02
				1.02	87.83	71.62	119.18	102.00	85.83	76.78	58.47	49.47	24.38	76.64
				1.38	119.56	95.79	152.88	138.00	115.82	104.84	81.37	73.55	52.64	103.46
				1.10	94.86	77.02	126.83	110.00	92.50	82.99	63.50	54.62	30.66	82.61
				1.27	109.85	88.43	142.77	127.00	106.67	96.24	74.30	65.96	44.01	95.27
				1.17	101.03	81.73	133.44	117.00	98.34	88.44	67.93	59.23	36.16	87.82
				1.17	101.03	81.73	133.44	117.00	98.34	88.44	67.93	59.23	36.16	87.82
				1.34	116.03	93.11	149.22	134.00	112.50	101.71	78.79	70.77	49.50	100.48
				1.40	121.33	97.12	154.70	140.00	117.49	106.41	82.66	74.95	54.21	104.95
11	Turonian	NMNS_DS00040_20180409_c1_wl_01_0001.jpg–0800.jpg	6	1.16	100.15	81.05	132.50	116.00	97.50	87.66	67.30	58.57	35.37	87.08
				2.22	194.22	151.30	226.19	222.00	185.58	171.13	136.82	137.25	118.59	165.84
				3.62	319.87	242.13	338.40	362.00	301.38	283.25	233.49	260.70	228.51	269.43
				1.97	171.93	134.88	204.98	197.00	164.85	151.30	120.07	117.34	98.96	147.30
				2.83	248.81	191.09	276.27	283.00	236.10	219.78	178.40	188.74	166.48	211.02
				1.06	91.35	74.32	123.02	106.00	89.16	79.88	60.98	52.03	27.52	79.63
15	Turonian	NMNS_DS00141_wl_02_0001.tif–1615.tif	3	1.76	153.25	121.03	186.80	176.00	147.42	134.71	106.15	101.21	82.48	131.71
				4.22	374.06	280.60	383.98	422.00	350.88	331.75	276.11	318.81	275.61	313.73
				1.05	90.47	73.65	122.06	105.00	88.33	79.11	60.35	51.39	26.74	78.88
16	Turonian	NMNS_DS00173_wl_01_0001.tif–1400.tif	1	2.60	228.20	176.13	257.64	260.00	217.06	201.39	162.61	168.87	148.43	194.00
17	Coniacian	NMNS_DS00034_20180207_c1_wl_01_0001.jpg–0800.jpg	5	1.62	140.82	111.75	174.47	162.00	135.79	123.68	96.95	90.78	71.49	121.30
				2.58	226.40	174.83	256.00	258.00	215.41	199.79	161.25	167.17	146.86	192.52
				0.87	74.67	61.47	104.54	87.00	73.30	65.17	49.14	40.15	12.60	65.45
				6.38	570.31	417.55	539.76	638.00	528.64	507.95	433.81	548.37	445.19	472.85
				1.57	136.38	108.44	170.02	157.00	131.63	119.75	93.69	87.12	67.56	117.59
19	Coniacian	NMNS_DS00083_20190130_c1_wl_01_0001.jpg–0900.jpg	15	1.04	89.59	72.97	121.10	104.00	87.50	78.33	59.73	50.75	25.95	78.13
				1.44	124.87	99.79	158.34	144.00	120.82	109.54	85.24	77.78	57.35	107.92
				2.64	231.78	178.73	260.90	264.00	220.37	204.59	165.35	172.29	151.57	196.96
				1.30	112.50	90.44	145.54	130.00	109.16	98.58	76.23	68.01	46.36	97.50
				1.84	160.36	126.31	193.77	184.00	154.06	141.02	111.43	107.28	88.76	137.65
				1.55	134.61	107.11	168.24	155.00	129.97	118.17	92.38	85.66	65.99	116.10
				0.85	72.92	60.11	102.56	85.00	71.63	63.63	47.91	38.95	11.03	63.96
				1.38	119.56	95.79	152.88	138.00	115.82	104.84	81.37	73.55	52.64	103.46
				1.15	99.27	80.38	131.56	115.00	96.67	86.88	66.66	57.90	34.59	86.33
				2.07	180.84	141.46	213.52	207.00	173.15	159.22	126.75	125.21	106.82	154.72
				1.87	163.03	128.29	196.37	187.00	156.55	143.39	113.42	109.58	91.11	139.87
				2.55	223.72	172.87	253.55	255.00	212.92	197.40	159.20	164.62	144.50	190.29
				3.71	327.99	247.92	345.32	371.00	308.81	290.51	239.84	269.24	235.57	276.08
				1.77	154.13	121.69	187.68	177.00	148.25	135.50	106.81	101.96	83.26	132.45
				2.04	178.16	139.49	210.97	204.00	170.66	156.85	124.74	122.84	104.46	152.49
20	Coniacian	NMNS_DS00089_20190223_c1_wl_01_0001.jpg–0836.jpg	3	2.96	260.48	199.52	286.69	296.00	246.85	230.19	187.38	200.19	176.69	220.64
				0.86	73.80	60.79	103.55	86.00	72.47	64.40	48.52	39.55	11.82	64.70
				1.89	164.81	129.61	198.10	189.00	158.21	144.97	114.75	111.12	92.68	141.36
22	Santonian	NMNS_DS00011_20170806_c1_wl_01_0001.jpg–1000.jpg	3	3.62	319.87	242.13	338.40	362.00	301.38	283.25	233.49	260.70	228.51	269.43
				3.12	274.86	209.88	299.39	312.00	260.08	243.02	198.48	214.51	189.25	232.48
				1.58	137.27	109.10	170.92	158.00	132.46	120.53	94.34	87.85	68.35	118.33

Table 7. (continued)

Sample No.	Geological age	Collection No. of cross-sectional image (NMNS: National Museum of Nature and Science, Tokyo)	Number of measurable teleost vertebrae	VL (mm)	TL (mm) estimated from the relationship between VL (mm) and TL (mm) of modern teleost fishes (Watt et al., 1997)[39]									
					Clupea harengus : exp(1.0204 × ln(VL) + 4.4552)	*Sprattus sprattus* : exp(0.9616 × ln(VL) + 4.2524)	*Salmo salar* & *S. trutta* : exp(0.8239 × ln(VL) + 4.7643)	*Argentina sphyraena* & *A. silus* : VL / 0.01	*Merluccius merluccius* : exp(0.9916 × ln(VL) + 4.4327)	*Molva molva* : exp(1.0306 × ln(VL) + 4.3205)	*Gaidropsarus vulgaris* : exp(1.0931 × ln(VL) + 4.0469)	*Rhinonemus cimbrius* : exp(1.3121 × ln(VL) + 3.8754)	*Ciliata mustela* : 78.51 × VL - 55.70	*Brosme brosme* : exp(0.9925 × ln(VL) + 4.3195)
23	Santonian	NMNS_DS00039_20180406_c1_wl_01_0001.jpg–0500.jpg	1	1.80	156.80	123.67	190.30	180.00	150.74	137.86	108.79	104.23	85.62	134.68
24	Santonian	NMNS_DS00042_20180419_c1_wl_02_0001.jpg–0601.jpg	3	4.83	429.31	319.50	429.15	483.00	401.14	381.28	320.01	380.60	323.50	358.72
				2.99	263.17	201.46	289.08	299.00	249.33	232.59	189.45	202.86	179.04	222.86
				6.48	579.43	423.84	546.72	648.00	536.85	516.15	441.24	559.67	453.04	480.20
25	Santonian	NMNS_DS00090_20190228_c1_wl_01_0001.jpg–0732.jpg	1	2.33	204.04	158.51	235.38	233.00	194.70	179.87	144.25	146.24	127.23	173.99
27	Campanian	NMNS_DS00073_20181212_c1_wl_01_0001.jpg–0893.jpg	10	1.46	126.64	101.12	160.15	146.00	122.48	111.11	86.54	79.20	58.92	109.41
				2.19	191.54	149.34	223.67	219.00	183.10	168.75	134.80	134.82	116.24	163.62
				0.93	79.93	65.54	110.44	93.00	78.31	69.81	52.86	43.82	17.31	69.93
				2.09	182.62	142.77	215.22	209.00	174.81	160.81	128.08	126.80	108.39	156.20
				0.93	79.93	65.54	110.44	93.00	78.31	69.81	52.86	43.82	17.31	69.93
				1.47	127.53	101.79	161.05	147.00	123.31	111.89	87.18	79.91	59.71	110.15
				1.59	138.16	109.76	171.81	159.00	133.29	121.32	94.99	88.58	69.13	119.08
				2.15	187.97	146.71	220.30	215.00	179.78	165.57	132.11	131.60	113.10	160.65
				1.75	152.36	120.36	185.93	175.00	146.59	133.92	105.49	100.45	81.69	130.96
				1.18	101.91	82.40	134.38	118.00	99.17	89.22	68.57	59.89	36.94	88.57
28	Campanian	NMNS_DS00097_wl_01_0001.jpg–0920.jpg	4	1.82	158.58	124.99	192.04	182.00	152.40	139.44	110.11	105.76	87.19	136.16
				2.64	231.78	178.73	260.90	264.00	220.37	204.59	165.35	172.29	151.57	196.96
				1.14	98.39	79.71	130.62	114.00	95.83	86.10	66.03	57.24	33.80	85.59
				2.87	252.40	193.68	279.48	287.00	239.40	222.98	181.16	192.24	169.62	213.98
29	Campanian	NMNS_DS00134_wl_01_0001.tif–1690.tif	1	2.46	215.66	167.00	246.15	246.00	205.47	190.22	153.07	157.04	137.43	183.63
30	Campanian	NMNS_DS00175_wl_01_0001.tif–1176.tif	9	2.70	237.16	182.64	265.77	270.00	225.34	209.38	169.46	177.44	156.28	201.40
				2.09	182.62	142.77	215.22	209.00	174.81	160.81	128.08	126.80	108.39	156.20
				1.03	88.71	72.30	120.14	103.00	86.66	77.55	59.10	50.11	25.17	77.39
				1.83	159.47	125.65	192.90	183.00	153.23	140.23	110.77	106.52	87.97	136.90
				1.73	150.58	119.04	184.18	173.00	144.93	132.34	104.17	98.95	80.12	129.48
				1.52	131.95	105.11	165.55	152.00	127.47	115.82	90.43	83.50	63.64	113.87
				2.33	204.04	158.51	235.38	233.00	194.70	179.87	144.25	146.24	127.23	173.99
				1.82	158.58	124.99	192.04	182.00	152.40	139.44	110.11	105.76	87.19	136.16
				2.01	175.49	137.51	208.41	201.00	168.17	154.47	122.74	120.47	102.11	150.26
31	Campanian	NMNS_DS00171_wl_01_0001.tif–1421.tif	2	2.52	221.03	170.92	251.09	252.00	210.44	195.01	157.15	162.08	142.15	188.07
				2.70	237.16	182.64	265.77	270.00	225.34	209.38	169.46	177.44	156.28	201.40
32	Campanian	NMNS_DS00182_wl_01_0001.tif–1060.tif	4	2.27	198.68	154.58	230.38	227.00	189.73	175.10	140.19	141.32	122.52	169.55
				3.20	282.05	215.05	305.70	320.00	266.69	249.45	204.04	221.75	195.53	238.39
				2.63	230.88	178.08	260.08	263.00	219.55	203.79	164.66	171.43	150.78	196.22
				3.28	289.25	220.22	311.99	328.00	273.30	255.88	209.63	229.06	201.81	244.31
33	Maastrichtian	NMNS_DS00128_wl_01_0001.jpg–1200.jpg	20	2.34	204.94	159.16	236.21	234.00	195.53	180.67	144.92	147.07	128.01	174.74
				1.88	163.92	128.95	197.24	188.00	157.38	144.18	114.08	110.35	91.90	140.62
				2.64	231.78	178.73	260.90	264.00	220.37	204.59	165.35	172.29	151.57	196.96
				1.72	149.69	118.38	183.30	172.00	144.09	131.55	103.51	98.20	79.34	128.74
				3.04	267.67	204.70	293.05	304.00	253.46	236.60	192.92	207.32	182.97	226.56
				3.00	264.07	202.11	289.87	300.00	250.16	233.39	190.15	203.75	179.83	223.60
				2.04	178.16	139.49	210.97	204.00	170.66	156.85	124.74	122.84	104.46	152.49
				2.59	227.30	175.48	256.82	259.00	216.23	200.59	161.93	168.02	147.64	193.26
				1.08	93.11	75.67	124.92	108.00	90.83	81.44	62.24	53.32	29.09	81.12
				1.42	123.10	98.45	156.52	142.00	119.15	107.97	83.95	76.36	55.78	106.43
				2.49	218.35	168.96	248.62	249.00	207.95	192.62	155.11	159.56	139.79	185.85
				2.52	221.03	170.92	251.09	252.00	210.44	195.01	157.15	162.08	142.15	188.07
				1.97	171.93	134.88	204.98	197.00	164.85	151.30	120.07	117.34	98.96	147.30
				2.67	234.47	180.69	263.34	267.00	222.86	206.98	167.40	174.86	153.92	199.18
				2.68	235.36	181.34	264.15	268.00	223.68	207.78	168.09	175.72	154.71	199.92
				1.89	164.81	129.61	198.10	189.00	158.21	144.97	114.75	111.12	92.68	141.36
				2.40	210.30	163.08	241.19	240.00	200.50	185.44	148.99	152.03	132.72	179.18
				2.70	237.16	182.64	265.77	270.00	225.34	209.38	169.46	177.44	156.28	201.40
				2.61	229.09	176.78	258.45	261.00	217.89	202.19	163.30	169.72	149.21	194.74
				2.79	245.22	188.49	273.05	279.00	232.79	216.58	175.65	185.24	163.34	208.06
34	Maastrichtian	NMNS_DS00172_wl_01_0001.tif–1310.tif	2	1.11	95.75	77.69	127.78	111.00	93.33	83.77	64.13	55.28	31.45	83.35
				4.49	398.49	297.85	404.11	449.00	373.13	353.65	295.47	345.84	296.81	333.65
35	Maastrichtian	NMNS_DS00174_wl_01_0001.tif–1159.tif	2	2.07	180.84	141.46	213.52	207.00	173.15	159.22	126.75	125.21	106.82	154.72
				3.33	293.75	223.45	315.90	333.00	277.43	259.90	213.12	233.65	205.74	248.01

Table 7. (continued)

Sample No.	Geological age	Collection No. of cross-sectional image (NMNS: National Museum of Nature and Science, Tokyo)	Number of measurable teleost vertebrae	VL (mm)	TL (mm) estimated from the relationship between VL (mm) and TL (mm) of modern teleost fishes (Watt et al., 1997)[39]											
					Melanogrammus aeglefinus : exp(0.9701 × ln(VL) + 4.3571)	*Trisopterus minutus* : 60.48 × VL + 13.51	*Micromesistius poutassou* : exp(0.8300 × ln(VL) + 4.6688)	*Merlangius merlangius* : 73.108 × VL + 1.906	*Pollachius pollachius* : 65.030 × VL + 4.0112	*Pollachius virens* : 57.800 × VL + 28.57	*Gadus morhua* : exp(0.9202 × ln(VL) + 4.3513)	*Labrus mixtus* : VL / 0.0175	*Crenilabrus melops* : VL / 0.0175	*Ctenolabrus rupestris* : VL / 0.0175	*Ammodytes marinus* & *Am. tobianus* : exp(1.0426 × ln(VL) + 4.4758)	*Trachurus trachurus* : VL / 0.0255
1	Albian	NMNS_DS00178_wl_01_0001.tif–1400.tif	3	2.58	195.69	169.55	234.03	190.52	171.79	177.69	185.57	147.43	147.43	147.43	236.03	101.18
				2.09	159.53	139.91	196.50	154.70	139.92	149.37	152.88	119.43	119.43	119.43	189.50	81.96
				2.50	189.80	164.71	227.99	184.68	166.59	173.07	180.27	142.86	142.86	142.86	228.41	98.04
3	Albian	NMNS_DS00224_wl_01_0001.tif–1485.tif	1	2.37	180.22	156.85	218.11	175.17	158.13	165.56	171.63	135.43	135.43	135.43	216.04	92.94
4	Albian	NMNS_DS00249_wl_01_0001.tif–1540.tif	1	1.54	118.63	106.65	152.50	114.49	104.16	117.58	115.43	88.00	88.00	88.00	137.82	60.39
8	Cenomanian	NMNS_DS00082_20190127_c1_wl_01_0001.jpg–0933.jpg	6	1.88	143.95	127.21	179.96	139.35	126.27	137.23	138.68	107.43	107.43	107.43	169.69	73.73
				2.16	164.71	144.15	201.94	159.82	144.48	153.42	157.58	123.43	123.43	123.43	196.12	84.71
				2.32	176.53	153.82	214.28	171.52	154.88	162.67	168.29	132.57	132.57	132.57	211.29	90.98
				1.57	120.87	108.46	154.96	116.69	106.11	119.32	117.49	89.71	89.71	89.71	140.62	61.57
				2.93	221.40	190.72	260.10	216.11	194.55	197.92	208.62	167.43	167.43	167.43	269.51	114.90
				2.36	179.48	156.24	217.35	174.44	157.48	164.98	170.96	134.86	134.86	134.86	215.09	92.55
10	Turonian	NMNS_DS00009_20170720_c1_wl_01_0001.jpg–1257.jpg	13	0.99	77.27	73.39	105.68	74.28	68.39	85.79	76.87	56.57	56.57	56.57	86.95	38.82
				1.44	111.15	100.60	144.24	107.18	97.65	111.80	108.51	82.29	82.29	82.29	128.51	56.47
				1.10	85.59	80.04	115.34	82.32	75.54	92.15	84.69	62.86	62.86	62.86	97.04	43.14
				1.43	110.40	100.00	143.40	106.45	97.00	111.22	107.82	81.71	81.71	81.71	127.58	56.08
				1.28	99.14	90.92	130.80	95.48	87.25	102.55	97.36	73.14	73.14	73.14	113.66	50.20
				1.02	79.54	75.20	108.34	76.48	70.34	87.53	79.01	58.29	58.29	58.29	89.70	40.00
				1.38	106.65	96.97	139.23	102.80	93.75	108.33	104.34	78.86	78.86	78.86	122.93	54.12
				1.10	85.59	80.04	115.34	82.32	75.54	92.15	84.69	62.86	62.86	62.86	97.04	43.14
				1.27	98.39	90.32	129.95	94.75	86.60	101.98	96.66	72.57	72.57	72.57	112.73	49.80
				1.17	90.87	84.27	121.40	87.44	80.10	96.20	89.64	66.86	66.86	66.86	103.49	45.88
				1.17	90.87	84.27	121.40	87.44	80.10	96.20	89.64	66.86	66.86	66.86	103.49	45.88
				1.34	103.65	94.55	135.87	99.87	91.15	106.02	101.56	76.57	76.57	76.57	119.22	52.55
				1.40	108.15	98.18	140.90	104.26	95.05	109.49	105.73	80.00	80.00	80.00	124.79	54.90
11	Turonian	NMNS_DS00040_20180409_c1_wl_01_0001.jpg–0800.jpg	6	1.16	90.11	83.67	120.54	86.71	79.45	95.62	88.93	66.29	66.29	66.29	102.57	45.49
				2.22	169.15	147.78	206.59	164.21	148.38	156.89	161.61	126.86	126.86	126.86	201.80	87.06
				3.62	271.81	232.45	310.00	266.56	239.42	237.81	253.44	206.86	206.86	206.86	335.99	141.96
				1.97	150.64	132.66	187.09	145.93	132.12	142.44	144.78	112.57	112.57	112.57	178.17	77.25
				2.83	214.06	184.67	252.71	208.80	188.05	192.14	202.06	161.71	161.71	161.71	259.92	110.98
				1.06	82.57	77.62	111.85	79.40	72.94	89.84	81.85	60.57	60.57	60.57	93.37	41.57
15	Turonian	NMNS_DS00141_wl_02_0001.tif–1615.tif	3	1.76	135.03	119.95	170.38	130.58	118.46	130.30	130.52	100.57	100.57	100.57	158.41	69.02
				4.22	315.41	268.74	352.08	310.42	278.44	272.49	291.85	241.14	241.14	241.14	394.24	165.49
				1.05	81.81	77.01	110.97	78.67	72.29	89.26	81.14	60.00	60.00	60.00	92.45	41.18
16	Turonian	NMNS_DS00173_wl_01_0001.tif–1400.tif	1	2.60	197.17	170.76	235.54	191.99	173.09	178.85	186.90	148.57	148.57	148.57	237.94	101.96
17	Coniacian	NMNS_DS00034_20180207_c1_wl_01_0001.jpg–0800.jpg	5	1.62	124.60	111.49	159.05	120.34	109.36	122.21	120.93	92.57	92.57	92.57	145.30	63.53
				2.58	195.69	169.55	234.03	190.52	171.79	177.69	185.57	147.43	147.43	147.43	236.03	101.18
				0.87	68.17	66.13	94.94	65.51	60.59	78.86	68.25	49.71	49.71	49.71	75.99	34.12
				6.38	471.00	399.37	496.18	468.34	418.90	397.33	426.92	364.57	364.57	364.57	606.63	250.20
				1.57	120.87	108.46	154.96	116.69	106.11	119.32	117.49	89.71	89.71	89.71	140.62	61.57
19	Coniacian	NMNS_DS00083_20190130_c1_wl_01_0001.jpg–0900.jpg	15	1.04	81.06	76.41	110.10	77.94	71.64	88.68	80.43	59.43	59.43	59.43	91.53	40.78
				1.44	111.15	100.60	144.24	107.18	97.65	111.80	108.51	82.29	82.29	82.29	128.51	56.47
				2.64	200.11	173.18	238.54	194.91	175.69	181.16	189.54	150.86	150.86	150.86	241.76	103.53
				1.30	100.65	92.13	132.50	96.95	88.55	103.71	98.76	74.29	74.29	74.29	115.51	50.98
				1.84	140.98	124.79	176.78	136.42	123.67	134.92	135.97	105.14	105.14	105.14	165.93	72.16
				1.55	119.37	107.25	153.32	115.22	104.81	118.16	116.12	88.57	88.57	88.57	138.76	60.78
				0.85	66.65	64.92	93.12	64.05	59.29	77.70	66.80	48.57	48.57	48.57	74.17	33.33
				1.38	106.65	96.97	139.23	102.80	93.75	108.33	104.34	78.86	78.86	78.86	122.93	54.12
				1.15	89.36	83.06	119.68	85.98	78.80	95.04	88.23	65.71	65.71	65.71	101.65	45.10
				2.07	158.05	138.70	194.93	153.24	138.62	148.22	151.53	118.29	118.29	118.29	187.61	81.18
				1.87	143.21	126.61	179.17	138.62	125.62	136.66	138.00	106.86	106.86	106.86	168.75	73.33
				2.55	193.49	167.73	231.77	188.33	169.84	175.96	183.59	145.71	145.71	145.71	233.17	100.00
				3.71	278.36	237.89	316.38	273.14	245.27	243.01	259.23	212.00	212.00	212.00	344.70	145.49
				1.77	135.78	120.56	171.18	131.31	119.11	130.88	131.20	101.14	101.14	101.14	159.35	69.41
				2.04	155.82	136.89	192.59	151.05	136.67	146.48	149.51	116.57	116.57	116.57	184.77	80.00
20	Coniacian	NMNS_DS00089_20190223_c1_wl_01_0001.jpg–0836.jpg	3	2.96	223.60	192.53	262.30	218.31	196.50	199.66	210.59	169.14	169.14	169.14	272.39	116.08
				0.86	67.41	65.52	94.03	64.78	59.94	78.28	67.53	49.14	49.14	49.14	75.08	33.73
				1.89	144.70	127.82	180.76	140.08	126.92	137.81	139.36	108.00	108.00	108.00	170.63	74.12
22	Santonian	NMNS_DS00011_20170806_c1_wl_01_0001.jpg–1000.jpg	3	3.62	271.81	232.45	310.00	266.56	239.42	237.81	253.44	206.86	206.86	206.86	335.99	141.96
				3.12	235.31	202.21	274.02	230.00	206.90	208.91	221.04	178.29	178.29	178.29	287.75	122.35
				1.58	121.61	109.07	155.78	117.42	106.76	119.89	118.18	90.29	90.29	90.29	141.56	61.96

Table 7. (continued)

Sample No.	Geological age	Collection No. of cross-sectional image (NMNS: National Museum of Nature and Science, Tokyo)	Number of measurable teleost vertebrae	VL (mm)	TL (mm) estimated from the relationship between VL (mm) and TL (mm) of modern teleost fishes (Watt et al., 1997)[39]											
					Melanogrammus aeglefinus : exp(0.9701 × ln(VL) + 4.3571)	*Trisopterus minutus* : 60.48 × VL + 13.51	*Micromesistius poutassou* : exp(0.8300 × ln(VL) + 4.6688)	*Merlangius merlangius* : 73.108 × VL + 1.906	*Pollachius pollachius* : 65.030 × VL + 4.0112	*Pollachius virens* : 57.800 × VL + 28.57	*Gadus morhua* : exp(0.9202 × ln(VL) + 4.3513)	*Labrus mixtus* : VL / 0.0175	*Crenilabrus melops* : VL / 0.0175	*Ctenolabrus rupestris* : VL / 0.0175	*Ammodytes marinus* & *Am. tobianus* : exp(1.0426 × ln(VL) + 4.4758)	*Trachurus trachurus* : VL / 0.0255
23	Santonian	NMNS_DS00039_20180406_c1_wl_01_0001.jpg–0500.jpg	1	1.80	138.01	122.37	173.58	133.50	121.07	132.61	133.24	102.86	102.86	102.86	162.17	70.59
24	Santonian	NMNS_DS00042_20180419_c1_wl_02_0001.jpg–0601.jpg	3	4.83	359.55	305.63	393.83	355.02	318.11	307.74	330.46	276.00	276.00	276.00	453.84	189.41
				2.99	225.79	194.35	264.51	220.50	198.45	201.39	212.55	170.86	170.86	170.86	275.26	117.25
				6.48	478.16	405.42	502.62	475.65	425.41	403.11	433.07	370.29	370.29	370.29	616.54	254.12
25	Santonian	NMNS_DS00090_20190228_c1_wl_01_0001.jpg–0732.jpg	1	2.33	177.27	154.43	215.05	172.25	155.53	163.24	168.96	133.14	133.14	133.14	212.24	91.37
27	Campanian	NMNS_DS00073_20181212_c1_wl_01_0001.jpg–0893.jpg	10	1.46	112.64	101.81	145.90	108.64	98.96	112.96	109.90	83.43	83.43	83.43	130.37	57.25
				2.19	166.93	145.96	204.27	162.01	146.43	155.15	159.60	125.14	125.14	125.14	198.96	85.88
				0.93	72.73	69.76	100.34	69.90	64.49	82.32	72.57	53.14	53.14	53.14	81.46	36.47
				2.09	159.53	139.91	196.50	154.70	139.92	149.37	152.88	119.43	119.43	119.43	189.50	81.96
				0.93	72.73	69.76	100.34	69.90	64.49	82.32	72.57	53.14	53.14	53.14	81.46	36.47
				1.47	113.39	102.42	146.73	109.37	99.61	113.54	110.59	84.00	84.00	84.00	131.30	57.65
				1.59	122.36	109.67	156.60	118.15	107.41	120.47	118.87	90.86	90.86	90.86	142.49	62.35
				2.15	163.97	143.54	201.17	159.09	143.83	152.84	156.91	122.86	122.86	122.86	195.17	84.31
				1.75	134.29	119.35	169.57	129.85	117.81	129.72	129.83	100.00	100.00	100.00	157.47	68.63
				1.18	91.62	84.88	122.26	88.17	80.75	96.77	90.34	67.43	67.43	67.43	104.41	46.27
28	Campanian	NMNS_DS00097_wl_01_0001.jpg–0920.jpg	4	1.82	139.50	123.58	175.18	134.96	122.37	133.77	134.61	104.00	104.00	104.00	164.05	71.37
				2.64	200.11	173.18	238.54	194.91	175.69	181.16	189.54	150.86	150.86	150.86	241.76	103.53
				1.14	88.61	82.46	118.81	85.25	78.15	94.46	87.52	65.14	65.14	65.14	100.73	44.71
				2.87	217.00	187.09	255.67	211.73	190.65	194.46	204.69	164.00	164.00	164.00	263.76	112.55
29	Campanian	NMNS_DS00134_wl_01_0001.tif–1690.tif	1	2.46	186.86	162.29	224.96	181.75	163.99	170.76	177.62	140.57	140.57	140.57	224.60	96.47
30	Campanian	NMNS_DS00175_wl_01_0001.tif–1176.tif	9	2.70	204.52	176.81	243.03	199.30	179.59	184.63	193.50	154.29	154.29	154.29	247.49	105.88
				2.09	159.53	139.91	196.50	154.70	139.92	149.37	152.88	119.43	119.43	119.43	189.50	81.96
				1.03	80.30	75.80	109.22	77.21	70.99	88.10	79.72	58.86	58.86	58.86	90.61	40.39
				1.83	140.24	124.19	175.98	135.69	123.02	134.34	135.29	104.57	104.57	104.57	164.99	71.76
				1.73	132.80	118.14	167.96	128.38	116.51	128.56	128.47	98.86	98.86	98.86	155.60	67.84
				1.52	117.13	105.44	150.86	113.03	102.86	116.43	114.05	86.86	86.86	86.86	135.96	59.61
				2.33	177.27	154.43	215.05	172.25	155.53	163.24	168.96	133.14	133.14	133.14	212.24	91.37
				1.82	139.50	123.58	175.18	134.96	122.37	133.77	134.61	104.00	104.00	104.00	164.05	71.37
				2.01	153.60	135.07	190.23	148.85	134.72	144.75	147.48	114.86	114.86	114.86	181.94	78.82
31	Campanian	NMNS_DS00171_wl_01_0001.tif–1421.tif	2	2.52	191.28	165.92	229.51	186.14	167.89	174.23	181.60	144.00	144.00	144.00	230.31	98.82
				2.70	204.52	176.81	243.03	199.30	179.59	184.63	193.50	154.29	154.29	154.29	247.49	105.88
32	Campanian	NMNS_DS00182_wl_01_0001.tif–1060.tif	4	2.27	172.84	150.80	210.44	167.86	151.63	159.78	164.95	129.71	129.71	129.71	206.54	89.02
				3.20	241.16	207.05	279.84	235.85	212.11	213.53	226.25	182.86	182.86	182.86	295.45	125.49
				2.63	199.37	172.57	237.79	194.18	175.04	180.58	188.88	150.29	150.29	150.29	240.80	103.14
				3.28	247.01	211.88	285.63	241.70	217.31	218.15	231.45	187.43	187.43	187.43	303.16	128.63
33	Maastrichtian	NMNS_DS00128_wl_01_0001.jpg–1200.jpg	20	2.34	178.01	155.03	215.82	172.98	156.18	163.82	169.63	133.71	133.71	133.71	213.19	91.76
				1.88	143.95	127.21	179.96	139.35	126.27	137.23	138.68	107.43	107.43	107.43	169.69	73.73
				2.64	200.11	173.18	238.54	194.91	175.69	181.16	189.54	150.86	150.86	150.86	241.76	103.53
				1.72	132.05	117.54	167.16	127.65	115.86	127.99	127.78	98.29	98.29	98.29	154.66	67.45
				3.04	229.46	197.37	268.18	224.15	201.70	204.28	215.82	173.71	173.71	173.71	280.07	119.22
				3.00	226.53	194.95	265.24	221.23	199.10	201.97	213.20	171.43	171.43	171.43	276.22	117.65
				2.04	155.82	136.89	192.59	151.05	136.67	146.48	149.51	116.57	116.57	116.57	184.77	80.00
				2.59	196.43	170.15	234.79	191.26	172.44	178.27	186.24	148.00	148.00	148.00	236.99	101.57
				1.08	84.08	78.83	113.60	80.86	74.24	90.99	83.27	61.71	61.71	61.71	95.21	42.35
				1.42	109.65	99.39	142.57	105.72	96.35	110.65	107.12	81.14	81.14	81.14	126.65	55.69
				2.49	189.07	164.11	227.24	183.94	165.94	172.49	179.61	142.29	142.29	142.29	227.45	97.65
				2.52	191.28	165.92	229.51	186.14	167.89	174.23	181.60	144.00	144.00	144.00	230.31	98.82
				1.97	150.64	132.66	187.09	145.93	132.12	142.44	144.78	112.57	112.57	112.57	178.17	77.25
				2.67	202.31	174.99	240.79	197.10	177.64	182.90	191.52	152.57	152.57	152.57	244.62	104.71
				2.68	203.05	175.60	241.54	197.84	178.29	183.47	192.18	153.14	153.14	153.14	245.58	105.10
				1.89	144.70	127.82	180.76	140.08	126.92	137.81	139.36	108.00	108.00	108.00	170.63	74.12
				2.40	182.43	158.66	220.40	177.37	160.08	167.29	173.63	137.14	137.14	137.14	218.89	94.12
				2.70	204.52	176.81	243.03	199.30	179.59	184.63	193.50	154.29	154.29	154.29	247.49	105.88
				2.61	197.90	171.36	236.29	192.72	173.74	179.43	187.56	149.14	149.14	149.14	238.89	102.35
				2.79	211.13	182.25	249.74	205.88	185.44	189.83	199.43	159.43	159.43	159.43	256.10	109.41
34	Maastrichtian	NMNS_DS00172_wl_01_0001.tif–1310.tif	2	1.11	86.34	80.64	116.21	83.06	76.19	92.73	85.40	63.43	63.43	63.43	97.96	43.53
				4.49	334.97	285.07	370.68	330.16	296.00	288.09	308.99	256.57	256.57	256.57	420.58	176.08
35	Maastrichtian	NMNS_DS00174_wl_01_0001.tif–1159.tif	2	2.07	158.05	138.70	194.93	153.24	138.62	148.22	151.53	118.29	118.29	118.29	187.61	81.18
				3.33	250.66	214.91	289.24	245.36	220.56	221.04	234.69	190.29	190.29	190.29	307.98	130.59

Table 7. (co□ti□u□d)

Table 7. (continued)

Sample No.	Geological age	Collection No. of cross-sectional image (NMNS: National Museum of Nature and Science, Tokyo)	Number of measurable teleost vertebrae	VL (mm)	TL (mm) estimated from the relationship between VL (mm) and TL (mm) of modern teleost fishes (Watt et al., 1997)[39]								
					Scomber scombrus : VL / 0.022	*Pomatoschistus minutus* : VL / 0.0185	*Gobius paganellus* : VL / 0.0185	*Callionymus lyra* & *C. maculatus* : VL / 0.0305	*Pholis gunnellus* : VL / 0.01	*Zoarces viviparus* : VL / 0.008	*Myoxocephalus scorpius* : VL / 0.0155	*Taurulus bubalis* : VL / 0.0155	*Cyclopterus lumpus* : VL / 0.02
1	Albian	NMNS_DS00178_wl_01_0001.tif–1400.tif	3	2.58	117.27	139.46	139.46	84.59	258.00	322.50	166.45	166.45	129.00
				2.09	95.00	112.97	112.97	68.52	209.00	261.25	134.84	134.84	104.50
				2.50	113.64	135.14	135.14	81.97	250.00	312.50	161.29	161.29	125.00
3	Albian	NMNS_DS00224_wl_01_0001.tif–1485.tif	1	2.37	107.73	128.11	128.11	77.70	237.00	296.25	152.90	152.90	118.50
4	Albian	NMNS_DS00249_wl_01_0001.tif–1540.tif	1	1.54	70.00	83.24	83.24	50.49	154.00	192.50	99.35	99.35	77.00
8	Cenomanian	NMNS_DS00082_20190127_c1_wl_01_0001.jpg–0933.jpg	6	1.88	85.45	101.62	101.62	61.64	188.00	235.00	121.29	121.29	94.00
				2.16	98.18	116.76	116.76	70.82	216.00	270.00	139.35	139.35	108.00
				2.32	105.45	125.41	125.41	76.07	232.00	290.00	149.68	149.68	116.00
				1.57	71.36	84.86	84.86	51.48	157.00	196.25	101.29	101.29	78.50
				2.93	133.18	158.38	158.38	96.07	293.00	366.25	189.03	189.03	146.50
				2.36	107.27	127.57	127.57	77.38	236.00	295.00	152.26	152.26	118.00
10	Turonian	NMNS_DS00009_20170720_c1_wl_01_0001.jpg–1257.jpg	13	0.99	45.00	53.51	53.51	32.46	99.00	123.75	63.87	63.87	49.50
				1.44	65.45	77.84	77.84	47.21	144.00	180.00	92.90	92.90	72.00
				1.10	50.00	59.46	59.46	36.07	110.00	137.50	70.97	70.97	55.00
				1.43	65.00	77.30	77.30	46.89	143.00	178.75	92.26	92.26	71.50
				1.28	58.18	69.19	69.19	41.97	128.00	160.00	82.58	82.58	64.00
				1.02	46.36	55.14	55.14	33.44	102.00	127.50	65.81	65.81	51.00
				1.38	62.73	74.59	74.59	45.25	138.00	172.50	89.03	89.03	69.00
				1.10	50.00	59.46	59.46	36.07	110.00	137.50	70.97	70.97	55.00
				1.27	57.73	68.65	68.65	41.64	127.00	158.75	81.94	81.94	63.50
				1.17	53.18	63.24	63.24	38.36	117.00	146.25	75.48	75.48	58.50
				1.17	53.18	63.24	63.24	38.36	117.00	146.25	75.48	75.48	58.50
				1.34	60.91	72.43	72.43	43.93	134.00	167.50	86.45	86.45	67.00
				1.40	63.64	75.68	75.68	45.90	140.00	175.00	90.32	90.32	70.00
11	Turonian	NMNS_DS00040_20180409_c1_wl_01_0001.jpg–0800.jpg	6	1.16	52.73	62.70	62.70	38.03	116.00	145.00	74.84	74.84	58.00
				2.22	100.91	120.00	120.00	72.79	222.00	277.50	143.23	143.23	111.00
				3.62	164.55	195.68	195.68	118.69	362.00	452.50	233.55	233.55	181.00
				1.97	89.55	106.49	106.49	64.59	197.00	246.25	127.10	127.10	98.50
				2.83	128.64	152.97	152.97	92.79	283.00	353.75	182.58	182.58	141.50
				1.06	48.18	57.30	57.30	34.75	106.00	132.50	68.39	68.39	53.00
15	Turonian	NMNS_DS00141_wl_02_0001.tif–1615.tif	3	1.76	80.00	95.14	95.14	57.70	176.00	220.00	113.55	113.55	88.00
				4.22	191.82	228.11	228.11	138.36	422.00	527.50	272.26	272.26	211.00
				1.05	47.73	56.76	56.76	34.43	105.00	131.25	67.74	67.74	52.50
16	Turonian	NMNS_DS00173_wl_01_0001.tif–1400.tif	1	2.60	118.18	140.54	140.54	85.25	260.00	325.00	167.74	167.74	130.00
17	Coniacian	NMNS_DS00034_20180207_c1_wl_01_0001.jpg–0800.jpg	5	1.62	73.64	87.57	87.57	53.11	162.00	202.50	104.52	104.52	81.00
				2.58	117.27	139.46	139.46	84.59	258.00	322.50	166.45	166.45	129.00
				0.87	39.55	47.03	47.03	28.52	87.00	108.75	56.13	56.13	43.50
				6.38	290.00	344.86	344.86	209.18	638.00	797.50	411.61	411.61	319.00
				1.57	71.36	84.86	84.86	51.48	157.00	196.25	101.29	101.29	78.50
19	Coniacian	NMNS_DS00083_20190130_c1_wl_01_0001.jpg–0900.jpg	15	1.04	47.27	56.22	56.22	34.10	104.00	130.00	67.10	67.10	52.00
				1.44	65.45	77.84	77.84	47.21	144.00	180.00	92.90	92.90	72.00
				2.64	120.00	142.70	142.70	86.56	264.00	330.00	170.32	170.32	132.00
				1.30	59.09	70.27	70.27	42.62	130.00	162.50	83.87	83.87	65.00
				1.84	83.64	99.46	99.46	60.33	184.00	230.00	118.71	118.71	92.00
				1.55	70.45	83.78	83.78	50.82	155.00	193.75	100.00	100.00	77.50
				0.85	38.64	45.95	45.95	27.87	85.00	106.25	54.84	54.84	42.50
				1.38	62.73	74.59	74.59	45.25	138.00	172.50	89.03	89.03	69.00
				1.15	52.27	62.16	62.16	37.70	115.00	143.75	74.19	74.19	57.50
				2.07	94.09	111.89	111.89	67.87	207.00	258.75	133.55	133.55	103.50
				1.87	85.00	101.08	101.08	61.31	187.00	233.75	120.65	120.65	93.50
				2.55	115.91	137.84	137.84	83.61	255.00	318.75	164.52	164.52	127.50
				3.71	168.64	200.54	200.54	121.64	371.00	463.75	239.35	239.35	185.50
				1.77	80.45	95.68	95.68	58.03	177.00	221.25	114.19	114.19	88.50
				2.04	92.73	110.27	110.27	66.89	204.00	255.00	131.61	131.61	102.00
20	Coniacian	NMNS_DS00089_20190223_c1_wl_01_0001.jpg–0836.jpg	3	2.96	134.55	160.00	160.00	97.05	296.00	370.00	190.97	190.97	148.00
				0.86	39.09	46.49	46.49	28.20	86.00	107.50	55.48	55.48	43.00
				1.89	85.91	102.16	102.16	61.97	189.00	236.25	121.94	121.94	94.50
22	Santonian	NMNS_DS00011_20170806_c1_wl_01_0001.jpg–1000.jpg	3	3.62	164.55	195.68	195.68	118.69	362.00	452.50	233.55	233.55	181.00
				3.12	141.82	168.65	168.65	102.30	312.00	390.00	201.29	201.29	156.00
				1.58	71.82	85.41	85.41	51.80	158.00	197.50	101.94	101.94	79.00

Table 7. (continued)

Sample No.	Geological age	Collection No. of cross-sectional image (NMNS: National Museum of Nature and Science, Tokyo)	Number of measurable teleost vertebrae	VL (mm)	TL (mm) estimated from the relationship between VL (mm) and TL (mm) of modern teleost fishes (Watt et al., 1997)[39]								
					Scomber scombrus : VL / 0.022	*Pomatoschistus minutus* : VL / 0.0185	*Gobius paganellus* : VL / 0.0185	*Callionymus lyra* & *C. maculatus* : VL / 0.0305	*Pholis gunnellus* : VL / 0.01	*Zoarces viviparus* : VL / 0.008	*Myoxocephalus scorpius* : VL / 0.0155	*Taurulus bubalis* : VL / 0.0155	*Cyclopterus lumpus* : VL / 0.02
23	Santonian	NMNS_DS00039_20180406_c1_wl_01_0001.jpg–0500.jpg	1	1.80	81.82	97.30	97.30	59.02	180.00	225.00	116.13	116.13	90.00
24	Santonian	NMNS_DS00042_20180419_c1_wl_02_0001.jpg–0601.jpg	3	4.83	219.55	261.08	261.08	158.36	483.00	603.75	311.61	311.61	241.50
				2.99	135.91	161.62	161.62	98.03	299.00	373.75	192.90	192.90	149.50
				6.48	294.55	350.27	350.27	212.46	648.00	810.00	418.06	418.06	324.00
25	Santonian	NMNS_DS00090_20190228_c1_wl_01_0001.jpg–0732.jpg	1	2.33	105.91	125.95	125.95	76.39	233.00	291.25	150.32	150.32	116.50
27	Campanian	NMNS_DS00073_20181212_c1_wl_01_0001.jpg–0893.jpg	10	1.46	66.36	78.92	78.92	47.87	146.00	182.50	94.19	94.19	73.00
				2.19	99.55	118.38	118.38	71.80	219.00	273.75	141.29	141.29	109.50
				0.93	42.27	50.27	50.27	30.49	93.00	116.25	60.00	60.00	46.50
				2.09	95.00	112.97	112.97	68.52	209.00	261.25	134.84	134.84	104.50
				0.93	42.27	50.27	50.27	30.49	93.00	116.25	60.00	60.00	46.50
				1.47	66.82	79.46	79.46	48.20	147.00	183.75	94.84	94.84	73.50
				1.59	72.27	85.95	85.95	52.13	159.00	198.75	102.58	102.58	79.50
				2.15	97.73	116.22	116.22	70.49	215.00	268.75	138.71	138.71	107.50
				1.75	79.55	94.59	94.59	57.38	175.00	218.75	112.90	112.90	87.50
				1.18	53.64	63.78	63.78	38.69	118.00	147.50	76.13	76.13	59.00
28	Campanian	NMNS_DS00097_wl_01_0001.jpg–0920.jpg	4	1.82	82.73	98.38	98.38	59.67	182.00	227.50	117.42	117.42	91.00
				2.64	120.00	142.70	142.70	86.56	264.00	330.00	170.32	170.32	132.00
				1.14	51.82	61.62	61.62	37.38	114.00	142.50	73.55	73.55	57.00
				2.87	130.45	155.14	155.14	94.10	287.00	358.75	185.16	185.16	143.50
29	Campanian	NMNS_DS00134_wl_01_0001.tif–1690.tif	1	2.46	111.82	132.97	132.97	80.66	246.00	307.50	158.71	158.71	123.00
30	Campanian	NMNS_DS00175_wl_01_0001.tif–1176.tif	9	2.70	122.73	145.95	145.95	88.52	270.00	337.50	174.19	174.19	135.00
				2.09	95.00	112.97	112.97	68.52	209.00	261.25	134.84	134.84	104.50
				1.03	46.82	55.68	55.68	33.77	103.00	128.75	66.45	66.45	51.50
				1.83	83.18	98.92	98.92	60.00	183.00	228.75	118.06	118.06	91.50
				1.73	78.64	93.51	93.51	56.72	173.00	216.25	111.61	111.61	86.50
				1.52	69.09	82.16	82.16	49.84	152.00	190.00	98.06	98.06	76.00
				2.33	105.91	125.95	125.95	76.39	233.00	291.25	150.32	150.32	116.50
				1.82	82.73	98.38	98.38	59.67	182.00	227.50	117.42	117.42	91.00
				2.01	91.36	108.65	108.65	65.90	201.00	251.25	129.68	129.68	100.50
31	Campanian	NMNS_DS00171_wl_01_0001.tif–1421.tif	2	2.52	114.55	136.22	136.22	82.62	252.00	315.00	162.58	162.58	126.00
				2.70	122.73	145.95	145.95	88.52	270.00	337.50	174.19	174.19	135.00
32	Campanian	NMNS_DS00182_wl_01_0001.tif–1060.tif	4	2.27	103.18	122.70	122.70	74.43	227.00	283.75	146.45	146.45	113.50
				3.20	145.45	172.97	172.97	104.92	320.00	400.00	206.45	206.45	160.00
				2.63	119.55	142.16	142.16	86.23	263.00	328.75	169.68	169.68	131.50
				3.28	149.09	177.30	177.30	107.54	328.00	410.00	211.61	211.61	164.00
33	Maastrichtian	NMNS_DS00128_wl_01_0001.jpg–1200.jpg	20	2.34	106.36	126.49	126.49	76.72	234.00	292.50	150.97	150.97	117.00
				1.88	85.45	101.62	101.62	61.64	188.00	235.00	121.29	121.29	94.00
				2.64	120.00	142.70	142.70	86.56	264.00	330.00	170.32	170.32	132.00
				1.72	78.18	92.97	92.97	56.39	172.00	215.00	110.97	110.97	86.00
				3.04	138.18	164.32	164.32	99.67	304.00	380.00	196.13	196.13	152.00
				3.00	136.36	162.16	162.16	98.36	300.00	375.00	193.55	193.55	150.00
				2.04	92.73	110.27	110.27	66.89	204.00	255.00	131.61	131.61	102.00
				2.59	117.73	140.00	140.00	84.92	259.00	323.75	167.10	167.10	129.50
				1.08	49.09	58.38	58.38	35.41	108.00	135.00	69.68	69.68	54.00
				1.42	64.55	76.76	76.76	46.56	142.00	177.50	91.61	91.61	71.00
				2.49	113.18	134.59	134.59	81.64	249.00	311.25	160.65	160.65	124.50
				2.52	114.55	136.22	136.22	82.62	252.00	315.00	162.58	162.58	126.00
				1.97	89.55	106.49	106.49	64.59	197.00	246.25	127.10	127.10	98.50
				2.67	121.36	144.32	144.32	87.54	267.00	333.75	172.26	172.26	133.50
				2.68	121.82	144.86	144.86	87.87	268.00	335.00	172.90	172.90	134.00
				1.89	85.91	102.16	102.16	61.97	189.00	236.25	121.94	121.94	94.50
				2.40	109.09	129.73	129.73	78.69	240.00	300.00	154.84	154.84	120.00
				2.70	122.73	145.95	145.95	88.52	270.00	337.50	174.19	174.19	135.00
				2.61	118.64	141.08	141.08	85.57	261.00	326.25	168.39	168.39	130.50
				2.79	126.82	150.81	150.81	91.48	279.00	348.75	180.00	180.00	139.50
34	Maastrichtian	NMNS_DS00172_wl_01_0001.tif–1310.tif	2	1.11	50.45	60.00	60.00	36.39	111.00	138.75	71.61	71.61	55.50
				4.49	204.09	242.70	242.70	147.21	449.00	561.25	289.68	289.68	224.50
35	Maastrichtian	NMNS_DS00174_wl_01_0001.tif–1159.tif	2	2.07	94.09	111.89	111.89	67.87	207.00	258.75	133.55	133.55	103.50
				3.33	151.36	180.00	180.00	109.18	333.00	416.25	214.84	214.84	166.50

Table 7. (continued)

Sample No.	Geological age	Collection No. of cross-sectional image (NMNS: National Museum of Nature and Science, Tokyo)	Number of measurable teleost vertebrae	VL (mm)	TL (mm) estimated from the relationship between VL (mm) and TL (mm) of modern teleost fishes (Watt et al., 1997)[39]									
					Scophthalmus maximus : exp(0.8568 × ln(VL) + 4.3694)	*Lepidorhombus whiffiagonis* : exp(0.9400 × ln(VL) + 4.2805)	*Pleuronectes platessa* : exp(0.9520 × ln(VL) + 4.4671)	*Limanda limanda* : exp(0.9802 × ln(VL) + 4.2920)	*Platichthys flesus* : exp(0.8605 × ln(VL) + 4.3757)	*Glyptocephalus cynoglossus* : exp(0.9135 × ln(VL) + 4.6402)	*Microstomus kitt* : exp(0.9124 × ln(VL) + 4.4164)	*Hippoglossoides platessoides* : exp(0.8832 × ln(VL) + 4.4390)	*Hippoglossus hippoglossus* : 84.52 × VL + 34.39	*Buglossidium luteum* : exp(0.9427 × ln(VL) + 4.2338)
1	Albian	NMNS_DS00178_wl_01_0001.tif–1400.tif	3	2.58	177.94	176.17	214.73	185.12	179.70	246.17	196.60	195.60	252.45	168.56
				2.09	148.56	144.52	175.72	150.59	149.91	203.08	162.23	162.40	211.04	138.20
				2.50	173.21	171.03	208.39	179.50	174.89	239.18	191.03	190.24	245.69	163.63
3	Albian	NMNS_DS00224_wl_01_0001.tif–1485.tif	1	2.37	165.46	162.65	198.06	170.34	167.04	227.80	181.94	181.47	234.70	155.59
4	Albian	NMNS_DS00249_wl_01_0001.tif–1540.tif	1	1.54	114.36	108.46	131.39	111.63	115.27	153.64	122.78	124.01	164.55	103.63
8	Cenomanian	NMNS_DS00082_20190127_c1_wl_01_0001.jpg–0933.jpg	6	1.88	135.68	130.83	158.87	135.74	136.85	184.36	147.29	147.90	193.29	125.07
				2.16	152.82	149.07	181.32	155.53	154.22	209.28	167.18	167.19	216.95	142.56
				2.32	162.46	159.42	194.08	166.82	164.00	223.40	178.44	178.09	230.48	152.50
				1.57	116.27	110.44	133.82	113.77	117.20	156.38	124.96	126.14	167.09	105.53
				2.93	198.44	198.54	242.38	209.71	200.49	276.50	220.79	218.86	282.03	190.03
				2.36	164.86	162.01	197.26	169.64	166.43	226.92	181.24	180.80	233.86	154.97
10	Turonian	NMNS_DS00009_20170720_c1_wl_01_0001.jpg–1257.jpg	13	0.99	78.32	71.60	86.27	72.40	78.81	102.62	82.04	83.94	118.06	68.33
				1.44	107.97	101.83	123.25	104.52	108.80	144.50	115.48	116.87	156.10	97.28
				1.10	85.72	79.05	95.38	80.27	86.29	112.99	90.32	92.13	127.36	75.46
				1.43	107.32	101.16	122.44	103.81	108.15	143.59	114.75	116.15	155.25	96.64
				1.28	97.60	91.15	110.18	93.13	98.31	129.76	103.71	105.32	142.58	87.05
				1.02	80.35	73.63	88.76	74.55	80.86	105.46	84.31	86.18	120.60	70.28
				1.38	104.10	97.83	118.36	100.25	104.88	138.99	111.08	112.56	151.03	93.45
				1.10	85.72	79.05	95.38	80.27	86.29	112.99	90.32	92.13	127.36	75.46
				1.27	96.95	90.48	109.36	92.41	97.65	128.84	102.97	104.60	141.73	86.41
				1.17	90.37	83.77	101.15	85.28	90.99	119.54	95.55	97.29	133.28	79.98
				1.17	90.37	83.77	101.15	85.28	90.99	119.54	95.55	97.29	133.28	79.98
				1.34	101.51	95.16	115.09	97.40	102.26	135.31	108.14	109.67	147.65	90.89
				1.40	105.39	99.16	119.99	101.68	106.19	140.83	112.55	114.00	152.72	94.73
11	Turonian	NMNS_DS00040_20180409_c1_wl_01_0001.jpg–0800.jpg	6	1.16	89.71	83.10	100.32	84.56	90.33	118.60	94.80	96.55	132.43	79.34
				2.22	156.44	152.96	186.11	159.77	157.90	214.59	171.41	171.29	222.02	146.29
				3.62	237.85	242.21	296.43	258.01	240.50	335.42	267.78	263.81	340.35	231.96
				1.97	141.22	136.71	166.10	142.11	142.47	192.40	153.71	154.14	200.89	130.71
				2.83	192.62	192.17	234.50	202.69	194.58	267.87	213.91	212.25	273.58	183.91
				1.06	83.04	76.35	92.07	77.41	83.58	109.23	87.32	89.16	123.98	72.87
15	Turonian	NMNS_DS00141_wl_02_0001.tif–1615.tif	3	1.76	128.22	122.96	149.20	127.25	129.30	173.58	138.68	139.53	183.15	117.53
				4.22	271.25	279.76	343.03	299.86	274.43	385.87	308.00	302.07	391.06	268.04
				1.05	82.37	75.67	91.25	76.69	82.90	108.29	86.57	88.42	123.14	72.23
16	Turonian	NMNS_DS00173_wl_01_0001.tif–1400.tif	1	2.60	179.12	177.45	216.32	186.53	180.90	247.91	197.99	196.94	254.14	169.79
17	Coniacian	NMNS_DS00034_20180207_c1_wl_01_0001.jpg–0800.jpg	5	1.62	119.43	113.75	137.88	117.32	120.40	160.92	128.58	129.68	171.31	108.70
				2.58	177.94	176.17	214.73	185.12	179.70	246.17	196.60	195.60	252.45	168.56
				0.87	70.11	63.41	76.29	63.78	70.52	91.19	72.92	74.89	107.92	60.49
				6.38	386.52	412.60	508.42	449.65	391.64	562.88	449.09	435.16	573.63	395.75
				1.57	116.27	110.44	133.82	113.77	117.20	156.38	124.96	126.14	167.09	105.53
19	Coniacian	NMNS_DS00083_20190130_c1_wl_01_0001.jpg–0900.jpg	15	1.04	81.70	74.99	90.42	75.98	82.22	107.34	85.81	87.68	122.29	71.58
				1.44	107.97	101.83	123.25	104.52	108.80	144.50	115.48	116.87	156.10	97.28
				2.64	181.48	180.01	219.48	189.34	183.29	251.39	200.77	199.62	257.52	172.25
				1.30	98.91	92.49	111.82	94.55	99.63	131.61	105.19	106.77	144.27	88.33
				1.84	133.20	128.21	155.65	132.91	134.34	180.77	144.42	145.12	189.91	122.56
				1.55	115.00	109.12	132.20	112.35	115.91	154.55	123.50	124.72	165.40	104.27
				0.85	68.73	62.04	74.62	62.35	69.12	89.28	71.39	73.37	106.23	59.18
				1.38	104.10	97.83	118.36	100.25	104.88	138.99	111.08	112.56	151.03	93.45
				1.15	89.05	82.42	99.50	83.85	89.65	117.67	94.06	95.82	131.59	78.69
				2.07	147.34	143.22	174.12	149.18	148.67	201.30	160.81	161.03	209.35	136.96
				1.87	135.06	130.18	158.06	135.04	136.23	183.46	146.57	147.21	192.44	124.45
				2.55	176.17	174.24	212.36	183.01	177.90	243.55	194.51	193.59	249.92	166.71
				3.71	242.91	247.86	303.45	264.30	245.63	343.03	273.85	269.59	347.96	237.39
				1.77	128.85	123.62	150.01	127.95	129.93	174.48	139.40	140.23	183.99	118.16
				2.04	145.51	141.27	171.71	147.06	146.82	198.64	158.68	158.96	206.81	135.08
20	Coniacian	NMNS_DS00089_20190223_c1_wl_01_0001.jpg–0836.jpg	3	2.96	200.17	200.45	244.74	211.81	202.25	279.09	222.86	220.84	284.57	191.87
				0.86	69.42	62.72	75.45	63.06	69.82	90.24	72.15	74.13	107.08	59.84
				1.89	136.29	131.48	159.67	136.45	137.48	185.25	148.00	148.60	194.13	125.70
22	Santonian	NMNS_DS00011_20170806_c1_wl_01_0001.jpg–1000.jpg	3	3.62	237.85	242.21	296.43	258.01	240.50	335.42	267.78	263.81	340.35	231.96
				3.12	209.41	210.62	257.32	223.03	211.62	292.84	233.82	231.35	298.09	201.63
				1.58	116.90	111.11	134.64	114.48	117.84	157.28	125.68	126.85	167.93	106.17

Table 7. (continued)

Sample No.	Geological age	Collection No. of cross-sectional image (NMNS: National Museum of Nature and Science, Tokyo)	Number of measurable teleost vertebrae	VL (mm)	TL (mm) estimated from the relationship between VL (mm) and TL (mm) of modern teleost fishes (Watt et al., 1997)[39]									
					Scophthalmus maximus : exp(0.8568 × ln(VL) + 4.3694)	*Lepidorhombus whiffiagonis* : exp(0.9400 × ln(VL) + 4.2805)	*Pleuronectes platessa* : exp(0.9520 × ln(VL) + 4.4671)	*Limanda limanda* : exp(0.9802 × ln(VL) + 4.2920)	*Platichthys flesus* : exp(0.8605 × ln(VL) + 4.3757)	*Glyptocephalus cynoglossus* : exp(0.9135 × ln(VL) + 4.6402)	*Microstomus kitt* : exp(0.9124 × ln(VL) + 4.4164)	*Hippoglossoides platessoides* : exp(0.8832 × ln(VL) + 4.4390)	*Hippoglossus hippoglossus* : 84.52 × VL + 34.39	*Buglossidium luteum* : exp(0.9427 × ln(VL) + 4.2338)
23	Santonian	NMNS_DS00039_20180406_c1_wl_01_0001.jpg–0500.jpg	1	1.80	130.71	125.59	152.43	130.08	131.83	177.18	141.56	142.33	186.53	120.05
24	Santonian	NMNS_DS00042_20180419_c1_wl_02_0001.jpg–0601.jpg	3	4.83	304.52	317.62	390.08	342.29	308.23	436.51	348.38	340.33	442.62	304.42
				2.99	201.91	202.36	247.10	213.92	204.01	281.67	224.92	222.82	287.10	193.70
				6.48	391.71	418.68	516.01	456.56	396.92	570.94	455.51	441.18	582.08	401.59
25	Santonian	NMNS_DS00090_20190228_c1_wl_01_0001.jpg–0732.jpg	1	2.33	163.06	160.07	194.88	167.52	164.61	224.28	179.14	178.76	231.32	153.12
27	Campanian	NMNS_DS00073_20181212_c1_wl_01_0001.jpg–0893.jpg	10	1.46	109.25	103.15	124.88	105.95	110.10	146.34	116.94	118.30	157.79	98.55
				2.19	154.63	151.01	183.71	157.65	156.06	211.94	169.29	169.24	219.49	144.43
				0.93	74.23	67.51	81.29	68.09	74.68	96.92	77.49	79.43	112.99	64.42
				2.09	148.56	144.52	175.72	150.59	149.91	203.08	162.23	162.40	211.04	138.20
				0.93	74.23	67.51	81.29	68.09	74.68	96.92	77.49	79.43	112.99	64.42
				1.47	109.89	103.82	125.70	106.66	110.74	147.25	117.67	119.02	158.63	99.19
				1.59	117.53	111.77	135.45	115.19	118.48	158.19	126.41	127.56	168.78	106.80
				2.15	152.21	148.42	180.52	154.83	153.61	208.40	166.47	166.51	216.11	141.94
				1.75	127.60	122.31	148.39	126.54	128.67	172.67	137.96	138.83	182.30	116.90
				1.18	91.03	84.44	101.97	85.99	91.66	120.47	96.29	98.02	134.12	80.63
28	Campanian	NMNS_DS00097_wl_01_0001.jpg–0920.jpg	4	1.82	131.96	126.90	154.04	131.50	133.09	178.97	142.99	143.72	188.22	121.31
				2.64	181.48	180.01	219.48	189.34	183.29	251.39	200.77	199.62	257.52	172.25
				1.14	88.38	81.75	98.68	83.13	88.98	116.73	93.31	95.08	130.74	78.05
				2.87	194.95	194.72	237.65	205.50	196.95	271.32	216.67	214.90	276.96	186.36
29	Campanian	NMNS_DS00134_wl_01_0001.tif–1690.tif	1	2.46	170.83	168.45	205.21	176.68	172.48	235.69	188.24	187.55	242.31	161.16
30	Campanian	NMNS_DS00175_wl_01_0001.tif–1176.tif	9	2.70	185.01	183.86	224.23	193.56	186.87	256.60	204.92	203.62	262.59	175.94
				2.09	148.56	144.52	175.72	150.59	149.91	203.08	162.23	162.40	211.04	138.20
				1.03	81.02	74.31	89.59	75.26	81.54	106.40	85.06	86.93	121.45	70.93
				1.83	132.58	127.56	154.84	132.20	133.72	179.87	143.71	144.42	189.06	121.94
				1.73	126.35	120.99	146.78	125.12	127.40	170.87	136.52	137.43	180.61	115.64
				1.52	113.09	107.13	129.76	110.21	113.98	151.82	121.32	122.59	162.86	102.36
				2.33	163.06	160.07	194.88	167.52	164.61	224.28	179.14	178.76	231.32	153.12
				1.82	131.96	126.90	154.04	131.50	133.09	178.97	142.99	143.72	188.22	121.31
				2.01	143.68	139.32	169.31	144.94	144.96	195.97	156.55	156.90	204.28	133.21
31	Campanian	NMNS_DS00171_wl_01_0001.tif–1421.tif	2	2.52	174.39	172.31	209.98	180.90	176.10	240.93	192.42	191.58	247.38	164.86
				2.70	185.01	183.86	224.23	193.56	186.87	256.60	204.92	203.62	262.59	175.94
32	Campanian	NMNS_DS00182_wl_01_0001.tif–1060.tif	4	2.27	159.46	156.19	190.10	163.29	160.95	219.00	174.93	174.69	226.25	149.40
				3.20	214.00	215.69	263.60	228.63	216.28	299.69	239.29	236.58	304.85	206.50
				2.63	180.89	179.37	218.69	188.64	182.69	250.52	200.07	198.95	256.68	171.64
				3.28	218.58	220.76	269.87	234.23	220.93	306.52	244.74	241.80	311.62	211.36
33	Maastrichtian	NMNS_DS00128_wl_01_0001.jpg–1200.jpg	20	2.34	163.66	160.72	195.67	168.23	165.22	225.16	179.84	179.44	232.17	153.74
				1.88	135.68	130.83	158.87	135.74	136.85	184.36	147.29	147.90	193.29	125.07
				2.64	181.48	180.01	219.48	189.34	183.29	251.39	200.77	199.62	257.52	172.25
				1.72	125.72	120.34	145.97	124.41	126.77	169.97	135.80	136.73	179.76	115.01
				3.04	204.80	205.54	251.03	217.42	206.95	285.97	228.35	226.10	291.33	196.75
				3.00	202.49	203.00	247.89	214.62	204.60	282.53	225.60	223.47	287.95	194.31
				2.04	145.51	141.27	171.71	147.06	146.82	198.64	158.68	158.96	206.81	135.08
				2.59	178.53	176.81	215.53	185.83	180.30	247.04	197.29	196.27	253.30	169.17
				1.08	84.38	77.70	93.73	78.84	84.94	111.11	88.82	90.65	125.67	74.17
				1.42	106.68	100.50	121.62	103.10	107.49	142.67	114.02	115.43	154.41	96.00
				2.49	172.61	170.38	207.60	178.79	174.29	238.31	190.33	189.56	244.84	163.01
				2.52	174.39	172.31	209.98	180.90	176.10	240.93	192.42	191.58	247.38	164.86
				1.97	141.22	136.71	166.10	142.11	142.47	192.40	153.71	154.14	200.89	130.71
				2.67	183.25	181.94	221.86	191.45	185.08	254.00	202.85	201.62	260.06	174.10
				2.68	183.84	182.58	222.65	192.15	185.67	254.87	203.54	202.28	260.90	174.71
				1.89	136.29	131.48	159.67	136.45	137.48	185.25	148.00	148.60	194.13	125.70
				2.40	167.25	164.59	200.45	172.45	168.86	230.43	184.04	183.50	237.24	157.45
				2.70	185.01	183.86	224.23	193.56	186.87	256.60	204.92	203.62	262.59	175.94
				2.61	179.71	178.09	217.11	187.23	181.49	248.78	198.68	197.61	254.99	170.41
				2.79	190.28	189.61	231.34	199.88	192.21	264.41	211.15	209.60	270.20	181.46
34	Maastrichtian	NMNS_DS00172_wl_01_0001.tif–1310.tif	2	1.11	86.39	79.73	96.20	80.99	86.96	113.92	91.07	92.87	128.21	76.11
				4.49	286.06	296.56	363.89	318.66	289.47	408.36	325.93	319.08	413.88	284.18
35	Maastrichtian	NMNS_DS00174_wl_01_0001.tif–1159.tif	2	2.07	147.34	143.22	174.12	149.18	148.67	201.30	160.81	161.03	209.35	136.96
				3.33	221.43	223.92	273.78	237.73	223.82	310.79	248.14	245.05	315.84	214.40

Table 8. Estimated body size of teleosts in the Late Cretaceous.

Geological age	Number of measurable vertebrae	Estimated total length (mm) (for details see Table 7)			
		Average	Median	Lower Quartile	Upper Quartile
Albian	5	160.22	159.53	126.80	189.50
Cenomanian	6	159.32	155.25	123.81	189.78
Turonian	23	122.06	100.91	78.08	143.11
Coniacian	23	144.52	122.21	87.00	173.01
Santonian	8	238.93	209.16	143.77	304.44
Campanian	30	145.70	140.06	101.84	182.23
Maastrichtian	24	172.68	169.07	127.05	205.77

References for Chapter 1

1. Tittensor, D. P. *et al.* Global patterns and predictors of marine biodiversity across taxa. *Nature* **466**, 1098–1101 (2010).
2. Boyle, P. & Rodhouse, P. *Cephalopods: Ecology and Fisheries*. (Blackwell Science, Oxford, 2005).
3. Cai, J., Townsend, J. P., Dodson, T. C., Heiney, P. A. & Sweeney, A. M. Eye patches: Protein assembly of index-gradient squid lenses. *Science* **357**, 564–569 (2017).
4. Huffard, C. L., Boneka, F. & Full, R. J. Underwater Bipedal Locomotion by Octopuses in Disguise. *Science* **307**, 1927–1927 (2005).
5. Albertin, C. B. *et al.* Genome and transcriptome mechanisms driving cephalopod evolution. *Nat. Commun.* **13**, 2427 (2022).
6. Amodio, P. *et al.* Grow smart and die young: why did cephalopods evolve intelligence? *Trends Ecol. Evol.* **34**, 45–56 (2019).
7. Packard, A. Cephalopods and fish: the limits of convergence. *Biol. Rev.* **47**, 241–307 (1972).
8. Visser, F. *et al.* Deep-sea predator niche segregation revealed by combined cetacean biologging and eDNA analysis of cephalopod prey. *Science Advances* **7**, eabf5908 (2021).
9. Dedman, S. *et al.* Ecological roles and importance of sharks in the Anthropocene Ocean. *Science* **385**, adl2362 (2024).
10. Kröger, B., Vinther, J. & Fuchs, D. Cephalopod origin and evolution: A congruent picture emerging from fossils, development and molecules. *BioEssays* **33**, 602–613 (2011).
11. Fuchs, D., & Iba, Y. The gladiuses in coleoid cephalopods: homology, parallelism, or convergence? *Swiss J. Palaeontol*. **134**, 187–197 (2015).
12. Neige, P., Lapierre, H. & Merle, D. New Eocene coleoid (Cephalopoda) diversity from statolith remains: taxonomic assignation, fossil record analysis, and new data for calibrating molecular phylogenies. *PLoS One* **11**, e0154062 (2016).
13. Tanner, A. R. *et al.* Molecular clocks indicate turnover and diversification of modern coleoid cephalopods during the Mesozoic Marine Revolution. *Proc. R. Soc. B.* **284**, 20162818 (2017).
14. López-Córdova, D. A., Avaria-Llautureo, J., Ulloa, P. M., Braid, H. E., Revell, L. J., Fuchs, D., & Ibáñez, C. M. Mesozoic origin of coleoid cephalopods and their abrupt shifts of diversification patterns. *Mol. Phylogenet. Evol*. **166**, 107331 (2022).
15. Clements, T., Colleary, C., De Baets, K. & Vinther, J. Buoyancy mechanisms limit preservation of coleoid cephalopod soft tissues in Mesozoic Lagerstätten. *Palaeontology* **60**, 1–14 (2017).
16. *Ammonoid Paleobiology: From Anatomy to Ecology*. vol. 43 (Springer, 2015).
17. Clarke, M. R. & Maddock, L. Beaks of living coleoid Cephalopoda. in *Paleontology and neontology of cephalopods* (eds. Clarke, M. R. & Trueman, E. R.) 123–131 (Academic Press, Cambridge, 1988).

18. Clarke, M. R. Significance of cephalopod beaks. *Nature* **193**, 560–561 (1962).

19. Clarke, M. R. *A Handbook for the Identification of Cephalopod Beaks*. (Clarendon Press, Oxford, 1986).

20. Hernández-García, V. Growth and pigmentation process of the beaks of *Todaropsis Eblanae* (Cephalopoda: Ommastrephidae). *Berl. Paläobiol. Abh.* **3**, 131–140 (2003).

21. Takashima, R. *et al.* Geology and stratigraphy of forearc basin sediments in Hokkaido, Japan: Cretaceous environmental events on the north-west Pacific margin. *Cret. Res.* **25**, 365–390 (2004).

22. Obradovich, J. D., Matsumoto, T., Nishida, T. & Inoue, Y. Integrated biostratigraphic and radiometric study on the Lower Cenomanian (Cretaceous) of Hokkaido, Japan. *Proc. Jap. Acad., Ser. B* **78**, 149–153 (2002).

23. Asai A. & Hirano H. Stratigraphy of the Upper Cretaceous in the Obira area, Northwestern Hokkaido. *Acad. Stud., Biol. Earth Sci, Sch. Edu., Waseda Univ.* **39**, p37-50 (1990).

24. Tanabe K., Hirano H., Matsumoto T. & Miyata Y. Stratigraphy of the Upper Cretaceous deposits in the Obira area, northwestern Hokkaido. *Sci. Rep., Dep. Geol., Kyushu Univ.* **12**, 181–202 (1977).

25. Takahashi, A., Hikida, Y., Jenkins, R. G. & Tanabe, K. Stratigraphy and megafauna of the Upper Cretaceous Yezo Supergroup in the Teshionakagawa area, northern Hokkaido, Japan. *Bull. Mikasa City Mus.* **11**, 25–59 (2007).

26. Okamoto T., Matsunaga T. & Okada M. Restudy of the Upper Cretaceous stratigraphy in the Haboro area, northwestern Hokkaido. *J. Geol. Soc. Jap.* **109**, 363–382 (2003).

27. Toshimitsu, S. Biostratigraphy of the Upper Cretaceous Santonian Stage in Northwestem Hokkaido. *Mem. Fac. Sci., Kyushu Univ., Ser. D, Geol.* **26**, 125–192 (1988).

28. Kawabe S. & Okamoto T. Restudy of the Upper Cretaceous megafossil biostratigraphy in the Migi-no-sawa area, a tributary of the Haboro River, northwestern Hokkaido. *J. Geol. Soc. Jap.* **118**, 769–781 (2012).

29. Osanai, H. Mitani, K. Takahashi, K. *Explanatory text of the geological map of Japan 'Kyowa' (scale 1:50000)*. (Geological Survey of Hokkaido, Sapporo, 1960).

30. Shigeta, Y. & Izukura, M. Discovery of the middle Campanian (late Cretaceous) "Soya Fauna" ammonoids in the Hidaka area, Hokkaido, Japan. *Bull. Hobetsu Mus.* **33**, 11–25 (2018).

31. Ando, H. & Tomosugi, T. Unconformity between the Upper Maastrichtian and Upper Paleocene in the Hakobuchi Formation, north Hokkaido, Japan: a major time gap within the Yezo forearc basin sediments. *Cret. Res.* **26**, 85–95 (2005).

32. Shigeta, Y., Izukura, M. & Tsutsumi, Y. An early Maastrichtian (latest Cretaceous) ammonoid fauna from the Soya Hill area, Hokkaido, northern Japan. *Bull. Hobetsu Mus.* **32**, 7–41 (2017).

33. Mehra, A., Watters, W. A., Grotzinger, J. P. & Maloof, A. C. Three-dimensional reconstructions of the putative metazoan *Namapoikia* show that it was a microbial construction. *Proc. Natl. Acad. Sci. USA* **117**, 19760–19766 (2020).

34. Tanabe, K., Hikida, Y. & Iba, Y. Two coleoid jaws from the Upper Cretaceous of Hokkaido, Japan. *J. Paleontol.* **80**, 138–145 (2006).

35. Tanabe, K., Misaki, A. & Ubukata, T. Late Cretaceous record of large soft-bodied coleoids based on lower jaw remains from Hokkaido, Japan. *Acta Palaeontol. Pol.* **60**, 27–38 (2015).

36. Tanabe, K. & Misaki, A. Upper Cretaceous record of non-belemnitid coleoid jaws from Hokkaido, Japan, and its evolutionary implications. *Cret. Res.* **151**, 105624 (2023).

37. Young, R. E., Clarke, M. R., Vecchione, M. & Mangold, K. M. Beak terminology. *Tree of Life* http://tolweb.org/notes/?note_id=1980 (2000).

38. International Commission on Zoological Nomenclature. Declaration 45 — Addition of Recommendations to Article 73 and of the term "specimen, preserved" to the Glossary. *Bull. Zool. Nomencl.* **73**, 96–97 (2017).

39. Watt, J., Pierce, G. & Boyle, P. R. Guide to the identification of North Sea fish using premaxillae and vertebrae. *ICES Coop. Res. Rep.* **220**, 1–235 (1997).

40. Lu, C.-C. A new family of myopsid squid from Australasian waters (Cephalopoda: Teuthida). *Phuket Mar. Biol. Center Res. Bull* **66**, 71–82 (2005).

41. Clarke, M. R. The identification of cephalopod 'beaks' and the relationship between beak size and total body weight. *Bull. Br. Mus. nat. Hist. (Zool.)* **8**, 419–480 (1962).

42. Young, R. E. Introduction to upper beak types. *Tree of Life* http://tolweb.org/notes/?note_id=5664 (2014).

43. Neige, P. & Dommergues, J. L. Disparity of beaks and statoliths of some coleoids: a morphometric approach to depict shape differentiation. *Abh. Geol. B. -A* **57**, 393–399 (2002).

44. Young, R. E. Beak structure and evolution. *Tree of Life* http://tolweb.org/notes/?note_id=4541 (2007).

45. Fuchs, D. *et al. Longibelus* gen. nov., A new Cretaceous coleoid genus linking Belemnoidea and early Decabrachia. *Palaeontology* **56**, 1081–1106 (2013).

46. Doyle, P. A review of the biogeography of Cretaceous belemnites. *Palaeogeography, Palaeoclimatology, Palaeoecology* **92**, 207–216 (1992).

47. Iba, Y. *et al.* Belemnite extinction and the origin of modern cephalopods 35 m.y. prior to the Cretaceous-Paleogene event. *Geology* **39**, 483–486 (2011).

48. Yoshida, H. *et al.* Early post-mortem formation of carbonate concretions around tusk-shells over week-month timescales. *Sci. Rep.* **5**, 1–7 (2015).

49. Nelson, J. S., Grande, T. C. & Wilson, M. V. H. *Fishes of the World*. (John Wiley & Sons, New York, 2016).

50. Tanabe, K. The feeding habits of ammonites. *Science* **331**, 37–38 (2011).

51. Arkhipkin, A. I. *et al.* World squid fisheries. *Rev. Fish. Sci. Aquac.* **23**, 92–252 (2015).

52. Roth, G. Convergent evolution of complex brains and high intelligence. *Philos. Trans. R. Soc. B: Biol.* **370**, 20150049 (2015).

53. Hatton, I. A., Heneghan, R. F., Bar-On, Y. M. & Galbraith, E. D. The global ocean size spectrum from bacteria to whales. *Sci. Adv.* **7**, eabh3732 (2021).

54. Marx, F. G. & Uhen, M. D. Climate, Critters, and Cetaceans: Cenozoic Drivers of the Evolution of Modern Whales. *Science* **327**, 993–996 (2010).

55. Alfaro, M. E. *et al.* Explosive diversification of marine fishes at the Cretaceous–Palaeogene boundary. *Nat. Ecol. Evol.* **2**, 688–696 (2018).

Chapter 2. Octopoda

Summary

Large-sized carnivorous vertebrates dominated the top of the marine food chain for 400 million years, impacting biodiversity and ecosystems. In response most invertebrates developed defence systems against these predators. Octopuses followed a different strategy, they attained sophisticated hunting organs and cognition systems, by convergent evolution with vertebrates. Like vertebrate top predators, octopuses and their stem groups developed several extremely large-sized taxa in their evolutionary history, but their feeding habits remain so far completely unknown. Here I report the oldest and largest octopuses, which were top predators in the marine ecosystem during the Late Cretaceous (~100–72 Ma). These findings are based on huge, exceptionally well-preserved fossil jaws and their wear. The calculated body size of ~7 to 18 meters makes these octopuses the largest invertebrates ever and matches the size of co-existing giant marine reptiles, including plesiosaurs and mosasaurs. Extensive wear on the fossil jaws provides evidence for a dynamic crushing of hard skeletons. Severe fractures in the wear indicate extremely strong biting forces that induce a high lethality. These findings reveal that this gigantism of octopuses transformed the long-established structure of the marine ecosystem, in which only vertebrates dominated the top of the food chain.

2.1. Introduction

Top predators are key drivers for changes in biodiversity and ecosystem structure by generating a high predation pressure[1–3]. The evolution of strong jaws and an increase in body size are principal factors that transform animals into top predators, by gaining physical strength, mobility, and cognition[3–7]. Advanced morphological complexity allowed vertebrates to become large and to occupy the top position in marine ecosystems for more than 400 million years, starting with the origination of the jaw[1,4,8–10]. This pattern was reinforced by iterative readaptations of tetrapod vertebrates since the early Mesozoic (~250 Ma), documented by the fossil record of marine reptiles and whales[8]. In the late Mesozoic (~200–66 Ma), the radiation of durophagous vertebrates, namely shell-crushing predators, opened a new phase in the predator-driven evolution, shaping the modern-type marine ecosystem[8,11–14]. Invertebrates of this interval primarily served as small prey, which survived this arms race by evolving hard, mineralised shells for protection[11,12,15–17].

Cephalopods followed an exceptional evolutionary pathway among invertebrates, which is convergent to that of vertebrates[18]. Jaws, an innovation that allowed efficient and carnivorous food intake, evolved contemporaneously in cephalopods and vertebrates[19]. The superorder Octobrachia, namely octopus and its stem groups, diverged in the late Mesozoic by abandoning protective shells, which improved their swimming ability[20,21]. This innovation increased the mobility, eyesight, and intelligence of octopuses, all of which rival those of vertebrates[20–22]. Octopuses are consequently thriving as mid-ranking carnivores in nowadays oceans[23–25]. The eight arms and jaws positioned at the base of these arms play a key role in their hunting behaviour[24]. Modern octopuses use their flexible arms to catch and restrain the prey. Their upper and lower jaws kill the prey by biting vital points and then dissect it into pieces. By using arms and jaws, modern octopuses prey on animals exceeding their own size[24]. The size increase of the body makes the arms longer, allowing the capture of larger prey. It also enlarges the muscles of the jaws, providing a stronger bite force that enhances their lethality[26].

Several fossil octobrachian genera of over 1 m body length have been documented from coastal and shelf environments by their chitinous jaws and imprints of soft tissues[27]. These giants were probably high-level carnivores at the time. As direct evidence like stomach content has not been found to date[28], their diet remains completely unknown. In fossil and extant cephalopods, the arm morphology does not provide any evidence for the type of food. Jaws are also no reliable indicators for specific feeding habits since their morphology varies considerably throughout cephalopod phylogeny[29]. This study uses a totally different approach, in which the wear of fossil jaws is documented and used to reconstruct the carnivorous feeding habits. The wear was caused by cracking skeletons of prey, which are harder than the jaws composed of stiffened chitin[26]. This pronounced wear of the jaws is a common feature of durophagous modern cephalopods[26,30]. To analyse the wear of fossil jaws, the jaws must be preserved three-dimensionally. Damages caused by post-mortem processes and physical preparation of the fossil must be excluded to avoid misidentification of the wear. Tracking ontogenetic changes is also necessary to distinguish erosion caused by wear from the original morphology. Extremely rare fossil specimens satisfy these requirements.

This study revisited 15 large-sized fossil jaws of Cretaceous finned octopus (order Cirrata) previously reported from Japan and Vancouver Island[31–34] (Table 9). Distinctive wear features have been observed on an exceptionally well-preserved specimen. Additionally, this study excavated 12 jaws of the Cirrata from Cretaceous rocks of Japan digitally, thus avoiding damages by physical preparation (Table 10). This technique uses high-resolution grinding tomography and a zero-shot learning AI (artificial

intelligence) model (Methods). The digital jaws include juvenile and adult specimens, allowing the identification of ontogenetic changes. All specimens originate from low-energy, outer shelf deposits without wave influence. Damage from re-sedimentation can thus be excluded. This approach enabled a precise identification of the wear and the reconstruction of the feeding habits of fossil Cirrata. Investigations on their taxonomy, stratigraphic ranges, and body size further allow a reconstruction of the position of the Cirrata in the Cretaceous marine ecosystems.

2.2. Material

The details of the previously reported specimens are documented in Table 1. That of the newly discovered ones are in Table 10. The new beaks were found from concretions formed in an outer shelf sea, low-energy environment without wave influence[35]. Their geological age assignment is based on previous chronostratigraphic studies. The studied concretions were collected by the authors and their crews in 2017–2022. All fieldwork was carried out under the permission of the Hokkaido Regional Forest Office. The detailed localities, geological ages, and horizons are documented in Table 10.

Institutional abbreviations

CDM: Courtenay and District Museum and Paleontological Center, Courtenay, British Columbia, Canada.
HMG: Hobetsu Museum, Mukawa, Hokkaido, Japan.
KMNH: Kitakyushu Museum of Natural History and Human History, Kitakyushu, Fukuoka, Japan.
NMA: Nakagawa Museum of Natural History, Nakagawa, Hokkaido, Japan.
NMNS and *NSMT*: National Museum of Nature and Science, Tsukuba, Ibaraki, Japan.

2.3. Methods

2.3.1. Digital fossil-mining and preparation

For a precise visualisation of wear on the surfaces of fossil octopod jaws, and for documenting these jaws from all ontogenetic stages, this study employed grinding tomography (Palaeobiology Lab, Hokkaido University) and a zero-shot learning artificial intelligence AI segmentation method[36].

Fossiliferous carbonate concretions were converted into sequential cross-sectional images by grinding tomography. The concretions were ground equidistant in 50 μm intervals by high-precision diamond cup wheels (diamond size ~15 μm: Asahi Diamond Industrial Co., Ltd; ~20 μm: Noritake Co., Ltd). Each surface was photographed with high-resolution digital cameras (8,688 x 5,792 pixels in EOS 5Ds, Canon; 19,008 x 12,672 pixels in α7R IV, SONY). These grinding–photographing processes were computerised, controlled numerically, and repeated automatically. The full-coloured image datasets of the fossil jaws were converted into mask data by applying a zero-shot learning AI model, the decoupled video segmentation approach (DEVA)[36]. Before segmentation, the image datasets of five jaws (Table 10) were processed by ImageJ 1.52a (National Institutes of Health) for the enhancement of contrast and denoising. This study improved the capabilities of DEVA, allowing it to use central processing units (CPU) on high-performance servers without requiring graphics processing units (GPU). The CPU-optimised DEVA was run on a Supermicro AS -4125GS-TNRT server. This unit is equipped with two CPUs (AMD EPYC 9374F, 32 cores, base clock 3.85 GHz) mounted on a motherboard (Supermicro Super H13DSG-O-CPU), 1.5 TB RAM configured with 24 modules of

64GB DDR5 (Micron MTC40F2046S1RC48BA1), and Ubuntu 24.04 through WSL2 on Microsoft Windows 11 Pro. These methods enabled a precise segmentation of the large dataset that comprises over 600 images with a dimension of 1,698 x 1,934 pixels. The sensitivity of object detection can be freely adjusted in the fork.

The output masks of the octopod jaws were unified and reconstructed as 3D models for the observations and documentation of wear, measurements, and taxonomical interpretations. These 3D models underwent minimal smoothing to avoid modifying their surface structures. They were painted in their original colours extracted from tomographic images. The operations to process the 3D models were conducted in Amira 3D 2023.2. (Thermo Fisher Scientific, Inc.). Blender 4.2.2 (Blender Foundation) was used to display the 3D models in figures.

2.3.2. Taxonomy

This study used published terminology and methods[37,38] (Fig. 17) with respect to the measurements and taxonomic classification of the octopod jaws. Only lower jaws are evaluated here since upper jaws do not show significant taxonomic features on the order level. The crest length and hood length were measured following these studies[37,38]. Additionally, in this study the length between the tip of the rostrum and a wing was measured. The previously reported specimens of fossil jaws, revisited in this study, were listed in Table 9. The data of the digitally extracted specimens, including accession numbers, measurements, and occurrences, are provided in Table 10. This document does not include nomenclatural acts. Taxonomic revisions coducted here will be published in other papers at appropriate journals.

Terminology and Measurements for Systematic Palaeontology

The following terms[37,38] were used for describing fossil squid jaws in this study.

Bridge: the strip of jaw material that connects the hood to the lateral wall on each side of the jaw (Fig. 17C).

Crest: the join at the top of the two lateral walls (Fig. 17B).

Hood: the outer part of the jaw attached to the lateral walls by the jaw edges or bridges, lying outside the lateral walls (Fig. 17B).

Hood notch: an indentation of the posterior edge of the pigmented hood in the dorsal midline.

Inner lamella: the inner one of two plates that form the jaw, consisting of two lateral walls and shoulders (Fig. 17A).

Jaw angle: the angle formed at the intersection of the jaw edge and the adjacent shoulder (Fig. 17C).

Jaw edge: the cutting edge of the lower jaw formed from the anterior ends of a lateral wall and the hood or from those of a lateral wall and the adjacent bridge (Fig. 17B).

Lateral wall: a sheet on each side of the jaw, running back from the jaw edge and medial to the hood (Fig. 17B).

Outer lamella: the inner one of the two plates that comprise the jaw, consisting of the rostrum, hood, and wings (Fig. 17B).

Rostrum: the anterior part of the hood consisting of the heavy, biting region of the jaw that includes the jaw edges (Fig. 17B).

Rostral tip: the anterior end of the rostrum where the jaw edges converge.

Shoulder: the join of wings with the anterior end of the nearest lateral wall, approximately bounded by the bridge posteriorly and including some of the wing laterally (Fig. 17C).

Wing: the part of the hood that extends anteroventrally (Fig. 17B).

Following measurements of lengths and angles[37,38] were used in this study. All measured values are documented in Table 10.

Crest length: the distance from the rostral tip to the posterior end of the crest (Fig. 17D).

Hood length: the distance from the rostral tip to the posterior end of the hood (Fig. 17D).

Length between the tip of the rostrum and a wing: the distance from the rostral tip to the posterior end of a wing (Fig. 17D)

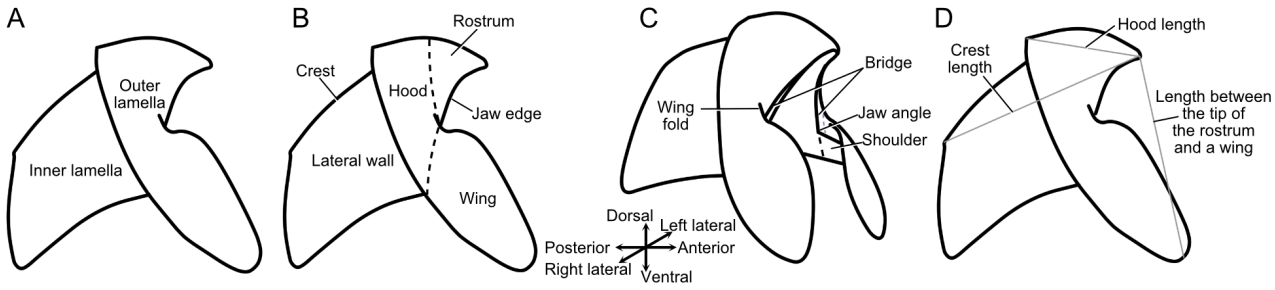


Fig. 17. Descriptive terms of the coleoid lower jaw.
(**A**) Inner and outer lamellae. (**B**) Terms for the individual parts of the lower jaw. (**C**) Morphological terms for the area near the jaw edges. (**D**) Measurements of lengths. The terms and measurements are based on published methods

2.3.3. Body size estimation

The maximum body sizes of *Nanaimoteuthis jeletzkyi* and *N. haggarti* were calculated from the largest jaw of each species based on 15 and 5 specimens, respectively. For the estimations of their mantle length (ML), this study applied measurements of these specimens to well-investigated data of the allometric relationship between the hood length (HL) and ML in extant Cirrata[39–41]. These data are documented as a correlation function at the species level, all used in this study. Among these extant species, *Cirroteuthis muelleri*, *Stauroteuthis syrtensis*, and *Grimpoteuthis* sp. belong to the long-bodied group. In contrast, the three species of *Opisthoteuthis* are assigned to the short-bodied group. The applied correlation functions and estimated mantle lengths are shown in Table 11. For estimating the maximum total length, the ratio between ML and the total length of the long-bodied group were calculated based on the comprehensive data of extant Cirrata[42] (Table 11). These data are documented for 18 species, covering all genera used for the estimations of ML.

The HL measured in fossil jaws becomes shorter than the actual value if there is a loss by erosion or wear. To avoid the underestimation induced by this false value, the original outline of the rostrum and the hood were reconstructed in the largest specimen of two fossil species. The former was identified by using striations on the jaw surface. In the lower jaw of the extant Cirrata, radial striations on the hood converge to the rostral tip[37]. The original position thus can be identified as the point where anteriorly extended lines of the striations cross. The latter were only considered in *N. jeletzkyi*, of which the posterior part of the hood is weathered. Its restoration was based on the form of the well-preserved

hood in the holotype. The estimated original HL and the depth of accumulated wear were measured based on these reconstructed outlines (Table 11).

2.3.4. Data availability

The image datasets of octopus beaks discovered here and the original tomographic images of carbonate concretions are archived in the National Museum of Nature and Science, Tokyo. The collection number of those images is listed in Table 9. The image datasets of octopus beaks include 3D models, mask data, and cross-sectional images that were cropped for annotation. These data are available from the Figshare repository at the following link: https://doi.org/10.6084/m9.figshare.27933759.

2.3.5. Code availability

The source code of the modified DEVA is available at GitHub (https://github.com/mehmetoguzderin/python-202404-nested).

2.4. Results

2.4.1. Systematic palaeontology

Superorder **Octobrachia** Fiorini, 1981

Order **Cirrata** Grimpe, 1916

Remarks. In the lower jaw of the Cirrata, the bridges are entirely hidden by the inner and outer lamellae, which in turn are exposed in the jaws of Vampyromorpha[37]. The lower jaw morphology of the Incirrata allows the recognition of a benthic and a pelagic type[37]. The lower jaws of the Cirrata differ from the benthic type by the elongated hood and from the pelagic-type by the significantly larger rostrum and gently curved jaw edges[37].

Family uncertain

Genus ***Nanaimoteuthis*** Tanabe in Tanabe et al., 2008

Emended diagnosis. The lower jaw, which has a crest length > 50 mm in adults, shows the following features. The outer lamella has almost the same height and width. The rostrum is not hooked and has no dents around the jaw edges. Jaw edges are strongly curved, single-edged, and smoothly connected to the anterior edge of a wing without forming a jaw angle. Bridges are entirely concealed by the merger part of the inner and outer lamellae. Anterior parts of the outer and inner lamellae merge directly. The hood is much longer than the rostrum. Its posterior edge shows nearly the same curvature of the lateral and medial parts in dorsal view. Wings are smooth and ventrally tapered.

Remarks. In previous studies of fossil jaws, *Nanaimoteuthis* was taxonomically included in the order Vampyromorpha, *Paleocirroteuthis* in the suborder Cirrata in the order Octopoda[31–34]. These assignments were based on an open angle of wings and the ratio between the crest and hood lengths, in which Vampyromorpha show an acuter angle[31]. These differences are, however, probably an artefact of incomplete preservation or mechanical preparation in the marginal parts of lateral walls and wings. According to the observations, both *Nanaimoteuthis* and *Paleocirroteuthis* have bridges that are entirely concealed by the merged part of the inner and outer lamellae (Fig. 18E, J, K–S, and X). With clear differences missing, both genera are here synonymised as *Nanaimoteuthis* and are classified as

Cirrata.

The diagnosis of *N. yokotai*[32,34] was based on poorly preserved jaws, the posterior parts of which are lost. These specimens are here identified as upper jaws by their wings, which are much smaller than the rostrum (Tanabe et al., 2010, Fig. 1[32]; Tanabe et al., 2017, Fig. 5[34]). Since no lower jaws of *N. yokotai* have been observed so far, the generic assignment of this species is here revised to uncertain.

Nanaimoteuthis differs from all other Cirrata genera by a nearly constant curvature of the posterior edge of the hood in its lower jaws. In other Cirrata genera this curvature in the lateral parts is less curved or slightly indented[37].

In most juveniles, the hood and lateral walls are often shorter than in adults (Fig. 18T and U). These characteristics are most probably caused by damage in depositional processes since the posterior part of the jaws shows a low stiffness in earlier ontogenetic stages[43].

Nanaimoteuthis jeletzkyi Tanabe in Tanabe et al., 2008

Paleocirroteuthis pacifica Tanabe in Tanabe et al., 2008, Fig. 7

Holotype. CDM 2006.1.1 (Tanabe et al., 2008, Fig. 3[31]).

Other materials. CDM2006.2.1 (Holotype of *P. pacifica*, Tanabe et al., 2008, Fig. 7.1–7.4[31]), NMA284 (Paratype of *P. pacifica*, Tanabe et al., 2008, Fig. 7.5–7.9[31]), KMNH IvP 902005 (Tanabe et al., 2017, Fig. 3.1[34]), HMG-1689 (Tanabe et al., 2017, Fig. 3.2[34]), NMNS_DS00068_x8HxByP.stl, NMNS_DS00173_P74Doy1.stl, NMNS_DS00042_3LmvTpM.stl, NMNS_DS00171_qbOIwTk.stl, NMNS_DS00171_kJTYO76.stl, NMNS_DS00171_qK5qb3p.stl, NMNS_DS00171_PgRMnJl.stl, NMNS_DS00171_r2SXbn2.stl, NMNS_DS00171_wmVpKjl.stl, and NMNS_DS00171_tLWPrwm.stl.

Emended diagnosis. The lower jaw, which reaches a crest length > 50 mm in adults, shows the following features. The outer lamella is as high as wide. The rostrum has no hook or dents. Jaw edges are strongly curved and single-edged. Jaw angles are absent. Bridges are entirely concealed by the merged part of the inner and outer lamellae. Anterior parts of the outer and inner lamellae merge directly. The hood is much longer than the rostrum. Its posterior edge shows nearly the same curvature for the lateral and medial parts in dorsal view. In the frontal sections of the hood, the medial part is strongly curved, and the lateral parts are nearly straight. Wings are smooth and ventrally tapered.

Description. The outer lamella shows almost the same height and width (Fig. 18E, J, and K–R). The rostrum is not hooked and has no dents outlined by a distinct fold around the jaw edges (Fig. 18A, B, F, and G). Jaw edges are strongly curved, single-edged, and smoothly connected to the anterior edge of the wing without forming a jaw angle (Fig. 18D and I). Bridges are entirely hidden under the merged part of the inner and outer lamellae (Fig. 18E, J, and K–R). Anterior parts of the outer and inner lamellae merge directly (Fig. 18D and I). The merger area of these lamellae tapers slightly toward the ventral ends. The shoulders and lateral walls lack any structure to mark their boundary (Fig. 18D and I). Wings are ventrally tapered and have no folds, steps, or grooves around them (Fig. 18A–D, and F–I). The hood is fairly long and has no notches (Fig. 18C and H). Its posterior edge shows nearly the same curvature at the lateral and medial parts in the dorsal view (Fig. 18C and H). In the frontal sections

of the hood, the medial part is strongly curved, and the lateral parts are nearly straight (Fig. 18E, J, and K–R). Lateral walls are significantly longer than the hood, have no folds, and gradually taper toward the posterior end (Fig. 18A and B). The outer surfaces of both inner and outer lamellae are ornamented with radial striations that become distinct posteriorly with a gentle curvature toward the ventral part (Fig. 18F and G).

Remarks. The lateral curvature of the frontal sections of the hood is much weaker in *N. jeletzkyi* than in *N. haggarti* (Fig. 18E, J, K–S, and X). Based on this criterion, *P. pacifica* is here identified as a synonym of *N. jeletzkyi*

Occurrence. earliest Cenomanian to Late Campanian; the Yezo Group in Hokkaido, Japan.

Nanaimoteuthis haggarti Tanabe in Tanabe et al., 2008 comb. nov.

Paleocirroteuthis haggarti Tanabe in Tanabe et al., 2008, Fig. 5

Nanaimoteuthis hikidai Tanabe, Misaki and Ubukata, 2015, Fig. 6

Holotype. CDM994.59.9 (Tanabe et al., 2008, Fig. 5.1–5.5[31]).

Other materials. CDM996.295.1 (Paratype of *P. haggarti,* Tanabe et al., 2008, Fig. 5.6–5.9[31]), KMNH IvP 902001 (Holotype of *N. hikidai,* Tanabe et al., 2015, Fig. 6[33]), NMNS_DS00171_tLWPrwm.stl, and NMNS_DS00182_Ru8pBBo.stl.

Emended diagnosis. The lower jaw, which reaches a crest length > 50 mm in adults, shows the following features. The outer lamella is as high as wide. The rostrum has no hook or dents. Jaw edges are strongly curved and single-edged. Jaw angles are absent. Bridges are entirely concealed by the merged part of the inner and outer lamellae. The anterior parts of the outer and inner lamellae merge directly. The hood is much longer than the rostrum. Its posterior edge shows the same curvature of the lateral and medial parts in dorsal view. The medial and lateral parts of the frontal sections of the hood are gently curved. Wings are smooth and ventrally tapered. Lateral walls are significantly longer than the hood, have no folds, and gradually taper toward the posterior end.

Description. The outer lamella shows almost the same height and width (Fig. 18S and X). The rostrum is not hooked and has no dents around the jaw edges (Fig. 18T and U). Jaw edges are strongly curved, single-edged, and smoothly connected to the anterior edge of a wing without forming a jaw angle (Fig. 18W). Bridges are entirely hidden under the merged part of the inner and outer lamellae (Fig. 18S and X). The anterior parts of the outer and inner lamellae merge directly (Fig. 18W). The merger area of these lamellae tapers slightly toward the ventral ends. Shoulders and lateral walls lack any structure to mark a boundary (Fig. 18W). Wings taper ventrally and are without folds, steps, or grooves (Fig. 18T–W). The hood is fairly long and has no notches (Fig. 18V). Its posterior edge shows nearly the same curvature of the lateral and medial parts in dorsal view (Fig. 18V). In the frontal sections of the hood, the medial and lateral parts are gently curved (Fig. 18S and X). Lateral walls are significantly longer than the hood, have no folds, and gradually taper toward the posterior end (Fig. 19B). The outer surface of both inner and outer lamellae is ornamented with radial striations that become distinct posteriorly with a gentle curvature toward the ventral part (Fig. 19B).

Remarks. *N. haggarti* differs from *N. jeletzkyi* by the frontal sections of the hood, which show a gentle curvature for both the medial and lateral parts (Fig. 18E, J, K–S, and X). Based on this feature, *N.*

hikidai is here identified as a synonym of *N. haggarti.*

Occurrence. Early to Late Campanian; the Yezo Group in Hokkaido, Japan.

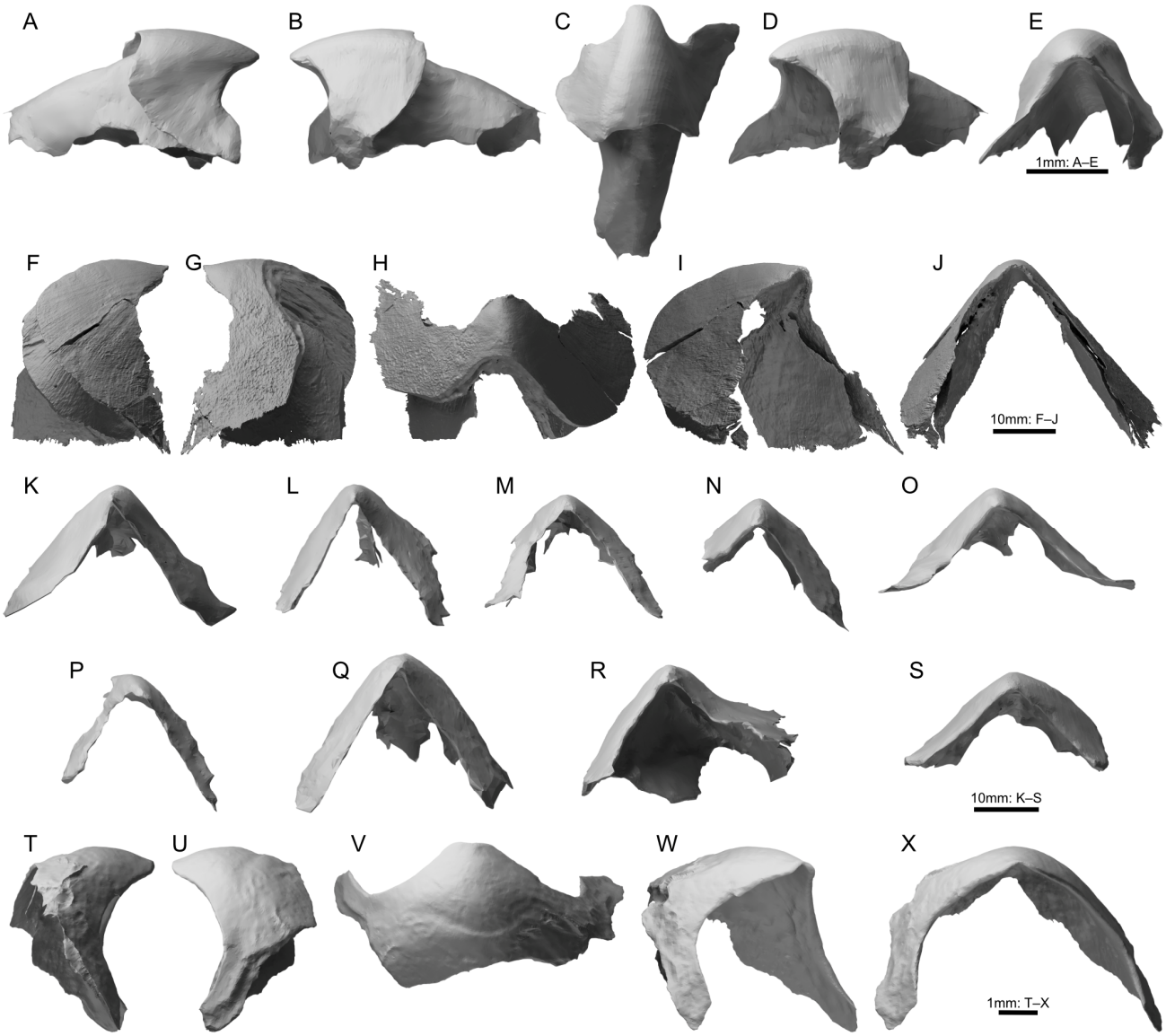


Fig. 18. Lower jaw of *Nanaimoteuthis.*

(**A** to **R**), *N. jeletzkyi*. (**S** to **X**), *N. haggarti.* (A–E) NMNS_DS00173_P74Doy1.stl; (F–J) NMNS_DS00042_3LmvTpM.stl; (K) NMNS_DS00068_x8HxByP.stl; (L) NMNS_DS00171_qbOIwTk.stl; (M) NMNS_DS00171_kJTYO76.stl; (N) NMNS_DS00171_qK5qb3p.stl; o, NMNS_DS00171_PgRMnJl.stl; (P) NMNS_DS00171_r2SXbn2.stl; (Q) NMNS_DS00171_wmVpKjl.stl; (R) NMNS_DS00171_tLWPrwm.stl; (S) NMNS_DS00171_gvo0eUY.stl; (T to X) NMNS_DS00182_Ru8pBBo.stl. (A, F, and K) left lateral view; (B, G, and L) right lateral view; (C, H, and M) dorsal view; (D, I, and N) oblique view; (E, J to S, and X) anterior view.

2.4.2. Taxonomical revisions

Five species of Octobrachia have been reported from Cretaceous sediments, based on fossil jaws in the past[31–34]. Here, these taxa are taxonomically reorganised as two species, *Nanaimoteuthis jeletzkyi* and *N. haggarti* (Fig. 19). *Nanaimoteuthis* is included in the order Cirrata (finned octopuses), previously it has been assigned to the order Vampyromorpha (vampire squids)[31–34]. The newly discovered specimens extend the stratigraphic range of *N. jeletzkyi* to the earliest Cenomanian–Late Campanian (~100–72 Ma), and that of *N. haggarti* to the Early–Late Campanian (~83–72 Ma) (Tables 9 and 10).

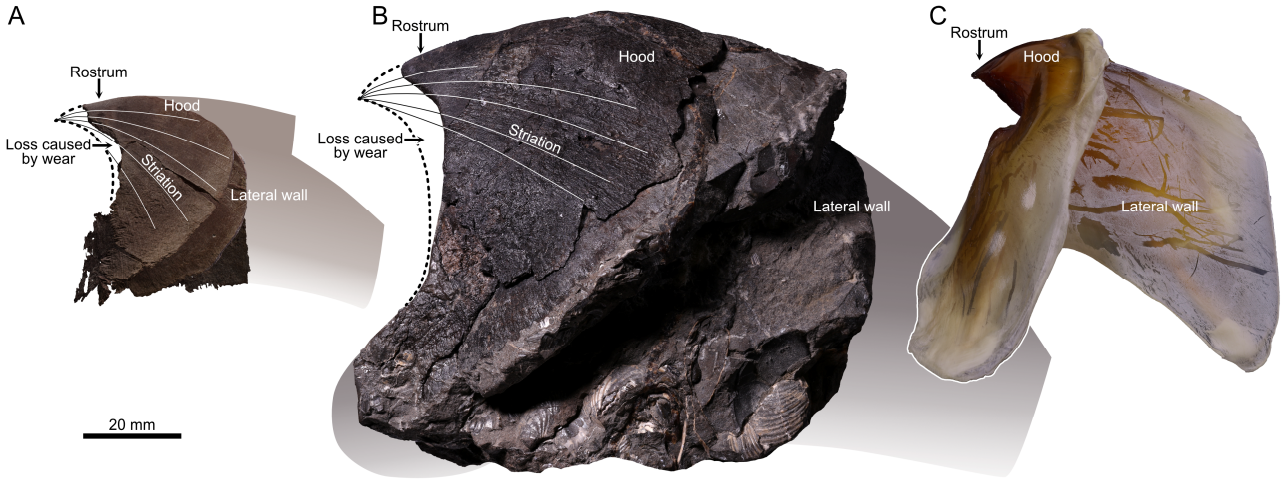


Fig. 19. Huge lower jaws of fossil octopuses and of an extant giant squid.
(**A** and **B**) The largest lower jaws of the Late Cretaceous finned octopus species *N. jeletzkyi* (A; NMNS_DS00042_3LmvTpM.stl) and *N. haggarti* (B; KMNH IvP 902001). Both specimens show extensive loss of jaw material caused by wear. (**C**) A lower jaw of the extant giant squid *Architeuthis dux* (NSMT-Mo 85956), a species having the largest jaw among modern cephalopods. (A) is a digital fossil jaw visualised as a 3D model, (B) is an exceptionally well-preserved non-digital fossil jaw, (C) is a modern jaw dissected from a carcass of ~10 m total body length. Solid lines indicate the extension of striation on the outer surface of the hood, and broken lines show the estimated outline of the rostrum without wear. The hood and lateral walls lost by weathering are shadowed in brown. (A) and (C) are exhibited in a mirrored position.

2.4.3. Body size estimations

The ontogenetic growth of jaws and soft body is allometric[37], well-documented data of the growth from extant species allow reliable body size calculations. The extant order Cirrata, which includes the genus *Nanaimoteuthis*, consists of two morphologically different groups, the long-bodied forms (family Cirroctopodidae, Cirroteuthidae, Grimpoteuthidae, and Stauroteuthidae) and the short-bodied forms (family Opisthoteuthidae)[42]. This study quantifies the maximum body size of *N. jeletzkyi* and *N. haggarti* based on the largest jaws observed for each species, using the known sizes of large- and short-bodied forms alternatively. The jaw of *N. jeletzkyi* was discovered digitally in this study (Fig. 19A), and that of *N. haggarti* is a non-digital specimen previously reported[33] (Fig. 19B). Mantle lengths of the largest specimens, encountered in this study, have been calculated using the well-documented jaws and body sizes recorded from extant Cirrata (Methods). A maximum mantle length of ~0.68–1.66 m and ~0.24–0.90 m, based on the data of long-bodied and short-bodied forms respectively, have been

Table 9. Previously reported specimens of fossil octobrachian jaws and their taxonomic revisions.

Specimen No.	Previous classification				Revised classification				Geological age	Horizon	Locality	Longitude	Deposition
	Order	Family	Genus	Species	Order	Family	Genus	Species					
CDM 2006.1.1 (Tanabe et al., 2008)[31]	Vampyromorpha	uncertain	*Nanaimoteuthis*	*jeletzkyi*	Cirrata	uncertain	*Nanaimoteuthis*	*jeletzkyi*	Early Campanian, Late Cretaceous	Pender Formation, Nanaimo Group	Black Creek, Courtenay, British Columbia, Canada	49° 48' 13" N 125° 09' 53" W	Courtenay and District Museum and Paleontological Center, Courtenay, British Columbia, Canada
KMNH IvP 902005 (Tanabe et al., 2017)[34]	Vampyromorpha	uncertain	*Nanaimoteuthis*	*jeletzkyi*	Cirrata	uncertain	*Nanaimoteuthis*	*jeletzkyi*	Santonian, Late Cretaceous	Upper part of Haborogawa Formation, Yezo Group	Kotanbetsu Creek, Tomamae, Hokkaido, Japan	44° 10' 58.3" N 141° 58' 20.6" E	Kitakyushu Museum of Natural History and Human History, Kitakyushu, Fukuoka, Japan.
HMG 1689 (Tanabe et al., 2017)[34]	Vampyromorpha	uncertain	*Nanaimoteuthis*	*jeletzkyi*	Cirrata	uncertain	*Nanaimoteuthis*	*jeletzkyi*	Santonian, Late Cretaceous	Middle part of Kashima Formation, Yezo Group	Tosanonosawa Creek, Mukawa, Hokkaido, Japan	42° 47' 44" N 142° 12' 49" E	Hobetsu Museum, Mukawa, Hokkaido, Japan.
UMUT MM 30337 (Tanabe and Hikida, 2010)[32]	Vampyromorpha	uncertain	*Nanaimoteuthis*	*yokotai*	uncertain	uncertain	indeterminate	indeterminate	Middle Turonian, Late Cretaceous	Upper part of Saku Formation, Yezo Group	Satonosawa Creek, Obira, Hokkaido, Japan	44° 03' 56" N 141° 59' 41" E	University Museum, University of Tokyo, Tokyo, Tokyo, Japan
NMA 580 (Tanabe and Hikida, 2010)[32]	Vampyromorpha	uncertain	*Nanaimoteuthis*	*yokotai*	uncertain	uncertain	indeterminate	indeterminate	Late Turonian, Late Cretaceous	Upper part of Saku Formation, Yezo Group	Sakugakkonosawa Creek, Nakagawa, Hokkaido, Japan	44° 44' 21" N 142° 00' 50" E	Nakagawa Museum of Natural History, Nakagawa, Hokkaido, Japan.
KMNH IvP 902003 (Tanabe et al., 2017)[34]	Vampyromorpha	uncertain	*Nanaimoteuthis*	*yokotai*	uncertain	uncertain	indeterminate	indeterminate	Early Campanian, Late Cretaceous	Upper part of Haborogawa Formation, Yezo Group	Sakasa Creek, Haboro, Hokkaido, Japan	44° 16' 26.1" N 141° 58' 24.7" E	Kitakyushu Museum of Natural History and Human History, Kitakyushu, Fukuoka, Japan.
KMNH IvP 902004 (Tanabe et al., 2017)[34]	Vampyromorpha	uncertain	*Nanaimoteuthis*	*yokotai*	uncertain	uncertain	indeterminate	indeterminate	Santonian, Late Cretaceous	Upper part of Haborogawa Formation, Yezo Group	Nakafutamata Creek, Haboro, Hokkaido, Japan	44° 18' 11.8" N 141° 58' 14.8" E	Kitakyushu Museum of Natural History and Human History, Kitakyushu, Fukuoka, Japan.
KMNH IvP 902001 (Tanabe et al., 2015)[33]	Vampyromorpha	uncertain	*Nanaimoteuthis*	*hikidai*	Cirrata	uncertain	*Nanaimoteuthis*	*haggarti*	Early Campanian, Late Cretaceous	Upper part of Haborogawa Formation, Yezo Group	Detofutamata Creek, Haboro, Hokkaido, Japan	44° 18' 19" N 141° 56' 40" E	Kitakyushu Museum of Natural History and Human History, Kitakyushu, Fukuoka, Japan.
CDM 994.59.9 (Tanabe et al., 2008)[31]	Cirrata	uncertain	*Paleocirroteuthis*	*haggarti*	Cirrata	uncertain	*Nanaimoteuthis*	*haggarti*	Santonian, Late Cretaceous	Haslam Formation, Nanaimo Group	Puntledge River, Courtenay, British Columbia, Canada	49° 41' 21" N 125° 02' 08" W	Courtenay and District Museum and Paleontological Center, Courtenay, British Columbia, Canada
CDM 996.295.1 (Tanabe et al., 2008)[31]	Cirrata	uncertain	*Paleocirroteuthis*	*haggarti*	Cirrata	uncertain	*Nanaimoteuthis*	*haggarti*	Early Campanian, Late Cretaceous	Pender Formation, Nanaimo Group	Puntledge River, Courtenay, British Columbia, Canada	49° 41' 17" N 125° 01' 40" W	Courtenay and District Museum and Paleontological Center, Courtenay, British Columbia, Canada
CDM 2006.2.1 (Tanabe et al., 2008)[31]	Cirrata	uncertain	*Paleocirroteuthis*	*pacifica*	Cirrata	uncertain	*Nanaimoteuthis*	*jeletzkyi*	Early Campanian, Late Cretaceous	Pender Formation, Nanaimo Group	Black Creek, Courtenay, British Columbia, Canada	49° 49' 52" N 125° 11' 27" W	Courtenay and District Museum and Paleontological Center, Courtenay, British Columbia, Canada
NMA 284 (Tanabe et al., 2008)[31]	Cirrata	uncertain	*Paleocirroteuthis*	*pacifica*	Cirrata	uncertain	*Nanaimoteuthis*	*jeletzkyi*	Early Campanian, Late Cretaceous	Osoushinai Formation, Yezo Group	Toyosato Tunnel, Nakagawa, Hokkaido, Japan	44° 45' N 141° 59' E	Nakagawa Museum of Natural History, Nakagawa, Hokkaido, Japan.
MCM A872 (lower jaw; Tanabe et al., 2017)[34]	Cirrata	uncertain	*Paleocirroteuthis*	sp.	Cirrata	uncertain	*Nanaimoteuthis*	sp.	Santonian, Late Cretaceous	Upper part of Haborogawa Formation, Yezo Group	Kaminosawa Creek, Tomamae, Hokkaido, Japan	44° 11' 56.0" N 141° 58' 59.0" E	Mikasa City Museum, Mikasa, Hokkaido, Japan
MCM A872 (upper jaw; Tanabe et al., 2017)[34]	Cirrata	uncertain	*Paleocirroteuthis*	sp.	uncertain	uncertain	indeterminate	indeterminate	Santonian, Late Cretaceous	Upper part of Haborogawa Formation, Yezo Group	Kaminosawa Creek, Tomamae, Hokkaido, Japan	44° 11' 56.0" N 141° 58' 59.0" E	Mikasa City Museum, Mikasa, Hokkaido, Japan
CDM 994.124.1 (Tanabe et al., 2008)[31]	Incirrata	uncertain	indeterminate	indeterminate	uncertain	uncertain	indeterminate	indeterminate	Early Campanian, Late Cretaceous	Haslam Formation, Nanaimo Group	Puntledge River, Courtenay, British Columbia, Canada	49° 40' 53" N 125° 03' 16" W	Courtenay and District Museum and Paleontological Center, Courtenay, British Columbia, Canada

Table 10. Newly discovered lower jaw specimens of Late Cretaceous Cirrata.

Specimen (3D model) No. Available from Figshare (doi: 10.6084/m9.figshare.27933759)	Classification			Measurements			Geological age	Horizon	Locality	Longitude and latitude
	Order	Genus	Species	CL (mm)	HL (mm)	RWL (mm)				
NMNS_DS00068_x8HxByP.stl	Cirrata	*Nanaimoteuthis*	*jeletzkyi*	-	2.23	2.33	earliest Cenomanian, Late Cretaceous	Unit My3, Yezo Group	Suribachi creek, Soeushinai, Horokanai, Hokkaido, Japan	44° 13' 29" N 142° 04' 07" E
NMNS_DS00173_P74Doy1.stl	Cirrata	*Nanaimoteuthis*	*jeletzkyi*	3.08	1.47	1.76	Late Turonian, Late Cretaceous	Upper part of Saku Formation, Yezo Group	A tributary of Kamikinenbetsu creek, Kawakami, Obira, Hokkaido, Japan	44° 03' 43" N 141° 58' 51" E
NMNS_DS00042_3LmvTpM.stl (entire jaw) NMNS_DS00042_nyw6tJu.stl (rostral part)	Cirrata	*Nanaimoteuthis*	*jeletzkyi*	-	-	32.32	Santonian, Late Cretaceous	Upper part of Haborogawa Fm., Yezo Group	Kumanosawa creek, a tributary of Kotanbetsu creek, Kiritachi, Tomamae, Hokkaido, Japan	44° 11' 24" N 141° 58' 14" E
NMNS_DS00171_qbOIwTk.stl	Cirrata	*Nanaimoteuthis*	*jeletzkyi*	2.36	1.59	1.87	Late Campanian, Late Cretaceous	Chinomigawa Formation, Yezo Group	Pankeushappu creek, Hidaka, Hidaka, Hokkaido, Japan	42° 54' 36" N 142° 25' 08" E
NMNS_DS00171_kJTYO76.stl	Cirrata	*Nanaimoteuthis*	*jeletzkyi*	-	1.20	2.57	Late Campanian, Late Cretaceous	Chinomigawa Formation, Yezo Group	Pankeushappu creek, Hidaka, Hidaka, Hokkaido, Japan	42° 54' 36" N 142° 25' 08" E
NMNS_DS00171_qK5qb3p.stl	Cirrata	*Nanaimoteuthis*	*jeletzkyi*	2.84	1.77	2.32	Late Campanian, Late Cretaceous	Chinomigawa Formation, Yezo Group	Pankeushappu creek, Hidaka, Hidaka, Hokkaido, Japan	42° 54' 36" N 142° 25' 08" E
NMNS_DS00171_PgRMnJl.stl	Cirrata	*Nanaimoteuthis*	*jeletzkyi*	2.47	1.55	2.05	Late Campanian, Late Cretaceous	Chinomigawa Formation, Yezo Group	Pankeushappu creek, Hidaka, Hidaka, Hokkaido, Japan	42° 54' 36" N 142° 25' 08" E
NMNS_DS00171_r2SXbn2.stl	Cirrata	*Nanaimoteuthis*	*jeletzkyi*	-	1.23	1.76	Late Campanian, Late Cretaceous	Chinomigawa Formation, Yezo Group	Pankeushappu creek, Hidaka, Hidaka, Hokkaido, Japan	42° 54' 36" N 142° 25' 08" E
NMNS_DS00171_wmVpKjl.stl	Cirrata	*Nanaimoteuthis*	*jeletzkyi*	2.48	1.90	2.04	Late Campanian, Late Cretaceous	Chinomigawa Formation, Yezo Group	Pankeushappu creek, Hidaka, Hidaka, Hokkaido, Japan	42° 54' 36" N 142° 25' 08" E
NMNS_DS00171_tLWPrwm.stl	Cirrata	*Nanaimoteuthis*	*jeletzkyi*	2.50	1.79	2.09	Late Campanian, Late Cretaceous	Chinomigawa Formation, Yezo Group	Pankeushappu creek, Hidaka, Hidaka, Hokkaido, Japan	42° 54' 36" N 142° 25' 08" E
NMNS_DS00171_gvo0eUY.stl	Cirrata	*Nanaimoteuthis*	*haggarti*	-	1.59	1.60	Late Campanian, Late Cretaceous	Chinomigawa Formation, Yezo Group	Pankeushappu creek, Hidaka, Hidaka, Hokkaido, Japan	42° 54' 36" N 142° 25' 08" E
NMNS_DS00182_Ru8pBBo.stl	Cirrata	*Nanaimoteuthis*	*haggarti*	-	-	5.77	Late Campanian, Late Cretaceous	Chinomigawa Formation, Yezo Group	Pankeushappu creek, Hidaka, Hidaka, Hokkaido, Japan	42° 54' 49" N 142° 24' 45" E

Table 10. (continued)

Specimen (3D model) No. Available from Figshare (doi: 10.6084/m9.figshare.27933759)	Image datasets			Resolution of mask data and cropped cross-sectional images		Image processing by ImageJ before segmentation	Figures
	Mask data for 3D models (doi: 10.6084/m9.figshare.27933759)	Cropped cross-sectional images (doi: 10.6084/m9.figshare.27933759)	Original cross-sectional images (doi: 10.6084/m9.figshare.27935904)	Pixel size (μm/pixel)	Interval (μm)		
NMNS_DS00068_x8HxByP.stl	L_NMNS_DS00068_20181123_c1_wl_01_0741_x8HxByP.tif–0796_x8HxByP.tif	C_NMNS_DS00068_20181123_c1_wl_01_0741_x8HxByP.jpg–0796_x8HxByP.jpg	NMNS_DS00068_20181123_c1_wl_01_0741.jpg–0796.jpg	10.715	50	Not processed	Fig. 16K
NMNS_DS00173_P74Doy1.stl	L_NMNS_DS00173_wl_01_0056_P74Doy1.tif–0094_P74Doy1.tif	C_NMNS_DS00173_wl_01_0056_P74Doy1.jpg–0094_P74Doy1.jpg	NMNS_DS00173_wl_01_0056.tif–0094.tif	5.339	50	Not processed	Fig. 16A–E
NMNS_DS00042_3LmvTpM.stl (entire jaw) NMNS_DS00042_nyw6tJu.stl (rostral part)	L_NMNS_DS00042_20180419_c1_wl_02_0001_3LmvTpM.tif–0601_3LmvTpM.tif (entire jaw) L_NMNS_DS00042_20180419_c1_wl_02_0052_nyw6tJu.tif–0305_nyw6tJu.tif (rostral part)	C_NMNS_DS00042_20180419_c1_wl_02_0001_3LmvTpM.jpg–0601_3LmvTpM.jpg (entire jaw) C_NMNS_DS00042_20180419_c1_wl_02_0052_nyw6tJu.jpg–0305_nyw6tJu.jpg (rostral part)	NMNS_DS00042_20180419_c1_wl_02_0001.jpg–0601.jpg	21.006 (entire jaw) 10.503 (rostral part)	50	Not processed	Figs 16F–J, 17A, & 18A, B, & D (entire jaw) Fig. 18C & E–G (rostral part)
NMNS_DS00171_qbOIwTk.stl	L_NMNS_DS00171_wl_01_0158_qbOIwTk.tif–0208_qbOIwTk.tif	C_NMNS_DS00171_wl_01_0158_qbOIwTk.jpg–0208_qbOIwTk.jpg	NMNS_DS00171_wl_01_0158.tif–0208.tif	5.805	50	Processed	Fig. 16L
NMNS_DS00171_kJTYO76.stl	L_NMNS_DS00171_wl_01_0266_kJTYO76.tif–0308_kJTYO76.tif	C_NMNS_DS00171_wl_01_0266_kJTYO76.jpg–0308_kJTYO76.jpg	NMNS_DS00171_wl_01_0266.tif–0308.tif	5.805	50	Processed	Fig. 16M
NMNS_DS00171_qK5qb3p.stl	L_NMNS_DS00171_wl_01_0337_qK5qb3p.tif–0389_qK5qb3p.tif	C_NMNS_DS00171_wl_01_0337_qK5qb3p.jpg–0389_qK5qb3p.jpg	NMNS_DS00171_wl_01_0337.tif–0389.tif	5.805	50	Not processed	Fig. 16N
NMNS_DS00171_PgRMnJl.stl	L_NMNS_DS00171_wl_01_0437_PgRMnJl.tif–0483_PgRMnJl.tif	C_NMNS_DS00171_wl_01_0437_PgRMnJl.jpg–0483_PgRMnJl.jpg	NMNS_DS00171_wl_01_0437.tif–0483.tif	5.805	50	Not processed	Fig. 16O
NMNS_DS00171_r2SXbn2.stl	L_NMNS_DS00171_wl_01_0434_r2SXbn2.tif–0473_r2SXbn2.tif	C_NMNS_DS00171_wl_01_0434_r2SXbn2.jpg–0473_r2SXbn2.jpg	NMNS_DS00171_wl_01_0434.tif–0473.tif	5.805	50	Processed	Fig. 16P
NMNS_DS00171_wmVpKjl.stl	L_NMNS_DS00171_wl_01_0434_wmVpKjl.tif–0485_wmVpKjl.tif	C_NMNS_DS00171_wl_01_0434_wmVpKjl.jpg–0485_wmVpKjl.jpg	NMNS_DS00171_wl_01_0434.tif–0485.tif	5.805	50	Processed	Fig. 16Q
NMNS_DS00171_tLWPrwm.stl	L_NMNS_DS00171_wl_01_0653_tLWPrwm.tif–0691_tLWPrwm.tif	C_NMNS_DS00171_wl_01_0653_tLWPrwm.jpg–0691_tLWPrwm.jpg	NMNS_DS00171_wl_01_0653.tif–0691.tif	5.805	50	Processed	Fig. 16R
NMNS_DS00171_gvo0eUY.stl	L_NMNS_DS00171_wl_01_0589_gvo0eUY.tif–0618_gvo0eUY.tif	C_NMNS_DS00171_wl_01_0589_gvo0eUY.jpg–0618_gvo0eUY.jpg	NMNS_DS00171_wl_01_0589.tif–0618.tif	5.805	50	Not processed	Fig. 16S
NMNS_DS00182_Ru8pBBo.stl	L_NMNS_DS00182_wl_01_0264_Ru8pBBo.tif–0419_Ru8pBBo.tif	C_NMNS_DS00182_wl_01_0264_Ru8pBBo.jpg–0419_Ru8pBBo.jpg	NMNS_DS00182_wl_01_0264.tif–0419.tif	4.756	50	Not processed	Fig. 16T–X

Table 11. Body size estimations of the Late Cretaceous Cirrata.

Classification			Specimen No.	Reconstructed HL (mm)	ML (m) estimated from the relationship between HL and ML of extant Cirrata					
					Long-bodied group			Short-bodied group		
Order	Genus	Species			*Stauroteuthis syrtensis*[39]: 15.37 × HL$^{1.27}$	*Cirroteuthis muelleri*[39]: 11.71 × HL$^{1.10}$	*Grimpoteuthis* sp.[40]: 31.36 × HL - 121.28	*Opisthoteuthis persephone*[40]: 6.74 × HL - 7.84	*Opisthoteuthis pluto*[40]: 5.98 × HL + 2.79	*Opisthoteuthis* sp.[41]: 23.03× HL - 13.76
Cirrata	*Nanaimoteuthis*	*jeletzkyi*	NMNS_DS00042_3LmvTpM.stl	39.6	1.64	0.67	1.12	0.26	0.24	0.90
Cirrata	*Nanaimoteuthis*	*haggarti*	KMNH IvP 902001	86.4	4.43	1.58	2.59	0.57	0.52	1.98

calculated for *N. jeletzkyi* (Table 11). The jaw-based maximum mantle length of *N. haggarti* is ~1.58–4.43 m and ~0.52–1.98 m for long- respectively short-bodied forms (Table 11).

2.4.4. Wear patterns

The largest specimens of *N. jeletzkyi* and *N. haggarti* have a blunt rostrum and rounded jaw edges due to intensive wear, both these jaw elements are sharp in juveniles (Fig. 19). The rostral part, which has been lost by wear, was reconstructed from striation, an original ornamentation of the jaw (Fig. 19). The length of this lost part is ~5.7 mm in *N. jeletzkyi* and ~10.6 mm in *N. haggarti*, which amounts to 10% of the total jaw length for each species (Fig. 19). The loss at the right jaw edge is more intense than at the left edge in both *N. jeletzkyi* and *N. hikidai* (Fig. 20F and M). The observed signs of wear include chips, scratches, and polish (Figs. 20 and 21). The chips and scratches in *N. jeletzkyi* have been precisely visualised in the digital 3D models (Fig. 20C–G). Those in *N. haggarti* are filled with sediment, indicating that they were not caused by mechanical preparation using dental tools (Figs. 20L and 21B–E). In both species, many chips that surpass 1 mm in size are preserved on the jaw edges (Fig. 20E and L). The outer surface of the rostrum is polished, causing an absence of the primary striation. It also shows numerous scratches that reach a length up to 5 mm superposed on the polished part (Fig. 20A, C, D, F, H, J, K, and N). The scratches extend vertically or obliquely to the jaw edges. The inner surface of *N. jeletzkyi*, facing the oral cavity for chewing, is more worn than the outer surface (Fig. 20G). The rostrum of *N. haggarti* shows many transverse cracks with a length of up to 5 mm (Figs. 20M and 21F and G).

2.5. Discussion

2.5.1. The largest marine invertebrates

Octopuses are classified into two taxonomic orders, the Cirrata (finned octopuses) and the Incirrata (finless octopuses)[37]. In modern oceans, the Cirrata primarily inhabit deep-sea environments, while the Incirrata are mainly found in coastal areas[42]. The discovery of *N. jeletzkyi*, described here, extends the oldest record of Cirrata[34] by ~15 million years and that of octopuses[27] by ~5 million years to the earliest Cenomanian (~100 Ma). The Cirrata extensively inhabited the Late Cretaceous shelf seas, all studied jaws come from shelf deposits of the circum-North Pacific, the largest ocean in the Mesozoic.

Numerous soft-body imprints of Mesozoic Octobrachia are known, so far 51 genera have been described based on these fossils[27]. All of these taxa, such as *Trachyteuthis* and *Palaeoctopus*, have an elongated body[27]. Molecular phylogenetic analyses covering all extant families of Cirrata show that the long-bodied group is ancestral to the short-bodied[44]. Both lines of evidence strongly suggest that the earliest species of Cirrata, *N. jeletzkyi* and *N. haggarti*, had a long body. Their mantle lengths can accordingly be reconstructed as ~0.68–1.66 m for *N. jeletzkyi* and ~1.58–4.43 m for *N. haggarti* (Fig. 22 and Table 11). In the long-bodied group of modern Cirrata, the total length, including their arms, is on average ~4.2 times the mantle length[42] (Table 12). Based on this ratio, *N. jeletzkyi* reached a total body length of ~2.8–7.0 m, and *N. haggarti* of ~6.6–18.6 m (Fig. 22). *N. jeletzkyi* has an earliest Cenomanian to the Late Campanian age, *N. haggarti* a Campanian age. These data show that the sizes of Cirrata significantly increased near the end of the Cretaceous (Fig. 19).

The lower jaw of *N. haggarti* is ~1.5 times larger in size than that of the giant squid (*Architeuthis dux*), which has the largest jaw in extant cephalopods (Fig. 19C; ~80 mm maximum length in the so far known specimens[37]). The giant squid, with a body length of ~12 m, is the biggest

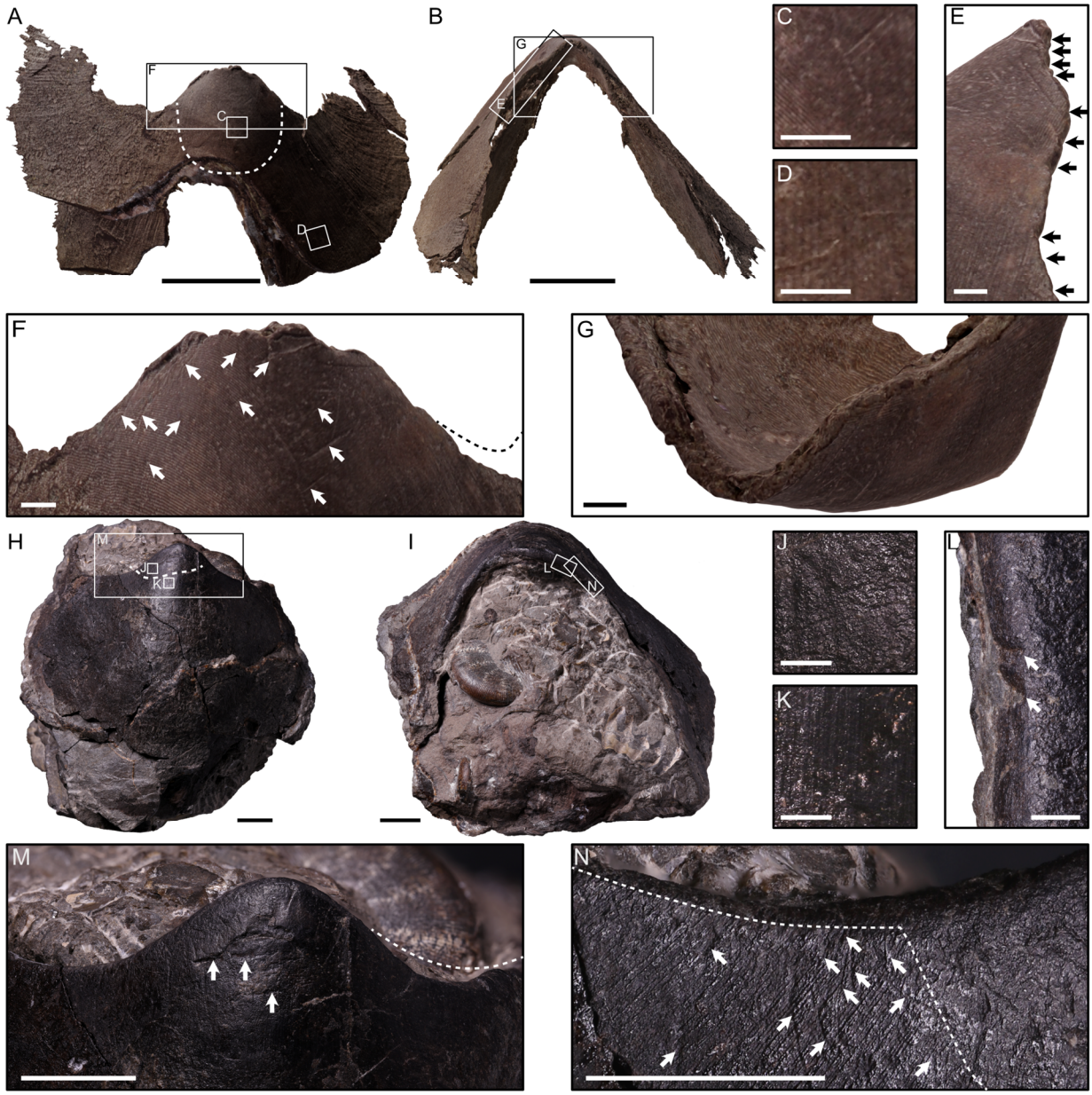


Fig. 20. Wear on the lower jaws of Late Cretaceous octopuses.
(**A** to **G**) The largest specimen of *N. jeletzkyi* (A, B, and D: NMNS_DS00042_3LmvTpM.stl, C, and E to G: NMNS_DS00042_nyw6tJu.stl). (**H** to **N**) The largest specimen of *N. haggarti* (KMNH IvP 902001). (C to G) and (J to N), Close-ups of the wear, of which the accurate positions are indicated by boxes in (A), (B), (H), and (I). (A) Dorsal view of the entire specimen. (B) Anterior view of the entire specimen. (C) Polished area where striation is lost. (D) Area showing striation, which extends vertically in this figure. (E) Lateral view of the right jaw edge with many chips. (F) Dorsal view of the rounded rostral part. (G) Oblique view of the rostral part with many chips. (H) Dorsal view of the entire specimen. (I) Anterior view of the entire specimen. (J) Polished area where striation is lost. (K) Area showing striation, which extends vertically in this figure. (L) Lateral view of the right jaw edge. (M) Dorsal view of the rounded rostral part. (N) Lateral view of the right jaw edge. Arrows indicate scratches in (F) and (N), chips in (E) and (L), and large transverse cracks in (M). The broken lines show the boundary where striation becomes lost in a, h, and n, and the position of the left jaw edge mirrored to the right side in f and m. Scale bars: 10 mm for (A), (B), (H), (I), (M), and (N); 1 mm for (C to G) and (J to N).

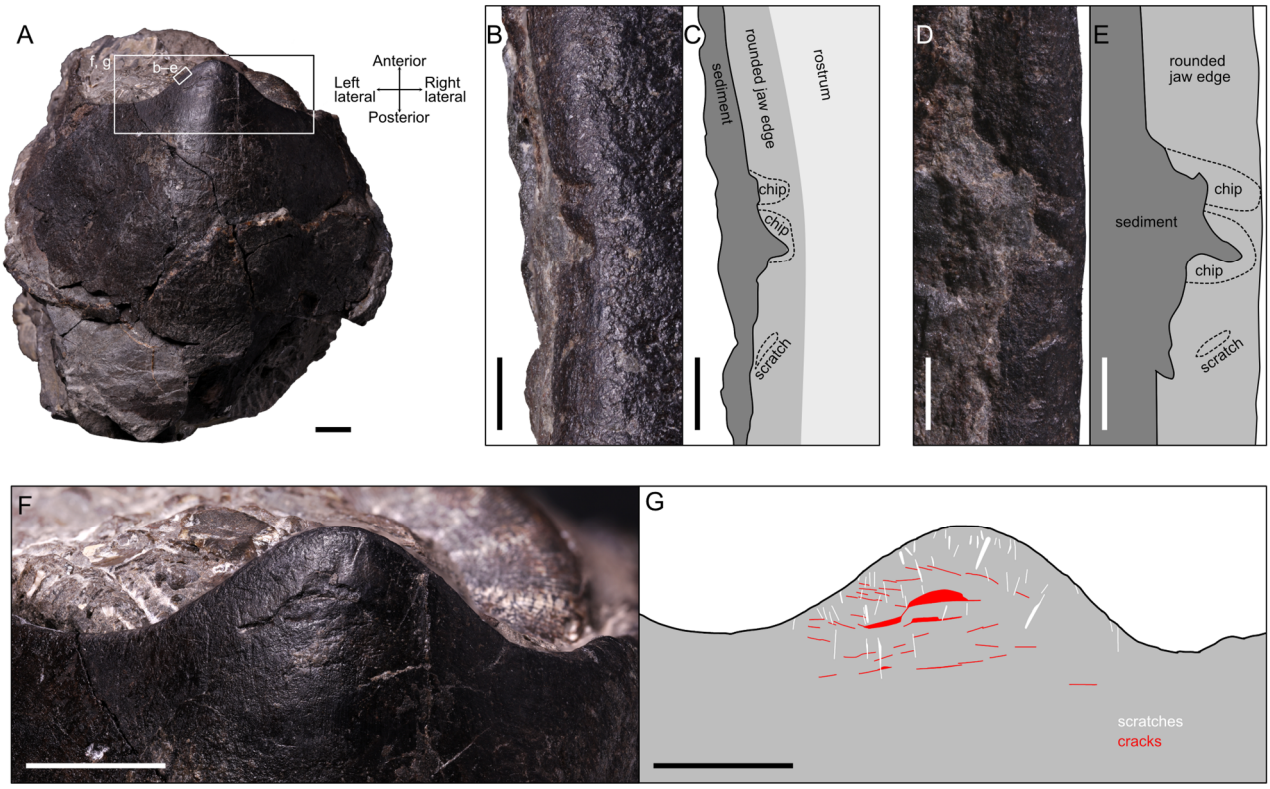


Fig. 21. Wear on the largest jaw of *N. haggarti* (KMNH IvP 902001).
(**A**) Dorsal view of the entire jaw. (**B** to **G**) Close-ups of the wear, the accurate positions are indicated by boxes in (A). (B), Lateral view of large chips and a scratch on the left jaw edge. (D), Anterior view of the same area shown in (B). (F), Dorsal view of scratches and cracks on the rostrum. Schematic drawing of (B), (D), and (F) are shown in (C), (E), and (G), respectively. Scale bars: 10 mm for (A); 1 mm for (B to E); 5 mm for (F) and (G).

species among all fossil and living invertebrates so far known[45]. The reconstruction in this study shows that *N. haggarti* is the largest invertebrate ever recorded, exceeding even the giant squid in size. It also rivals the dimensions of the largest bony fish (*Xiphactinus audax*, ~5 m)[46], chondrichthyans (*Ptychodus mortoni*, ~10 m)[47], plesiosaurs (*Styxosaurus* sp., ~12 m)[48], and mosasaurs (*Mosasaurus hoffmannii*, ~17 m)[49] known from the Cretaceous (Fig. 22). Cirrata thus had top-tier body sizes in the Cretaceous oceans.

2.5.2. Giant octopuses – top predators in Cretaceous ocean

Most extant octopuses and cuttlefishes are generalist carnivores that consume soft and hard prey, mainly crustaceans, shelled molluscs, other cephalopods, and bony fishes[50]. Frequent durophagous predation on hard-shelled prey causes wear of their jaw tips and jaw edges (Fig. 23), which is absent in non-durophagous cephalopods like squids[26,30]. This wear provides reliable evidence of durophagy, in a broader sense carnivory, in fossil cephalopods. The loss of jaw material caused by the accumulated wear reaches 10% of the total jaw length in *N. jeletzkyi* and *N. haggarti*, which is more severe than in modern cephalopods[26,30]. These wear patterns indicate that Late Cretaceous Cirrata were active carnivores, which frequently crushed hard shells and bones. The long scratches distributed on wide areas of their jaw reflect the dynamic use of the entire jaw for dismantling the prey. Asymmetric loss

Table 12. The ratio between the mantle length and total length in extant Cirrata.

Body form	Family	Genus	Species	Mantle length[42] (mm)	Total length[42] (mm)	Total length/ Mantle length
Long-bodied group	Cirroctopodidae	*Cirroctopus*	*glacialis*	165	600	3.6
		Cirroctopus	*hochbergi*	160	493	3.1
		Cirroctopus	*mawsoni*	12	32	2.7
	Cirroteuthidae	*Cirrothauma*	*magna*	330	1700	5.2
	Grimpoteuthidae	*Grimpoteuthis*	*wuelkeri*	115	400	3.5
		Grimpoteuthis	*abyssicola*	75	305	4.1
		Grimpoteuthis	*bathynectes*	85	240	2.8
		Grimpoteuthis	*boylei*	115	470	4.1
		Grimpoteuthis	*challengeri*	75	370	4.9
		Grimpoteuthis	*discoveryi*	58	210	3.6
		Grimpoteuthis	*innominata*	43	156	3.6
		Grimpoteuthis	*plena*	57	185	3.2
		Grimpoteuthis	*tuftsi*	102	475	4.7
		Grimpoteuthis	*umbellata*	46	250	5.4
		Luteuthis	*dentatus*	98	524	5.3
		Luteuthis	*shuishi*	87.5	300	3.4
	Stauroteuthidae	*Stauroteuthis*	*syrtensis*	114	500	4.4
		Stauroteuthis	*gilchristi*	70	540	7.7
					Average	4.2
Short-bodied group	Opisthoteuthidae	*Opisthoteuthis*	*agassizii*	55	186	3.4
		Opisthoteuthis	*albatrossi*	36	200	5.6
		Opisthoteuthis	*calypso*	50	482	9.6
		Opisthoteuthis	*chathamensis*	54	180	3.3
		Opisthoteuthis	*dongshaensis*	46	226	4.9
		Opisthoteuthis	*grimaldii*	50	250	5.0
		Opisthoteuthis	*hardyi*	64	285	4.5
		Opisthoteuthis	*massyae*	76	350	4.6
		Opisthoteuthis	*mero*	90	340	3.8
		Opisthoteuthis	*philipii*	140	470	3.4
		Opisthoteuthis	*robsoni*	65	362	5.6
		Cryptoteuthis	*brevibracchiata*	35	121	3.5
					Average	4.8

in the jaw edges implies that individuality already existed in earliest octopuses, as lateralisation in behaviour presumably resulted from a highly developed brain and cognition[51]. Given that modern octopuses act individually, including laterality[51,52], the approach of this study allows to understand the behaviour of individual ancient animals. The exceptionally large jaws of adult *N. jeletzkyi* and *N. haggarti* indicate a strong bite force since cephalopod jaw muscles enlarge as the jaw size increases[26]. The chips on both the rostrum and jaw edge were caused by strong shear stress beyond the yield point of the most robust part of the jaw. The transverse cracks in *N. haggarti* are probably a trace of larger shear failures. These large fractures thus suggest an overloadingly powerful biting. In giant Cirrata, the jaws are smaller than those of vertebrate top predators, which measure nearly 1 m in length[47]. Their eight arms instead function like the large mouth of vertebrate predators[24]. The giant Cirrata caught large prey with these arms and killed it with their robust jaws, playing the role of a top predator in the Cretaceous marine ecosystem.

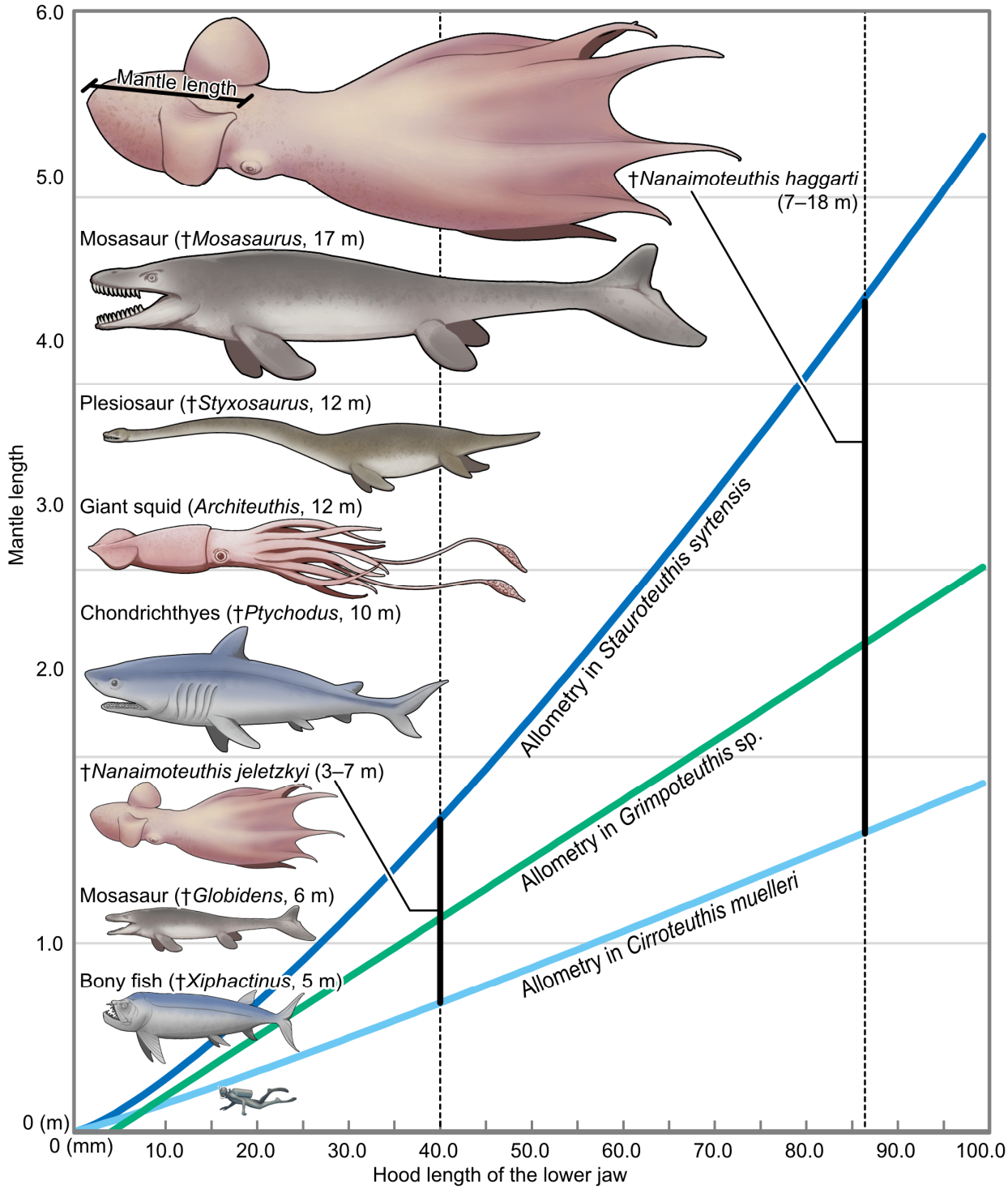


Fig. 22. Body size estimation of Late Cretaceous octopuses.
The graph shows an allometric relationship between the length of the jaw and mantle in extant finned octopus species. The dark blue line stands for *Stauroteuthis syrtensis*[39], the green line for *Grimpoteuthis* sp.[40], and the light blue line for *Cirroteuthis muelleri*[39]. The maximum size of *N. jeletzkyi* and *N. haggarti* is indicated by a grey vertical line. Reconstruction of these two species and gigantic vertebrate predators in the Late Cretaceous[46–49] are shown.

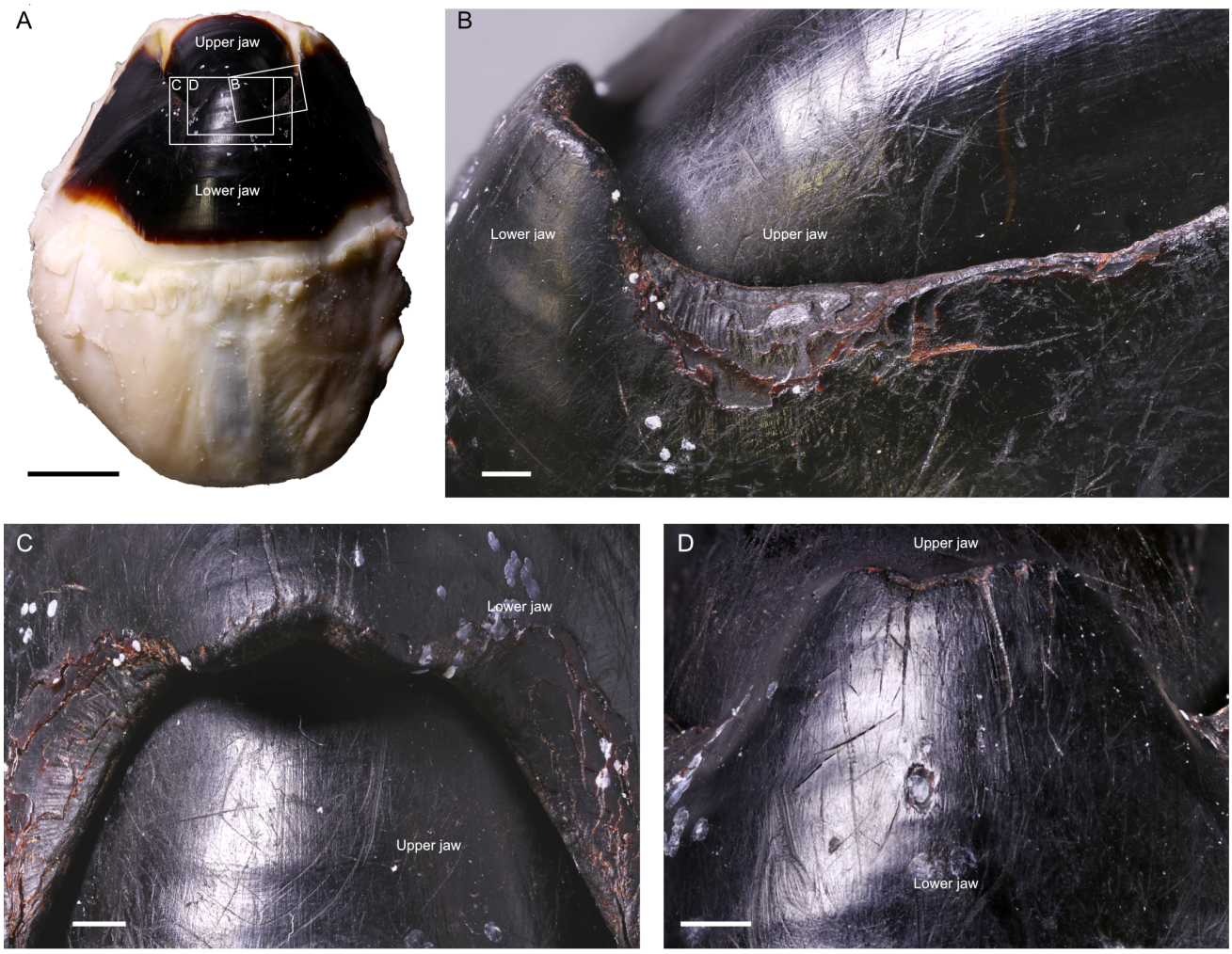


Fig. 23. Wear on the lower jaw of a modern octopus (*Enteroctopus dofleini*: NSMT-Mo 85957). (**A**) Dorsal view of the entire buccal mass. (**B** to **D**) Close-ups of the wear, the accurate positions are indicated by boxes in (A). (B) Lateral view of the right jaw edge. (C) Anterior view around the rostrum. (D) Dorsal view of the rostrum. Scale bars: 10 mm for (A); 1 mm for (B to D).

2.5.3. Innovations of marine top predators

The increase of durophagous predation in the late Mesozoic oceans enhanced both taxonomic and ecological diversity, shaping the modern-type marine ecosystem[3–7]. The Cretaceous, the final phase of this interval, saw a peak of this predator-prey arms race[3–7]. Previous studies have recognised only large vertebrates as durophagous top predators that drove this coevolution, represented by chondrichthyans (e.g., *Ptychodus* and *Coupatezia*) and mosasaurs (e.g., *Globidens* and *Carinodens*) (Fig. 22)[8,11–14,49]. Cretaceous invertebrates have been regarded as prey or mid-ranking predators, which underwent protective adaptations[3–7]. This study, however, sheds light on the only invertebrates that invaded a top position in the food chain, namely the earliest octopuses that evolved strong biting. The convergent evolution of octopuses and vertebrates highlights that the combination of robust jaws and the dismantlement of external skeletons is essential for becoming a top predator. Jawless carnivorous invertebrates like gastropods, including naked forms, occupied the lower trophic levels throughout their evolutionary history[4,5] due to less efficient food intake[19]. Likewise, other jawed carnivorous invertebrates, like arthropods, could not rival vertebrate top predators[4,5]. Their disadvantage is the external skeleton, which limits growth rates, agility, and behavioural flexibility[53]. Without these

constraints, the earliest octopuses mounted huge body sizes, and probably high mobility and sophisticated cognition. They were most likely generalist carnivores, accelerating the evolution of prey animals and competing successfully with vertebrate predators. The rise of octopuses in the Late Cretaceous transformed the long-established structure of the marine ecosystem, in which only vertebrates occupied a top position in the food chain.

References for Chapter 2

1. Rossberg, A. G., Gaedke, U. & Kratina, P. Dome patterns in pelagic size spectra reveal strong trophic cascades. *Nat. Commun.* **10**, 4396 (2019).
2. Atkins, J. L. *et al.* Cascading impacts of large-carnivore extirpation in an African ecosystem. *Science* **364**, 173–177 (2019).
3. Hughes, B. B. *et al.* Top-predator recovery abates geomorphic decline of a coastal ecosystem. *Nature* **626**, 111–118 (2024).
4. Brett, C. E. & Walker, S. E. Predators and predation in Paleozoic marine environments. *Paleontol. Soc. Pap.* **8**, 93–118 (2002).
5. Andersen, K. H. *et al.* Characteristic sizes of life in the oceans, from bacteria to whales. *Annu. Rev. Mar. Sci.* **8**, 217–241 (2016).
6. Brose, U. *et al.* Predator traits determine food-web architecture across ecosystems. *Nat. Ecol. Evol.* **3**, 919–927 (2019).
7. Woodward, G. *et al.* Body size in ecological networks. *Trends Ecol. Evol.* **20**, 402–409 (2005).
8. Kelley, N. P. & Pyenson, N. D. Evolutionary innovation and ecology in marine tetrapods from the Triassic to the Anthropocene. *Science* **348**, aaa3716 (2015).
9. Long, J. A. The first jaws. *Science* **354**, 280–281 (2016).
10. Bonner, J. T. Perspective: the size-complexity rule. *Evolution* **58**, 1883–1890 (2004).
11. Vermeij, G. J. The Mesozoic marine revolution: evidence from snails, predators and grazers. *Paleobiology* **3**, 245–258 (1977).
12. Zuschin, M., Stachowitsch, M. & Stanton, R. J. Patterns and processes of shell fragmentation in modern and ancient marine environments. *Earth-Sci. Rev.* **63**, 33–82 (2003).
13. Foffa, D., Young, M. T., Stubbs, T. L., Dexter, K. G. & Brusatte, S. L. The long-term ecology and evolution of marine reptiles in a Jurassic seaway. *Nat. Ecol. Evol.* **2**, 1548–1555 (2018).
14. Guinot, G. & Condamine, F. L. Global impact and selectivity of the Cretaceous-Paleogene mass extinction among sharks, skates, and rays. *Science* **379**, 802–806 (2023).
15. Alroy, J. The shifting balance of diversity among major marine animal groups. *Science* **329**, 1191–1194 (2010).
16. Huntley, J. W. & Kowalewski, M. Strong coupling of predation intensity and diversity in the Phanerozoic fossil record. *Proc. Natl. Acad. Sci.* **104**, 15006–15010 (2007).
17. Klompmaker, A. A., Kowalewski, M., Huntley, J. W. & Finnegan, S. Increase in predator-prey size ratios throughout the Phanerozoic history of marine ecosystems. *Science* **356**, 1178–1180 (2017).
18. Albertin, C. B. *et al.* Genome and transcriptome mechanisms driving cephalopod evolution. *Nat. Commun.* **13**, 2427 (2022).
19. Klug, C., Frey, L., Korn, D., Jattiot, R. & Rücklin, M. The oldest Gondwanan cephalopod mandibles (Hangenberg Black Shale, Late Devonian) and the mid-Palaeozoic rise of jaws. *Palaeontology* **59**, 611–629 (2016).

20. Amodio, P. *et al.* Grow smart and die young: why did cephalopods evolve intelligence? *Trends Ecol. Evol.* **34**, 45–56 (2019).

21. Kröger, B., Vinther, J. & Fuchs, D. Cephalopod origin and evolution: A congruent picture emerging from fossils, development and molecules. *BioEssays* **33**, 602–613 (2011).

22. Gilbert, P. U. P. A. *et al.* Biomineralization: Integrating mechanism and evolutionary history. *Sci. Adv.* **8**, eabl9653 (2022).

23. Hatton, I. A., Heneghan, R. F., Bar-On, Y. M. & Galbraith, E. D. The global ocean size spectrum from bacteria to whales. *Sci. Adv.* **7**, eabh3732 (2021).

24. Packard, A. Cephalopods and fish: the limits of convergence. *Biol. Rev.* **47**, 241–307 (1972).

25. Tittensor, D. P. *et al.* Global patterns and predictors of marine biodiversity across taxa. *Nature* **466**, 1098–1101 (2010).

26. Souquet, L. *et al.* The growth of the buccal mass in *Sepia officinalis*: functional changes throughout ontogeny. *Mar. Biol.* **170**, 82 (2023).

27. Fuchs, D. Part M, Chapter 23G: Systematic descriptions: Octobrachia. *Treatise Online* **138**, 1–52 (2020).

28. Hoffmann, R., Stevens, K., Keupp, H., Simonsen, S. & Schweigert, G. Regurgitalites – a window into the trophic ecology of fossil cephalopods. *J. Geol. Soc.* **177**, 82–102 (2020).

29. Clarke, M. R. & Maddock, L. Beaks of living coleoid Cephalopoda. in *Paleontology and neontology of cephalopods* (eds. Clarke, M. R. & Trueman, E. R.) 123–131 (Academic Press, Cambridge, 1988).

30. Clarke, M. R. The identification of cephalopod 'beaks' and the relationship between beak size and total body weight. *Bull. Br. Mus. Nat. Hist. Zool.* **8**, 419–480 (1962).

31. Tanabe, K., Trask, P., Ross, R. & Hikida, Y. Late Cretaceous octobrachiate coleoid lower jaws from the North Pacific regions. *J. Paleontol.* **82**, 398–408 (2008).

32. Tanabe, K. & Hikida, Y. Jaws of a New Species of *Nanaimoteuthis* (Coleoidea: Vampyromorphida) from the Tuironian of Hokkaido, Japan. *Paleontol. Res.* **14**, 145–150 (2010).

33. Tanabe, K., Misaki, A. & Ubukata, T. Late Cretaceous record of large soft-bodied coleoids based on lower jaw remains from Hokkaido, Japan. *Acta Palaeontol. Pol.* **60**, 27–38 (2015).

34. Tanabe, K., Misaki, A., Hikida, Y. & Nishimura, T. New records of coleoid cephalopod jaws from the Upper Cretaceous of Hokkaido, Japan, and their paleobiogeographic and evolutionary implications. *Cretac. Res.* **70**, 128–141 (2017).

35. Takashima, R. *et al.* Geology and stratigraphy of forearc basin sediments in Hokkaido, Japan: Cretaceous environmental events on the north-west Pacific margin. *Cretac. Res.* **25**, 365–390 (2004).

36. Cheng, H. K., Oh, S. W., Price, B., Schwing, A. & Lee, J.-Y. Tracking anything with decoupled video segmentation. *Proc. Int. Conf. Comput. Vis.* 1316–1326 (2023).

37. Clarke, M. R. *A Handbook for the Identification of Cephalopod Beaks*. (Clarendon Press, Oxford, 1986).

38. Young, R. E., Clarke, M. R., Vecchione, M. & Mangold, K. M. Beak terminology. *Tree of Life* http://tolweb.org/notes/?note_id=1980 (2000).

39. Golikov, A. V. *et al.* Deep and cold: are Boreal and Arctic finned octopods, *Stauroteuthis syrtensis* and *Cirroteuthis muelleri* (Cephalopoda, Octopoda, Cirrata), ecological analogues? *Deep Sea Res. Part Oceanogr. Res. Pap.* **181**, 103706 (2022).

40. Lu, C. C. & Ickeringill, R. Cephalopod beak identification and biomass estimation techniques: tools for dietary studies of southern Australian finfishes. *Mus. Vic. Sci. Rep.* **6**, 1–65 (2002).

41. Smale, M. J., Clarke, M. R., Klages, N. T. W. & Roeleveld, M. A. C. Octopod beak identification — resolution at a regional level (Cephalopoda, Octopoda: southern Africa). *South Afr. J. Mar. Sci.* **13**, 269–293 (1993).

42. Jereb, P., Roper, C. F. E., Norman, M. D. & Finn, J. K. *Cephalopods of the World. An Annotated and Illustrated Catalogue of Cephalopod Species Known to Date: Volume 3. Octopods and Vampire Squids*. (Food and Agriculture Organization of the United Nations, Rome, 2016).

43. Tan, Y. *et al.* Infiltration of chitin by protein coacervates defines the squid beak mechanical gradient. *Nat. Chem. Biol.* **11**, 488–495 (2015).

44. Taite, M. *et al.* Genome skimming elucidates the evolutionary history of Octopoda. *Mol. Phylogenet. Evol.* **182**, 107729 (2023).

45. Rosa, R., Lopes, V. M., Guerreiro, M., Bolstad, K. & Xavier, J. C. Biology and ecology of the world's largest invertebrate, the colossal squid (*Mesonychoteuthis hamiltoni*): a short review. *Polar Biol.* **40**, 1871–1883 (2017).

46. Ferrón, H. G. Evidence of endothermy in the extinct macropredatory osteichthyan *Xiphactinus audax* (Teleostei, Ichthyodectiformes). *J. Vertebr. Paleontol.* **39**, (2020).

47. Shimada, K., Everhart, M. J., Decker, R. & Decker, P. D. A new skeletal remain of the durophagous shark, *Ptychodus mortoni*, from the Upper Cretaceous of North America: an indication of gigantic body size. *Cretac. Res.* **31**, 249–254 (2010).

48. Gutarra, S., Stubbs, T. L., Moon, B. C., Palmer, C. & Benton, M. J. Large size in aquatic tetrapods compensates for high drag caused by extreme body proportions. *Commun. Biol.* **5**, 1–12 (2022).

49. Polcyn, M. J., Jacobs, L. L., Araújo, R., Schulp, A. S. & Mateus, O. Physical drivers of mosasaur evolution. *Palaeogeogr. Palaeoclimatol. Palaeoecol.* **400**, 17–27 (2014).

50. Villanueva, R., Perricone, V. & Fiorito, G. Cephalopods as Predators: A Short Journey among Behavioral Flexibilities, Adaptions, and Feeding Habits. *Front. Physiol.* **8**, (2017).

51. Güntürkün, O., Ströckens, F. & Ocklenburg, S. Brain Lateralization: A Comparative Perspective. *Physiol. Rev.* **100**, 1019–1063 (2020).

52. Pronk, R., Wilson, D. R. & Harcourt, R. Video playback demonstrates episodic personality in the gloomy octopus. *J. Exp. Biol.* **213**, 1035–1041 (2010).

53. Currey, J. D. The failure of exoskeletons and endoskeletons. *J. Morphol.* **123**, 1–16 (1967).

Chapter 3. Vampyromorpha

Summary

The vampire squid (*Vampyroteuthis infernalis*) is an iconic deep-sea cephalopod reported from oxygen-minimum zones of tropical and temperate regions worldwide, mainly at a depth of 600–1500 m. Its ancestral groups, in contrast, inhabited shallow marine and were active predators fed on fishes and other cephalopods. It has attracted significant interest in how it migrated from shallow water to deep sea and developed its unique ecology. However, a gap of 90 Ma (from the Early Aptian to the Oligocene) exists in fossil records of the vampire squid lineage, Vampyromorpha. Due to this gap, the precise understanding of how vampyromorphid habitats have shifted from the shallow marine to the abyss is hampered by the long-time absence of fossil records.

In this study, 45 beak fossils were obtained from the Upper Cretaceous Yezo Group of Japan. Those beaks can be classified into six species of three genera, considerably close to the extant *V. infernalis*. Beak fossils fill the middle 30 Myr of the gap in vampyromorphid fossil records. The morphological resemblance indicates similar feeding habits to extant ones, which mainly feed on small and soft prey. The body size of the Cretaceous vampire squids was small like extant ones, estimated to be less than 30 mm in mantle length of adults. It might be the cause of the gap since the Pacific region lacks lagerstätten. Vampire squids are commonly found throughout the Late Cretaceous, and their habitats probably include neritic zones with high-oxygen levels inferred from the depositional environment of samples. These results suggest that ecological shifts might precede the migration into the deep sea. The migration of vampire squids was probably gradual, and the Late Cretaceous records represent the middle stage of their decline.

3.1. Introduction

Niche expansions are considered signals of significant shifts like morphological novelties, competitions, or environmental changes[1]. When and how creatures have advanced into new ecospaces is a primary concern of evolutionary biology and geoscience. Soft-bodied cephalopods, including squids, cuttlefishes, and octopuses, show global distribution and tremendous biomass in the current oceans[2,3]. In this group, a significant number of species inhabit abyssal zones with manifold ecology and morphological features[2–4]. Therefore, those taxa have attracted considerable interest as model cases of adaptive evolution and niche expansion to severe environments[4,5].

Vampire squid (*Vampyroteuthis infernalis*) is an iconic deep-sea cephalopod reported from oxygen minimum zones of worldwide tropical to temperate regions mainly in a depth of 600–1500 m[6–9]. Laboratory experiments and in situ observation in previous studies showed that feeding strategy as an opportunistic detritivore and inactive locomotion allowed its success in such zones with few predators and competitors[8]. The vampire squid is relatively small and shows characteristic ecology of the lowest metabolic rate among extant cephalopods[8]. It is often regarded as a phylogenetic relic due to the mosaic morphology of squids and octopuses[6]. Owing to this peculiar feature, *V. infernalis* composes a monophyletic order and family, Vampyromorpha and Vampyroteuthidae, in the extant cephalopods[9,10]. However, a large number of related fossil taxa have been known from lagerstätten of the world, including the Pacific, Tethys, Australia, and the Western Interior Seaway[11–14]. Recent morphological examinations and molecular analyses suggested that vampire squid belongs to the clade Vampyropoda, which includes octopuses and differentiated from the squid lineage in the Paleozoic[15–18]. This clade is characterized by the demineralized gladius or complete loss of shell vestige[19]. Vampyropoda has its oldest indisputable record in the Late Triassic and diverged in the Early Jurassic[13]. Mesozoic vampyropods show high diversity in gladius morphology and are divided into three suborders: Prototeuthina, Teudopseina, and Loligosepiina[12,13]. The vampire squid is presumed to have originated from Loligosepiina, implied by changes in gladius form in the Jurassic and the Cretaceous[20]. Mesozoic vampyromorpha probably inhabited shallow marine on continental shelves, inferred from the depositional environment of those localities[14], and were active predators fed on fishes and other cephalopods, as suggested by specimens fossilized with possible prey[21,22].

Despite abundant specimens, vampyropod fossils are seldom discovered from sediments other than lagerstätten due to a low fossilization potential induced by the lack of mineralized tissues[12,23]. Major sources of their fossils are concentrated on Mesozoic Tethyan deposits and provide significantly restricted clues for their evolutionary history[24]. Therefore, a gap of 90 Myr exists in vampyromorphid fossil records from the Early Aptian to the Oligocene[14]. The Oligocene species *Necroteuthis hungarica* from Hungary is placed in a close position to extant *V. infernalis* (the same family) and is presumed to inhabit bathyal, oxygen-depleted zones by geological settings[14]. However, the precise understanding of how vampyromorphid habitats have shifted from the shallow marine to the abyss is hampered by the long-time absence of fossil records.

This study describe 48 beak fossils obtained from the Upper Cretaceous Yezo Group of Japan. Beaks are paired feeding organs consisting of the upper and lower ones, made of chemically tolerant chitin-protein complex, and unique to cephalopods[25]. Beak form is subjected to taxonomic differences and enables species-level identification, especially in the lower one of extant coleoids[26]. All described fossils are lower beaks and exhibit traits similar to the sole extant Vampyromorpha, *V. infernalis*. Those discoveries brought new insights into the evolutionary history, ecology, and biogeography of

vampire squids.

3.2. Material

In this study, I searched for squid beaks in 35 fist-sized carbonate concretions covering the Middle Albian to Early Maastrichtian interval (110–70 Ma: Table 1). Carbonate concretions reflect a faunal cross-section of a short period of time because they were formed within several weeks or months and were not reworked[27,28]. The material studied here comes from stratigraphically well-dated shelf deposits of northern Japan, the Cretaceous standard section of the circum-North Pacific[27].

Institutional abbreviations

NMNS: National Museum of Nature and Science, Tokyo, Japan.

3.3. Methods

3.3.1. Destructive tomography and extraction as a digital 3D model

This study used a new grinding tomography system (Paleobiology Lab, Hokkaido University: Fig. 1) that scans rocks in their original colors with high-resolution. In a first step, whole rocks were automatically converted into sequential cross-sectional images, along with numerous fossils hidden inside the rocks. The rock samples were embedded into a plaster jacket and ground at equal intervals of 10, 25, or 50 μm (Table 1). High-precision diamond cup wheels were used for surface grinding (diamond size ~15 μm: Asahi Diamond Industrial Co., Ltd; ~20 μm: Noritake Co., Ltd). The new surfaces were then thinly coated with an oil-based coolant to make the images clear. Each surface was then photographed in color with high-resolution digital cameras (8,688 x 5,792 pixels/image in EOS 5Ds, Canon; 19,008 x 12,672 pixels/image in α7R IV, SONY). These grinding–photographing processes were computerized, controlled numerically, and repeated automatically.

In a second step, the fossil beaks were discovered from each image dataset and its animation. The beak fossils were then extracted from the host rocks individually as digital 3D models. In a following process, the areas of the beak fossils were masked by RGB values in the IV-Seg (IVLab Co., Ltd.) and subsequently imported to Amira 6.2.0 (Thermo Fisher Scientific, Inc.) for 3D reconstruction. The 3D models underwent minimal smoothing consistent with imported masks to avoid modifying the diagnostic characters. All measurements and taxonomical interpretations are based on these 3D models.

3.3.2. Taxonomy

The same terminology and methods as Chapter 1 were used here. All measurements are documented in Table 13.

3.3.3. Body size estimation

Methods to estimate the body lengths of extant vampire squids from the size of their isolated lower beaks have been established in the past. Based on biometric measurements, a correlation between HL and mantle length has been calculated as an allometric equation for the extant species[26]. The equations were here used to calculate the mantle lengths of the Late Cretaceous vampire squids.

3.4. Systematic palaeontology

Subclass **Coleoidea** Bather, 1888
Order **Vampyromorpha** Robison, 1929
Family **Vampyroteuthidae** Thiele, 1915

Remarks. The lower beak of *Vampyroteuthis* Chun, 1903, the only extant genus of this family, is described as follows in Clarke (1986)[26]; *"characterized by a jaw angle which is close to a right angle, a very high wing fold which is thickened to form a cutting edge which obscures the jaw angle and more than half the jaw edge in profile, a small, flat ledge between the wing fold and the shoulder which may sometimes be cartilage, no shoulder ridge, a very broad hood which obscures over four-fifths of the crest in profile and has no notch, a broadly rounded, unthickened crest, and a lateral wall with no notch near the crest and a slight, inwardly directed fold towards the anterior end (this may be absent)."* The flat ledge and wing folds in this description were reinterpreted as the bridges and their product in a later work[29]. The lower beak of Vampyroteuthidae can be distinguished from that of all other known cephalopod families by the bridges, which extend from the hookless rostral tip to the ventral end of lateral walls, are nearly parallel to the transverse axis in horizontal sections, and are connected to a wing at its outer edge.

Genus ***Vampyrobeccus*** gen. nov.

Etymology. Latinized form of the Slavic word 'vampyr' (vampire) + Latin 'beccus' (beak).
Type species. *Vampyrobeccus pusillus* sp. nov.
Diagnosis. The lower beak is small, less than 10 mm in crest length. JELL/EJEL ranges from 0.27 to 0.44, and LRL/RW from 0.85 to 1.07. No hooks or dents exist around the rostrum. Bridges extend from the rostral tip to the ventral end of the inner lamella, are nearly parallel to the transverse axis in horizontal sections, and broaden ventrally. Shoulder blades are small. Wings are thin, but in certain species, they become thick around the joint with the adjacent bridge. The wings rise from the lateral edge of a bridge without forming a wing fold. The hood is long and has no notch. Lateral walls are as high as long.
Discussion. The lower beak morphology of this genus is almost identical to *Vampyroteuthis*. Since diagnostic characters in other organs cannot be observed by discovered fossils, this genus is here regarded as a parataxon of the extant family, Vampyroteuthidae. It differs from *Angustivampyrus* gen. nov. by its wider rostrum (LRL/RW is 0.85–1.07 in *Vampyrobeccus*, 1.27–1.33 in *Angustivampyrus*: Table 13). It also differs from *Mysticivampyrus* gen. nov. by its smaller rostrum (JELL/EJEL is 0.27–0.44 in *Vampyrobeccus*, 0.54–0.64 in *Mysticivampyrus*: Table 13). It can be distinguished from *Paleothauma* gen. nov. by its thin anterior part of the wings and shorter lateral walls.
Occurrence. earliest Cenomanian to Early Maastrichtian; the Yezo Group in Hokkaido, Japan.

Vampyrobeccus pusillus sp. nov.
Fig. 24A–E

Etymology. Latin 'pusillus' (tiny).
Diagnosis. The lower beak is small, less than 10 mm in crest length. JELL/EJEL ranges from 0.27 to 0.43, and LRL/RW from 0.87 to 1.03. No hooks or dents exist around the rostrum. Bridges extend

from the rostral tip to the ventral end of the inner lamella, are nearly parallel to the transverse axis in horizontal sections, and broaden ventrally. Shoulder blades are very thin and small. Wings are entirely thin. The wings rise from the lateral edge of a bridge without forming a wing fold. Both the anterior and posterior margins of the wings are almost straight. Wing angles range from 109.0° to 126.4°. The hood is long and has no notch. Lateral walls are as high as long.

Description. The lower beaks obtained in this study are all smaller than 10 mm in crest length. The rostrum is small, in which JELL/EJEL ranges from 0.27 to 0.43. It is moderately wide, showing LRL/RW that ranges from 0.87 to 1.03. No hooks or dents exist around the rostrum. Bridges extend from the rostral tip to the ventral end of the inner lamella, form distinct edges at their medial and lateral margins, and broaden ventrally. They are gently curved and nearly parallel to the transverse axis in horizontal sections. Shoulder blades are very thin and small. Wings are entirely thin. The wings rise from the lateral edge of a bridge without forming a wing fold. Both the anterior and posterior margins of the wings are almost straight. The anterior margin of the wings becomes anterodorsally convex or forms a subangular corner with the lateral edge of a bridge. Wing angles range from 109.0° to 126.4°. The hood is long and has no notch. Lateral walls are as high as long and parallelogram-shaped.

Comparison. This species differs from *V. rupis* sp. nov. by acuter wing angles (109.0°–126.4° in *V. pusillus*, 136.5°–148.0° in *V. rupis*: Table 13). The basal part of the wings becomes anterodorsally convex or forms a subangular corner in *V. pusillus*, whereas it forms a rounded corner in *V. rupis*. This species can be distinguished from *V. robustus* by its shoulder blades that are not connected to the adjacent wing, and from *V. ornatus* by the nearly straight anterior margin of the wings.

Occurrence. Late Cenomanian to Early Maastrichtian; the Yezo Group in Hokkaido, Japan.

Vampyrobeccus rupis sp. nov.
Fig. 24F–J

Etymology. Latin ‘rupes’ (cliff), referring to wings extending ventrally at a steep angle.

Diagnosis. The lower beak is small, less than 10 mm in crest length. JELL/EJEL ranges from 0.27 to 0.44, and LRL/RW from 0.86 to 1.02. No hooks or dents exist around the rostrum. Bridges extend from the rostral tip to the ventral end of the inner lamella, are nearly parallel to the transverse axis in horizontal sections, and broaden ventrally. Shoulder blades are very thin and small. Wings are entirely thin. The wings rise from the lateral edge of a bridge without forming a wing fold. Wing angles range from 136.5° to 148.0°. Both the anterior and posterior margins of the wings are almost straight. The hood is long and has no notch. Lateral walls are as high as long.

Description. The lower beaks obtained in this study are all smaller than 10 mm in crest length. The rostrum is small, in which JELL/EJEL ranges from 0.27 to 0.44. It is moderately wide, showing LRL/RW that ranges from 0.86 to 1.02. No hooks or dents exist around the rostrum. Bridges extend from the rostral tip to the ventral end of the inner lamella, form distinct edges at their medial and lateral margins, and broaden ventrally. They are gently curved and nearly parallel to the transverse axis in horizontal sections. Shoulder blades are very thin and small. Wings are entirely thin. The wings rise from the lateral edge of a bridge without forming a wing fold. Both the anterior and posterior margins of the wings are almost straight. The anterior margin of the wings forms a rounded corner with the lateral edge of a bridge. Wing angles range from 136.5° to 148.0°. The hood is long and has no notch. Lateral walls are as high as long and parallelogram-shaped.

Comparison. This species differs from *V. pusillus* sp. nov. by more obtuse wing angles (136.5°–148.0°

in *V. rupis*, 109.0°–126.4° in *V. pusillus*: Table 13). The basal part of the wings forms a rounded corner in *V. rupis*, whereas it becomes anterodorsally convex or forms a subangular corner in *V. pusillus*. This species can be distinguished from *V. robustus* by its shoulder blades that are not connected to the adjacent wing, and from *V. ornatus* by the nearly straight anterior margin of the wings.
Occurrence. Middle Turonian to Late Campanian; the Yezo Group in Hokkaido, Japan.

Vampyrobeccus robustus sp. nov.
Fig. 24K–O

Etymology. Latin 'robustus' (robust), referring to wings strongly connected to a bridge.
Diagnosis. The lower beak is small, less than 10 mm in crest length. JELL/EJEL ranges from 0.29 to 0.44, and LRL/RW from 0.85 to 1.07. No hooks or dents exist around the rostrum. Bridges extend from the rostral tip to the ventral end of the inner lamella, are nearly parallel to the transverse axis in horizontal sections, and broaden ventrally. Wings become thick around the joint with the adjacent bridge. The wings rise from the lateral edge of a bridge without forming a wing fold. Both the anterior and posterior margins of the wings are almost straight. Wing angles range from 130.1° to 154.5°. Shoulder blades are small. Planar shoulders connect the dorsal margin of a shoulder blade and that of the adjacent wing. The hood is long and has no notch. Lateral walls are as high as long.
Description. The lower beaks obtained in this study are all smaller than 10 mm in crest length. The rostrum is small, in which JELL/EJEL ranges from 0.29 to 0.44. It is moderately wide, showing LRL/RW that ranges from 0.85 to 1.07. No hooks or dents exist around the rostrum. Bridges extend from the rostral tip to the ventral end of the inner lamella, form distinct edges at their medial and lateral margins, and broaden ventrally. They are gently curved and nearly parallel to the transverse axis in horizontal sections. Wings become thick around the joint with the adjacent bridge. The wings rise from the lateral edge of a bridge without forming a wing fold. Both the anterior and posterior margins of the wings are almost straight. The anterior margin of the wings forms a rounded corner with the lateral edge of a bridge. Wing angles range from 136.5° to 148.0°. Shoulder blades are small. Planar shoulders connect the dorsal margin of a shoulder blade and that of the adjacent wing, covering the ventral part of a bridge. The hood is long and has no notch. Lateral walls are as high as long and parallelogram-shaped.
Comparison. This species differs from the other species of *Vampyrobeccus* by its shoulders that cover the ventral part of the neighbouring bridge.
Occurrence. Middle Turonian to Late Campanian; the Yezo Group in Hokkaido, Japan.

Vampyrobeccus ornatus sp. nov.
Fig. 24P–T

Etymology. Latin 'ornatus' (decorated).
Diagnosis. The lower beak is small, less than 10 mm in crest length. JELL/EJEL is ~0.37. The ratio of EJEL and the distance between the anteroventral end of the two lateral walls is ~0.88. No hooks or dents exist around the rostrum. Bridges extend from the rostral tip to the ventral end of the inner lamella, are nearly parallel to the transverse axis in horizontal sections, and broaden ventrally. The anterior margin of the wings forms a pointed tip at its basal part. Wing angles are ~137.9°. The wings rise from the lateral edge of a bridge without forming a wing fold. Wings are entirely thin. The hood is long and

has no notch.

Description. The lower beak obtained in this study is smaller than 10 mm in crest length. The rostrum is small, showing JELL/EJEL of ~0.37. It is moderately wide, in which the ratio of EJEL and the distance between the anteroventral end of the two lateral walls is ~0.88. No hooks or dents exist around the rostrum. Bridges extend from the rostral tip to the ventral end of the inner lamella and form distinct edges at their medial and lateral margins. They broaden ventrally with a high expansion rate, and the ration between their width at the ventral end and EJEL is ~0.17. The bridges are gently curved and nearly parallel to the transverse axis in horizontal sections. Shoulder blades are absent in the observed beak. The anterior margin of the wings forms a pointed tip at its basal part and a subangular corner with the lateral edge of a bridge. This character is probably not the result of deformation, inferred from symmetrically preserved wings. Wings are entirely thin. The wings rise from the lateral edge of a bridge without forming a wing fold. Wing angles are ~137.9°. The hood is long and has no notch. Lateral walls are as high as long.

Comparison. *V. ornatus* can be easily distinguished from other species by its peculiar wing form and a high expansion rate of bridges.

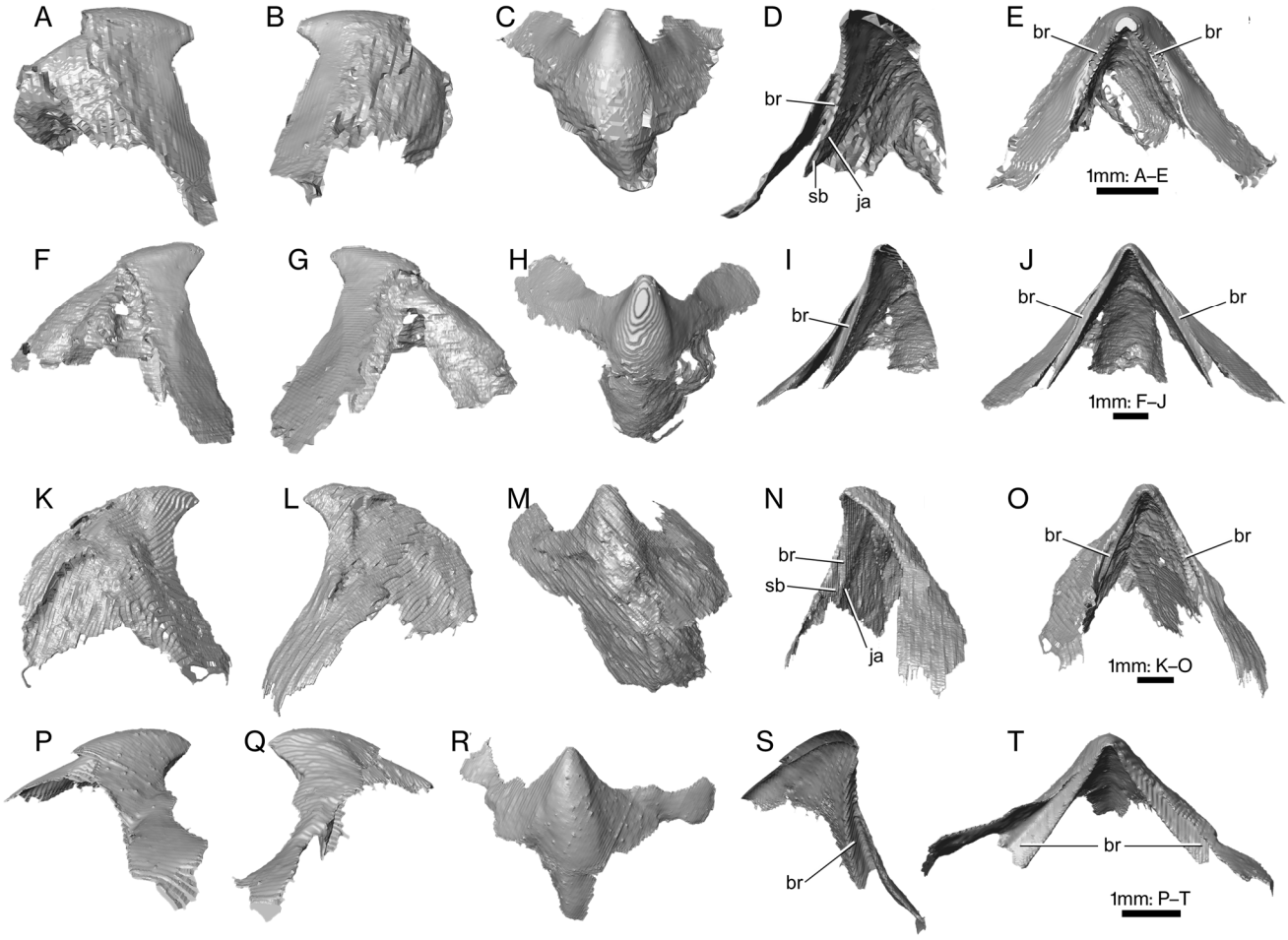


Fig. 24. Lower beaks of *Vampyrobeccus*.
(**A** to **E**) *Vampyrobeccus pusillus* sp. nov., NMNS_DS00009_SikV7tD.stl. (**F** to **J**) *Vampyrobeccus rupis* sp. nov., NMNS_DS00041_3kNoelr.stl. (**K** to **O**) *Vampyrobeccus robustus* sp. nov., NMNS_DS00171_hflEysv.stl. (**P** to **T**) *Vampyrobeccus ornatus* sp. nov., NMNS_DS00068_fE0GOBN.stl. (A, F, K, and P) left lateral view; (B, G, L, and Q) right lateral view; (C, H, M, and R) dorsal view; (D, I, N, and S) oblique view around jaw edge and shoulder; (E, J, O, and T) frontal view. br, bridge; ja, jaw angle; sb, shoulder blade.

Occurrence. earliest Cenomanian; the Yezo Group in Hokkaido, Japan.

Genus ***Angustivampyrus*** gen. nov.

Etymology. Latin 'angustus' (narrow) + Latinized form of the Slavic word 'vampyr' (vampire).
Type species. *Angustivampyrus gracilis* sp. nov.
Diagnosis. The lower beak is small, less than 10 mm in crest length. JELL/EJEL ranges from 0.30 to 0.35, and LRL/RW from 1.27 to 1.33. No hooks or dents exist around the rostrum. Bridges extend from the rostral tip to the ventral end of the inner lamella, are nearly parallel to the transverse axis in horizontal sections, and broaden ventrally. Shoulder blades are very thin and small. Wings are entirely thin. The wings rise from the lateral edge of a bridge without forming a wing fold. Both the anterior and posterior margins of the wings are almost straight. The hood is long and has no notch. Lateral walls are as high as long.
Comparison. This genus differs from *Vampyrobeccus* gen. nov. by its narrower rostrum (LRL/RW is 1.27–1.33 in *Angustivampyrus*, 0.85–1.07 in *Vampyrobeccus*: Table 13). It also differs from *Mysticivampyrus* gen. nov. by its smaller rostrum (JELL/EJEL is 0.30–0.35 in *Angustivampyrus*, 0.54–0.64 in *Mysticivampyrus*: Table 13). It can be distinguished from *Paleothauma* gen. nov. by its thin anterior part of the wings and shorter lateral walls.
Occurrence. Late Cenomanian to Late Turonian; the Yezo Group in Hokkaido, Japan.

Angustivampyrus gracilis sp. nov.
Fig. 25A–E

Etymology. Latin 'gracilis (thin).
Diagnosis. Same as for genus due to monotypy.
Description. The lower beaks obtained in this study are all smaller than 10 mm in crest length. The rostrum is small, in which JELL/EJEL ranges from 0.30 to 0.35. It is narrow, showing LRL/RW that ranges from 1.27 to 1.33. No hooks or dents exist around the rostrum. Bridges extend from the rostral tip to the ventral end of the inner lamella, form distinct edges at their medial and lateral margins, and

broaden ventrally. They are gently curved and nearly parallel to the transverse axis in horizontal sections. Shoulder blades are very thin, small, and not connected to the adjacent wing. Wings are entirely thin. The wings rise from the lateral edge of a bridge without forming a wing fold. Both the anterior and posterior margins of the wings are almost straight. The anterior margin of the wings becomes anterodorsally convex or forms a subangular corner with the lateral edge of a bridge. Wing angles range from 132.0° to 134.9°. The hood is long and has no notch. Lateral walls are as high as long and parallelogram-shaped.
Comparison. See the comparison of the genus.
Occurrence. Late Cenomanian to Late Turonian; the Yezo Group in Hokkaido, Japan.

Genus ***Mysticivampyrus*** gen. nov.

Etymology. Latin 'mysticus' (mystic) + Latinized form of the Slavic word 'vampyr' (vampire).

Type species. *Mysticivampyrus megachasma* sp. nov.
Diagnosis. The lower beak is small, less than 10 mm in crest length. JELL/EJEL ranges from 0.54 to 0.64. The ratio of EJEL and the distance between the anteroventral end of the two lateral walls is from 0.97 to 1.00. No hooks or dents exist around the rostrum. Bridges extend from the rostral tip to the ventral end of the inner lamella, are nearly parallel to the transverse axis in horizontal sections, and broaden ventrally. Wings become thick around the joint with the adjacent bridge. The wings rise from the lateral edge of a bridge without forming a wing fold. Both the anterior and posterior margins of the wings are almost straight. The hood is long and has no notch. Lateral walls are as high as long.
Comparison. This genus differs from *Vampyrobeccus* gen. nov. and *Angustivampyrus* gen. nov. by its larger rostrum (JELL/EJEL is 0.54–0.64 in *Mysticivampyrus,* 0.27–0.44 in *Vampyrobeccus,* 0.30–0.35 in *Angustivampyrus*: Table 13). It can be distinguished from *Paleothauma* gen. nov. by its thin anterior part of the wings and shorter lateral walls.
Occurrence. earliest Cenomanian and Santonian; the Yezo Group in Hokkaido, Japan.

Mysticivampyrus megachasma sp. nov.
Fig. 25F–J

Etymology. After the Ancient Greek '*megas*' (large) + the Ancient Greek '*khasma*' (open mouth).
Diagnosis. Same as for the genus due to monotypy.
Description. The lower beaks obtained in this study are all smaller than 10 mm in crest length. The rostrum shows moderate size, in which JELL/EJEL ranges from 0.54–0.64. It is moderately wide, in which the ratio of EJEL and the distance between the anteroventral end of the two lateral walls is 0.97–1.00. No hooks or dents exist around the rostrum. Bridges extend from the rostral tip to the ventral end of the inner lamella, form distinct edges at their medial and lateral margins, and broaden ventrally. They are gently curved and nearly parallel to the transverse axis in horizontal sections. Shoulder blades are absent in the observed beaks. Wings become thick around the joint with the adjacent bridge, making a rounded boundary between the two parts. The wings rise from the lateral edge of a bridge without forming a wing fold. Both the anterior and posterior margins of the wings are almost straight. The anterior margin of the wings becomes anterodorsally convex or forms a subangular corner with the lateral edge of a bridge. Wing angles range from 129.9° to 134.8°. The anterior margin of the wings forms a rounded corner with the lateral edge of a bridge. The hood is long and has no notch. Lateral walls are as high as long.
Comparison. Same as for the genus.
Occurrence. earliest Cenomanian and Santonian; the Yezo Group in Hokkaido, Japan.

Genus ***Paleothauma*** gen. nov.

Etymology. After the Ancient Greek 'palaios' (ancient) + the Ancient Greek 'thauma' (wonder).
Type species. *Paleothauma aprophata* sp. nov.
Diagnosis. The lower beak is small, less than 10 mm in crest length. JELL/EJEL ranges from 0.25 to 0.37, and LRL/RW is ~0.86. No hooks or dents exist around the rostrum. Bridges extend from the rostral tip to the ventral end of the inner lamella and are nearly parallel to the transverse axis in horizontal sections. Their width increases ventrally in the dorsal half and is almost constant in the ventral half. Shoulder blades are very thin and small. Wings are thickened in the anterior part. The

wings rise from the lateral edge of a bridge without forming a wing fold. The hood is long and has no notch. Lateral walls are twice as long as high.
Comparison. *Paleothauma* gen. nov. differs from all other genera of Vampyroteuthidae Thiele, 1915 by its thickened anterior part of the wings and longer lateral walls.
Occurrence. Late Coniacian; the Yezo Group in Hokkaido, Japan.

Paleothauma aprophata sp. nov.
Fig. 25K–O

Etymology. After the Ancient Greek 'aprophatos' (unforetold).
Diagnosis. Same as for the genus due to monotypy.
Description. The lower beaks obtained in this study are smaller than 10 mm in crest length. The rostrum is small, in which JELL/EJEL ranges from 0.25 to 0.37. It is narrow, showing LRL/RW of ~0.86. No hooks or dents exist around the rostrum. Bridges extend from the rostral tip to the ventral end of the inner lamella and form distinct edges at their medial and lateral margins. Their width increases ventrally in the dorsal half and is almost constant in the ventral half. The bridges are gently curved and nearly parallel to the transverse axis in horizontal sections. Shoulder blades are very thin, small, and not connected to the adjacent wing. Both the anterior and posterior margins of the wings are almost straight. The anterior margin of the wings forms a rounded corner with the lateral edge of a bridge and is thickened. Wing angles range from 119.0° to 125.6°. The hood is long and has no notch. Lateral walls are twice as long as high and parallelogram-shaped.
Comparison. See the comparison of the genus.
Occurrence. Late Coniacian; the Yezo Group in Hokkaido, Japan.

3.5. Discussion & Conclusion

3.5.1. Chronostratigraphic ranges and diversity

The number of discovered vampyroteuthid beaks was approximately one-sixth of co-occurring squid beaks (Table 2). The proportion is small among all coleoids but still significantly larger than the current oceans[30]. Discovered beaks were classified into seven species of four genera (Table 13). *Angustivampyrus* has a narrower rostrum than *Vampyrobeccus*, but the phylogenetic relationship of the two genera is probably very close since changes in the rostral width have occurred frequently within the same families in extant squids[26]. *Mysticivampyrus* is also presumed to be close to *Vampyrobeccus* considering the resemblances in bridges and the outer lamella, which are rarely affected by lower taxonomic differences, although it shows more peculiar traits: a relatively large rostrum and the pigmentation pattern that preferentially progresses in the crest like squids[26,31]. The strongly curved outline around the rostrum in a profile view and the relatively long inner and outer lamellae in *Paleothauma* are similar to some extant Cirroctopoda. However, a close phylogenetic relationship between them is implausible because obvious bridges are never seen in extant octopods[26], which are predicted to have differentiated from Vampyromorphid lineage in the Early Jurassic. Beak forms of fossil vampyropods are poorly known due to flattened preservation[32], but extreme morphological similarity suggests a close relationship between new taxa and Vampyroteuthidae because beak forms of extant coleoids become entirely different in family-level comparison in most cases[26].

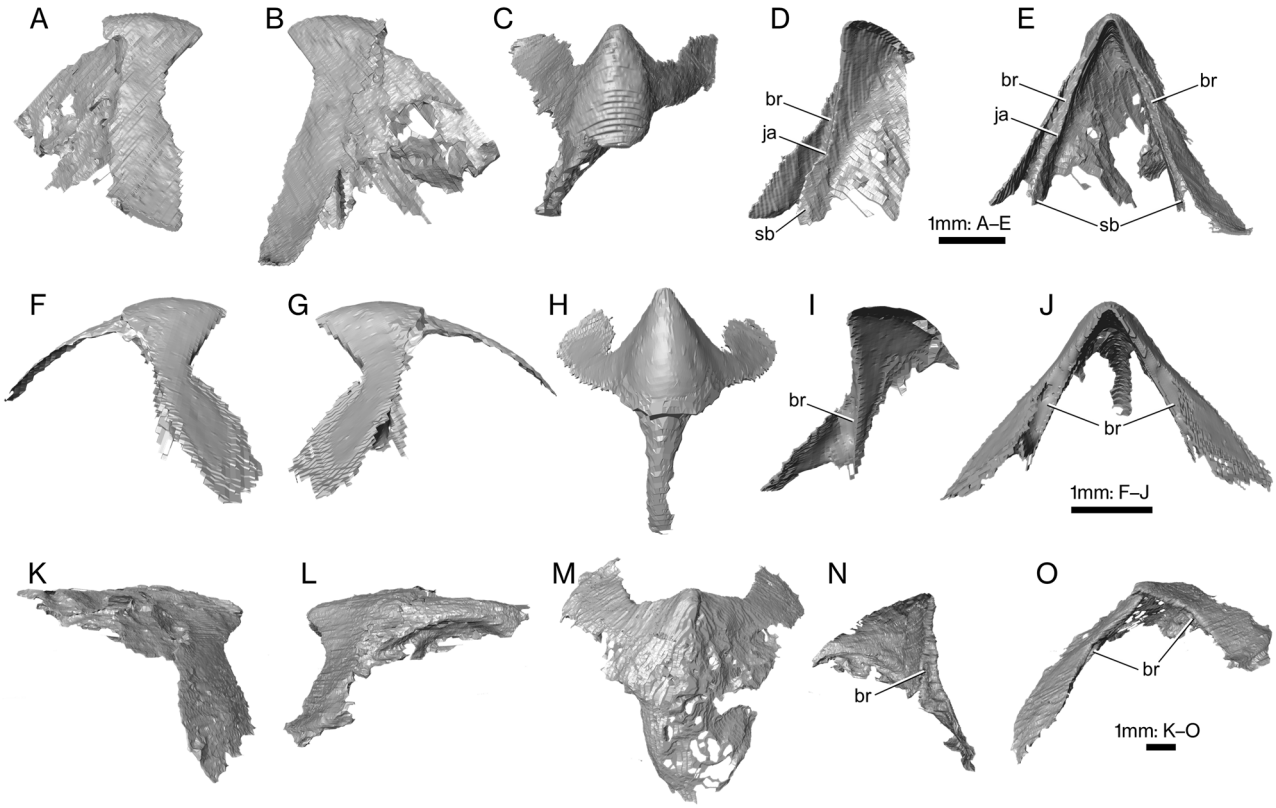


Fig. 25. Lower beaks of *Angustivampyrus*, *Mysticivampyrus*, & *Paleothauma*.
(**A** to **E**) *Angustivampyrus gracilis* sp. nov., NMNS_DS00173_H7WmleW.stl. (**F** to **J**) *Mysticivampyrus megachasma* sp. nov., NMNS_DS00011_riK07H1.stl. (**K** to **O**) *Paleothauma aprophata* sp. nov., NMNS_DS00083_fj8UthX.stl. (A, F, and K) left lateral view; (B, G, and L) right lateral view; (C, H, and M) dorsal view; (D, I, and N) oblique view around jaw edge and shoulder; (E, J, and O) frontal view. br, bridge; ja, jaw angle; sb, shoulder blade.

Three species with a relatively large number of individuals, *V. pusillus*, *V. rupis*, and *V. robustus*, occurred from a broad chronological range, which might mean 10 Myr of survival (Fig. 26). Especially the first ones were confirmed from all stages of the Late Cretaceous. The occurrence from the earliest Cenomanian (around 99 Ma)[33] is the oldest record of the family Vampyroteuthidae. At most, five species coexist in the same geological stage (Turonian and Coniacian: Fig 24). The diversity of Cretaceous vampire squids is high compared to the current state in that only a single species remains. The number of species and individuals, however, sharply dropped in the Maastrichtian (Fig. 26 and Table 13), the last stage of the Late Cretaceous. Despite the number of newly described species, their morphological disparity is not so high, as seen in that only seven characters have variations among discovered taxa, whereas more than thirty characters vary among squids in the current oceans[26].

3.5.2. Body size and implications for taphonomy

Obtained beak fossils were all less than 10 mm in their longest part (Table 13). In extant *V. infernalis*, the relationship between the size of beaks and the body size is formulated as a linear function of the hood length (HL) in the lower beak and the mantle length (ML)[26]. According to this formula, the original body sizes of discovered beaks are expected to fall between 5 to 30 mm ML (Table 13). This assumption shows that most of those individuals are smaller than the adults of extant *V. infernalis*, in

Table 13. Summary of Vampyromorphid lower beaks.

No.	Classification			Geological age	Measurements										Estimated mantle length (mm) = 9.02 × HL - 5.8
	Family	Genus	Species		CL (mm)	HL (mm)	WL (mm)	WA (degree)	LRL (mm)	RW (mm)	LRL/ RW	EJEL (mm)	JELL (mm)	JELL/ EJEL	
1	Vampyroteuthidae	*Vampyrobeccus*	*pusillus*	Middle Turonian	2.94	1.83	2.05	119.3	1.62	1.67	0.97	2.18	0.72	0.33	10.71
2	Vampyroteuthidae	*Vampyrobeccus*	*pusillus*	Late Turonian	2.13	1.26	2.00	118.9	-	-	-	1.35	0.47	0.35	5.57
3	Vampyroteuthidae	*Vampyrobeccus*	*pusillus*	Late Turonian	-	1.32	1.23	119.3	1.15	1.15	1.00	1.54	0.51	0.33	6.11
4	Vampyroteuthidae	*Vampyrobeccus*	*pusillus*	Late Cenomanian	-	1.16	1.47	119.2	1.47	1.54	0.95	1.72	0.69	0.40	4.66
5	Vampyroteuthidae	*Vampyrobeccus*	*pusillus*	Late Cenomanian	-	1.80	1.89	120.5	-	-	-	1.50	0.60	0.40	10.44
6	Vampyroteuthidae	*Vampyrobeccus*	*pusillus*	Late Coniacian	2.26	1.48	1.67	-	-	-	-	1.48	0.64	0.43	7.55
7	Vampyroteuthidae	*Vampyrobeccus*	*pusillus*	Santonian	2.23	1.43	1.45	124.1	1.10	1.27	0.87	1.54	0.56	0.36	7.10
8	Vampyroteuthidae	*Vampyrobeccus*	*pusillus*	Late Campanian	2.69	1.32	1.63	124.2	1.59	1.75	0.91	2.10	0.62	0.30	6.11
9	Vampyroteuthidae	*Vampyrobeccus*	*pusillus*	Early Maastrichtian	-	1.90	2.00	121.1	-	-	-	-	0.92	-	11.34
10	Vampyroteuthidae	*Vampyrobeccus*	*pusillus*	Late Turonian	3.24	2.29	1.68	109.0	1.53	1.62	0.94	2.21	0.76	0.34	14.86
11	Vampyroteuthidae	*Vampyrobeccus*	*pusillus*	Late Turonian	2.27	1.28	1.76	114.4	1.10	1.07	1.03	1.52	0.54	0.36	5.75
12	Vampyroteuthidae	*Vampyrobeccus*	*pusillus*	Late Turonian	3.15	2.05	2.61	120.7	-	-	-	2.00	0.54	0.27	12.69
13	Vampyroteuthidae	*Vampyrobeccus*	*pusillus*	Late Turonian	2.54	1.90	1.82	126.4	-	-	-	1.76	0.55	0.31	11.34
14	Vampyroteuthidae	*Vampyrobeccus*	*pusillus*	Late Turonian	1.47	1.12	1.23	125.0	-	-	-	0.96	0.32	0.33	4.30
15	Vampyroteuthidae	*Vampyrobeccus*	*rupis*	Santonian	3.32	2.09	3.44	148.0	2.31	2.33	0.99	2.75	0.84	0.31	13.05
16	Vampyroteuthidae	*Vampyrobeccus*	*rupis*	Late Turonian	6.25	-	4.25	140.2	3.13	3.20	0.98	4.55	1.57	0.35	-
17	Vampyroteuthidae	*Vampyrobeccus*	*rupis*	Late Turonian	-	2.18	2.62	136.7	1.83	1.96	0.93	2.77	0.76	0.27	13.86
18	Vampyroteuthidae	*Vampyrobeccus*	*rupis*	Santonian	6.05	3.82	4.32	136.5	2.63	2.60	1.01	4.05	1.20	0.30	28.66
19	Vampyroteuthidae	*Vampyrobeccus*	*rupis*	Late Turonian	-	1.93	1.59	144.4	1.63	1.75	0.93	1.93	0.66	0.34	11.61
20	Vampyroteuthidae	*Vampyrobeccus*	*rupis*	Late Coniacian	3.70	2.15	3.52	137.2	1.92	-	-	2.45	0.94	0.38	13.59
21	Vampyroteuthidae	*Vampyrobeccus*	*rupis*	Late Coniacian	-	-	1.69	146.3	2.57	-	-	3.03	1.10	0.36	-
22	Vampyroteuthidae	*Vampyrobeccus*	*rupis*	Late Coniacian	7.44	-	-	-	-	-	-	4.53	1.34	0.30	-
23	Vampyroteuthidae	*Vampyrobeccus*	*rupis*	Santonian	-	1.33	1.57	138.2	1.25	1.23	1.02	1.68	0.73	0.44	6.20
24	Vampyroteuthidae	*Vampyrobeccus*	*rupis*	Late Campanian	-	1.81	2.24	139.8	-	-	-	2.50	0.94	0.38	10.53
25	Vampyroteuthidae	*Vampyrobeccus*	*rupis*	Late Campanian	2.89	1.53	1.61	138.2	1.94	-	-	2.59	0.75	0.29	8.00
26	Vampyroteuthidae	*Vampyrobeccus*	*rupis*	Late Turonian	3.38	2.19	1.83	138.2	1.48	1.73	0.86	2.07	0.61	0.29	13.95
27	Vampyroteuthidae	*Vampyrobeccus*	*rupis*	Late Turonian	-	1.74	2.09	137.0	1.24	1.30	0.95	2.25	0.63	0.28	9.89
28	Vampyroteuthidae	*Vampyrobeccus*	*robustus*	Santonian	2.75	1.74	2.06	138.3	1.74	1.70	1.02	2.20	0.66	0.30	9.89
29	Vampyroteuthidae	*Vampyrobeccus*	*robustus*	Late Turonian	4.19	1.86	2.73	144.4	2.15	-	-	2.85	1.04	0.36	10.98
30	Vampyroteuthidae	*Vampyrobeccus*	*robustus*	Late Coniacian	-	1.94	2.99	142.3	2.78	-	-	3.13	1.07	0.34	11.70
31	Vampyroteuthidae	*Vampyrobeccus*	*robustus*	Late Coniacian	2.62	2.30	1.54	-	1.72	-	-	1.85	0.81	0.44	14.95
32	Vampyroteuthidae	*Vampyrobeccus*	*robustus*	Late Campanian	4.44	2.59	3.12	140.4	2.02	2.11	0.96	2.58	1.05	0.41	17.56
33	Vampyroteuthidae	*Vampyrobeccus*	*robustus*	Late Campanian	5.08	3.51	3.75	-	2.78	2.60	1.07	3.34	1.36	0.41	25.86
34	Vampyroteuthidae	*Vampyrobeccus*	*robustus*	Late Campanian	6.40	4.05	4.27	130.1	2.89	-	-	4.10	1.77	0.43	30.73
35	Vampyroteuthidae	*Vampyrobeccus*	*robustus*	Late Campanian	-	1.43	1.69	144.3	2.02	2.18	0.93	2.94	1.20	0.41	7.10
36	Vampyroteuthidae	*Vampyrobeccus*	*robustus*	Late Campanian	4.28	2.00	2.60	135.0	2.14	2.52	0.85	2.42	0.95	0.39	12.24
37	Vampyroteuthidae	*Vampyrobeccus*	*robustus*	Late Campanian	-	-	4.05	-	2.68	-	-	3.42	1.32	0.39	-
38	Vampyroteuthidae	*Vampyrobeccus*	*robustus*	Late Campanian	4.16	2.47	1.69	132.2	2.21	-	-	2.70	0.78	0.29	16.48
39	Vampyroteuthidae	*Vampyrobeccus*	*robustus*	Late Campanian	4.84	3.24	3.98	141.6	3.01	3.10	0.97	3.67	1.59	0.43	23.42
40	Vampyroteuthidae	*Vampyrobeccus*	*robustus*	Late Campanian	-	1.46	1.73	154.5	2.02	-	-	2.44	1.02	0.42	7.37
41	Vampyroteuthidae	*Vampyrobeccus*	*ornatus*	earliest Cenomanian	3.35	2.13	2.54	137.9	-	-	-	2.70	1.01	0.37	13.41
42	Vampyroteuthidae	*Angustivampyrus*	*gracilis*	Late Cenomanian	3.64	2.14	3.12	132.0	1.50	1.13	1.33	2.15	0.64	0.30	13.50
43	Vampyroteuthidae	*Angustivampyrus*	*gracilis*	Late Turonian	3.76	1.52	2.83	134.9	2.04	1.61	1.27	3.10	1.09	0.35	7.91
44	Vampyroteuthidae	*Mysticivampyrus*	*megachasma*	Santonian	3.12	1.27	1.37	129.9	-	-	-	1.98	1.26	0.64	5.66
45	Vampyroteuthidae	*Mysticivampyrus*	*megachasma*	Late Turonian	2.26	1.48	2.05	134.8	-	-	-	1.66	0.89	0.54	7.55
46	Vampyroteuthidae	*Paleothauma*	*aprophata*	Late Coniacian	7.59	3.27	4.46	125.6	-	-	-	4.13	1.04	0.25	23.70
47	Vampyroteuthidae	*Paleothauma*	*aprophata*	Late Coniacian	5.26	-	-	-	1.39	-	-	3.43	1.19	0.35	-
48	Vampyroteuthidae	*Paleothauma*	*aprophata*	Late Coniacian	4.27	2.74	1.84?	119.0	1.06	1.23	0.86	2.60	0.95	0.37	18.91

Table 13. (continued)

No.	Dataset and Collection No. (NMNS: National Museum of Nature and Science, Tokyo)			
	3D model	Label data of 3D models	Cross-sectional images of 3D models	Original cross-sectional images of carbonate concretions
1	NMNS_DS00009_SikV7tD.stl	L_NMNS_DS00009_20170720_c1_wl_01_0596_SikV7tD.tif –0656_SikV7tD.tif	C_NMNS_DS00009_20170720_c1_wl_01_0596_SikV7tD.jpg –0656_SikV7tD.jpg	NMNS_DS00009_20170720_c1_wl_01_0596.jpg–0656.jpg
2	NMNS_DS00041_JFWihOr.stl	L_NMNS_DS00041_20180414_c1_wl_01_0517_JFWihOr.tif –0555_JFWihOr.tif	C_NMNS_DS00041_20180414_c1_wl_01_0517_JFWihOr.jpg –0555_JFWihOr.jpg	NMNS_DS00041_20180414_c1_wl_01_0517.jpg–0555.jpg
3	NMNS_DS00041_roSbpAy.stl	L_NMNS_DS00041_20180414_c1_wl_01_0573_roSbpAy.tif –0600_roSbpAy.tif	C_NMNS_DS00041_20180414_c1_wl_01_0573_roSbpAy.jpg –0600_roSbpAy.jpg	NMNS_DS00041_20180414_c1_wl_01_0573.jpg–0600.jpg
4	NMNS_DS00082_RdxHRsF.stl	L_NMNS_DS00082_20190127_c1_wl_01_0012_RdxHRsF.tif –0044_RdxHRsF.tif	C_NMNS_DS00082_20190127_c1_wl_01_0012_RdxHRsF.jpg –0044_RdxHRsF.jpg	NMNS_DS00082_20190127_c1_wl_01_0012.jpg–0044.jpg
5	NMNS_DS00082_dLRRx1U.stl	L_NMNS_DS00082_20190127_c1_wl_01_0034_dLRRx1U.tif –0074_dLRRx1U.tif	C_NMNS_DS00082_20190127_c1_wl_01_0034_dLRRx1U.jpg –0074_dLRRx1U.jpg	NMNS_DS00082_20190127_c1_wl_01_0034.jpg–0074.jpg
6	NMNS_DS00083_NrHLTR5.stl	L_NMNS_DS00083_20190130_c1_wl_01_0153_NrHLTR5.tif –0188_NrHLTR5.tif	C_NMNS_DS00083_20190130_c1_wl_01_0153_NrHLTR5.jpg –0188_NrHLTR5.jpg	NMNS_DS00083_20190130_c1_wl_01_0153.jpg–0188.jpg
7	NMNS_DS00090_yUGkyCU.stl	L_NMNS_DS00090_20190228_c1_wl_01_0374_yUGkyCU.tif –0413_yUGkyCU.tif	C_NMNS_DS00090_20190228_c1_wl_01_0374_yUGkyCU.jpg –0413_yUGkyCU.jpg	NMNS_DS00090_20190228_c1_wl_01_0374.jpg–0413.jpg
8	NMNS_DS00171_JX0P0m5.stl	L_NMNS_DS00171_wl_01_0168_JX0P0m5.tif–0222_JX0P0m5.tif	C_NMNS_DS00171_wl_01_0168_JX0P0m5.tif–0222_JX0P0m5.tif	NMNS_DS00171_wl_01_0168.tif–0222.tif
9	NMNS_DS00174_e1pwpuB.stl	L_NMNS_DS00174_wl_01_0549_e1pwpuB.tif–0590_e1pwpuB.tif	C_NMNS_DS00174_wl_01_0549_e1pwpuB.tif–0590_e1pwpuB.tif	NMNS_DS00174_wl_01_0549.tif–0590.tif
10	NMNS_DS00173_64soRis.stl	L_NMNS_DS00173_wl_01_0342_64soRis.tif–0398_64soRis.tif	C_NMNS_DS00173_wl_01_0342_64soRis.tif–0398_64soRis.tif	NMNS_DS00173_wl_01_0342.tif–0398.tif
11	NMNS_DS00173_JdlfVEt.stl	L_NMNS_DS00173_wl_01_0734_JdlfVEt.tif–0778_JdlfVEt.tif	C_NMNS_DS00173_wl_01_0734_JdlfVEt.tif–0778_JdlfVEt.tif	NMNS_DS00173_wl_01_0734.tif–0778.tif
12	NMNS_DS00173_baur4Rp.stl	L_NMNS_DS00173_wl_01_0770_baur4Rp.tif–0833_baur4Rp.tif	C_NMNS_DS00173_wl_01_0770_baur4Rp.tif–0833_baur4Rp.tif	NMNS_DS00173_wl_01_0770.tif–0833.tif
13	NMNS_DS00173_KEeFCOM.stl	L_NMNS_DS00173_wl_01_1303_KEeFCOM.tif–1348_KEeFCOM.tif	C_NMNS_DS00173_wl_01_1303_KEeFCOM.tif–1348_KEeFCOM.tif	NMNS_DS00173_wl_01_1303.tif–1348.tif
14	NMNS_DS00173_s2Rcd4I.stl	L_NMNS_DS00173_wl_01_1321_s2Rcd4I.tif–1345_s2Rcd4I.tif	C_NMNS_DS00173_wl_01_1321_s2Rcd4I.tif–1345_s2Rcd4I.tif	NMNS_DS00173_wl_01_1321.tif–1345.tif
15	NMNS_DS00004_vaujIdF.stl	L_NMNS_DS00004_20170519_c1_wl_01_0527_vaujIdF.tif –0605_vaujIdF.tif	C_NMNS_DS00004_20170519_c1_wl_01_0527_vaujIdF.jpg –0605_vaujIdF.jpg	NMNS_DS00004_20170519_c1_wl_01_0527.jpg–0605.jpg
16	NMNS_DS00041_3kNoeIr.stl	L_NMNS_DS00041_20180414_c1_wl_01_0126_3kNoeIr.tif –0230_3kNoeIr.tif	C_NMNS_DS00041_20180414_c1_wl_01_0126_3kNoeIr.jpg –0230_3kNoeIr.jpg	NMNS_DS00041_20180414_c1_wl_01_0126.jpg–0230.jpg
17	NMNS_DS00041_jdpBU5c.stl	L_NMNS_DS00041_20180414_c1_wl_01_0517_jdpBU5c.tif –0577_jdpBU5c.tif	C_NMNS_DS00041_20180414_c1_wl_01_0517_jdpBU5c.jpg –0577_jdpBU5c.jpg	NMNS_DS00041_20180414_c1_wl_01_0517.jpg–0577.jpg
18	NMNS_DS00042_4QE2uVD.stl	L_NMNS_DS00042_20180419_c1_wl_02_0001_4QE2uVD.tif –0077_4QE2uVD.tif	C_NMNS_DS00042_20180419_c1_wl_02_0001_4QE2uVD.jpg –0077_4QE2uVD.jpg	NMNS_DS00042_20180419_c1_wl_02_0001.jpg–0077.jpg
19	NMNS_DS00046_cUcSyXm.stl	L_NMNS_DS00046_20180709_c1_wl_01_0427_cUcSyXm.tif –0464_cUcSyXm.tif	C_NMNS_DS00046_20180709_c1_wl_01_0427_cUcSyXm.jpg –0464_cUcSyXm.jpg	NMNS_DS00046_20180709_c1_wl_01_0427.jpg–0464.jpg
20	NMNS_DS00081_ndfIUoT.stl	L_NMNS_DS00081_20190124_c1_wl_01_0178_ndfIUoT.tif –0248_ndfIUoT.tif	C_NMNS_DS00081_20190124_c1_wl_01_0178_ndfIUoT.jpg –0248_ndfIUoT.jpg	NMNS_DS00081_20190124_c1_wl_01_0178.jpg–0248.jpg
21	NMNS_DS00083_CRJbYpV.stl	L_NMNS_DS00083_20190130_c1_wl_01_0576_CRJbYpV.tif –0621_CRJbYpV.tif	C_NMNS_DS00083_20190130_c1_wl_01_0576_CRJbYpV.jpg –0621_CRJbYpV.jpg	NMNS_DS00083_20190130_c1_wl_01_0576.jpg–0621.jpg
22	NMNS_DS00089_3IKFu5E.stl	L_NMNS_DS00089_20190223_c1_wl_01_0020_3IKFu5E.tif –0145_3IKFu5E.tif	C_NMNS_DS00089_20190223_c1_wl_01_0020_3IKFu5E.jpg –0145_3IKFu5E.jpg	NMNS_DS00089_20190223_c1_wl_01_0020.jpg–0145.jpg
23	NMNS_DS00090_63yn0UE.stl	L_NMNS_DS00090_20190228_c1_wl_01_0542_63yn0UE.tif –0591_63yn0UE.tif	C_NMNS_DS00090_20190228_c1_wl_01_0542_63yn0UE.jpg –0591_63yn0UE.jpg	NMNS_DS00090_20190228_c1_wl_01_0542.jpg–0591.jpg
24	NMNS_DS00171_HJp26PY.stl	L_NMNS_DS00171_wl_01_0326_HJp26PY.tif–0370_HJp26PY.tif	C_NMNS_DS00171_wl_01_0326_HJp26PY.tif–0370_HJp26PY.tif	NMNS_DS00171_wl_01_0326.tif–0370.tif
25	NMNS_DS00171_K8R4qou.stl	L_NMNS_DS00171_wl_01_0558_K8R4qou.tif–0612_K8R4qou.tif	C_NMNS_DS00171_wl_01_0558_K8R4qou.tif–0612_K8R4qou.tif	NMNS_DS00171_wl_01_0558.tif–0612.tif
26	NMNS_DS00173_B7GkHio.stl	L_NMNS_DS00173_wl_01_0774_B7GkHio.tif–0826_B7GkHio.tif	C_NMNS_DS00173_wl_01_0774_B7GkHio.tif–0826_B7GkHio.tif	NMNS_DS00173_wl_01_0774.tif–0826.tif
27	NMNS_DS00173_AyUVdYq.stl	L_NMNS_DS00173_wl_01_1208_AyUVdYq.tif–1262_AyUVdYq.tif	C_NMNS_DS00173_wl_01_1208_AyUVdYq.tif–1262_AyUVdYq.tif	NMNS_DS00173_wl_01_1208.tif–1262.tif
28	NMNS_DS00011_fwhtNUY.stl	L_NMNS_DS00011_20170806_c1_wl_01_0679_fwhtNUY.tif –0742_fwhtNUY.tif	C_NMNS_DS00011_20170806_c1_wl_01_0679_fwhtNUY.jpg –0742_fwhtNUY.jpg	NMNS_DS00011_20170806_c1_wl_01_0679.jpg–0742.jpg
29	NMNS_DS00046_K6pGHWQ.stl	L_NMNS_DS00046_20180709_c1_wl_01_0774_K6pGHWQ.tif –0851_K6pGHWQ.tif	C_NMNS_DS00046_20180709_c1_wl_01_0774_K6pGHWQ.jpg –0851_K6pGHWQ.jpg	NMNS_DS00046_20180709_c1_wl_01_0774.jpg–0851.jpg
30	NMNS_DS00083_fTXQf6h.stl	L_NMNS_DS00083_20190130_c1_wl_01_0216_fTXQf6h.tif –0275_fTXQf6h.tif	C_NMNS_DS00083_20190130_c1_wl_01_0216_fTXQf6h.jpg –0275_fTXQf6h.jpg	NMNS_DS00083_20190130_c1_wl_01_0216.jpg–0275.jpg
31	NMNS_DS00083_GodW17x.stl	L_NMNS_DS00083_20190130_c1_wl_01_0477_GodW17x.tif –0530_GodW17x.tif	C_NMNS_DS00083_20190130_c1_wl_01_0477_GodW17x.jpg –0530_GodW17x.jpg	NMNS_DS00083_20190130_c1_wl_01_0477.jpg–0530.jpg
32	NMNS_DS00171_3u5tfbp.stl	L_NMNS_DS00171_wl_01_0100_3u5tfbp.tif–0174_3u5tfbp.tif	C_NMNS_DS00171_wl_01_0100_3u5tfbp.tif–0174_3u5tfbp.tif	NMNS_DS00171_wl_01_0100.tif–0174.tif
33	NMNS_DS00171_hflEysv.stl	L_NMNS_DS00171_wl_01_0082_hflEysv.tif–0171_hflEysv.tif	C_NMNS_DS00171_wl_01_0082_hflEysv.tif–0171_hflEysv.tif	NMNS_DS00171_wl_01_0082.tif–0171.tif
34	NMNS_DS00171_rV3Qnex.stl	L_NMNS_DS00171_wl_01_0161_rV3Qnex.tif–0272_rV3Qnex.tif	C_NMNS_DS00171_wl_01_0161_rV3Qnex.tif–0272_rV3Qnex.tif	NMNS_DS00171_wl_01_0161.tif–0272.tif
35	NMNS_DS00171_fQB6E7C.stl	L_NMNS_DS00171_wl_01_0710_fQB6E7C.tif–0766_fQB6E7C.tif	C_NMNS_DS00171_wl_01_0710_fQB6E7C.tif–0766_fQB6E7C.tif	NMNS_DS00171_wl_01_0710.tif–0766.tif
36	NMNS_DS00171_mpwGk3N.stl	L_NMNS_DS00171_wl_01_0739_mpwGk3N.tif–0818_mpwGk3N.tif	C_NMNS_DS00171_wl_01_0739_mpwGk3N.tif–0818_mpwGk3N.tif	NMNS_DS00171_wl_01_0739.tif–0818.tif
37	NMNS_DS00171_uQxv4C0.stl	L_NMNS_DS00171_wl_01_0736_uQxv4C0.tif–0850_uQxv4C0.tif	C_NMNS_DS00171_wl_01_0736_uQxv4C0.tif–0850_uQxv4C0.tif	NMNS_DS00171_wl_01_0736.tif–0850.tif
38	NMNS_DS00171_pe6Kbga.stl	L_NMNS_DS00171_wl_01_0853_pe6Kbga.tif–0907_pe6Kbga.tif	C_NMNS_DS00171_wl_01_0853_pe6Kbga.tif–0907_pe6Kbga.tif	NMNS_DS00171_wl_01_0853.tif–0907.tif
39	NMNS_DS00171_Hw6o6u0.stl	L_NMNS_DS00171_wl_01_1086_Hw6o6u0.tif–1193_Hw6o6u0.tif	C_NMNS_DS00171_wl_01_1086_Hw6o6u0.tif–1193_Hw6o6u0.tif	NMNS_DS00171_wl_01_1086.tif–1193.tif
40	NMNS_DS00171_SQeQVkb.stl	L_NMNS_DS00171_wl_01_1128_SQeQVkb.tif–1173_SQeQVkb.tif	C_NMNS_DS00171_wl_01_1128_SQeQVkb.tif–1173_SQeQVkb.tif	NMNS_DS00171_wl_01_1128.tif–1173.tif
41	NMNS_DS00068_fE0GOBN.stl	L_NMNS_DS00068_20181123_c1_wl_01_0338_fE0GOBN.tif –0444_fE0GOBN.tif	C_NMNS_DS00068_20181123_c1_wl_01_0338_fE0GOBN.jpg –0444_fE0GOBN.jpg	NMNS_DS00068_20181123_c1_wl_01_0338.jpg–0444.jpg
42	NMNS_DS00082_jhTRMGQ.stl	L_NMNS_DS00082_20190127_c1_wl_01_0689_jhTRMGQ.tif –0734_jhTRMGQ.tif	C_NMNS_DS00082_20190127_c1_wl_01_0689_jhTRMGQ.jpg –0734_jhTRMGQ.jpg	NMNS_DS00082_20190127_c1_wl_01_0689.jpg–0734.jpg
43	NMNS_DS00173_H7WmleW.stl	L_NMNS_DS00173_wl_01_0342_H7WmleW.tif–0407_H7WmleW.tif	C_NMNS_DS00173_wl_01_0342_H7WmleW.tif–0407_H7WmleW.tif	NMNS_DS00173_wl_01_0342.tif–0407.tif
44	NMNS_DS00011_riK07H1.stl	L_NMNS_DS00011_20170806_c1_wl_01_0838_riK07H1.tif –0901_riK07H1.tif	C_NMNS_DS00011_20170806_c1_wl_01_0838_riK07H1.jpg –0901_riK07H1.jpg	NMNS_DS00011_20170806_c1_wl_01_0838.jpg–0901.jpg
45	NMNS_DS00041_ty14Te8.stl	L_NMNS_DS00041_20180414_c1_wl_01_0713_ty14Te8.tif –0760_ty14Te8.tif	C_NMNS_DS00041_20180414_c1_wl_01_0713_ty14Te8.jpg –0760_ty14Te8.jpg	NMNS_DS00041_20180414_c1_wl_01_0713.jpg–0760.jpg
46	NMNS_DS00083_fj8UthX.stl	L_NMNS_DS00083_20190130_c1_wl_01_0108_fj8UthX.tif –0199_fj8UthX.tif	C_NMNS_DS00083_20190130_c1_wl_01_0108_fj8UthX.jpg –0199_fj8UthX.jpg	NMNS_DS00083_20190130_c1_wl_01_0108.jpg–0199.jpg
47	NMNS_DS00083_ikh1myp.stl	L_NMNS_DS00083_20190130_c1_wl_01_0208_ikh1myp.tif –0283_ikh1myp.tif	C_NMNS_DS00083_20190130_c1_wl_01_0208_ikh1myp.jpg –0283_ikh1myp.jpg	NMNS_DS00083_20190130_c1_wl_01_0208.jpg–0283.jpg
48	NMNS_DS00083_jGPOPwW.stl	L_NMNS_DS00083_20190130_c1_wl_01_0600_jGPOPwW.tif –0667_jGPOPwW.tif	C_NMNS_DS00083_20190130_c1_wl_01_0600_jGPOPwW.jpg –0667_jGPOPwW.jpg	NMNS_DS00083_20190130_c1_wl_01_0600.jpg–0667.jpg

which the female matures at 78 mm, the male at 44 mm ML, and the largest specimen was 210mm ML[7]. In extant coleoids, the growth stage can be estimated from the degree of pigmentation (i.e. the proportion of blackened area)[31]. In obtained beaks, more than half of them (25 individuals) do not retain the posteroventral corner of lateral walls, indicating their immaturity. Thus, the adult body sizes of the Late Cretaceous vampire squids were probably as large as or slightly smaller than that of the extant species. Vampyropod gladius fossils have never been reported from the Cretaceous North Pacific regions except for huge specimens of *Actinosepia* that reach 300 mm from Nanaimo Group, Canada[13,34]. These results imply that the small gladius of early vampire squids had insufficient fossilization potential for those regions that lack konservat-lagerstätten and subsequently led the oversight in previous studies.

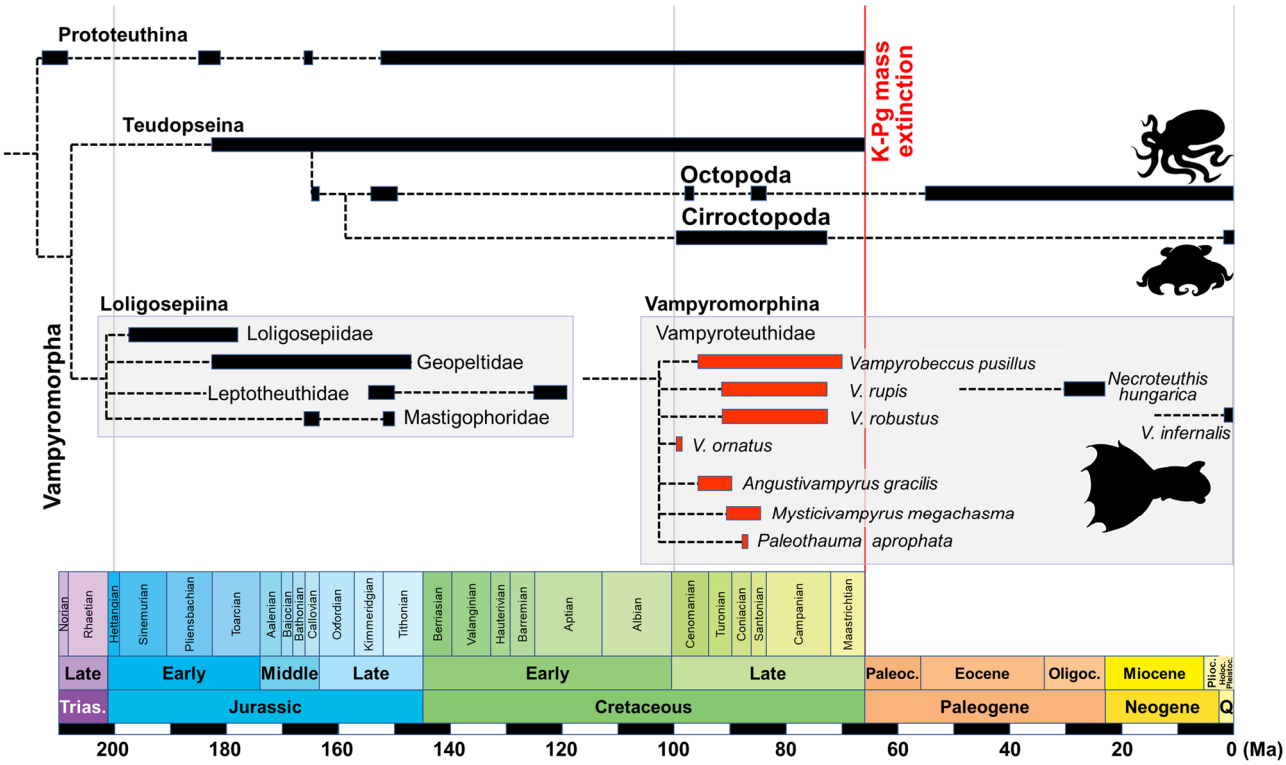


Fig. 26. Stratigraphic distribution of fossil Vampyromorpha in the Cretaceous North Pacific. Red bars show the stratigraphic range revealed by this study. The phylogenetic tree and fossil records shown as black bars are from Fuchs (2020)[13] and Fuchs et al. (2020)[14].

3.5.3. Feeding habits

The beaks reflect differences in feeding habits in their entire outline since they are directly involved in biting[35]. Morphological immutability indicates that the Late Cretaceous vampire squids fed on similar prey to present ones. Preys of present *V. infernalis* examined by crop contents mainly consist of small or soft prey like plankton and gelatinous animals and also contain little amount of fragmented tissues of fishes and cephalopods[4]. Based on this observation, the fossil taxa are expected to be planktivores or scavengers. This prediction might be consistent with the small body size which was estimated above. As the concept proposed in 1930's known as Kleiber's Law, larger animals show a larger metabolic rate and subsequently require larger food intakes[36]. It is previously confirmed that cephalopods in the current oceans follow this rule as well[37,38]. Thus, the estimated body size suggests little food intake of the Cretaceous vampire squids. Smaller individuals of cephalopods tend to be placed on lower trophic levels regardless of the maximum body size and the activity-level in cephalopods[39,40]. Stomach

contents analyses of various extant taxa showed that smaller individuals mainly prey on planktonic crustaceans[41]. It is also applied for voracious neritic cephalopods, of which feeding habits change ontogenetically[41]. The body size at which the shift of diets occurs is poorly documented, but Vovk and Khvichiya (1980)[42] detected the shift in the range from 80 to 120 mm ML in *Loligo pealeii.* All fossil vampyropod specimens preserved with large prey surpass 100 mm ML[21,22]. These lines of evidence suggest that Late Cretaceous vampire squids had an inactive feeding strategy.

3.5.4. Habitats and the evolutionary history

The Upper Cretaceous of the Yezo Group was formed on various environments ranging from the continental slope to the non-marine areas of the Yezo Forearc Basin[27]. The depositional environment is considered to be the upper bathyal zone of 300–600 m depth in the late Early Cretaceous (Albian) and became shallower with time, based on lithology and benthic foraminiferal assemblages[27]. Vampyroteuthid beaks in this study were yielded from sediments of shallow, highly oxygenated zones as well as deep, deoxygenated ones[43].The sudden decline in the Maastrichtian implies the upper limit of habitable zones in the Cretaceous vampire squids since the sample rocks from the Maastrichtian were formed under shallower water (the inner shelf) than the other samples[44].

Vampyromorphids in the Jurassic–Early Cretaceous interval occur from sediments deposited in very shallow seas, while extant ones inhabit the deep sea[8,24]. The gap in their fossil record is probably due to the migration of vampyromorphids into the deep sea[14]. A previous study presumed that the expansion of oxygen minimum zones associated with OAEs in the mid-Cretaceous might have triggered this migration[14]. The findings of this study, however, showed that they inhabited shelf seas probably throughout the Late Cretaceous. These zones are at an intermediate depth between the habitats of earlier and extant vampyromorphids, suggesting a gradual migration rather than that associated with geological events like OAEs. The relative abundance, diversity, body size, and habitats all suggest that vampyromorphids experienced a gradual decline in the Cretaceous.

References for Chapter 3

1. Pearman, P. B., Guisan, A., Broennimann, O. & Randin, C. F. Niche dynamics in space and time. *Trends Ecol. Evol.* **23**, 149–158 (2008).
2. Boyle, P. & Rodhouse, P. *Cephalopods: Ecology and Fisheries*. (Blackwell Science, Oxford, 2005).
3. Hanlon, R. T. & Messenger, J. B. *Cephalopod Behaviour*. (Cambridge University Press, Cambridge, 2018).
4. Hoving, H. T. *et al.* The Study of Deep-Sea Cephalopods. *Adv. Mar. Biol.* **67**, 235–359 (2014).
5. Warrant, E. J. & Locket, N. A. Vision in the deep sea. *Biol. Rev.* **79**, 671–712 (2004).
6. Seibel, B. A., Chausson, F., Lallier, F. H., Zal, F. & Childress, J. J. Vampire blood: respiratory physiology of the vampire squid (Cephalopoda: Vampyromorpha) in relation to the oxygen minimum layer. *Exp. Biol. Online* **4**, 1–10 (1999).
7. Nixon, M. & Young, J. Z. *The Brains and Lives of Cephalopods*. (Oxford University Press, Oxford, 2003).
8. Hoving, H. J. T. & Robison, B. H. Vampire squid: detritivores in the oxygen minimum zone. *Proc. R. Soc. B Biol. Sci.* **279**, 4559–4567 (2012).
9. Jereb, P., Roper, C. F. E., Norman, M. D. & Finn, J. K. *Cephalopods of the World. An Annotated and Illustrated Catalogue of Cephalopod Species Known to Date: Volume 3. Octopods and Vampire Squids*. (Food and Agriculture Organization of the United Nations, Rome, 2016).
10. Doyle, P., Donovan, D. T. & Nixon, M. Phylogeny and Systematics of the Coleoidea. *Paleontol. Contrib. - Univ. Kans.* (1994).
11. Jeletzky, J. A. Comparative morphology, phylogeny, and classification of fossil Coleoidea. (1966).
12. Fuchs, D. Part M, Chapter 9B: The Gladius and Gladius Vestige in Fossil Coleoidea. *Treatise Online* **83**, 1–23 (2016).
13. Fuchs, D. Part M, Chapter 23G: Systematic descriptions: Octobrachia. *Treatise Online* **138**, 1–52 (2020).
14. Košťák, M. *et al.* Fossil evidence for vampire squid inhabiting oxygen-depleted ocean zones since at least the Oligocene. *Commun. Biol.* **4**, 216 (2021).
15. Lindgren, A. R., Giribet, G. & Nishiguchi, M. K. A combined approach to the phylogeny of Cephalopoda (Mollusca). *Cladistics* **20**, 454–486 (2004).
16. Tanner, A. R. *et al.* Molecular clocks indicate turnover and diversification of modern coleoid cephalopods during the Mesozoic Marine Revolution. *Proc. R. Soc. B Biol. Sci.* **284**, 20162818 (2017).
17. Uribe, J. E. & Zardoya, R. Revisiting the phylogeny of Cephalopoda using complete mitochondrial genomes. *J. Molluscan Stud.* **83**, 133–144 (2017).
18. Sanchez, G. *et al.* Genus-level phylogeny of cephalopods using molecular markers: current status and problematic areas. *PeerJ* **6**, e4331 (2018).
19. Whalen, C. D. & Landman, N. H. Fossil coleoid cephalopod from the Mississippian Bear Gulch

Lagerstätte sheds light on early vampyropod evolution. *Nat. Commun.* **13**, 1107 (2022).

20. Fuchs, D., Iba, Y., Tischlinger, H., Keupp, H. & Klug, C. The locomotion system of Mesozoic Coleoidea (Cephalopoda) and its phylogenetic significance. *Lethaia* **49**, 433–454 (2016).
21. Klug, C., Schweigert, G., Fuchs, D. & De Baets, K. Distraction sinking and fossilized coleoid predatory behaviour from the German Early Jurassic. *Swiss J. Palaeontol.* **140**, 7 (2021).
22. Fuchs, D., Weis, R. & Thuy, B. *Simoniteuthis*, a new vampyromorph coleoid with prey in its arms from the Early Jurassic of Luxembourg. *Swiss J. Palaeontol.* **143**, 6 (2024).
23. Raup, D. M. & Sepkoski, J. J. Mass extinctions in the marine fossil record. *Science* **215**, 1501–1503 (1982).
24. Donovan, D. & Fuchs, D. Fossilized Soft Tissues in Coleoidea. *Treatise Online* **73**, (2016).
25. Tanabe, K., Kruta, I. & Landman, N. H. Ammonoid Buccal Mass and Jaw Apparatus. in *Ammonoid Paleobiology: From anatomy to ecology* (eds. Klug, C., Korn, D., De Baets, K., Kruta, I. & Mapes, R. H.) vol. 43 429–484 (Springer Netherlands, Dordrecht, 2015).
26. Clarke, M. R. *A Handbook for the Identification of Cephalopod Beaks*. (Clarendon Press, Oxford, 1986).
27. Takashima, R. *et al.* Geology and stratigraphy of forearc basin sediments in Hokkaido, Japan: Cretaceous environmental events on the north-west Pacific margin. *Cretac. Res.* **25**, 365–390 (2004).
28. Yoshida, H. *et al.* Early post-mortem formation of carbonate concretions around tusk-shells over week-month timescales. *Sci. Rep.* **5**, 1–7 (2015).
29. Young, R. E. Beak structure and evolution. *Tree of Life* http://tolweb.org/notes/?note_id=4541 (2007).
30. Shea, E. K. *et al.* Cephalopod biodiversity in the vicinity of Bear Seamount, western North Atlantic based on exploratory trawling from 2000 to 2014. *Mar. Biodivers.* **47**, 699–722 (2017).
31. Hernández-García, V. Growth and pigmentation process of the beaks of *Todaropsis Eblanae* (Cephalopoda: Ommastrephidae). *Berl. Paläobiologische Abh.* **3**, 131–140 (2003).
32. Klug, C., Schweigert, G., Dietl, G. & Fuchs, D. Coleoid beaks from the Nusplingen Lithographic Limestone (Upper Kimmeridgian, SW Germany). *Lethaia* **38**, 173–192 (2005).
33. Obradovich, J. D., Matsumoto, T., Nishida, T. & Inoue, Y. Integrated biostratigraphic and radiometric study on the Lower Cenomanian (Cretaceous) of Hokkaido, Japan. *Proc. Jpn. Acad. Ser. B* **78**, 149–153 (2002).
34. Ludvigsen, R. & Beard, G. *West Coast Fossils: A Guide to the Ancient Life of Vancouver Island*. (Harbour Pub., Vancouver, 2001).
35. Roscian, M. *et al.* Every hooked beak is maintained by a prey: Ecological signal in cephalopod beak shape. *Funct. Ecol.* **36**, 2015–2028 (2022).
36. Kleiber, M. Body size and metabolism. *Hilgardia* **6**, 315–353 (1932).
37. Katsanevakis, S., Stephanopoulou, S., Miliou, H., Moraitou-Apostolopoulou, M. & Verriopoulos, G. Oxygen consumption and ammonia excretion of Octopus vulgaris (Cephalopoda) in relation to

body mass and temperature. *Mar. Biol.* **146**, 725–732 (2005).

38. Kooijman, S. A. & Augustine, S. The comparative energetics of the cephalopods: they neither grow nor reproduce fast. *J. Sea Res.* **184**, 102205 (2022).
39. Murphy, K. J. *et al.* Functional traits explain trophic allometries of cephalopods. *J. Anim. Ecol.* **89**, 2692–2703 (2020).
40. Cherel, Y., Ridoux, V., Spitz, J. & Richard, P. Stable isotopes document the trophic structure of a deep-sea cephalopod assemblage including giant octopod and giant squid. *Biol. Lett.* **5**, 364–367 (2009).
41. Boletzky, S. V. & Hanlon, R. T. A review of the laboratory maintenance, rearing and culture of cephalopod molluscs. *Mem. Natl. Mus. Vic. Melb.* **44**, 147–187 (1983).
42. Vovk, A. N. & Khvichiya, L. A. On feeding of long-finned squid (Loligo pealei) juveniles in Subareas 5 and 6. *Northwest Atl Fish OrgNAFO Sci Counc Res Doc* **80**, (1980).
43. Kaiho, K., Fujiwara, O. & Motoyama, I. Mid-Cretaceous faunal turnover of intermediate-water benthic foraminifera in the northwestern Pacific Ocean margin. *Mar. Micropaleontol.* **23**, 13–49 (1993).
44. Ando, H., Tomosugi, T. & Kanakubo, T. Upper Cretaceous to Paleocene Hakobuchi Group, Nakatonbetsu area, northern Hokkaido-lithostratigraphy and megafossil biostratigraphy. *J. Geol. Soc. Jpn.* **107**, 142–162 (2001).

Chapter 4. New groups

Summary

Soft-bodied cephalopods thrive in modern oceans, but their evolutionary history remains unclear due to the scarcity of their fossil record. The current understanding of their phylogeny primarily relies on extant species, resulting in the unlikely scenario that their long-lasting evolutionary radiation is solely covered by extant orders in taxonomy. Here, I report four new orders of soft-bodied cephalopods based on fossil beaks discovered from the Upper Cretaceous (~100–72 Ma) of Japan. These orders are not included in the known eight- and ten-armed groups, namely in any of the existing superorders. Each of these four groups represents an extinct lineage without leaving modern descendants. These results indicate that a significant number of soft-bodied cephalopods has hitherto not been recognized, causing a substantial underestimation of their past biodiversity. These discoveries highlight the complexity and diversity in the evolution of soft-bodied cephalopods, which are not recognizable from extant species alone.

4.1. Introduction

Cephalopods have flourished in oceans worldwide since the Late Cambrian (500 Ma), experiencing several phases of extensive radiation and extinction[1–3]. In the last stage of their history, they underwent a major evolutionary innovation, transforming from shelled (e.g., ammonites) to soft-bodied forms (e.g., octopuses and squids)[4–7]. This change gave them enhanced swimming and cognitive capabilities, leading to the expansion of soft-bodied cephalopods in modern oceans[4,5,8–10]. The loss of the shell, however, reduced their fossil record since the shell has the highest fossilization potential of the cephalopod body[4,5]. It is thus extremely challenging to understand their evolutionary history. Previous research, which tried to reconstruct the evolution of soft-bodied groups, relied on molecular analyses and exceptionally well-preserved fossil records[7,9,11–13]. The former approach exclusively addresses phylogenetic relationships of extant lineages, and the latter focuses on pursuing modern relatives. The drawback of these approaches is the non-consideration of extinct groups which have no modern descendants. The currently known fossil and recent soft-bodied cephalopods are included in six taxonomic orders, all of which are based on living species[4]. It seems, however, unlikely that the long-lasting evolutionary radiation of soft-bodied cephalopods is covered by these six extant orders only.

Here, I report four new species of soft-bodied cephalopods, each representing a new extinct order. These new taxa are based on fossil lower beaks, which required specific techniques to be extracted from hard rocks. discovery was achieved by grinding tomography and extraction as digital 3D models. These digitized fossil beaks are derived from shelf deposits of the Cretaceous Yezo Group in northern Japan. The Yezo Group is recognized as a chronostratigraphic standard for the Cretaceous in the circum-North Pacific[14]. The morphology of the cephalopod lower beak, discussed here, is strongly constrained by phylogenetic relationships[15]. These stratigraphic and morphological data enabled assignments of these fossil beaks to new taxonomic orders. The discovery of the new orders sheds light on the presence of hidden lineages in soft-bodied cephalopods and is a first step toward a precise understanding of their evolutionary history.

4.2. Material

The fossil beaks of the new coleoid orders were extracted from sediments of the Yezo Group, Cretaceous shelf deposits in Hokkaido, northern Japan. The geological ages given here are based on published chronostratigraphic studies[16–26] (Table 14). All fieldwork was carried out in compliance with local, national, and international laws. Detailed informations for the localities, geological ages, and horizons studied here are documented in Table 14.

Institutional abbreviations

NMNS: National Museum of Nature and Science, Tokyo, Japan.

4.3. Methods

4.3.1. Grinding tomography and image processing

The carbonate concretions were scanned by a grinding tomography system (Paleobiology Lab, Hokkaido University). The rock samples were ground at equal intervals of 10, 25, or 50 μm. Information on each sample and corresponding image dataset is documented in Table 15. High-precision diamond cup wheels were used for surface grinding (diamond size 15 μm: Asahi Diamond Industrial Co., Ltd; 20 μm: Noritake Co., Ltd). Each surface was photographed by a digital camera in

Table 14. Carbonate concretions and contained cephalopod beaks.

Sample No. of carbonate concretion	Dimensions (cm^3)	Geological age	Horizon	Longitude and latitude	Number of fossil beaks				
					All cephalopods	*Globosimilvus amabilis*	*Monachicothauma aenigmatica*	*Cryptaroter vociferans*	*Amblystoma delicatum*
1	590	middle to late Albian, Late Cretaceous[S1]	Middle part of Hikagenosawa Formation, Yezo Group	43° 17' 38" N 141° 59' 55" E	1	0	0	0	0
2	290	middle to late Albian, Late Cretaceous[S1]	Middle part of Hikagenosawa Formation, Yezo Group	43° 18' 02" N 142° 00' 02" E	7	0	0	0	0
3	640	middle to late Albian, Late Cretaceous[S1]	Middle part of Hikagenosawa Formation, Yezo Group	43° 19' 55" N 142° 01' 35" E	2	0	0	0	0
4	600	middle to late Albian, Late Cretaceous[S1]	Middle part of Hikagenosawa Formation, Yezo Group	43° 19' 20" N 142° 00' 18" E	3	0	0	0	0
5	350	middle to late Albian, Late Cretaceous[S1]	Middle part of Hikagenosawa Formation, Yezo Group	43° 18' 50" N 142° 00' 44" E	5	0	0	0	0
6	100	earliest Cenomanian, Late Cretaceous[S2]	Unit My3, Yezo Group	44° 13' 29" N 142° 04' 07" E	68	4	0	0	0
7	140	Early Cenomanian, Late Cretaceous[S2]	Unit My4, Yezo Group	44° 14' 30" N 142° 04' 57" E	26	1	0	0	0
8	270	Late Cenomanian, Late Cretaceous[S3]	Lower part of Saku Formation, Yezo Group	44° 05' 58" N 142° 00' 50" E	55	1	0	0	0
9	570	Early Turonian, Late Cretaceous[S1]	Lower part of Saku Formation, Yezo Group	43° 07' 49" N 142° 08' 00" E	17	0	0	0	0
10	200	Middle Turonian, Late Cretaceous[S4]	Upper part of Saku Formation, Yezo Group	44° 02' 07" N 141° 35' 33" E	18	0	0	0	0
11	180	Late Turonian, Late Cretaceous[S1]	Upper part of Mikasa Formation, Yezo Group	43° 17' 52" N 142° 05' 16" E	46	0	0	0	0
12	100	Late Turonian, Late Cretaceous[S4]	Upper part of Saku Formation, Yezo Group	44° 03' 47" N 141° 58' 55" E	34	1	1	0	0
13	580	Late Turonian, Late Cretaceous[S4]	Upper part of Saku Formation, Yezo Group	44° 03' 30" N 141° 59' 28" E	20	0	0	0	0
14	100	Late Turonian, Late Cretaceous[S7]	Upper part of Saku Formation, Yezo Group	44° 45' 41" N 142° 01' 40" E	15	0	0	0	0
15	100	Late Turonian, Late Cretaceous[S7]	Upper part of Saku Formation, Yezo Group	44° 44' 15" N 142° 00' 43" E	33	0	0	0	0
16	460	Late Turonian, Late Cretaceous[S4]	Upper part of Saku Formation, Yezo Group	44° 03' 43" N 141° 58' 51" E	207	7	0	0	0
17	150	Early Coniacian, Late Cretaceous[S8]	Lower part of Haborogawa Formation, Yezo Group	44° 17' 20" N 141° 00' 23" E	31	0	0	0	0
18	310	Late Coniacian, Late Cretaceous[S8]	Lower part of Haborogawa Formation, Yezo Group	44° 17' 43" N 142° 00' 10" E	16	0	0	0	0
19	180	Late Coniacian, Late Cretaceous[S8]	Lower part of Haborogawa Formation, Yezo Group	44° 17' 55" N 142° 00' 04" E	58	0	0	0	0
20	170	Late Coniacian, Late Cretaceous[S4]	Lower part of Haborogawa Formation, Yezo Group	44° 05' 42" N 141° 58' 42" E	39	3	0	1	0
21	380	Santonian, Late Cretaceous[S5]	Upper part of Haborogawa Formation, Yezo Group	44° 10' 41" N 141° 58' 34" E	15	1	0	0	0
22	550	Santonian, Late Cretaceous[S5]	Upper part of Haborogawa Formation, Yezo Group	44° 19' 26" N 141° 57' 25" E	18	0	0	0	0
23	140	Santonian, Late Cretaceous[S5]	Upper part of Haborogawa Formation, Yezo Group	44° 18' 05" N 141° 57' 42" E	1	0	0	0	0
24	140	Santonian, Late Cretaceous[S5]	Upper part of Haborogawa Formation, Yezo Group	44° 11' 24" N 141° 58' 14" E	4	0	0	0	0
25	200	Santonian, Late Cretaceous[S5]	Upper part of Haborogawa Formation, Yezo Group	44° 18' 04" N 141° 58' 56" E	10	0	0	0	0
26	210	Santonian, Late Cretaceous[S5]	Unit Ug, Haborogawa Formation, Yezo Group	44° 18' 06" N 141° 58' 04" E	36	2	0	0	0
27	150	Early Campanian, Late Cretaceous[S9]	Nagareya Formation, Yezo Group	44° 16' 50" N 141° 53' 16" E	5	0	0	0	0
28	200	Early Campanian, Late Cretaceous[S10]	Nigorigawa Formation, Yezo Group	44° 38' 00" N 141° 59' 16" E	31	0	0	0	0
29	100	Early Campanian, Late Cretaceous[S7]	Osoushinai Formation, Yezo Group	44° 40' 30" N 142° 01' 22" E	0	0	0	0	0
30	310	Early Campanian, Late Cretaceous[S9]	Nagareya Formation, Yezo Group	44° 16' 50" N 141° 53' 16" E	20	0	0	0	0
31	280	Late Campanian, Late Cretaceous[S6]	Chinomigawa Formation, Yezo Group	42° 54' 36" N 142° 25' 08" E	66	0	0	0	1
32	290	Late Campanian, Late Cretaceous[S6]	Chinomigawa Formation, Yezo Group	42° 54' 49" N 142° 24' 45" E	34	0	0	0	0
33	360	Early Maastrichtian, Late Cretaceous[S11]	Lower part of Heitaro-zawa Member, Hakobuchi Formation, Yezo Group	45° 01' 25" N 142° 12' 44" E	13	0	0	0	0
34	500	Early Maastrichtian, Late Cretaceous[S12]	Etanpakku Formation, Yezo Group	45° 18' 09" N 141° 59' 24" E	8	0	0	0	0
35	390	Early Maastrichtian, Late Cretaceous[S11]	Lower part of Heitaro-zawa Member, Hakobuchi Formation, Yezo Group	45° 01' 27" N 142° 12' 03" E	38	0	0	0	0
				Total	1000	20	1	1	1

its original colors in high resolution (50 million pixels/image in EOS 5Ds, Canon; 245 million pixels/image in α7R IV, SONY). These grinding–photographing processes were computerized and repeated automatically.

This study discovered fossil beaks in each image dataset. The fossil beaks were then extracted from the host rocks individually as digital 3D models. The areas of the fossil beaks were segmented by RGB values in the IV-Seg 1.3.2.0 (IVLab Co., Ltd.) and subsequently imported to Amira 6.2.0 (Thermo Fisher Scientific, Inc.) for 3D reconstruction. The 3D models underwent minimal smoothing consistent with imported masks to avoid modifying the diagnostic characters. All measurements and taxonomical interpretations are based on these 3D models. Blender 3.2.1 (Blender Foundation) was used to display the models in figures.

4.3.2. Taxonomic evaluations of fossil coleoid lower beaks

The measurements and descriptions of the coleoid lower beaks (Fig. 3) use published terminology and methods[27,28]. The crest length, hood length, lower rostral length, wing length, and wing angle were measured according to these methods. Additionally, the following measurements were raised in this study (Fig. 3): extended jaw edge length, jaw edge length in lateral view, angle between a jaw edge and the adjacent shoulder blade, and rostral width. All measured values are documented in Table 15. Growth stages were defined based on their degree of pigmentation[29] (Table 15).

4.3.3. Taxonomy

The International Code of Zoological Nomenclature allows “typeless species” in specific situations, with several recommended actions[30]. This study was conducted in accordance with these regulations. The collection numbers of the image data, which define the new species, are documented in Tables 14 and 15. This document does not include nomenclatural acts. New taxonomic names shown here will be published in other papers at appropriate journals.

4.3.4. Data availability

The 3D models, the label data, and the cropped cross-sectional images of the discovered beaks are available from Figshare (https://doi.org/10.6084/m9.figshare.27678570). All tomographic images of the carbonate concretions (~30 TB) are archived in the National Museum of Nature and Science, Tokyo. The collection numbers of these data are listed in Tables 14 and 15.

4.4. Systematic palaeontology

Coleoidea Bather, 1888

Remarks. Coleoid lower beaks differ from those of external-shelled cephalopods (ammonoids and nautiloids) by a well-developed, arched inner lamella and the absence of a calcareous cover[31]. Due to these morphological features, all beaks encountered in this study have been identified as coleoid lower beaks.

Globosimilvida ord. nov.

Diagnosis. The rostrum has a distinct hook. The ratio of the lower rostral length to the rostral width ranges from 0.72 to 0.94. In lateral view, 42–63 % the jaw edges are hidden by the wings. The bridges

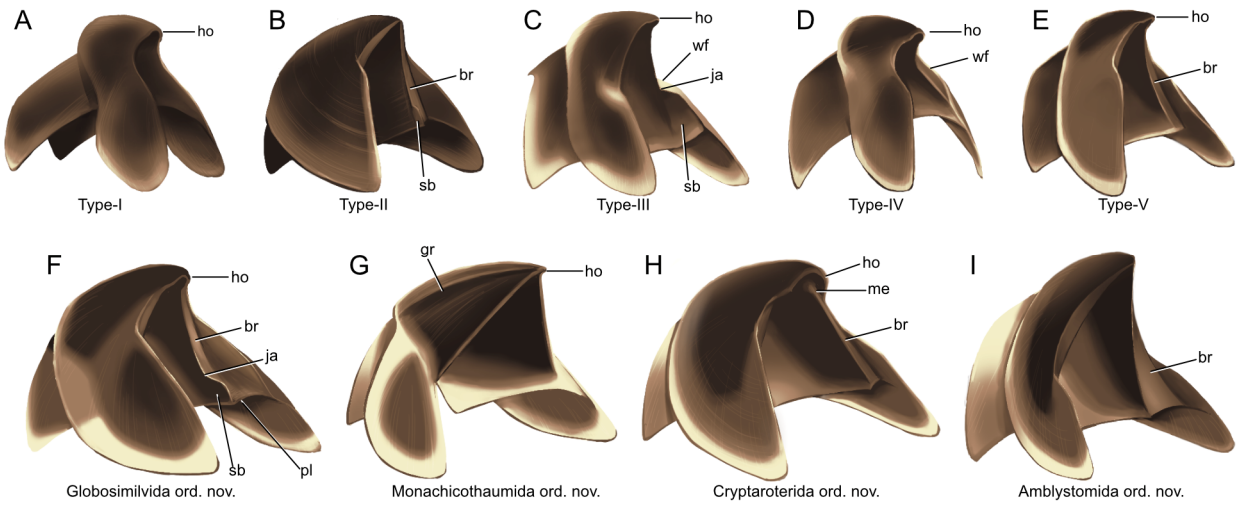


Fig. 27. Morphological types of coleoid lower beaks.
(**A** to **E**) The types of known coleoid lower beaks. (A) Type-I; (B) type-II; (C) type-III; (D) type-IV; (E) type-V. (**F** to **I**) Reconstruction of the new orders. (F) Globosimilvida ord. nov.; (G) Monachicothaumida ord. nov.; (H) Cryptaroterida ord. nov.; (I) Amblystomida ord. nov. Abbreviations: br, bridge; gr, groove on the hood; ho, rostral hook; me, medial edge of a bridge; ja, jaw angle; pl, plate at the ventral margin of the shoulders; sb, shoulder blade; wf, wing fold.

are entirely exposed, inclined posterolaterally in horizontal sections, and extend from the rostral tip to the ventral end of the inner lamella. The shoulder blades are thin and small. The shoulders have a thin pigmented plate at their ventral margin. This plate is smoothly connected to a bridge posteriorly, to the ventral edge of the adjacent shoulder blade medially, and to the adjacent wing laterally. The wings are thin, smooth, and constricted around the nearest jaw edge. They rise from the outer edge of the bridge and do not extend posteriorly from this edge. Wing folds are absent. The hood is relatively long and broadly arched. The height of the lateral walls is almost the same as their length.

Comparison. The Globosimilvida can be clearly distinguished from all other coleoid orders by the presence of a plate at the ventral margin of the shoulders (Fig. 27). A relatively small rostrum, bridges that extend from the top to the bottom of the inner lamella, and a broadly arched hood are in common with Vampyromorpha (Fig. 27B)[27,32]. The rostral hook and the constriction of the wings are rather similar to those of the Oegopsida (Fig. 27C)[27].

Globosimilvidae fam. nov.
Globosimilvus amabilis gen. et sp. nov.
Etymology. From Latin *globosus* (globular), *milvus* (kyte), and *amabilis* (attractive).
Material. Documented in Table 15.
Diagnosis. Same as the diagnosis of the order.
Description. The crest length does not surpass 2.5 mm, not even in adults (Table 15). The rostrum has a distinct hook on its tip (Fig. 28A, B, F, and G). The ratio of the lower rostral length to the rostral width ranges from 0.72 to 0.94 (Fig. 28E, J, and Table 15). In lateral view, 42–63 % the jaw edges are hidden by the wings (Table 15). Bridges extend to the ventral end of the lateral walls (Fig. 28D) but are not discernible below the jaw angles in early growth stages (Fig. 28I). The bridges are entirely exposed and inclined posterolaterally in horizontal sections (Fig. 28D, and I). Thin and small shoulder blades are distinct in the early growth stage (Fig. 28F and G). They do not become larger with growth

(Fig. 28D). The anterior edge of the shoulder blades does not reach that of the adjacent wing (Fig. 28D). The angle between the jaw edge and the adjacent shoulder blade is obtuse (Fig. 28D, and Table 15). Thin wings rise from the lateral margin of the bridges (Fig. 28D and I). Their anterodorsal part is free from the other pigmented regions and is often damaged (Fig. 28D). The wings are constricted around a jaw edge and do not extend posteriorly from the bridges (Fig. 28A–C). The hood is fairly elongated, broadly arched, and has no notches (Fig. 28A–C, and F–H). Lateral walls have the shape of a parallelogram that is as long as high (Fig. 28A and B). Ontogenetically, pigmented regions expand laterally from the jaw edges in the outer lamella (Fig. 28E and J) and ventrally from the crest in the inner lamella (Fig. 28F and G). Juveniles often exhibit a broad and large hood (Fig. 28H), jaw edges that are free from the outer lamella (Fig. 28J), a small shoulder blade (Fig. 28I), and lateral walls retaining only a narrow crest part (Fig. 28F–H). Adults have a faint dent on the lateral sides of the rostrum (Fig. 28D).
Occurrence. Earliest Cenomanian to Santonian; Yezo Group in Hokkaido, Japan (Tables 14 and 15).

Monachicothaumida ord. nov.
Diagnosis. The rostrum is strongly protruded forward and slightly hooked. Deep grooves extend posteriorly from the rostral tip to the posterior end of the hood. They gradually become shallow in the posterior part and slightly curve downward. The dorsal margin of these grooves forms an angular ridge. Jaw edges are sharp and single-edged. The hood is relatively long and broadly arched. Both the inner and outer lamellae are very thin. These lamellae fuse in narrow fields around their anterior margin and medial part.
Comparison. The Monachicothaumida can be clearly distinguished from all other coleoid orders by the deep grooves on the hood with the angular dorsal margin (Fig. 27). Extraordinarily thin outer and inner lamellae are seen in the pelagic groups of the Incirrata[27], but this order differs by its large and strongly protruded rostrum (Fig. 27A and G).

Monachicothaumidae fam. nov.
Monachicothauma aenigmatica gen. et. sp. nov.
Etymology. From Ancient Greek *monachikos* (lonely), *thauma* (wonder), and Latin *aenigmaticus* (enigmatic).
Material. Documented in Table 15.
Diagnosis. Same as the diagnosis of the order due to monotypy.
Description. The rostrum strongly protrudes forward and has a small hook on its tip (Fig. 28K and L). The size and width cannot be measured since the only discovered beak lacks jaw angles, but the length between the ventral end of both jaw edges is longer than the jaw edge length (Fig. 28O). The outer and inner lamellae are extremely thin, even in jaw edges, but the rostrum probably retains the original morphology inferred from its fairly symmetrical outline (Fig. 28M and O). These lamellae fuse in narrow fields around their anterior margin and medial part. Jaw edges are straight, sharp, and single-edged (Fig. 28K–O). Bridges, shoulder blades, and wings are not discernible (Fig. 28N). The hood is relatively long, very broadly arched, and not notched (Fig. 28M and O). The hood has a deep groove on both sides (Fig. 28K, and L). These grooves extend posteriorly from the rostral tip to the posterior end of the hood and slightly curve downward. They have the deepest part around their midpoint and gradually become shallow in the rear part. The dorsal margin of these grooves forms an angular ridge.
Occurrence. Late Turonian; Yezo Group in Hokkaido, Japan (Tables 14 and 15).

Cryptaroterida ord. nov.
Diagnosis. The rostrum is broadly arched and has a strong, broad hook. No dents exist on the outer surface around the jaw edges. Bridges are entirely exposed and form a sharp edge on both lateral and medial sides. The ventral part of the bridges is almost parallel to the transverse axis in horizontal sections. The medial edge of the bridges extends on the medial surface of the rostrum, forming a low step tapering off dorsally.
Comparison. This order can be distinguished from all other coleoids by the medial edge of the bridges that extend on the medial surface of the rostrum. The large, broad rostral hook is also seen in Cirrata, Incirrata, and Sepiida (Fig. 27A and D)[27]. The Cryptarotida differs from these three orders by the presence of clearly defined bridges (Fig. 27G).

Cryptaroteridae fam. nov.
Cryptaroter vociferans gen. et sp. nov.
Etymology. From Ancient Greek *kruptos* (hidden), *aroter* (plower), and Latin *vociferans* (shouting).
Material. Documented in Table 15.
Diagnosis. Same as the diagnosis of the genus due to monotypy.
Description. The broadly arched rostrum has a strong and broad hook on its tip (Fig. 28P–R and T). The size and width of the rostrum cannot be measured due to the absence of jaw angles, but the length between the ventral end of both jaw edges is longer than the jaw edge length (Fig. 28T). Bridges are entirely exposed, forming a sharp edge on both lateral and medial sides. They show gentle curvature and broaden ventrally (Fig. 28S and T). The ventral part of the bridges is almost parallel to the transverse axis in horizontal sections (Fig. 28P and Q). From the base of the rostral hook, the inner edge of the bridges slightly extends on the inner surface of the rostrum, forming a low step fading dorsally (Fig. 28S). Shoulder blades and wings are not discernible (Fig. 28S). Wing folds and dents on the rostrum around jaw edges are absent (Fig. 28P, and Q). The hood has no notches (Fig. 28R).
Occurrence. Late Coniacian; Yezo Group in Hokkaido, Japan (Tables 14 and 15).

Amblystomida ord. nov.
Diagnosis. The rostrum is narrowly arched, not hooked, and has no dents. Bridges are entirely exposed, form a sharp edge on both lateral and medial sides, and significantly broaden ventrally. The lateral edge of the bridge curves strongly, while the medial edge curves gently. The ventral part of the lateral edges extends anteriorly to run across the medial edge in lateral view.
Comparison. Other than Amblystomida ord. nov., the distinct bridges are also seen in Oegopsida, Vampyromorpha, Belemnitida, Globosimilvida ord. nov., and Cryptarotida ord. nov. (Fig. 27)[27,32,33]. The bridges of the Amblystomida show, however, the highest expansion rate and remarkably increase their curvature laterally, unlike the narrow and planular bridges of the other orders. With these characters, Amblystomida can be easily distinguished from the other coleoid orders.

Amblystomidae fam. nov.
Amblystoma delicatum gen. et sp. nov.
Etymology. From Ancient Greek *amblys* (blunt), *stoma* (mouth), and Latin *delicatus* (delicate).

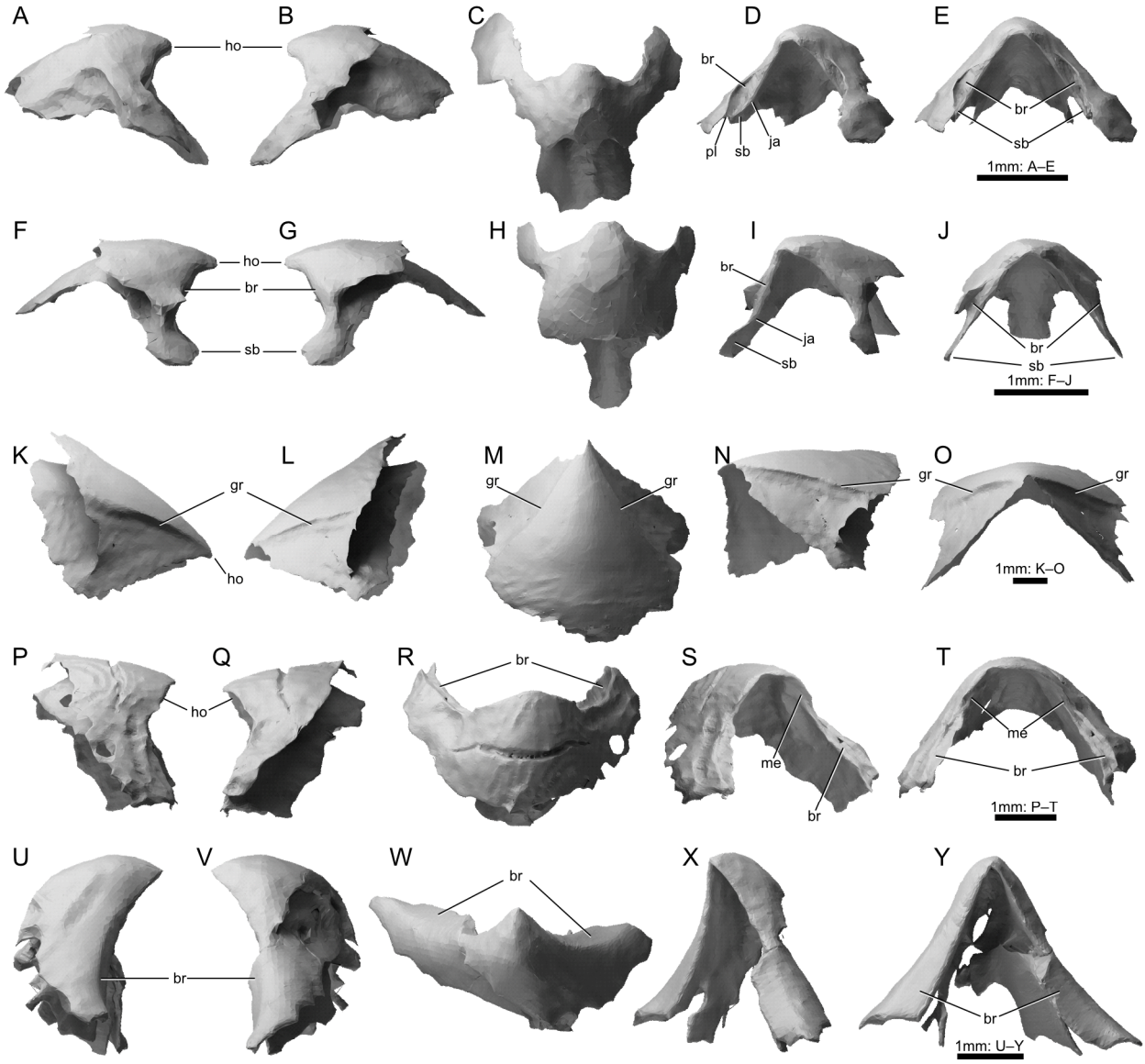


Fig. 28. Lower beaks of the new species.
(**A** to **J**) *Globosimilvus amabilis* gen. et sp. nov. (**K** to **O**) *Monachicothauma aenigmatica* gen. et sp. nov. (**P** to **T**) *Cryptaroter vociferans* gen. et sp. nov. (**U** to **Y**) *Amblystoma delicatum* gen. et sp. nov. (A, F, K, P, and U) Left lateral view; (B, G, L, Q, and V) right lateral view; (C, H, M, R, and W) dorsal view; (D, I, N, S, and X) oblique view; (E, J, O, T, and Y) frontal view. For G. amabilis, both adult (A to E) and juvenile (F to J) are shown. Information on the specimens is provided in Table S1. The 3D models are available from Figshare (https://doi.org/10.6084/m9.figshare.27678570). Abbreviations: br, bridge; gr, groove on the hood; ho, rostral hook; me, medial edge of a bridge; ja, jaw angle; pl, plate at the ventral margin of the shoulders; sb, shoulder blade.

Material. Documented in Table 15.

Diagnosis. Same as the diagnosis of the order due to monotypy.

Description. The rostrum is narrowly arched, not hooked, and has no dents (Fig. 28U–W and Y). The size and width cannot be measured due to the absence of jaw angles, but the jaw edge length is longer than the presumed length between the ventral end of both jaw edges (Fig. 28Y). Bridges are entirely exposed in preserved parts, form a sharp edge on both lateral and medial sides, and broaden ventrally

Table 15. Summary of described lower beaks.

Classification		Geological age	Sample No. of concretion	Growth stage	Measurements											Dataset and Collection No. (NMNS; National Museum of			Resolution		Figures
Genus	Species				CL (mm)	EJEL (mm)	HL (mm)	JELL (mm)	JELL/ EJEL	LRL (mm)	RW (mm)	LRL/ RW	WL (mm)	AJS (degree)	WA (degree)	3D model	Label data of 3D models	Cross-sectional images for 3D models	Pixel size (μm/pixel)	Interval (μm)	
Globosimilvus	*amabilis*	earliest Cenomanian	6	subadult	1.90	1.27	1.23	0.65	0.51	0.78	0.98	0.80	-	146.1	-	NMNS_DS00068_hleQr5Y.stl	L_NMNS_DS00068_20181123_c1_wl_01_0123_hleQr5Y.tif–0145_hleQr5Y.tif	C_NMNS_DS00068_20181123_c1_wl_01_0123_hleQr5Y.jpg–0145_hleQr5Y.jpg	10.715	50	-
Globosimilvus	*amabilis*	earliest Cenomanian	6	adult	1.89	1.30	0.98	0.47	0.36	1.03	1.26	0.82	1.14	148.7	133.3	NMNS_DS00068_VFw7InD.stl	L_NMNS_DS00068_20181123_c1_wl_01_0141_VFw7InD.tif–0180_VFw7InD.tif	C_NMNS_DS00068_20181123_c1_wl_01_0141_VFw7InD.jpg–0180_VFw7InD.jpg	10.715	50	Fig. 26A–E
Globosimilvus	*amabilis*	earliest Cenomanian	6	juvenile	1.51	1.28	1.19	0.75	0.58	0.90	1.08	0.84	-	126.0	-	NMNS_DS00068_Cl5TvPs.stl	L_NMNS_DS00068_20181123_c1_wl_01_0188_Cl5TvPs.tif–0216_Cl5TvPs.tif	C_NMNS_DS00068_20181123_c1_wl_01_0188_Cl5TvPs.jpg–0216_Cl5TvPs.jpg	10.715	50	-
Globosimilvus	*amabilis*	earliest Cenomanian	6	subadult	1.78	1.32	0.94	0.51	0.39	0.97	1.09	0.89	-	122.4	-	NMNS_DS00068_cGlGquN.stl	L_NMNS_DS00068_20181123_c1_wl_01_0779_cGlGquN.tif–0809_cGlGquN.tif	C_NMNS_DS00068_20181123_c1_wl_01_0779_cGlGquN.jpg–0809_cGlGquN.jpg	10.715	50	-
Globosimilvus	*amabilis*	Early Cenomanian	7	subadult	2.10	1.83	1.34	0.77	0.42	1.09	-	-	-	117.4	-	NMNS_DS00084_D51Wcvg.stl	L_NMNS_DS00084_20190202_c1_wl_01_0113_D51Wcvg.tif–0146_D51Wcvg.tif	C_NMNS_DS00084_20190202_c1_wl_01_0113_D51Wcvg.jpg–0146_D51Wcvg.jpg	10.316	50	-
Globosimilvus	*amabilis*	Late Cenomanian	8	subadult	1.94	1.39	1.08	0.68	0.49	1.03	1.24	0.83	-	105.3	-	NMNS_DS00082_kSrDgJd.stl	L_NMNS_DS00082_20190127_c1_wl_01_0659_kSrDgJd.tif–0690_kSrDgJd.tif	C_NMNS_DS00082_20190127_c1_wl_01_0659_kSrDgJd.jpg–0690_kSrDgJd.jpg	11.864	50	-
Globosimilvus	*amabilis*	Late Turonian	12	juvenile	1.50	1.01	0.99	-	-	0.56	0.69	0.81	-	143.4	-	NMNS_DS00041_0H8sJu5.stl	L_NMNS_DS00041_20180414_c1_wl_01_0526_0H8sJu5.tif–0550_0H8sJu5.tif	C_NMNS_DS00041_20180414_c1_wl_01_0526_0H8sJu5.jpg–0550_0H8sJu5.jpg	12.287	50	-
Globosimilvus	*amabilis*	Late Turonian	16	juvenile	1.48	1.27	0.99	-	-	1.19	1.27	0.94	-	-	-	NMNS_DS00173_1dxkPLA.stl	L_NMNS_DS00173_wl_01_0059_1dxkPLA.tif–0089_1dxkPLA.tif	C_NMNS_DS00173_wl_01_0059_1dxkPLA.tif–0089_1dxkPLA.tif	5.339	50	-
Globosimilvus	*amabilis*	Late Turonian	16	juvenile	1.85	1.21	1.21	-	-	1.07	-	-	-	-	-	NMNS_DS00173_BYbf08O.stl	L_NMNS_DS00173_wl_01_0143_BYbf08O.tif–0168_BYbf08O.tif	C_NMNS_DS00173_wl_01_0143_BYbf08O.tif–0168_BYbf08O.tif	5.339	50	-
Globosimilvus	*amabilis*	Late Turonian	16	subadult	1.91	1.37	1.13	-	-	1.01	1.40	0.72	-	-	-	NMNS_DS00173_LnfY1uq.stl	L_NMNS_DS00173_wl_01_0257_LnfY1uq.tif–0279_LnfY1uq.tif	C_NMNS_DS00173_wl_01_0257_LnfY1uq.tif–0279_LnfY1uq.tif	5.339	50	-
Globosimilvus	*amabilis*	Late Turonian	16	juvenile	2.15	1.43	1.20	-	-	1.13	1.29	0.88	-	115.0	-	NMNS_DS00173_So8W1S2.stl	L_NMNS_DS00173_wl_01_0984_So8W1S2.tif–1010_So8W1S2.tif	C_NMNS_DS00173_wl_01_0984_So8W1S2.tif–1010_So8W1S2.tif	5.339	50	-
Globosimilvus	*amabilis*	Late Turonian	16	juvenile	2.10	1.39	1.07	-	-	1.11	1.42	0.78	-	96.1	-	NMNS_DS00173_namBOfY.stl	L_NMNS_DS00173_wl_01_1059_namBOfY.tif–1085_namBOfY.tif	C_NMNS_DS00173_wl_01_1059_namBOfY.tif–1085_namBOfY.tif	5.339	50	-
Globosimilvus	*amabilis*	Late Turonian	16	juvenile	-	1.19	0.93	-	-	0.93	1.11	0.83	-	-	-	NMNS_DS00173_kHB54lC.stl	L_NMNS_DS00173_wl_01_1130_kHB54lC.tif–1153_kHB54lC.tif	C_NMNS_DS00173_wl_01_1130_kHB54lC.tif–1153_kHB54lC.tif	5.339	50	-
Globosimilvus	*amabilis*	Late Turonian	16	juvenile	1.60	1.23	0.99	-	-	0.91	1.11	0.82	-	-	-	NMNS_DS00173_RnM3wfq.stl	L_NMNS_DS00173_wl_01_1199_RnM3wfq.tif–1228_RnM3wfq.tif	C_NMNS_DS00173_wl_01_1199_RnM3wfq.tif–1228_RnM3wfq.tif	5.339	50	-
Globosimilvus	*amabilis*	Late Coniacian	20	subadult	2.25	1.48	1.32	0.60	0.40	1.02	1.36	0.75	-	-	-	NMNS_DS00089_aAhgCur.stl	L_NMNS_DS00089_20190223_c1_wl_01_0237_aAhgCur.tif–0278_aAhgCur.tif	C_NMNS_DS00089_20190223_c1_wl_01_0237_aAhgCur.jpg–0278_aAhgCur.jpg	8.871	50	-
Globosimilvus	*amabilis*	Late Coniacian	20	adult	1.92	1.27	1.35	0.51	0.40	0.85	1.15	0.74	-	-	-	NMNS_DS00089_x2MorFu.stl	L_NMNS_DS00089_20190223_c1_wl_01_0398_x2MorFu.tif–0440_x2MorFu.tif	C_NMNS_DS00089_20190223_c1_wl_01_0398_x2MorFu.jpg–0440_x2MorFu.jpg	8.871	50	-
Globosimilvus	*amabilis*	Late Coniacian	20	adult	1.97	1.40	1.29	0.57	0.41	1.23	1.37	0.90	1.18	119.6	-	NMNS_DS00089_W3S5OcS.stl	L_NMNS_DS00089_20190223_c1_wl_01_0477_W3S5OcS.tif–0509_W3S5OcS.tif	C_NMNS_DS00089_20190223_c1_wl_01_0477_W3S5OcS.jpg–0509_W3S5OcS.jpg	8.871	50	-
Globosimilvus	*amabilis*	Santonian	21	juvenile	2.28	1.51	1.31	0.87	0.58	1.10	1.40	0.79	-	121.0	-	NMNS_DS00004_vj51kJF.stl	L_NMNS_DS00004_20170519_c1_wl_01_0348_vj51kJF.tif–0376_vj51kJF.tif	C_NMNS_DS00004_20170519_c1_wl_01_0348_vj51kJF.jpg–0376_vj51kJF.jpg	17.852	50	Fig. 26F–J
Globosimilvus	*amabilis*	Santonian	26	juvenile	-	1.30	1.13	0.48	0.37	0.98	1.22	0.80	-	-	-	NMNS_DS00104_UkrKuyx.stl	L_NMNS_DS00104_wl_01_0375_UkrKuyx.tif–0401_UkrKuyx.tif	C_NMNS_DS00104_wl_01_0375_UkrKuyx.tif–0401_UkrKuyx.tif	9.768	50	-
Globosimilvus	*amabilis*	Santonian	26	juvenile	1.67	1.20	0.99	-	-	1.03	1.22	0.84	-	-	-	NMNS_DS00104_0Q7mSuK.stl	L_NMNS_DS00104_wl_01_0437_0Q7mSuK.tif–0470_0Q7mSuK.tif	C_NMNS_DS00104_wl_01_0437_0Q7mSuK.tif–0470_0Q7mSuK.tif	9.768	50	-
Monachicothauma	*aenigmatica*	Late Turonian	12	subadult	-	4.66	5.87	-	-	-	-	-	-	-	-	NMNS_DS00041_aH7yQ7u.stl	L_NMNS_DS00041_20180414_c1_wl_01_0435_aH7yQ7u.tif–0554_aH7yQ7u.tif	C_NMNS_DS00041_20180414_c1_wl_01_0435_aH7yQ7u.jpg–0554_aH7yQ7u.jpg	12.287	50	Fig. 26K–O
Cryptaroter	*vociferans*	Late Turonian	20	uncertain	-	2.40	2.22	-	-	-	-	-	-	-	-	NMNS_DS00089_k15wqI8.stl	L_NMNS_DS00089_20190223_c1_wl_01_0113_k15wqI8.tif–0179_k15wqI8.tif	C_NMNS_DS00089_20190223_c1_wl_01_0113_k15wqI8.jpg–0179_k15wqI8.jpg	8.871	50	Fig. 26P–T
Amblystoma	*delicatum*	Late Campanian	31	uncertain	-	1.92	1.65	-	-	-	-	-	-	-	-	NMNS_DS00171_eFfEVfb.stl	L_NMNS_DS00171_wl_01_0911_eFfEVfb.tif–0943_eFfEVfb.tif	C_NMNS_DS00171_wl_01_0911_eFfEVfb.tif–0943_eFfEVfb.tif	5.805	50	Fig. 26U–Y

Table 16. Comparison of morphological features among coleoid lower beaks.

Morphological type		Known types					New types			
		Type-I	**Type-II**	**Type-III**	**Type-IV**	**Type-V**	**Type VI**	**Type-VII**	**Type VIII**	**Type IX**
Orders included		Cirrata, Incirrata	Vampyromorpha	Oegopsida, Myopsida, Sepiolida, and Spirulida	Sepiida	Belemnitida	Globosimilvida ord. nov.	Monachicothaumida ord. nov.	Cryptaroterida ord. nov.	Amblystomida ord. nov.
Morphological features	1. Bridges	Unrecognizable	Distinct	Unrecognizable or reduced	Unrecognizable	Distinct	Distinct	Unrecognizable	Distinct	Distinct
	2. Width of bridges	No bridges	Narrow	Narrow	No bridges	Narrow	Narrow	No bridges	Narrow	Broad
	3. Rostral hook	Large and broad	Absent	Small and sharp	Large and broad	Small and sharp	Small and sharp	Small and sharp	Large and broad	Absent
	4. Jaw angle	Rounded	Indistinct	Angular	Rounded	Indistinct	Indistinct	Uncertain	Uncertain	Uncertain
	5. Shoulder blade	Unrecognizable	Indistinct	Distinct	Unrecognizable	Indistinct	Distinct	Uncertain	Uncertain	Uncertain
	6. Basal part of wings	Connected to a shoulder blade	Free edge	Form wing folds	Form wing folds	Free edge	Free edge	Uncertain	Uncertain	Uncertain
	7. Ventral edge of shoulder blades	Not defined	Free edge	Free edge	Not defined	Free edge	Connected to a wing and a bridge	Uncertain	Uncertain	Uncertain
	8. Grooves on lateral sides of the hood	Absent	Absent	Absent	Absent	Absent	Absent	Present	Absent	Absent
	9. Medial edge of bridges	No bridges	Converged to the rostral tip	Converged to the rostral tip	No bridges	Converged to the rostral tip	Converged to the rostral tip	No bridges	Extended on the medial surface	Converged to the rostral tip
	10. Lataral edge of bridges	No bridges	Parallel to the medial edge	Parallel to the medial edge	No bridges	Parallel to the medial edge	Parallel to the medial edge	No bridges	Parallel to the medial edge	Curving stronger than the medial edge

with a significantly large expansion rate (Fig. 28X). The curvature of these edges is stronger in the lateral one than in the inner one (Fig. 28U, V, and X). The ventral part of the lateral edges extends anteriorly to run across the inner edges in lateral view. The hood is relatively short (Fig. 28W). Shoulder blades, wings, and wing folds are not discernible (Fig. 28X).

Occurrence. Late Campanian; Yezo Group in Hokkaido, Japan (Tables 14 and 15).

4.5. Discussion

4.5.1. The discovery of four new orders in coleoid cephalopods

Coleoids, a cephalopod group without external shells, are classified into three superorders: eight-armed Octobrachia, ten-armed Decabrachia, and ten-armed Belemnoidea[12,34]. The Octobrachia consist of octopuses and vampire squids[11,12,34]. The Decabrachia include squids, bobtail squids, cuttlefishes, and ram's horn squids[4,34]. Belemnoidea, the stem group of Decabrachia, comprises all groups of belemnites[12,35,36]. Based on their body plan, coleoids can be divided into soft-bodied and internal shelled groups[4,34]. The soft-bodied group (octopuses, vampire squids, squids, and bobtail squids) represents the majority of extant cephalopods with respect to species diversity and biomass[4,37]. Most taxa of the internal shelled group belong to the Belemnoidea and became extinct at the Cretaceous-Paleogene boundary (~66 Ma)[4,5]. Nowadays shelled coleoids are represented by the cuttlefishes and the ram's horn squids, which have survived into modern oceans.[4,5]

The morphology of cephalopod beaks is constrained by phylogenetic relationships rather than by feeding habits[15]. The known lower beaks of coleoids can be classified into five morphological types (Fig. 27 and Table 16): type-I (octopuses), II (vampire squids), III (squids, bobtail squids, and ram's horn squids), IV (cuttlefishes), and V (belemnites). The identification of these types is not affected by ontogenetic changes[29,38,39]. The four new taxa described in this study do not correspond to any of the five morphological types, and are significantly different from each other. They thus represent distinct taxonomic groups at the order level (Fig. 27 and Table 16). The taxa newly described are different to any representatives of the known eight- and ten-armed cephalopods.

4.5.2. Are the new taxa shelled or soft-bodied?

In cephalopods, the large mineralized shell is more likely to be fossilized and discovered than the beaks. Over a century of research has provided many fossils of the coleoid internal shell from the Northwest Pacific region[6,35,40–42]. Belemnite shells are abundant in the Lower Cretaceous (~145–100 Ma) of this region but they are absent in the Upper Cretaceous due to their regional extinction at the Early-Late Cretaceous boundary[6]. Only two species of shelled coleoids are known from the Upper Cretaceous of this region: *Conoteuthis hayakawai* (Belemnoidea) and *Longibelus matsumotoi* (a stem group of ram's horn squids)[35].

The descriptions of *C. hayakawai* and *L. matsumotoi* are both based on shell fossils, their beaks have yet to be found. Both species are interpreted to represent intermediate groups between Belemnitida and Spirulida[35,42]. Thus, their beaks are thought to be either type-III[43], type-V, or intermediate between both types. In contrast, the beak morphologies of the four new orders described here do not correspond to these potential beak types of the two shelled species. *C. hayakawai* occurs in the Lower Cenomanian to the Upper Turonian[42]. Despite being the thinnest-shelled coleoid, *L. matsumotoi* has been discovered continuously from the Lower Cenomanian to the Lower Maastrichtian (Fig. 29)[35]. The stratigraphic ranges of the four new taxa, described here, do not correlate with those

of *C. hayakawai* and *L. matsumotoi* (Fig. 29). Since this study have obtained 1,000 fossil cephalopod beaks continuously from the Middle Albian to the Lower Maastrichtian, the different stratigraphic ranges are not reflecting a sampling bias of this study. These lines of evidence demonstrate that the four new taxa were soft-bodied coleoids, lacking shells.

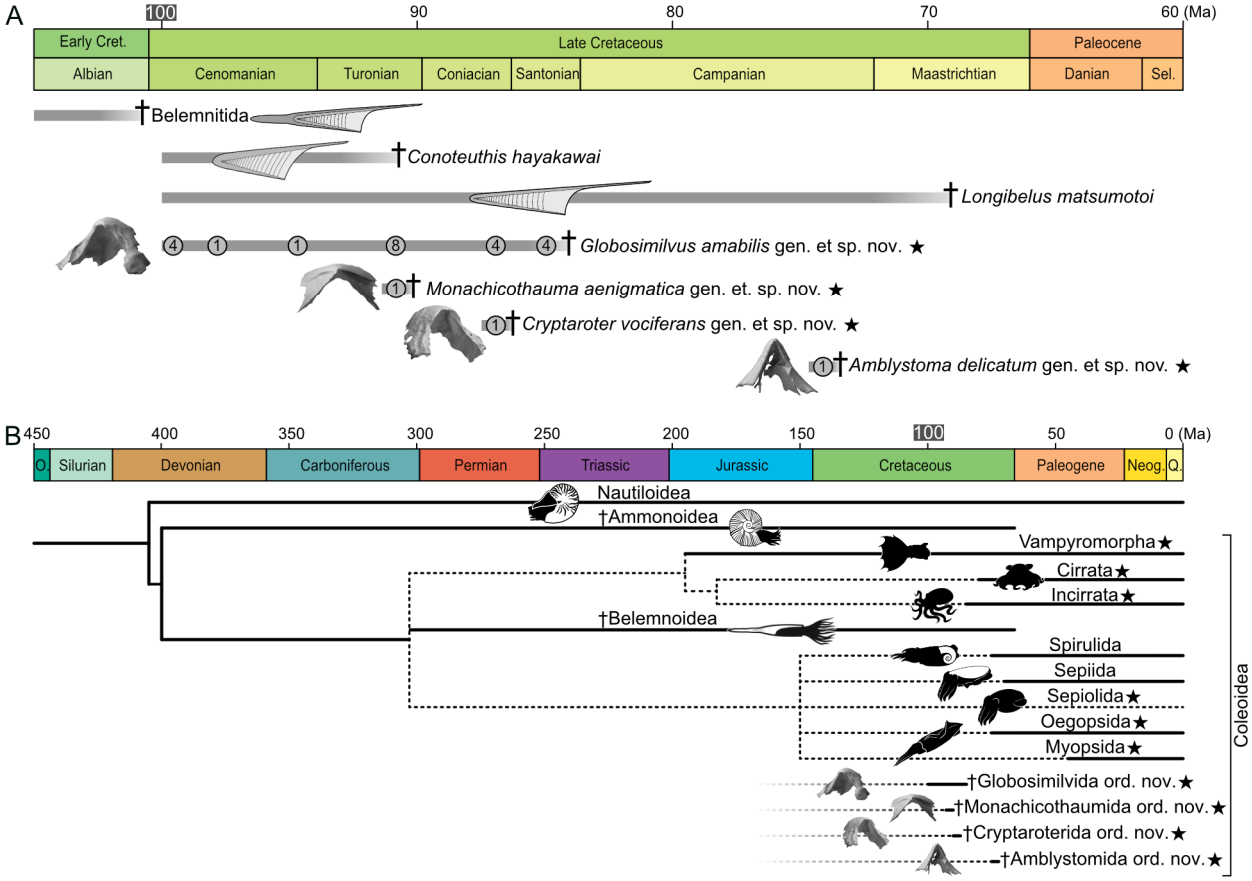


Fig. 29. Stratigraphic ranges and phylogenetic relationships of cephalopods.
(**A**) Stratigraphic ranges of known internal shelled coleoids and of the four new species from the Late Cretaceous of the Northwest Pacific. The beak numbers of the new species are shown in the grey circles. (**B**) Chronological distribution and phylogenetic tree of cephalopods. Lineages confirmed by fossil records are shown as solid lines, while hypothetical ones are indicated by dashed lines. Stars indicate the soft-bodied lineages. The phylogenetic tree and fossil records of the known groups are from previous studies.

4.5.3. Decoding soft-bodied cephalopod evolution

Beaks are one of the few hard tissues that fossilize in soft-bodied cephalopods, useful for taxonomy[13,27,38]. So far only few fossil beaks have been described, limiting the knowledge of the evolution of soft-bodied cephalopods. In this study, we introduce four new taxonomic groups (orders) by examining a large number of fossil beaks. These are the first discoveries of extinct orders of soft-bodied coleoids. The findings of this study suggest that a substantial number of unknown soft-bodied cephalopods is still hidden in the sedimentological archives.

Previous studies which aimed at reconstructing the evolutionary history of soft-bodied cephalopods used two approaches. One procedure uses molecular analyses to reconstruct the phylogenetic trees of extant species[7,9]. Albertin et al.[9] investigated the genome evolution of modern cephalopods by using mitochondrial protein-coding genes of 19 species. Their results suggest that the

genetic innovation, supporting the novelty of soft-bodied groups, likely occurred before the split of octopuses and squids in the Permian at ~275 Ma. The second approach focuses on tracing fossil records of extant clades through geological time. Fuchs[11] established a systematic of all soft-bodied groups known from Mesozoic Lagerstätten. He assigned them into the affinity of the octopuses and vampire squids, including groups of which the order-level classification remains uncertain. Whalen and Landman[12] reported the oldest fossil of soft-bodied cephalopods and compared its morphology with those of fossils and extant species. Their results suggest that the origin of the octopus lineage goes back to the Carboniferous, which is ~82 million years earlier than previously assumed. Both of these approaches can, however, only reconstruct the phylogenetic lineage of extant species, extinct ones are unrecognized. In contrast, this study reveals that multiple lineages of soft-bodied cephalopods without extant descendants repeatedly originated and declined in the Late Cretaceous Oceans (Fig. 29).

References for Chapter 4

1. Alroy, J. The shifting balance of diversity among major marine animal groups. *Science* **329**, 1191–1194 (2010).
2. Tittensor, D. P. *et al.* Global patterns and predictors of marine biodiversity across taxa. *Nature* **466**, 1098–1101 (2010).
3. Close, R. A., Benson, R. B. J., Saupe, E. E., Clapham, M. E. & Butler, R. J. The spatial structure of Phanerozoic marine animal diversity. *Science* **368**, 420–424 (2020).
4. Kröger, B., Vinther, J. & Fuchs, D. Cephalopod origin and evolution: A congruent picture emerging from fossils, development and molecules. *BioEssays* **33**, 602–613 (2011).
5. Maderspacher, F. Thinking outside the shell. *Curr. Biol.* **33**, R1071–R1078 (2023).
6. Iba, Y. *et al.* Belemnite extinction and the origin of modern cephalopods 35 m.y. prior to the Cretaceous-Paleogene event. *Geology* **39**, 483–486 (2011).
7. Tanner, A. R. *et al.* Molecular clocks indicate turnover and diversification of modern coleoid cephalopods during the Mesozoic Marine Revolution. *Proc. R. Soc. B Biol. Sci.* **284**, 20162818 (2017).
8. Amodio, P. *et al.* Grow smart and die young: why did cephalopods evolve intelligence? *Trends Ecol. Evol.* **34**, 45–56 (2019).
9. Albertin, C. B. *et al.* Genome and transcriptome mechanisms driving cephalopod evolution. *Nat. Commun.* **13**, 2427 (2022).
10. Gilbert, P. U. P. A. *et al.* Biomineralization: Integrating mechanism and evolutionary history. *Sci. Adv.* **8**, eabl9653 (2022).
11. Fuchs, D. Part M, Chapter 23G: Systematic descriptions: Octobrachia. *Treatise Online* **138**, 1–52 (2020).
12. Whalen, C. D. & Landman, N. H. Fossil coleoid cephalopod from the Mississippian Bear Gulch Lagerstätte sheds light on early vampyropod evolution. *Nat. Commun.* **13**, 1107 (2022).
13. Tanabe, K., Misaki, A. & Ubukata, T. Late Cretaceous record of large soft-bodied coleoids based on lower jaw remains from Hokkaido, Japan. *Acta Palaeontol. Pol.* **60**, 27–38 (2015).
14. Takashima, R. *et al.* Geology and stratigraphy of forearc basin sediments in Hokkaido, Japan: Cretaceous environmental events on the north-west Pacific margin. *Cretac. Res.* **25**, 365–390 (2004).
15. Clarke, M. R. & Maddock, L. Beaks of living coleoid Cephalopoda. in *Paleontology and neontology of cephalopods* (eds. Clarke, M. R. & Trueman, E. R.) 123–131 (Academic Press, Cambridge, 1988).
16. Obradovich, J. D., Matsumoto, T., Nishida, T. & Inoue, Y. Integrated biostratigraphic and radiometric study on the Lower Cenomanian (Cretaceous) of Hokkaido, Japan. *Proc. Jpn. Acad. Ser. B* **78**, 149–153 (2002).
17. Asai A. & Hirano H. Stratigraphy of the Upper Cretaceous in the Obira area, Northwestern

Hokkaido. *Acad. Stud. Biol. Earth Sci. Sch. Educ. Waseda Univ.* **39**, p37-50 (1990).

18. Tanabe K., Hirano H., Matsumoto T. & Miyata Y. Stratigraphy of the Upper Cretaceous deposits in the Obira area, northwestern Hokkaido. *Sci. Rep. Dep. Geol. Kyushu Univ.* **12**, 181–202 (1977).
19. Toshimitsu, S. Biostratigraphy of the Upper Cretaceous Santonian Stage in Northwestem Hokkaido. *Mem. Fac. Sci. Kyushu Univ. Ser. Geol.* **26**, 125–192 (1988).
20. Shigeta, Y. & Izukura, M. Discovery of the middle Campanian (late Cretaceous) "Soya Fauna" ammonoids in the Hidaka area, Hokkaido, Japan. *Bull. Hobetsu Mus.* **33**, 11–25 (2018).
21. Takahashi, A., Hikida, Y., Jenkins, R. G. & Tanabe, K. Stratigraphy and megafauna of the Upper Cretaceous Yezo Supergroup in the Teshionakagawa area, northern Hokkaido, Japan. *Bull. Mikasa City Mus.* **11**, 25–59 (2007).
22. Okamoto T., Matsunaga T. & Okada M. Restudy of the Upper Cretaceous stratigraphy in the Haboro area, northwestern Hokkaido. *J. Geol. Soc. Jpn.* **109**, 363–382 (2003).
23. Kawabe S. & Okamoto T. Restudy of the Upper Cretaceous megafossil biostratigraphy in the Migi-no-sawa area, a tributary of the Haboro River, northwestern Hokkaido. *J. Geol. Soc. Jpn.* **118**, 769–781 (2012).
24. Osanai, H. Mitani, K. Takahashi, K. *Explanatory text of the geological map of Japan 'Kyowa' (scale 1:50000)*. (Geological Survey of Hokkaido, Sapporo, 1960).
25. Ando, H. & Tomosugi, T. Unconformity between the Upper Maastrichtian and Upper Paleocene in the Hakobuchi Formation, north Hokkaido, Japan: a major time gap within the Yezo forearc basin sediments. *Cretac. Res.* **26**, 85–95 (2005).
26. Shigeta, Y., Izukura, M. & Tsutsumi, Y. An early Maastrichtian (latest Cretaceous) ammonoid fauna from the Soya Hill area, Hokkaido, northern Japan. *Bull. Hobetsu Mus.* **32**, 7–41 (2017).
27. Clarke, M. R. *A Handbook for the Identification of Cephalopod Beaks*. (Clarendon Press, Oxford, 1986).
28. Young, R. E., Clarke, M. R., Vecchione, M. & Mangold, K. M. Beak terminology. *Tree of Life* http://tolweb.org/notes/?note_id=1980 (2000).
29. Hernández-García, V. Growth and pigmentation process of the beaks of *Todaropsis Eblanae* (Cephalopoda: Ommastrephidae). *Berl. Paläobiologische Abh.* **3**, 131–140 (2003).
30. International Commission on Zoological Nomenclature. Declaration 45 — Addition of Recommendations to Article 73 and of the term "specimen, preserved" to the Glossary. *Bull. Zool. Nomencl.* **73**, 96–97 (2017).
31. Tanabe, K., Kruta, I. & Landman, N. H. Ammonoid Buccal Mass and Jaw Apparatus. in *Ammonoid Paleobiology: From anatomy to ecology* (eds. Klug, C., Korn, D., De Baets, K., Kruta, I. & Mapes, R. H.) vol. 43 429–484 (Springer Netherlands, Dordrecht, 2015).
32. Young, R. E. Beak structure and evolution. *Tree of Life* http://tolweb.org/notes/?note_id=4541 (2007).
33. Klug, C., Etter, W., Hoffmann, R., Fuchs, D. & De Baets, K. Jaws of a large belemnite and an ammonite from the Aalenian (Middle Jurassic) of Switzerland. *Swiss J. Palaeontol.* **139**, 7 (2020).

34. Boyle, P. & Rodhouse, P. *Cephalopods: Ecology and Fisheries*. (Blackwell Science, Oxford, 2005).

35. Fuchs, D. *et al. Longibelus* gen. nov., A new Cretaceous coleoid genus linking Belemnoidea and early Decabrachia. *Palaeontology* **56**, 1081–1106 (2013).

36. Hoffmann, R. & Stevens, K. The palaeobiology of belemnites – foundation for the interpretation of rostrum geochemistry. *Biol. Rev.* **95**, 94–123 (2020).

37. Nesis, K. N. Distribution of recent Cephalopoda and implications for Plio-Pleistocene events. *Berl. Paläobiologische Abh.* **3**, 199–224 (2003).

38. Clarke, M. R. The identification of cephalopod 'beaks' and the relationship between beak size and total body weight. *Bull. Br. Mus. Nat. Hist. Zool.* **8**, 419–480 (1962).

39. Klug, C., Schweigert, G., Fuchs, D. & Dietl, G. First record of a belemnite preserved with beaks, arms and ink sac from the Nusplingen Lithographic Limestone (Kimmeridgian, SW Germany). *Lethaia* **43**, 445–456 (2010).

40. Yabe H. Discovery of Belemnites from the Cretaceous of Hokkaido. *Jpn. J. Geol. Geogr.* **9**, 36 (1902).

41. Hewitt, R. A., Yoshiike, T. & Westermann, G. E. G. Shell microstructure and ecology of the Cretaceous coleoid cephalopod *Naefia* from the Santonian of Japan. *Cretac. Res.* **12**, 47–54 (1991).

42. Fuchs, D., Keupp, H. & Wiese, F. Protoconch morphology of *Conoteuthis* (Diplobelida, Coleoidea) and its implications on the presumed origin of the Sepiida. *Cretac. Res.* **34**, 200–207 (2012).

43. Tanabe, K. & Misaki, A. Upper Cretaceous record of non-belemnitid coleoid jaws from Hokkaido, Japan, and its evolutionary implications. *Cretac. Res.* **151**, 105624 (2023).

General Discussion

This study has addressed the challenges in researching the evolutionary history of soft-bodied cephalopods by overcoming the incompleteness of fossil record. A novel approach was taken in this study, which transfers the entire process from fossil-mining to curation into cyberspace. By that, this study succeeded in discovering 671 fossil beaks of coleoid cephalopods (Table 2), for which only 37 specimens were previously known in the studied section[1–7]. These fossils are "microfossils" being smaller than 5 mm on average, which can currently be discovered and extracted only in the digital fossil-mining method. Additionally, the digital 3D models can be easily enlarged, rotated, and measured without damaging the fossils. Consequently, this enables the accurate observation and measurement of more traits. This study established the beak identification methods that can be used for both fossil and extant coleoids. A total of 4 orders, 8 families, 30 genera, and 50 species were discovered here as possible new taxa among the Late Cretaceous soft-bodied cephalopods (these taxa will be formally described in future papers at appropriate journals). This discovery was made from only 35 samples from the Yezo group, which have been thoroughly investigated over 100 years. Thus, the digital fossil mining of beak fossils will facilitate further discoveries of numerous previously overlooked taxa.

The findings of new fossil beaks provide continuous records of various soft-bodied groups during the Cretaceous period. This result reveals the origins of squids and the Cirrata, and identifies four unknown groups that cannot be identified even at the superorder level (Fig. 29). These unknown groups represent "lineages not connected to extant species," highlighting the unrecognized biases in previous evolutionary history studies (Chapter 4). In Vampyromorpha, this research fills a 90-million-year gap from the Early Cretaceous to the Oligocene[8] (Fig. 26). Unbiased discovery and identification of a significant number of beak fossils have demonstrated that groups such as the Incirrata did not inhabit the northwestern Pacific in the Late Cretaceous.

Since each cephalopod lower jaw corresponds to a single individual, and the fossilization potential is expected to be consistent across different taxonomic groups[9], it allows for a comparative analysis of the population sizes of various cephalopod groups, which is not feasible with shell fossils. This comparison revealed that soft-bodied cephalopods exhibited overwhelmingly high proportions during the Late Cretaceous. Squids were the most abundant group, surpassing even the ammonites (Fig. 16 and Table 2). This was followed by the Vampyromorpha, the unknown groups, and the Cirrata, all of which were found in greater numbers than the shelled Nautiloids. Added to that, the estimated body size (Tables 4–6) indicated that soft-bodied cephalopods were larger than ammonites, suggesting that the Late Cretaceous Pacific was dominated by soft-bodied cephalopods. This study also revealed that the biomass of soft-bodied cephalopods exceeded that of teleost fishes, which are currently their ecological competitors[10], by more than tenfold (Fig. 16 and Table 2, 4–8). The dominance of squids indicates that the modern-type diversity and biomass composition of cephalopods have already been established in the Late Cretaceous. Today, cephalopods are central predators in marine ecosystems, alongside teleost fishes and marine mammals, all characterised by advanced bodily functions and intelligence[11,12]. This study suggests that cephalopods, through innovations such as the transition to soft-bodied forms, were the first to thrive among these groups. Consequently, the Late Cretaceous rise of cephalopods likely accelerated the evolution of body manipulation and intelligence in marine organisms, significantly contributing to the formation of the current marine ecosystem framework.

These findings on the origin, diversification, and biomass illuminate a significant shift in cephalopods from shelled to soft-bodied forms at the Early/Late Cretaceous boundary (Fig. 15). This boundary marked the extinction of belemnites in regions outside the polar areas[13,14] and the emergence and diversification of squids, octopuses[15] and unknown orders. It was followed by the later appearance of orders such as Spirulida[16] and Sepiida[17]. These findings demonstrate that soft-bodied cephalopods diversified during the Late Cretaceous, challenging the traditional hypothesis of the phylogeny and the Cenozoic diversification of soft-bodied groups. Since the fluctuations in their diversity seem unrelated to geological events like OAEs[18], biological interactions such as niche competitions have probably been the principal factors of their evolution.

The absence of certain groups from the northwestern Pacific has provided new insights into the paleobiogeography of early soft-bodied cephalopods. According to the oldest records in prior research, Incirrata originated in the Tethys Sea[15], the Spirulida in the northeastern Pacific[16], the Sepiida in the northern Atlantic[17], and the Sepiolida in North America (Sugiura: personal communications), each in different regions. These records indicate that the various cephalopod groups, now widespread, had contemporarily originated and evolved in separate regions during the Late Cretaceous.

An ecological comparison focusing on body size and diet indicated the niche diversity of Late Cretaceous soft-bodied cephalopods. Most squid were relatively small, and their beak morphology, with sharp jaw edges and large rostrum similar to modern squids, suggests that many were predatory on fish and other cephalopods. In contrast, the Cirrata were of gigantic size, comparable to sharks and marine reptiles, and were likely durophagous predators, preying on hard-shelled organisms. The Cretaceous is known to be in the middle of the Mesozoic Marine Revolution, characterized by the acceleration of durophagy and the evolution of defensive shell morphology in prey[19]. Despite numerous extant cephalopods being known for durophagy, previous studies have considered cephalopods to be less related to this event[20]. However, the Cirrata, occupying an apex predator role in benthic ecosystems, might have contributed significantly to these marine food web transformations. The Vampyromorpha, considered living fossils from the Mesozoic[21], were likely extremely small plankton feeders. The unidentified groups, all small in size and lacking beak morphology indicative of piscivory or durophagy, were probably plankton feeders as well. These findings suggest that various groups of soft-bodied cephalopods occupied different niches within the same habitats, diversifying through differences in body size and the mode of feeding. They might have controlled the evolutions of marine animals through food webs with their huge biomass and diverse ecological niches.

References for General Discussion

1. Kanie, Y. New vampyromorph (Coleoidea: Cephalopoda) jaw apparatuses from the Late Cretaceous of Japan. *Bull. Gumma Mus. Nat. Hist.* **2**, 23–34 (1998).
2. Tanabe, K., Hikida, Y. & Iba, Y. Two coleoid jaws from the Upper Cretaceous of Hokkaido, Japan. *J. Paleontol.* **80**, 138–145 (2006).
3. Tanabe, K., Trask, P., Ross, R. & Hikida, Y. Late Cretaceous octobrachiate coleoid lower jaws from the North Pacific regions. *J. Paleontol.* **82**, 398–408 (2008).
4. Tanabe, K. & Hikida, Y. Jaws of a New Species of *Nanaimoteuthis* (Coleoidea: Vampyromorphida) from the Tuironian of Hokkaido, Japan. *Paleontol. Res.* **14**, 145–150 (2010).
5. Tanabe, K., Misaki, A. & Ubukata, T. Late Cretaceous record of large soft-bodied coleoids based on lower jaw remains from Hokkaido, Japan. *Acta Palaeontol. Pol.* **60**, 27–38 (2015).
6. Tanabe, K., Misaki, A., Hikida, Y. & Nishimura, T. New records of coleoid cephalopod jaws from the Upper Cretaceous of Hokkaido, Japan, and their paleobiogeographic and evolutionary implications. *Cret. Res.* **70**, 128–141 (2017).
7. Tanabe, K. & Misaki, A. Upper Cretaceous record of non-belemnitid coleoid jaws from Hokkaido, Japan, and its evolutionary implications. *Cret. Res.* **151**, 105624 (2023).
8. Košťák, M. *et al.* Fossil evidence for vampire squid inhabiting oxygen-depleted ocean zones since at least the Oligocene. *Commun. Biol.* **4**, 216 (2021).
9. Tanabe, K. & Fukuda, Y. Morphology and function of cephalopod buccal mass. in *Functional Morphology of the Invertebrate Skeleton* (ed. Savazzi, E.) 245–262 (John Wiley & Sons, New York, 1999).
10. Packard, A. Cephalopods and fish: the limits of convergence. *Biol. Rev.* **47**, 241–307 (1972).
11. Amodio, P. *et al.* Grow smart and die young: why did cephalopods evolve intelligence? *Trends Ecol. Evol.* **34**, 45–56 (2019).
12. Roth, G. Convergent evolution of complex brains and high intelligence. *Philos. Trans. R. Soc. B Biol. Sci.* **370**, 20150049 (2015).
13. Doyle, P. A review of the biogeography of Cretaceous belemnites. *Palaeogeogr. Palaeoclimatol. Palaeoecol.* **92**, 207–216 (1992).
14. Iba, Y. *et al.* Belemnite extinction and the origin of modern cephalopods 35 m.y. prior to the Cretaceous-Paleogene event. *Geology* **39**, 483–486 (2011).
15. Fuchs, D., Bracchi, G. & Weis, R. New octopods (cephalopoda: Coleoidea) from the late cretaceous (upper cenomanian) of Hâkel and Hâdjoula, Lebanon. *Palaeontology* **52**, 65–81 (2009).
16. Fuchs, D. *et al. Longibelus* gen. nov., A new Cretaceous coleoid genus linking Belemnoidea and early Decabrachia. *Palaeontology* **56**, 1081–1106 (2013).
17. Košt'ák, M., Jagt, J. W., Speijer, R. P., Stassen, P. & Steurbaut, E. New Paleocene sepiid coleoids (Cephalopoda) from Egypt: evolutionary significance and origin of the sepiid 'rostrum'. *PloS One* **8**, e81180 (2013).
18. Takashima, R. *et al.* Geology and stratigraphy of forearc basin sediments in Hokkaido, Japan:

Cretaceous environmental events on the north-west Pacific margin. *Cret. Res.* **25**, 365–390 (2004).

19. Vermeij, G. J. The Mesozoic marine revolution: evidence from snails, predators and grazers. *Paleobiology* **3**, 245–258 (1977).
20. Walker, S. E. & Brett, C. E. Post-Paleozoic patterns in marine predation: was there a Mesozoic and Cenozoic marine predatory revolution? *Paleontol. Soc. Pap.* **8**, 119–194 (2002).
21. Fuchs, D. Part M, Chapter 23G: Systematic descriptions: Octobrachia. *Treatise Online* **138**, 1–52 (2020)

Acknowledgements

I deeply thank my supervisor Prof. Yasuhiro Iba for extraordinarily kind and patient guidance in my study. I am thankful to Prof. Yoshitsugu Kobayashi and Prof. Toshihiro Yamada for willingly accepting to be sub-chief examiner of my doctoral dissertation. I am also thankful to Prof. Jörg Mutterlose of Ruhr University Bochum, Prof. Neil H. Landman of the American Museum of Natural History, Prof. Alexander J. Hetherington of the University of Edinburgh, Prof. Yuichiro Kashiyama of Fukui University of Technology, Prof. Shinichi Sano of Toyama University for valuable comments on the manuscript. I am grateful to Prof. Makoto Manabe, Ms. Chisako Sakata, Dr. Takuma Haga, and Prof. Kazunori Hasegawa of National Museum of Nature and Science, Prof. Takenori Sasaki of The University Museum, The University of Tokyo, Dr. Akihiro Misaki of Kitakyushu Museum of Natural History and Human History, Dr. Daisuke Aiba of Fukada Geological Institute (Mikasa City Museum), Dr. Yoshinori Hikida of Nakagawa Museum of Natural History, Dr. Kenichiro Shibata of Yokosuka City Museum, and Dr. Tomohiro Nishimura of Hobetsu Museum for access to the previously described specimens. Dr. Mehmet Oguz Derin and Dr. Takahiro Harada of Morgenrot Inc. supported me in developing AI segmentation methods. Dr. Kentaro Uesugi and Dr. Masato Hoshino of Japan Synchrotron Radiation Research Institute gave me kind instructions on the analyses at SPring-8. I am thankful to Dr. Yusuke Takeda of Japan Synchrotron Radiation Research Institute, Dr. Ryuji Takasaki of Okayama University of Science, Dr. Aya Kubota of National Institute of Advanced Industrial Science and Technology, Dr. Keisuke Nakamoto, Ms. Yumi Adachi, Mr. Shintaro Sasaki, Dr. Kota Kubo, Dr. Ryo Taniguchi, Mr. Tomoyuki Ueda for various assistances in this study. Mr. Rintaro Murakami, Mr. Sande An, Mr. Jun Kato, Mr. Yo Uemura, Mr. Tokio Moriguchi, and Mr. Kei Nakayauchi assisted me in fieldwork. Mr. Rinto Noguchi, Mr. Yudai Azuma, and Mr. Kanta Sugiura supported me with the work on image processing.

This work was supported by the Japan Society for the Promotion of Science (grant No. 22J13936), the Japan Science Society (grant No. 2020-6024), and the Fukada Geological Institute. The X-ray data in Figure 2 was acquired at SPring-8 with the approval of the Japan Synchrotron Radiation Research Institute (Proposal Nos. 2018A1703 and 2021B1810).